New atmosphere models for massive stars: line-blanketing effects and wind properties of O stars

Fabrice Martins

UNIVERSITE TOULOUSE III - PAUL SABATIER
U.F.R. PHYSIQUE, CHIMIE, AUTOMATIQUE

New atmosphere models for massive stars: line-blanketing effects and wind properties of O stars

THESIS

submitted for the Degree of

DOCTOR OF THE UNIVERSITY TOULOUSE III
Astrophysics

by

Fabrice MARTINS

Supervisor : Daniel SCHAERER
Co-supervisor : Mohammad HEYDARI-MALAYERI

October 1st 2004

Jury

Pr. Sylvie Vauclair
Pr. D. John Hillier
Dr. Artemio Herrero
Pr. André Maeder
Dr. Daniel Schaerer
Dr. Mohammad Heydari-Malayeri

Contents

Remerciements

Après ces quatre années consacrées aux étoiles non seulement à Toulouse et à Genève mais aussi à travers le monde (Chili, Etats-Unis, Australie... je n'avais jamais autant voyagé !), je voudrais en tout premier lieu adresser mes plus sincères remerciements à Daniel. En plus de ses qualités scientifiques remarquables qui m'ont permis d'apprendre beaucoup et sans cesse, il possède des qualités humaines précieuses qui ont rendu notre collaboration particulièrement agréable et je pense durable. Merci pour tout !

Je voudrais bien sûr associer Mohammad à ces remerciements car il possède lui aussi un sens de l'accueil et une gentillesse que j'ai toujours grandement appréciés lors de nos multiples rencontres.

I also want to warmly acknowldege John Hillier for his constant interest in my work, his precious advice concerning the modelling with CMFGEN and his disposal to answer my questions. I also greatly appreciate his kindness each time we have the chance to meet. And thanks a lot for revising my thesis and attending the french presentation !

A propos de la soutenance, je tiens aussi à remercier les diverses paeronnes qui ont accepté de faire partie du jury, et notamment Artemio Herrero qui a su trouver un peu de place dans son emploi du temps chargé pour lire et faire son rapport sur ma thèse, et qui lui aussi a toujours montré de l'intérêt pour mon travail. Une autre personne à l'emploi du temps bien rempli a accepté de présider ce jury de thèse: merci à Sylvie Vauclair. Enfin, je suis reconnaissant à André Maeder d'avoir accepté le rôle d'examinateur, mais aussi de communiquer avec toujours le même enthousiasme sa passion des étoiles (et pour le cor des Alpes), même au milieu des montagnes !

J'aimerais à cet instant exprimer ma profonde gratitude à mes parents pour leur soutien de tous les jours. Si aujourd'hui j'ai des étoiles plein la tête, c'est qu'ils m'ont toujours laissé libre de mes choix et m'ont constamment encouragé á suivre mes idées et à atteindre mes objectifs. C'est d'ailleurs grâce a eux que je me suis un jour retrouvé avec un livre d'astronomie entre les mains et que j'ai attrapé le virus. Je ne voudrais pas oublier non plus ma sœur Nadège qui a toujours été là, même quand je ne le voyais pas. Merci a tous !

Enfin, je voudrais remercier toutes les personnes que j'ai pu rencontrer lors de ces quatres années. Les "Toulousaings" tout d'abord: Nicolas, Hubert, Olivier, Samuel pour avoir fait avec moi et plus ou moins directement la transition ingénieur / chercheur (même si certains.. non certain a finalement résisté); toute l'équipe de feu-le-bureau-152 (version très élargie): Gregory, Ana, Isabelle, Marie, Pascal, Sylvie, Nathalie, Noëlle, David, Valérie pour les "randos-en-montagne-avec-un-lac-et-option-pique-nique", la coinche (et l'invention du coup du Fabrice) et les diverses soirées

délires; et tous les gens du labo que j'ai pu cotoyer. J'ai également une pensée pour les "Jneuvoas", et en particulier Mirka (et Luc) et Yves (et Céline) qui m'ont permis de découvrir la haute montagne, là où l'homme retrouve une place à sa juste valeur; Frédéric et Xavier également, pour, "Oh my God!", les mythiques soirées "Friends"; Raphaël, Veruska, Leticia, Anne, Max, Thibaut, Nuno et j'en oublie sûrement (pardon) pour avoir partagé ces deux dernières années; et toutes les personnes de l'Observatoire de Genève.

Enfin, merci à la Nature de faire que les étoiles brillent.

Outline

This thesis is dedicated to the study of massive stars thanks to new generation atmosphere models. By this expression, we mean atmosphere models including the three main ingredients of the modelling of massive stars atmospheres: non-LTE, spherical extension and line-blanketing.

In a first part, we focus on line-blanketing. Indeed, this ingredient has been included only recently in a reliable way in the models and although its effects were known qualitatively, a quantitative description was lacking. We first concentrate on the effect of line-blanketing on the atmospheric structure and show that the inclusion of metals strongly modifies the behaviour of ionisation and temperature throughout the atmosphere (Sect. 3). This affects the He optical lines used for the spectral classification in a way such that a lower effective temperature is required to achieve a given ionisation and then a given He line strength. Hence, the relation effective temperature - spectral type is shifted towards lower values when line-blanketing is included compared to pure H He models. The difference goes from 1500 K at spectral type O9.7V to 4000 K at spectral type O3V (Sect. 3.3). The new $T_{\rm eff}$ - scale we propose based on a small grid of models is in good agreement with spectroscopic determinations of effective temperatures of individual stars with the new generation atmosphere models, at least for spectral types later than O5V. For earlier spectral types, more studies are required to draw any conclusion (Sect. 3.3.2). We also show that adoptiong a metallicity of 1/8 $Z_\odot$ translates to a reduction of the $T_{\rm eff}$ - scale roughly half the shift obtained in the solar case (Sect. 3.3.3).

In a second step, we study the behaviour of the spectral energy distribution of O stars when line-blanketing is included in the models. We show that the He II ionising flux is strongly reduced, whereas the H ionising flux is essentially unchanged *for a given* $T_{\rm eff}$ (Sect. 4.1). This is due to the blocking of flux at short wavelength by numerous bound-free opacities and line forests of metals and its redistribution to longer wavelengths below the Lyman break. Besides this, we show that the inclusion of all lines as weak as they are is crucial to correctly predict the ionising fluxes. Indeed, we take the example of Iron lines coupled to He II λ304 which sensitively modify the He ionisation structure and thus the Helium continua (Sect. 4.2). Statistical methods to include line-blanketing may miss such weak

lines. Finally, we test the SEDs of O stars through their impact on nebular lines emitted by compact Galactic star forming regions observed by ISO (Sect. 4.3). This study reveals that atmosphere models including a non-LTE aproach, spherical extension and line-blanketing give the best - although not perfect - fit of the excitation sequences observed (defined by the ratio of lines from two successive ionisation states of the same element).

The second part of this thesis deals with the determination of wind properties of O dwarfs. The knowledge of mass loss rates of massive stars is indeed crucial since it controles the evolution of massive stars and quantitative determinations are required to produce reliable evolutionary models. Moreover, mass loss is known to depend on several parameters, especially luminosity and metallicity but again, a quantitative estimate of such dependencies based on analysis of individual massive stars must be done. We take part to such an effort by first studying the stellar components of the High Excitation Blob N81 in the Small Magellanic Cloud. The analysis reveals that those stars are mid to late O dwarfs fainter than typical O dwarfs and showing very weak winds (Sect. 6). Indeed the mass loss rates are of the order $10^{-8..-9}$ $M_\odot$ yr^{-1} which is smaller than observed so far for O dwarfs and lower than predicted by the current hydrodynamical simulations (Sect. 7). The modified wind momenta of these stars are also much lower than expected from the relation modified wind momentum - luminosity (WLR) established for brighter stars and lower than predicted by hydrodynamical simulations, even at low metallicity. We investigate several reasons for such a weakness of the wind, one of them being a possible link between youth of the star and weakness of the wind. Indeed, the combination of subluminosity and weak winds may be a characteristics of Vz stars which are O stars thought to lie near the Zero Age Main Sequence.

The second step of the study of O stars winds consists in the spectroscopic analysis of a sample of Galactic O dwarfs with both low and high luminosities and including Vz stars (Sect. 8). The aim is to see if weak winds also happen in a solar environment and to better characterise the physical conditions under which such weak winds appear. We also want to examine the behaviour of the WLR at low luminosities. The main result is that we find several stars with extremely low mass loss rates (down to 10^{-10} $M_\odot$ yr^{-1}) for luminosities below $\log \frac{L}{L_\odot} = 5.2$. Again, these values are much lower than the theoretical predictions. There does not seem to be a relation with the youth of the star since the stars with the weakest winds are not the youngest. For stars brighter than $\log \frac{L}{L_\odot} = 5.2$, the mass loss are slightly reduced (factor $\lesssim 5$) compared to previous determinations in this luminosity range, mainly due to the introduction of clumping. The WLR show a significant break near the transition luminosity. Although the exact reason for the weakness of the winds is still unknown, metallicity and youth of the star can be discarded.

Chapter 1

Introduction

La caractéristique la plus importante d'une étoile est sa masse. En effet, toute l'évolution stellaire est gouvernée par un subtil jeu d'équilibre entre les forces de gravité qui tendent a faire se contracter l'étoile et les forces de pression qui, elles, engendrent une dilatation. La gravité dépend directement de la masse de l'étoile, alors que les forces de pression dépendent de la température. Plus l'étoile est massive, plus la gravité est grande, et plus la température est élevée. Il s'en suit des changements de comportement et de structure qui expliquent en grande partie des différences de comportement entre les étoiles de petite masse (une masse solaire et moins) et les étoiles dites "massives" (au dela de 10 masses solaires).

Ces dernières sont les plus extrêmes à plus d'un titre. Tout d'abord, ce sont les plus rares: pour une étoile de 40 masses solaires, il existe environ 10000 étoiles de type solaire. Ensuite, ce sont les plus lumineuses : leur luminosité peut atteindre plusieurs centaines de milliers, voire plusieurs millions de fois celle du Soleil. A ce titre, les étoiles massives sont visibles à de très longues distances, bien au-delà de notre Galaxie. Par ailleurs, les étoiles massives sont également les plus chaudes puisque leurs températures effectives dépassent généralement 20 000 K. Cela révèle d'ailleurs que les étoiles massives émettent l'essentiel de leur énergie dans le domaine UV. Ainsi, les étoiles massives émettent une énorme quantité d'énergie sous forme de rayonnement, ce qui n'est pas sans conséquence car cela implique qu'elles brûlent très rapidement leurs réserves d'énergie. La conséquence directe est un temps de vie très court : une étoile de 60 $M_\odot$ vivra typiquement quelques millions d'années, alors que le Soleil a une espérance de vie de dix milliards d'années. Les étoiles massives sont donc peu nombreuses et vivent peu de temps : est-ce à dire qu'elles n'ont qu'un rôle insignifiant dans l'Univers ? Bien au contraire...

Le caractère extrême des étoiles massives a de nombreuses implications, et pas seulement dans le domaine de la physique stellaire. Du fait de leur masse élevée, les étoiles massives sont les seules à pouvoir dépasser le stade de fusion du carbone et sont donc les principaux pourvoyeurs en éléments

plus lourds que l'Oxygène de l'Univers (e.g. Chiosi & Maeder, 1986). Elles sont ainsi la principale source d'enrichissement en métaux du milieu interstellaire. Leur rôle est donc fondamental dans l'évolution chimique des galaxies (et de façon plus générale, de l'Univers). En outre, à cause de leur forte luminosité UV, les étoiles massives sont de formidables sources de rayonnement ionisant à l'origine de régions HII. Le milieu interstellaire environnant subit donc de plein fouet le fort rayonnement de ces étoiles, auquel s'ajoute en outre un fort dégagement d'énergie mécanique tout au long de la vie de l'étoile (Leitherer, Robert & Drissen, 1992). En effet, les étoiles massives perdent continuellement de la masse au cours de leur évolution, que ce soit via de forts vents stellaires, ou bien lors de leur explosion en supernova, phase dans laquelle elles éjectent l'essentiel de leur enveloppe à des vitesses de l'ordre de 10% de la vitesse de la lumière. Cette constante perte de masse est à l'origine de l'ensemencement des éléments lourds dans le milieu interstellaire, mais elle a également une grande influence sur la dynamique du milieu interstellaire environnant. En effet, le dépôt d'énergie mécanique va créer des bulles (Nazé et al., 2002) (voire mêmes des super-bulles - Oey (2004) - lorsque l'on a affaire à un amas d'étoiles massives) de matière en expansion. De plus, l'énergie mécanique injectée dans les nuages moléculaires peut être suffisante pour en déclencher l'effondrement (Deharveng et al., 2003a,b). A ce titre, les étoiles massives sont à l'origine de nouveaux épisodes de formation stellaire dans leur voisinage proche : c'est typiquement ce que l'on voit dans la région de 30 Dor dans le Grand Nuage de Magellan où une seconde génération d'étoiles est en formation autour de l'amas central d'étoiles massives (Walborn et al., 1999; Walborn, Maíz-Apellániz & Barbá, 2002). Les propriétés ionisantes des étoiles massives sont un facteur important dans le cadre des études cosmologiques. En effet, la première génération d'étoiles (les étoiles dites de population III) a probablement été essentiellement composée d'étoiles très massives au pouvoir ionisant supérieur à ce que l'on observe aujourd'hui (Abel et al., 1998; Bromm et al., 1999; Nakamura & Umemura, 2001; Schaerer, 2002, 2003). Or, on sait que l'Univers actuel est majoritairement ionisé, ce qui n'a pas toujours été le cas (la recombinaison ayant eu lieu au moment où le fond diffus cosmologique a été émis environ 300000 ans après le Big-Bang). Une hypothèse pour expliquer cette re-ionisation consiste à invoquer cette population d'étoiles massives de population III et son flux ionisant particulièrement fort (Sokasian et al., 2004). D'un point de vue cosmologique, on peut également mentionner que les étoiles massives sont encore invoquées pour rendre compte de l'existence des mystérieux sursauts gamma, explosions extrêmement intenses et lumineuses dans le domaine gamma, et également très brèves. Il se pourrait que des explosions d'un type particulier (collapsar model Woosley & Weaver, 1995) d'étoiles massives de populations I et II soient à l'origine de ce phénomène. Un autre scenario explicatif indique que les

sursauts gamma pourraient résulter de l'explosion d'étoiles de population III en supernovae (Bromm & Larson, 2004, et références incluses). Sans aller aussi loin dans l'Univers, il est possible de voir l'effet des étoiles massives sur leur environnement dans les galaxies dites starbursts. Ces dernières sont des galaxies abritant un épisode de formation stellaire quasiment généralisé. Or dans un tel événement, les étoiles massives nouvellement créées et en nombre important dominent complètement le spectre de la galaxie, révélant leur influence sur leur environnement (Leitherer & Lamers, 1991; Schaerer, 2002). Les sursauts de formation stellaire existent bien sûr à des échelles plus petites, à l'intérieur de galaxies "classiques", mais les propriétés générales (forte émission UV, interaction avec le milieu interstellaire...) restent qualitativement identiques.

Ce bref tour d'horizon montre que les étoiles massives, en dépit de leur petit nombre et de leur temps de vie court, sont à un carrefour entre divers domaines de l'astrophysique, allant de la physique stellaire à celle du milieu interstellaire, à celle des galaxies et même à la cosmologie. Il est donc fondamental de bien les comprendre, ce qui passe par une bonne connaissance de leurs propriétés. Or, il reste bien des zones d'ombre en ce qui les concerne. Même si les grandes lignes de leur évolution sont bien caractérisées qualitativement, une description quantitative reste encore à établir. Par ailleurs, certaines phases de la vie des étoiles massives sont encore méconnues : c'est la cas de la phase de formation. Nous avons vu que la masse était le facteur principal de l'évolution de toute étoile. Dans le cas des étoiles massives, cette masse diminue sans cesse au cours de l'évolution : il est donc indispensable de connaître quantitativement la perte de masse de ces étoiles pour être capable de bien suivre leur évolution. Or, cette connaissance reste partielle à l'heure actuelle. Dans les paragraphes suivants, nous revenons sur ces diverses méconnaisances ou incertitudes.

1.1 Formation des étoiles massives

La formation des étoiles reste l'une des grandes questions de l'astrophysique moderne. En effet, on ne dispose pas à l'heure actuelle d'un schéma quantitatif permettant d'expliquer comment on passe d'un réservoir de matière peu dense (nuage moléculaire) à une étoile brûlant son hydrogène. Le scenario actuel qui semble le plus probable et qui est en tout cas celui reconnu comme tel est celui de l'effondrement/accrétion. Dans ce modèle, une étoile se forme par effondrement d'un nuage moléculaire conduisant à un cœur dense qui accrète peu à peu de la matière. Il se forme d'abord un disque circumstellaire depuis lequel la matière est accrétée sur l'étoile. La contraction de la proto-étoile ainsi formée génère l'allumage des réactions nucléaires permettant la combustion de l'hydrogène : l'étoile est alors née. Les diverses phases semblent correspondre à différents objets classés selon

leur apparence spectrale et regroupés dans le désormais célèbre schéma de Lada (1987) montré en Fig. 1.1. On y voit tout d'abord un nuage moléculaire en effondrement donnant naissance à un coeur pré-stellaire qui va ensuite évoluer en un objet proto-stellaire accrétant de la matière via un disque d'accrétion, puis va devenir une étoile pré-séquence principale encore entourée de ce qui reste de son disque d'accrétion. Ce scenario représente les grandes étapes de la formation des étoiles mais ses détails sont encore loin d'être bien connus. Et s'il semble être largement adopté pour décrire la formation des étoiles de faible masse, il est incertain pour les étoiles massives. La raison principale en est qu'à partir d'une certaine masse, divers effets d'interaction dus à l'étoile elle-même vont perturber ce schéma (Larson & Starrfield, 1971). En effet, dans le cas d'une proto-étoile suffisamment massive la luminosité de l'objet en formation va être suffisante pour générer une pression de radiation capable de ralentir voire même de stopper le processus d'accrétion. La formation des étoiles massives par accrétion est donc loin d'être établie de façon certaine. Pour que ce scenario reste valide, il faut modifier sensiblement certains paramètres tels que la taille des grains de poussière du nuage moléculaire parent (Wolfire & Cassinelli, 1986, 1987). On peut aussi préserver ce mécanisme de formation en admettant que le taux d'accrétion augmente avec la masse de la proto-étoile (Behrend & Maeder, 2001). Cela reste néanmoins spéculatif, car les observations d'étoiles massives en formation font cruellement défaut. Ceci est dû au fait que les échelles de temps pour la formation des étoiles massives sont plus courtes que pour leurs homologues de faible masse, de sorte qu'il est possible qu'elles entrent sur la séquence principale alors qu'elles sont encore en train d'accréter de la matière (si elles se forment bien par accrétion; voir Bernasconi & Maeder, 1996). Par ailleurs, les phases précoces de l'évolution sont la plupart du temps invisibles car elles ont lieu au coeur de nuages encore suffisamment denses pour empêcher toute émission directe de rayonnement. Elles sont donc extrêment difficiles à observer. Malgré cela, divers indices d'une formation par accrétion apparaissent peu à peu. En particulier, la présence de jets de matière (caractéristique courante dans les proto-étoiles de faible masse) dans des zones de formation d'étoiles massives se confirme (Stecklum et al., 1995; Shepherd et al., 2000). Aucune véritable observation de disque autour d'objets massifs n'a en revanche été réalisée jusqu'ici, contrairement à ce que l'on voit couramment pour les étoiles de faible masse (Hoare et al., 2003), si ce n'est la toute récente observation de Chini et al. (2004) qui semble montrer l'existence d'un disque autour d'un objet de grande masse en formation.

Cette incertitude sur le mécanisme de formation des étoiles massives a conduit à l'élaboration d'un autre scenario selon lequel des collisions d'objets de masses faibles ou intermédiaires dans des amas denses pourraient conduire à des proto-étoiles massives (Bonnell, Bate & Zinnecker,

1998). Cette hypothèse a l'avantage de rendre compte du fait que l'essentiel des étoiles massives jeunes sont observées dans des amas. Toutefois, les densités requises (de l'ordre de 10^6 pc^{-3}) rendent cette solution friable. Pour mieux comprendre la formation des étoiles massives, il est crucial d'obtenir des observations sinon de ces jeunes étoiles elles-mêmes, du moins des régions dans lesquelles elles se forment.

Les stades les plus précoces observés jusqu'à présent correspondent aux objets "hot cores" (Hofner et al., 1996) caractérisés par une densité électronique et une température élevées ($n_e > 10^7$ cm^{-3}, T > 100 K). Ils sont de plus très compacts (diamètre < 0.1 pc) (Kurtz et al., 2000, et références incluses). Ces objets sont optiquement épais de sorte que l'on ne distingue leurs composantes dans aucun domaine spectral. La présence d'étoiles massives est seulement supposée d'après la température observée dans le nuage. Le stade suivant de la formation correspond vraisemblablement aux régions HII ultra-compactes ("UCHII regions", see Churchwell, 2002) qui montrent des densités réduites par rapport aux hot cores, mais encore sensiblement élevées ($n_e > 10^5$ cm^{-3}). Ces régions sont aussi un peu plus étendues ($\sim$ 1 pc) et contiennent une ou plusieurs étoiles massives jeunes (Kurtz et al., 2000). Ces dernières sont suffisamment chaudes pour émettre la majorité de leur flux dans le domaine UV. La conséquence immédiate est que le milieu environnant proche est ionisé par ce rayonnement UV intense et donne ainsi naissance à une région HII ultra-compacte. Là encore, on n'observe pas l'étoile (ou les étoiles) responsable de cette ionisation, mais on en déduit ses propriétés via des raies émises dans la nébuleuse et dont l'intensité dépend directement de l'étoile contenue dans la région. Au cours du temps, cette région HII s'étend à cause du dépôt continu de photons ionisants (Jaffe et al., 2003), révélant peu à peu le contenu stellaire et devenant une région HII classique au sein de laquelle les étoiles massives vont poursuivre leur évolution. Dans cette phase, les étoiles massives sont directement observables dans divers domaines de longueur d'onde, mais elles sont déjà significativement évoluées. L'idéal pour étudier de jeunes étoiles massives serait donc de trouver des régions de formation stellaire intermédiaires entre la phase UCHII et la phase HII classique. C'est l'opportunité qui est offerte par les "High Excitation Blobs" (HEBs), une classe d'objets découverte par Heydari-Malayeri & Testor (1982) et qui semble bien être le chaînon manquant entre ces diverses régions ionisées. En effet, ces HEBs sont d'un point de vue morphologique plus étendus que des régions UCHII (de 1 à quelques parsecs de diamètre) mais moins que des régions HII classiques (une dizaine de parsecs de diamètre et plus). En outre, leur forte excitation (mesurée par le rapport O III λ5007 / H$_\beta$) laisse penser que ce sont des objets relativement jeunes et compacts au sein desquels le rayonnement UV est intense et interagit fortement avec la matière interstellaire. Ces objets n'ont jusqu'à présent été observés que dans les Nuages de Magellan et sont au nombre

d'une dizaine (Heydari-Malayeri et al., 1999a,c,b, 2001, 2002c). La Fig. 1.2 montre l'un de ces HEBs dans le Grand Nuage de Magellan. On y reconnaît les caractéristiques principales de régions de formation stellaire, à savoir une cavité ionisée, des fronts d'ionisation, des chocs, diverses structures turbulentes... Et ce qui est le plus intéressant, c'est que l'on distingue très clairement les étoiles contenues dans ces régions ! Ainsi, ces HEBs qui, en plus d'être de véritables régions de formation stellaire, sont suffisamment transparents pour révéler leur contenu stellaire sont une opportunité intéressante d'observer de jeunes étoiles massives peu évoluées, et donc d'améliorer notre connaisance des étoiles massives jeunes.

Une partie importante de cette thèse a été consacrée à l'étude des étoiles de l'une de ces régions. Les motivations qui ont conduit à cette étude ont été de divers ordres. L'étude de jeunes étoiles massives faisait partie de ces motivations qui incluaient aussi la caractérisation des propriétés des vents des étoiles massives dans un environnement de métallicité sous-solaire. C'est cette motivation que nous developpons dans le paragraphe suivant.

1.2 Les vents des étoiles massives

Comme nous l'avons déjà mentionné, la masse est le paramètre fondamental de l'évolution stellaire, et dans le cas des étoiles massives, cette masse est sensiblement modifiée au cours de la vie de l'étoile à cause des vents violents qui expulsent sans cesse de la matière stellaire dans le milieu interstellaire (Chiosi & Maeder, 1986; Maeder & Conti, 1994). Les taux de perte de masse peuvent atteindre des valeurs de $10^{-4/-3}$ $M_\odot$ yr^{-1} et la vitesse à laquelle est éjectée cette matière peut être aussi élevée que 3000 km s^{-1} (soit 1 % de la vitesse de la lumière). On comprend ainsi que les quantités d'énergie mécanique relâchée par l'étoile (de l'ordre de 10^{51} erg au cours de la vie d'une étoile massive) soient de nature à influencer fortement le milieu environnant. Pour l'étoile également cette perte de masse est fondamentale : une étoile de 100 $M_\odot$ peut perdre plus de 90 % de sa masse au cours de sa vie (Maeder, 1992). Il est donc crucial de connaître quantitativement la perte de masse des étoiles massives si l'on veut mieux comprendre non seulement leur évolution, mais aussi leur impact sur l'environnement.

Quelle est donc l'origine du vent des étoiles massives ? Le mécanisme de base est relativement simple. Il s'agit d'un transfert de quantité de mouvement entre les photons émis par l'étoile, et les éléments présents à la surface de celle-ci. En d'autres termes, c'est l'accélération radiative des couches externes de l'étoile qui génère ce flot de matière. Ce mécanisme est particulièrement efficace pour les étoiles massives car la très forte luminosité des étoiles engendre un grand nombre de photons susceptibles d'interagir avec les espèces présentes dans l'atmosphère. Il s'en suit un

fort couplage entre matière et rayonnement qui produit une accélération radiative suffisante pour contrebalancer et même surpasser la gravité. La quantité de matière éjectée sera d'autant plus grande que l'accélération sera importante, et donc que la luminosité de l'étoile sera élévée (le nombre de photons émis et susceptible d'interagir avec la matière étant plus grand). Cela explique que la perte de masse d'une étoile massive augmente quand l'étoile évolue depuis la séquence principale vers les phases plus avancées.

Les déterminations de taux de perte de masse reposent sur diverses techniques basées soit sur l'estimation de l'excès d'émission millimétrique et radio dû aux interactions libre-libre des électrons du vent stellaire (Lamers & Leitherer, 1993; Leitherer et al., 1995), soit sur l'ajustement de diverses raies sensibles aux propriétés du vent de l'étoile (essentiellement des raies UV, extrême UV et H_α). Un certain nombre de travaux réalisés au cours des deux dernières décennies ont permis d'acquérir une bonne connaissance des taux de perte de masse et vitesses terminales (vitesse maximale atteinte au sommet de l'atmosphère) pour les étoiles de la Galaxie (Howarth & Prinja, 1989; Chlebowski & Garmany, 1991; Leitherer, 1988; Puls et al., 1996; Herrero, Puls & Najarro, 2002; Repolust, Puls & Herrero, 2004). Plusieurs étoiles des Nuages de Magellan ont aussi été analysées (Puls et al., 1996; Crowther et al., 2002a; Hillier et al., 2003; Bouret et al., 2003).

La figure 1.3 montre les déterminations de vitesses terminales pour des étoiles Galactiques. On y voit en particulier que v_∞ est très bien corrélé à la vitesse d'échappement v_{esc}. Cette relation de proportionnalité dépend de la température de l'étoile, mais pour des étoiles de type O, elle est quasiment la même (ces étoiles ayant des températures supérieures à 21000 K qui est la limite du premier saut). Ce type de décrochement (appelé "bistability jump") a été mis en évidence par Lamers et al. (1995) et est dû à un changement dans la répartition des ions présents dans l'atmosphère, lui-même dû à une modification de l'ionisation (voir Vink, de Koter & Lamers, 1999).

En ce qui concerne la perte de masse, la figure 1.4 montre les résultats de diverses études récentes en fonction de la luminosité de l'étoile. Ces travaux sont basés sur l'étude de la raie H_α. On constate que luminosité et perte de masse sont bien corrélées comme la théorie le prévoit (voir Sect. 5). Par ailleurs, si le nombre de supergéantes analysées est important, ce n'est en revanche pas le cas des naines. De plus, le domaine de luminosité en dessous d'une valeur de $log\frac{L}{L_\odot} \sim 5.3$ reste relativement peu exploré. Ceci peut s'expliquer par la plus faible luminosité des objets, et donc la plus grande difficulté pour obtenir des données observationnelles de bonne qualité. Ceci est confirmé par la Fig. 1.5 qui montre les déterminations de perte de masse effectuées au moyen d'analyses dans le domaine radio: il est encore plus flagrant que les études quantitatives des propriétés des vents des étoiles massives peu lumineuses et des naines en particulier font défaut.

Une autre question qui reste en suspens concerne la dépendance de ces propriétés de vent avec la métallicité. En effet, les éléments responsables de l'accélération radiative qui génère le vent sont en majorité des métaux (C, N, O et Fe pour les principaux). Cela implique nécessairement que selon la métallicité de l'étoile, le vent sera plus ou moins fort (avec les diverses conséquences que cela peut avoir sur l'évolution de l'étoile). De manière théorique, on s'attend à ce que la perte de masse suive une variation avec la métallicité du type $\dot{M} \propto Z^r$ où l'exposant r est de l'ordre de 0.5-1.0 (Abbott, 1982; Leitherer, Robert & Drissen, 1992; Vink, de Koter & Lamers, 2001). De même, la vitesse terminale doit varier avec la métallicité selon une loi de puissance d'exposant ~ 0.13 (Leitherer, Robert & Drissen, 1992), bien que, selon Evans et al. (2004), cette dépendance ne soit pas complètement évidente. D'un point de vue observationnel, la question reste ouverte, même si la figure 1.6 montre que qualitativement, la réduction de la force du vent lorsque la métallicité diminue semble être bien avérée. Au début de cette thèse, les analyses quantitatives dans des environnements déficients en métaux étaient quasiment inexistantes, à l'exception des travaux de Puls et al. (1996) qui n'incluaient cependant que quelques étoiles des Nuages de Magellan. Leurs résultats indiquent une possible réduction de la perte de masse lorsque la métallicité diminue, mais le nombre d'étoiles analysées reste insuffisant pour tirer des conclusions générales, comme on le voit sur la figure 1.7. Même chose du côté des métallicités super-solaires où les seules études quantitatives étaient (et sont toujours) celles de Krabbe et al. (1995) et Najarro et al. (1994), Najarro et al. (1997) et concernent des étoiles sensiblement évoluées (étoiles HeI, voir Krabbe et al., 1995). Le besoin de nouvelles contraintes relatives aux propriétés de vents d'étoiles massives tant à haute que basse métallicité était donc criant, et cette thèse a pris part à cet effort global.

Outre la perte de masse et la vitesse terminale des étoiles massives, une autre grandeur restait mal connue dans des environnement de métallicity autre que solaire : la quantité de mouvement modifiée (notée MWM). Cette grandeur qui est simplement la quantité de mouvement du vent multipliée par la racine carrée du rayon de l'étoile ($\dot{M} v_\infty \sqrt{R}$) doit dépendre uniquement de la luminosité de l'étoile comme le prédit la théorie (Kudritzki & Puls, 2000, + Sect. 5). La Fig. 1.8 montre cette relation pour une grande partie des étoiles Galactiques étudiées avant 2000. On y voit que le relation est légèrement différente entre les supergéantes et les naines. Toutefois, on constate qu'il existe bien une corrélation entre quantité de mouvement modifiée et luminosité. Cela est particulièrement intéressant car si cette relation est calibrée correctement, elle peut servir d'indicateur de distance jusqu'à des distances de plusieurs Mpc (Kudritzki, 1998). En effet, la dérivation de la MWM au moyen de spectres donne directement

accès à la luminosité de l'étoile, et donc à la distance (Kudritzki, Lennon & Puls, 1995). Néanmoins, tout comme les paramètres de vent dont elle dépend directement, cette quantité varie avec la métallicité. Des études dans différents environnements sont donc nécessaires pour bien calibrer cette relation.

Les étoiles du HEB que nous avons étudiées dans cette thèse étaient ainsi parfaitement adaptées à ce type d'étude des propriétés de vents et de calibration de la relation quantité de mouvement modifiée - luminosité. Cette étude a très largement reposé sur l'utilisation de modèles d'atmosphères "nouvelle génération" dont nous donnons les principales caractéristiques dans le paragraphe suivant.

1.3 Modèles d'atmosphères pour étoiles massives

L'analyse quantitative des propriétés des étoiles massives repose en grande partie sur l'utilisation de modèles d'atmosphères. Ceux-ci permettent de reproduire les différentes structures (densité, température, ionisation) et le champ de rayonnement à l'intérieur de l'atmosphère et de synthétiser le spectre émis par celle-ci. L'ajustement de spectres observés par ces derniers spectres synthétiques permet de remonter directement aux principales propriétés de l'étoile (température effective, gravité, composition chimique, perte de masse...). L'analyse spectroscopique au moyen de modèles d'atmosphères se révèle ainsi être un puissant outil d'analyse. Toutefois, cette modélisation n'est pas triviale car la complexité des atmosphères des étoiles massives requiert la prise en compte d'un grand nombre de phénomènes physiques. De façon générale, on peut résumer comme suit les principaux ingrédients à prendre en compte :

- traitement hors-ETL:

  A cause de leur forte luminosité, les étoiles massives ont un champ de rayonnement particulièrement intense, de sorte que les phénomènes radiatifs prennent le pas sur les phénomènes collisionnels dans leurs atmosphères. Cela implique l'absence de tout équilibre thermodynamique, même local. Il s'en suit que la détermination des populations des divers niveaux d'énergie inclus dans les modèles doit impérativement se faire individuellement, en calculant un équilibre détaillé entre les phénomènes peuplant et dépeuplant le niveau en question. Bref, il faut résoudre les équations d'équilibre statistique une à une. En pratique, cela demande un temps de calcul important, et d'autant plus grand que le nombre de niveaux pour lesquels on souhaite avoir les populations est élevé.

- extension sphérique:

  Comme nous l'avons vu précédemment, les étoiles massives émettent continuellement un vent qui crée autour d'elles une atmosphère pouvant s'étendre jusqu'à une centaine de rayons stellaires. Dans ce cas, l'approximation classique consistant à dire que la hauteur de l'atmosphère est très inférieure au rayon stellaire, de sorte que l'on peut considérer cette atmosphère comme une couche plane (cas plan-parallèle), n'est plus valide. Il est donc nécessaire de résoudre les différents problèmes en géométrie sphérique. L'atmosphère étant par ailleurs en expansion, il faut prendre en compte la structure de vitesse, ce qui complique encore la modélisation car les décalages Doppler qui en découlent introduisent un couplage non local entre les diverses équations, un photon émis à un endroit à une certaine fréquence pouvant être absorbé loin de son lieu d'émission par une raie de fréquence plus basse.

- line-lanketing:

  Pour que les prédictions des modèles soient les plus réalistes possible, il est nécessaire de prendre en compte le plus d'éléments possible, notamment les métaux. Or, ces derniers ont une influence qui ne se limite pas au simple spectre émergent où ils sont à l'origine de nombreuses raies, mais elle s'étend aussi à la structure de l'atmosphère. En effet, les diverses opacités de ces métaux modifient sensiblement le transfert de rayonnement et donc la structure globale de l'atmosphère.

En pratique, le traitement hors ETL et l'extension sphérique ont été les deux premiers ingrédients introduits dans les modèles (voir Sects. 2.1, 2.2). Le line-blanketing en revanche n'a été implémenté que récemment et même si ses effets étaient connus qualitativement auparavant, une étude quantitative restait à faire au début de cette thèse.

Le degré de sophistication des modèles actuels permet d'envisager des études quantitatives d'une précision accrue. En particulier, les spectres produits sont d'une qualité remarquable et ouvrent la voie à des analyses spectroscopiques poussées. Diverses questions vont ainsi pouvoir être abordées. Notons-en simplement quelques unes :

- déterminations d'abondances dans les étoiles massives : l'inclusion de métaux et la simulation des spectres détaillés montrant les signatures des éléments CNO et Fe (entre autres) permettent désormais une détermination de métallicité et des abondances fiables. Grâce à cela, les modèles d'évolution des étoiles massives vont pouvoir être testés, en particulier les mécanismes d'enrichissement/appauvrissement en éléments CNO. Nous sommes donc entrés dans une période où le contenu en éléments autres que l'Hydrogène et l'Hélium peut être déterminé.

- détermination précise des masses: Herrero et al. (1992) ont montré que les masses déterminées de façon spectroscopique (via la gravité) étaient systématiquement inférieures à celle déduites des modèles d'évolution (par le biais de diagramme HR). Les erreurs proviennent probablement à la fois des modèles d'atmosphères et des modèles d'évolution, mais l'utilisation de spectres synthétiques plus réalistes doit sans aucun doute permettre de réduire le désaccord. Cela a d'ailleurs été montré récemment par Herrero, Puls & Najarro (2002).

- estimations pécises des températures effectives et luminosités : l'analyse spectroscopique peut fournir des valeurs plus précises de ces deux paramètres fondamentaux des étoiles chaudes. Une fois connus, ils conduisent à une estimation du stade évolutif de l'objet étudié, autrement dit de son âge. De nouvelles contraintes sur l'âge d'amas jeunes peuvent ainsi être envisagées.

- propriétés des vents : l'obtention de profils de raies détaillés couplée à l'obtention de spectres observés à des résolutions importantes laisse présager une précision accrue dans la détermination des paramètres des vents, notamment la perte de masse. En particulier, l'inclusion des métaux dans les modèles doit permettre de contraindre la dépendance de ces paramètres avec la métallicité.

- flux ionisants : les effets du line-blanketing modifient la forme de la SED des étoiles massives. Il en résulte que les nouveaux modèles doivent prévoir des flux ionisants quelque peu différents comparés à la précédente génération de modèles. Les études de régions HII doivent en bénéficier.

Ces exemples n'en sont que quelques-uns parmi bien d'autres. Ils montrent simplement le potentiel de la nouvelle génération de modèles d'atmosphères pour étoiles chaudes. Bien sûr, des améliorations sont encore à venir. En particulier, l'essentiel des simulations actuelles adopte une géométrie unidimensionnelle. Or, on sait que la rotation brise cette géométrie en introduisant une dépendance en latitude des paramètres stellaires et du vent (voir Maeder & Meynet, 2000). De plus, des phénomènes temporels existent dans les vents, alors que les modèles font souvent l'hypothèse de stationnarité (voir néanmoins Owocki, Castor & Rybicki, 1988) Les modèles actuels ne sont pas non plus dans la majorité des cas complètement cohérents dans le sens où la structure de vitesse (et par là même de densité) est imposée en entrée et ne varie pas au cours de la simulation. Or, le développement des vents, et par conséquent l'évolution de la structure, dépend principalement des populations et de la température dans l'atmophère. Un modèle complet nécessiterait donc le traitement du couplage entre l'hydrodynamique et le calcul de l'atmosphère

à proprement parler. Ce type d'approche existe déjà (voir par exemple Pauldrach, Hoffmann & Lennon, 2001) mais au prix d'un traitement de l'atmosphère (i.e. transfert de rayonnement + populations) moins performants que d'autres simulations n'incluant pas la partie hydrodynamique. Malgré tout, l'utilisation de modèles empiriques (i.e. sans traitement de l'hydrodynamique) reste fondamentale pour la détermination des paramètres de vents qui peuvent être ajustés pour reproduire les observations.

Malgré l'absence de ces ingrédients, la nouvelle génération de modèles d'atmosphères incluant de façon robuste le line-blanketing ouvre la voie à des avancées importantes dans l'analyse spectroscopique des étoiles massives et dans la compréhension de leur évolution en général.

1.4 Dans cette thèse

Compte tenu des différentes questions mentionnées dans les paragraphes précédents, cette thèse s'est focalisée essentiellement sur deux aspects principaux :

- Les effets du line-blanketing.

  Dans cette partie, nous nous sommes penchés sur l'étude quantitative du line-blanketing et sur ses effets principaux sur les modèles d'atmosphères d'étoiles massives. Nous nous sommes tout particulièrement intéressés à l'échelle de température des étoiles O et en avons donné une nouvelle version. D'autre part, nous avons étudié l'effet du line-blanketing sur la distribution spectrale d'énergie des étoiles O et nous avons testé cette dernière via son effet sur des raies nébulaires émises dans des régions HII compactes.

- Les vents des jeunes étoiles O.

  Dans le but de mieux connaître les propriétés des vents des étoiles massives et de type O en particulier, nous avons mené diverses analyses spectroscopiques d'étoiles à la fois dans la Galaxie et dans les Nuages de Magellan. Cette étude a pris part à un effort global visant à 1) contraindre la dépendance avec la métallicité des paramètres de vent, 2) calibrer le relation quantité de mouvement modifiée - luminosité, 3) apporter des contraintes sur le taux de perte de masse d'étoiles de faible luminosité. Ces études s'inscrivent également dans le cadre d'une meilleure compréhension de la formation des étoiles massives.

Ces deux types d'analyse ont reposé sur la modélisation d'atmosphères d'étoiles massives au moyen du code CMFGEN (CoMoving Frame GENeral) développé par John Hillier de l'Université de Pittsburgh, USA.

D'un point de vue pratique, la suite de ce manuscrit s'organise ainsi:

◇ chapitre 2: Ce chapitre fait une présentation générale des modèles d'atmosphère d'étoiles massives en en rappelant les principaux ingrédients et en montrant leurs effets. Une brève description de CMFGEN est également donnée.

◇ chapitre 3: Nous étudions ici les effets du line-blanketing sur la température effective des étoiles O naines. Après un bref rappel historique, nous montrons que l'inclusion du line-blanketing dans les modèles conduit à une réduction de l'échelle de température de ces étoiles. Les effets de la métallicité sont aussi abordés.

◇ chapitre 4: Nous nous intéressons dans ce chapitre au flux ionisant des étoiles O et étudions leurs variations sous l'effet du line-blanketing. Un test de leur validité est mené au moyen de l'étude de raies nébulaires infra-rouges émises dans des régions HII compactes.

◇ chapitre 5: Ce chapitre présente une vue globale de la théorie des vents radiatifs et en rappelle les principaux concepts et résultats.

◇ chapitre 6: Ici, le contenu stellaire du HEB N81 dans le SMC est analysé de façon qualitative. Une classification spectrale approximative est réalisée et des contraintes sur les propriétés stellaires et de vent sont apportées.

◇ chapitre 7: Une analyse quantitative des étoiles de N81 est menée dans ce chapitre au moyen des modèles CMFGEN. Les paramètres de vents sont particulièrement étudiés car ils témoignent d'un vent très faible. L'origine de cette surprenante faiblesse est étudiée.

◇ chapitre 8: Ce chapitre s'inscrit dans la continuité du précédent et s'intéresse aux propriétés de vent d'étoiles Galactiques soupçonnées de montrer elles-aussi des pertes de masse faibles. Le comportement de la relation quantité de mouvement modifiée - luminosité des étoiles naines est inspecté.

◇ chapitre 9: Il s'agit du chapitre de conclusion qui rassemble les résultats et mentionne diverses perspectives.

Chapter 1

Introduction

The main characteristic of a star is its mass. Indeed, the entire stellar evolution is governed by a balance between gravitational forces which make the star contract and the pressure forces which make the star expand. Gravity is directly related to mass, while pressure forces are sensitive to temperature. The more massive the star, the higher the gravity and the higher the temperature. This implies important changes of the internal structure, explaining the main differences in the behaviour of low mass stars (one solar mass and below) and massive stars (mass greater than $\sim$ 10 $M_\odot$). The latter are extreme stars for several reasons. First of all, they are rare: there is only one 40 $M_\odot$ star for 10000 solar type stars. Then, with luminosities reaching a million times the solar luminosity they are the most luminous stars. This renders them visible at high distances, and at least outside the Galaxy. Moreover, massive stars are also very hot since their effective temperature easily reaches 20000 K. As their emission resembles that of a black body at "zeroth" order, this shows that most of their luminosity is emitted in the UV range. Due to their high luminosity, massive stars release huge quantities of radiative energy with the consequence that they burn rapidly their central hydrogen and have short lifetimes. Indeed, a 60 $M_\odot$ star dies after 4-5 million years while the Sun has a lifetime of ten billion years. Thus, there are few massive stars and they quickly disappear: does it mean that they have no role in the Universe? Not at all...

The extreme properties of massive stars has a number of implications, not only for the field of stellar astrophysics. Due to their high mass, massive stars are the only one to go beyond the He burning phases, which means that they are the only star to produce elements heavier than Oxygen (e.g. Chiosi & Maeder, 1986). And they are the main source of most of the metals (in the chemical sense) of the Universe. Consequently, they have an important role to play in the chemical evolution of galaxies (Rana, 1991). Besides this, because of their high luminosity, massive stars are incredible sources of ionising photons creating HII regions. The interstellar

medium neighbouring massive stars is influenced by the effect of the ionising fluxes of massive stars, and also by a strong release of mechanical energy (Leitherer, Robert & Drissen, 1992). Indeed, massive stars continuously lose mass during their life, either through stellar winds or through the supernova phase in which the outer layers of the stars are expelled into the interstellar medium. These mass loss events allows the ISM to be enriched in the elements produced by massive stars, but they also have important consequences on the dynamics of the ISM. Indeed, the release of mechanical energy will create bubbles (Nazé et al., 2002) or super-bubbles depending on the number of massive stars ejecting mass (Oey, 2004) and can trigger the collapse of molecular clouds (Deharveng et al., 2003a,b). This explains why massive stars can be at the origin of star formation events: this is typically what we see in the 30 Doradus region of the Large Magellanic Cloud where a second generation of stars is in formation in the molecular clouds surrounding the central cluster of massive stars (Walborn et al., 1999; Walborn, Maíz-Apellániz & Barbá, 2002).

The ionising properties of massive stars are also an important ingredient in the context of cosmological studies. Indeed, the first generation of massive stars is thought to be composed mostly of very massive stars (the so-called population III stars, see Abel et al., 1998; Bromm et al., 1999; Nakamura & Umemura, 2001) with ionising fluxes even higher than present day massive stars (see Schaerer, 2002, 2003). However, we know that the Universe is now mostly ionised, which has not always been the case since the recombination at the origin of the emission of the cosmic microwave background (CMB) took place nearly 300000 years after the big-bang. This means that between this period and now, a reionisation should have happen, and population III stars are possibly responsible for it due to their strong Lyman fluxes (e.g. Sokasian et al., 2004). From a cosmological point of view, massive stars are also invoked to explain the mysterious gamma-ray bursts, these extremely powerful and short explosions observed in the early Universe at high energy. They may be the result of a special explosion of a population I or II star (collapsar model, see Woosley & Weaver, 1995), or they could be the result of the supernova explosion of population III stars (Bromm & Larson, 2004, and references therein).

Without going this far in the Universe, the influence of massive stars on their surrounding medium can be seen in starburst galaxies. They are galaxies experiencing a star formation event so intense that the spectrum of the galaxy is dominated by the spectrum of the region where stars are being formed. As in such starburst phenomenon massive stars are formed, and as they dominate the luminosity of the region, the observed spectrum is a combination of the direct spectrum of massive stars recently formed and of the ionised gas suffering the strong influence of massive stars (Leitherer & Lamers, 1991; Schaerer, 2002). Of course, starbursts happen on

much lower scales in more classical galaxies, but the main properties of the observed spectrum (strong UV emission of massive stars + effect on the environment) remains qualitatively identical.

This short overview show that massive stars, in spite of their rarity and short lifetimes, are involved in several fields of astrophysics, going from stellar physics to the physics of interstellar medium, to the physics of galaxies and to cosmology. It is thus crucial to know in detail their evolution and physical properties. However, several questions remain to be answered. Although the main phases of their evolution are qualitatively known, a quantitative description of their evolution (in particular as a function of their initial mass) has to be defined. Moreover, the mass loss experienced by massive stars is crucial since mass is the main factor of the evolution: quantitative determinations of mass loss rates must be completed. And we do not know how massive stars form, since in their special case, several phenomenon render the classical scenario of accretion more complex. In the next sections, we go back to these uncertainties concerning massive stars.

1.1 Massive star formation

The formation of stars remains one of the biggest questions of modern astrophysics. Indeed, we do not have at present a quantitative scenario explaining how we can go from a low density molecular cloud to a star burning Hydrogen in its core. The present explanation is that of a collapse of the molecular cloud followed by an accretion phase. In this picture, the collapse gives birth to a central object, denser than its environment, on which matter is, little by little, accreted. The accretion takes place in a disk from which matter is transferred to the central objects. The contraction of the protostellar object because of the increasing mass triggers the burning of hydrogen, giving birth to the star. The various phases of the formation of stars according to this scenario have observational counterparts which are gathered in the famous picture by Lada (1987) and shown in Fig. 1.1. We first see that a collapsing molecular cloud creates a pre-stellar object which then evolves into a protostellar object on which accretion takes place through a disk. This object then becomes a pre main sequence star surrounded by the debris of the disk. All these phases are distinguishable on the shape of the spectral energy distribution which depends on the matter around the central object and the evolutionary state of this object. This scenario explains the main steps of star formation, but the details are still poorly known.

In the case of massive stars, the formation scenario is even more uncertain. Indeed, above a given mass for the central object, feedback effects

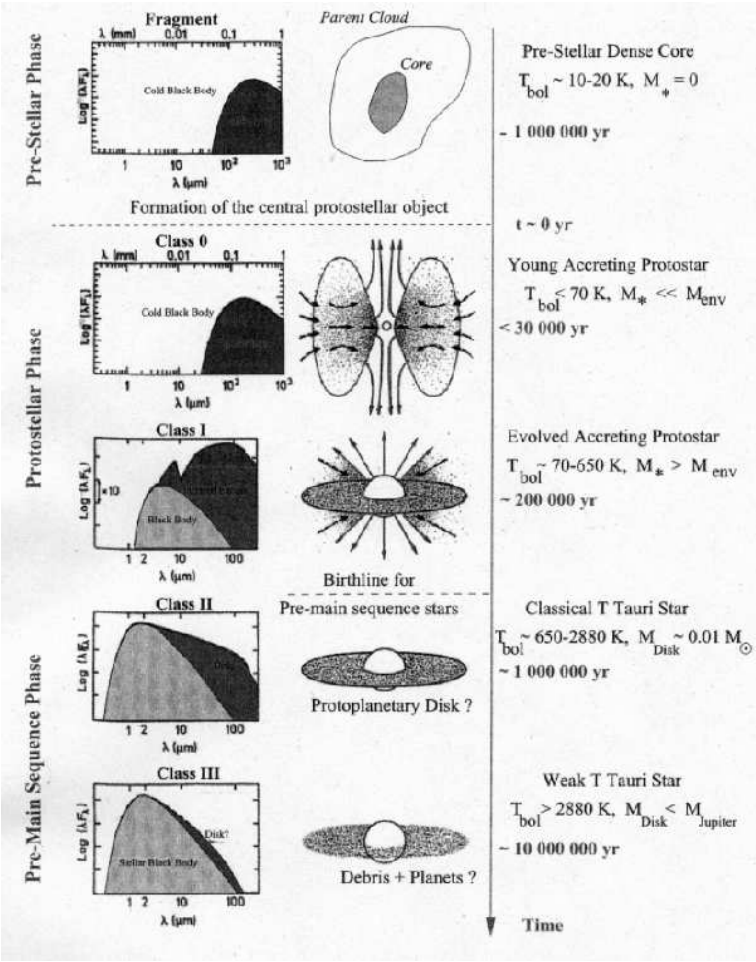

Figure 1.1: Picture of the formation of a low mass stars via the accretion process. After the collapse of a molecular cloud, a proto-star grows thanks to accretion through a disk. Then accretion stops, leaving a pre main sequence star surrounded by what remains of the disk which will be later evaporated. From (Lada, 1987).

from this object will strongly modify the picture. Hence, for a proto-star massive enough, the luminosity of this object will be sufficient to create a radiative pressure acting against accretion (Larson & Starrfield, 1971). This explains why the formation of massive stars via accretion remains to be established. If we want the classical picture to remain valid, several parameters have to be modified, such as the size and composition of the dust grain present in the parent cloud (Wolfire & Cassinelli, 1986, 1987). Another possibility is the increase of the mass loss rate with the mass of the star in formation (see Behrend & Maeder, 2001). This remains speculative since the observations of massive star in formation are missing. This is mainly due to the short timescales of the evolution of massive stars, so that it is possible that they enter the main sequence while they are still

accreting (Bernasconi & Maeder, 1996). Moreover, since their evolution is rapid, they are significantly evolved when they emerge from their parental cloud. Observing massive stars in formation is then a formidable task. There are nonetheless several hints pointing to the possible formation of massive stars via accretion. In particular, the presence of jets of matter (a typical property of low mass star formation by accretion) in sites of massive star formation is well established (Stecklum et al., 1995; Shepherd et al., 2000). But no real observation of disks around massive stars has been made so far (Hoare et al., 2003), except perhaps the very recent one by Chini et al. (2004).

This uncertainty on the formation of massive stars has lead people to think in another process according to which massive stars would be the result of collisions and mergers of low mass proto-stars (Bonnell, Bate & Zinnecker, 1998). This hypothesis has the advantage of explaining why we observe most of the massive stars in clusters. However, the densities required for such a process to happen are high (of the order of 10^6 pc^{-3}). In order to better understand the formation of massive stars, it is then crucial to observe them as soon as possible.

The earliest phases of massive stars formation observed so far seem to consist in the "hot cores" objects (Hofner et al., 1996). They are very compact regions (diameter < 0.1 pc) with a high electron density and temperature ($n_e > 10^7$ cm^{-3}, T$>$ 100 K) (Kurtz et al., 2000, and references therein). They are usually optically thick so that we do not see any component of these regions at any wavelength. The presence of one or several massive stars is only inferred from the temperature of the cloud. The next phase of the formation corresponds probably to the ultra compact HII regions (UCHII, see Churchwell, 2002) which display reduced densities compared to hot cores, although they are still high ($n_e > 10^5$ cm^{-3}). These regions are little extended (~ 1 pc) and harbour one or several massive stars which ionise the circumstellar medium giving birth to the ultra compact HII region (Kurtz et al., 2000). Once again, the stellar components are not observed, but their properties are deduced from nebular lines sensitive to the spectral energy distribution of the central object (s). With time, the HII region expands because of the release of ionising photons (Jaffe et al., 2003), revealing the stellar content and becoming a classical HII region. In the latter phase, massive stars are observable directly at different wavelengths, but they are significantly evolved. Hence, the best way to observe young massive stars would be be to find star forming regions intermediate between UCHII and classical HII regions. This is the opportunity offered by the "High Excitation Blobs" (HEBs), a class of objects first observed by Heydari-Malayeri & Testor (1982) and which seems to be the missing links in the above description. Indeed, morphologically the HEBs are more extended than UCHII regions (1 to a few parsecs wide), but less than classical HII regions (which have diameters of more

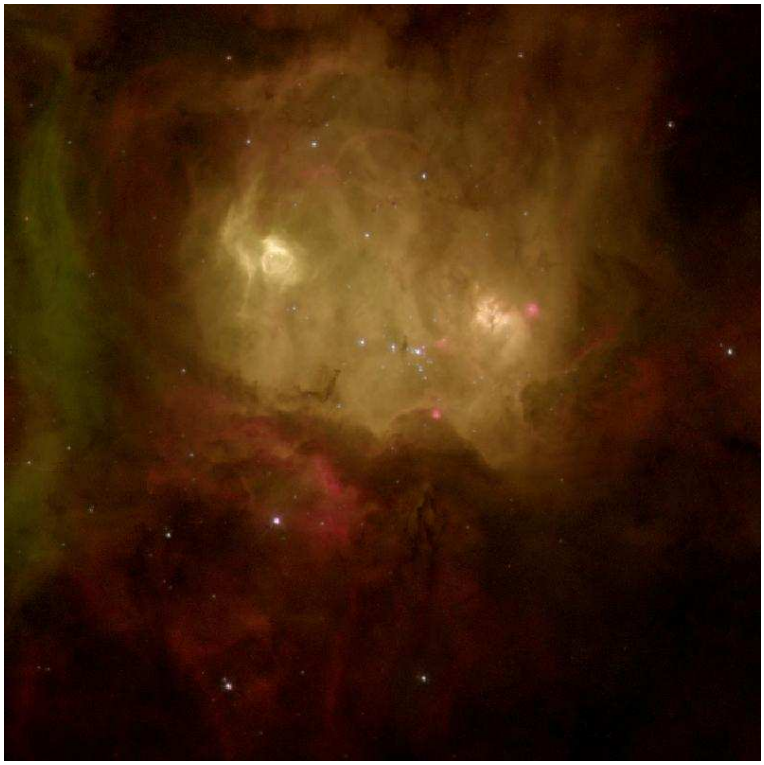

Figure 1.2: High Excitation Blob N160 in the Large Magellanic Cloud. This star forming region is probably in an intermediate state between between Ultra Compact HII region and classical HII region. It represents a good opportunity to observe young massive stars just emerging from their parental molecular cloud. The picture results from three exposure in different filters. Its was taken in May 2000 by WFPC2 on HST and has a size of 67×67 ".

than a few parsecs). Moreover, their strong excitation (measured by the ratio O III λ5007 / H_β) is an indication that they are certainly young objects in which the intense radiation field of young stars is not diluted and interact a lot with the environment. So far, HEBs have only been observed in the Magellanic Clouds (Heydari-Malayeri et al., 1999a,b,c, 2001, 2002c). Their total number amounts to roughly ten. Fig. 1.2 shows one of these HEBs and we recognise the typical characteristics of star forming regions: ionised cavity, ionisation fronts, shocks, turbulent structures... And the most interesting is that we clearly see the stellar components! Hence, the HEBs are young star forming regions transparent enough to reveal their stellar content. They represent a unique opportunity to study recently formed massive stars.

An important part of this thesis was devoted to the study of stars in one of these HEBS (N81 in the SMC). The motivations were manyfold. The analysis of the properties of young massive stars was one of the reasons,

but the analysis of wind properties of massive stars in a metal deficient environment was another important one. This is the topic of the next section.

1.2 Massive stars winds

As we already mentioned it, mass is the fundamental parameter of stellar evolution. In the case of massive stars, the mass is modified by the mass loss phenomenon due to strong stellar winds which expel continuously mass in the interstellar medium (Chiosi & Maeder, 1986; Maeder & Conti, 1994). Such outflows were first observed by Morton, Jenkins & Bohlin (1968) thanks to rocket UV observations. The mass loss rates can reach $10^{-4..-3}$ $M_\odot$ yr^{-1} and the terminal velocities can be 1 % of the light speed, or 3000 km s^{-1}. Hence, the total mechanical energy released by the star during its life (of the order of 10^{51} ergs, see Leitherer, Robert & Drissen, 1992) strongly influences the neighbouring interstellar medium. But this mass loss is crucial for the star too. Indeed, a 100 solar mass star can loose more than 90 % of its mass during its life (Maeder, 1992). It is then fundamental to know qualitatively as well as quantitatively the mass loss rates of massive stars to understand not only their own evolution, but also their influence on the environment.

What is the origin of the wind of massive stars? The basic mechanism is quite simple. It simply consists of a transfer of momentum between the photon emitted by the star and the elements at the surface of the star. Said differently, it is the radiative acceleration suffered by the external layers of the star which create this outflow. This mechanism is especially important in the case of massive stars since the luminosity is high and lots of photons interact with lines. The resulting strong coupling between matter and radiation creates a radiative acceleration sufficient to balance and even surpass gravity (Milne, 1926). The quantity of matter ejected will be all the more important as the number of photons, and then the luminosity, will be high. This explains that the mass loss rate increases from late O stars towards early O stars. For more evolved stars close to the Eddington limit, instabilities can increase the mass loss rate even more.

The determination of mass loss rates relies on various methods based on either the estimate of the excess of infrared and millimeter radiation due to free-free interactions of electrons in the wind (Lamers & Leitherer, 1993; Leitherer et al., 1995), or on fits of several spectral lines sensitive to wind properties (mainly (extreme) UV and H_α). A number of studies in the past two decades lead to a good knowledge of the mass loss rates and terminal velocities of Galactic stars (Howarth & Prinja, 1989; Chlebowski

& Garmany, 1991; Leitherer, 1988; Puls et al., 1996; Herrero, Puls & Najarro, 2002; Repolust, Puls & Herrero, 2004). Several Magellanic Clouds objects have also been studied in the last years (Puls et al., 1996; Crowther et al., 2002a; Hillier et al., 2003; Bouret et al., 2003).

Fig. 1.3 shows the result of determinations of terminal velocities (v_∞) for Galactic stars. We see that v_∞ is well correlated with the escape velocity (v_{esc}). The coefficient of proportionality of this relation depends on the effective temperature of the star, but for O stars it is essentially the same since they are usually hotter than 21000 K where a first jump occurs in the relation, the coefficient of proportionality becoming smaller below this value. This kind of jump was called the "bistability jump" by Lamers et al. (1995) who first highlighted its existence. It is mainly due to a change in the ions responsible for the radiative acceleration, due itself to a modification of the ionisation (see Vink, de Koter & Lamers, 1999). In simple descriptive term, the correlation between v_∞ and v_{esc} can be understood as follows: in the upper atmosphere, thermal pressure and radiative acceleration becomes much less important than gravity so that the velocity is mainly governed by gravity. Hence, the higher the gravity (and thus to first order the higher the escape velocity), the higher the terminal velocity.

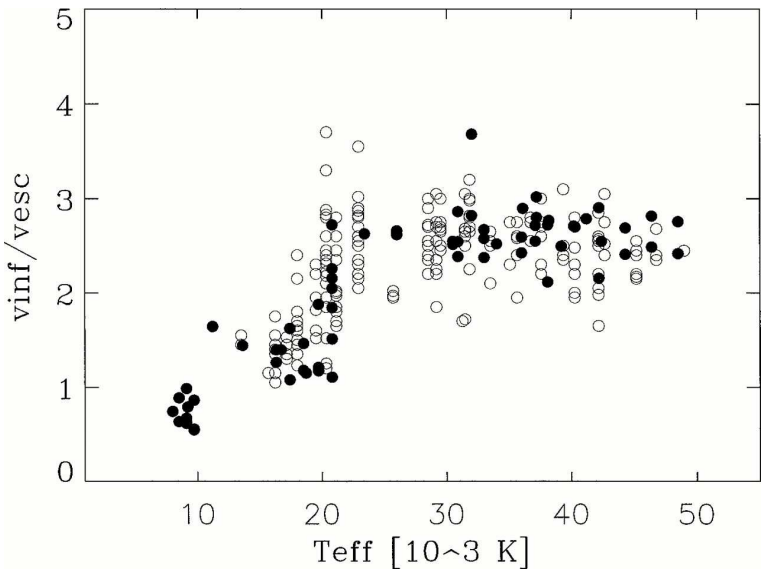

Figure 1.3: Ratio of terminal velocity (v_∞) to escape velocity (v_{esc}) for various galactic stars. Supergiants are shown by filled circles, other luminosity classes by open circles. Data are from Prinja, Barlow & Howarth (1990), Prinja & Massa (1998), Lamers et al. (1995) and Howarth et al. (1997). From Kudritzki & Puls (2000).

As regards mass loss, Fig. 1.4 displays results of various recent studies

as a function of luminosity. These studies are based on determinations of mass loss rates thanks to the H_α line. We see that mass loss rate and luminosity are well correlated as expected from the previous qualitative argument and from theory (see Sect. 5). The number of studies for supergiants is significant, which is not the case of dwarfs. Moreover, the luminosity range below $\log \frac{L}{L_\odot} \lesssim 5.3$ remains little explored. This may be explained by the lower magnitude of the objects in this range, rendering them more difficult to observe. In addition, the determination of wind parameters in weak wind stars is more difficult since classical indicators such as H_α and radio excess become almost insensitive to $\dot{M}$ when it decreases and reaches values as low as $10^{-8..9}$ $M_\odot$ yr^{-1}. This is confirmed by Fig. 1.5 showing determinations of mass loss rates based on radio measurements: it is even more obvious that quantitative studies of massive stars with low luminosity (especially dwarfs) are missing.

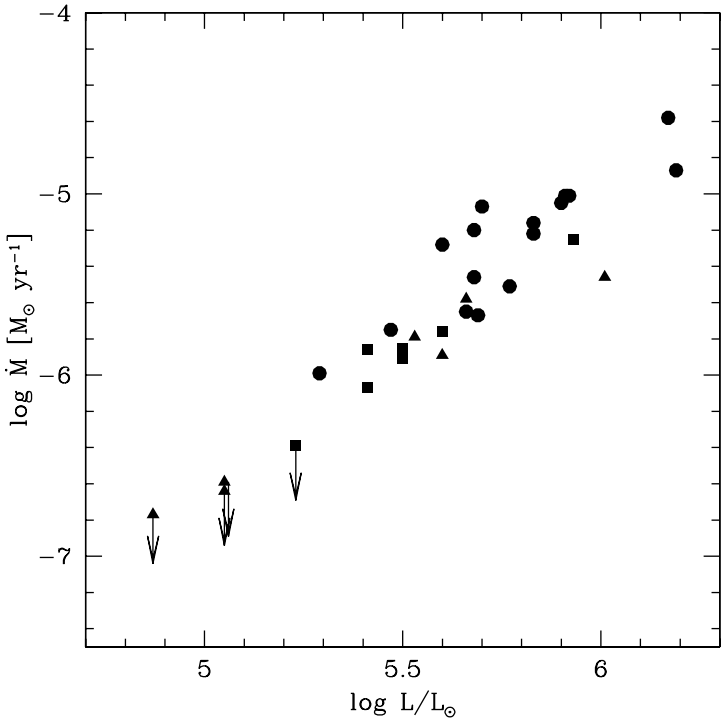

Figure 1.4: Mass loss rates of Galactic O stars as a function of luminosity. Circles (squares, triangles) are for supergiants (giants, dwarfs). Determinations are from Repolust, Puls & Herrero (2004) and Herrero, Puls & Najarro (2002) and are based on H_α.

Another question waiting to be answered is the metallicity dependence of wind properties. Indeed, the elements responsible for the radiative acceleration are mainly metals (C, N, O and Fe). This implies that the strength

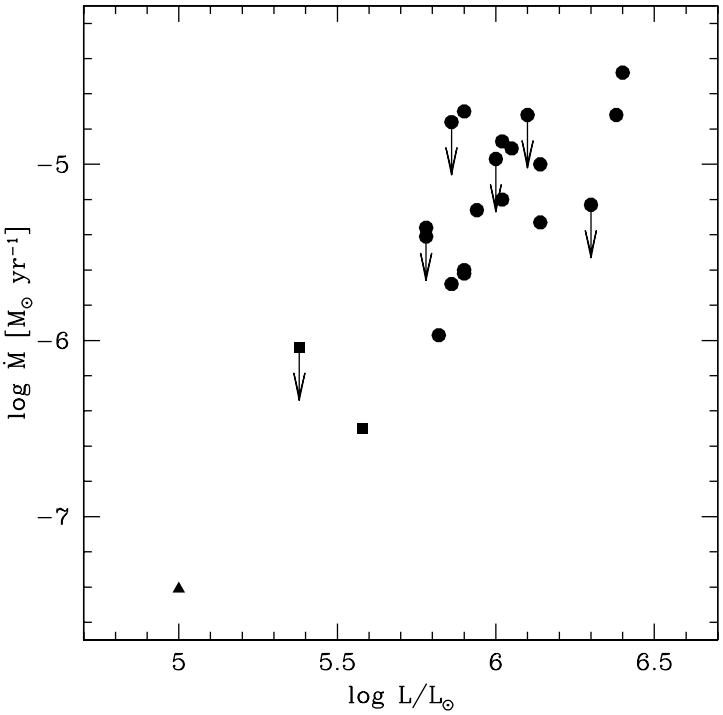

Figure 1.5: Mass loss rates of Galactic O stars derived from radio fluxes Symbols are the same as in Fig. 1.4 and data are from Lamers & Leitherer (1993), Leitherer (1988) and Howarth & Prinja (1989).

of the wind will vary with the metal content, the radiative acceleration changing with the abundances of absorbing ions. From a theoretical point of view, the mass loss rates is expected to follow the relation $\dot{M} \propto Z^r$ where r is of the order 0.5-1.0 (see Abbott, 1982; Leitherer, Robert & Drissen, 1992; Vink, de Koter & Lamers, 2001). Similarly, the terminal velocity should scale with metallicity according to a power law with exponent 0.13 (Leitherer, Robert & Drissen, 1992). A reduction of terminal velocities in the SMC was observed by Walborn et al. (1995) but recently Evans et al. (2004) did not find such an obvious trend. As for mass loss rates, although Fig. 1.6 shows that the reduction of the wind strength at low metallicity seems to exist *qualitatively*, there are only few *quantitative* studies. At the beginning of this thesis, the only work was that of Puls et al. (1996) which included only a few stars of the Magellanic Clouds. Their results indicated a possible decrease of mass loss rates with metallicity, but the small number of stars studied did not allow to draw general conclusions, as seen in Fig. 1.7. Concerning super-solar metallicities, the only studies where that of Krabbe et al. (1995) and Najarro et al. (1994), Najarro et al. (1997) and concerned evolved stars for which mass loss rates are poorly known, even at solar metallicity, so that no conclusion as regards the metallicity

dependence could be drawn. New constraints on the wind properties of massive stars at super solar as well as at sub solar metallicities were then needed, and this thesis took part in this global effort.

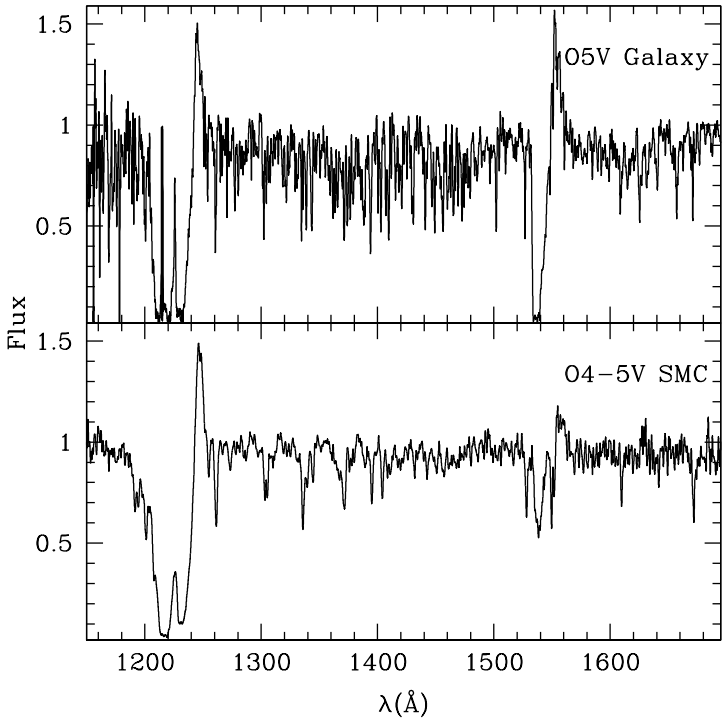

Figure 1.6: Metallicity effect on the UV spectrum of star of spectral type O5V. A lower metal content reduces the strength of wind sensitive lines (especially C IV $\lambda\lambda$1548,1551), indicating a lower mass loss rate.

Besides mass loss rates and terminal velocities, another quantity was poorly known at non solar metallicities: the modified wind momentum (noted MWM). This quantity is the wind momentum times the square root of the radius of the stars ($\dot{M}v_\infty\sqrt{R}$) and is predicted to be a function of the only luminosity (Kudritzki, Lennon & Puls, 1995; Kudritzki & Puls, 2000, + Sect. 5). In fact, historically, the term $\sqrt{R}$ was added to $\dot{M}v_\infty$ to obtain a quantity depending only on L. Fig. 1.8 shows this relation for various Galactic stars. We see that there is indeed a good correlation between the MWM and the luminosity (giving the so-called modified wind momentum - luminosity relation, hereafter WLR). The relation is however different for supergiants and giants + dwarfs, which is not predicted by the radiation driven wind theory. This relation is particularly interesting since in the case it is well calibrated, it can be used as a distance indicator up to several Mpc (Kudritzki, 1998). Indeed, the determination of the MWM through quantitative spectroscopy gives the luminosity, and then the dis-

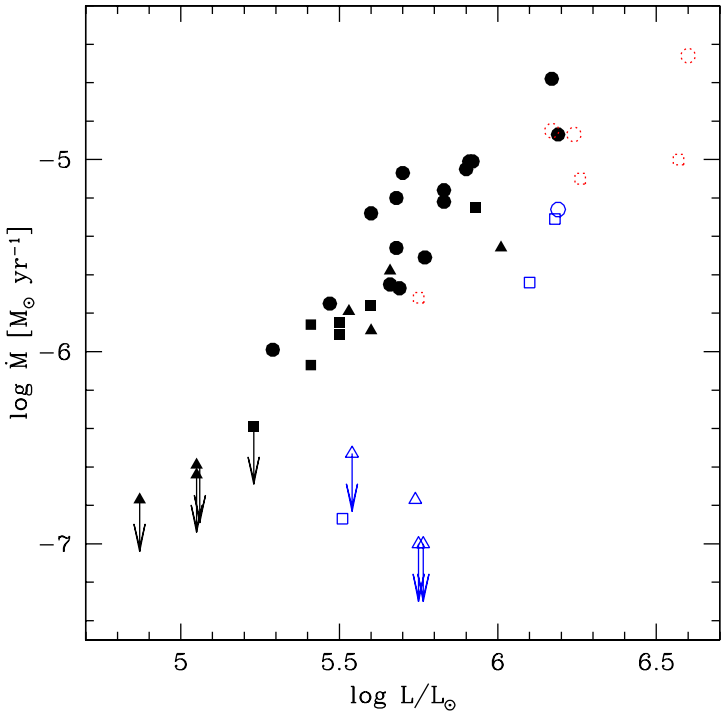

Figure 1.7: Mass loss rate of O stars in the Galaxy (filled symbols) and in the Magellanic Clouds (open symbols, red + dotted: LMC, blue + solid, SMC) as a function of their luminosity. Circles (squares, triangles) are for supergiants (giants, dwarfs). From Repolust, Puls & Herrero (2004) and Herrero, Puls & Najarro (2002).

tance. Nonetheless, just as the wind parameters entering its definition, the MWM depends on metallicity and quantitative studies are required to calibrate the WLR in non solar environments.

The HEB stars studied in this thesis are perfectly suited for these different kind of studies of the wind parameters and the WLR in a low metallicity environment. Moreover, the study of the wind properties of dwarfs with low luminosities was completed through the analysis of winds of Galactic stars. The various studies carried on during this thesis relied heavily on "new generation" atmosphere models which are introduced in the following section.

1.3 Atmosphere models for massive stars

Quantitative analysis of the wind properties of massive stars relies mainly on the use of atmosphere models. Such models help to reproduce the dif-

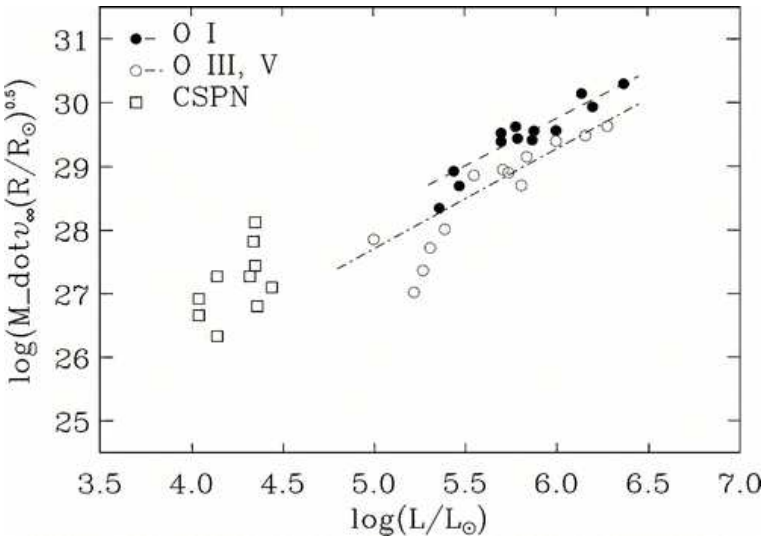

Figure 1.8: Relation between modified wind momentum ($\dot{M}v_\infty\sqrt{R}$) and luminosity of Galactic O stars and planetary nebulae. From Kudritzki & Puls (2000).

ferent structures (density, temperature, ionisation) and the radiative field in the atmosphere. They also provide synthetic spectra emitted by the star through its atmosphere. The fit of observed lines thanks to such spectra gives informations on the physical properties of the star (effective temperature, gravity, chemical composition, mass loss rate...). Spectroscopic analysis of stars with atmosphere models turns out to be a powerful tool. However, the modelling of massive stars atmospheres is not a trivial task since several physical ingredients have to be taken into account. From a general point of view, one can summarise them as follows:

- non-LTE treatment:

  Due to their high luminosity, massive stars have a strong radiation field so that radiative phenomenon are dominant other collisional processes. This implies the absence of thermodynamical equilibrium, even locally. Hence, the determination of the populations of the energy levels must result from a detailed statistical equilibrium calculation for each level where all the populating and depopulating processes have to be taken into account. Practically, this requires a lot of cpu time which increases as the number of level populations increases.

- spherical extension:

  As we have seen before, massive stars continuously emit a wind which creates an atmosphere extending up to a hundred of stellar radii. In that case, the classical approximation of plane parallel geometry (i.e.

the atmosphere height is much lower than the stellar radius) breaks down. It is thus necessary to solve the various equations in spherical geometry. Moreover, the atmosphere is accelerated so that Doppler shifts appear and create a non local coupling between the various equations, a photon emitted at a given place having the possibility to be absorbed far from its emission point by a line with lower frequency.

- line blanketing:

  The inclusion of metals in the atmosphere models is required to obtain synthetic spectra as realistic as possible. Indeed, metals shape the emergent spectrum through their numerous lines, but they also strongly modify the atmospheric structure. Indeed, metal opacities influence the radiative transfer which have important consequences for the ionisation and temperature structure, and thus indirectly on the emergent spectrum.

Historically, non-LTE treatment and spherical extension were the two first ingredients to be included in the atmosphere models of massive stars (see Sect. 2.1). However, line-blanketing in O stars has been taken into account only very recently and even though its effects were known *qualitatively*, only one partial quantitative study based on new atmosphere models was completed before this thesis (Hubeny, Heap & Lanz, 1998).

Now, the atmosphere models including line-blanketing are sufficiently developed to lead such a quantitative study. In particular, the very realistic synthetic spectra produced render possible detailed spectroscopic analysis. Various questions concerning massive stars can be tackled. Let us just mention a few ones:

- abundances determinations in massive stars: the inclusion of metals and the creation of detailed synthetic spectra showing signatures of CNO and Fe (among others) allows to determine reliable metallicities and individual abundances. Such determinations are crucial to test evolutionary models of massive stars including different mechanisms (e.g. rotation) leading to enrichment or depletion of elements, especially C, N and O (e.g. Walborn et al., 2004).

- determination of masses: Herrero et al. (1992) have shown that masses determined from spectroscopy (through log g) were systematically lower than the masses deduced from evolutionary models in the HR diagram. The discrepancy probably comes from uncertainties in both atmosphere models and evolutionary models, but the use of improved synthetic spectra will certainly allow a reduction of this discrepancy. And indeed, first results presented by Herrero, Puls & Najarro (Herrero, Puls & Najarro (2002)) indicate that the

agreement is better, although not perfect. This is due to a better determination of gravity through improved atmosphere structures and better synthetic spectra, and to new determinations of evolutionary masses from revised stellar parameters and HR diagrams.

- effective temperatures and luminosities: spectroscopic analysis of massive stars with new atmosphere models leads to better constraints on these two important parameters which can be used to build the HR diagram and estimate the evolutionary status of the star and its age. New constraints of the age of young clusters can be considered, together with determinations of IMF (e.g. Massey et al., 1995a,b).

- wind properties: detailed synthetic spectra coupled to high resolution / high S/N ratios can lead to improved determinations of wind properties, especially as regards mass loss rates. In particular, the inclusion of metals in atmosphere models should help to constrain the metallicity dependence of wind parameters.

- ionising fluxes: line blanketing effects modify the spectral energy distribution (SED) of massive stars (see Sect. 4.1) with the consequence of new ionising fluxes. This is important for nebular analysis of HII regions which rely heavily on such ionising fluxes.

The previous examples are only a few among others. They just show the potential of the new generation of atmosphere models for massive stars. Of course, improvements can still be brought. Let us mention that at present, all models use a 1D geometry. However, it is well known that rotation breaks this global symmetry, introducing a dependence of all the stellar and wind parameters with latitude (e.g. Maeder & Meynet, 2000). Moreover, time variable phenomenon take place in the winds whereas models usually compute stationary atmospheres (see however Owocki, Castor & Rybicki, 1988). Also, the majority of current models are not consistent in the sense that they simply assume a velocity and density structure, but do not compute it self-consistently with the populations and radiative field. A complete models would require the treatment of the hydrodynamics together with the radiative transfer. Such an approach already exists (see Pauldrach et al., 1994; Pauldrach, Hoffmann & Lennon, 2001), but at the price of a treatment of the radiative transfer of lower quality than in other models not including the hydrodynamics. However, the use of empirical models not including the hydrodynamics is crucial to determine freely the wind parameters through spectroscopic analysis.

In spite of the absence of these last ingredients, the new generation of massive star atmospheres including a reliable treatment of line-blanketing allows to expect important progress in the spectroscopic analysis of massive stars and the understanding of their evolution in general.

1.4 In this thesis

In view of the various questions presented in the previous sections, this thesis focused mainly on two main aspects of the physics of massive stars:

- Line-blanketing effects:

  Here, we have studied quantitatively the the line-blanketing effects on the atmosphere models of massive stars. We were especially interested in the effective temperature of O stars and in the relation between $T_{\rm eff}$ and the spectral types (effective temperature scale) for which we have given a revised version. Moreover, we have studied the improvements brought by line-blanketing in terms of spectral energy distributions and we have tested them through their effect on the nebular emission of compact HII regions.

- Winds of young O stars:

  In order to better know the wind properties of massive stars and of O stars in particular, we have lead various spectroscopic analysis in the Galaxy and the Magellanic Clouds. Such studies took part in a global effort to 1) constrain the metallicity dependence of wind parameters, 2) calibrate the modified wind momentum - luminosity relation, and 3) to bring constraints on the mass loss rates of O stars with low luminosity.

These two types of analysis relied on the modelling of massive star atmospheres with the code CMFGEN (CoMoving Frame GENeral) developed by John Hillier, University of Pittsburgh, USA.

The manuscript is organised as follows:

◇ chapter 2: this chapter makes a general presentation of atmosphere models for massive stars and recalls the main ingredients to be included and their effects. A short description of CMFGEN is also given.

◇ chapter 3: Here, we study the effects of line blanketing on the effective temperature of O dwarfs. After a brief historical overview, we show that the inclusion of line-blanketing in atmosphere models leads to a reduction of the effective temperature scale of such stars. Metallicity effects on this $T_{\rm eff}$ - scale are also investigated.

◇ chapter 4: In this chapter, we study the influence of line-blanketing on the ionising fluxes of O stars. A test of these spectral energy distributions in the (extreme) UV is done through the analysis of mid IR nebular lines emitted in compact HII regions observed with ISO.

- ◇ chapter 5: A brief presentation of the radiation driven wind theory is made, with special emphasis on the main ideas and the results.
- ◇ chapter 6: The stellar content of the HEB SMC-N81 is qualitatively analysed here. An approximate spectral classification is done and constraints on the stellar and wind properties are derived.
- ◇ chapter 7: A quantitative analysis of the SMC-N81 stars is performed using atmosphere models computed with CMFGEN. Special care is given to the derivation of the wind parameters since they indicate very weak winds. The origin of this weakness is investigated.
- ◇ chapter 8: This chapter focuses on the spectroscopic analysis of Galactic dwarfs with weak winds. Quantitative constraints on the wind parameters are given and the behaviour of the modified wind momentum - luminosity relation of O dwarfs is investigated.
- ◇ chapter 9: This is the concluding chapter where the summary of the results is made and perspectives are mentioned.

Part I

Line-Blanketing

The first part of these thesis is dedicated to the study of line-blanketing. Under this designation, we mean all effects related to the inclusion of metals in atmosphere models. Modifications of both the atmosphere structure and the emergent spectrum are investigated, with special emphasis on the temperature structure and the spectral energy distribution of O stars.

Chapter 2

Atmosphere models for massive stars

French summary

Ce chapitre est consacré à la descrition des modèles d'atmosphères pour étoiles massives.

Nous montrons tout d'abord qu'une approche hors équilibre thermodynamique local (hors-ETL) est fondamentale. En effet, les étoiles massives émettent une quantité de photons gigantesque à cause de leur forte luminosité. Il en découle un champ de rayonnement très intense qui rend les phénomènes radiatifs très largement dominants par rapport aux phénomènes collisionnels (excitation, ionisation, recombinaison...). Ainsi, une approche où populations et rayonnement sont calculés au moyen de l'hypothèse que localement l'équilibre thermodynamique local est atteint n'est pas valable. On doit s'en remettre à l'utilisation et à la résolution des équations d'équilibre statistique, ce qui est beaucoup plus compliqué.

Les premières tentatives de calculs hors-ETL ont été menées dans les années 70 notamment par Auer et Mihalas. Au moyen de modèles ne contenant que quelques niveaux d'H et He en plus des continus, ils ont montré toute l'importance des effets hors-ETL. En particulier, la température ne décroît plus continûment à travers l'atmosphère, mais subit une remontée lorsque les continus deviennent optiquement minces et qu'un rayonnement plus intense venant de couches plus profondes peut re-ioniser le milieu. Par la suite, la température diminue à nouveau à cause d'un mécanisme de refroidissement par les raies fortes devenant elles aussi optiquement minces. Le spectre émergent est également significativement modifié, tant au niveau de la distribution spectral d'énergie (SED) que des raies individuelles, et ce à cause des modifications de la structure d'ionisation et du champ radiatif. Cela a d'importantes conséquence pour l'analyse spectro-

scopique d'étoiles individuelles.

Ensuite, l'adoption d'une géométrie sphérique est nécessaire pour obtenir des modèles réalistes. Ceci tient au fait que les étoiles massives émettent sans cesse un vent qui crée une atmosphère s'étendant jusqu'à plusieurs dizaines de rayons stellaires, rendant caduque l'approximation d'une atmosphère plan-parallèle. Dans ce domaine, les travaux de Gabler et al. (1989) sont majeurs. Ils montrent en particulier que les gradients de vitesse dans l'atmosphère conduisent à une désaturation de certaines transitions. Cela produit une remontée de la température encore plus importante que dans le cas hors-ETL sans extension sphérique. D'autre part, la structure d'ionisation de l'He est significativement modifiée, ce qui a pour effet d'augmenter considérablement le flux dans le continu d'He II. Enfin, de nombreuses raies en émission apparaissent dans le spectre.

Puis nous nous intéressons au line-blanketing. Cet effet n'a été introduit que récemment dans les modèles, mais il était connu qualitativement depuis longtemps. Il est dû à l'inclusion de métaux dans les modèles, chose impossible il y a quelques années en raison des ressources informatiques importantes que cela demande. Ses principales manifestations sont 1) une modification du spectre émergent, 2) un blocage du flux aux courtes longueurs d'ondes, 3) un réchauffement des couches intérieures, 4) un refroidissement des couches extérieures et 5) un changement de l'ionisation de l'atmosphère. Diverses approximations ont d'abord été utilisées pour inclure le line-blanketing, et nous en donnons une brève description. Les chapitres 3 et 4 seront consacrés à l'étude de cet effet.

Finalement, nous donnons une description du code d'atmosphère CMFGEN qui a été utilisé pour nos simulations. Celui-ci inclue les trois ingrédients majeurs présentés ci-dessus et permet une étude approfondie des effets du line-blanketing quasiment sans approximation.

In this chapter, we recall the basic ingredients of the modelling of massive stars atmospheres. An historical overview of the improvements achieved within the last decades is given, with special emphasis on the inclusion of non-LTE effects, winds and line-blanketing in the models. We also make a brief presentation of CMFGEN, the atmosphere code we have used in this thesis.

What is an atmosphere model and what is it used for? The atmosphere of a star is simply the interface between the stellar interior and the observer so that it behaves as a filter which modifies the spectral energy distribution (SED) emitted by the star. This SED is essentially a black body emission in the optically thick stellar interior, and is strongly affected by the various opacities when it goes through the atmosphere so that when it reaches the observer, the SED is not the simple smooth black body function but shows continuum jumps and thousands of lines. The aim of an atmosphere model is to predict as precisely as possible this emergent SED. This implies a modelling of the radiative transfer and the knowledge of the various opacities which depends on the populations of the individual levels of all the elements. This requires the knowledge of the temperature and density structure in the atmosphere. Hence, predicting the SED emerging of a stellar atmosphere is a complex task since many physical quantities must be predicted. Moreover, all phenomena are coupled. Indeed, the radiation field depends on the opacities, which in turn depend on the populations set by collisional and radiative processes depending themselves on the radiation field!

One of the main characteristics of massive stars is that they continuously emit a wind which creates an atmosphere expanding up to several tens of stellar radii. Moreover, the effective temperature of these stars is so high (20000 to 80000 K for the hottest WR stars, e.g. Crowther et al., 2002b) that their radiative field is especially strong. This implies that the radiative processes are dominant over collisional processes. These two characteristics (expanding atmosphere + importance of radiative processes) must be included in the atmosphere models of massive stars: this requires a **non-LTE** approach to be used and **spherical geometry** to be adopted. Moreover, many lines from various elements other than H and He (especially Iron) must be included to make the models as realistic as possible. The effects caused by these metals on the atmosphere models are called **line-blanketing** effects. From the above requirements, atmosphere models of massive stars must solve the following set of equations:

- radiative transfer equation: it determines the radiative field.
- statistical equilibrium equations: they determine the non-LTE populations for each level included in the model.

- radiative equilibrium equation: it is a special case of the more general equation of energy conservation and leads to the temperature structure in a non convective environment.

- momentum conservation equation: it determines the velocity structure.

- mass conservation equation: it determines the density in the atmosphere.

As mentioned above, all these equations are coupled together: populations give the opacities and thus the radiative field, but the latter modifies the populations through radiative transitions; the radiative field is used for the computation of the radiative acceleration which enters the momentum conservation equation; the velocity law modifies the density and consequently the opacities; and the Doppler shifts due the velocity law create a coupling between different lines at different places, a photon emitted in a line at a given place being able to interact with another line far from its emission point; moreover, the radiative field modifies the temperature structure through the radiative equilibrium equation, and the temperature has an influence on collisional processes entering the computation of populations. Hence, the computation of an atmosphere model is a very complex task which explains that it took more than 30 years to obtain the first models including all the main ingredients. However, this does not mean that the current generation of models can not be improved. In particular, one of the remaining approximation is that of stationarity, since the inclusion of time-dependent variables is complex and the models which take into account time variations must use approximation concerning radiative transfer, statistical equilibrium or temperature structure. Moreover, most of the current models are still 1D models.

In order to better understand the evolution of massive stars atmosphere models, we will show in the next sections the improvements brought by the inclusion of the three main ingredients: non-LTE, spherical geometry and line-blanketing.

2.1 Non-LTE models

The first step towards realistic atmosphere models was the handling of non-LTE effects. The pioneering works in this field are those of Auer & Mihalas in the 70's. Due to the limited computational facilities, their first attempts included only a few non-LTE levels of H and He in addition to continua. However, their studies showed how important it was to make such a non-LTE treatment for which a good summary can be found in Mihalas (1978).

Let us first have a look at the temperature structure. Fig. 2.1 shows its behaviour in different types of models. The dotted line is the structure of a LTE model: the temperature decreases continuously form the interior toward the exterior. This can be explained as follows: at the top of the atmosphere, the mean free path of photons is high so that they can escape easily form the atmosphere. But when we go deeper in the atmosphere, this mean free path is reduced so that photons are more absorbed and scattered, leading to a more isotropic radiation field. As the flux must be conserved, this means that the same quantity of energy must go out the atmosphere in the inner layers and in the outer layers. This conservation can be achieved by an increase of the temperature gradient from the top down to the bottom of the atmosphere, leading to a constant increase of the temperature as displayed in Fig. 2.1.

When the assumption of thermodynamic equilibrium is dropped, things behave differently. Let us first consider the case where only continua are included in the models (dashed line in Fig. 2.1). The temperature first decreases, then reaches a minimum, increases and stabilises at a constant value. The explanation is rooted in the fact that in the non-LTE case, radiative processes can dominate other collisional processes and can set the temperature structure. In particular, the different continua can propagate through the atmosphere when they become optically thin and can interact with matter far from the place where they are emitted, but with the same distribution, say the same radiative temperature. This last temperature being high (since it comes from deeper layers), it leads to photoionisations which provide a high energy excess for the electrons, so that the temperature is increased. Hence, it is the non local interaction if radiation and matter which causes this increases of temperature. In Fig. 2.1, one sees that the temperature increase happens when the H (and to a lower extend HeI) continuum becomes optically thin.

If lines are added to the continua in the non-LTE models, the solid line of Fig. 2.1 is obtained. As in the previous case, the temperature begins to drop, reaches a minimum, but then increases even more, reaches a maximum and finally decreases outward. To understand this behaviour, let us examine the effect of a line. Close to the top of the atmosphere, a line is optically thin so that photons can easily escape the atmosphere through this line, leading to a downward transition of electrons from the upper to the lower levels. Consequently, energy is transferred from the thermal pool to the radiation field: the temperature decreases (line cooling effect). This fully explains the drop of temperature in the outer atmosphere seen in Fig. 2.1. However, this does not mean that effect of lines is systematically to decrease the temperature. Indeed, the cascade induced by the escape of photons leads to an overpopulation of the lower levels from which photoionisations usually happen. In Fig. 2.1, we see that when H_α becomes optically thin, the temperature increases. This due to the fact that in

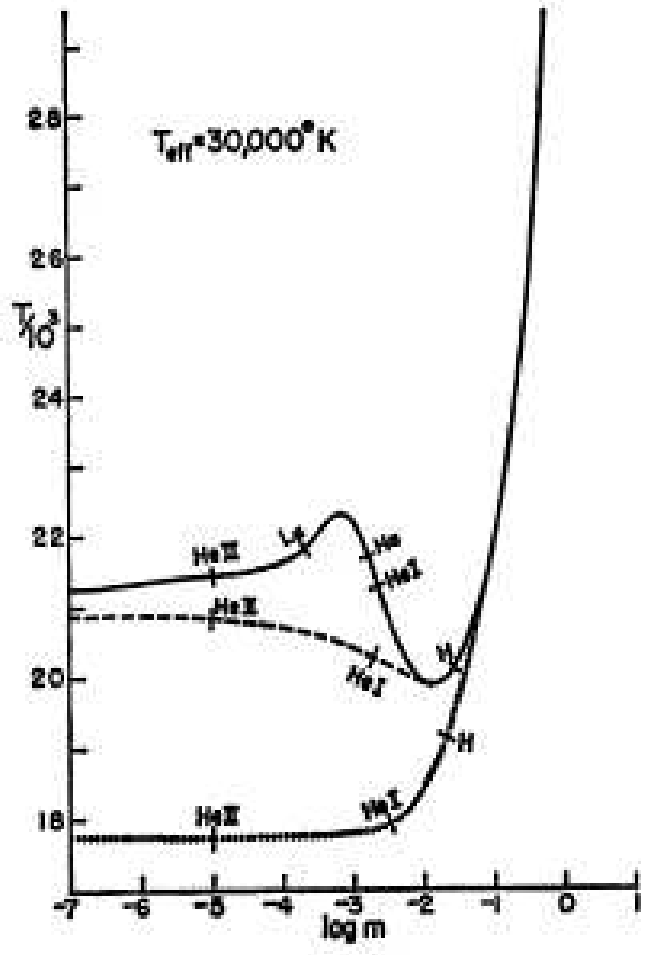

Figure 2.1: Temperature structure in a LTE model (dotted line) and in two non-LTE models, one including only continua (dashed line), the other including also lines (solid line). The tick marks indicate the formation depth of the various continua and of Ly_α and H_α. Taken from Mihalas & Auer (1970).

that case, the n=2 level becomes overpopulated (due to transitions from level 3): photoionisation from level 2 are then more frequent, which leads to an increase of the temperature (which adds to the increase due to the continua). Higher in the atmosphere, Lyman α becomes optically thin and induces a decrease of temperature as explained above (line cooling effect).

The spectral energy distribution (SED) is also modified by the non-LTE treatment. Fig. 2.2 shows the EUV/UV spectral range for a $T_{\rm eff}$ = 30000 K and log g = 4.0 star in the case of LTE (solid line) and non-LTE (dotted line). The He jumps are different in the two cases, while the Lyman jump is almost the same. The detailed understanding of the behaviour of a given

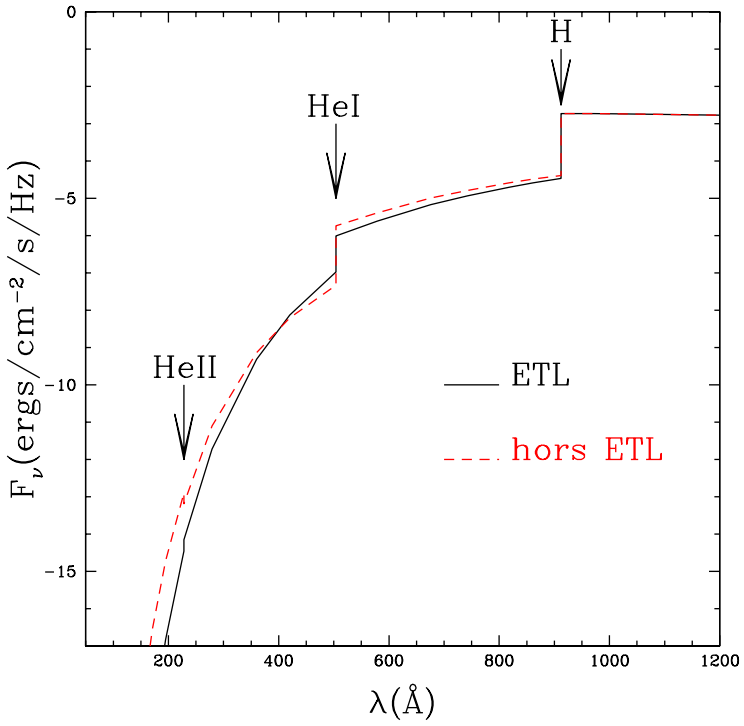

Figure 2.2: SED of a pure H He model with $T_{\rm eff}$ = 30000 K and log g = 4.0 in the LTE approximation (solid line) and non-LTE approximation (dotted line). The H, HeI and HeII discontinuities are indicated. Models are from Mihalas & Auer (1970). See text for discussion.

jump depends on a subtle competition between change of temperature and over(under)population of the ground state levels. Hence, an increase of temperature where the continuum is emitted leads to an increase of the flux, but an overpopulation of the ground state increases the opacity and reduces the emitted flux: the final result depends on the relative effect of both effects. Examples can be found in Mihalas & Auer (1970).

Spectral lines are also modified when one goes from LTE to non-LTE as shown in Fig. 2.3. The main conclusion is that depending on which type of model are used (LTE vs non-LTE), different results can be obtained from the fitting of observed spectra. Once again, the exact behaviour of a line is specific. However, the main mechanism is the over(under)population of levels involved in the transition. As in certain cases radiative mechanisms can dominate the physics of the transition, this explains that the non-LTE profiles can be very different of the LTE case. Various examples can be found in Auer & Mihalas (1972), Kudritzki (1988) or Kudritzki & Hummer (1990).

This quick overview of the non-LTE effects in the atmosphere models of massive stars show that their inclusion is fundamental to derive reli-

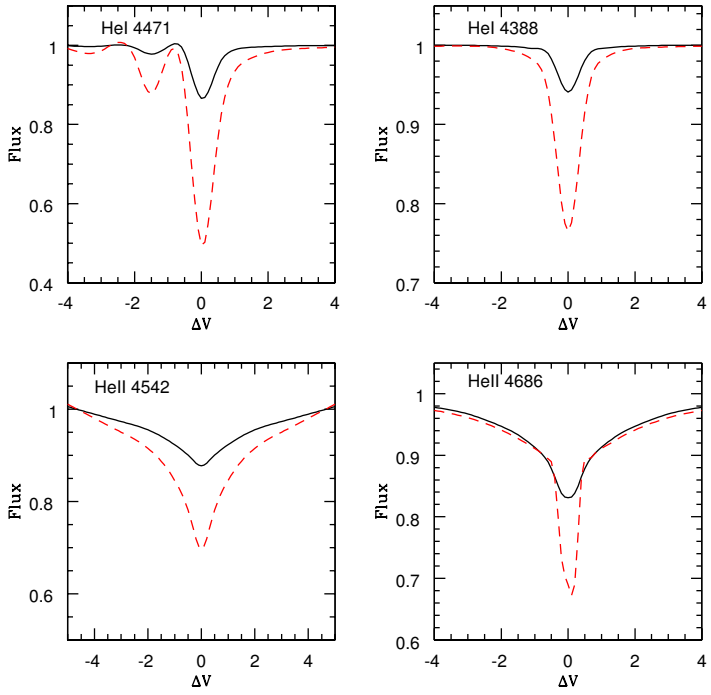

Figure 2.3: He lines profiles computed in the LTE case (solid line) and in the non-LTE case (dashed line). Models are from Auer & Mihalas (1972) for a star with $T_{\rm eff}$ = 40000 K and log g = 4.0.

able stellar parameters from the fit of observed spectra. Nowadays, all atmosphere models of massive stars take those effects into account for all levels.

2.2 Wind extension

The second crucial ingredient for the modelling of massive stars atmospheres is the extension due to the wind. Why is it the case? First, the fact that the wind may extend up to several tens of stellar radii renders possible the emission of continua and lines well above the stellar surface where the emitting surface is much larger than the photosphere. Moreover, the temperature at such places can be significantly different form the photospheric temperature, so that the emitted flux can be altered compared to a plane parallel case where all is supposed to be emitted close to the photosphere. Second, the atmosphere is accelerated which implies Doppler shifts rendering the radiative transfer problem more complex, a photon emitted at a given place in a line being able to interact with another line far form its emission point. The effects of spherical extension in

WR stars have been deeply studied by Hillier (1987a,b). For O stars, the work of Gabler et al. (1989) and Schaerer & de Koter (1997) give the main results.

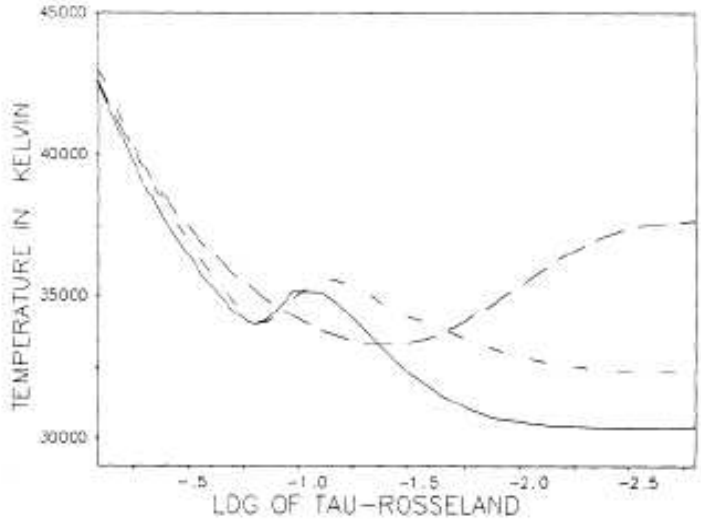

Figure 2.4: Temperature structure in a model without wind (long dashed line) and two models with wind (solid line: H and He lines included; short dashed line: H lines only). See text for discussion. From Gabler et al. (1989).

As in the previous section, let us first have a look at the temperature structure. Fig. 2.4 shows such a structure in a plane parallel pure H He model (dashed line). One sees the typical decrease in the interior followed by the increase near log τ = -2.0 due to the downward cascade of electrons in the ground state levels from which photoionisations heat the atmosphere (non LTE effect, see previous section). The decrease of T beyond log τ = -3.0 is not shown. The two other curves are temperature structures of models with winds, one with H and He lines (solid line), the other including only H lines (short dashed line). On average, the shape of the temperature profile is the same in the three cases. However, various modifications can be noted. First, the temperature decreases much faster with decreasing τ in the spherical models, because the flux dilutes more rapidly in an expanding atmosphere. Second, the increase of temperature happens much earlier than in the plane parallel case. This is mainly due to the velocity gradient which creates Doppler shifts leading to the desaturation of lines. Indeed, as we go outward, the profiles are more and more redshifted so that bluer photons can be absorbed, leading to a pumping of electrons in the n=2 levels in resonance lines. More photoionisations happen from these levels, increasing the temperature deeper in the atmosphere than in the plane parallel case (see Gabler et al., 1989; Schaerer & de Koter, 1997).

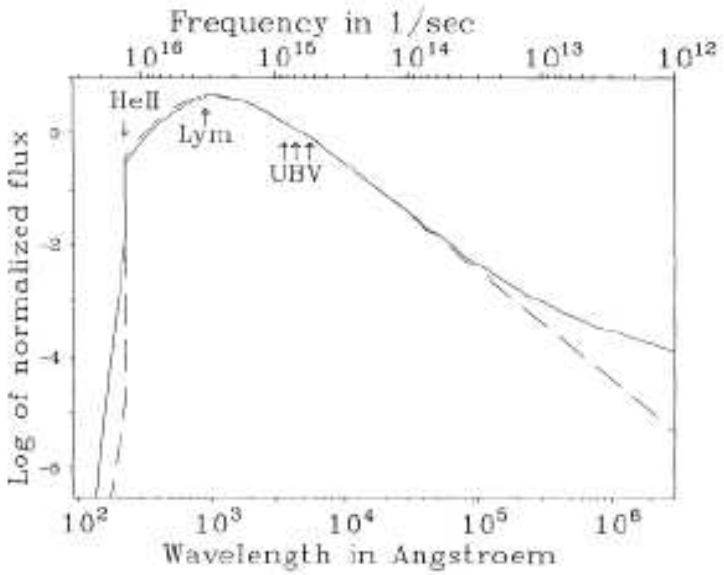

Figure 2.5: Wind effects on the SED. SED of a model without wind (dotted line) and with wind (solid line). The inclusion of the extension due to the wind create an excess of emission in the far-IR and mm ranges, together with a strong HeII continuum. From Gabler et al. (1989).

Further out, the desaturation of lines thanks to Doppler shifts allows the photons to escape earlier, causing the decrease of temperature in external layers.

Concerning the SED, winds imply two main changes. First, the existence of and extended ionised zone gives birth to an excess of free-free emission (arising from the interaction of ions and electrons) in the far-IR and mm ranges as displayed in Fig. 2.5. This excess is usually observed in atmospheres of massive stars and its predictions is one of the successes of the models. The other important change is in the extreme UV range, more precisely in the HeII continuum (below 218 Å). Here, the inclusion of the wind translates to an increase of the emission. The velocity field can explain this behaviour: due to Doppler shifts caused by the acceleration of the wind, the HeII Ly_α line (i.e. He II λ504) desaturates, implying a pumping of electrons to the n=2 level by a hotter and bluer radiation coming form deeper layers (as explained above; see also Hillier, 1987a). Hence, the ground state is underpopulated, leading to a reduced opacity and consequently to a higher flux emission below 228 Å (see Gabler et al., 1989; Schaerer & de Koter, 1997). This is what is clearly shown in Fig. 2.5.

The inclusion of the wind modifies also the line profiles. A first effect has already been mentioned: the extension of the wind allows certain lines to be emitted high in the atmosphere where the emitting surface is large,

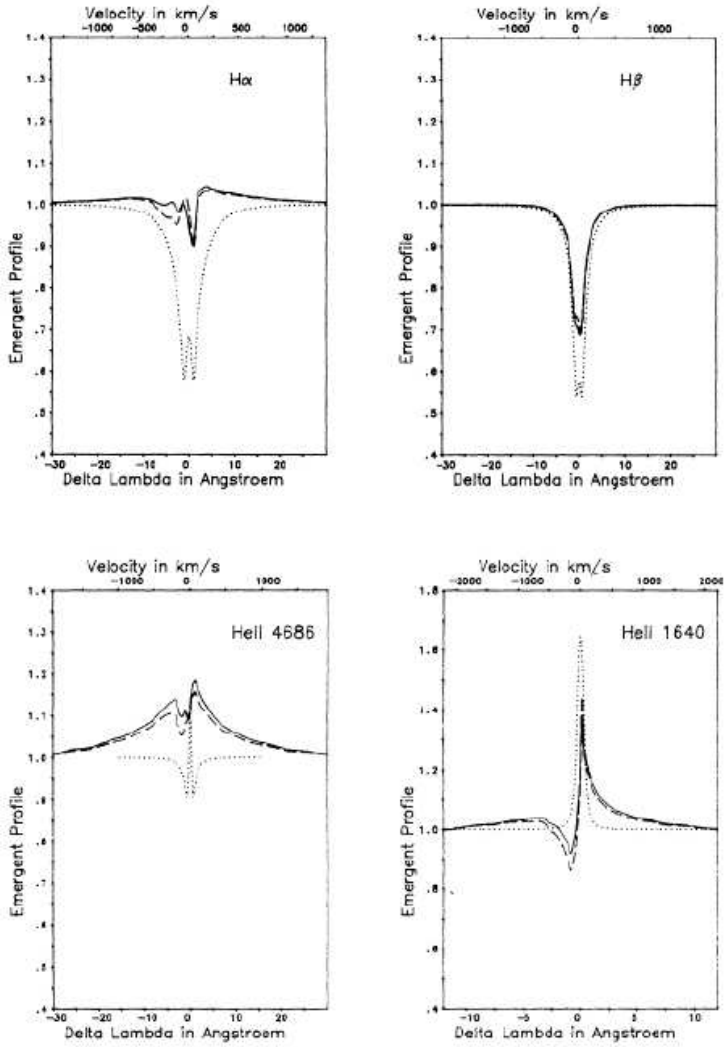

Figure 2.6: Wind effects on lines. Dotted line: plane-parallel model; solid line: model with wind. The inclusion of wind have important effects on the line profiles. Quantitative analysis of massive stars must include this ingredient. From Gabler et al. (1989).

possibly larger than the emitting surface of the neighbouring continuum. In that case, the line appears in emission. Moreover, the velocity gradients and related Doppler shifts modify the transfer of radiation (optical depths and escape probabilities being changed) and the level populations (see the case of the SED explained above). Fig. 2.6 show various profiles with (solid line) and without (dotted line) wind. The differences can be important in term of derived parameters from quantitative analysis of observed spectra.

More details concerning the effect of winds on atmosphere models can be found in (among others) Mihalas (1978), Gabler et al. (1989) and Schaerer & de Koter (1997). It is clear from the above discussion that the inclusion of winds in atmosphere models of massive stars is crucial in view of quantitative analysis of observed spectra. A word of caution however: all the effects presented so far are for pure H He atmospheres. We will see (e.g. Sect. 4.1) that the inclusion of metals has also strong implications for the SEDs of hot stars.

2.3 Line-blanketing

The third main ingredient of the modelling of massive stars atmospheres is called line-blanketing. Various effects are gathered within this name, but all have the same origin: opacities of metals. Indeed, although the abundances of metals are small, they have much more transitions than lighter elements (H and He). Moreover, they have a number of bound-free transitions. Hence, they contribute a major part of the total opacities of the atmosphere and have a major influence on the structure of the atmosphere (especially the temperature structure) and of course the emergent spectrum. Line blanketing is especially efficient in hot stars since the emission peak is in the UV where there are many bound-free opacities of metals. In addition, the numerous metallic lines interact a lot with the huge number of photons emitted by massive stars.

The main difficulty to take line-blanketing effects into account is the computational cost. Indeed, calculating the populations and radiative field in an atmosphere with thousands of transitions and energy levels with a non-LTE approach is very expensive in terms of cpu time. Thus, the first attempts to include line-blanketing were restricted to LTE atmospheres (Kurucz, 1979). Although this approximation was crude for O stars as we have seen above (it is reasonable for cooler stars), it highlighted the main effects of line-blanketing which can be summarised as follows:

- modification of the emergent spectrum. Adding forests of metallic lines greatly change the shape of the spectrum and new continuum opacities introduces new discontinuities in the SED.

- blocking: thousands of lines behave like a wall which disturbs the

outward transportation of energy. The radiation field is modified and must adapt to evacuate the energy. This translates to a redistribution of flux from the EUV range to longer wavelengths where opacities are weaker.

- backwarming : the blocking of radiation by the opacities of metals implies an increase of the temperature gradients, and consequently of the temperature itself, to ensure flux conservation.

- surface cooling: this effect has already been mentioned in Sect. 2.1. Due to the great number of lines becoming optically thin in the outer atmosphere, the escape of photons through these lines is favoured so that the transfer of energy from the thermal pool to the radiative pool, and thus the cooling of the atmosphere, is strengthened.

More details concerning these mechanisms can be found in Mihalas (1978) or Hubeny (1999).

Qualitatively, for massive stars, the effects of line-blanketing have been known for a while, but no quantitative study could be done until complete models were available (i.e. non-LTE models with winds and line-blanketing). The first attempts were made in the early 90's but they still made crude approximations as regards the treatment of line-blanketing in order to reduce the complexity of the problem. In particular, sampling methods were used (Pauldrach et al., 1994) to reduce the number of transitions. In such approaches, all opacities of all the lines are not included, but a sampling is made to estimate the total opacity. The drawback is that important lines can be missed. Another method was that of the opacity distribution function (Hubeny & Lanz, 1995) which estimates the number of transitions of given strength by wavelength interval. Again, it is a statistical approach which can introduce errors. An interesting idea was introduced by Anderson (1991) with the concept of super-levels. The principle is to gather levels of close energy in a single super-level and to make the computations with these super-levels. The underlying idea is that levels with similar energy will have roughly the same populations. It allows to reduce significantly the number of levels included in the models and thus the computational cost. Other methods consisted in estimating ionisations of various metals from that of H and He, and then to compute the radiative transfer with Monte-Carlo methods (see Abbott & Lucy, 1985; Lucy & Abbott, 1993; Schaerer & Schmutz, 1994; Schaerer et al., 1996). We will go back to the history of line-blanketing in model atmospheres for massive stars in Sect. 3.1.

Within the last few years, the improvements brought by the different methods together with the developments of computers have lead to the emergence of reliable and realistic models in terms of line-blanketing. It is now possible to quantitatively study its effects since models without any

approximations (as regards line-blanketing) can now be computed. This is especially true with the code CMFGEN to which the following section is devoted.

2.4 CMFGEN: atmosphere code for the modelling of massive stars

This thesis relied heavily on the computation of atmosphere models. The code CMFGEN developed by John Hillier (University of Pittsburgh) was chosen to run such simulations since it is one (if not The) most reliable code devoted to the modelling of massive stars atmospheres with winds. Other codes usually refer to CMFGEN to test their own results (see Herrero, Puls & Najarro, 2002). This is mainly due to the fact that CMFGEN makes the least assumptions as possible, at the cost of cpu time. We give below the basic ingredients of CMFGEN. Note that the detailed description can be found in Hillier & Miller (1998) and references therein.

First of all, CMFGEN includes the three main ingredients of the modelling of massive stars atmospheres already mentioned above:

- **non-LTE**: all statistical equilibrium equations are solved individually to give access to the populations of the different energy levels. The processes involved are collisional and radiative transitions (bound-bound terms), collisional and radiative ionisations (bound-free terms) from ground-state and excited states, Auger ionisations and dielectronic recombinations.

- **sphericity**: spherical geometry is adopted for all the equations, which allows to take into account the extension due to the wind. The atmosphere is chosen to extend to several times the stellar radius. Generally, the computations extend typically up to 100 stellar radii. Lower values (20 $R_\odot$) can be adopted if the wind density is low.

- **line-blanketing**: CMFGEN is the only code which includes directly the treatment of line-blanketing. No statistical approach as those mentioned in Sect. 2.3 is used and all populations and opacities from the energy levels of metals are computed individually. This is of course very demanding in terms of CPU time. The only assumption used is that of super-levels (see Sect. 2.3: levels of close energy are grouped in a single super-level for which the non-LTE population is computed, and the levels included in the super-level are assumed to have the same departure coefficient from LTE). Note that computations without any super-levels are possible but requires huge amounts of cpu time and memory and that the effects of super-levels

assignment can be easily checked. Basically, the approach adopted in CMFGEN is to treat the metals (especially Iron) as H and He in the previous models. The main difficulty is that the number of levels in those metals is much higher (up to a factor of 100 higher in the case of Iron) than for H or He. Typically, a complete model including C, N, O, Si, S and Fe in addition to H and He has $\sim$ 900 super levels, $\sim$ 2500 levels and $\sim$ 25000 lines.

Once again, the inclusion of these three main ingredient renders possible the computation of detailed and reliable atmosphere models for massive stars. The other main characteristics of the code are summarised in the following.

- $\diamond$ *stationarity*: CMFGEN solves all the equations under the assumption of stationarity. Although there are evidences that the winds of massive stars show time-dependent features, it is presently not conceivable to run time-dependent models. Moreover, time-independent models can be regarded as snapshots of the spectral evolution of massive stars. Hydrodynamical simulations (see Owocki, Castor & Rybicki, 1988) reveal that the atmospheric structure (velocity and density) is influenced by time-dependent processes (related to instabilities inherent to the basic mechanism driving the winds). However, the time-averaged velocity (and density) structures are equivalent to time-independent structures (see below and Fig. 8.25 of Lamers & Cassinelli, 1999).

- $\diamond$ *velocity structure*: CMFGEN does not compute self-consistently the hydrodynamical structure of the wind which has to be given. This is at present one of the main limitations of the code. But the coupling of hydrodynamics and radiative transfer remains a very difficult task in astrophysics today. Hence, the velocity structure is estimated as follows: the photospheric part is taken from other atmosphere codes. Either ISA-WIND (see de Koter, 1996) or TLUSTY (see Hubeny & Lanz, 1995) is used. Both codes estimate the different terms entering the momentum conservation equation. TLUSTY makes a more detailed treatment, but the computation of TLUSTY models is much longer than ISA-WIND models which make more approximations (especially as for the temperature structure which is simply assumed to be grey). The wind part of the velocity structure is given by a classical β-law

$$v = v_\infty (1 - \tfrac{r}{R_\star})^\beta$$

  where $R_\star$ is the stellar radius and v_∞ is the terminal velocity reached at the top of the atmosphere. This velocity law is expected to well

represent the velocity in this part of the atmosphere (see Sect. 5). The two velocity fields -inner + outer atmosphere- are smoothly connected to give a monotonic function. Note that the accuracy of such hydrostatic and velocity structures can be checked through spectroscopic analysis.

◇ *density structure*: the density structure is simply given by the mass conservation equation

$$\dot{M} = 4\pi r^2 \rho v$$

where $\dot{M}$ is the mass loss rate and ρ the density.

◇ *temperature structure*: the temperature is determined by the equation of energy conservation in the atmosphere. In the particular case where energy is fully transported by radiation, and if there is no source of energy in the atmosphere (i.e. the radiation simply transports the energy), then this equation boils down to the radiative equilibrium equation which simply says that the amount of energy entering a slab must be the same as the amount of energy going outward. This condition thus sets the temperature structure.

Other details can be found in Hillier & Miller (1998). Another important thing to mention is the fact that the computation of the radiative transfer equation and statistical equilibrium equations are made in the frame co-moving with the wind outflow. This is especially important since it allows a detailed modelling which avoids any approximations necessary when the computations are done in the observer frame. In particular, the Sobolev approximation which assumes that the interaction of a photon with a line can happen only in a very local region, but which can be violated in the case of a too low acceleration, is not used. The Doppler shift implied by the expansion of the wind are taken into account directly in the radiative transfer equation and thus the interaction of photons and matter is correctly simulated.

The most difficult part of the simulation comes from the computation of the radiative field and the populations. Indeed, as populations depend on the radiation field (through radiative transitions) and as in return the radiation field depends on populations (through opacities and source functions), there is a strong coupling between radiative transfer and statistical equations which implies an iterative process. In practice, the whole set of equation is solved using a linearisation technique which basically expresses the changes in radiation field in term of changes in populations, leaving a set of equations which only depend on the populations. Once again, details concerning the modelling and techniques are given in Hillier & Miller (1998). A model is estimated to be converged when the maximum

relative change of populations between two successive iterations is lower than a typical value of a few percent (which can be adjusted). A sketch of the behaviour of CMFGEN during the computation of a model is given in Appendix A.

Once the model is computed, a formal solution of the radiative transfer in the observer frame is done to give the detailed emergent spectrum. This means that the populations are held fixed and the radiative transfer equation is solved with fixed opacities. In this part of the simulations, more accurate line profiles are included. In particular, Stark broadening functions is included to represent correctly the H and He optical lines. A depth variable micro-turbulent velocity can also be used to give more realistic line profiles.

Practically, a CMFGEN model can be summarised as follows:

- Input: The main input parameters are:
  - → stellar parameters: Luminosity (L), stellar radius ($R_\star$), mass (M), chemical abundances.
  - → wind parameters: mass loss rate ($\dot{M}$), terminal velocity (v_∞), slope of the velocity field (β).
  - → "pseudo-physical" parameters: input velocity structure, extension of the atmosphere, number of depth points, number of levels/super-levels for each element.
  - → modelling parameters: there are many parameters controlling the behaviour of CMFGEN. They are first the "continuum and line" parameters saying how the frequency sampling must be done, which type of profile must be used for the lines, what value of microturbulent velocity is chosen, how to treat overlapping lines... The second set of parameters tells which physical processes are to be included in the model: adiabatic cooling, X-rays, charge exchange reactions... Third, the "numerical" parameters tell which method to use to estimate optical depths, Eddington factors... Finally, several parameters control the convergence: they allow to fix the temperature, to fix the populations, they tell which are the maximum changes allowed for the populations within an iteration of weakly populated levels or they tell when to stop the computation. A typical input file containing these modelling parameters is given in Appendix B.
- Output: the two main outputs are:
  - → atmospheric structure: the temperature structure and the populations are given. Other outputs related to the opacities, radia-

tive accelerations, collisional rates, recombinations and photo-ionisation rates are also given and allow a detailed investigation of the atmosphere structure and a check on the computations..

→ emergent spectrum: a detailed spectrum for any wavelength range is produced.

The output spectrum is the useful output in terms of spectroscopic analysis, whereas the details concerning the atmospheric structure are necessary to understand the effects of various parameters and ingredients, especially the effect of line-blanketing as we are now going to see in more detail.

Chapter 3

Line blanketing and the effective temperature scale of O stars

French summary

Ce chapitre est dédié à l'étude des effets du line-blanketing sur la structure de l'atmosphère et sur le comportement des raies utilisées pour la classification spectrale des étoiles naines de type O. Nous nous intéressons en particulier à la relation température effective - type spectral dont nous donnons une nouvelle version.

Dans un premier temps, nous revenons brièvement sur l'historique de l'inclusion du line-blanketing dans les modèles d'atmosphère. Ce sont d'abord Abbott & Hummer (1985) qui ont utilisé une méthode basée sur l'estimation de fonctions d'albédo pour rendre compte du blocage du flux par l'atmosphère. Ensuite, Abbott & Lucy (1985), Lucy & Abbott (1993) puis Schaerer & Schmutz (1994) ont réalisé des simulations Monte-Carlo pour étudier le transfert radiatif en présence de métaux et en déduire les conséquences sur la structure et le spectre émergent. Puis des méthodes statistiques ont été dévelopées par Pauldrach et al. (1994) - méthode d'échantillonnage d'opacité - et Hubeny & Lanz (1995) - méthode de fonction de distribution d'opacités dans les atmosphères *sans* vent. Toutes ces approches ont confirmé les effets attendus du line-blanketing (modifications de la structure de température, du spectre émergent) mais ont toujours souffert d'une ou plusieurs approximation, ce qui est beaucoup moins le cas pour le code CMFGEN que nous utilisons par la suite puisqu'aucune méthode statistique n'est employée.

Nous avons donc construit une grille de modèles représentative des

différents types spectraux d'étoiles O naines afin d'étudier quantitativement l'influence du line-blanketing. Cela nous a permis de montrer que l'inclusion de métaux amenait 1) un champ de rayonnement plus isotrope à cause du plus grand nombre de diffusions, 2) une ionisation plus forte à l'intérieur de l'atmosphère et moins forte à l'extérieure, et 3) une température accrue dans les couches profondes et diminuée à l'extérieur. La conséquence directe est un type spectral plus précoce pour une température effective donnée (en raison du changement d'ionisation), ou bien de façon équivalente une température effective plus basse pour un type spectral donné. La réduction de $T_{\rm eff}$ va de 1500 K pour les types spectraux tardifs à 4000 K pour les types les plus précoces. Ces résultats sont valables pour une métallicité solaire, mais nous avons par ailleurs montré que pour une métallicité typique du SMC (Z = 1/8 $Z_{\odot}$) la réduction de la température effective était environ deux fois moindre.

Diverses études menées par d'autres groupes par la suite ont confirmé ces résultats de façon théorique. Par ailleurs, plusieurs étoiles ont été analysées au moyen de la nouvelle génération de modèles d'atmosphères, et les résultats sont en bon accord avec notre relation $T_{\rm eff}$ - type spectral, du moins pour ce qui concerne les étoiles plus tardives que O5. Pour les étoiles plus précoces, la question reste ouverte.

We have seen in Sect. 2.3 that line-blanketing have different kinds of effects of the atmospheres of O stars. In particular, this does not reduce to a simple modification of the emergent spectrum, but important changes of the structure happen when metals are included in the models. In this section, we investigate the effects of line-blanketing through its impact on the effective temperature of O stars.

3.1 Brief historical overview of line-blanketing

Before studying in detail the effects of line-blanketing, let us first review quickly the different steps that have lead to the present generation of fully blanketed atmosphere models for massive stars.

The first attempt to build non-LTE, spherically extended, line-blanketed models was made by Abbott & Hummer (1985) who improved the non-LTE models of Mihalas (1972) by adding a wind component above the photosphere in a so-called core-halo approach in which the wind is simply superimposed on the photosphere, both parts being independent. Their main improvement was due to their treatment of the wind-blanketing effect. Indeed, due to the presence of the wind, a significant fraction of the radiation is backscattered towards the photosphere by line and electron scattering, with the immediate consequence of an increase of the photospheric temperature. The main idea of their study was to estimate this fraction of backscattered radiation (quantified by an albedo function) through Monte-Carlo simulations. Their results show an increase of the temperature more important in the outer atmosphere than in the inner parts. This is mainly due to the core-halo approach: in such models the albedo function is used to estimate the amount of radiation going back to the photosphere so that most changes are expected to occur near this transition region, heating the material at this place and leading to a stronger continuum emission which can propagate outward and heat the wind, whereas the inner parts are not too much modified as they do not feel so strongly the effect of backscattered radiation. Abbott & Hummer (1985) estimate that the temperature increase can be as high as 19 % in the case with the stronger mass loss. This first study of blanketing effects was not directly related to metals, but only to the presence of the wind. This explains why Abbott & Hummer had only a few non-LTE levels from H and He in their models, but no levels from heavier elements.

The first real attempt to include metals in atmosphere models with winds was that of Abbott & Lucy (1985) and Lucy & Abbott (1993) who developed Monte-Carlo simulations to model the winds of O supergiants and Wolf-Rayet stars. For the first time, metals are included in the com-

putation and their level populations are estimated using a nebular approximation. This allows an estimate of opacities which are then used to compute the mass loss rate under the assumption of a given velocity law. In practise, their result confirm the wind blanketing effect of Abbott & Hummer (1985) and they show that lines increases even more the temperature. However, all line interactions are supposed to be scattering, which is in fact only valid for the strongest resonance lines.

Such Monte-Carlo simulations were improved by Schaerer & Schmutz (1994). Their models were aimed at reproducing in a consistent way the hydrodynamic structure and the spectral energy distribution. In an iterative process, they determined the atmospheric structure (temperature, populations), the opacities and the radiative field, and the radiative forces used for the hydrodynamics. Their simulations can be summarised in three steps:

- atmospheric structure: the statistical equilibrium equations for H and He are solved together with radiative transfer with modified absorptive and Thomson scattering opacities to take line-blanketing into account.

- estimate of opacities: Monte-Carlo simulation to estimate the opacities. This is the line-blanketing part. An opacity sampling method is used in this formal solution of the radiative transfer equation to follow the fate of photons in the atmosphere and determine the opacities due to metals. Metal level populations are estimated by a modified nebular approximation where the non-LTE populations of H and He are used to compute ionisation equilibrium of metals.

- hydrodynamic solution: the momentum conservation equation is solved together with the energy conservation in a grey atmosphere to yield the velocity and density structure.

Practically, the hydrodynamical structure and opacities obtained in the two last steps are used in a following iteration cycle to compute the atmospheric structure until convergence is achieved. These simulations yielded a number of results as regards line-blanketing:

- the temperature is increased, mostly in the intermediate part of the atmosphere. In the outer part, the computations in the nebular approximation do not allow a reliable temperature structure and effects of metals are not seen.

- the radiation field becomes more isotropic due to the increase of scattering events.

- the ionisation is increased. Basically, this is due to the increase of the mean intensity (due to the higher isotropy) which favours photoionisations.

- the EUV radiation below 228 Å is increased due to the higher ionisation of He.

- the strength of optical He lines is modified according to the change of ionisation.

These results were the first quantitative results concerning line-blanketing. However, the approach used still involved approximation especially as regards the computation of opacities and non-LTE levels of metals. Note also that the inclusion of Iron is much more complicated than the inclusion of CNO elements due to the much larger number of lines.

In parallel to the work of Schaerer & Schmutz (1994), Pauldrach et al. (1994) developed the first hydrodynamical models of massive star winds. They computed the detailed radiative acceleration with the CAK formalism (see Sect. 5) from which they derived the hydrodynamical structure of the wind. As the computation of the radiative acceleration requires the knowledge of thousands of line opacities, they had to include metals, first in the hydrodynamical part of their code (WM-BASIC) and more recently in the radiative transfer part (Pauldrach, Hoffmann & Lennon, 2001) thanks to an opacity sampling method.

Another statistical method to include line-blanketing in atmosphere models of massive stars *without winds* was developed by Hubeny & Lanz (1995) and Hubeny, Heap & Lanz (1998). They used their plane-parallel non-LTE code TLUSTY and an opacity distribution function (ODF) method to treat metals as correctly as possible. The ODF simply gives the number of lines of given opacity by wavelength interval. It is a statistical approach which allows the inclusion of a number of levels from metals. In addition to the previous models, the computations of Hubeny, Heap & Lanz (1998) also solve the statistical equilibrium equations for all metallic levels, giving the first reliable non-LTE populations of metals. Their results are the following:

- the temperature is increased in the deeper layers when line-blanketing is included, due to the backscattering of radiation (backwarming effect).

- the UV flux is increased since due to backwarming, the emission is stronger.

- the He ionisation is increased, leading to modified optical lines.

From a practical point of view, this last effect is important for the assignment of effective temperature, since a line-blanketed model with lower temperature will be necessary to fit the same spectrum (i.e. the spectrum of a star of given spectral type) as an unblanketed model. Hubeny, Heap & Lanz (1998) provide the first quantitative indication that the effective temperature scale of O stars should be revised downward (by $\sim$ 10 %). The main caveat in the TLUSTY models was the absence of winds which can significantly alter the atmosphere structure (see Sect. 2.2).

The code CMFGEN (see Sect. 2.4) now includes a realistic treatment of line-blanketing and is the first to include it directly without any statistical approach to estimate the opacities. Non-LTE level populations of metals are consistently computed with the radiation field and the temperature

structure, yielding accurate and reliable atmospheric structure and spectral energy distribution. Thus, it can be used for a quantitative study of line-blanketing in massive stars atmospheres and on the $T_{\rm eff}$ - scale in particular.

3.2 Effective temperature of O stars

The effective temperature of any star is the temperature of the blackboby emitting exactly the same amount of radiative energy as the star. It is then defined as follows:

$$L = 4\pi R^2 \sigma T_{\rm eff}^4$$

where L is the stellar luminosity and σ is the Stefan-Boltzmann constant. Practically, this means that the effective temperature is similar to the temperature of the star at the point where the flux is emitted. This point is usually close to the photosphere. Of course, the temperature in the atmosphere of any star is not constant: it decreases from the interior (where the energy is produced) towards the outer atmosphere (where the radiative energy escapes). The exact profile of the temperature structure depends on the detailed physics of the atmosphere, especially the opacities. Indeed, the role of the atmosphere is to transport the radiative energy outward. In massive stars, this is mostly done by radiative transfer, which depends on the temperature gradient: the higher the temperature gradient, the more efficient the transfer of energy. On the contrary, opacities behave as a fence which blocks the flux, which means that if the opacities in the atmosphere are high, it is more difficult for the radiative energy to go out. In order to maintain an efficient energy transport, a balance between temperature gradient and opacities must be found. This explains why the inclusion of metals may significantly alter the temperature structure of O stars *at fixed effective temperature*. It is thus crucial to understand to which extend the inclusion of metals in massive stars atmospheres modifies the temperature distribution, since such a change will imply modifications of the ionisation structure, thus of the spectral lines and consequently of the spectral types. In other words, the relation between spectral-type and effective temperature may be changed.

How can we estimate the effective temperature of O stars? Massive stars emit most of their luminosity in the UV which is the wavelength range sensitive to $T_{\rm eff}$ (and gravity to a lesser extent) for massive stars (see Abbott & Hummer, 1985; Bohannan et al., 1986). The optical range is in the Rayleigh-Jeans part of the spectral distribution and is essentially independent of the temperature so that photometry can not be used to estimate $T_{\rm eff}$.

Thus, $T_{\rm eff}$ must be determined through spectroscopy (e.g. Massey, 2004) and it is crucial to have a relation between a spectroscopic quantity and $T_{\rm eff}$. This simplest quantity is the spectral type which is determined by the ratio of equivalent widths of He optical lines (Conti & Alschuler, 1971; Mathys, 1988). Such a relation between spectral type and effective temperature is called a $T_{\rm eff}$ - scale. Basically, it gives the average effective temperature of O stars of a given spectral type.

The knowledge of $T_{\rm eff}$ is crucial for a number of studies. Given this quantity and the luminosity of the star, a HR diagram can be constructed and used to assign ages or evolutionary masses which is useful in order to understand the evolution of massive stars (de Koter et al., 1998; Massey & Hunter, 1998). In the case of clusters of massive stars, the accurate determination of effective temperatures will give access to the Initial Mass Function and the star formation history (Massey et al., 1995a,b). Moreover, the effective temperature is directly correlated to the number of ionising photons responsible for the existence of HII regions.

There have been a number of studies in the past three decades to calibrate the effective temperature scale of O stars. The first attempt was done by (Conti, 1973) and relied on the comparison between measured equivalent widths and equivalent widths from the non-LTE models of Auer & Mihalas (1972). Schmidt-Kaler (1982) made a compilation of various studies (Conti, 1975; Kudritzki, 1980; Lamers, 1981) to produce a new temperature scale relying on non-LTE models. Note that the work of Kudritzki (1980) was the first to use detailed fitting of line profiles to assign effective temperatures. Conti (1988) updated his former temperature scale including results from various methods. No significant change on the scale was noticed. The first attempt to go beyond non-LTE models was the calibration of Howarth & Prinja (1989) who took advantage of various spectroscopic analysis of individual stars, some of which incorporating the first studies of blanketing (Abbott & Hummer, 1985). The resulting $T_{\rm eff}$-scale was slightly cooler at intermediate spectral types. No new calibrations were produced until the study of Vacca, Garmany & Schull (1996) who compiled various results based on spectroscopic analysis with plane-parallel non-LTE models and produced a temperature scale significantly hotter than the previous calibrations. Although this work relied on the best models available at that time, neither the wind effects nor the line blanketing effects were taken into account, which was a serious caveat. Analysis of binary stars (e.g. Hilditch, Harries & Bell, 1996) indeed revealed that the temperature scale of O stars should be revised downward. Such a revision is now possible thanks to the existence of the new generation atmosphere models including line-blanketing. This question is tackled in the next sections.

3.3 The effect of line-blanketing on the effective temperature scale of O dwarfs

In order to improve the calibration of Vacca, Garmany & Schull (1996), both winds and metals had to be included. This is now possible with the current generation of atmosphere models such as CMFGEN. Our strategy has been to concentrate first on the effects of line-blanketing since this ingredient has been included only recently in the models. That is the reason why we have restricted ourselves to the study of dwarf stars. Indeed, luminosity class V stars have only moderate winds (e.g. Puls et al., 1996) so that most of the changes between the non-LTE plane-parallel models involved in the work by Vacca, Garmany & Schull (1996) and the present one can be attributed to the inclusion of metals.

3.3.1 Effective temperature of O dwarfs at solar metallicity

The results of this work are summarised in the following paper.

A&A 382, 999–1004 (2002)
DOI: 10.1051/0004-6361:20011703

Astronomy & Astrophysics

On the effective temperature scale of O stars

F. Martins[1], D. Schaerer[1], and D. J. Hillier[2]

[1] Observatoire Midi-Pyrénées, Laboratoire d'Astrophysique, 14 Av. E. Belin, 31400 Toulouse, France
[2] Department of Physics and Astronomy, University of Pittsburgh, Pittsburgh, PA 15260, USA

Received 18 September 2001 / Accepted 16 November 2001

Abstract. We rediscuss the temperature of O dwarfs based on new non-LTE line blanketed atmosphere models including stellar winds computed with the *CMFGEN* code of Hillier & Miller (1998). Compared to the latest calibration of Vacca et al. (1996), the inclusion of line blanketing leads to lower effective temperatures, typically by ∼4000 to 1500 K for O3 to O9.5 dwarf stars. The dependence of the $T_{\rm eff}$–scale on stellar and model parameters – such as mass loss, microturbulence, and metallicity – is explored, and model predictions are compared to optical observations of O stars. Even for an SMC metallicity we find a non-negligible effect of line blanketing on the $T_{\rm eff}$–scale. The temperature reduction implies downward revisions of luminosities by ∼0.1 dex and Lyman continuum fluxes Q_0 by approximately 40% for dwarfs of a given spectral type.

Key words. stars: general – stars: temperature – stars: fundamental parameters – stars: atmospheres

1. Introduction

As a significant fraction of the flux of O stars is emitted in the inaccessible Lyman continuum ($\lambda < 912$ Å) reliable direct determinations of their effective temperatures are not possible. Indirect methods, primarily based on atmospheric modeling, are therefore employed (e.g. Böhm-Vitense 1981; Crowther 1998). Given the need for a detailed treatment of non-LTE effects and the presence of stellar winds (Kudritzki & Hummer 1990), a complete modeling of such atmospheres including also the effects of numerous metal-lines ("line blanketing") remains a complex task (cf. Schaerer & Schmutz 1994; Hillier & Miller 1998; Pauldrach et al. 2001).

For these reasons, most published spectral analysis have so far been based on simple non-LTE models. For example, the most recent calibration of stellar parameters of O and early B type stars of Vacca et al. (1996, hereafter VGS96) is based only on results from plane parallel, pure hydrogen and helium (H-He) non-LTE models. Their derived temperature scale for O stars is found to be significantly hotter than most earlier calibrations (see references in VGS96). Such differences lead to non-negligible changes in the fundamental parameters of O stars – e.g. luminosities, Lyman continuum fluxes etc. – when estimated from spectral types. Accurate calibrations are crucial for various astrophysical topics, such as comparisons with stellar evolution models, determinations of the initial mass function and cluster ages, studies of H II regions, and others.

Indications for a decrease of $T_{\rm eff}$ due to line blanketing effects have been found since the first non-LTE + wind modeling attempts by Abbott & Hummer (1985, and subsequent investigations based on the same "wind blanketed" models), the improved models of Schaerer & Schmutz (1994) and Schmutz (1998), and the fully-blanketed plane parallel non-LTE models of Hubeny et al. (1998). Similar indications are obtained by Fullerton et al. (2000) from recent modeling of *FUSE* spectra with the code of Pauldrach et al. (2001) and by Crowther et al. (2001).

The effective temperature scale of O stars is revised here based on the recent *CMFGEN* code of Hillier & Miller (1998), which treats the problem of a non-LTE line blanketed atmosphere with a stellar wind in a direct way, thereby avoiding possible shortcomings due to opacity sampling techniques employed by Schaerer & Schmutz (1994), Schmutz (1998), and Pauldrach et al. (2001). First results on the dwarf sequence are presented here. A more detailed account including all luminosity classes will be presented in a subsequent publication.

In Sect. 2 we describe our method and the calculated models. The results, their dependence on model/stellar parameters, and first comparison with observations are

Send offprint requests to: F. Martins,
e-mail: martins@ast.obs-mip.fr

presented in Sect. 3. Implications of the revised $T_{\rm eff}$ scale and remaining uncertainties are discussed in Sect. 4.

2. Model ingredients

We have constructed spherically expanding non-LTE line-blanketed model atmospheres using the *CMFGEN* comoving-frame code of Hillier & Miller (1998). This code solves the equations of statistical equilibrium, radiative transfer, and radiative equilibrium, and allows for a direct treatment of line blanketing through the use of a super-level approach. The following ions are included in our calculations: H, He I–II, C II–IV, N II–V, O II–VI, Si II–IV, S IV–VI, and Fe III–VII, whose ∼2000 levels are described by ∼700 super-levels, corresponding to a total of ∼20 000 bound-bound transitions.

For simplicity a constant Doppler profile (thermal width corresponding to the mass of Helium and T = 20 000 K plus a microturbulent velocity of $v_{\rm turb}$ = 20 km s^{-1}) is assumed for all lines in the statistical equilibrium and radiative transfer computation. To examine if a constant thermal width and the use of the large microturbulent velocity does not artificially enhance the photospheric blanketing, we have made test calculations with the correct depth and ion dependent thermal width and $v_{\rm turb} = 0.1$ km s^{-1}. No significant changes in atmospheric structure, level populations, and the emergent spectrum were found. This is explained in part by the high density of lines in the UV part of the spectrum, which implies an average spacing between lines which is smaller than the typical Doppler width. The opacity in the wing of a line is therefore mostly dominated by the core opacity of the neighbouring line, and the exact intrinsic line profile is of little importance. With our standard choice, ∼80 000 frequency points are necessary to correctly sample all lines.

The input atmospheric structure, connecting smoothly the spherically extended hydrostatic layers with the wind (parametrised by the usual β-law), is calculated as in Schaerer & de Koter (1997) with the *ISA-WIND* code of de Koter et al. (1996) As the approximate temperature structure in *ISA-WIND* differs from the final radiative equilibrium temperature structure, the atmosphere structure in the quasi-hydrostatic part may be inconsistent with the final gas pressure gradient. However, for the issues discussed here the differences are small (corresponding to a change of $\lesssim$0.1 dex in $\log g$). In any case, the lines considered here are formed in the transition region whose structure/dynamics remain largely parametrised. The formal solution of the radiative transfer equation yielding the detailed emergent spectrum allows for incoherent electron scattering and includes standard Stark broadening tables for H, He I, and He II lines. Our standard calculations assume $v_{\rm turb} = 5$ km s^{-1}.

We have computed a grid of models representative of O dwarfs in the temperature range between ∼30 000 and 50 000 K. The model parameters are taken from the *CoStar* models A2-E2 of Schaerer & de Koter (1997), with an additional model Y2 at ($T_{\rm eff}$, $\log g$) ∼ (31 500, 4.0) and the remaining parameters[1] taken from stellar tracks of Meynet et al. (1994). For each parameter set a line blanketed model with solar metallicity and a pure H-He model was computed.

3. Results

3.1. Blanketing effect on the temperature scale

The optical He I λ4471 and He II λ4542 classification lines are used to assign spectral types to our models. Figure 1 shows the effective temperature as a function of $\log W' \equiv \log W(4471) - \log W(4542)$ and the corresponding spectral type according to Mathys (1988). The pure H-He models (open circles) follow closely the $T_{\rm eff}$–scale for dwarfs of VGS96, which is based on a compilation of stellar parameters determined using pure H-He plane parallel non-LTE model atmospheres. The comparison shows that if we neglect line blanketing our dwarf model grid would yield nearly the same absolute $T_{\rm eff}$–scale as the pure H-He plane parallel models adopted for the spectral analysis included in the compilation of VGS96.

The line blanketed model sequence (Fig. 1, filled symbols) shows a systematic shift to earlier spectral types for a given temperature, or equivalently a shift to *lower $T_{\rm eff}$ for line blanketed models at a given spectral type.* The difference ranges from ∼1500 K at spectral type O9.5 to ∼4000 K at spectral type O3 (cf. Fig. 1, solid line in lower panel). The difference with the VGS96 scale is shown as the dotted line. Our line blanketed scale smoothly joins earlier calibrations at O9.7V (see VGS96, Fig. 1).

As a spectral type corresponds to a given ionisation state of Helium in the line formation region, blanketed models must be more ionised than unblanketed models. The introduction of line blanketing leads to three main effects illustrated in Fig. 2 for the case of model C2 (cf. Figs. 13 and 14 of Schaerer & Schmutz 1994). Qualitatively the same trends are obtained for all models.

1) Blanketing leads to the backscattering of photons towards the inner atmosphere which forces the local temperature to rise so that flux conservation is fulfilled (backwarming effect; see upper panel);
2) At the same time the radiation field becomes more diffuse, as quantified by the dilution factor $\tilde{W} = 1 - \frac{1}{4}F/J$ shown in the middle panel, causing an increase of the mean intensity (cf. Abbott & Hummer 1985; Schaerer & Schmutz 1994);
3) In the outer part of the atmosphere ($\log \tau_{\rm Ross} \lesssim -2$ in Fig. 2) the ionisation is essentially controlled by the EUV flux, which is quite strongly reduced due to the blocking by numerous metal lines shown in Fig. 3. Here this effect dominates over 2), in contrast with the finding of Schaerer & Schmutz (1994), leading to a lower ionisation.

[1] $M = 16.83\ M_\odot$, $\log T_{\rm eff} = 4.498$, $\log(L/L_\odot) = 4.552$, $R = 6.358\ R_\odot$, $\log \dot{M} = -7.204\ M_\odot$/yr, and $v_\infty = 2500$ km s^{-1}.

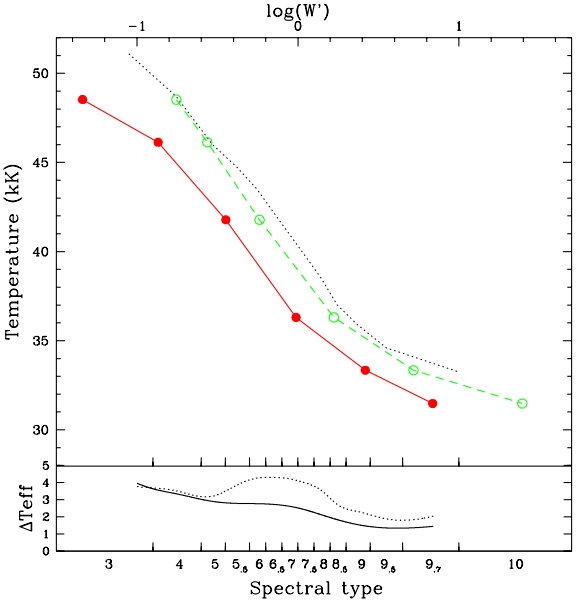

Fig. 1. *Upper panel:* effective temperature of O dwarfs as a function of the spectral subtype (lower scale). The correspondance between $\log W'$ (upper scale) and spectral type is given by Mathys (1988). For values $\log W' > 1.0$ we assign a spectral type of 10. Filled circles show our line blanketed models, open circles pure H-He models. The VGS96 relation (dotted line) is well reproduced by our pure H-He models. *Lower panel:* $T_{\rm eff}$ shift between H-He and line blanketed models (solid line) and between VGS96 scale and our line blanketed models (dotted line). Note the decrease of $T_{\rm eff}$ due to line blanketing.

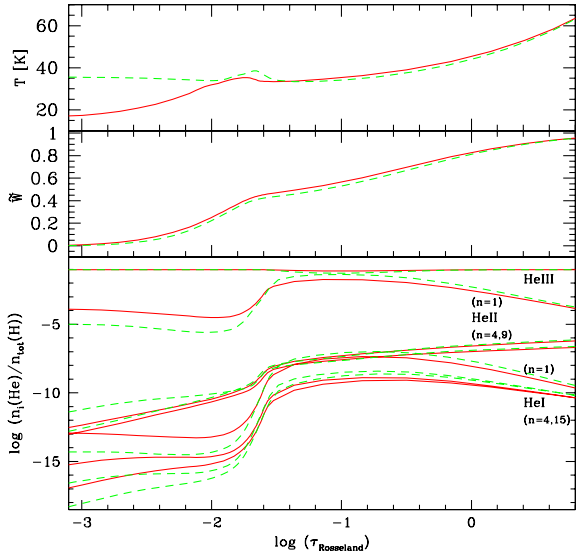

Fig. 2. Comparison of atmosphere structures of model C2 ($T_{\rm eff}$ = 41.8 kK, $\log g$ = 4.0). Solid line is for the line-blanketed model and dashed line for the pure H-He model. *Upper panel:* temperature structure. *Middle panel:* dilution factor $\tilde{W} = 1 - \frac{1}{4}F/J$ where F is the flux and J the frequency averaged mean intensity (cf. Schaerer & Schmutz 1994). *Lower panel:* Populations of the ground levels of Helium and of the lower and upper levels of the transitions He I λ4471 and He II λ4542. Given are the relative number population n_i with respect to total H population $n_{\rm tot}$(H).

Effects 1) and 2) lead to a higher ionisation in the formation region of the classification lines. This results predominantly in an increase of W(4542) at $T_{\rm eff} \lesssim 38\,000$ K and a decrease of W(4471) at higher $T_{\rm eff}$ (cf. Fig. 4).

Given the stronger mass loss and the corresponding increase of the wind density, one expects even larger temperature differences between non-blanketed and line blanketed models for giant and supergiant luminosity classes (cf. Abbott & Hummer 1985; Schmutz 1998; Crowther et al. 2001).

3.2. Dependence on model and stellar parameters

How strongly do our results depend on poorly known parameters such as the velocity law in the photosphere-wind transition zone, $v_{\rm turb}$, and variations of gravity and $\dot{M}$ expected within the dwarf class? Do our calculations still miss opacity sources?

As pointed out by Schaerer & Schmutz (1994) changes in He line profiles due to modifications of the velocity law $v(r)$ in the photosphere–wind transition zone can lead to similar equivalent widths variations as line blanketing. Test calculations for models A2 and C2 varying the slope β from 0.8 (our standard value) to 1.5 show that both H-He and line blanketed models exhibit a similar shift in $\log(W')$. The obtained *relative* $T_{\rm eff}$ difference between H-He and blanketed models remains thus identical. The blanketed models with $\beta = 1.5$ have $\log(W')$ lowered by $\sim$0.1–0.2 dex. However, as Hα profile fits for O dwarfs are generally quite compatible with $\beta \sim 0.8$ (e.g. Puls et al. 1996), we do not expect drastic changes of the absolute scale from this effect.

An increase of the microturbulent velocity $v_{\rm turb}$ from 5 to 20 km s^{-1} in blanketed models increases the strength of He I λ4471 (cf. Smith & Howarth 1998; Villamariz & Herrero 2000), and leads to a shift of $\sim$+0.05 to 0.1 dex in $\log(W')$ (i.e. towards later types) for models with $T_{\rm eff} \lesssim$ 42 000 K. For hotter stars the difference is negligible.

The effect of line blanketing is strengthened further in denser winds (cf. Abbott & Hummer 1985; Schmutz 1998). Models C2 and D2 with an increased mass loss rate by a factor of 2 show a shift of $\log(W')$ between ~-0.05 and -0.1 dex.

Test calculations for model C2 including also Nickel (Ni IV–VI) show unchanged He lines. Other models

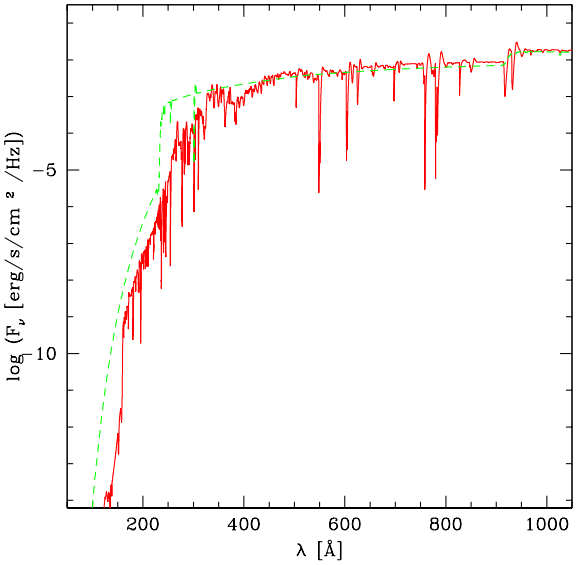

Fig. 3. UV spectrum of model C2 with line blanketing (solid line) and pure H-He model (dashed line). Note the reduction of the EUV flux below ∼500 Å due to the inclusion of metals.

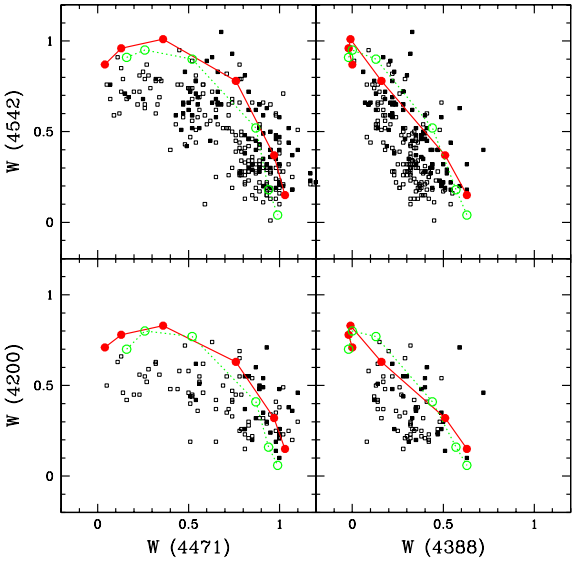

Fig. 4. Comparison between observed (filled squares: luminosity class V; open squares: other luminosity classes) and calculated equivalent widths of He I λ4471, He I λ4388, He II λ4542, and He II λ4200 (in Å). Line blanketed models are indicated by full circles, pure H-He models by open circles. See discussion in text.

including also Ar, Ne, and Ca confirm that Fe blanketing dominates.

While microturbulence and mass loss affect (though in opposite ways) the exact $T_{\rm eff}$-scale, their exact importance will have to be studied in future comparisons.

3.3. Comparison with observations

As a first comparison of our models with observations we show in Fig. 4 the predicted and observed equivalent widths of He I and He II classification lines and other strong He lines frequently used in spectral analysis. The observational data is taken from Mathys (1988, 1989) and Conti & Alschuler (1971). The observational scatter is real, as the typical measurement errors are ∼5–7%. The general trend is that the He I λ4471 and He I λ4388 equivalent widths are well represented by the models, while He II λ4542 seems to be overestimated by ∼20% for spectral types earlier than O7. He II λ4200 behaves as He II λ4542. The other equivalent widths remain essentially unchanged by all other parameter variations discussed above (Sect. 3.2). A value of $\beta \gtrsim 1.5$, a stronger increase of $\dot{M}$, or an unrealisticly large reduction of $\log g$ would be necessary to reduce the predicted equivalent widths of the Stark broadened He II lines.

Strictly speaking, if we were simply to reduce $W(4542)$ by ∼20% while keeping $W(4471)$ constant for early spectral types, this would result in a change of ~ -0.08 dex in $\log(W')$ thus reducing the shift in the $T_{\rm eff}$–scale between line blanketed and pure H-He models from ∼4000 K to 3000 K in the high temperature part. Future tailored spectral analysis should allow to assess more precisely the achievable fit accuracy and the precise importance of the parameters discussed in Sect. 3.2 on the stellar parameters.

3.4. Comparison with previous analysis

As discussed in Sect. 1, few earlier studies have addressed the effect of line blanketing in O stars. Essentially all investigations concur with a reduction of $T_{\rm eff}$ when blanketing is included.

Abbott & Hummer (1985) have constructed a core-halo model where backscattered radiation due to multiple line scattering in the wind modifies the plane parallel photosphere. Their so-called "wind blanketed" models yield a decrease of $T_{\rm eff}$ by ∼10% for O4 types (similar to our results), ~ -2000 K for an O9.5 supergiant, but essentially no shift for O9.5 dwarfs (Bohannan et al. 1990; Voels et al. 1989). The latter finding is likely due to lack of photospheric blanketing (inherent to their method) and modest wind blanketing due to the comparatively low mass loss rates of O9.5 dwarfs.

An improved Monte-Carlo opacity sampling method of a unified photosphere–wind model was used by Schaerer & Schmutz (1994), Schaerer & de Koter (1997), and subsequently applied to a larger parameter space by Schmutz (1998). For mass loss rates comparable to the values

adopted here (typical for dwarfs with low mass loss) the models of Schmutz (1998) indicate differences from $\sim$−600 K at O8 to $\sim$−2000 K at O4, which is half the shift deduced from Fig. 1 and roughly the difference obtained with $Z = 1/8\ Z_\odot$ (see Sect. 4). This indicates that their method underestimates line blanketing compared to *CMFGEN*.

Using plane parallel line blanketed non-LTE models based on opacity distribution functions Hubeny et al. (1998) found that a pure H-He model with $T_{\rm eff} \sim 37\,500$ K and $\log g = 4.0$ is necessary to reproduce the H and He lines of a line blanketed model with $T_{\rm eff} = 35\,000$ K and same gravity. As can be seen from Fig. 1 our results are in excellent agreement with their result.

LTE line blocking has been included in plane parallel models by Herrero et al. (2000) primarily to resolve discrepancies between He I singlet and triplet lines. For stars with $T_{\rm eff} \gtrsim 40\,000$ K this leads to a strengthening of He I λ4471, opposite to the effect found in all above studies including ours. This results must be due to an incomplete treatment of the various effects of line blanketing (cf. above), and appears to be unphysical. This discrepancy with line blanketed models has also been noted by the authors.

4. Implications and concluding remarks

The importance of line blanketing obviously depends on metallicity Z. Therefore one may wonder at which Z the stellar parameters will again correspond to the results obtained with pure H-He (metal-free) atmosphere models, i.e. close to the VGS96 scale. Test calculations for models A2 and D2 with a metallicity close to the SMC value ($1/8\ Z_\odot$) show still a reduction of $T_{\rm eff}$ compared to pure H-He models: $\Delta T_{\rm eff}$ is $\sim$60% that found at solar metallicity.

As the bolometric correction is essentially unchanged by line blanketing, and the M_V versus spectral type (Sp) calibration independent to first order from modeling, we can use the BC-$T_{\rm eff}$ relation of VGS96 to derive luminosities through $\log(L/L_\odot) = 2.736 \log\ T_{\rm eff}({\rm Sp}) - 0.4\ M_V({\rm Sp}) - 9.164$. This relation shows that the predicted reduction of $T_{\rm eff}$ by $\lesssim$0.04 dex implies a downward revision of L by $\lesssim$0.1 dex for dwarfs of a given spectral type.

Since line blanketing is mostly efficient in the EUV, the ionising spectrum below 912 Å is modified. The total number of Lyman continuum photons Q_0 predicted by our models is in good agreement with the calculations of Schaerer & de Koter (1997). The change of Q_0 due to the shift in the $T_{\rm eff}$-Sp calibration, taking into account the change of both the radius and the ionising flux per unit surface area q_0, is given by $\Delta(\log Q_0) = -1.264\Delta(\log T_{\rm eff}) + \Delta(\log q_0(T_{\rm eff}))$, where the latter term is dominant (see Schaerer & de Koter 1997). For a given spectral type between O4V and O9V this amounts typically to a reduction of Q_0 by $\sim$40%.

While the results presented here provide a clear improvement over earlier calibrations, and a general reduction of $T_{\rm eff}$ due to line blanketing is unavoidable, we wish to caution that the absolute $T_{\rm eff}$ scale may still be subject to revisions for the following reasons. First, tailored multi-wavelength analysis of individual objects are required to test the present models in more depth for O stars, as recently started by Bouret et al. (2001), Hillier et al. (2001), and Crowther et al. (2001). Second, the effect of X-rays on the overall ionisation balance and in particular on the Helium lines remains to be studied. Indeed for late O and B stars, depending on the relative X-ray to photospheric flux at energies close to the relevant ionisation potentials and the wind density, X-ray emission (likely due to shocks) is expected to increase the ionisation of most ions (MacFarlane et al. 1994). Nonetheless, first test calculations with *CMFGEN* seem to indicate that photospheric lines are not affected by X-rays generated in the wind. Finally, we note that comparisons of photoionisation models calculated using fluxes from recent atmosphere models (including *CMFGEN* and Pauldrach et al. 2001 models) with *ISO* observations of H II regions possibly reveal a flux deficiency at energies $\gtrsim$34.8–40.9 eV (Morisset et al. 2001, but cf. Giveon et al. 2001). The importance of the latter two findings – possibly related to each other – on the lines used here as $T_{\rm eff}$ indicators remains to be studied.

As UV and optical classification lines of O stars depend in fact on several parameters ($T_{\rm eff}$, gravity, mass loss rate, metallicity, rotation; e.g. Abbott & Hummer 1985; Schmutz 1998; Walborn et al. 1995), spectral type and luminosity class calibrations must ultimately account for this multi dimensionality. Some of these issues will be addressed in subsequent publications.

Acknowledgements. We thank the "Programme National de Physique Stellaire" (PNPS) for support for this project and the CALMIP center in Toulouse for generous allocation of computing time. D. John Hillier acknowlodeges partial support for this work from NASA grant NAG 5-8211.

References

Abbott, D. C., & Hummer, D. G. 1985, ApJ, 294, 286
Bohannan, B., Voels, S. A., Hummer, D. G., & Abbott, D. C. 1990, ApJ, 365, 729
Böhm-Vitense, E. 1981, ARA&A, 19, 295
Bouret, J. C., Heap, S. R., Hubeny, I., et al. 2001, ApJ, in preparation
Conti, P. S., & Alschuler, W. R. 1971, ApJ, 170, 325
Crowther, P. A. 1998, IAU Symp., 189, 137
Crowther, P. A., Fullerton, A. W., Hillier, D. J., et al. 2001, in preparation
de Koter, A., Lamers, H. J. G. L. M., & Schmutz, W. 1996, A&A, 306, 501
Fullerton, A. W., Crowther, P. A., De Marco, O., et al. 2000, ApJ, 538, L43
Giveon, U, Sternberg, A., Lutz, D., Feuchtgruber, H., & Pauldrach, A. 2001, ApJ, in press
Herrero, A., Puls, J., & Villamariz, M. R. 2000, A&A, 354, 193

Hillier, D. J., Lanz, T., Hubeny, I., et al. 2001, in preparation
Hillier, D. J., & Miller, D. L. 1998, ApJ, 497, 407
Hubeny, I., Heap, S. R., & Lanz, T. 1998, ASP Conf. Ser., 131, 108
Kudritzki, R. P., & Hummer, D. G. 1990, ARA&A, 28, 303
MacFarlane, J. J., Cohen, D. H., & Wang, P. 1994, ApJ, 437, 351
Mathys, G. 1998, A&AS, 76, 427
Mathys, G. 1989, A&AS, 81, 237
Meynet, G., Maeder, A., Schaller, G., Schaerer, D., & Charbonnel, C. 1994, A&AS, 103, 97
Morisset, C., Schaerer, D., Bouret, J. C., & Martins, F. 2001, A&A, in preparation
Pauldrach, A. W. A., Hoffmann, T. L., & Lennon, M. 2001, A&A, 375, 161
Puls, J., Kudritzki, R. P., Herrero, A., et al. 1996, A&A, 305, 171
Schaerer, D., & de Koter, A. 1997, A&A, 322, 598
Schaerer, D., & Schmutz, W. 1994, A&A, 288, 231
Schmutz, W. 1998, in Boulder-Munich II: Properties of Hot, Luminous stars, ed. I. D. Howarth, ASP Conf. Ser., 131, 119
Smith, K. C., & Howarth, I. D. 1998, MNRAS, 299, 1146
Vacca, W. D., Garmany, C. D., & Shull, J. M. 1996, ApJ, 460, 914 (VGS96)
Villamariz, M. R., & Herrero, A. 2000, A&A, 357, 597
Voels, S. A., Bohannan, B., Abbott, D. C., & Hummer, D. G. 1989, ApJ, 340, 1073
Walborn, N. R., Lennon, J. L., Haser, S. M., et al. 1995, PASP, 107, 104

In the study presented in the above paper, we mentioned several tests to estimate the sensitivity of the results to the details of the modelling. We now give more information about these test models and in particular, we show the dependence of the line profile of the He classification lines of various model parameters.

Turbulent velocity:

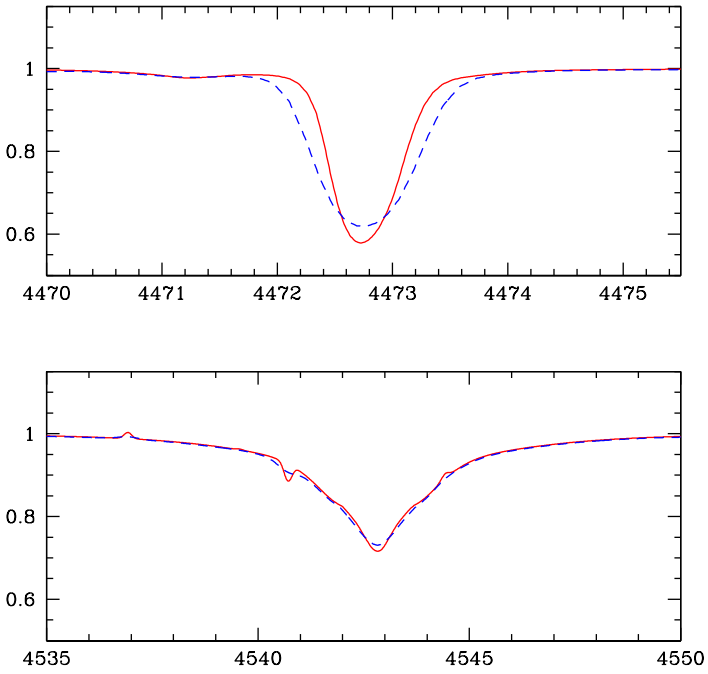

Figure 3.1: Effect of microturbulent velocity on the He line profiles (top: He I λ4471 ; bottom: He II λ4542). The solid line is the initial model with v_{turb}= 5 km s^{-1} and the dashed line is for a model with v_{turb}= 20 km s^{-1}. Increasing the microturbulent velocity translates to a shift of +0.08 dex in terms of log W'.

Let us first examine the effect of microturbulent velocity. In Fig. 3.1, we show the original model (solid line) compared to a model in which v_{turb} has been increased from 5 to 20 km s^{-1}. Note that we have modified the value of the microturbulent velocity used in the formal solution of the radiative transfer giving the detailed emergent emergent spectrum, and not the value used in the computation of the model atmosphere which is still fixed at 20 km s^{-1}. Whereas He II λ4542 is hardly modified, He I λ4471 displays a broader profile so that the equivalent width increases from 0.345 Å to 0.429 Å (for He II λ4542 the equivalent width is 0.968 Å when v_{turb}= 5 km s^{-1} and 1.000 Å when v_{turb}= 20 km s^{-1}). This translates

to a shift of +0.08 dex in $\log W' = \log(EW(\text{He I } \lambda4471\ )/EW(\text{He II } \lambda4542\ ))$ (where EW is for equivalent width).

We note in Fig. 3.1 that lines behave differently as regards microturbulence. This result was noted by various people (see Mc Erlean, Lennon & Dufton, 1997; Smith & Howarth, 1998; Villamariz & Herrero, 2000) in detailed studies of microturbulence. The general trend is that He I lines are more affected than He II lines since the latter are usually more sensitive to Stark broadening which leads to wider lines. The inclusion of a microturbulent velocity in the models is necessary to reproduce observed He lines. In particular, the use of such a velocity is useful to overcome the "dilution effect" problem. This issue was noted by Voels et al. (1989) who pointed out that it was not possible to simultaneously fit the singlet and triplet He I lines, an effect attributed to the reduction of the surface temperature in expanding atmospheres. Smith & Howarth (1998) claim that microturbulent can solve the dilution effect problem, although the conclusion are not so strong in other studies (see Villamariz & Herrero, 2000). As regards the effective temperature scale, a change of v_{turb} has little influence on the results (Martins et al., 2002; Mokiem et al., 2004) since a shift of less than 0.1 dex is lower than the typical extension of the log W' range within a given spectral type ($\sim$ 0.1 dex).

Wind parameters:

Let us now have a look at the influence of two wind parameters: the mass loss rate and the slope of the velocity field (the so-called β parameter). Fig. 3.2 shows the behaviour of the He lines when $\dot{M}$ is increased by a factor of 2 (dashed line) and 10 (dotted line). The lines are weaker when the mass loss rate is increased since they are filled by wind emission. Note that an increase of the mass loss rate acn also modify the level population (due to a higher blanketing). In the case of a moderate increase of $\dot{M}$ (factor 2), log W' is reduced by 0.03 dex whereas for a stronger mass loss rate, the reduction reaches 0.3 dex. Hence, $\dot{M}$ can potentially strongly affects the effective temperature scale (see also Mokiem et al., 2004). This is fact the main reason for the cooler $T_{\rm eff}$ - scale of giants and supergiants (Crowther et al., 2002a; Markova et al., 2004). However, variation of a factor of 10 within dwarfs of the same spectral type are not expected. Dispersion of a factor of 2 are more realistic and in that case, the effect of $\dot{M}$ on the $T_{\rm eff}$ scale is much less critical.

Concerning the slope of the velocity field, an increase of β corresponds to a softer velocity gradient, which means a higher density in the atmosphere (due to mass conservation, a lower velocity implies a higher density). This modifies the atmospheric structure and thus changes the strength of the He lines. This is shown in Fig. 3.3 where the dashed (dotted) line is a model where β has been increased from 0.8 to 1.5 (2.0). Log W' is decreased from -0.448 to -0.666 (-1.016) in the case where $\beta = 1.5$ (2.0).

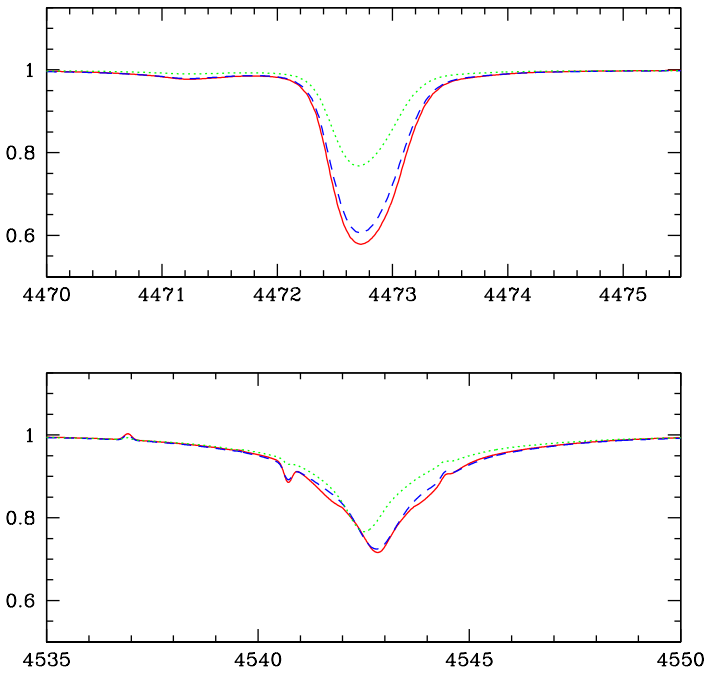

Figure 3.2: Effect of mass loss rate on the He line profiles. The solid line is the initial model ($T_{\rm eff}$=41783 K, $\log g$=4.02, $\dot{M}$=$10^{-6.17}$ $M_\odot$ yr^{-1}), the dashed line is for a model with a mass loss rate increased by a factor of 2, and the dotted line is for a model with a mass loss rate increased by a factor of 10. He lines are filled by wind emission when $\dot{M}$ is increased. Only a strong increase of the mass loss rate have a significant impact on the $T_{\rm eff}$ scale.

A detailed explanation of the effect of β on the line profiles will be given in Sect. 7.1. As mentioned in the above paper, dwarfs usually have values of β close to 0.8. Hence, although log W' can be significantly changed for high β (2.0 or even more), a reasonable change (from 0.8 to 1.2) will not make the spectral type change by more than a subclass.

Note that the effects highlighted in the above example in fact depend on the model parameters. But this example illustrates the uncertainty we can expect on the effective temperature scale of O stars.

Additional metals:

Finally, let us examine how the ionisation changes when new elements are added to the model (in addition to H, He, C, N, O, Si, S and Fe). Indeed, there are other elements from the iron peak which may increase the blanketing effect. Among them, Ni has the highest abundance. We have then run a model in which this element was included. Fig. 3.4 shows the He

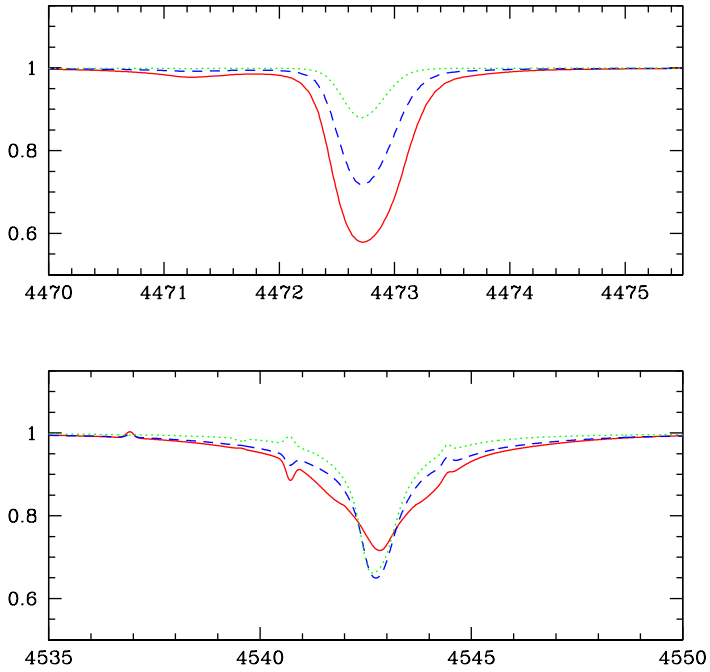

Figure 3.3: Effect of β on the He line profiles. The solid line is the initial model ($\beta = 0.8$), the dashed line is for a model with $\beta = 1.5$, and the dotted line is for a model with $\beta = 2.0$. For high values of β, log W' can be significantly changed and the $T_{\rm eff}$ scale can be shifted.

lines for this model (dashed line) compared to the initial model (solid line). We note very little changes: log W' is only reduced by 0.04 dex. This indicates that most of the line-blanketing effect can be accounted for by Iron.

3.3.2 Comparison with observations

In this short section we want to compare our prediction (Martins et al., 2002) for the relation between spectral type and effective temperature with determinations of $T_{\rm eff}$ based on spectroscopic analysis of observed stars.

The first comparison we can do is with older $T_{\rm eff}$ - scales since they often rely on compilations of spectroscopic determinations thanks to model atmospheres. In Fig. 3.5, we show the result of such a comparison. We see that our scale is cooler than any other scales (except at spectral types O9 and later compared to the scale of Howarth & Prinja (1989)), revealing once again the strong effect of line-blanketing (all other results lacking this ingredient). But does it mean that our $T_{\rm eff}$ - scale is correct? The

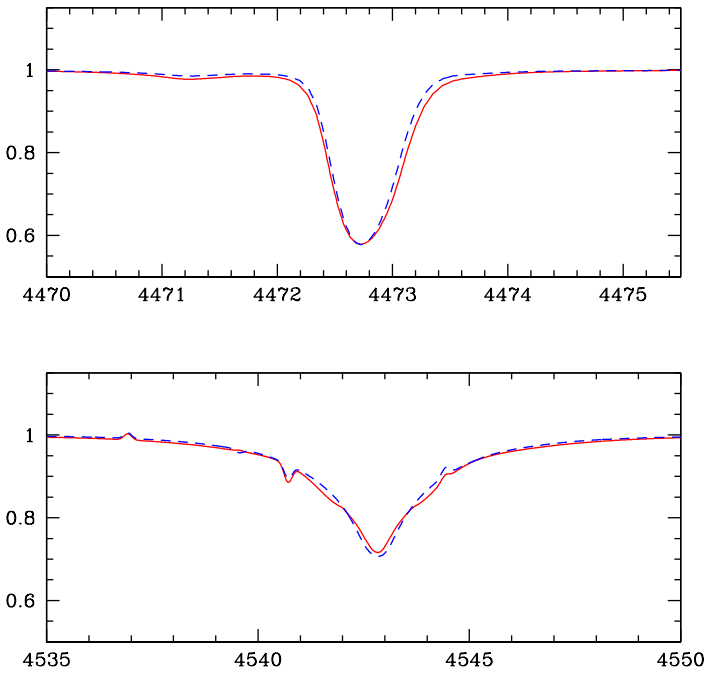

Figure 3.4: Effect of the addition of Ni on the He line profiles. The solid line is the initial model and the dashed line is for a model in which Ni has been added. He lines are little affected which means that most of the line-blanketing effect is due to Iron.

answer must come from the comparison with determinations of effective temperatures thanks to new models including line-blanketing. This is not a proof that our scale gives the real $T_{\rm eff}$, but it is at least a consistent check since the models include the same ingredients. Hence, a difference between our result and the spectroscopic determinations should reveal problems in the physical parameters we have adopted for the computation of our models.

Since the publication of the paper presented in Sect. 3.3.1, there have been several spectroscopic studies of O stars with new atmosphere models (Crowther et al., 2002a; Herrero, Puls & Najarro, 2002; Bianchi & Garcia, 2002; Hillier et al., 2003; Repolust, Puls & Herrero, 2004; Bouret et al., 2003; Markova et al., 2004; Garcia & Bianchi, 2004), but few results concern dwarfs. Moreover, a comparison with our $T_{\rm eff}$-scale must be based on Galactic stars since metallicity is expected to change the $T_{\rm eff}$ - scale (see Sect. 3.3.3), which reduces the total number of objects to 17 (from Bianchi & Garcia, 2002; Repolust, Puls & Herrero, 2004; Markova et al., 2004; Garcia & Bianchi, 2004). In addition to this sample, one can include our own study of Galactic dwarfs given in Sect. 8. this brings the total

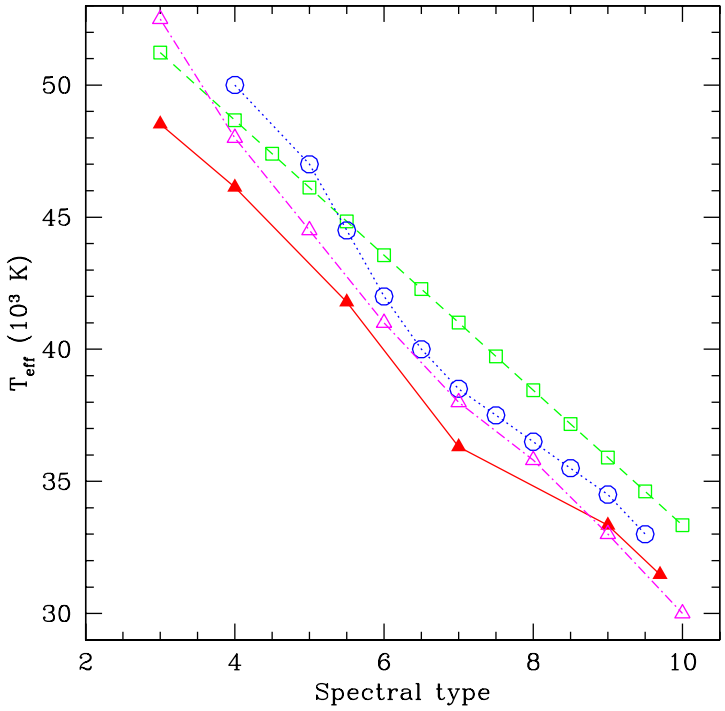

Figure 3.5: Comparison between our $T_{\rm eff}$-scale for O dwarfs (filled triangles) and previous scales. The dotted line + open circles is the $T_{\rm eff}$ - scale of Conti (1973), the dashed line + open squares is that of Vacca, Garmany & Schull (1996) and the dot-dashed line + open triangles that of Howarth & Prinja (1989). Our scale is cooler than the other ones, revealing the effect of line-blanketing.

number of objects to $\sim$ 25, which is reasonable for a relevant comparison. All the stars have been analysis with new generation atmosphere codes including winds and line blanketing (WM-BASIC, FASTWIND or CMFGEN). With the exception of the work by Bianchi & Garcia (2002); Garcia & Bianchi (2004) which was restricted to the UV range, all other studies derived effective temperatures from He optical lines including He I λ4471 and He II λ4542 used for the spectral classification.

In Fig. 3.6, we show the result of the comparison between $T_{\rm eff}$ derived from spectroscopic analysis, and $T_{\rm eff}$ predicted by our effective temperature scale. Filled triangles are results of optical analysis, while open triangles are for studies based *only* on UV lines. The $T_{\rm eff}$ - scale of Vacca, Garmany & Schull (1996) is also shown by the dashed line and is hotter than the latest spectroscopic determinations of $T_{\rm eff}$. As regards our $T_{\rm eff}$ - scale, the main conclusion is:

- if we do not make difference between the various analysis, it seems that our $T_{\rm eff}$-scale is still too hot compared to observations, especially

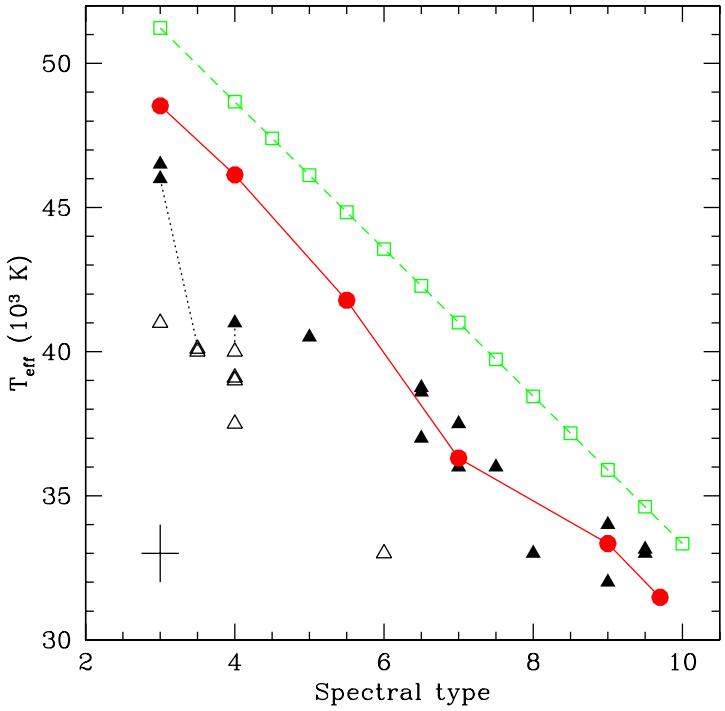

Figure 3.6: Comparison between our $T_{\rm eff}$-scale for dwarfs and the results of spectroscopic analysis of Galactic O dwarfs. The solid line is the predicted effective temperature scale, while triangles are the spectroscopic determinations of $T_{\rm eff}$ based on optical lines (filled symbols) and UV lines (open symbols). Dotted lines indicated stars analysed with both optical and UV lines. Data are from Bianchi & Garcia (2002); Repolust, Puls & Herrero (2004); Markova et al. (2004); Garcia & Bianchi (2004) and Sect. 8 of this thesis. The dashed line and open squares give the $T_{\rm eff}$ - scale of Vacca, Garmany & Schull (1996) and typical error bars on the spectral type (one subclass) and the effective temperature ($\pm$ 1000 K) are indicated by the cross symbol.

at early spectral types. The difference can reach 6000-7000 K!

- if we discard the analysis based on the only UV lines, the agreement is much better. For clarity, we have plotted this comparison in Fig. 3.7. In that case, between spectral types O5 and O9.7, our predicted scale agrees very well with the observational points. A scatter in natural due to the uncertainty of the $T_{\rm eff}$ determination, and due to the fact that a given spectral type include a range of values of the ratio log(EW(HeIλ4471)/EW(HeIIλ4542)). For earlier spectral types, the agreement seems to be not so good. However, several words of caution are necessary. First, there are only four stars with

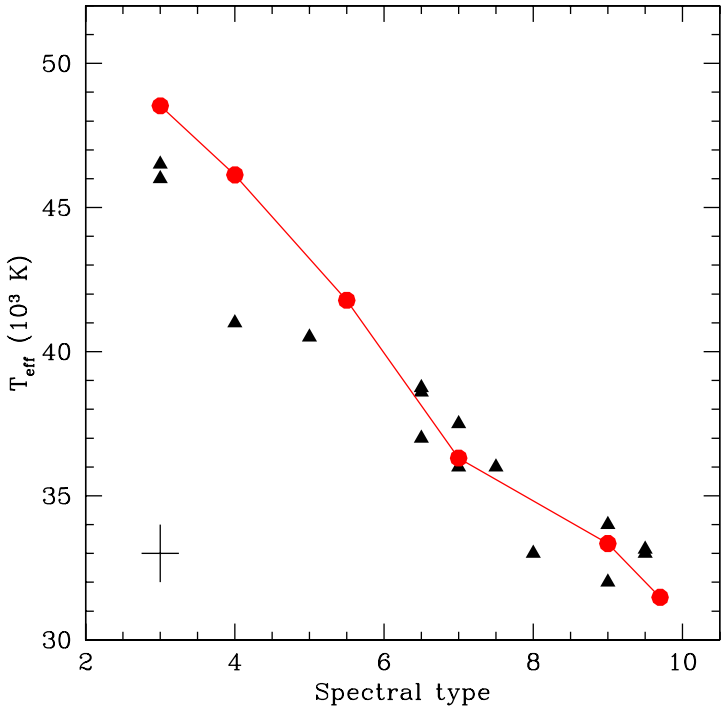

Figure 3.7: Same as Fig. 3.6 except that the determinations based on UV have been removed.

spectral types earlier than O5, which is too few to draw any general conclusion. Second, the star with spectral type O4 (HDE303308) is possibly member of a binary (Repolust, Puls & Herrero, 2004), so that the determination of effective temperature may be influenced by the contribution of the companion star. Taken together, these arguments do not allow to conclude as for the agreement or not of our $T_{\rm eff}$-scale with observations for spectral types earlier than O5.

Why do we separate between analysis based on UV only and optical? First, the disagreement between both type of study is surprising, especially since it is huge. Moreover, various comparisons between different atmosphere codes do not reveal extreme discrepancies between them so that we would expect that they give the same result. Does it mean that UV and optical indicate different temperatures? This is doubtful since several studies using the optical spectrum to derive the effective temperature *also* used the UV range to estimate other parameters and checked that the derived $T_{\rm eff}$ gave consistent fits of the UV range (Crowther et al., 2002a; Bouret et al., 2003; Hillier et al., 2003). Small adjustments may be necessary, but usually the difference between optically and UV estimated is lower than 1000-2000 K. Given that, what could be the reason for such a discrepancy observed in Fig. 3.6?

To try to understand this problem, let us mention the method used by Bianchi & Garcia (2002) and Garcia & Bianchi (2004) to derive effective temperatures. The upper limit on $T_{\rm eff}$ is given by the behaviour of O V λ1371 which shows a too extended profile at high temperatures. The lower limit on $T_{\rm eff}$ is given by P V $\lambda\lambda$ 1118, 1128 (and C IV $\lambda\lambda$1548,1551 as a secondary indicator) which is too strong at low temperatures. However, this strategy may suffer from difficulties. Indeed, the behaviour of O V λ1371 has been known for a long time to be somewhat mysterious above $\sim$ 40000 K since the line profile was always stronger in the models than in the observed spectra (e.g. de Koter et al., 1998). Recently, Bouret et al. (2003) have shown that this long standing problem could be alleviated by the inclusion of clumping in the wind models. In that case O V, which is the dominant ionisation state of Oxygen above 40000 K, recombines to O IV and the O V λ1371 line is reduced, giving a much better agreement with observations. This means that if clumping is included in the models (keeping the same $\dot{M}$), the upper limit on $T_{\rm eff}$ assigned by O V λ1371 can be increased, the line being comparatively weaker than for unclumped models. The second consequence of the inclusion of clumping is the expected strengthening of P V $\lambda\lambda$ 1118, 1128 . Indeed, P V has nearly the same ionisation potential as C IV. And C V recombines to C IV when clumping is included (again for a given $\dot{M}$), strengthening the C IV $\lambda\lambda$1548,1551 line. If indeed P V has the same behaviour, one expects a stronger P V $\lambda\lambda$ 1118, 1128 line in clumped models for a given $T_{\rm eff}$. This means that a higher $T_{\rm eff}$ must be used to reduce P V $\lambda\lambda$ 1118, 1128 and make it fit the observed spectrum: the lower limit on $T_{\rm eff}$ must be increased. The same conclusion is reached for the C IV $\lambda\lambda$1548,1551 line. Note that the behaviour of UV lines described above is only expected to be valid when both O V and P V are not the dominant ionisation states of O and P (otherwise, recombination due to clumping should not strongly modify the shape of the lines). Hence, the results are temperature dependent. However, they should be valid around $T_{\rm eff}$ = 42000 K where the discrepancy between UV determination and our $T_{\rm eff}$ - scale is the highest. Taken together, these arguments indicate that the effective temperature of the stars studied by Bianchi & Garcia (2002) and Garcia & Bianchi (2004) may be underestimated, which could explain the disagreement with our prediction. Note however that Bianchi & Garcia (2002) and Garcia & Bianchi (2004) use also C III λ1176 and C IV λ1169 to derive $T_{\rm eff}$. However, these lines are also sensitive to $\dot{M}$ which weakens their potential as effective temperature indicators. The possible underestimation of $T_{\rm eff}$ determined by UV analysis is strengthened by the fact that two O dwarfs (HD 93250 and HDE 303308) have been analysed using both optical and UV lines. The optical analysis leads respectively to 46000 K and 41000 K (Repolust, Puls & Herrero, 2004), while the UV analysis leads to 40000 K for both stars. The underestimation of $T_{\rm eff}$ derived by UV analyses is of 6000 K for HD 93250,

while it is only of 1000 K for HDE 303308. The latter being probably a binary, the results for this stars are less reliable (see above discussion). Moreover, Bianchi & Garcia (2002) analysed the (extreme) UV spectrum of the O6If supergiant HD210839 and found $T_{\rm eff} = 34000$ K, while Repolust, Puls & Herrero (2004) found 36000 K from optical lines. This is again an indication that UV analyses lead to lower effective temperatures. Hence, there are indications that determinations of $T_{\rm eff}$ from UV lines which are sensitive to several other parameters (especially clumping) underestimate the effective temperatures by several thousands K.

Of course, there could also be problems with our models which could predict too high effective temperatures. We have estimated the various sources of uncertainty, the main ones being the mass loss rate and the slope of the velocity field. However, they do not indicate reduction of the effective temperature by 6000 K as would be necessary to reconcile the predictions with the UV based $T_{\rm eff}$ at early spectral types. An alternative possibility (put forward by Bianchi & Garcia, 2002; Garcia & Bianchi, 2004) would be that effective temperatures derived by UV lines are systematically lower than effective temperatures derived by optical lines. This would explain that our $T_{\rm eff}$ - scale shows a rather good agreement with spectroscopic analyses based on optical lines, while it seems hotter than $T_{\rm eff}$ derived from UV lines. But again the reason for such a discrepancy is unclear.

In conclusion, we can say that the agreement between our $T_{\rm eff}$-scale for dwarfs and the results of spectroscopic analyses is satisfying for spectral types later than O5, while for earlier spectral types, no conclusion can be drawn with the current limited sample of Galactic stars studied. We should also mention here that there are indirect indications that our $T_{\rm eff}$ - scale is probably not too wrong. Maybe the most relevant is the derivation of masses of binaries through spectroscopy using our scale by Gies (2002) who found very good agreement with evolutionary masses (see also Sect. 4.3).

3.3.3 Effect of metallicity on the effective temperature scale of O dwarfs

In this section, we study the effects of a change of metallicity on the results presented above.

Metallicity in the Universe spans a wide range of values. The first generation of stars are thought to be composed of only H and He, whereas metal rich environments are found in the local Universe, the best example being the Galactic center. Even in the Milky Way, metallicity is not uniform. Shaver et al. (1983), Deharveng et al. (2000), Rolleston et al. (2000),

Martín-Hernández et al. (2002) (among others) have proven the existence of a galactic metallicity gradient: the metal content decrease from the Galactic center towards the outer part of the galactic disk. The difference between high and low metallicity regions can reach a factor of 5 depending on the element.

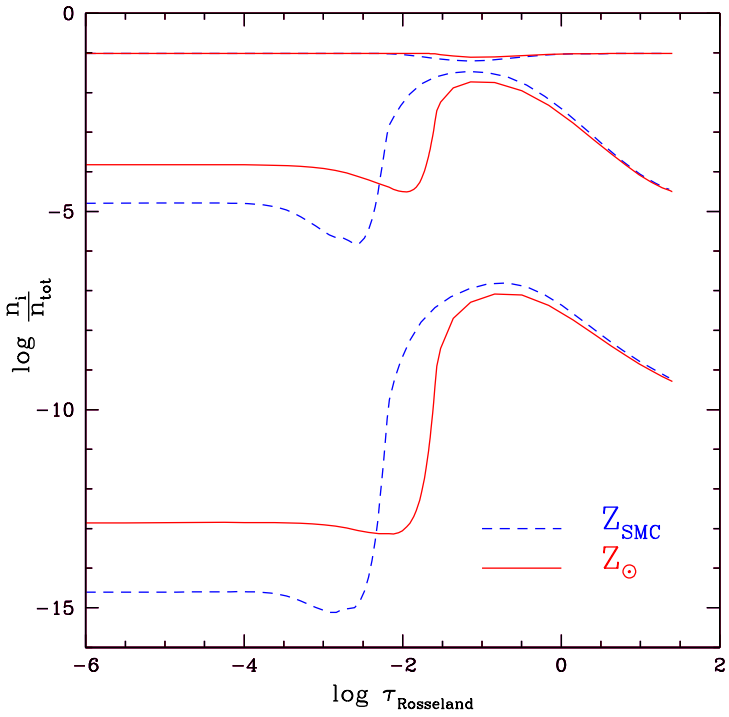

Figure 3.8: Metallicity effect on the He ionisation structure. The dashed line is for a model with Z = 1/8 $Z_\odot$ while the solid line is the solar metallicity model. The reduction of the metal content leads to a lower ionisation in the inner atmosphere.

Hence, it is crucial to take metallicity effects into account in the atmosphere models of massive stars. Indeed, as line-blanketing effects depend on the metal content, and as this metal content shows significant variations even in the local Universe, massive stars should show different properties according to their environment. This is especially true for the effective temperature. We have shown in the previous section that the inclusion of metals could lead to a significant reduction of the $T_{\rm eff}$ scale of O dwarfs. One can expect that a lower metallicity will diminish this effect.

In order to have a quantitative picture of the metallicity effect on the effective temperature scale of O dwarfs, we have run new CMFGEN models with a metallicity reduced by a factor of 8 (Z = 1/8 $Z_\odot$). This value is thought to be typical of the Small Magellanic Cloud (Venn, 1999; Hill, 1999; Vermeij et al., 2002). Practically, we have used the same grid of

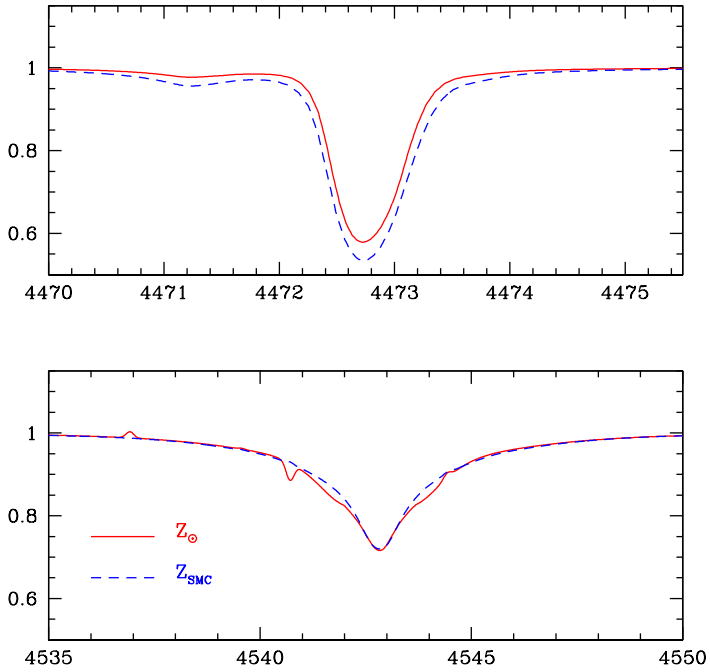

Figure 3.9: Metallicity effect on the optical He lines used for spectral classification. The dashed line is for a model with Z = 1/8 $Z_\odot$ while the solid line is the solar metallicity model. The lower ionisation in the Z = 1/8 $Z_\odot$ model leads to a stronger He I λ4471 line. The He II λ4542 line is hardly modified so that the larger ration of EW(He I λ4471)/EW(He II λ4542) implies a shift towards later spectral types.

models as the one used in the previous study with the following changes:

- the C, N, O, Si, S and Fe abundances have been reduced by a factor of 8.

- the wind parameters have been reduced. Indeed, the mass loss rate and terminal velocity of massive star are known to vary with Z (see Sect. 5). Practically, the mass loss rates are thought to be proportional to $Z^{0.8}$ (Vink, de Koter & Lamers, 2001) and the terminal velocities to $Z^{0.13}$ (Leitherer, Robert & Drissen, 1992). We have thus used these relations to scale the values of the wind parameters in the models with Z = 1/8 $Z_\odot$.

The main parameters of the models are summarised in Table 3.1.

The reduction of the metallicity will simply reduce the effect of line-blanketing. In particular, one can expect a smaller increase of the ionisation in the inner atmosphere and consequently a smaller shift of the spectral type for a given $T_{\rm eff}$. This is indeed what is seen in Fig. 3.8 and

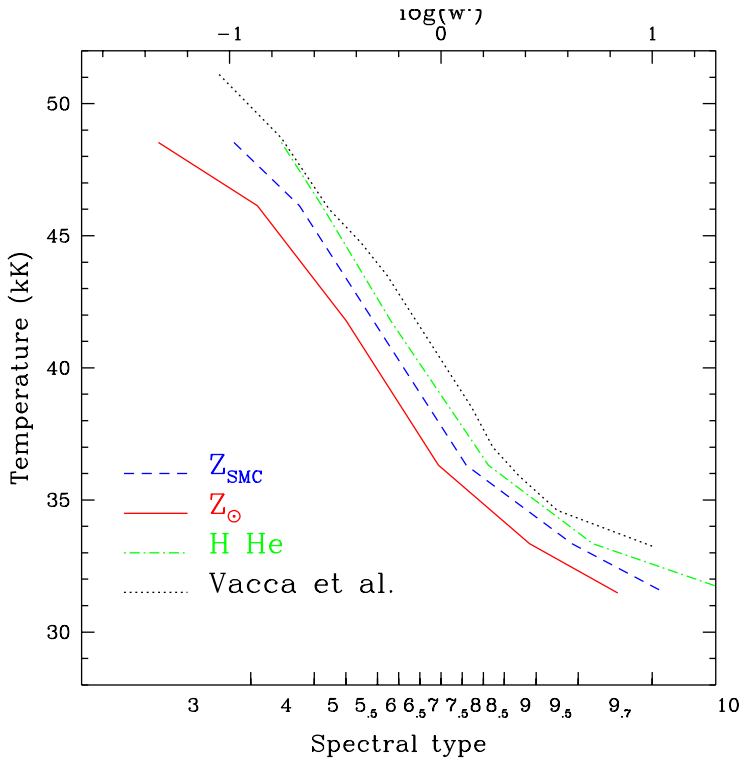

Figure 3.10: Metallicity effect on the effective temperature scale of O dwarfs. The dashed line is for a model with Z = 1/8 $Z_\odot$ while the solid line is the solar metallicity model. The dot-dashed line gives the relation for a pure H He model. A lower metal content leads to a reduction of $T_{\rm eff}$ for a given spectral type which is roughly half the reduction obtained in the solar metallicity case. Even for an SMC metallicity, the $T_{\rm eff}$ scale is cooler than the Vacca et al. (Vacca, Garmany & Schull (1996)) scale.

Table 3.1: Parameters of models used in the study of metallicity on the effective temperature scale of O dwarfs. The parameters come from the grid of CoStar models (Schaerer & de Koter, 1997) and the wind parameters have been scaled according to the relation mentioned above.

Model	Y2	A2	B2	C2	D2	E2
$T_{\rm eff}$ [K]	31477	33343	36308	41783	46132	48529
$\log \frac{L}{L_\odot}$	4.552	4.767	4.997	5.447	5.766	6.034
R [$R_\odot$]	6.358	7.268	7.994	10.152	12.010	14.780
M [$M_\odot$]	16.83	19.60	24.48	39.25	59.20	82.84
$\log \dot{M}$ [$M_\odot$ yr^{-1}]	-7.93	-7.58	-7.32	-6.89	-6.58	-6.10
v_∞ [km s^{-1}]	1900	1940	1970	2050	2200	2270

3.9 where the models with a lower metal content are shown by the dashed

lines and the solar metallicity model by the solid line. The He ionisation is lower in the low Z model in the region where the diagnostic lines are formed (around $\log \tau_{Rosseland}$ = -1.5). It results that the He I λ4471 line is stronger while the He II λ4542 line remains almost unchanged. This is equivalent to shift toward later spectral types and means that the shift towards earlier spectral types obtained in solar metallicity models compared to pure H He models is reduced in the case where Z = 1/8 $Z_\odot$. In terms of $T_{\rm eff}$ scale, this boils down to a scale between the pure H He case and the solar metallicity case. Fig. 3.10 shows this behaviour: reducing the metal content by a factor of 8 translates to a lowering of the $T_{\rm eff}$ scale by roughly half the reduction obtained in the Z = $Z_\odot$ case, which means a reduction of 1000 to 2000 K depending on the spectral type. Even if the reduction of the $T_{\rm eff}$ scale is smaller for Z = 1/8 $Z_\odot$, it leads to a relation cooler than that of Vacca, Garmany & Schull (1996). Note also that the effects of line-blanketing are reduced in the outer atmosphere: due to the weaker blocking of flux, the ionisation is higher for Z = 1/8 $Z_\odot$ than for the solar case (see Fig. 3.8).

In conclusion to this section, we have shown quantitatively that for Z = 1/8 $Z_\odot$, the reduction of the $T_{\rm eff}$ - scale compared to a pure H He case is roughly half the reduction obtained for solar metallicity. This is the first quantitative study of such an effect, and it may have important consequences since it means that for a given spectral type, O dwarfs are 1000 to 2000 K hotter in the SMC than in the Galaxy.

Chapter 4

Ionising radiation of O stars

French summary

Dans ce chapitre, nous nous concentrons sur l'effet du line-blanketing sur la distribution spectrale d'énergie des étoiles de type O.

Nous montrons tout d'abord que les principales manifestations du line-blanketing sont: 1) l'apparition d'une forêt de raies superposée au continu, 2) la modification de ce même continu sous l'influence d'opacités libre-liées, et 3) la redistribution du flux émis en dessous de $\sim$ 500 Å à des longueurs d'onde plus grandes. Ces effets sont plus ou moins importants selon la température effective de l'étoile (sans tendance générale). Le rapport de flux ionisants q_1/q_0 est légèrement augmenté quand les métaux sont inclus, alors que le rapport q_2/q_0 est lui diminué, traduisant entre autres la redistribution du flux (point 3 ci dessus).

Une comparaison avec des modèles précédents révèle que les flux ionisant l'Hydrogène (q_0) restent essentiellement inchangés pour une $T_{\rm eff}$ donnée, une fois encore à cause de la redistribution du flux qui se produit pratiquement totalement sous 912 Å. Le flux ionisant He I (q_1) est lui aussi peu modifié alors que le flux ionisant He II (q_2) est fortement réduit par la présence du line-blanketing. Pour un type spectral donné, la réduction de l'échelle de température conduit nécessairement à une réduction de tous les flux ionisants.

Ensuite, nous nous penchons sur un problème de transfert radiatif dans la raie Ly_α de He II afin de monter l'importance de l'inclusion de toutes les transitions et les risques encourus par des méthodes statistiques. En effet, nous montrons que l'inclusion ou non de raies de Fe VI voisines de He II λ304 peut passablement modifier l'ionisation d'He et le flux émis en dessous de 228 Å. L'explication réside dans un couplage entre ces diverses

raies conduisant à une surpeuplement du second niveau d'He II depuis lequel la photo-ionisation est possible de façon efficace.

Enfin, nous donnons les principaux résultats d'une étude visant à tester la distribution spectrale d'énergie des étoiles O au moyen de son effet sur des raies nébulaires émises dans des régions compactes de formation stellaire observées par le satellite ISO. La conclusion majeure en ce qui concerne les étoiles O est que la nouvelle génération de modèles permet de mieux reproduire les observations comparé aux modèles n'incluant pas le line-blanketing, les vents ou bien les deux. L'accord n'est toutefois pas parfait, et il s'avère qu'une distribution de corps noir donne finalement les meilleurs résultats, ce qui signifie que les flux ionisant les diverses espèces donnant naissance aux raies observées doivent être dans le même rapport que dans le cas d'un corps noir. Cette étude montre d'autre part que la séquence d'excitation observée dans ces régions jeunes est majoritairement dominée par la métallicité.

One of the main characteristics of O stars is their strong emission of ionising photons. Indeed, due to their $T_{\rm eff}$ of the order of a few ten thousands K, their spectral energy distribution peaks at around 1000 Å so that an important part of their luminosity is below the Lyman break (912 Å $\simeq$ 13.6 eV). This ionising radiation interacts with the surrounding medium and creates HII regions. Such regions can have different sizes depending on the number of ionising photons (and thus on the population of massive stars inside the region), on density and on the age of the region (since the continuous release of ionising flux makes the region expand). The knowledge is the ionising fluxes of massive stars is crucial for a number of studies including, of course, HII regions and starbursts in which the high number of massive stars produces a lot of ionising photons. A detailed modelling of massive stars atmospheres is then required, all ingredients being important to produce realistic SEDs as we have seen in Sect. 2.1 and 2.2. The computations of Vacca, Garmany & Schull (1996) (based on non-LTE plane parallel models without line-blanketing) and of Schaerer & de Koter (1997) (non-LTE spherical models with approximate treatment of line-blanketing) reveal that significant differences can be obtained depending on the ingredients included. In particular, the extension due to the wind enhances the emission below 228 Å (see Sect. 2.2).

As we have already noticed, the UV / extreme UV part of the spectrum corresponds to the region where the density of metallic lines is the highest. As a consequence, line-blanketing effects are expected to be very important in this region, not only because many metallic lines will shape the SED, but also because the change of the atmospheric structure will imply modifications on the flux emission due to new or changed opacities. This was noticed by Schaerer & Schmutz (1994) in their quantitative study of line-blanketing. A common statement is that due to the increased opacities in the EUV part of the spectrum, and due to the flux conservation, the photons which are blocked at low wavelengths must be redistributed to longer wavelengths where opacities are lower and where emission is possible. But modifications of the ionisations in the atmosphere can also *increase* the short wavelength emission (see Schaerer & Schmutz, 1994).

In this section, we show the results of the modelling of O stars SEDs thanks to the non-LTE spherically extended line-blanketed models computed with CMFGEN. As line-blanketing is included directly without approximation (except super-levels), we expect the results to reflect the correct effects of line-blanketing. We first show the general behaviour of the SED when metals are included, then we focus on the critical effect of metallic lines around 304 Å (near the HeII Lyman α line) and finally we test the ionising radiation of O stars thanks to their impact on nebular lines of young HII regions.

4.1 General effect of line-blanketing on the SED of O stars

In this section, we show the effect of the inclusion of metals on the spectral energy distribution of O stars and compare this SED to pure H-He models and previous atmosphere models results. We also try to estimate quantitatively the impact of line-blanketing on the ionising fluxes of O stars.

Let us first investigate the behaviour of the SED when metals are included. The results have already been mentioned in Sect. 3.3 so that we do not spend too much time on them. Fig. 4.1 shows the SED of a typical O star ($T_{\rm eff} = 41783$ K, $\log g = 4.02$, $\dot{M}$= 6.76 10^{-7} $M_\odot$ yr^{-1} and $v_\infty = 2690$ km s^{-1}) with (solid line) and without metals (pure H He model, dashed line). The following conclusions can be drawn:

- continuum:

  below $\sim$ 500 Å, the flux in the blanketed model is strongly reduced compared to the pure H He model. Moreover, additional discontinuities are present due to new bound-free edges of metals. This is in particular the case near 160 Å where the flux is used to ionise O IV, N IV and Fe V and is thus strongly reduced, creating a discontinuity.

- lines:

  the presence of numerous lines of metals creates a veil which modifies the very shape of the spectrum. This is particularly spectacular near the He II edge (228 Å) where the discontinuity almost disappears. Strong lines in the He I continuum are also seen in the blanketed model.

- flux conservation:

  It is clear form Fig. 4.1 that below $\sim$ 500 Å the blanketed model has a lower flux, while above this threshold, the opposite is true. This is required by the flux conservation and confirms the fact that the short wavelength photons blocked in the EUV part of the spectrum are processed and re- emitted at longer wavelength.

The effect of metallic lines on the shape of the SED is easy to understand: metallic lines simply behave as a line forest which blocks the flux. The modification of the continuum flux is more complex to understand. The continuum emission depends on the temperature and on the ground state level population of He II where the flux is emitted. Schaerer & de Koter highlighted two main effects of line-blanketing on the ionising fluxes:

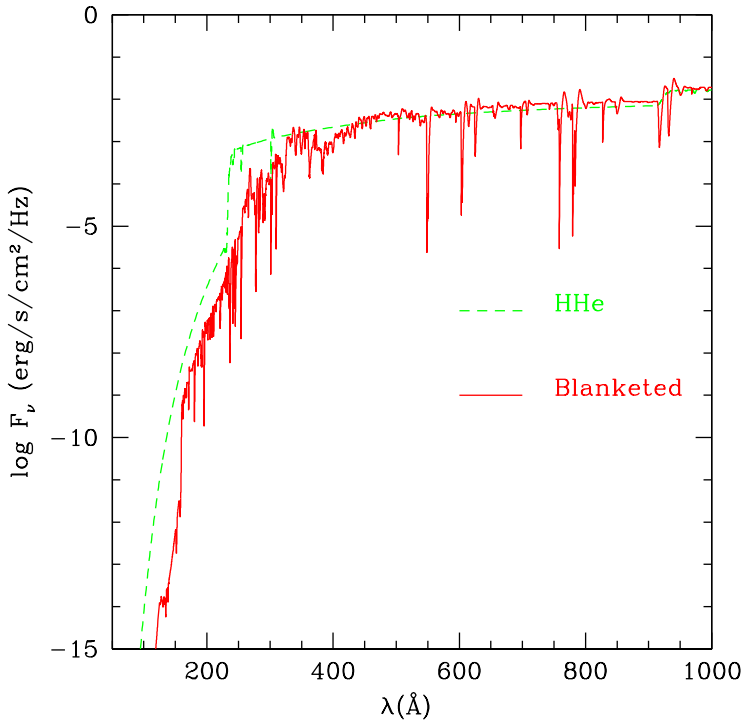

Figure 4.1: Effect of line-blanketing on the spectral energy distribution of a typical O star. The dashed line is a pure H He model and the solid one is a model with line-blanketing. The flux below $\sim$ 500 Å is strongly reduced when metals are included and lines affect the very shape of the spectrum. New discontinuities due to bound-free opacities of metals appear in the model with line-blanketing.

- first, the blocking of photospheric flux by opacities of metals leads to a decrease of the He ionisation and to an increase of the He II ground state population which boils down to a lower flux emission.

- second, as shown by Schaerer & Schmutz (1994) and confirmed by our investigations (see Sect. 3.3), line-blanketing renders the mean radiation field J more isotropic, which in turn increases the ionisation and then decreases the He II population, leading finally to a higher flux emission.

These two effects are very difficult to disentangle with simple arguments and depend on the detailed condition existing in each model. Fig. 4.2 indeed show that we can not draw any general conclusion concerning the influence of metals on the SED in CMFGEN models. For example, the reduction of the extreme UV flux is huge for the model at $T_{\rm eff}$ = 36308 K, but it is much weaker for the models at $T_{\rm eff}$ = 48529 K or 31477 K.

This statement is confirmed by Fig. 4.3 which gives the ionising fluxes

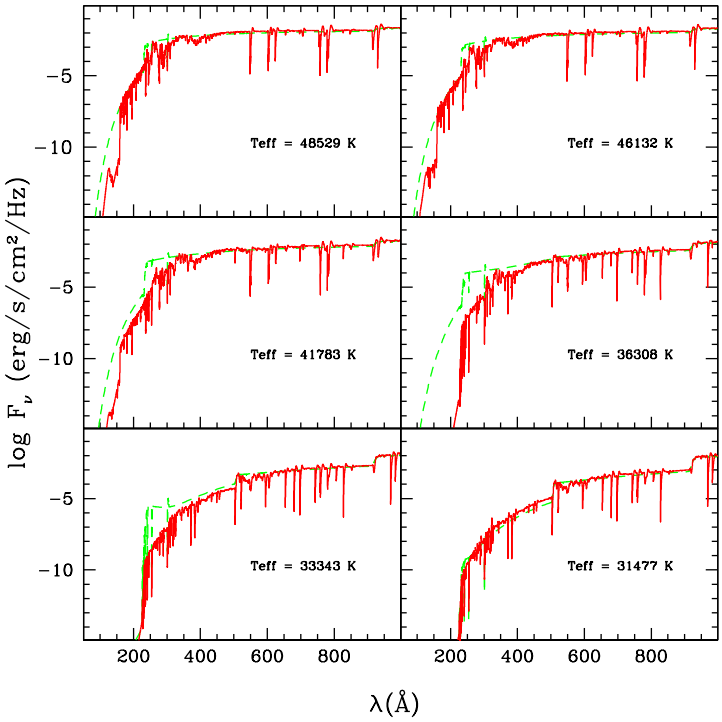

Figure 4.2: Same as Fig. 4.1 but with additional models. Although the EUV flux is reduced in all models including metals (compared to pure H He models), there is no general trend with $T_{\rm eff}$. This is mainly due to the complex behaviour of the continua in the models.

defined as follows:

$$q_i = \int_0^{\lambda_i} \frac{\pi \lambda F_\lambda}{hc} d\lambda \tag{4.1}$$

In this figure one sees that the He II ionising flux (i.e. q_2, below 228 Å) is strongly reduced in models with $T_{\rm eff}$ between 32000 and 44000 K, whereas it is almost unchanged out of this range. The largest difference (model with $T_{\rm eff} = 36308$ K) can reach 6 orders of magnitude. This is just the translation in terms of ionising photons of the trends observed in the SEDs of Fig. 4.2. Quantitatively, one notes that the He I ionising fluxes (q_1) are hardly changed when metals are included (upper right panel of Fig. 4.3), whereas the H ionising fluxes (q_0, upper left panel of Fig. 4.3) are slightly increased. Quantitatively, the increase goes from a factor of 1.13 for the hottest model to 1.77 for the cooler model. The fact that the H ionising fluxes are little modified when metals are added in the models indicates that the redistribution of the flux blocked at short wavelength

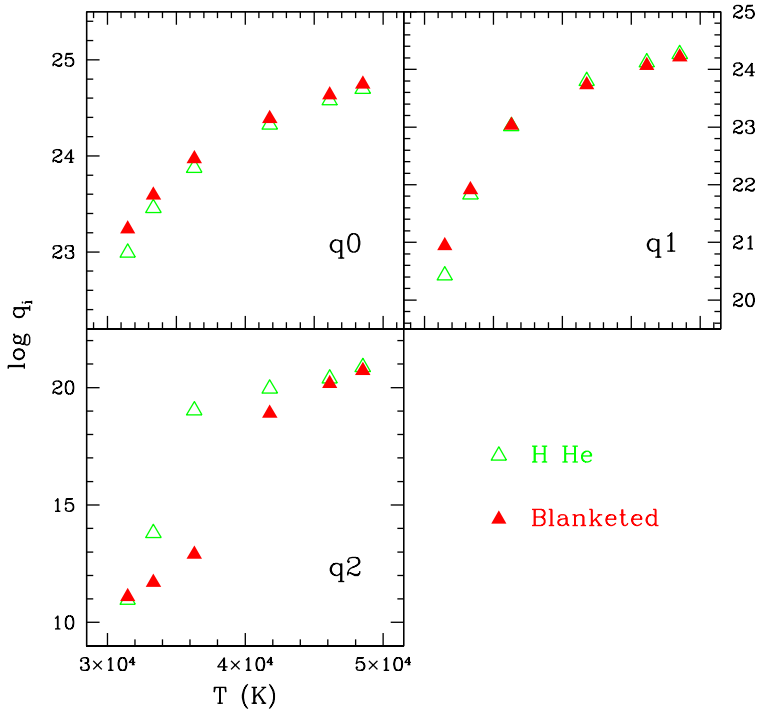

Figure 4.3: Ionising fluxes in the He II (q_2, upper left panel), He II (q_1, upper right panel) and H (q_0, lower panel) of CMFGEN models with (filled symbols) and without (open symbols) line-blanketing. q_0 and q_1 are slightly modified while q_2 can show reduction by more than 6 orders of magnitudes at intermediate $T_{\rm eff}$ (around 35000 K).

is almost - but not fully - entirely redistributed shortward of the Lyman break (see also Mokiem et al., 2004). The slight increase of q_0 in models with line blanketing reflects the changes in the atmospheric structure, in particular the increase of the temperature and ionisation in the layers where the continuum is emitted (see Sect. 3.3). Fig. 4.4 shows the ratios of ionising fluxes q_1/q_0 and q_2/q_0 as a function of effective temperature. We see that the inclusion of line-blanketing redistributes the flux from short wavelengths to longer wavelengths. Indeed, both ratios are lower in the models with metals than in the models without metals. The reduction is stronger for q_2/q_0 revealing that q_2 in more affected by the blocking of radiation. Note however that this part of the spectrum is affected by X-rays emission and can be significantly altered when such an emission is included in the models (Pauldrach et al., 1994; Santolaya-Rey, Puls & Herrero, 1997; Pauldrach, Hoffmann & Lennon, 2001).

The above discussion relies on the comparison between H He models and models with line-blanketing. As the CMFGEN models include the main ingredients of the modelling of massive stars atmospheres, a com-

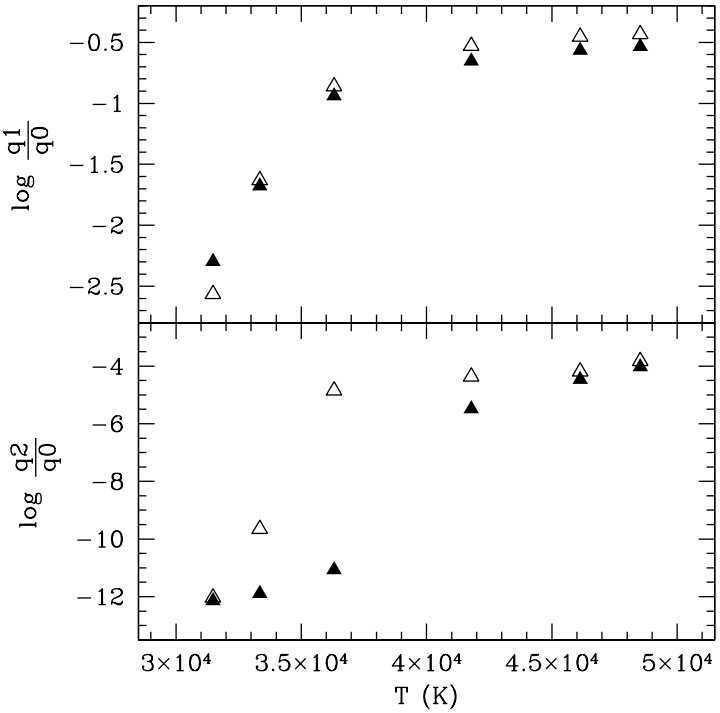

Figure 4.4: Ratio of HeI ionising flux (q_1, upper panel) and HeII ionising flux (q_2, lower panel) to Hydrogen ionising flux (q_0) of CMFGEN models with (filled symbols) and without (open symbols) line-blanketing. Due to the stronger blocking of flux at short wavelength, this ratio is lower when metals are included. This is especially the case for q_2/q_0.

parison with previous published ionising fluxes should highlight the main improvements of the new models. For that purpose, we use the CoStar models of Schaerer & de Koter (1997) and the ionising fluxes of Vacca, Garmany & Schull (1996). Fig. 4.5 gives the spectral energy distributions of CMFGEN (solid line) and CoStar models (dashed line). The main characteristic is the strong reduction of the flux below $\sim$ 300 Å in the CMFGEN models. As the difference between the two sets of models is the treatment of line-blanketing, we can conclude that the improved treatment of this ingredient in CMFGEN is the reason for the differences. Once again, these differences are the highest for intermediate temperatures. One of the most obvious improvement of the CMFGEN models is the presence of strong breaks due to bound-free opacities of metals (especially around 160 Å where N IV, O IV and Fe V ionisation potentials are located). The important modifications of the SED should influence the results of nebular analysis based on photoionisation models as we will see in Sect. 4.3. Quantitatively, the reduction of the ionising fluxes in the CMFGEN models are displayed in Fig. 4.6. For q_0 and q_1 the conclusion are the same as

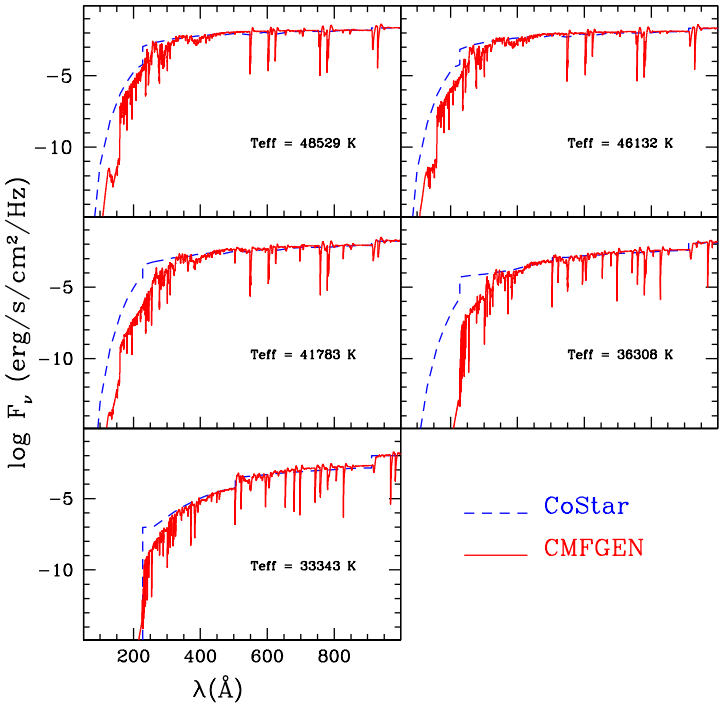

Figure 4.5: Spectral energy distribution of CMFGEN (solid line) and CoStar (dashed line) models. The improved treatment of line-blanketing in CMFGEN results in a lower flux below $\sim$ 300 Å.

in the previous comparison with H He models: q_0 is slightly increased in the CMFGEN models (for a given $T_{\rm eff}$) whereas q_1 is hardly modified. The main differences occur for q_2 which can be reduced by more than 8 orders of magnitude. This reflects the trend observed in the SEDs below $\sim$ 300 Å. Fig. 4.6 also shows the ionising fluxes of Vacca, Garmany & Schull (1996) which rely on plane parallel H He models. q_0 remains essentially unchanged for a given $T_{\rm eff}$ while q_1 is slightly stronger in the CMFGEN (and CoStar) models. Vacca, Garmany & Schull (1996) do not provide He II ionising fluxes since as shown by Gabler et al. (1989) the SED below 228 Å is strongly influenced by wind effects (see also Sect. 2.2). Fig. 4.7 displays the ratios of He ionising fluxes to H ionising flux for the CMFGEN and CoStar models and for the ionising fluxes of Vacca, Garmany & Schull (1996). q_1/q_0 is essentially the same in the CoStar and CMFGEN models, whereas the Vacca, Garmany & Schull (1996) results are lower. As line-blanketing (not included in the latter models) reduces this ratio (see Fig. 4.4) the main difference between the CoStar+CMFGEN models and the Vacca, Garmany & Schull (1996) results comes probably from the absence of winds in the latter. Indeed, we have shown in Fig. 2.2 that the inclusion of winds lead to an increase of the ionising fluxes at short

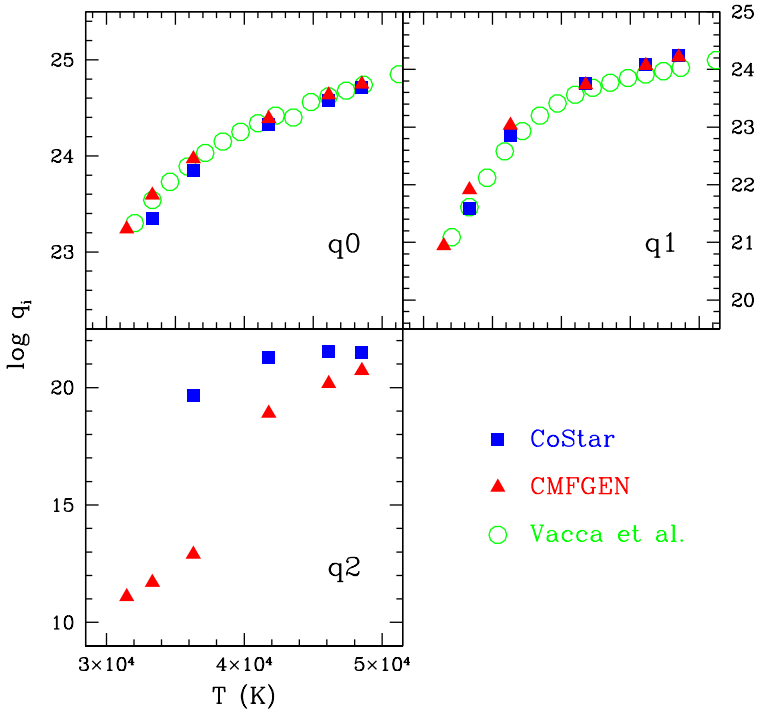

Figure 4.6: Ionising fluxes (in terms of q_i) for CMFGEN (filled triangles), CoStar (filled squares) and Vacca et al. (1996, open circles). The H and He I ionising fluxes are hardly affected while q_2 is strongly reduced in the CMFGEN models, in agreement with the trend observed for the SEDs.

wavelength. This is mainly the case in the He II continuum which explains that Vacca, Garmany & Schull (1996) do not provide values of q_2. q_2/q_0 is much lower in the CMFGEN models than in the CoStar models due to the approximate treatment of line-blanketing in the latter models.

In conclusion, one can say that:

- the inclusion of line-blanketing does not strongly modifies the H and He I ionising fluxes *for a given* $T_{\rm eff}$. This is mainly due to the fact that the flux blocked at short wavelength is almost entirely redistributed below 912 Å. However, this does not mean that the SED are the same, since q_i are integrated values. This is seen in Fig. 4.1 for example: the detailed shape of the spectrum is modified so that "intermediate" ionising fluxes (responsible for the ionisation of metals in nebulae) are changed (see also Sect. 4.3).

- the He II ionising flux is modified by the inclusion of metals, but no general trend can be put forward, the modification being either weak or huge depending on $T_{\rm eff}$. This is due to the complex interaction of various effects such as change of ionisation, different temperature

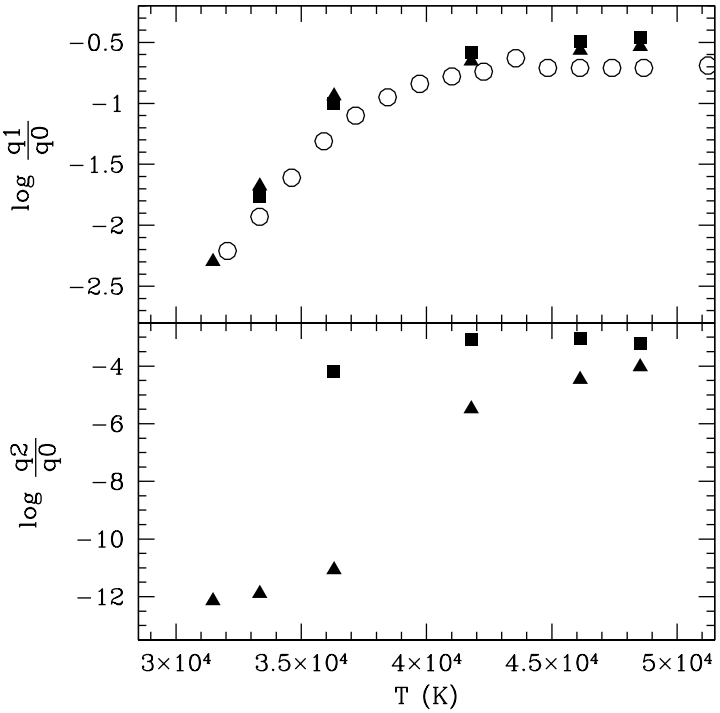

Figure 4.7: Ratio of HeI ionising flux (q_1, upper panel) and HeII ionising flux (q_2, lower panel) to Hydrogen ionising flux (q_0) of CMFGEN models (filled triangles), CoStar models (filled squares) and from Vacca, Garmany & Schull (1996) (open circles).

structures, isotropy of radiation field and blocking of flux. This continuum is also strongly sensitive to X-rays which are not included in the present models (see Pauldrach et al., 1994; Santolaya-Rey, Puls & Herrero, 1997; Pauldrach, Hoffmann & Lennon, 2001). Hence, the values given by CMFGEN must be taken with care.

4.2 Radiative transfer near He II λ304

Here, we investigate the effects of metal lines in the radiative transfer in the He II *λ304 line and show that the inclusion or not of such lines influences the ionising fluxes.*

In the previous section we have seen that most of the changes in the SEDs of O stars due to line-blanketing occur below $\sim$ 300 Å, Practically, it is essentially the He II continuum flux which is modified. This means that the He II continuum opacity, and thus the He II populations, must be strongly influenced by the presence of metals. Hence, it is important

to understand the influence of line-blanketing on the populations of the low energy levels of He II. In the following, we show that the inclusion of metallic lines can affect the radiative transfer in the He II Ly_α line (He II λ304) and the He II populations. This highlights the role of weak lines from metals in radiative transfer processes and shows that they may be crucial to set the ionisation structure despite their weakness. More generally, this is a warning for the opacity sampling methods which may miss such weak but important lines. To study this effect, we have restricted ourselves to a typical models of massive stars: the effective temperature is 40000 K and $\log g \sim 4.0$. These parameters are typical of a mid O dwarf.

Table 4.1: Fe ions included in models used to study the line-blanketing effects on the extreme UV part of the spectrum of a typical O stars with $T_{\rm eff}$ = 41783 K, $\log g$ = 4.02, $\dot{M}$= 6.76 10^{-7} $M_\odot$ yr^{-1} and v_∞ = 2690 km s^{-1}.

Model	Fe ions included				Fe VI lines around 304 Å
C2_noFe					No
C2_noFe456				VII	No
C2_noFe45			VI	VII	Yes
C2_noFe4		V	VI	VII	Yes
C2_noFe45noFe6l			VI	VII	No
C2_noFe6l	IV	V	VI	VII	No
C2	IV	V	VI	VII	Yes

Fig. 4.8 shows the ionisation rates as a function of mean Rosseland optical depth in the atmosphere of a typical O star. Ionisation from the ground state dominates the photoionisation of He II, but we see that photoionisation from the first excited level (dashed line) is also important and even higher around $\log \tau_{Rosseland} = -1.5.. - 2$ (see also Fig. 4.14). This indicates that any depopulation or overpopulation of the ground state and first excited level can modify the He II ionisation and then the emergent spectrum. In order to test this hypothesis, we have run several test models starting from a model without Iron and in which we have successively added different Fe ions (from Fe VII to Fe IV). As Iron is the main contributor to line-blanketing (see Sect. 3.3), we expect to see the main effects of metals on the He II populations. Table 4.1 gives the Fe ions included in the various models. Fig. 4.9 shows the results of this study in terms of SED. One can draw two conclusions:

→ Although we could expect that the addition of metals would reduce the extreme UV flux (due to higher new opacities of metals), *the inclusion of more and more Fe ions increases the flux below 228 Å.*

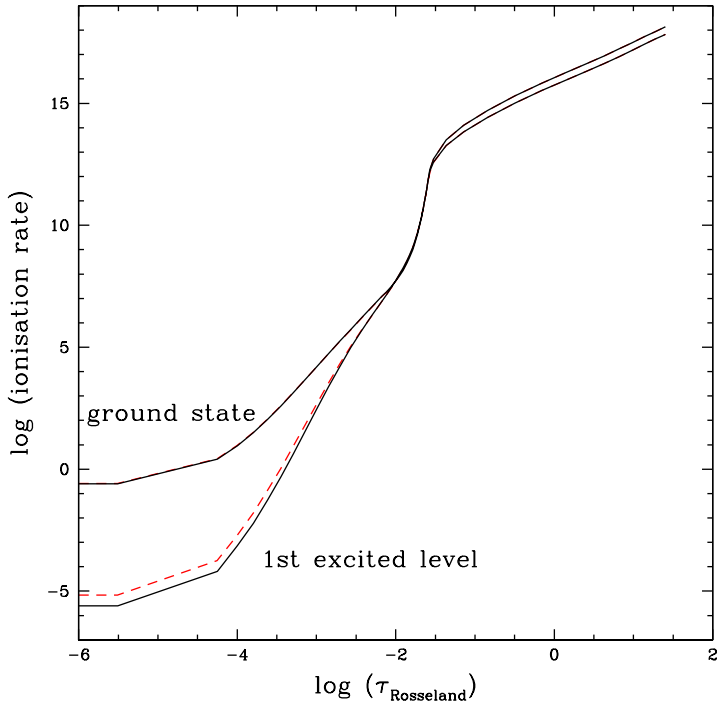

Figure 4.8: Ionisation rate from the ground state and first excited level in a model. The solid line is a model for which the Fe VI lines close to He II λ304 are included, and the dashed line is the case where they are not present.

→ The major flux increase occurs when Fe VI is included in the model.

As the main source of opacity below 228 Å is He II bound-free absorption, the changes observed in Fig. 4.9 are certainly due to an increase of the He ionisation and thus a reduction of the He II ground state population. How could the He ionisation be increased? A possible explanation relies on a photon loss mechanism similar to that described by Schmutz (1998): photons with $\lambda \sim 304$ Å are either absorbed or injected by metallic lines of similar wavelength and modify the radiative transfer in the He II λ304 line, leading to over or under population of the ground state and first excited level and thus to a new He ionisation. Schmutz (1998) points that iron lines could be responsible for such a photon loss (or photon gain depending on whether photons are absorbed or injected). The analysis of Fig. 4.9 seems to confirm that hypothesis and indicates moreover that Fe VI lines are probably the main contributors to this effect. Hence, we have searched for possible Fe VI lines with wavelength close to 304 Å in the line list of the CMFGEN model studied here. We have found two lines which could well have such an interaction with He II λ304 : one has $\lambda = 303.802$ Å and the

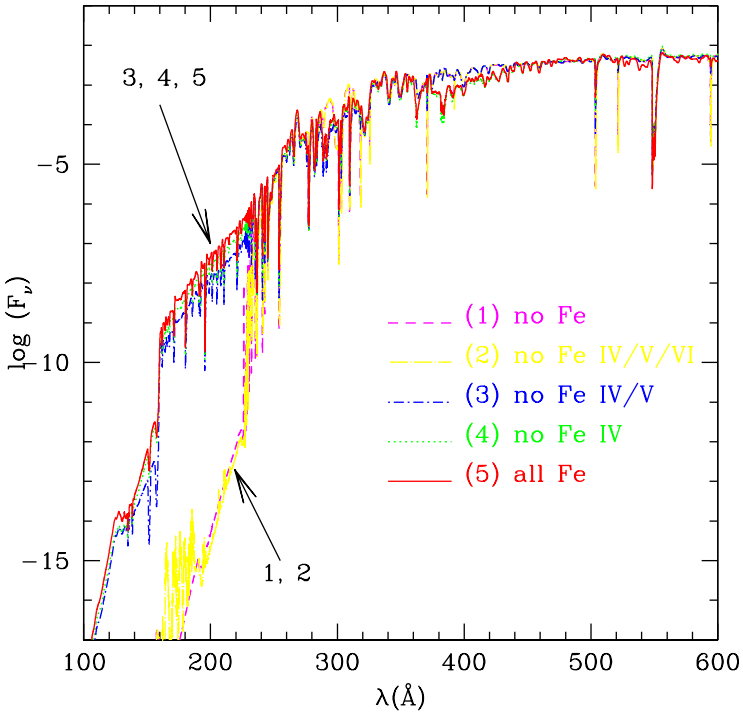

Figure 4.9: Effect of the addition of different Fe ions on the extreme UV spectral energy distribution of a typical O stars with $T_{\rm eff}$ = 41783 K, $\log g$ = 4.02, $\dot{M}$= 6.76 10^{-7} $M_\odot$ yr^{-1} and v_∞ = 2690 km s^{-1}. The details of the models are given in Table 4.1.

other has $\lambda = 303.834$ Å[1]. Note that in the atomic data used by CMFGEN, He II λ304 is at 303.783 Å so that the Fe VI lines are separated by no more than 50 km s^{-1} from this He line. We have then run a new model with Fe VII and Fe VI but without these two lines (practically, we have simply set their oscillator strength to 0). The characteristics of the model are given in Table 4.1. The result of this test is displayed in Fig. 4.10: the inclusion of the two Fe VI lines strongly enhances the He II continuum flux. In fact, a model with Fe VI but without the two Fe VI lines around 304 Å has roughly the same SED as a model without any Fe VI level. From this test, we can conclude that the direct inclusion of line-blanketing in massive stars atmosphere is necessary to produce reliable SEDs, at least in the extreme UV. Indeed, statistical approaches such as the opacity sampling method may miss important lines such as the FeVI lines tested here and then predict erroneous He ionisation. It is also important to compute the detailed statistical equilibrium equations for the individual levels re-

[1]they correspond respectively to transitions between levels $3d^2(1D)4p\ ^2P^0_{3/2}$ and $3d^3\ ^2D_{5/2}$, and between $3d^2(1D)4p\ ^2P^0_{3/2}$ and $3d^3\ ^2D_{3/2}$

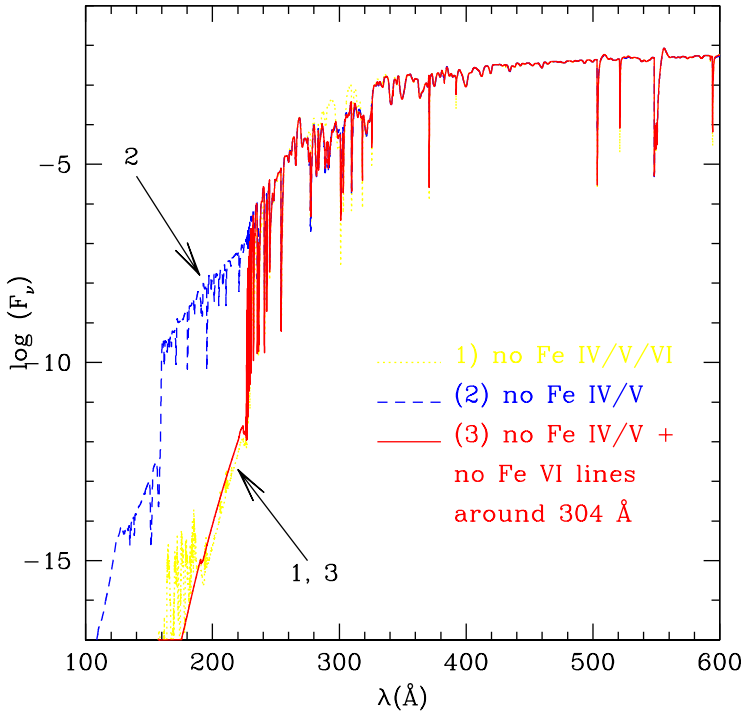

Figure 4.10: Determination of the exact factor governing the change of ionising flux below 228 Å. Fe VI lines close to He II λ304 seem to be very important to set the He ionisation since their addition strongly enhances the flux in the He II continuum.

sponsible for the transitions neighbouring He II λ304 , which means that they should not be grouped in super-levels. Indeed, such a gathering may slightly modify the level populations and thus the strength of the lines. As a consequence, the He II continuum may be modified. That is why after this test we have always excluded super-levels for Fe VI in our calculations. Fig. 4.11 confirm the above result in a test where all the ionisation states of Fe are included in the models except that the 304 Å Fe VI lines are not included (see Table 4.1 for the characteristics of the model). Again, the effect of these lines on the He II continuum is obvious. It turns out that the effect of the addition of these two lines is comparable to the addition of both all Fe IV and Fe V opacities.

To be more quantitative, Table 4.2 gives the ionisation fluxes below 228 Å (q_2), 504 Å (q_1) and 912 Å (q_0) by surface unit (q_i) and integrated ($Q_i = 4\pi R^2 q_i$). Including Fe VI lines in the model with all the Fe ions boils down to an increase of q_2 by 0.56 dex, or a factor 3.6. This increase is of 3.28 dex in the models without Fe IV and Fe V!

What is the physical explanation for the influence of these two lines? The answer is that given by Schmutz (1998): injection of photons in the

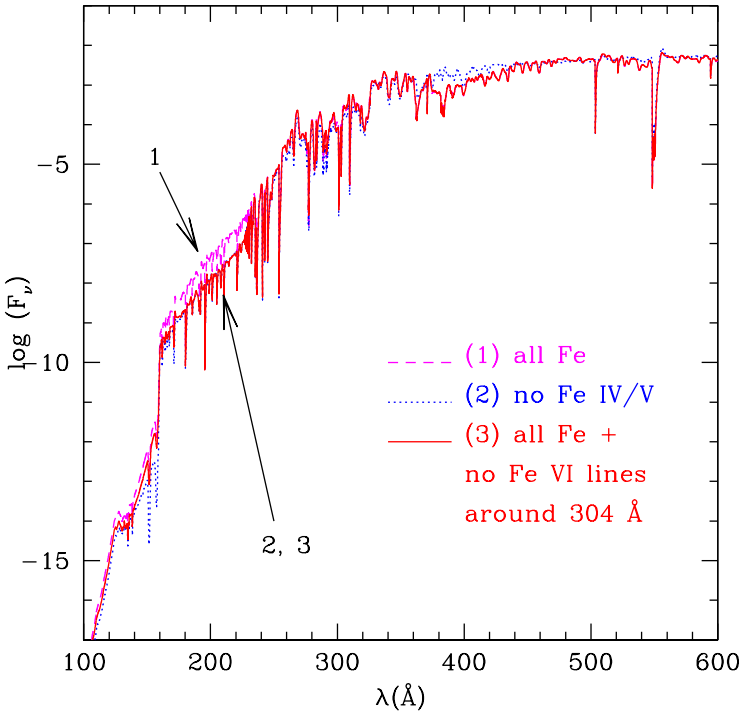

Figure 4.11: Effect of Fe VI lines close to He II λ304 on the extreme UV spectral energy distribution of a typical O star. The inclusion of these lines modifies the radiative transfer in the He II λ304 line and have important effects on the He ionisation in the wind. See text for discussion.

Table 4.2: Ionising fluxes below 228 Å(q_2 and Q_2), 504 Å(q_1 and Q_1) and 912 Å(q_0 and Q_0) fot the models given in Table 4.1

Model	q_0	q_1	q_2	Q_0	Q_1	Q_2
C2_noFe	24.332	23.700	15.600	49.130	48.497	40.397
C2_noFe456	24.333	23.702	13.623	49.131	48.499	38.421
C2_noFe45	24.336	23.697	18.454	49.133	48.494	43.251
C2_noFe4	24.340	23.599	18.777	49.137	48.396	43.575
C2_noFe45noFe6l	24.336	23.697	15.174	49.133	48.494	39.971
C2_noFe6l	24.342	23.633	18.454	49.139	48.431	43.252
C2	24.342	23.633	19.018	49.139	48.431	43.815

He II λ304 line. Let us be more precise. The Fe VI lines have wavelength close to that of He II λ304 so that they can inject photons in this line. Fig. 4.12 demonstrates that these Fe VI lines indeed inject photons in the He II λ304 line since around $\log \tau = -1.5.. - 2$, where photoionisations from level 2 are important, the net radiative rates in these lines are positive. These rates (Z) are defined as follows:

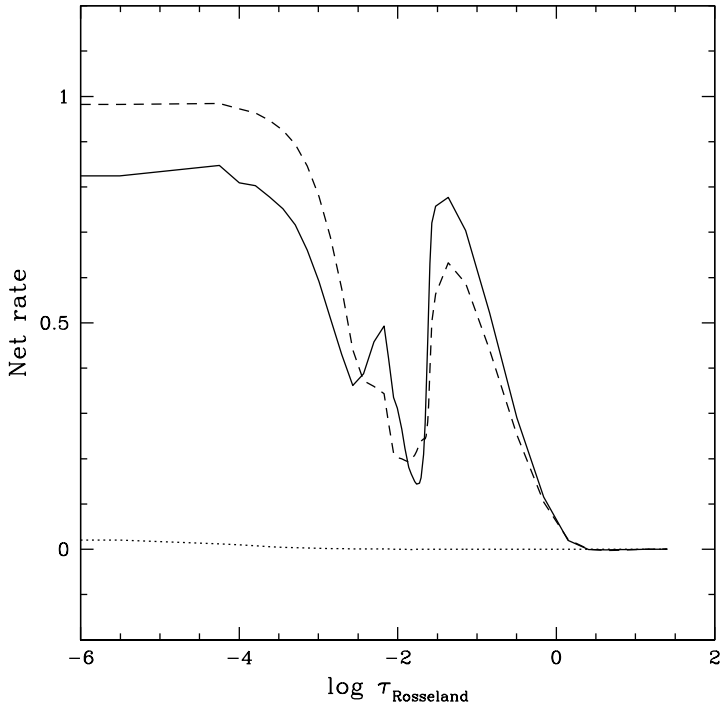

Figure 4.12: Net radiative rates in He II λ304 (dotted line) and in the two neighbouring Fe VI lines (solid and dashed line). The positive values of the net rates of the two latter lines indicate that downward transitions are more frequent than upward transitions, which means that photons are produced in these lines. He II λ304 is in detailed balanced almost everywhere.

$$n_j A_{ji} Z_{ji} = n_j (A_{ji} + B_{ji} J_{ij}) - n_i B_{ij} J_{ij} \tag{4.2}$$

$$Z_{ji} = 1 - \frac{n_i B_{ij} - n_j B_{ji}}{n_j A_{ji}} J_{ij} \tag{4.3}$$

$$Z_{ji} = 1 - \frac{J_{ij}}{S_{ij}} \tag{4.4}$$

where n_i, n_j are the populations, J_{ij} the mean intensity of the radiation field in the transition, S_{ij} the source function and A_{ji}, B_{ij} and B_{ji} the Einstein coefficients. A positive value of Z_{ji} means that the number of downward transitions is higher than the number of upward transitions, or that photons are emitted more than they are absorbed, which is the case of the Fe VI lines shown in Fig. 4.12. The dotted line in this figures is for the He II λ304 line and shows that its net rate is almost all the time zero, which means that the transition is in detailed balanced.

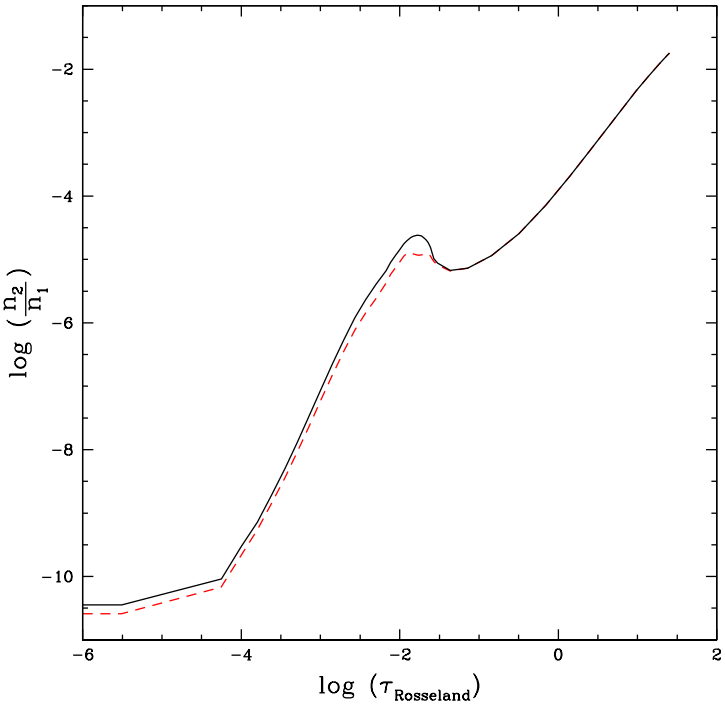

Figure 4.13: Effect of Fe VI lines close to He II λ304 on the ratio of first excited level to the ground state population of He II. Solid (dashed) line: model with (without) Fe VI lines. Including these lines pumps electrons in the first excited level. See text for discussion.

This global downward transitions in the Fe VI lines means that more photons will be available for this He II line and that electrons will be pumped from the ground state to the first excited level. An overpopulation of level 2 (first excited level) relative to level 1 (ground state) will result as demonstrated by Fig. 4.13. But we have seen in Fig. 4.14 that photoionisation from level 2 can be equal or even higher than from level 1. This means that an overpopulation of level 2 will result in an increase of photoionisation from this level: this is shown in Fig. 4.14 where one sees that at the depth where photoionisation from level 2 exceeds that from level 1, the addition of Fe VI lines increases the former and reduces the latter. The global effect is an increase of the all He ionisation from this point and in the outer atmosphere, as displayed in Fig. 4.15. The reduced He II continuum opacity implies a higher flux emission shortward of 228 Å.

Despite this apparently reasonable explanation to the change of the He II ionisong flux when different Iron ionisation states and lines are included, we have to mention that the model we investigate here is in the temperature range where q_2 deacrease dramatically (see Fig. 4.3). Hence,

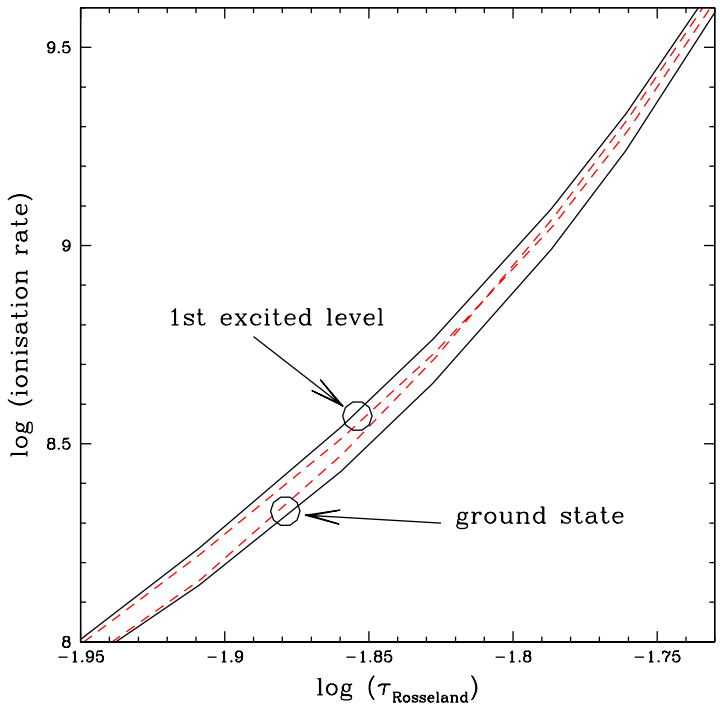

Figure 4.14: Effect of Fe VI lines close to He II λ304 on the photoionisation rates from level 1 and 2. The inclusion of the Fe VI lines increases photoionisations from level 2 and reduces those from level 1, has a result of pumping of photons from the ground state to the first excited level. Solid (dashed) line: model with (without) Fe VI lines. See text for discussion.

it may be possible that a small change in the model parameters (such as the inclusion of two Fe VI lines) can strongly affect the atmosphere structure and the emergent flux. Models with different effective temperatures should be checked to see if this "weak lines" effect also takes place in other temperature ranges.

In conclusion, this study reveals the importance of the inclusion of all transitions in the rediative transfer problem without approximation, since interactions between lines can modify the atmospheric structure (especially the ionisation structure) and the emergent spectrum.

4.3 Observational test of the ionising radiation of O stars

This section is dedicated to the test of the ionising fluxes predicted by the new generation of model atmospheres for massive stars thanks to the anal-

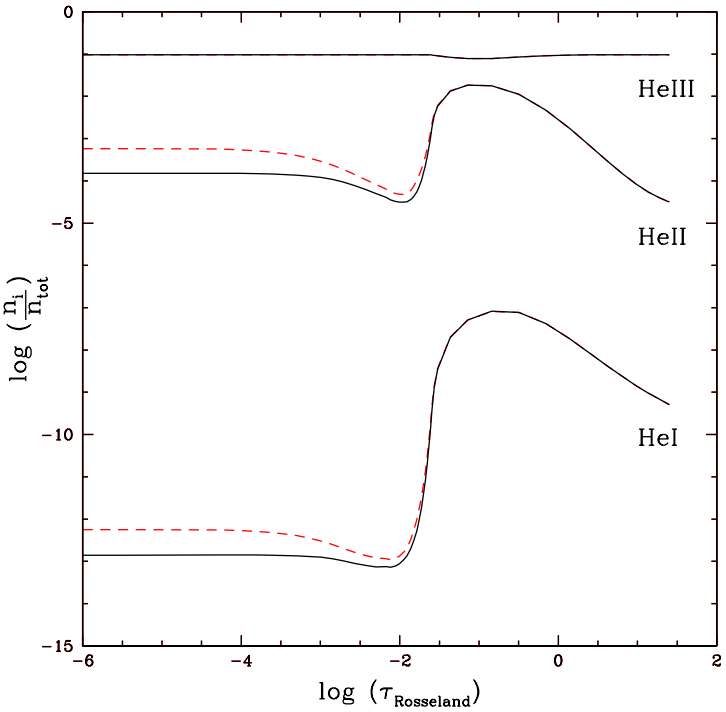

Figure 4.15: Effect of Fe VI lines close to He II λ304 on the ionisation of He. The inclusion of these two lines increases the global He ionisation (solid line). The dashed line is the case where these Fe VI lines are not included.

ysis of mid-IR lines emitted by compact HII regions observed by ISO.

We have seen in the previous section that the inclusion of line-blanketing in the atmosphere models of O stars lead to important changes of the atmospheric structure and the emergent spectrum. However, the question of how realistic these new results are remains. As for the effective temperature scale, one of the indication that the lower effective temperatures are in better agreement with real values has been given by Gies (2002). He studied spectroscopic binaries and derived masses which were compared to masses predicted by evolutionary models. The latter were derived by interpolation in the $T_{\rm eff}$ - log L plane. If previous, hotter temperature are used, the evolutionary masses are systematically higher than the observed masses, whereas the adoption of our revised $T_{\rm eff}$ - scale leads to much better agreement. Although indirect, this is a strong evidence that lower effective temperatures are preferred.

What about the ionising radiation of O stars? There are in fact two ways of testing such SEDs. The first one is to study directly individual stars in different wavelength ranges to reconstruct the SED. But constrain-

ing the ionising radiation requires observations in the extreme UV range which suffers from huge interstellar and atmospheric absorption. Space observations are thus required. At present, FUSE can probe the far-UV range (above 900 Å) and the Chandra and XMM observatories explore the X ranges, so that the ionising radiation between the He II and Lyman breaks can now be observed. Archive data exist but only for a few stars. And as already mentioned, interstellar absorption introduces a source of uncertainty in the exact level of emission. Hence, another technique has to be used: it consists in studying *indirectly* the SEDs of O stars through its effect on the surrounding interstellar medium. Indeed, the ionising radiation creates HII regions in which excited elements emit various observable lines. The strength of these lines depends on the conditions in the nebula (density, electron temperature) but also on the amount of ionising photons at different wavelength. Hence, the ionisation of different elements traced by the strength of the lines they emit will depend on the shape of the SED of the ionising star (or star cluster). We have chosen this solution to test the ionising radiation of O stars and have studied a sample of compact HII regions observed by the ISO observatory in the mid IR range. Such objects are well suited for this kind of study since they probably host one or a few massive stars not too evolved. The interaction of ionising radiation with the interstellar medium leads to the emission of IR lines from different elements. The important point is that IR radiation suffers from much lower extinction than shorter wavelength ranges, so that reliable measures of the continuum and line strength can be done. These measures are then compared to predictions of photoionisation models which predict the behaviour of nebular lines as a function of the properties of the nebula and of the ionising radiation of the central star(s). The results of the study are given in the following paper. In the context of testing the ionising radiation of O stars, the main conclusion is that the new generation of atmosphere models including non-LTE, winds and line-blanketing leads to improvements in the predictions of IR lines from HII regions. This is an indirect evidence that the SEDs of O stars are better represented by these new models.

A&A 415, 577–594 (2004)
DOI: 10.1051/0004-6361:20034622

Astronomy & Astrophysics

Mid-IR observations of Galactic H II regions: Constraining ionizing spectra of massive stars and the nature of the observed excitation sequences

C. Morisset[1,2], D. Schaerer[3,4], J.-C. Bouret[2], and F. Martins[4,3]

[1] Instituto de Astronomía, Universidad Nacional Autónoma de México, Apdo. postal 70–264, Ciudad Universitaria, México DF 04510, México
[2] Laboratoire d'Astrophysique de Marseille, CNRS, BP 8, 13376 Marseille Cedex 12, France
[3] Observatoire de Genève, 51 Ch. des Maillettes, 1290 Sauverny, Switzerland
[4] Laboratoire d'Astrophysique, UMR 5572, Observatoire Midi-Pyrénées, 14 Av. E. Belin, 31400 Toulouse, France

Received 3 June 2003 / Accepted 1 October 2003

Abstract. Extensive photoionization model grids for single star H II regions using state-of-the-art stellar atmosphere models have been computed to test their predicted ionizing spectra against recent ISO mid-IR observations of Galactic H II regions. Particular care has been paid to examining in detail the dependences of the nebular properties on the numerous nebular parameters which are generally unconstrained. Provided the ionization parameter U is fairly constant on average and the atomic data is correct these comparisons show the following:

- Both recent non-LTE codes including line blanketing and stellar winds (*WM-Basic* and *CMFGEN*) show a reasonable agreement with the observations, although non-negligible differences between their predicted ionizing spectra are found. Recurrently none of the models can be preferred over the other.
- The softening of the ionizing spectra with increasing metallicity predicted by the *WM-Basic* models is found to be too strong.
- We confirm earlier indications that the *CoStar* atmospheres, including an approximate treatment of line blanketing, overpredict somewhat the ionizing flux at high energies.
- Both LTE and non-LTE plane parallel hydrostatic atmosphere codes predict ionizing spectra that are too soft, especially over the energy range between 27.6, 35.0, and 41.1 eV and above. The inclusion of wind effects is crucial for accurate predictions of ionizing fluxes.

These conclusions are found to be robust to effects such as changes of U, stellar metallicity changes, and the inclusion of dust. Uncertainties due to atomic data (especially for Ar) are discussed. We also discuss the difficulties in estimating absolute stellar temperatures from mid-IR line ratios. Finally we have examined which parameters are chiefly responsible for the observed mid-IR excitation sequences. The galactic gradient of metallicity changing the shape of the stellar emission is found to be one of the drivers for the excitation sequence of Galactic H II regions, the actual contribution of this effect being finally atmosphere model dependent. The observed excitation scatter can be explained by effects due to statistical sampling of the IMF leading to a $T_{\rm eff}$ dispersion plus additional dispersion of U.

Key words. ISM: abundances – ISM: dust, extinction – ISM: HII regions – ISM: lines and bands – atomic data – stars: atmospheres

1. Introduction

Despite their paucity, hot massive stars are prominent contributors to the chemical and dynamical evolution of their host galaxies. Because of their intense nucleosynthesis, they process large amounts of material, on very short time scales. Furthermore, in addition to type II supernovae, of which they are progenitors, massive stars drive the dynamics and energetics of the ISM through their supersonic massive winds, thus affecting the subsequent star formation process in their surrounding environment. Their strong UV radiative fluxes ionize the ISM and create H II regions. The ionization structure of the latter is therefore, for the most part, controlled by the EUV radiation field of their massive stars content. In order to determine the properties of H II regions, it is therefore essential to understand the physical properties of massive stars and most importantly, to constrain their FUV and EUV (H-ionizing continuum) flux distribution. Yet, this part of the stellar spectrum

Send offprint requests to: C. Morisset,
e-mail: Morisset@AstroScu.UNAM.mx

is generally unaccessible to direct observations and it is crucial to find indirect tests to constrain it. In this context, nebular observations of H II regions combined with extensive grids of photoionization models including state-of-the-art model atmospheres offer the best opportunity to achieve this goal.

A large number of galactic H II regions have been observed with the ISO satellite (see e.g. Martín-Hernández 2002, and references therein). These spectra provide a wealth of spectral information, through fine-structure lines of ions whose ionization/excitation threshold are located below 912 Å. The shape of the SED in the EUV, and more specifically the number of ionizing photons in this region, is directly probed by ratios of successive ionization states such as [Ar III] 8.98 μm/[Ar II] 6.98 μm, [N III] 57.3 μm/[N II] 121.8 μm, [S IV] 10.5 μm/[S III] 18.7 μm, and [Ne III] 15.5 μm/[Ne II] 12.8 μm. Building line ratios diagrams for these species that are very sensitive to different parts of the flux distribution below the Lyman threshold allow one to derive informations on the actual spectral energy distribution at wavelengths usually unaccessible to direct observations. This not only provides valuable informations on the physical properties of the H II regions but on their stellar content as well. As a matter of fact, it is nowadays often used to estimate the spectral type of the ionizing source of single star H II regions, and offers a useful counterparts to more classical techniques of typing, based on optical or near-infrared absorption features (Mathys 1988; Hanson et al. 1996; Watson & Hanson 1997; Kaper et al. 2002).

On the other hand, modeling tools to analyze the photosphere and winds of hot, massive stars with a high level of accuracy and reliability have become available in recent years. In particular, major progress has been achieved modeling the stellar photosphere and stellar wind in a unified approach incorporating also a treatment of non-LTE line blanketing for the major opacity sources (Hillier & Miller 1998; Pauldrach et al. 2001; Hubeny & Lanz 1995; Lanz & Hubeny 2003a,b).

The impact of the first generation of atmosphere models including stellar winds and non-LTE line blanketing on nebular diagnostics was studied by Stasińska & Schaerer (1997) using the *CoStar* atmosphere models of Schaerer & de Koter (1997). This study showed already several improvements with respect to the widely used LTE models of Kurucz (1991). More recently Martín-Hernández (2002); Martín-Hernández et al. (2004) have investigated the metallicity dependence of the spectral energy distribution of O stars and the ionization structure of H II regions, using the *CMFGEN* code by Hillier & Miller (1998). They also compared the EUV fluxes from *CMFGEN* to those of the *CoStar* (Schaerer & de Koter 1997) and *WM-Basic* (Pauldrach et al. 2001) codes. They concluded that different treatment of line-blanketing between *CoStar* on the one hand and *WM-Basic* and *CMFGEN* on the other hand results in significant differences in the predicted EUV SEDs and ionizing fluxes.

In this context, it is of special interest to investigate how the different models available nowadays compare to each other in predicting nebular lines ratios. Similarly, it is of importance to test the role that a handful of various nebular parameters might have on the line ratios diagrams provided by ISO observations. The parameters influencing the ionization structure of a photoionized region are: 1) the geometry, the density distribution, the metallicity of the gas, and the possible absorption of the ionizing radiation by dust, 2) any physical quantity affecting the shape of the ionizing flux like, for example, the effective temperature of the ionizing star, its metallicity, the presence of a wind and the characteristics of the latter, 3) the hypothesis used to model the atmosphere like the number of elements taken into account, the treatment of the line-blanketing, etc. in summary: the physical ingredients and the related assumptions used to model the emitting atmosphere.

The present paper describes photoionization models performed with various atmosphere models, separating the effects of all these parameters. The paper is structured as follows: The various adopted atmosphere models are briefly described and compared in Sect. 2. The ionizing spectra from these models are then used as input to our photoionization code for the calculation of extended grids of nebular models (Sect. 3). The compilation of ISO observations of H II regions is described in Sect. 4. In Sect. 5 we compare our photoionization models to the observations and discuss the effect of changing parameters one by one on the excitation diagnostics. In Sect. 6 we test the validity of the different excitation diagnostics and softness radiation parameters for the determination of $T_{\rm eff}$. The discussion takes place in Sect. 7. Our main conclusions are summarized in Sect. 8.

2. O star atmosphere models

Among the key ingredients for the description of O star model atmospheres are the treatment of non-LTE effects, the inclusion of stellar winds, and a treatment of line blanketing (see e.g. Abbott & Hummer 1985; Kudritzki et al. 1988; Gabler et al. 1989). In recent years considerable improvements have been made in the modeling of these processes and model grids computed with various sophisticated atmosphere codes have become available (see e.g. the recent conference on "Stellar atmosphere modeling", Hubeny et al. 2003). For our photoionization models, we adopt the ionizing spectra predicted from five different codes (*Kurucz*, *TLUSTY*, *CoStar*, *WM-Basic*, *CMFGEN*) briefly described hereafter. With the exception of the *TLUSTY* and *Kurucz* models, which assume a plane parallel geometry and thus no wind, all models describe the photosphere and winds in spherical geometry, in a unified manner.

Except mentioned otherwise, we have used atmosphere models computed for solar abundances: He, C, N, O, Ne, Si, S, Ar and Fe being 0.1, 4.7×10^{-4}, 9.8×10^{-5}, 8.3×10^{-4}, 5.4×10^{-5}, 4×10^{-5}, 1.6×10^{-5}, 6.8×10^{-6} and 4×10^{-5} resp.

2.1. Kurucz models

We use the well-known plane parallel LTE line blanketed models of Kurucz (1991, 1994). Computations were done for models with $T_{\rm eff}$ (and $\log(g)$) between 26 and 50 kK (3.0 and 5.0). For stability reasons, the available high $T_{\rm eff}$ models are restricted to cases of high gravity. The employed *Kurucz* models are therefore representative of dwarfs rather than supergiants mostly considered for the other model atmospheres (cf. below).

2.2. TLUSTY

A grid of plane-parallel non-LTE line blanketed models based on the *TLUSTY* code of Hubeny & Lanz (1995) has recently been calculated using a super-level approach and an Opacity distribution function or a modified opacity sampling (Lanz & Hubeny 2003a,b). About 100 000 individual atomic levels have been included, for more than 40 ions of H, He, C, N, O, Ne, Si, P, S, Fe and Ni, using a superlevel approach. For all the models, a standard microturbulent velocity $V_{\rm turb}$ = 10 km s^{-1} has been used. The parameter space of the grid covers 27 500 K $\leq T_{\rm eff} \leq$ 55 000 K with 2500 K steps and 3.0 $\leq \log(g) \leq$ 4.75 with 0.25 dex steps. Up to 10 different metallicities, from 2 times solar to metal free chemical composition, have been considered by Lanz & Hubeny (2003a,b)[1]. We extracted from this database models with $T_{\rm eff}$ ($\log(g)$) ranging from 30 to 50 kK (3.0 to 4.0), with solar metallicity.

2.3. CoStar

The *CoStar* models of Schaerer & de Koter (1997) include stellar winds, treat H−He in full non-LTE, and include line blanketing effects with an opacity sampling method based on Monte-Carlo simulations (Schmutz 1991). The impact of these effects on the ionizing fluxes and nebular diagnostics of H II regions has been discussed in detail by Stasińska & Schaerer (1997).

For our computations we use *CoStar* models with the lowest value for $\log(g)$, i.e. models D5, D4, D3, E3, F3, F2 and F1 from the *CoStar* grid of Schaerer & de Koter (1997). The $T_{\rm eff}$ (and $\log(g)$) range from 27 kK (2.9) to 53 kK (4.1).

2.4. WM-Basic

The *WM-Basic* models of Pauldrach et al. (2001) treat a large number of ions in non-LTE and include their line blocking effect by means of an opacity sampling technique. The atmospheric structure is computed from the hydrodynamic equations including radiative acceleration from numerous metal-lines and continua. We used the grid available on the web[2] and described in Pauldrach et al. (2001) for Supergiant models with $T_{\rm eff}$ (and $\log(g)$) ranging from 30 kK (3.0) to 50 kK (3.9).

2.5. CMFGEN

We have constructed spherically symmetric wind models, using the non-LTE, comoving frame code *CMFGEN* (Hillier & Miller 1998). This code solves the radiative transfer equation, together with the statistical equilibrium equations, and line blanketing is self-consistently taken into account, using a super-level formulation. The chemical elements included in our model calculations are H, He, C, N, O, S, Si and Fe. For the 28 ions explicitly treated, a total of 2292 levels distributed in 819 superlevels are included, representing 22 762 bound-bound transitions. Atomic data for Fe IV and Fe V have been slightly improved, compared to those first introduced in *CMFGEN* (Hillier & Miller 1998) and made consistent with those used in *TLUSTY*. As shown in Bouret et al. (2003), this was required to get a very good agreement in the determination of iron abundances, when fitting lines of these two successive ionization stages in individual O stars in NGC 346, the largest H II region in the SMC. The temperature structure is calculated from the assumption of radiative equilibrium. The atmospheric structure consists of the wind, parameterized by the classical β-law, which is connected to hydrostatic layers obtained from the ISA-Wind code of de Koter et al. (1996), such that at the connecting point both the velocity and velocity gradient match. We assume a constant Doppler profile of 20 km s^{-1} for all lines. As shown by Martins et al. (2002) for dwarfs and by additional test calculations this assumption leads to negligible changes of emergent spectrum. The stellar parameters, including the abundances, used to compute the *CMFGEN* grid of supergiants are identical to those used by *WM-Basic* and described in Pauldrach et al. (2001).

2.6. Atmosphere models for Dwarf stars

The main results of the present paper are obtained for Supergiant stars. Nevertheless, we also computed grids of photoionization models using Dwarf stellar atmosphere models as ionizing spectrum, to check the effect of $\log(g)$ on the excitation of the nebula. In this purpose, *WM-Basic* D models from Pauldrach et al. (2001) have been used. We have also computed *CMFGEN* models using the same set of parameters than those used for the *WM-Basic* D models.

The models using Dwarf stellar atmosphere are discussed in Sect. 5.3.

2.7. Rebinning of the ionizing spectra

For subsequent use in our photoionization code NEBU (described in Sect. 3) the different atmosphere models have to be rebinned to the energy grid used in this code. The SEDs are first converted to the units used in NEBU (number of photons/eV/s/cm^2). The SED is then interpolated on the NEBU grid, such as to preserve the integrated number of photons in each energy interval in NEBU. For most of the energy intervals, the number of points in the original stellar atmosphere domain is some tens to some hundreds, giving a good accuracy for the rebinning. Note that despite the much lower number of points used to describe the ionizing spectrum in NEBU, the results are reliable, as the most important quantities are the number of photons able to ionize the different ions. The grid points actually fully takes into account the discontinuities at the ionisation thersholds of the differents ions.

2.8. Comparing the EUV spectra

Figure 1 present all the Supergiant models used in this paper in a $\log(g)$ versus $T_{\rm eff}$ diagram. The values for $\log(g)$ at a given $T_{\rm eff}$ are very close together, with the exception of the *Kurucz* models, which have a systematic higher value

[1] This grid is available at `http://tlusty.gsfc.nasa.gov`

[2] `http://www.usm.uni-muenchen.de/people/adi/Models/`

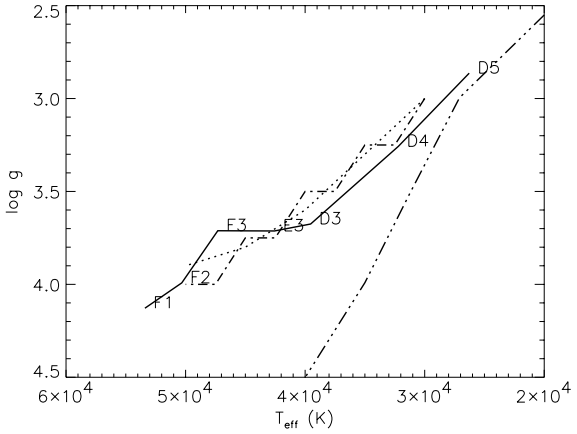

Fig. 1. Position in a log (g) versus $T_{\rm eff}$ diagram of the Supergiant models and the *Kurucz* dwarf models used in this paper. See Fig. 2 for the line symbols. *CoStar* models are labeled according to the original naming convention. *CMFGEN* models have the same parameters than *WM-Basic* models and are not drawn here.

for log (g), up to be even higher than the value adopted for Dwarf models (see also Fig. 1 in Schaerer & de Koter 1997).

Figure 2 illustrates the differences in the SED obtained from different atmosphere models after the rebinning procedure described above, for the same $T_{\rm eff}$, here 35 and 40 kK, with the exception of *CoStar* model for which no value at 35 kK is available in the Supergiant subset of models used here, model D4 at 32.2 kK is plotted. While the five models agree quite well in the domain of energies lower than 20 eV (and very well in the optical and IR range, not shown here), their differences can be as big as 4 orders of magnitudes just before 4 Rydberg. In this paper, we will use IR lines to trace the SED between 27, 35 and 41 eV (see next section), where the models differences already reach 1 to 2 orders of magnitude.

Of more interest for the analysis of the behavior of the fine-structure lines is the distribution of the ionizing photons at each energy. This is quantified by Q_E, which is the number of photons with energy greater than E, shown in right panels of Fig. 2. More precisely, the relevant quantity determining the nebular structure and properties would be the photon output weighted by the photoionization cross section. In the range of energy traced by the excitation diagnostics, 27−41 eV, the behavior of the four models is very different. We will discuss this further in Sects. 5.1 and 6.1.

3. Grid of photoionization models

Extensive grids of photoionization models were computed with the NEBU code (Morisset & Péquignot 1996; Péquignot et al. 2001; Morisset et al. 2002) in order to evaluate in detail the dependence of the mid-IR atomic fine-structure line emission of Galactic H II regions on the atmosphere models, and the stellar and nebular properties. Our main aims are a) to derive constraints on the stellar ionizing spectra and b) to examine the origin of the observed excitation gradients in (compact) Galactic H II regions.

In principle nebular emission line properties depend on fairly a large number of parameters, namely:

- the shape of the stellar ionizing spectrum, determined (mostly) by the stellar temperature $T_{\rm eff}$, gravity, and metallicity $Z_\star$;
- the ionization parameter $U(r) = Q_{13.6}/N_{\rm e}4\pi r^2 c$. As the geometry of the H II regions modeled here is an empty cavity surrounded by an ionized shell, we prefer to use hereafter the mean ionization parameter $\bar{U} = U(\bar{r})$, computed following Evans & Dopita (1985) at a distance from the ionizing star $\bar{r} = r_{\rm empty} + \Delta R/2$, where $r_{\rm empty}$ is the size of the empty cavity and ΔR the thickness of the H II shell[3]. $\bar{U}$ is essentially given by the ratio of the ionizing photon density over the nebular particle density, i.e. properties of the ionizing source and the nebular geometry;
- the nebular abundances/metallicity $Z_{\rm gas}$;
- atomic parameters driving the ionization equilibrium and line emissivities, e.g. photoionization cross section, recombination coefficients (radiative and dielectronic), collisional excitation cross sections, etc.;
- other secondary parameters like the presence of dust.

There is no doubt the existence of a systematic metallicity variation among the observed sources considered below. On the other hand, as for most of these objects (compact/ultra-compact H II regions) the properties of the ionizing source(s) and their geometry are not known, it is imperative to assess the impact of all parameters on the observables and to establish that the conclusions drawn from comparisons with observations are robust in this respect. The dependence of the emission line properties on the above parameters is examined in Sect. 5 with the help of photoionization models computed for a wide range of model parameters.

The bulk of "standard" models were computed for the following cases/assumptions. The ionizing spectra from the five atmosphere models described in Sect. 2 and plotted in Fig. 2 plus blackbody spectra are adopted. Stellar $T_{\rm eff}$ ranging from 30 to 50 kK were used. This range in $T_{\rm eff}$ is likely to describe the physical conditions of the sample of H II regions (Morisset 2003). For most cases we assume a solar composition for the nebular and stellar abundances. Metallicity variations are considered in Sect. 5.5. For each of these stellar atmosphere, series of photoionization models were computed for the following nebular parameters. We set the electron density to 10^3 cm^{-3}, one order of magnitude below the lowest critical density of the lines under consideration (cf. Martín-Hernández et al. 2002a). An empty cavity of radius 3×10^{17} cm is assumed. The luminosity of the ionizing star is adjusted to lead to a constant number of Lyman continuum photons ($Q_{13.6} = 1.5\times10^{49}$ s^{-1}) corresponding to an ionization parameter log (U) = −1.5. Additional models quantifying the effect of variations of $\bar{U}$ are presented in Sects. 5.2, 5.4, and 6.2.

[3] For U derived at the Strömgren radius without empty cavity one has $U \propto (QN_{\rm e}\epsilon^2)^{1/3}$, with the filling factor ϵ.

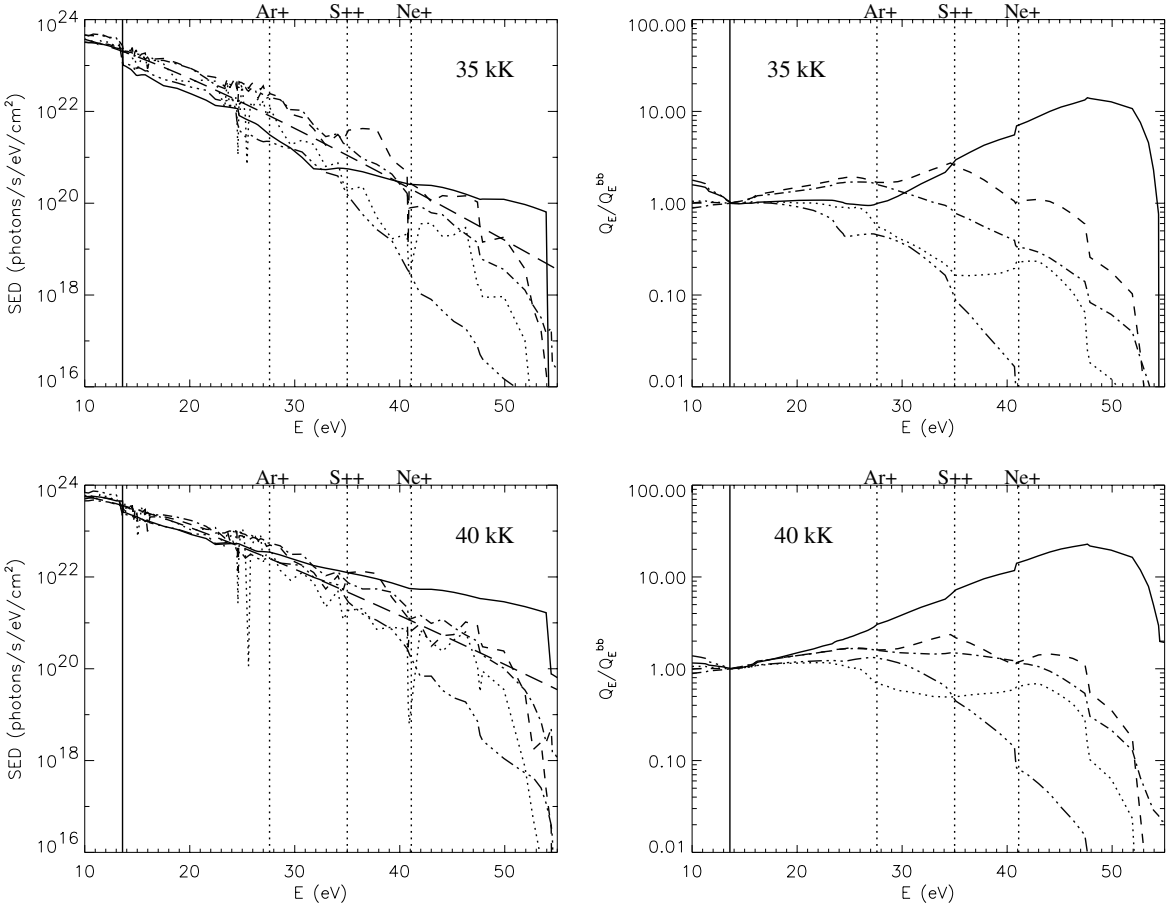

Fig. 2. Comparison between the 6 stellar atmosphere models: *CoStar* (solid), *WM-Basic* (dotted), *CMFGEN* (dashed), *TLUSTY* (dash dot), *Kurucz* (dash dot dot) and the Blackbody (long dashes, left panels only), for the same $T_{\rm eff}$ of 35 kK (upper plots), except for *CoStar* model (see text), and 40 kK (lower plots). The left panels show the Spectral Energy Distribution and the right panels show, for any energy E (eV), the number Q_E of photons with energy greater than E, relative to the corresponding number for the Blackbody emission, all the spectra having the same value for $Q_{13.6}$. Vertical lines are plotted at 13.6 eV (solid) and 27.6, 35.0 and 41.1 eV (dotted), corresponding to the ionization potentials of the ions considered in this paper (Ar^+, S^{++}, and Ne^+ resp.).

The effect of dust can be included in the photoionization computation, with two different optical properties corresponding to graphite or astronomical silicate (see Sect. 5.6).

The observables predicted from these extensive model grids will be compared to observations in Sect. 5.1.

4. The ISO H II regions catalogs

Infra-red spectra between 2.3 and 196 μm were taken from a sample of 43 compact H II regions using the two spectrometers (SWS and LWS) on board ISO (Peeters et al. 2002). Details about the data reduction and a first analysis of the ionic lines in terms of abundances can be found in Martín-Hernández et al. (2002a). Error bars on the lines intensities are within 10% to 20%. Note that a detailed study of one source has been achieved in Morisset et al. (2002).

Giveon et al. (2002b) published a catalog of 112 H II regions observed by ISO SWS spectrometer. Some of the sources are common with the Martín-Hernández et al. (2002a) catalog. The two catalogs are very coherent in terms of line intensities, as concluded by Giveon et al. (2002a), and are therefore included in our analysis. The effect of local and interstellar attenuation, even if lower in the IR range used in this work than for the optical domain, can be important and need to be corrected for. We correct the observed line intensities from the reddening using the extinction law described in Table 2 of Giveon et al. (2002a).

In the SWS and LWS spectral domain, 4 fine-structure line ratios are sensitive to the ionizing flux distribution: [Ar III] 8.98 μm/[Ar II] 6.98 μm, [N III] 57.3 μm/[N II] 121.8 μm, [S IV] 10.5 μm/[S III] 18.7 μm, and [Ne III] 15.5 μm/[Ne II] 12.8 μm, hereafter [Ar III/II], [N III/II], [S IV/III], and [Ne III/II] respectively.

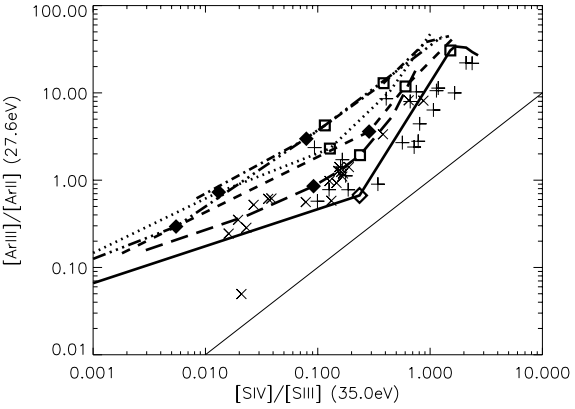

Fig. 3. Dereddened observed values for the excitation sensitive line ratio [Ar III/II] versus [S IV/III] (the corresponding ionization potentials are also given). Source with a galactocentric distance lower than 7 kpc are symbolized with a +, otherwise with an X. Results from the photoionization model grid are line plotted using the same codes as in Fig. 2. The plot have been done such as the lowest ionization potential (indicated in braces) is always on the y-axis. Models obtained with 35 and 40 kK stars are shown using filled diamonds and empty squares respectively (except for *CoStar* model at 32.2 kK, empty diamond, see text). The $y = x$ line is also drawn.

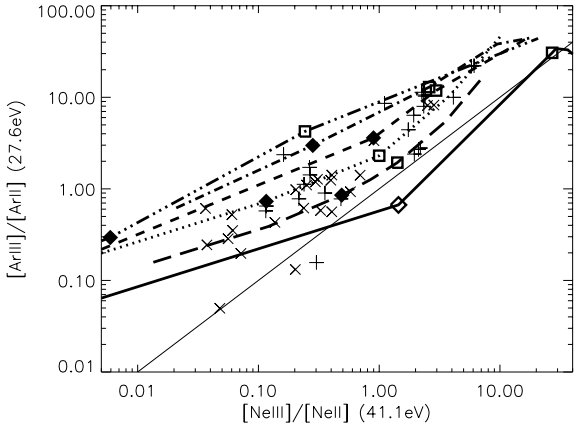

Fig. 4. Same as Fig. 3 for the excitation sensitive line ratio [Ar III/II] versus [Ne III/II].

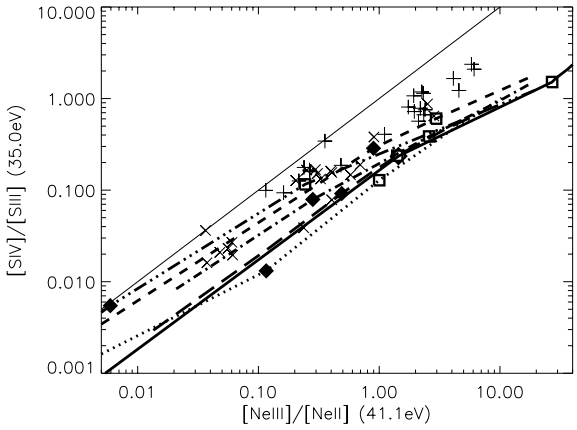

Fig. 5. Same as Fig. 3 for the excitation sensitive line ratio [S IV/III] versus [Ne III/II].

The excitation ratio implying nitrogen lines will not be used in the next discussion, since: 1) the two nitrogen lines are observed by LWS spectrometer, with a larger aperture size than the SWS: some nitrogen emission can arise from regions not seen in the other lines; 2) Giveon et al. (2002b) have observations only with SWS and then the number of observational constraints strongly decrease when using only Martín-Hernández et al. (2002a) data; 3) the critical densities of the nitrogen lines are very low compared to the one of the other lines (see Martín-Hernández et al. 2002a) and will not be emitted by medium density gas which can still emit the other lines, and 4) the ionization potential of N^{++} is very close to the one of Ar^{++} (29.7 and 27.6 eV resp.), so the main conclusions regarding the 30 eV energy domain will be obtained from argon lines.

Depending on the element, the number of sources for which we have finite value for the corrected excitation ratios is ranging from 45 to 51. Error bars on the line intensities are approximately 10 to 20%.

5. Excitation diagnostics

Figures 3 to 5 show the main results of the photoionization models using different atmosphere models for the ionizing star (lines), and the deredenned observed values, for the two merged catalogs (Martín-Hernández et al. 2002a; Giveon et al. 2002b). As we consider 3 diagnostic ratios, 3 plots can be drawn. The models obtained with $T_{\rm eff}$ = 35 and 40 kK are symbolized by filled diamonds and open squares respectively. The open diamond indicates a *CoStar* model at 32.2 kK as no model at 35 kK is available.

In principle the position of a model in such diagrams depends on all the following parameters: the hardness of the stellar SED (parametrized here for each set of model atmospheres by $T_{\rm eff}$ for a fixed stellar metallicity) and the main nebular parameters, i.e. the ionization parameter $\bar{U}$ and the nebular composition. Let us consider first the case of constant (solar) metallicity and constant $\bar{U}$ (but see Sects. 5.2, 5.4 and 5.5). In this case the location of a point on such diagnostic diagrams depends only on *a)* the global excitation of the gas and *b)* the "slope" of the ionizing photon distribution between the two corresponding ionization potentials. For constant $\bar{U}$ and a given set of atmosphere models the excitation (*a*) is determined by $T_{\rm eff}$. In other words, when $T_{\rm eff}$ increases, the number of ionizing photons at all the energies traced by the observed ions increases, and the points in the excitation diagrams will essentially move along the diagonal ($y = x$) direction. Note, however, that different atmosphere models with the same $T_{\rm eff}$

predict fairly different absolute positions in these plots. This simply reflects the differences in the predicted number of ionizing photons above the relevant energy (cf. Fig. 2).

For a given line ratio the other line ratios depend to the first order on the "slope" of the ionizing spectra (b). More precisely, the relevant quantity is the slope of the cumulative number of ionizing photon flux Q_E between the corresponding ionization potentials (see right panels in Fig. 2). For example, *TLUSTY* and *Kurucz* models show in general the softest spectra (i.e. steepest slopes) between 27.6 and 41.1 eV. For a given [Ne III/II] these models therefore show the highest [Ar III/II] values.

For the assumptions made here (constant $\bar{U}$ and metallicity) each location of the model results in the three excitation diagrams can be approximately understood in terms of the ionizing photon distributions Q_E. The correspondence is not always exact, as some competitive processes take place in the use of the ionizing photons, but the overall trends can be simply understood from the shapes of the spectra. Other additional assumptions (e.g. on the luminosity class of the exciting sources, the presence of dust, and uncertainties of the atomic data) also affect the predicted excitation diagrams. These effects are discussed below.

The observed excitations, correlated between the three excitation ratios [Ar III/II], [S IV/III], and [Ne III/II], can be decomposed into two components: an excitation sequence showing a global increase of the excitation ratios over ∼2 orders of magnitude, following to first order a trend parallel to $y = x$ in the excitation diagrams, and a superposed excitation scatter of typically ∼0.5−1 order of magnitude around the mean excitation (cf. Figs. 3 to 5, but see also Figs. 19 and 20, where excitations versus metallicity are plotted).

5.1. First comparison with the observations

The zero-th order trend of the observations plotted in Figs. 3 to 5 is reproduced by the models: the excitation of the ionized gas, traced by the X^{i+1}/X^i ratios, are well correlated. A $T_{\rm eff}$ sequence from ∼30 to 45 kK succeeds in reproducing the entire range of gas excitations. Note however, that, as discussed below (Sect. 7.2), this does not imply that the ionizing stars of our objects indeed cover this range of $T_{\rm eff}$.

Fairly large differences are found in the predicted excitation diagnostic diagrams (Figs. 3 to 5) when using different atmosphere models. As expected from the intrinsic SEDs, the largest differences are found in Fig. 4, which traces the largest energy domain (∼28 to 41 eV) corresponding to the [Ar III/II] and [Ne III/II] ratios.

When taken literally (i.e. assuming a fixed constant value of $\bar{U}$ for all atmosphere model sets and a fixed solar metallicity) Figs. 3 to 5 indicate the following concerning the shape of the ionizing spectra.

1. Both recent codes, *WM-Basic* and *CMFGEN*, show a reasonable agreement with the observations. Given their different behavior in the three excitation diagnostics depending on luminosity class (cf. Sect. 5.3), and other remaining uncertainties discussed subsequently, it seems quite clear that none of the models can be preferred on this basis. Despite these similarities we note, however, that an important offset is found in the excitation ratios predicted by these codes for a given absolute value of $T_{\rm eff}$ (cf. Sect. 6.1).
2. Both plane parallel hydrostatic codes (*Kurucz*, *TLUSTY*) predict spectra which are too soft, especially over the energy range between 27.6 and 41.1 eV and above. For the *Kurucz* LTE models this problem is just a manifestation of the well-known "Ne III" problem (Rubin et al. 1988; Simpson et al. 1995; Stasińska & Schaerer 1997). This problem is persistently found with the non-LTE *TLUSTY* models. Although not completely clear, this "softness" is likely due the neglect of wind effects which are known to alter the ionizing spectrum (cf. Gabler et al. 1989; Stasińska & Schaerer 1997) albeit in fairly complex way involving line blanketing from large numbers of metal-lines.
3. As already found in other investigations (cf. Oey et al. 2000; Schaerer 2000, and references therein) we see that the *CoStar* models (showing the hardest spectra among the ones considered here) overpredict somewhat the ionizing flux at high energies. This likely overestimate of the ionizing flux at high energy (cf. below) must be due to the approximate and incomplete treatment of line blanketing (see also Crowther et al. 1999; Martín-Hernández et al. 2004).
4. Interestingly blackbodies reproduce best the observed excitation diagrams, which indicates a posteriori that the ionizing spectra should have relative ionizing photon flux productions (Q_E at energies 27.6, 35.0 and 41.1 eV) close to that of blackbody spectra. This will be discussed in more detail in Sect. 7.

We note that the results concerning *CMFGEN*, *WM-Basic*, *CoStar*, and *Kurucz* models presented here confirm and support those presented by Stasińska et al. (2002) in terms of position of the models between each other in the [Ar III/II] versus [Ne III/II] excitation diagram and distance to the H II regions observations (cf. below).

5.2. Main dependences: Stellar temperature, ionization parameter, metallicity

For clarity it is useful to discuss first the dependences of the excitation diagnostics on the main parameters, i.e. the stellar temperature, ionization parameter, and metallicity. This is illustrated here somewhat schematically for the case of the [Ne III/II] versus [Ar III/II] diagnostic. Qualitatively the same results are found for the other excitation diagrams.

An increase of the stellar temperature $T_{\rm eff}$ or ionization parameter $\bar{U}$ or a decrease of the metallicity all lead overall to a higher excitation of the nebula, which e.g. manifests itself by larger [Ne III/II] and [Ar III/II] line ratios. However, although both line ratios change in similar ways, their effect is distinguishable to some extent. This is illustrated in Fig. 6, which shows for blackbody (and *WM-Basic*, see Sect. 5.5) spectra the implied shift in the [Ne III/II] versus [Ar III/II] excitation diagnostics due to a change of $T_{\rm eff}$, $\bar{U}$ and $Z_{\rm gas}$ (consistent changes of both the stellar and nebular metallicity are discussed

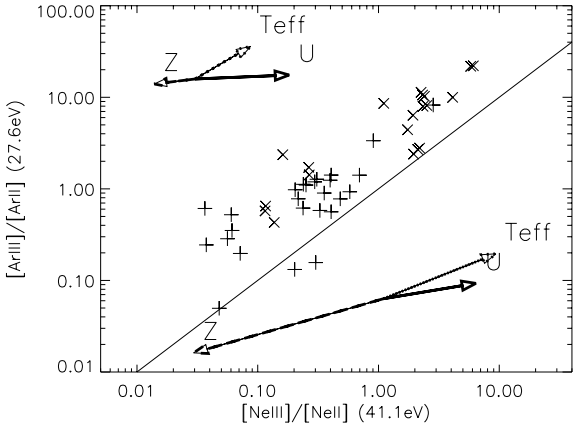

Fig. 6. Increase of the excitation diagnostics [Ar III/II] versus [Ne III/II], when $\log(\bar{U})$ is increased from −2.6 to −0.8 (solid arrows), when the metallicity of the gas is increased from half solar to twice solar (dashed arrows), and when $T_{\rm eff}$ is increasing from 35 to 40 kK (dotted arrows). Upper set of arrows are for BlackBody models, and lower set for *WM-Basic* models. In the latter case the metallicity is changes coherently for both the gas and the star. Codes are the same than in Figs. 2, 3.

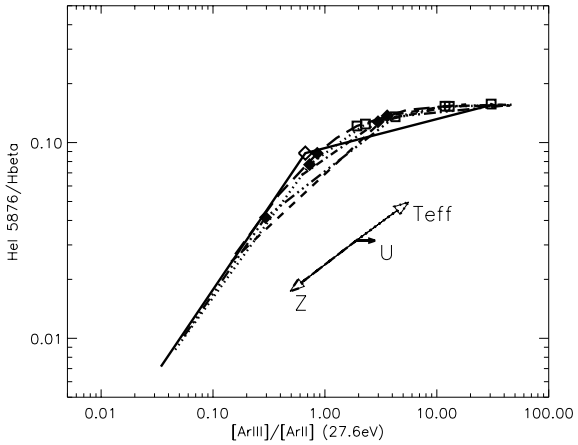

Fig. 7. Correlation between He I 5876 Å/H_β and [Ar III/II]. The line styles are the same as in Fig. 2. Arrows have the same meaning as in Fig. 6, for *WM-Basic* models only.

in Sect. 5.5). From this figure we see that $T_{\rm eff}$ and $\bar{U}$ variations are not completely degenerate (i.e. "parallel").

Also, an increase of the nebular metallicity leads to a (very) small decrease of the excitation diagnostics, quite parallel to the variations induced by changing $\bar{U}$. The effect of changing coherently the metallicity of both the H II region and the star (which is principally acting on excitation diagnostics) are considered in Sect. 5.5.

The effect of continuum absorption by dust inside the H II region on the excitation diagnostics is also parallel to changes of $T_{\rm eff}$, and is discussed in Sect. 5.6. Although quantitatively these variations depend e.g. on the adopted SED (and of the point in the $T_{\rm eff}$-$\bar{U}$-Z space chosen to compute the partial derivatives traced by the arrows in Fig. 6), these qualitative distinctions remain valid for the entire parameter space considered in the present paper and will be useful for the discussions below.

Note that earlier investigations have considered that changes of $\bar{U}$ are completely degenerate with $T_{\rm eff}$ (Giveon et al. 2002b; Martín-Hernández et al. 2002b)[4], or have simply assumed an arbitrarily fixed, constant value of $\bar{U}$ (Martín-Hernández et al. 2004).

As apparent from Fig. 6, [Ar III/II] varies little with $\bar{U}$ in comparison with other mid-IR excitation ratios. This behavior is easily understood, as explained in the following brief digression.

In $T_{\rm eff}$ and $\bar{U}$ domain used in this work, the [Ar III/II] ratio is controlled by the helium equilibrium: the IPs of Ar^+ and He^0 are closed together (27.7 and 24.6 eV resp.); in this energy domain the photon dominant predator is He^0. The Ar^{++} region (Ar^+) is then cospatial with the He^+ (He^0) region (Some Ar^+ can also be present in the He^+ region, depending on the ionization parameter). The H II regions modeled here are all radiation bounded, the size (and the emission) of the He^+ and Ar^{++} region is mainly proportional to $Q_{24.6}$, while the size of the He^0 and Ar^+ region is controlled by the size of the H II region removing the He^+ region. [Ar III/II] is then mainly controlled by $Q_{24.6}/Q_{13.6}$. The previous argumentation is valid only if the recombination of Ar^{++} remains quite small, which is not the case when strong dielectronic recombination occurs. In this case, the Ar^+ region penetrates inside the He^+ region, and the [Ar III/II] is decreased (see Sect. 5.7 for the effects of dielectronic recombinations of Ar^{++}.) Nevertheless, using atmosphere models instead of BlackBody leads to a more important increase of [Ar III/II] while increasing $\bar{U}$, as seen in Fig. 6.

The extreme correlation between He^+/H and Ar^{++}/Ar^+ can be verified in Fig. 7, where He I 5876 Å/H_β versus [Ar III/II] is plotted, for all the atmosphere models. While the He I 5876 Å/H_β ratio saturate at a value between 0.1 and 0.2, the [Ar III/II] excitation diagnostic still evolve with $T_{\rm eff}$. This will be discussed further in Sect. 6.1.

5.3. Comparing results of Supergiant and Dwarf stars

The results shown in previous sections are obtained for Supergiant stars. Models were also performed using Dwarfs stars (see description in Sect. 2.6). The decrease of $\log(g)$ changes the shape of the ionizing radiation, as shown in Fig. 8, where Q_E is shown for Supergiants and Dwarfs atmosphere models obtained using *CMFGEN* and *WM-Basic*, all at 35 kK. The main effect of increasing $\log(g)$, observed on the two models, is to decrease strongly Q_E at 41 eV, and to increase the slope of Q_E between 27 and 41 eV. This overall hardening of the ionizing flux for stars with lower gravity is due mostly to an

[4] For their grids the ionization parameter U defined at the Strömgren radius vary actually by ∼0.1 (supergiant grid) and 0.3 dex (dwarfs).

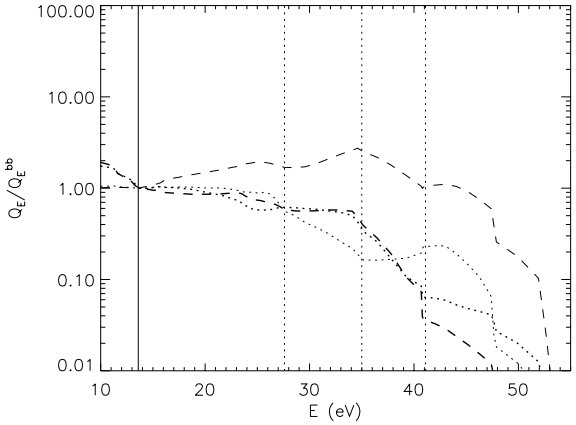

Fig. 8. Comparison between energy distribution (same as right panels of Fig. 2) between Supergiants (light curves) and Dwarfs (bold curves) of *WM-Basic* (dotted) and *CMFGEN* (dashed) models, all at 35 kK.

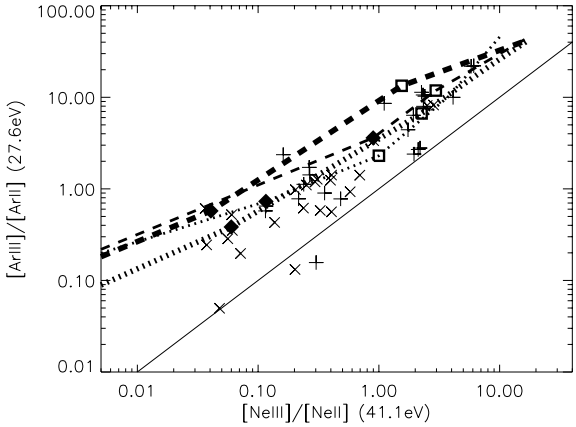

Fig. 9. Comparison between excitation diagnostic [Ar III/II] obtained with Supergiants (light curves) and Dwarfs stars (bold curves), for *WM-Basic* (dotted) and *CMFGEN* (dashed) atmosphere models. Models at 35 and 40 kK are shown by filled diamonds and empty squares respectively.

increased ionization in the continuum forming layers, the latter effect resulting from the increased wind density (mass-loss rate).

Figure 9 shows the excitation diagram [Ne III/II] versus [Ar III/II] performed using the models described above, comparing the Supergiant (light curves) and Dwarf (bold curves) results for both *CMFGEN* (dashed) and *WM-Basic* (dotted).

As expected from the increased hardness of the ionizing fluxes for supergiants, the use of dwarf atmospheres leads in general to an excitation decrease which is more important at the highest energies (i.e. [Ne III/II] decreases more rapidly than [Ar III/II])[5]. Overall the differences between supergiant and dwarf spectra do not importantly affect our conclusions.

5.4. Effect of changing the mean ionization parameter $\bar{U}$

Given that the ionizing sources and the nebular geometry of the observed objects are essentially unknown and $\bar{U}$ therefore as well, it is important to examine how robust the above results are with respect to changes of $\bar{U}$. E.g. is it possible to reconcile the discrepant predictions using the *Kurucz* and *TLUSTY* atmosphere models (i.e. to increase the predicted [Ne III/II] ratio of a given [Ar III/II]) by invoking a larger ionization parameter toward the low excitation end of the observed sequence? As shown in Sect. 5.2 and by detailed model calculations, variations of $\bar{U}$ imply changes nearly parallel to the "standard" sequences for the *Kurucz* and *TLUSTY* atmosphere models, similar to the case of *WM-Basic* models shown in Fig. 6.

We can therefore quite safely conclude that variations of $\bar{U}$ cannot reconcile the *Kurucz* and *TLUSTY* atmosphere models with the observation. However, for the other model atmospheres showing more "curved" predictions in the excitation diagrams, variations of $\bar{U}$ might be invoked to improve/alter the predicted sequences for constant $\bar{U}$.

5.5. Effect of adopting a metallicity gradient, for both the stellar atmosphere and the ionized gas

It is well known that the metallicity decreases in the Galaxy when the distance to the center increases (e.g. Giveon et al. 2002a; Martín-Hernández et al. 2002a, and references therein). The metallicity varies approximately by a factor 4 from the center out to 15 kpc, where the most external regions used in this work are located (cf. Fig. 19).

Figure 6 shows the effect of changing the metallicity Z coherently in the ionizing star's SED computation and of the ionized gas in the photoionization computation, from half solar to twice solar. A metallicity increase in the atmospheres leads to a stronger blanketing with the effect of softening the EUV spectra of early type stars (e.g. Pauldrach et al. 2001), leading thus to a lower nebular excitation. As seen by comparing the Z-arrows in Fig. 6 and by additional test calculations, the increase of the nebular abundance plays a minor role in the resulting excitation shift.

In fact the *WM-Basic* models used here show that the ionizing spectra soften too strongly with increasing metallicity, leading to a stronger reduction of [Ne III/II] compared to [Ar III/II]. This results in a progressive shift away from the observed sequence toward higher metallicity. This discrepant trend, also found by Giveon et al. (2002b), was actually used by these authors to argue that the observed excitation sequence was mostly driven by $T_{\rm eff}$ variations. However, as abundances of these sources are known to vary by approximately the same factor as the Z variations considered here for the *WM-Basic* models, metallicity cannot be neglected. Therefore the

[5] The *WM-Basic* model at 35 kK shown here is an exception to this trend, however.

discrepancy between the observations and the expected changes of [Ne III/II] and [Ar III/II] show that the predicted softening of the *WM-Basic* ionizing spectra with metallicity at high energies ($\gtrsim$41 eV) is probably incorrect. Alternate solutions to this puzzle include postulating a increase of $\bar{U}$ toward higher Z (cf. above), or processes currently not accounted for in the *WM-Basic* models altering the high energy part of the SED (cf. Sect. 5.8), or changes in atomic physics parameters (cf. Sect. 5.7).

5.6. Effect of the dust

The effect of the presence of dust inside an H II region is firstly to decrease the global amount of ionizing photons from the point of view of the ionized gas, the effect being then to reduce the ionization parameter. On the other hand, the efficiency of dust in absorbing of the ionizing photons inside the H II region decreases with the energy of the photons after about 18 eV (e.g. Mathis 1985; Aannestad 1989), the global effect being to increase the excitation of the gas when increasing the amount of dust, for a given ionization parameter. As already pointed out by Morisset et al. (2002) for the case of ISO observations of G29.96−0.02, if dust is present in H II regions, quite the same excitation of the gas will be recovered using an higher ionization parameter and a lower $T_{\rm eff}$. As illustration, inclusion of Graphite and Astronomical Silicate dusts, in proportion of 2.5×10^{-3} relative to hydrogen, for each type of dust, leads to an increase of all the excitation diagnostic ratios by a factor close to 2. The excitation increase due to dust is found to be "parallel" to a $T_{\rm eff}$ increase to reasonable accuracy, when keeping $\bar{U}$ constant.

5.7. Effect of the atomic data

Could uncertainties in the atomic data affect the results? Indeed, from Figs. 3 to 5, we could suspect the argon ionization equilibrium to be wrong, favoring the emission of [Ar III]. This could e.g. be due to an overestimation of the ionizing flux at 27.6 eV with respect to higher energies, or to a systematic error in the observed intensities of one of the two lines involved in the [Ar III/II] ratio ([Ar III] 8.98 μm is affected by silicate band). However, we cannot exclude also the effect of atomic data in the photoionization computation. Collisional rates are generally believed to be accurate within 20%, while our knowledge of recombination coefficients are less probant. Dielectronic recombination coefficients for the elements of the third row of the periodic Table are poorly known, and even the new computations done today are usually only for the first and second rows, corresponding to highly charged elements of the third rows, which is not the case for Ar^{++} (see e.g. Savin & Laming 2002). Dielectronic recombination coefficients have been computed for less charged third row elements by e.g. Mazzotta et al. (1998), but only for high electron temperature (coronal gas), which is not the case for H II regions. Very recently, new dielectronic recombination rates have been computed for Ar^{++} (Zatsarinny et al. 2003, private communication), but the results these authors obtain have still to be checked (dielectronic recombination rates reach values as 10^3 times the classical recombination rates for electron temperature closed to 10^4 K!).

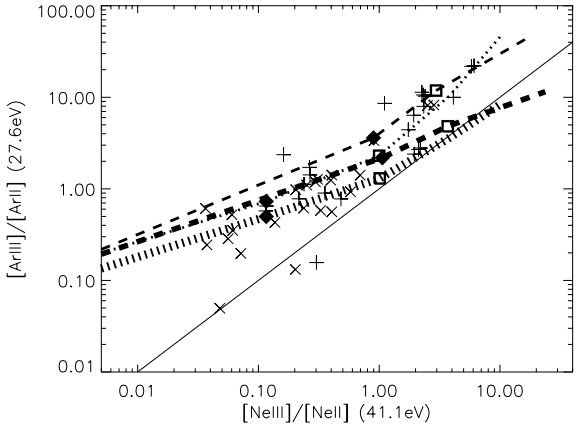

Fig. 10. Variation of the excitation diagnostics [Ne III/II] versus [Ar III/II] for the same atmosphere models (here *WM-Basic* and *CMFGEN*, dotted and dashed thin lines respectively), multiplying the effective recombination coefficient for only Ar^{++} by 10 (bold lines).

To simulate the effect of dielectronic recombination and charge transfer reactions we have multiplied the classical recombination coefficient for Ar^{++} by factors up to 20. Figure 10 shows the effects of multiplying this coefficient arbitrarily by 10, on the excitation diagnostics [Ar III/II] versus [Ne III/II]. The figure shows results using *WM-Basic* and *CMFGEN* models, but the same effect can be observed with any of the atmosphere models used in this paper.

The increase of the recombination coefficient improves overall the agreement with the observed sequence, although new discrepancies appear now at the high excitation end. However, no dependence of the dielectronic recombination coefficient on the electron temperature $T_{\rm e}$ has been taken into account here. As $T_{\rm e}$ is known to vary along the excitation sequence this could in fact "twist" the global shape of the predicted excitation sequence. Currently both the exact "direction" and importance of this effect remain, however, unknown. Note, that the uncertainties due to atomic data of Ar were already pointed out by Stasińska et al. (2002). We join these authors in encouraging atomic physicists to improve our knowledge of such data.

5.8. Effects not included in atmosphere models

What could be the limitations of the most sophisticated atmosphere models currently available, capable of altering the excitation diagnostics discussed here? Although an exhaustive discussion is obviously not possible, one can suspect one major process, namely the presence of X-rays, to alter in a non-negligible way the ionizing spectra of O stars. This has been shown clearly by Macfarlane et al. (1994), and has been discussed later e.g. by Schaerer & de Koter (1997). The relative importance of X-rays compared to normal photospheric

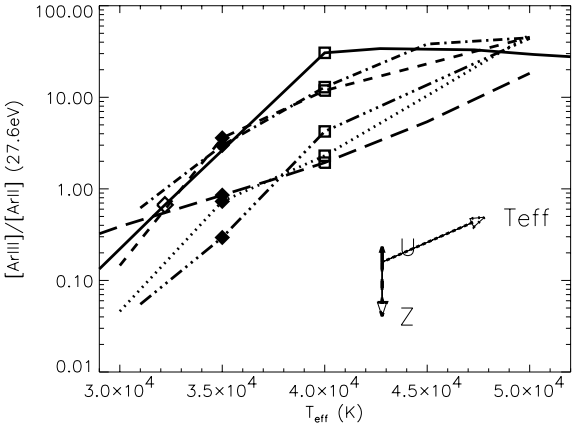

Fig. 11. Variation of the excitation diagnostic [Ar III/II] according to the $T_{\rm eff}$ of the ionizing star. Codes are the same as in Figs. 2, 3. The set of arrows have the same meaning as in Fig. 6, for *WM-Basic* models only.

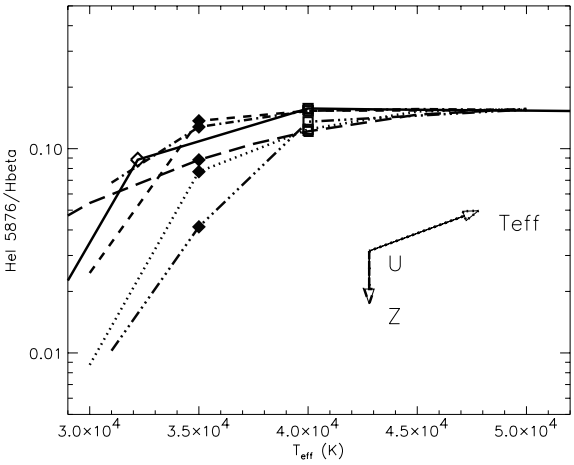

Fig. 12. Variation of the optical excitation diagnostic He I 5876 Å/H$_\beta$ with $T_{\rm eff}$ for supergiant stars. Codes are the same as in Figs. 2, 3. The set of arrows have the same meaning as in Fig. 6, for *WM-Basic* models only.

emission is expected to increase for stars with weaker winds and toward later spectral types. In late O types their contribution can be non-negligible down to energies ≳30 eV, see e.g. Macfarlane et al. (1994) and a model at $T_{\rm eff}$ = 30 kK by Pauldrach et al. (2001), with obvious consequences on nebular diagnostics. Regrettably few models treating the X-ray emission in O stars exist, their impact on the overall emergent spectrum including the EUV has hardly been studied with complete non-LTE codes including winds and blanketing, and their dependence with stellar parameters (wind density, stellar temperature, even metallicity?!) remains basically unknown.

For now, we can only qualitatively expect the inclusion of X-rays to harden the ionizing spectra, probably down to the energy range probed by (some) mid-IR diagnostics. While this could in principle improve some difficulties observed by the *CMFGEN* and *WM-Basic* models (e.g. increasing [Ne III/II]) their precise effect remains open.

6. $T_{\rm eff}$ diagnostics and "second-order" diagnostic diagrams

6.1. Using excitation diagnostic to determine $T_{\rm eff}$

Since the excitation of the gas increases with $T_{\rm eff}$, it is tempting to infer stellar temperatures from excitation diagnostic ratios. However, such an approach is intrinsically highly uncertain, as the nebular excitation is also strongly dependent on other parameters (see Sect. 3), such as the ionization parameter $\bar{U}$, which remain in most cases poorly known, cf. Mathis (1982) for optical lines and Schaerer & Stasińska (1999) for mid-IR ratios. These cautionary remarks should be kept in mind when e.g. using single line ratios or even several line ratios (e.g. Takahashi et al. 2000; Okamoto et al. 2001, 2003), but see also Morisset (2003), to estimate stellar properties of individual objects from nebular observations. Tailored photoionization models including numerous constraints can lead to substantially different results and should clearly be the preferred method (see e.g. Morisset et al. 2002).

For illustration we show in Fig. 11 the dependence of the [Ar III/II] excitation ratio on $T_{\rm eff}$ for a fixed $\bar{U}$ and metallicity. Other mid-IR excitation diagnostics show similar behaviors as can already be seen from various figures above, except that their dependence upon $\bar{U}$ are higher than for [Ar III/II], as already discussed in Sect. 5.2. The discussion of $T_{\rm eff}$ and $\bar{U}$ determinations using mid-IR excitation diagnostics and the H II regions metallicities is developed in Morisset (2003).

The most important conclusion from Fig. 11 is the important difference of the excitation of the gas ionized by *WM-Basic* (dotted line) and *CMFGEN* (dashed line) stars, for the same $T_{\rm eff}$ and $\bar{U}$, even if the two types of models are showing the same behavior in Figs. 3 to 5. In other words, taking for example a value of 10. For [Ar III/II], we can determine a $T_{\rm eff}$ of 39 kK using *CMFGEN* and a value of 45 kK using *WM-Basic*. This behavior can easily be understood when comparing the Q_E distribution, as shown in Fig. 2 and discussed in Sect. 2.8.

Two of the classical ways to constrain $T_{\rm eff}$ from optical observations are to use the He I 5876 Å/H$_\beta$ ratio (e.g. Kennicutt et al. 2000) or the [O III] 5007 Å/[O II] 3727,29 Å ratio (Dors & Copetti 2003). The predictions for He I 5876 Å/H$_\beta$ are shown in Fig. 12. As for [Ar III/II], this line ratio is fairly independent of $\bar{U}$. This diagnostic line ratio saturates above $T_{\rm eff} \gtrsim$ 40 kK, when helium is completely ionized to He^+. Note that even among *WM-Basic* and *CMFGEN*, which treat very similar physics, some differences in this $T_{\rm eff}$ indicator remain. Furthermore note that the predicted $Q_{24.6}/Q_{13.6}$ and hence He I 5876 Å/H$_\beta$ vary non-negligibly between dwarfs and supergiants (see e.g. Pauldrach et al. 2001; Smith et al. 2002). The predictions for [O III] 5007 Å/[O II] 3727,29 Å are presented in Fig. 13. As for the He I 5876 Å/H$_\beta$ ratio, the results differ strongly from one atmosphere model to another one. The Oxygen excitation diagnostic is also strongly sensitive to $\bar{U}$

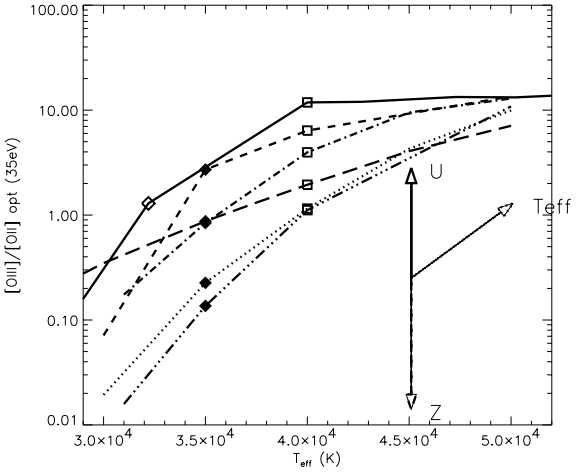

Fig. 13. Variation of the optical excitation diagnostic [O III] 5007 Å/[O II] 3727,29 Å with $T_{\rm eff}$ for supergiant stars. Codes are the same as in Figs. 2, 3. The set of arrows have the same meaning as in Fig. 6, for *WM-Basic* models only.

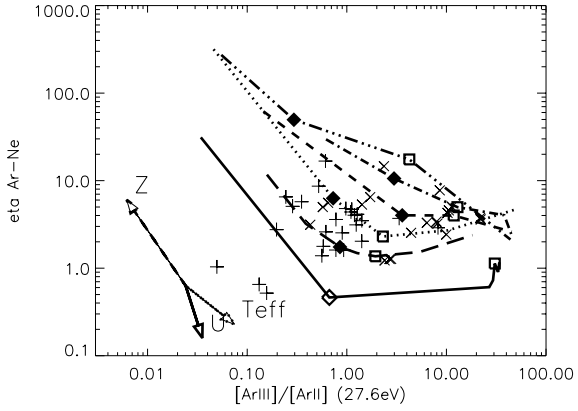

Fig. 14. Variation of the radiation softness parameter $\eta_{\rm Ar-Ne}$ versus [Ar III/II]. The codes are the same than in Figs. 2, 3. Note that the model predictions for both axis depend also on the assumed ionization parameter $\bar{U}$. Arrows as in Fig. 6 for *WM-Basic* models.

and Z, the effect of Z being slightly more important than found by Dors & Copetti (2003), but these authors used *WM-Basic* dwarfs atmosphere models.

We can conclude from the above examples that any determination of $T_{\rm eff}$ based on diagnostic ratios can be reliable only if the metallicity of the star is coherently taken into account, and if $\bar{U}$ is also determined at the same time, as shown in Morisset (2003).

6.2. Radiation softness parameters η

Following Vilchez & Pagel (1988), radiation softness parameters can be defined combining the excitation diagnostic ratios, namely: $\eta_{\rm Ar-Ne} = \frac{\rm [Ar\,III/II]}{\rm [Ne\,III/II]}$ and so on for the other diagnostic ratios.

To first order (but see the discussion on [Ar III/II] in Sect. 5.2) an excitation ratio X^{i+1}/X^i depends on the ionization parameter $\bar{U}$ and the hardness of the ionizing radiation and is given by

$$\frac{X^{i+1}}{X^i} \propto \bar{U} \frac{\int_{\nu(X^i)}^{\infty} \frac{J_\nu}{h\nu} {\rm d}\nu}{\int_{\nu(H^0)}^{\infty} \frac{J_\nu}{h\nu} {\rm d}\nu} = \bar{U} \frac{Q_{E(X^i)}}{Q_{13.6}}. \quad (1)$$

Therefore one has:

$$\eta_{X-Y} \propto \frac{Q_{E(X^i)}}{Q_{E(Y^i)}}, \quad (2)$$

where $E(X^i)$ is the ionization potential of the ion X^i. η is thus in principle independent of the ionization parameter $\bar{U}$, and a measure of the "slope" of the ionizing spectrum between the ionization energies $E(X^i)$ and $E(Y^i)$ respectively[6]. Therefore such quantities – used so far for optical lines only – have often been thought to be good estimators of stellar effective temperatures, see e.g. Garnett (1989), Kennicutt et al. (2000) but also Skillman (1989), Bresolin et al. (1999), Oey et al. (2002). For this reason we here explore whether the observed mid-IR fine structure lines offer, both from the empirical and theoretical standpoint, such a diagnostic power.

Figure 14 shows the variation of $\eta_{\rm Ne-Ar}$ versus [Ar III/II]. No correlation between these two observables is found. While a galactic gradient is found for [Ar III/II] (Martín-Hernández et al. 2002a; Giveon et al. 2002b), $\eta_{\rm Ne-Ar}$ and none of the other mid-IR η's which can be constructed show a galactic gradient. This can also be seen from the correlations between the various excitation ratios plotted by Martín-Hernández et al. (2002a), their Fig. 10. Already this finding indicates empirically that mid-IR softness parameters do not carry important information on the stellar ionizing sources.

How do the models compare with the observed softness parameters? Given the considerable spread between photoionization models using different stellar atmospheres and the various discrepancies already found earlier, it is not surprising that overall a large spread is also found here (Fig. 14). Compared to the observations the blackbody SED seems again to fit best. The *WM-Basic*, *CMFGEN* and *CoStar* models are marginally compatible with the observations each one on one side, while the *TLUSTY* and *Kurucz* results are definitively far away from the observed values. Note, however, that both theoretical quantities plotted here (including η) depend also on the ionization parameter.

In Fig. 15 we illustrate theoretical predictions of mid-IR softness parameters as a function of $T_{\rm eff}$ for the case of $\eta_{\rm Ne-Ar}$. Note that most of the model atmospheres predict that $\eta_{\rm Ne-Ar}$ becomes insensitive to $T_{\rm eff}$ above a certain value, here of the order of $T_{\rm eff} \gtrsim 35\,000$ K (the exact value also depending on $\bar{U}$). Similar dependencies on the adopted model atmosphere and "saturation effects" have also been found for the traditional

[6] However, note that e.g. any η involving [Ar III/II] will likely depend on $\bar{U}$, as [Ar III/II] itself depends already little on $\bar{U}$.

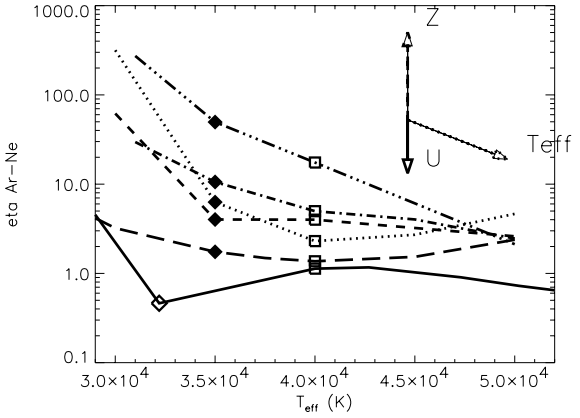

Fig. 15. Variation of the radiation softness parameter $\eta_{\rm Ar-Ne}$ according to the $T_{\rm eff}$ of the ionizing star. Codes are the same as in Figs. 2, 3. Arrows have the same meaning as in Fig. 6, for *WM-Basic* models.

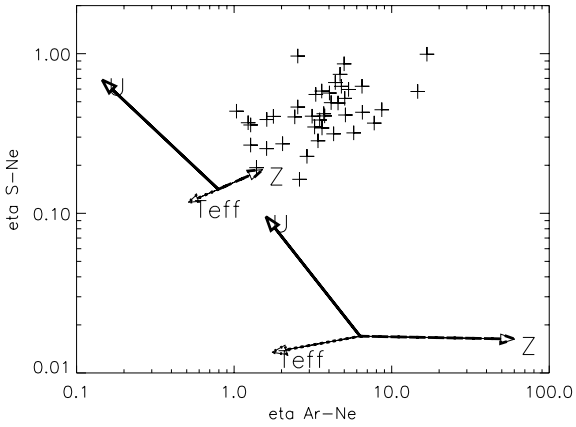

Fig. 17. Variation of the radiation softness parameter $\eta_{\rm S-Ne}$ versus $\eta_{\rm Ar-Ne}$, when changing $\bar{U}$, $T_{\rm eff}$ or Z. Arrows codes are the same as in Fig. 6.

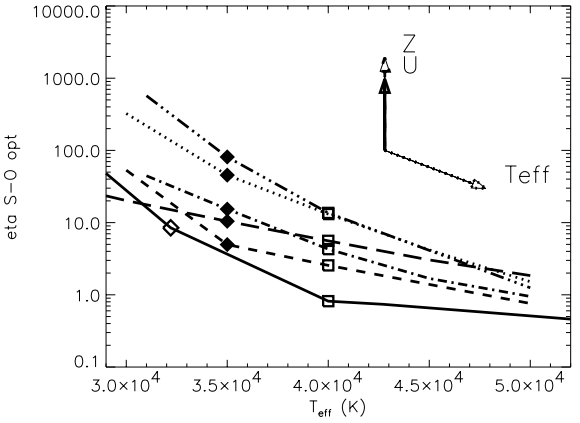

Fig. 16. Variation of the radiation softness parameter $\eta_{\rm S-O}$ (defined by Vilchez & Pagel 1988, see note 8), according to the $T_{\rm eff}$ of the ionizing star. Codes are the same as in Figs. 2, 3. Arrows have the same meaning as in Fig. 6, for *WM-Basic* models, for *WM-Basic* models only.

optical softness parameter (cf. Oey et al. 2002; Kennicutt et al. 2000).

Furthermore model calculations also show that all the mid-IR η depend quite strongly on the ionization parameter $\bar{U}$ and on metallicity, as shown here for the case of the *WM-Basic* models[7] (see Fig. 17). From the theoretical point of view, and without tailored photoionization modeling including constraints on $\bar{U}$ and Z, the use of mid-IR η's appears therefore highly compromised. Again, similar difficulties have also been found for the optical softness parameter, cf. Skillman (1989), Bresolin et al. (1999), Oey et al. (2002), but Kennicutt et al. (2000) and hereafter.

Last but not least, as each η implies 4 line intensities, the softness parameters are more sensitive to any observational uncertainty (as the attenuation correction or detector calibration), possible collisional effects, uncertainties in the atomic data etc. In view of all these considerations and the model results presented above, applications of softness parameters in the mid-IR appear therefore to be of very limited use.

For completeness we show in Fig. 16 the behavior of the traditional optical softness parameter $\eta_{\rm O-S}$[8] for all model atmospheres. Again a considerable spread between different atmosphere models and a dependence on $\bar{U}$ and Z is found.

7. Discussion

From the comparisons of the extensive model calculations with the observed excitation diagnostics we can draw some rather general conclusions about the shape of the ionizing spectra of early type stars and the on the nature of the ionizing sources of the Galactic H II regions.

7.1. Implications on stellar SEDs

Overall the "best fit" SED to the observed excitation diagrams (Figs. 3 to 4) was found with blackbody spectra. Does this imply that the ionizing fluxes of hot stars are best described by the Planck function? The overall answer is no, but. The observations probe (to 1st order) the relative number of ionizing photons with energies above the relevant ionization potentials, i.e. what was called the "slope" in Sect. 5. Therefore if we considered that all observed 3 line ratios are correctly reproduced by a blackbody this would imply that the 27.6−35.0 and 27.6–41.1 eV slopes (and hence also 35.0–41.1 eV) be

[7] Note that the metallicity dependence predicted by the *WM-Basic* models is probably overestimated as already discussed earlier (Sect. 5.5).

[8] Defined by Vilchez & Pagel (1988) as: ([O II] 3726,27 Å/[O III] 4959,5007 Å) / ([S II] 6717,31 Å/[S III] 9069,9532 Å).

equal to that of the Planck function (bb) of the same $T_{\rm eff}$, i.e. $Q_{27.6}/Q_{35.0} = Q^{\rm bb}_{27.6}/Q^{\rm bb}_{35.0}$ and $Q_{27.6}/Q_{41.1} = Q^{\rm bb}_{27.6}/Q^{\rm bb}_{41.1}$. This would therefore represent three "integral" constraints on the stellar SED. This is rather strong, but still leaves room for the detailed shape of the SED between these energies. Actually the agreement between blackbody spectra and [Ar III/II] vs. [Ne III/II] is better than diagrams involving [S IV/III]. This indicates that the constraint on the $Q_{27.6}/Q_{41.1}$ is better than at intermediate energies.

However, it is important to remember that these constraints on the underlying SED can be deduced only if the observed excitation diagram (Figs. 3 to 5) is essentially driven by a temperature sequence (i.e. $\bar{U}$ = const.). Note also the effects of uncertainties on the atomic data, as discussed in Sect. 5.7.

7.2. On the origin of the observed excitation sequences

The origin of the observed mid-IR excitation sequences and their correlation with galactocentric distance has been discussed recently by Giveon et al. (2002b); Martín-Hernández et al. (2002b). As both studies present somewhat limited arguments a more general discussion is appropriate here. The basic question is whether variations of the stellar effective temperature or metallicity variations are responsible for the observed decrease of excitation toward the Galactic Center?

Giveon et al. (2002b) have noted from photoionization models using *WM-Basic* spectra that [Ne III/II] is predicted to decrease more rapidly than [Ar III/II] with increasing metallicity – a finding also confirmed here (cf. Fig. 6). However, as the observed sequence does NOT follow this trend, they conclude that the decrease of excitation must be due to a reduction of $T_{\rm eff}$ as opposed to a softening of the stellar SED with increasing metallicity. Obviously as such this conclusion cannot be upheld as the same mid-IR observations, allowing fairly accurate abundance determinations, clearly establish the existence of a metallicity gradient (Giveon et al. 2002a). In fact, the apparent contradiction between the observed trend with metallicity and the one predicted with *WM-Basic* model atmospheres indicates quite likely that the stellar SEDs soften too quickly with increasing metallicity and/or that the ionization parameter in regions at small galactocentric distance must be larger than assumed (cf. Sect. 5.5).

In contrast to the above study, Martín-Hernández et al. (2002b) show a loose correlation between excitation and metal abundances (e.g. between [Ne III/II] and Ne/H), stress the importance of metallicity effects on the SED (see also Martín-Hernández et al. 2004), and conclude that at least partly the observed decrease of [Ne III/II] must be due to a softening of the stellar SEDs with increasing metallicity.

7.2.1. Stellar evolution effects

From what we know, three effects are related to metallicity and must all be taken into account. First, higher metallicity is known in stellar evolution to lead to a cooler zero age main sequence and to an overall shift to cooler temperatures (e.g. Schaller et al. 1992). Second, blanketing effects in the atmospheres become stronger with increasing metallicity and lead to softer ionizing spectra (e.g. Sect. 5.5; Pauldrach et al. 2001; Martín-Hernández et al. 2004). Finally, an increased nebular abundance leads also to a somewhat lower excitation of the gas in the H II regions (cf. Sect. 5.5). The remaining questions are then *a)* which of these effects dominate and *b)* whether taken together they can indeed quantitatively reproduce the entire range of observed excitation variations in the Galactic H II regions.

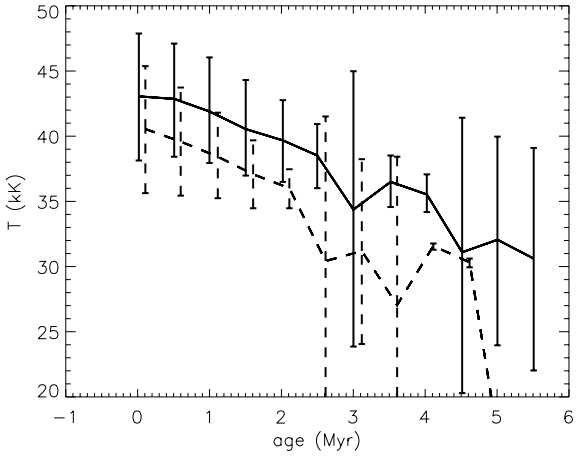

Fig. 18. Average stellar effective temperature and dispersion as a function of time for metallicities Z = 0.008 (1/2.5 $Z_\odot$, solid lines) and 0.04 (2 $Z_\odot$, dashed) predicted for an ensemble of single star H II regions for a Salpeter IMF with $M_{\rm up}$ = 120 $M_\odot$ and a minimum Lyman continuum flux $\log(Q_{\rm lim}) \geq 48.$. Note the rather small differences in average $T_{\rm eff}$ and the large intrinsic dispersion for each given metallicity.

Although the content of stellar ionizing sources of the objects considered is not known (but see Morisset 2003) we can estimate the $T_{\rm eff}$ variations expected from stellar evolution, e.g. by assuming a single ionizing source. We then perform Monte Carlo simulations of single star H II regions of different metallicities assuming that the ionizing stars are drawn from a Salpeter IMF with a given upper mass cut-off $M_{\rm up}$. In order to compute the mean properties of these stars, such as their average $T_{\rm eff}$, the predicted variation with metallicity and their dispersion, the equivalent of a lower mass limit must also be specified. This is done by imposing a lower limit on the total Lyman continuum photon flux $Q_{\rm lim}$. Only stars with $Q > Q_{\rm lim}$ at a given age are retained for this computation. In practice we use the Meynet et al. (1994) stellar tracks, we consider metallicities between ∼1/2 and 2 times solar, as indicated by the observed range of Ne/H or Ar/H abundances and we adopt $\log(Q_{\rm lim}) = 48.$, corresponding a typical lower limit for the H II regions of Martín-Hernández et al. (2002a). Very massive stars entering the Wolf-Rayet phase already on the main sequence are also excluded.

The resulting average and spread of $T_{\rm eff}$ as a function of age is shown in Fig. 18 for Z = 0.04 and 0.008 respectively. This figure shows the following: first, the reduction of the average

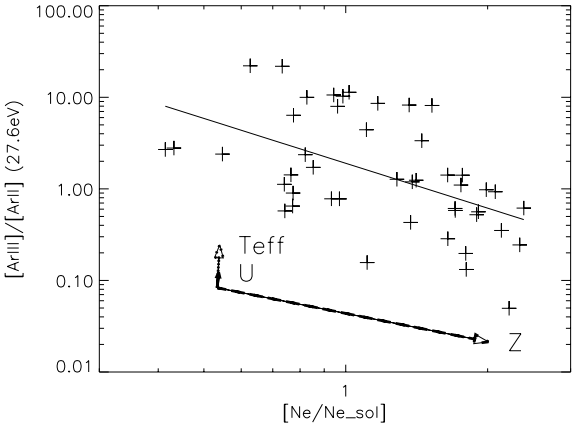

Fig. 19. [Ar III/II] versus metallicity, measured here by the Ne abundance (see text). The line is a linear fit to the observations in log-log space. Arrows as in Fig. 6, for *WM-Basic* models.

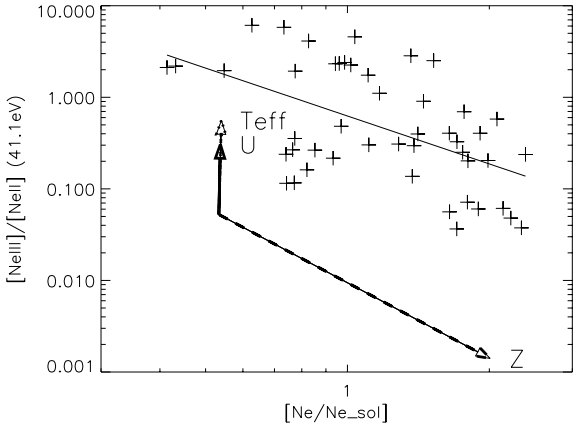

Fig. 20. [Ne III/II] versus metallicity, as in Fig. 19. A very similar plot is obtained for [S IV/III].

stellar temperature due to a metallicity increase by a factor 4 is rather modest, of the order of ∼3−4 kK. Second, for a given metallicity the predicted dispersion in $T_{\rm eff}$ is larger; typically of the order of ∼3−9 kK for reasonable ages. Although the absolute values of these $T_{\rm eff}$ depend for obvious reasons on the exact choice of $Q_{\rm lim}$, the $T_{\rm eff}$ differences and dispersion depend little on this value. From all the models considered above, the decrease of the mean $T_{\rm eff}$ due to stellar evolution effects appears to be too small to explain the full range of excitations.

On the other hand the fairly large $T_{\rm eff}$ dispersion at a given Z will induce quite important variations in the excitation. This effect probably dominates the observed excitation scatter (defined at the end of Sect. 5), as also suggested by the observations of a large spread of the excitation diagnostics Figs. 19 and 20 for a given metallicity measured here by Ne/Ne$_\odot$[9]. Indeed the observed spread of [Ar III/II] and [Ne III/II] at a given Z is somewhat larger than or similar to the decrease of the mean excitation with increasing Z. Taken together these findings imply that while undeniably metallicity effects on stellar evolution and nebular abundances must be present, statistical fluctuations of the effective stellar temperature due to the IMF are likely the dominant source of scatter for the observed mid-IR excitation sequence of Galactic H II regions, while the excitation sequences must be predominantly driven by other effects which we will discuss now.

7.2.2. Stellar atmospheres and nebular effects

As apparent from our modeling (see Figs. 19 and 20) the effects of metallicity on the shape of the stellar ionizing spectra strongly alter the predicted excitation. The magnitude of the predicted effect is found to be comparable to the observed variation. Both these findings and the above results concerning stellar evolution effects indicate the Z dependence of the ionizing spectra is the main driver for the correlation of the excitation with galactocentric distance.

As this result depends on a specific set of model atmospheres (*WM-Basic*) a few words of caution are, however, necessary here. First, we note that the effects of $T_{\rm eff}$ and Z are not exactly the same for [Ar III/II], [Ne III/II], and [S IV/III]. The predicted excitation variation (shown here for a change of $T_{\rm eff}$ from 35 to 40 kK) tends to be somewhat larger (smaller) for [Ne III/II] and [S IV/III] ([Ar III/II]) than the observed variations. Second, it must be remembered that the *WM-Basic* atmosphere models employed here could predict too strong a softening with increasing Z as suspected from Fig. 20 and already discussed in Sect. 5.5. Despite these imperfections there is little doubt that the above result remains valid.

Finally we may also comment on excitation changes related to the ionization parameter. Again, as for $T_{\rm eff}$, the above Monte Carlo simulations show small differences between the average ionizing photon flux $Q_{13.6}$ with metallicity, but a considerable dispersion for each Z. Combined with the observational fact of fairly similar nebular densities in our objects this could be a justification for a constant ionization parameter, at least on average. Random variations of $\bar{U}$ are, however, expected to contribute to the excitation scatter at a given metallicity.

In conclusion we see little doubt that the observed excitation sequence of Galactic H II regions is shaped by the joint effects of metallicity on stellar evolution, atmospheric line blanketing, and cooling of the ISM. From our investigations it seems, however, that metallicity effects on ionizing stellar flux is the dominant effect causing the excitation gradients while statistical fluctuations of $T_{\rm eff}$ and $\bar{U}$ are likely the dominant source of scatter in the observed excitations. A more detailed study of possible systematic $T_{\rm eff}$ and ionization parameter gradients is presented in Morisset (2003): no clear gradient of $T_{\rm eff}$

[9] Ne abundances were obtained using reddening and $T_{\rm elec}$ corrected abundances from Giveon et al. (2002a). Ne is preferred to Ar or S because Ar abundance is not reliable for high $T_{\rm eff}$, Ar^{3+} being present but unobserved, the same applying at low $T_{\rm eff}$ for S^+. The solar abundance for Ne is determined using the abundance gradient obtained by Giveon et al. (2002a) at 8.5 kpc.

nor $\bar{U}$ versus the galactocentric distance are found by this author, but some trends of increase (decrease) of $T_{\rm eff}$ ($\bar{U}$) with the metallicity are observed. Importance of taking into account the effect of the metallicity on the stellar spectral shape is addressed.

8. Summary and conclusion

We have presented results from extensive photoionization model grids for single star H II regions using a variety of recent state-of-the-art stellar atmosphere models such as *CMFGEN*, *WM-Basic*, *TLUSTY*, *CoStar*, and *Kurucz* models. Even among the two recent non-LTE line blanketed codes including stellar winds (*WM-Basic* and *CMFGEN*) the predicted ionizing spectra differ by amounts leading to observable differences in nebular spectra[10].

The main aim of this investigation was to compare these model predictions to recent catalogs of ISO mid-IR observations of Galactic H II regions, which present rich spectra probing the ionizing spectrum between ∼24 to 41 eV thanks to the measurements of [Ar III/II], [Ne III/II], and [S IV/III] line ratios. Particular care has been paid to examining in detail the dependences of the nebular properties on the numerous nebular parameters (ionization parameter $\bar{U}$, abundances, dust etc.) which are generally unconstrained for the objects considered here.

Most excitation diagnostics are found to be fairly degenerate, but not completely so, with respect to increases of $T_{\rm eff}$, $\bar{U}$, a change from dwarf to supergiant spectra, a decrease of the nebular metallicity (Sects. 5.2 and 5.3), and the presence of dust in the H II region (Sect. 5.6). Each of these parameters increases the overall excitation of the gas, and in absence of constraints on them, a derivation of such a parameter, e.g. an estimate of the stellar $T_{\rm eff}$ of the ionizing source, is intrinsically uncertain. In consequence, while for sets of objects with similar gas properties statistical inferences are probably meaningful, such estimates for individual objects must be taken with care.

Provided the ionization parameter is fairly constant on average and the atomic data is correct (but cf. below) the comparisons between the photoionization model predictions and the observations allow us to conclude the following concerning the different stellar atmosphere models (Sect. 5.1):

- Both recent non-LTE codes including line blanketing and stellar winds (*WM-Basic* and *CMFGEN*) show a reasonable agreement with the observations. Given their different behavior in the three excitation diagnostics, depending on luminosity class, and other remaining uncertainties, it appears that none of the models can be preferred on this basis.
- The plane parallel hydrostatic codes (*Kurucz*, *TLUSTY*) predict spectra which are too soft, especially over the energy range between 27.6, 35.0, and 41.1 eV and above. Although a good agreement is found for UV to optical spectra predicted by the hydrostatic *TLUSTY* code and the photosphere-wind code *CMFGEN* (Hillier 2003; Bouret et al. 2003) important differences are found in the EUV range probed by the present observations and photoionization models. Apparently the full non-LTE treatment of numerous elements accounted for by *TLUSTY* is insufficient to accurately predict the ionizing spectra at these energies, and the inclusion of stellar winds is imperative.
- We confirm the finding of earlier investigations (e.g. Oey et al. 2000) showing that the *CoStar* models overpredict somewhat the ionizing flux at high energies.
- Interestingly blackbodies reproduce best the observed excitation diagrams, which indicates that the ionizing spectra of our observed object should have relative ionizing photon flux productions Q_E at energies 27.6, 35.0 and 41.1 eV close to that of blackbody spectra. Although this integral constraint on the SED remains approximate, it should still be useful to guide future improvements in atmosphere modeling.
- Finally, the softening of the ionizing spectra with increasing metallicity predicted by the *WM-Basic* models is found to be too strong. As already apparent from observed correlations between excitation diagnostics probing various energies, the observed softening of the radiation field (in part due to metallicity) affects fairly equally the range between ∼27 and 41 eV (Martín-Hernández et al. 2002a) in contrast to the atmosphere model predictions, which soften most at the highest energies.

These conclusions are found to be fairly robust to effects such as changes of $\bar{U}$, nebular and stellar metallicity changes, and the inclusion of dust. We suggest that the main uncertainty which could alter the above conclusions is the poorly known atomic data for Ar^{++} (especially dielectronic recombination coefficients) as also pointed out by Stasińska et al. (2002). Reliable computations for such data are strongly needed. From the perspective of atmosphere codes probably the most important step toward improving the reliability of ionizing fluxes resides in a quantitative exploration of the influence of X-rays on the emergent spectra at lower energy.

The potential of mid-IR line ratios or "softness parameters", defined in analogy to the well known η parameter for optical emission lines, has been explored (Sect. 6.1). The following main results have been obtained:

- Given the non-negligible differences between the various atmosphere models it is not surprising that individual line ratios (e.g. [Ar III/II], [Ne III/II]) show quite different dependences on $T_{\rm eff}$. We find that [Ar III/II] depends little on the ionization parameter as the ionization of Ar^+ is closely coupled to that of He. This suggests that [Ar III] 8.98 μm/[Ar II] 6.98 μm should in principle be a fairly robust temperature indicator, provided the atmosphere models are sufficiently accurate up to ∼24−27 eV and the atomic data is reliable (cf. above).
  In comparison to He I/H indicators (e.g. He I 6678 Å/Hβ or He I 2.06 μm/Brγ in Kennicutt et al. 2000; Lumsden et al. 2003,and references therein), [Ar III/II] does not show a saturation effect but remain sensitive to $T_{\rm eff}$ up to the highest temperature examined here ($T_{\rm eff}$ ∼ 50 kK). Due to the large uncertainties of dielectronic recombination

[10] Presumably these differences are due to the use of different methods to treat line blanketing (opacity sampling method versus superlevel approach in the comoving frame) and different atomic data.

coefficient of Ar^{++}, Morisset (2003) prefer to use [S IV/III] and [Ne III/II] to determine $T_{\rm eff}$ and $\bar{U}$ simultaneously, for the H II regions used in this work.

– Both empirically and theoretically the mid-IR softness parameters which can be constructed from [Ar III/II], [S IV/III], and [Ne III/II] are found to provide little if any information on stellar temperatures if not used to determine $\bar{U}$ at the same time (Morisset 2003). Observationally little / no correlation is found between the η's and excitation ratios. Furthermore, our photoionization models show a considerable dependence of η on the ionization parameter. We therefore conclude that mid-IR η's appear to be of limited diagnostic power.

Finally we have examined which parameter(s) is (are) chiefly responsible for the observed mid-IR excitation sequences. Combining the results from our extensive photoionization model grids with Monte Carlo simulations of ensembles of single star H II regions of different metallicity and age we conclude the following (Sect. 7). While metallicity effects on stellar evolution, atmospheres and the nebulae all have an undeniable influence, they are probably of minor importance compared to the fairly large dispersion of $T_{\rm eff}$ expected at each metallicity from a simple statistical sampling of the IMF. The $T_{\rm eff}$ scatter plus additional scatter in the ionization parameter are probably the dominant driver for the observed mid-IR excitation scatter of Galactic H II regions, while the effect of metallicity on the shape of the ionizing spectra is partially responsible of the global excitation sequence, the proportion of this effect being strongly dependent of the reliability of the atmosphere models (Morisset 2003).

Acknowledgements. We wish to thank various persons who have contributed directly and indirectly to the shape of this paper, over its rather long gestation time. Among those are in particular Grazyna Stasińska and Daniel Péquignot who have been consulted on photoionization codes and atomic physics, and Leticia Martín-Hernandez. Thierry Lanz kindly provided model atmosphere results prior to publication. We are also grateful to John Hillier for assistance in adapting and modifying his atmosphere code to our purpose. We thank Ryszard Szczerba for helping introducing dust in NEBU code. DS thanks the CNRS, the French Programme National de Galaxies, and the Swiss National Fund for Research for support. DS and FM thank the CALMIP and IDRIS centers for generous allocation of computing time. CM thanks the IA/UANM in Mexico for offering him the opportunity to finish this work and investigate many others in the future. This work was partly supported by the CONACyT (México) grant 40096-F.

References

Aannestad, P. A. 1989, ApJ, 338, 162
Abbott, D. C., & Hummer, D. G. 1985, ApJ, 294, 286
Bouret, J., Lanz, T., Hillier, D. J., et al. 2003, ApJ, 595, 1182
Bresolin, F., Kennicutt, R. C., & Garnett, D. R. 1999, ApJ, 510, 104
Crowther, P. A., Pasquali, A., de Marco, O., et al. 1999, A&A, 350, 1007
de Koter, A., Lamers, H. J. G. L. M., & Schmutz, W. 1996, A&A, 306, 501
Dors, O. L., & Copetti, M. V. F. 2003, A&A, 404, 969
Evans, I. N., & Dopita, M. A. 1985, ApJS, 58, 125
Gabler, R., Gabler, A., Kudritzki, R. P., Puls, J., & Pauldrach, A. 1989, A&A, 226, 162
Garnett, D. R. 1989, ApJ, 345, 282
Giveon, U., Morisset, C., & Sternberg, A. 2002a, A&A, 392, 501
Giveon, U., Sternberg, A., Lutz, D., Feuchtgruber, H., & Pauldrach, A. W. A. 2002b, ApJ, 566, 880
Hanson, M. M., Conti, P. S., & Rieke, M. J. 1996, ApJS, 107, 281
Hillier, D. J. 2003, in Stellar Atmosphere Modeling, ed. I. Hubeny, D. Mihalas, & K. Werner, ASP Conf. Ser., 288
Hillier, D. J., & Miller, D. L. 1998, ApJ, 496, 407
Hubeny, I., & Lanz, T. 1995, ApJ, 439, 875
Hubeny, I., Mihalas, D., & Werner, K. 2003, Stellar Atmosphere Modeling, ASP Conf. Ser., 288
Kaper, L., Bik, A., Hanson, M. M., & Comerón, F. 2002, in Hot Star Workshop III, The Earliest Stages of Massive Star Birth, ed. P. A. Crowther, ISBN: 1-58381-107-9 (San Francisco: Astronomical Society of the Pacific), ASP Conf. Proc., 267, 95
Kennicutt, R. C., Bresolin, F., French, H., & Martin, P. 2000, ApJ, 537, 589
Kudritzki, R. P., Yorke, H. W., & Frisch, H. 1988, Research supported by the Swiss Academy of Sciences and DFG. Sauverny, Switzerland, Observatoire de Genève, 458 p., 89, 50499
Kurucz, R. 1991, in Stellar Atmospheres: Beyond Classical Models, ed. L. Crivellari, I. Hubeny, & D. Hummer, NATO ASI Series C, 341, 441
Kurucz, R. 1994, Solar abundance model atmospheres for 0, 1, 2, 4, 8 km/s. Kurucz CD-ROM No. 19. Cambridge, Mass.: Smithsonian Astrophysical Observatory, 1994, 19
Lanz, T., & Hubeny, I. 2003a, ApJS, 146, 417
Lanz, T., & Hubeny, I. 2003b, ApJS, 147, 225, erratum
Lumsden, S. L., Puxley, P. J., Hoare, M. G., Moore, T. J. T., & Ridge, N. A. 2003, MNRAS, 340, 799
Macfarlane, J. J., Cohen, D. H., & Wang, P. 1994, ApJ, 437, 351
Martín-Hernández, N., Peeters, E., Damour, F., et al. 2002a, A&A, 381, 606
Martín-Hernández, N. L. 2002, Ph.D. Thesis, Rijksuniversiteit Groningen
Martín-Hernández, N. L., Mokiem, M., de Koter, A., & Tielens, A. G. G. M. 2004, A&A, submited
Martín-Hernández, N. L., Vermeij, R., Tielens, A. G. G. M., van der Hulst, J. M., & Peeters, E. 2002b, A&A, 389, 286
Martins, F., Schaerer, D., & Hillier, D. J. 2002, A&A, 382, 999
Mathis, J. S. 1982, ApJ, 261, 195
Mathis, J. S. 1985, ApJ, 291, 247
Mathys, G. 1988, A&AS, 76, 427
Mazzotta, P., Mazzitelli, G., Colafrancesco, S., & Vittorio, N. 1998, A&AS, 133, 403
Meynet, G., Maeder, A., Schaller, G., Schaerer, D., & Charbonnel, C. 1994, A&AS, 103, 97
Morisset, C. 2003, ApJ, in press [astro-ph/0310275]
Morisset, C., & Péquignot, D. 1996, A&A, 312, 135
Morisset, C., Schaerer, D., Martín-Hernández, N. L., et al. 2002, A&A, 386, 558
Oey, M. S., Dopita, M. A., Shields, J. C., & Smith, R. C. 2000, ApJS, 128, 511
Oey, M. S., Shields, J. C., Dopita, M. A., & Smith, R. C. 2002, in Rev. Mex. Astron. Astrofis. Conf. Ser., 77
Okamoto, Y. K., Kataza, H., Yamashita, T., Miyata, T., & Onaka, T. 2001, ApJ, 553, 254

Okamoto, Y. K., Kataza, H., Yamashita, T., et al. 2003, ApJ, 584, 368
Péquignot, D., Ferland, G., Netzer, H., et al. 2001, in Spectroscopic Challenges of Photoionized Plasmas, ASP Conf. Ser., 247, 533
Pauldrach, A. W. A., Hoffmann, T. L., & Lennon, M. 2001, A&A, 375, 161
Peeters, E., Martín-Hernández, N. E., Damour, F., et al. 2002, A&A, 381, 571
Rubin, R. H., Simpson, J. P., Erickson, E. F., & Haas, M. R. 1988, ApJ, 327, 377
Savin, D. W., & Laming, J. M. 2002, ApJ, 566, 1166
Schaerer, D. 2000, in Stars, Gas and Dust in Galaxies: Exploring the Links, ASP Conf. Ser., 221, 99
Schaerer, D., & de Koter, A. 1997, A&A, 322, 598
Schaerer, D., & Stasińska, G. 1999, in ESA SP-427: The Universe as Seen by ISO, 751
Schaller, G., Schaerer, D., Meynet, G., & Maeder, A. 1992, A&AS, 96, 269
Schmutz, W. 1991, in NATO ASIC Proc. 341: Stellar Atmospheres – Beyond Classical Models, 191
Simpson, J. P., Colgan, S. W. J., Rubin, R. H., Erickson, E. F., & Haas, M. R. 1995, ApJ, 444, 721
Skillman, E. D. 1989, ApJ, 347, 883
Smith, L. J., Norris, R. P. F., & Crowther, P. A. 2002, MNRAS, 337, 1309
Stasińska, G., & Schaerer, D. 1997, A&A, 322, 615
Stasińska, G., Schaerer, D., & Zeipen, C. 2002, in A Massive Star Odyssey, from Main Sequence to Supernovae, ed. K. van der Hucht, A. Herrero, & C. Esteban, IAU Symp., 212
Takahashi, H., Matsuhara, H., Watarai, H., & Matsumoto, T. 2000, ApJ, 541, 779
Vilchez, J. M., & Pagel, B. E. J. 1988, MNRAS, 231, 257
Watson, A. M., & Hanson, M. M. 1997, ApJ, 490, L165

Part II

Winds of O stars

The second part of this thesis focuses on the spectroscopic analysis of stellar and wind properties of O dwarfs. We first study the stars in the High Excitation Blob SMC-N81 and then move to Galactic stars. The main result is the discodery of stars with extremely weak winds. The reason for such a weakness is investigated but remains unclear in the end.

Chapter 5

Overview of the radiation driven wind theory

French summary

Ce chapitre est consacré à un rappel des principales bases de la théorie des vents radiatifs dévelopée par Lucy & Salomon (1971), Castor, Abbott & Klein (1975) et Kudritzki et al. (1989).

Dans une première partie, nous donnons les équations fondamentales. Ensuite, nous dérivons l'expression de l'accélération radiative due à un ensemble de raies au moyen du formalisme de Castor, Abbott & Klein (1975). Cela nous amène à introduire l'approximation Sobolev, la fonction de distribution des forces oscillatrices et les paramètres CAK (k, α, δ) dont nous donnons une interprétation physique. Par la suite, nous résolvons partiellement les équations de la structure hydrodynamique et donnons leurs solutions que nous discutons brièvement. Nous pouvons ainsi dériver les expressions de la perte de masse et de la vitesse terminale en fonction des paramètres stellaires et CAK. Nous examinons la dépendance de ces expressions avec la métallicité et introduisons enfin la relation quantité de mouvement modifiée - luminosité que nous discuterons largement par la suite.

This chapter gives an overview of the radiation driven wind theory and recalls the basic equations and relations.

The observation of massive stars reveals that they lose mass at extremely high rates compared to solar type stars. Strong P-Cygni profiles in the UV (and sometimes optical) ranges witnesses the presence of outflows accelerated at velocities reaching typically up to 1 % of the light speed (e.g. Abbott, 1978; Prinja, Barlow & Howarth, 1990; Lamers et al., 1995). Excess of emission compared to thermal emission in the mm and radio ranges are other indicators of the presence of an extended atmosphere (up to several tens of stellar radii) in which free-free radiation due to electrons is important. Moreover, direct imaging of Wolf-Rayet stars shows huge outflows of material (Grosdidier et al., 1998). Indirect evidences of winds of massive stars also come from the existence of cavities in the interstellar medium surrounding massive stars resulting from the blowing of interstellar matter by outflows (Nazé et al., 2002). X-ray emission in high mass binaries is also attributed to the presence of colliding winds (Pittard et al., 2002; Rauw et al., 2002; Sana et al., 2004). These are just a few examples of the evidences of massive star winds. This phenomenon has been known for a long time and is crucial to understand the evolution of massive stars (see Sect. 1.2, Chiosi & Maeder, 1986; Maeder & Conti, 1994). Its origin is simply rooted in the transfer of momentum from photon to matter. As massive stars are very luminous, they emit huge quantities of photons. And as they are very hot, the emission peaks around 1000 Å where the density of spectral lines is very high. The resulting interaction between radiation and matter leads to a radiative acceleration sufficient to overcome gravity, so that the upper layers of the star are lifted and blown in a wind giving birth to an extended atmosphere.

The first quantitative description of such winds (called radiation driven winds) was given by Lucy & Salomon (1971). In their numerical simulations they derived values for the mass loss rate and showed that the position of stars predicted to lose mass through radiation driven winds in the log $T_{\rm eff}$ - log g diagram corresponded qualitatively to the observations. However, their models suffered from a crude approximation: they considered only UV resonances lines in their estimate of the radiative acceleration. As a consequence, their mass loss rates were low (of the order of $10^{-7..-10}$ $M_\odot$ yr^{-1}). The next step towards a quantitative description of radiation driven winds was due to Castor, Abbott & Klein (1975). They developed a formalism to take into account the acceleration due to an ensemble of lines and not just a few strong lines. This allowed them to predict mass loss rates nearly 100 times higher than those of Lucy & Salomon. Moreover, they derived the main dependencies of the wind parameters ($\dot{M}$ and v_∞) as a function of stellar parameters (luminosity, stellar radius...). The theory was then refined by Pauldrach et al. (1986) and Kudritzki et al.

(1989). In particular, they dropped the approximation of a point source for the star in the computation of the radiative acceleration, which lead to an increase of the terminal velocities and a decrease of the mass loss rates. In the following, we give the main ingredients of the radiation driven wind theory as developed by Castor, Abbot & Klein. A more detailed and well described discussion can be found in Lamers & Cassinelli (1999).

5.1 Hydrodynamical equations

The basic equations of the radiation driven wind theory are the same as for any hydrodynamical problem:

- momentum conservation:

$$\frac{vdv}{dr} = -\frac{GM}{r^2} + \frac{1}{\rho}\frac{dp}{dr} + g^e + g^l \tag{5.1}$$

where the first term is the variation of velocity (in steady state approximation), the second term is the gravitational acceleration, the third one the thermal acceleration, the fourth one the acceleration due to electron scattering and the last one the acceleration due to lines.

- mass conservation:

$$\dot{M} = 4\pi r^2 \rho v \tag{5.2}$$

the mass conservation is expressed in term of mass loss rate $\dot{M}$ and ρ is the density.

- energy equation:

$$e = \frac{v^2}{r} - \frac{GM}{r} + \frac{5\mathcal{R}T}{2\mu} \tag{5.3}$$

The first term is the kinetic energy per unit mass, the second one is the gravitational energy by unit mass and the last one is the enthalpy per unit mass. A simple assumption of constant temperature is made here for a simplified approach.

- state equation:

$$P = \frac{\mathcal{R}\rho T}{\mu} \tag{5.4}$$

which is the perfect gas equation.

With these equations, the solution for the velocity and density structure of the atmosphere can be derived provided that the radiative acceleration is given. We show in the following how this can be done.

5.2 Radiative acceleration

The main difficulty to solve the previous set of equations comes from eq. 5.1 where the radiative accelerations have to be expressed. It is quite simple for the acceleration due to electron scattering which is:

$$g^e = \frac{\sigma^e L}{4\pi r^2 c} \tag{5.5}$$

where σ^e is the absorption cross section for electron scattering.

The main idea of Castor, Abbott & Klein was to express the radiative acceleration due to lines as a multiple of the acceleration due to electron scattering:

$$g^l = g^e M(t) \tag{5.6}$$

where M(t) is called the *force multiplier* and simply represents the amount by which the acceleration is increased compared to a simple electron scattering acceleration. The parameter t is a dimensionless optical depth and is expressed by:

$$t = \sigma^e v_{th} \rho \frac{dr}{dv} \tag{5.7}$$

where v_{th} is the thermal velocity of particles (mainly H atoms).

Again, the difficulty is to express $M(t)$ as a function of physical parameters. Castor, Abbott & Klein (hereafter CAK) have shown that the force multiplier can be well approximated by a power law of t. Indeed, the detailed calculations of radiative accelerations of Abbott (1982) and Shimada et al. (1994) reveal that the logarithm of the force multiplier decreases linearly when $\log(t)$ increases. This can be seen in Fig. 5.1 where

the connected symbols are the results of the calculations of force multipliers for different temperatures. CAK introduced two parameters to represent the behaviour of $M(t)$: $kand\alpha$. Later, Abbott (1982) introduced a third parameter -δ- to take into account the variation of the ionisation throughout the wind. Taken together, these parameters allow to express the force multiplier as follows:

$$M(t) = kt^{-\alpha}\left(10^{-11}\frac{n_e}{W}\right)^{\delta} \tag{5.8}$$

where n_e is the electron density and W a geometrical factor ($W = \frac{1}{2}\{1 - \sqrt{1-(\frac{R}{r})^2}\}$).

The dotted line in Fig. 5.1 shows the parameterisation of the force multiplier with this formalism and indicates a good agreement between detailed calculations and analytical function.

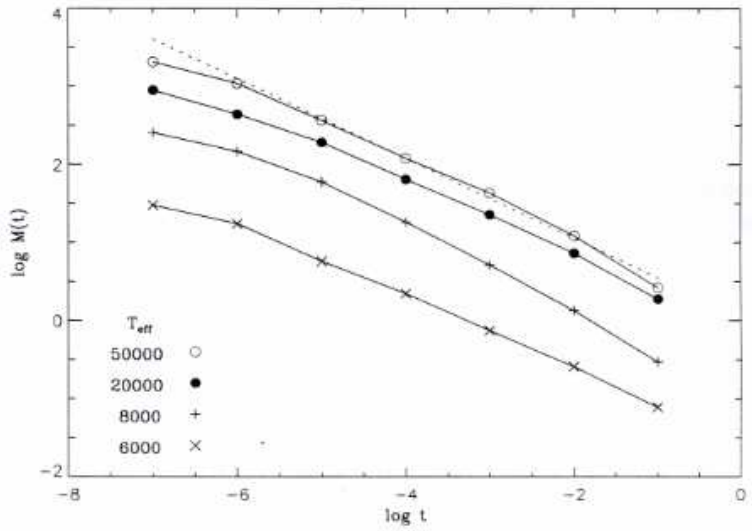

Figure 5.1: Force multiplier. The symbols connected by solid lines are radiative acceleration resulting from the detailed calculations of Shimada et al. (1994) and Abbott (1982) for different temperatures. The dotted line is a fit of the 50000 K model with the CAK parameters. M(t) can be well represented by the CAK parameterisation.

Let us give a short physical description of the CAK parameters. From simple arguments, we can say that the intensity of the acceleration is closely related to the properties of the absorbing lines. The more lines are involved in the transfer of momentum, the more acceleration is produced. But the exact amount of acceleration also depends on the efficiency of the transfer or the opacity of the lines: an optically thick line will absorb more photons

and transfer more momentum. However, this does not mean that only optically thick lines are important for the hydrodynamics, because the number of optically thin lines is generally high so that the number compensates the weak efficiency. This means that the nature of the radiative acceleration due to lines is rooted in the physical properties of the ensemble of lines, say their number and their strength. A distribution function of lines will gather these information. After these general considerations, let us go to a more detailed description.

To better understand the physics of radiative acceleration, let us first go back to the acceleration provided by one line. It is simply the number of photons absorbed by the line per time and mass unit multiplied by the momentum of the photons. This can be expressed as follows:

$$\begin{aligned} g_{rad} &= \frac{1}{4\pi r^2 \rho dr} N_\nu d_\nu \frac{h\nu}{c}(1 - e^{-\tau_S}) \\ &= \frac{1}{4\pi r^2 c^2} L_\nu \nu \frac{1}{\rho} \frac{dv}{dr}(1 - e^{-\tau_S}) \end{aligned} \tag{5.9}$$

In this expression, the probability of absorption of a photon is given by $1 - e^{-\tau_S}$ where τ_S is the Sobolev optical depth, which is the optical depth under the assumption that the velocity gradient in the atmosphere is high enough so that the interaction of a photon with a line can be restricted to a very local area (due to Doppler shifts in the frequency of the photon). It is possible to show that in the approximation of a point source star, the Sobolev optical depth can be written as follows:

$$\tau_S = \frac{\pi e^2}{m_e c} gf \left(\frac{n_l}{g_l} - \frac{n_u}{g_u} \right) \lambda \frac{dr}{dv} \tag{5.10}$$

where gf is the Gaunt factor and n_i and g_i are the occupation numbers and statistical weights. Introducing a dimensionless line strength for a line (k_L) the Sobolev optical depth can be written:

$$\tau_S = \frac{\sigma_e v_{th}}{dv/dr} k_L = t k_L \tag{5.11}$$

Given the expression of the Sobolev optical depth (Eq. 5.10), it is easy to show with Eq. 5.9 that the acceleration due to an optically thick line is directly proportional to $\frac{dv}{dr}$ and is independent of the number of absorbers: this is simply because due to the thickness of the line, all the radiation will be absorbed independently of the number of absorbers. Also, due

to this independence on the number of absorbers, all optically thick lines produce the same acceleration. In the case of an optically thin line, the acceleration is independent of the velocity gradient but depends on the number of absorbers: the radiation being unattenuated, more absorbers will produce more acceleration.

Once the acceleration of one line is estimated, the sum over all lines must be done to have the total acceleration. This requires the knowledge of the line distribution function which gives the number of lines of given oscillator strength by frequency and line strength range. A differential form of this function is (see Puls et al., 1996):

$$dN(\nu, k_L) = -N_0 f_\nu(\nu) k_L^{\alpha-2} d\nu dk_L \tag{5.12}$$

In this expression, N_0 is a normalisation constant directly related to the total number of lines and f_ν gives the dependence of the function on the frequency range.

If we now sum the contribution of all lines to the acceleration taking this distribution into account, one finds:

$$g_{rad}^{tot} = \frac{s_e v_{th}}{4\pi r^2 c^2} t^{-1} \int_0^\infty \int_0^\infty L_\nu \nu (1 - e^{-tk_L}) dN(\nu, k_L) \tag{5.13}$$

where $s_e = \sigma_e/\rho$.

Introducing k_1 as the value of k for which τ_S =1 (i.e. $k_1 = t^{-1}$) and separating the case of optically thick ($\tau_S > 1$) and thin ($\tau_S < 1$) lines, one finds:

$$\begin{aligned} g_{rad}^{tot} &= \frac{s_e v_{th} N_0 \int_0^\infty L_\nu \nu f_\nu d\nu}{4\pi r^2 c^2} \left\{ \frac{1}{\alpha(1-\alpha)} \right\} k_1^\alpha \\ &= \frac{s_e L}{4\pi r^2 c} \frac{\int_0^\infty L_\nu \nu f_\nu d\nu}{L} \frac{v_{th}}{c} \frac{N_0}{\alpha(1-\alpha)} t^{-\alpha} \\ &= g_e M(t) \end{aligned} \tag{5.14}$$

With Eq. 5.8 and 5.14, it is possible to give a physical interpretation of the CAK parameters:

◇ k : from Eq. 5.14, we have

$$k = \frac{\int_0^\infty L_\nu \nu f_\nu d\nu}{L} \frac{v_{th}}{c} \frac{N_0}{\alpha(1-\alpha)} \tag{5.15}$$

Hence, we see that k is directly proportional to the total number of lines (through N_0). It also depends on α which among other interpretation, is also the ratio of the acceleration due to optically thick lines to the total acceleration (this can be derived from Eq. 5.14). The physical properties of the radiative acceleration due to lines highlighted above appear then naturally in the derivation of the total acceleration.

- $\diamond$ α : as already mentioned above, α can be interpretated as the ratio of the acceleration due to optically thick lines to the total acceleration. But one sees that α has a more fundamental origin. Indeed, it comes directly from the line strength distribution function. As one could expect, it is then the detailed statistics of lines which governs the radiative acceleration of produced by those lines. A very detailed study of the line statistics can be found in Puls, Springmann & Lennon (2000). The typical value of α is 2/3.

- $\diamond$ δ : this parameter does not appear in our derivation of the total acceleration. It is due to an implicit assumption we have made. Indeed, adopting a constant value for the normalisation factor N_0, we have assumed that the ionisation in the wind was constant (and that the total number of lines was the same). However, this ionisation will change since recombinations (which scales with the density square) and photoionisations (scaling with density times the mean radiation field, being itself dependent on the dilution geometrical factor W) are changed as one goes outward. Hence, the normalisation factor N_0 should vary with $\frac{n_e}{W}$ where n_e is the electron density. Practically, Abbott (1982) introduced the parameter δ to take this effect into account according to

$$N_0' = N_0 \left(10^{-11} \frac{n_e}{W}\right)^{\delta} \tag{5.16}$$

  δ is usually of the order 0.05..0.1.

Thanks to the CAK formalism, we have a mean to express the radiative acceleration, which is the main difficulty of the theory of radiatively driven winds. We can go on and derive the solutions for the hydrodynamical structure.

5.3 Hydrodynamical structure

Now that we have an expression for the radiative acceleration due to lines, we can rewrite Eq. 5.1. Let us introduce the factor Γ_e to express the radia-

tive acceleration due to electron scattering as a function of gravitational acceleration:

$$g^e = \frac{\sigma_e L}{4\pi r^2 c} = \frac{GM}{r^2}\Gamma_e \tag{5.17}$$

If moreover we express the state equation in an isothermal wind, we have $P = \rho a^2$ where a is the sound speed. Hence, the momentum conservation equation writes:

$$\frac{vdv}{dr} = -\frac{GM(1-\Gamma_e}{r^2} + \frac{a2}{v}\frac{dv}{dr} + \frac{2a^2}{r} + g^e k t^{-\alpha}\left\{\frac{10^{-11}n_e}{M}\right\}^{\delta} \tag{5.18}$$

Using Eq. 5.7 and 5.2 we obtain:

$$\left(1-\frac{a^2}{v^2}\right) r^2 \frac{vdv}{dr} = -GM(1-\Gamma_e) + 2a^2 r + C\left(r^2\frac{vdv}{dr}\right)^{\alpha} \tag{5.19}$$

where the constant C is

$$C = \frac{\sigma_e L k}{a\pi c}\left\{\frac{\sigma_e v_{th}\dot{M}}{4\pi}\right\}^{-\alpha}\left\{\frac{10^{-11}n_e}{W}\right\}^{\delta} \tag{5.20}$$

Following Lamers & Cassinelli (1999), we write Eq. 5.20 as

$$F(r, v, v') = 0 \tag{5.21}$$

where $v' = \frac{dv}{dr}$

Eq. 5.19 is a non linear equation of the variable $r^2 v\frac{dv}{dr}$. It can be numerically solved. Castor, Abbott & Klein (1975, see also Lamers & Cassinelli, 1999) have derived the various solution of this equation which are shown in Fig. 5.2. Let us describe this figure. It gives the ratio of velocity to sound speed as a function of radius. Regions A and B are forbidden regions in which no solution exists. r_P is the Parker point defined as

$$-GM(1-\Gamma_e) + 2a^2 r_P = 0 \tag{5.22}$$

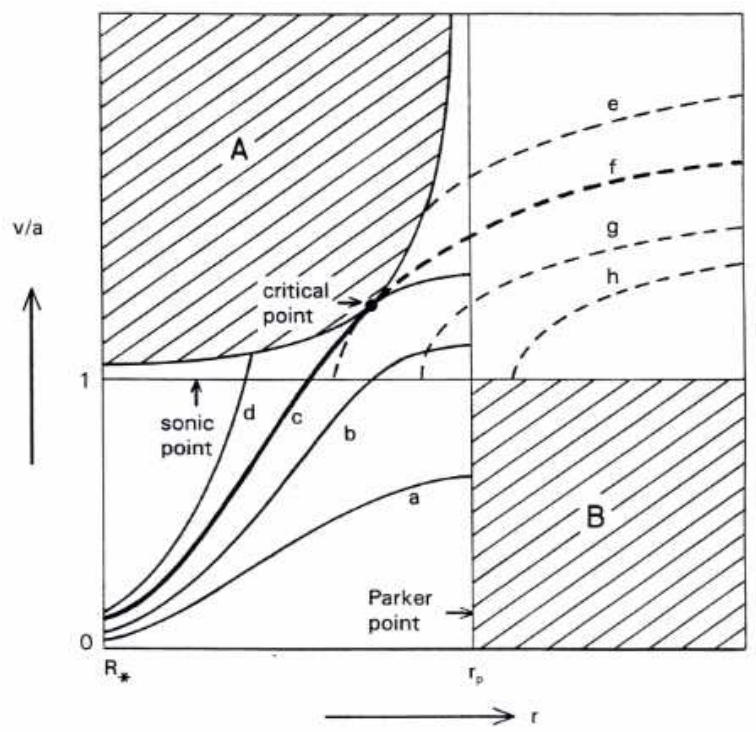

Figure 5.2: Topology of the solutions of the hydrodynamical equations in an expanding atmosphere in terms of velocity as a function of radius. a is the sound speed. Regions A and B are forbidden regions where no solution exist. a,b,c...g,h are the various types of solutions. The only solution connecting smoothly the stellar photosphere and the outer wind is a combination of solution c and f which join at the critical point. From Lamers & Cassinelli (1999).

Historically, this point corresponds to the singularity point of the momentum conservation equation in the solar atmosphere. a,b,c...g,h lines are various solution of the momentum conservation equation, some starting subsonic, some starting supersonic. From this figure, one sees that there is only one solution that start subsonic, then goes through the sonic point and end supersonic in the outer atmosphere: it is a combination of solutions c and f. How do these two solutions connect? Physically, the velocity must be a smooth function of the radius, which means that the velocity gradient must be continuous at the connecting point (regularity condition). Moreover, there should be only one solution for the velocity at the connecting point (singularity condition). These two conditions can be mathematically expressed as:

$$v'' = \frac{d^2v}{dr^2} = 0 \tag{5.23}$$

$$\left(\frac{\partial F}{\partial v'}\right) = 0 \tag{5.24}$$

both equations being valid at the connecting point, which is also called critical point (for a discussion of the critical point, see Lamers & Cassinelli, 1999).

The momentum conservation equation requires that F is constant (=0), in the atmosphere, so that we have $\frac{dF}{dr} = 0$. Developing this expression, one finds:

$$\frac{dF}{dr} = \frac{\partial F}{\partial r} + v'\frac{\partial F}{\partial v} + v''\frac{\partial F}{\partial v'} = 0 \tag{5.25}$$

from which we obtain

$$v'' = -\frac{\frac{\partial F}{\partial r} + v'\frac{\partial F}{\partial v}}{\frac{\partial F}{\partial v'}} \tag{5.26}$$

so that Eq. 5.23 can be rewritten

$$\frac{\partial F}{\partial r} + v'\frac{\partial F}{\partial v} = 0 \tag{5.27}$$

With the three equations 5.21, 5.26 and 5.27 written at the critical point, it is possible to derive the following results (see Lamers & Cassinelli 1999 p. 229 for a detailed derivation):

$$r_c^2 v_c v_c^{'} = \left(\frac{\alpha}{1-\alpha}\right)\{GM(1-\Gamma_e) - 2a^2 r_c\}\left\{1 - \frac{a^2}{v_c^2}\right\}^{-1} \tag{5.28}$$

$$v_c = a^2 + \left(\frac{\alpha}{1-\alpha}\right)\left\{\frac{GM(1-\Gamma_e)}{r_c} - 2a^2\right\} \tag{5.29}$$

$$\begin{aligned}\dot{M} &= \left(\frac{4\pi}{\sigma_e v_{th}}\right)\left(\frac{\sigma_e k}{4\pi c}\right)^{\frac{1}{\alpha}}(1-\alpha)^{\frac{1}{\alpha}} L^{\frac{1}{\alpha}}\left\{\frac{10^{-11} n_e}{W}\right\}^{\frac{\delta}{\alpha}} \\ &\quad \{GM(1-\Gamma_e) - 2a^2 r_c\}^{-\frac{1}{\alpha}} \\ &\quad \left[\left(\frac{\alpha}{1-\alpha}\right) GM(1-\Gamma_e) - 2a^2 r_c + a^2 r_c\right]\end{aligned} \tag{5.30}$$

where r_c is the radius of the critical point. As we will justify below, the critical point is most of the time well above the sonic point, so that the escape velocity at the critical point is much higher than the sound speed ($\frac{GM(1-\Gamma_e)}{r_c} \gg a^2$) so that Eq. 5.30 can be approximated by

$$\begin{aligned}\dot{M} &\simeq \left(\frac{4\pi}{\sigma_e v_{th}}\right)\left(\frac{\sigma_e k}{4\pi}\right)^{\frac{1}{\alpha}}(k\alpha)^{\frac{1}{\alpha}}\left(\frac{\alpha}{1-\alpha}\right)^{\frac{1-\alpha}{\alpha}}\left(\frac{L}{c}\right)^{\frac{1}{\alpha}} \\ &\quad \{GM(1-\Gamma_e)\}^{\frac{\alpha-1}{\alpha}}\left(\frac{10^{-11} n_e}{W}\right)^{\frac{\delta}{\alpha}}\end{aligned} \tag{5.31}$$

Here, we have to note that n_e/W, which enters the constant C, is not strictly constant throughout the atmosphere since both n_e and W vary. However, as δ is usually low (of the order of 0.05), the dependence with depth is very small which allows us to consider C as a constant in the previous steps of the reasoning. If now we take into account the fact that n_e is directly proportional to the density, and then to the mass loss rate, we can simply derive from Eq. 5.31

$$\dot{M} \propto L^{\frac{1}{\alpha-\delta}}\{GM(1-\Gamma_e)\}^{\frac{\alpha-1}{\alpha-\delta}} \tag{5.32}$$

Usually, the notation $\alpha' = \alpha - \delta$ is introduced.

We can apply the same approximation as we used in Eq. 5.31 to rewrite the momentum conservation equation 5.19

$$rvv' + GM(1-\Gamma_e) - C(rvv')^{\alpha} = 0 \tag{5.33}$$

which implies that rvv' must be constant and equal to its value at the critical point given by Eq. 5.28. Hence, we have

$$rv\frac{dv}{dr} \simeq \left(\frac{\alpha}{1-\alpha}\right) GM(1-\Gamma_e) \tag{5.34}$$

The solution of this equation is

$$v^2 = v_c^2 + 2\left(\frac{\alpha}{1-\alpha}\right) GM(1-\Gamma_e)\left(\frac{1}{r_c} - \frac{1}{r}\right) \tag{5.35}$$

Substituting Eq. 5.29 into Eq. 5.36 gives

$$v^2 = \left(\frac{\alpha}{1-\alpha}\right) v_{esc}^2 \left\{\frac{3}{2}\frac{R}{r_c} - \frac{R}{r}\right\} \tag{5.36}$$

Here, we can assume for a second that the velocity at r=R is close to the sound speed (since the sonic point is very close to the stellar surface), which yields

$$r_c = \frac{3}{2}R\left\{1 + \frac{1-\alpha}{\alpha}\frac{a^2}{v_{esc}^2}\right\}^{-1} \tag{5.37}$$

so that we can estimate that $r_c \simeq 1.5$ R, justifying the assumption that the critical point is higher than the sonic point so that thermal terms can be neglected compared to gravitational terms in Eq. 5.36 and 5.31.

The final substitution of Eq. 5.37 in Eq. 5.36 leads to

$$v^2 = a^2 + \left(\frac{\alpha}{1-\alpha}\right) v_{esc}^2 \left\{1 - \frac{R}{r}\right\} \tag{5.38}$$

which can again be again approximated by

$$v \simeq v_\infty \sqrt{1 - \frac{R}{r}} \tag{5.39}$$

where

$$v_\infty = \sqrt{\frac{\alpha}{1-\alpha}} v_{esc} \tag{5.40}$$

We have derived the expressions for the mass loss rate and the terminal velocity of a wind driven by line acceleration. A comment to make is that the mass loss rate is set by the regularity and singularity conditions at the critical point. This is because there is only one solution for the velocity law to connect the inner and outer atmosphere, and this solution exists only for a given value of the acceleration at this point. But the acceleration depends on the density, and thus on the mass loss rate, so that only one value of the mass loss rate is allowed.

5.4 Scaling relations

Let us now examine the dependencies of the terminal velocity and of the mass loss rate on stellar parameters. First, from Eq. 5.40, we see that the terminal velocity does not depend on the mass loss rate (or the density). As the acceleration depends on $\rho^{-\alpha}$ one could expect such a dependence. However, due to the uniqueness of the solution for velocity, a given mass loss rate is imposed, so that $\dot{M}$ is not a free parameter of the solution. Hence, the terminal velocity depends on the processes giving birth to the acceleration (i.e. the statistics of the lines) but not on the mass loss rates which is a consequence of the acceleration, just as the velocity field. The terminal velocity depends on the escape velocity, which means that a higher gravity will imply a higher velocity. This reflects the fact that a higher velocity is required to escape the star's gravity.

As regards the mass loss rate, Eq. 5.31 reveals that $\dot{M}$ depends also on the line statistics through the parameters k and α. It depends also on $L^{\frac{1}{\alpha'}}$. The higher the luminosity, the higher the number of photons available to be absorbed by the lines and the higher the transfer of momentum. Hence, more material can be accelerated and a higher mass loss rate results. $\dot{M}$ is also proportional to $(GM(1-\Gamma_e))^{\frac{\alpha-1}{\alpha'}}$. We have seen that α is the ratio of acceleration due to optically thick lines to optically thin lines, so that $\alpha < 1$. Hence a higher mass will result in a lower mass loss rate. This can

be understood by saying that a higher mass will lead to a higher gravity, and thus to a lower total acceleration (provided the radiative acceleration is given), so that less material will be lifted.

To quantify the strength of a radiatively driven wind, the natural quantity which comes to mind is the wind momentum $\dot{M} \times \mathrm{v}_\infty$. From Eq. 5.32 and 5.40, we have

$$\dot{M} v_\infty \propto L^{\frac{1}{\alpha'}} \{GM(1-\Gamma_e)\}^{\frac{\alpha-1}{\alpha'}+\frac{1}{2}} R^{-\frac{1}{2}} \tag{5.41}$$

If we now multiply this wind momentum by $\sqrt{R}$, we obtain the so-called modified wind momentum

$$\dot{M} v_\infty \sqrt{R} \propto L^{\frac{1}{\alpha'}} \{GM(1-\Gamma_e)\}^{\frac{1}{2}+\frac{\alpha}{\alpha'}-\frac{1}{\alpha'}} \tag{5.42}$$

We see that this quantity depends only on the luminosity of the star and on its effective mass. But the interesting thing is that usually, $\alpha \sim \alpha' \sim 2/3$ so that this last dependency disappears! We are left with a quantity which depends only on the luminosity. This property was discovered by Kudritzki, Lennon & Puls (1995) who highlighted its potential as a distance indicator. Indeed, if the relation between the modified wind momentum can be calibrated, the spectroscopic analysis will give the wind and stellar parameters necessary to compute $\dot{M} v_\infty \sqrt{R}$ which in turn will give the absolute luminosity, and thus the distance. We will go back to this important relation in the next sections.

In the above discussion, we have given the basic ideas of the radiation driven wind theory. More details can be found in Castor, Abbott & Klein (1975), Pauldrach et al. (1986), Kudritzki et al. (1989), Puls et al. (1996), Lamers & Cassinelli (1999) and Kudritzki & Puls (2000).

In our previous derivation of the wind parameters as a function of stellar parameters, we have made the implicit assumption that the star was considered as a point source. In reality, this is of course not the case, especially for the parts of the atmosphere closest to the photosphere. In practice, this means that the radiative accelerations will be slightly changed. First, due to a pure geometrical effect, the momentum gained by an absorbing element will be lower if the absorbed photon comes with a non radial direction (the correction being simply $cos\theta$ where θ is the angle between the photon's direction and the radial direction). Second, an extension of the stellar surface will lead to modifications of the optical depth since the radial velocities of the photons will be modified (due again to the geometrical effect). Hence, the global radiative acceleration will

be modified together with the wind properties. Friend & Abbott (1986) were the first to study this effect which was further deeply investigated by Kudritzki et al. (1989). The main quantitative effects of a finite disk compared to the point source approximation are the following:

- Mass loss rate: the mass loss rate is reduced by a factor $\lesssim 2$. This is due to the reduced acceleration close to the star and to the critical point where the mass loss rate is set.
- Terminal velocity: v_∞ is increased by a factor ~ 1.85 (see Lamers & Cassinelli, 1999). The Sobolev optical depth is reduced (due to the reduced wind density) which increases the radiative acceleration (since it is proportional to t^{-1}, see Eq. 5.7, 5.8). This leads to a higher terminal velocity.
- Slope of the velocity field: in the finite disk case, the velocity is as follows

$$v(r) \propto v_\infty \left(1 - \frac{R}{r}\right)^\beta \tag{5.43}$$

  which is a generalisation of Eq. 5.39 where we had $\beta = 0.5$. Here, with the modified accelerations due to the finite size of the disk, we have $\beta \sim 0.8$.

Scaling relations between the point source and finite disk predictions of the wind parameters are given by Kudritzki et al. (1989).

One other important point concerns the metallicity dependence of the radiation driven winds. We have already seen that due to the nature of the mechanism, the wind properties are expected to scale with the metal content. Abbott (1982) first quantified this effect and showed that $\dot{M}$ should be a power law of metallicity Z with an exponent of ~ 0.94. More recent hydrodynamical simulations by Vink, de Koter & Lamers (2001) indicate an exponent ~ 0.7. The terminal velocity is also expected to be reduced with lower Z. Leitherer, Robert & Drissen (1992) claimed a dependence with $Z^{0.13}$. Quantitative studies of the metallicity dependence of wind properties have been pursued by Puls, Springmann & Lennon (2000). Their very detailed investigations traced the origin of the effects of the metal content on the wind properties. We give the main results of their work.

First, due to the definition of k_L (see Eq. 5.10) we have the simple scaling

$$k_L(Z) = k_L(Z_\odot) \left(\frac{Z}{Z_\odot} \right) \tag{5.44}$$

Injecting this relation in Eq. 5.12

$$dN(\nu, k_L, Z) = -N_0 \left(\frac{Z}{Z_\odot} \right)^{\alpha-1} f_\nu(\nu) k_L^{\alpha-2} d\nu dk_L \tag{5.45}$$

from which we can derive

$$N_0(Z) = N_0(Z_\odot) Z^{1-\alpha} \tag{5.46}$$

Using Eq. 5.15 and 5.31, we are left with the following scaling relation

$$\dot{M}(Z) = \dot{M}(Z_\odot) \left(\frac{Z}{Z_\odot} \right)^{\frac{1-\alpha}{\alpha'}} \tag{5.47}$$

This is what Puls, Springmann & Lennon (2000) call the direct metallicity effect. It is directly due to the change of the metal content, leading to a lower acceleration (lower k) and to a lower mass loss rate. There is however another effect of metallicity which appears less clearly. Indeed, a modification of the metallicity will change the line strength distribution function. In particular, as the wind will be thinner, the importance of strong lines will increase. But the line strength distribution function shows a significant curvature for large line strength, with corresponding lower values of α. Hence, on a global point of view, the reduction of the metallicity will lead to lower α so that the mass loss rates will be changed according to Eq. 5.31, *independently of the modification of k* (direct effect). Note that at high metallicity, this effect should not happen and only the direct metallicity effect is expected. The change of α modifies the terminal velocity according to Eq. 5.40. We will go back to this metallicity dependence in Sect. 7.2.2.

Hence, as expected from the very mechanism of radiation driven winds, metallicity plays an important role in the properties of massive stars winds.

With these basic concepts in mind, we can now move to the analysis of the massive stars of the star forming region N81 of the SMC. As we have already highlighted (see Sect. 1.1), such stars are perfect targets to study both the properties of young massive stars and the wind properties in general and their metallicity dependence in particular.

Chapter 6

Qualitative analysis of massive stars in SMC-N81

French summary

Ce chapitre contient une analyse qualitative des étoiles massives à l'intérieur du "High Excitation Blob" N81 dans le Petit Nuage de Magellan.

Cette région de formation stellaire représente une bonne opportunité d'observer des étoiles massives récemment formées car elle est probablement dans un stade suivant juste la phase de région HII ultra-compacte dans laquelle les étoiles en formation et/ou formées récemment sont inaccessibles. De plus, ces étoiles de N81 sont intéressantes à analyser car elles appartiennent à un environnement déficient en métaux. L'étude de l'influence de la métallicité sur les propeiétés de vent est donc possible.

Les étoiles de N81 ont été résolues pour la première fois par le télescope spatial (Heydari-Malayeri et al., 1999a) grâce à sa résolution spatiale incomparable. De plus, son accès au domaine ultraviolet (instrument STIS) a permis d'obtenir des spectres contenant des raies traditionnellement sensibles aux paramètres de vent d'une qualité suffisante pour une analyse spectroscopique. Une étude qualitative de ces spectres a révélé les caractéristiques suivantes:

- Les étoiles les plus brillantes de l'amas de N81 sont des naines de type O intermédiaire à tardif.
- Ces étoiles ont des faibles luminosités qui correspondent à des magnitudes environ 2 unités plus basses que des naines O classiques.
- Elles montrent des signatures de vent très faibles sans aucune émission dans les fortes raies de résonance UV traditionnellement sensibles aux vents.

- Leur faible luminosité accompagnée d'une faiblesse évidente des vents les rend de possibles candidates pour appartenir à la classe des étoiles Vz qui sont des étoiles massives jeunes supposées être encore sur - ou non loin de - la séquence principale d'âge zéro (Walborn & Parker, 1992).

L'appartenance à la classe Vz ne peut pas être affirmée avec certitude car elle repose par définition sur le comportement de la raie He II λ4686 qui doit avoir une absorption plus forte que toutes les autres raies d'He du domaine optique. Malheureusement, nous ne disposons pas de spectres optiques pour ces étoiles. Néanmoins, la proximité de la ZAMS doit se traduire par une relative sous-luminosité et par un vent plus faible car la perte de masse grandit au cours de l'évolution, remplissant ainsi la raie He II λ4686 par l'émission se produisant dans l'atmosphère.

In this chapter, we make a qualitative analysis of the stellar component of the High Excitation Blob SMC-N81. The main stellar and wind properties are derived and an approximate spectral classification is made.

We have previously put forward the great opportunity High Excitation Blobs represented for the study of young massive stars in a metal poor environment. N81 is one of these HEBs. It is especially interesting for the following two reasons: first, it belongs to the Small Magellanic Cloud, which has the lowest metallicity of the two Clouds, rendering easier the study of any dependence on the metal content; second, it hosts a small cluster of massive stars that have been revealed for the first time by HST (Heydari-Malayeri et al., 1999a). This has motivated the spectroscopic observations of its components with HST, which is the only available telescope with both sufficient spatial resolution and sensitivity in the UV (due to its position out of Earth atmosphere). Several stars powering the HII regions inside N81 were observed thanks to STIS. UV spectra were obtained with a resolution of ~ 1.2 Å and a signal to noise ratio of the order of 10 to 30.

A qualitative analysis of these spectra revealed the following properties:

- The brightest stars of the N81 cluster are mid to late O dwarfs.
- They have low luminosities, being nearly 2 magnitudes fainter than typical O dwarfs of the same spectral type.
- They show signatures of very weak winds with no emission in the strong resonance lines.
- Their low luminosity and weakness of the wind render them possible Vz candidates.

Vz stars are dwarf O stars thought to be lying close to the Zero Age Main Sequence. The exact definition of this class of stars relies on the strength of the He II λ4686 line which is stronger than any other He II lines in these stars. This is thought to be a property of young massive stars with weak winds since the He II λ4686 line has not yet been filled by wind emission. The first Vz stars were observed by Walborn & Parker (1992). Unfortunately, in our case, we do not have optical spectra of the N81 stars so that we can not firmly establish that they indeed belong to this class of objects.

The details of the qualitative analysis are given in the following paper.

A&A 381, 951–958 (2002)
DOI: 10.1051/0004-6361:20011574

Astronomy & Astrophysics

STIS spectroscopy of newborn massive stars in SMC N81⋆

M. Heydari-Malayeri[1], M. R. Rosa[2,⋆⋆], D. Schaerer[3], F. Martins[3], and V. Charmandaris[4]

[1] DEMIRM, Observatoire de Paris, 61 avenue de l'Observatoire, 75014 Paris, France
[2] Space Telescope European Coordinating Facility, European Southern Observatory, Karl-Schwarzschild-Strasse-2, 85748 Garching bei München, Germany
[3] Laboratoire d'Astrophysique, Observatoire Midi-Pyrénées, 14 avenue É. Belin, 31400 Toulouse, France
[4] Cornell University, Astronomy Department, 106 Space Sciences Bldg., Ithaca, NY 14853, USA

Received 14 August 2001 / Accepted 25 October 2001

Abstract. Using *Hubble Space Telescope* observations with STIS, we study the main exciting stars of N81, a high excitation compact H II region in the Small Magellanic Cloud (SMC). These far UV observations are the first spectroscopic measurements of stars in such a region and reveal features characteristic of an O6–O8 stellar type. The astonishing weakness of their wind profiles and their sub-luminosity (up to ∼2 mag fainter in M_V than the corresponding dwarfs) make these stars a unique stellar population in the Magellanic Clouds. Our analysis suggests that they are probably in the Hertzsprung-Russell diagram locus of a particularly young class of massive stars, the so-called Vz luminosity class, as they are arriving at the zero age main sequence.

Key words. stars: early-type – ISM: dust, extinction – ISM: H II regions – ISM: individual objects: N81 – galaxies: magellanic clouds

1. Introduction

Understanding the formation of massive stars, which is still a largely unsolved problem, requires studying them at the earliest phases where they can be reached through the enshrouding material at different wavelengths. While high resolution radio continuum observations allow the investigation of ultracompact H II regions formed around newborn massive stars (Churchwell 1990), high angular resolution observations in the ultraviolet, visible, and infrared are also necessary to access accurate physical parameters of these stars in order to identify their evolutionary states (Walborn & Fitzpatrick 1990; Walborn et al. 1995b; Hanson et al. 1996). In particular, UV observations are of prime importance since massive stars emit the bulk of their energy in this wavelength range. In practice, though, observing newborn massive stars is not straightforward for several reasons. Mainly, they are very rare, and the relatively small evolutionary timescales involved make it difficult to catch them just at this very point in their evolution, that is when they become observable in the UV and visible (Yorke & Krügel 1977; Shu et al. 1987; Palla & Stahler 1990; Beech & Mitalas 1994; Bernasconi & Maeder 1996).

We have amply argued that the compact H II regions known as HEBs (High Excitation Blobs) provide the best opportunities for a direct access to massive stars at very early stages of their evolution (Heydari-Malayeri et al. 2001a and references therein). The members of this distinct and very rare class of ionized nebulae in the Magellanic Clouds are small and compact (∼ 5″ to 10″ in diameter corresponding to ∼1.5–3.0 pc), in contrast to the typical H II regions in those galaxies, which are extended structures (sizes of several arcmin corresponding to more than 50 pc, powered by a large number of exciting stars). In general, HEBs are also heavily affected by local dust, as one would expect from their very young age (Heydari-Malayeri et al. 2001a and references therein, see also Israel & Koornneef 1991). Also their study is pertinent to understanding the process of massive star formation, especially in the context of the Magellanic Clouds.

Our recent high-resolution imaging with the *Hubble Space Telescope* (GO 6563, GO 8246) using the Wide Field Planetary Camera (WFPC2) has for the first time resolved

Send offprint requests to: M. Heydari-Malayeri,
e-mail: heydari@obspm.fr

⋆ Based on observations with the NASA/ESA Hubble Space Telescope obtained at the Space Telescope Science Institute, which is operated by the Association of Universities for Research in Astronomy, Inc., under NASA contract NAS 5-26555.

⋆⋆ Affiliated to the Astrophysics Division, Space Science Department of the European Space Agency.

several HEBs which had appeared featureless to ground-based telescopes: SMC N81, N88A, LMC 159-5 (the Papillon nebula), N83B, and N11A (Heydari-Malayeri et al. 1999a, 1999b, 1999c, 2001a, 2001b). The *HST* observations uncover the stellar content hidden thus far, as well as the nebular features of these compact nebulae and display a turbulent environment typical of newborn massive star formation sites: outstanding emission ridges created by shocks and cavities sculpted in the ionized gas by the powerful winds of massive stars, prominent dust structures protruding from hot gas. The observations also bring to light even more compact H II blobs, immersed in the HEBs, harboring newborn, hot stars.

The present paper is devoted to N81, also known as DEM 138 (Henize 1956; Davies et al. 1976), a nebula only $\sim 10''$ across and located in the Shapley Wing at $\sim 1\overset{\circ}{.}2$ ($\sim$1.2 kpc) from the main body of the SMC. A first detailed study of this compact H II region, carried out by Heydari-Malayeri et al. (1988), revealed its nature and some of its physical characteristics: gas density and temperature, chemical composition, mass, age, etc. Subsequently, near infrared observations showed the presence of H_2 emission towards N81 (Israel & Koornneef 1988), while ^{12}CO(1–0) emission at two points towards this H II region was also detected (Israel et al. 1993). However, due to the lack of sufficient spatial resolution, it was not possible to view and study the exciting star(s) hidden inside the ionized gas. Therefore, the rather important question, which is often raised by star formation theories, of whether N81 was powered by a single massive star or a cluster of them, remained unanswered. This is, however, a critical question for theories of star formation.

High spatial resolution imaging with *HST* allowed us to resolve N81 and revealed the presence of a tight cluster of newborn massive stars embedded in this compact nebula (Heydari-Malayeri et al. 1999, hereafter Paper I). Six of the stars are grouped in the core region of $\sim 2''$ diameter, with a pair of the main exciting stars in the very center separated by only $0''.27$ or 0.08 pc. The images also displayed conspicuous marks of strong stellar winds, shocks, and ionization fronts characterising turbulent massive star forming regions. Moreover they revealed prominent dust lanes dividing the nebula into three lobes. One of the lanes, running over $15''$ (4.5 pc), ends in a magnificent curved plume. A remarkable absorption "hole" or dark globule of radius $\sim 0''.25$ ($\sim$0.07 pc) is situated towards the center of the H II region, where the extinction reaches higher values ($A_V = 1.3$ mag). These absorption features are probably parts of the molecular cloud which have given birth to the massive stars.

From the Strömgren *uvby* imaging with WFPC2 we carried out the photometry of some 50 stars towards N81. This allowed us, using color-magnitude diagrams, to select the main exciting stars of the region. This paper is devoted to the spectroscopy of these stars. We derive spectral classification for these very young massive stars and study their nature.

2. Observations and reduction

The General Observer Program No. 8246 devoted to observations of N81 was performed with Space Telescope Imaging Spectrograph, STIS (Woodgate et al. 1998) on board *HST* on 28 and 31 October 1999. The spectra were obtained with the far-UV Multi-Anode Microchannel Array (MAMA) detector in the G140L mode covering the wavelength range 1120–1715 Å. All the observations were made through the $52''\times 0''.2$ entrance slit. The effective resolution was 0.6 Å per pixel of 25 μm, corresponding to a dispersion of 24 Å mm^{-1}, or a resolution of 1.2 Å ($FWHM$). The exposure times were set according to the apparent magnitudes of the stars in order to equalize the signal-to-noise ratios (S/N) of the spectrograms. Total exposure times varied from 1229 s (stars #1 and #2) to 3169 s (stars #3, #4, and #8). Three relatively faint stars (#5, #7, #10), not initially scheduled for observations, happened to lie on the slit when observing their adjacent stars (#3 and #11). The S/N ratio is particularly weak for these stars, yet we present the spectrogram of star #5 which shows some interesting features. STIS was also used to obtain the spectra of the N81 stars in the visible domain. The grating G430L covered the range of 2900 to 5700 Å with a resolution of of 2.73 Å per pixel. The CCD pixels of 21 μm yielded a dispersion of 130 Å mm^{-1}. The exposure times ranged from 24 s (star #1) to 750 s (star #8).

The calibrated output products from the standard pipeline use a default extraction aperture of 22 pixels ($0''.53$ on the sky). We carefully reprocessed the 2D images using the most recent calibration reference files applicable to the observations and extracted the spectra using slits of both 6 and 2 pixels. We verified the centering of the stars on the slits, and tested for the effects of different sky background extraction on our spectra. The 6 pixel slit yielded spectra which are very similar to those produced by the standard pipeline with an insignificant loss in S/N. Even the 2 pixel slit did not indicate any extraction effect due to its size other than the expected loss in S/N. Comparing the resulting line profiles as a function of the aperture width, we found that other than an increase in noise when going to the smaller slits, and slightly modifying the slope of the spectra (because of a slight tilt of the spectral images), the line profiles do not change by any significant amount. The spectra displayed in Figs. 1 and 2 are based on 6 pixel extraction apertures.

3. Results

The N81 stars observed with STIS are listed in Table 1, and their physical location can be seen in Fig. 2 of Paper I. The table also presents the corresponding photometry of the stars (Paper I). The color excesses $E(B-V)$ were derived from $E(b-y)$ using the intrinsic color $(b-y)_0 = -0.15$ mag for hot stars (Relyea & Kurucz 1978) and assuming that our observed colors represent the standard Strömgren system. The relation $E(B-V) = 1.49\ E(b-y)$

Table 1. SMC N81 stars observed with STIS.

Star number	α (J2000)	δ (J2000)	y (F547M) (mag)	$b-y$ (mag)	A_V (mag)	M_V (mag)
1	01:09:13.1	−73:11:38.3	14.38	−0.10	0.22	−4.84
2	01:09:13.0	−73:11:38.0	14.87	−0.11	0.19	−4.32
3	01:09:13.4	−73:11:38.4	16.10	−0.08	0.31	−3.21
4	01:09:12.8	−73:11:38.3	17.41	+0.07	1.02	−2.61
5	01:09:13.3	−73:11:37.6	18.29	−0.05	0.46	−1.17
8	01:09:12.8	−73:11:40.2	17.84	+0.15	1.40	−2.56
11	01:09:13.7	−73:11:33.3	15.74	−0.10	0.22	−3.48
13	01:09:16.1	−73:11:29.1	16.65	−0.08	0.31	−2.66

(Kaltcheva & Georgiev 1992) was then used to transform into the Johnson system, which finally yielded the extinctions $A_V = 3.1\ E(B-V)$. The estimated absolute magnitudes are based on a distance modulus $M - m =$ 19.0 mag (corresponding to a distance of 63.2 kpc, e.g. Di Benedetto 1997 and references therein) and assuming that the Strömgren y filter is equal to the Johnson V.

The final reduced spectrograms are presented in Figs. 1 and 2, where the former figure includes the four brightest stars of the sample, whereas Fig. 2 displays the fainter ones. The main stellar features (C III λ1176, N V λ1239, 1243, O V λ1371, Si IV $\lambda\lambda$1394, 1403, C IV λ 1548, 1551, and He II λ1640) are distinguished with tick marks. The labels appearing below the features indicate cases where contamination with an interstellar component is possible. The identification of S V λ1502 Å is based on the work of Werner & Rauch (2001).

An outstanding aspect of these spectra is the extreme weakness of the UV wind profiles. Weak stellar wind features in SMC O stars have already been found by several workers (Hatchings 1982; Garmany & Conti 1985; Walborn et al. 1995b), who ascribed them to the metal deficiency of the SMC leading to a reduced radiation pressure responsible for driving the winds of early-type stars. More recent observations have further confirmed this result (Smith Neubig & Bruhweiler 1997; Walborn et al. 2000). However, the wind features observed in the stars of N81 are even weaker. If we consider the usually stronger wind lines seen in O stars (such as the N V λ1239, 1243 and C IV λ1548, 1551 in dwarfs, or the Si IV $\lambda\lambda$1394, 1403 in giants/supergiants), with the exception perhaps of star #5, none shows the emission part of a P-Cygni profile and the absorption is extremely weak, particularly for N V $\lambda\lambda$1239, 1243. For stars which we classify as O types (see below), such a behavior is observed for the first time.

3.1. Spectral classification

Traditionally the spectral classification schemes of stars are based on their optical spectra. However, recent studies comparing spectral features in the optical and UV have resulted in a global, coherent picture of classification criteria (Walborn et al. 1985, 1995a; Smith Neubig & Bruhweiler 1997, 1999). In particular, Smith Neubig & Bruhweiler (1997) have proposed a UV classification system for O and B stars of the SMC which is defined by a set of standard, low resolution spectra observed with the *International Ultraviolet Explorer (IUE)*. This UV scheme, which was used by the authors to derive classifications for 133 O and B stars of the SMC, while independent of the MK system, shows general agreement with those deduced from visual data.

The low S/N ratio of our STIS optical spectra and in particular their contamination with strong nebular emission lines limit their practical use for spectral classification. This can be understood since N81 is a very bright compact H II region with strong nebular emission lines in the visible part of the spectrum (Paper I). Although nebular emission lines are present also in the UV part, they are much less troublesome. Therefore, we will use the method put forward by Smith Neubig & Bruhweiler (1997). However, given some morphological differences of the N81 UV spectra with previously well studied stars, the limitations of the optical part of the spectrum mentioned earlier, and the constraints available from the UV classification scheme (Smith Neubig & Bruhweiler 1997), it is clear that there is no unique solution to the spectral classification of our targets.

The presence of He II λ1640 and O V λ1371 in all spectra, except perhaps in stars #13 and #8 which have lower S/N ratios, is the first and strongest evidence that we are observing O type stars. These spectra though display characteristics suggesting that the stars also belong to the dwarf luminosity class since the features Si IV $\lambda\lambda$1394, 1403 as well as N V $\lambda\lambda$1239, 1243 and C IV $\lambda\lambda$1548, 1551 are weak (even weaker than usual). Star #5 may be a different case as explained below. These features are known to increase with luminosity, ranging from weak P-Cyg profiles on the main sequence to very pronounced P-Cyg profiles in the supergiants (Walborn et al. 1995a; Smith Neubig & Bruhweiler 1997). A dwarf luminosity class is also supported by the optical spectra which show no He II λ 4686 and N III λ4640 emission. Although the morphology of the N81 spectra differs qualitatively from that of the known O types, we may classify them as "zero age main sequence dwarf" Vz, based on the weakness of the wind lines (Walborn & Parker 1992; Walborn & Blades 1997; Walborn et al. 2000). Note that

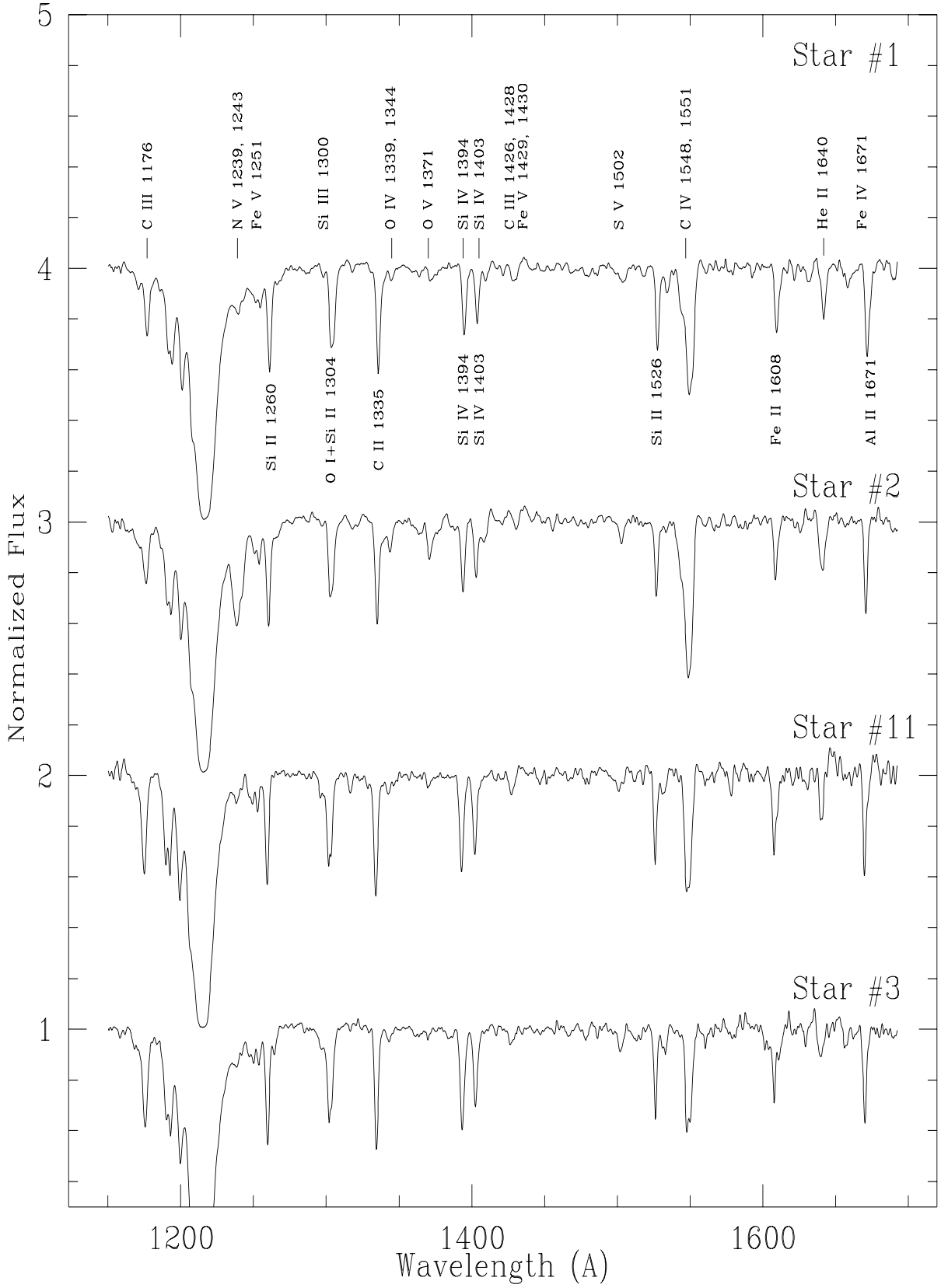

Fig. 1. Rectified *HST*/STIS ultraviolet spectrograms of the four brightest stars in SMC N81. The prominent absorption feature at $\lambda\,1210$ Å is due to the Ly α. The wind profiles are indicated with tick marks and the features possibly contaminated by an interstellar component are labelled below the lines.

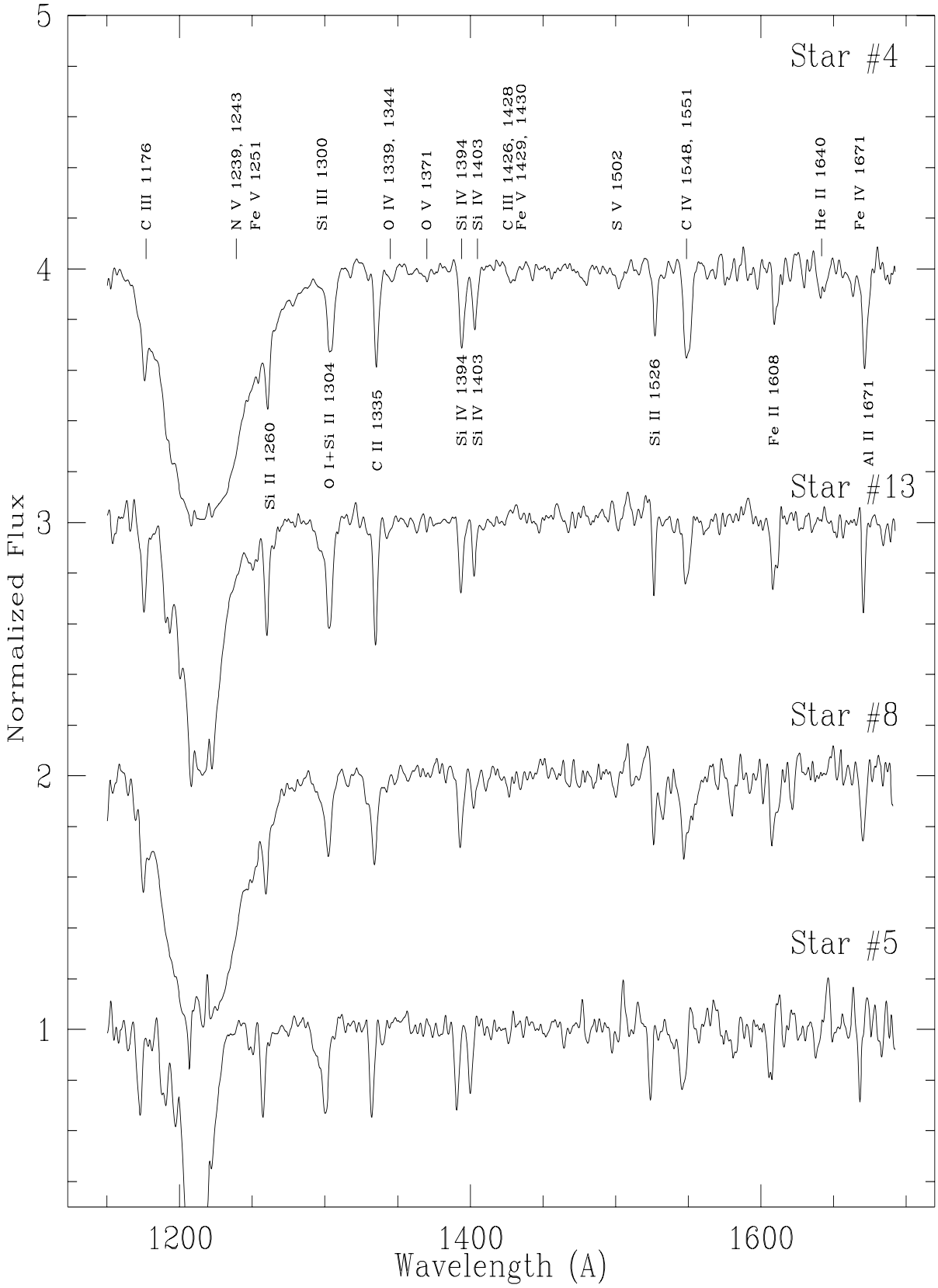

Fig. 2. Spectrograms for the remaining four less bright stars of N81. The notation is the same as in Fig. 1.

the original definition of the Vz class is He II λ4686 absorption much stronger than He II λ4541 or He I λ4471, and therefore the association of these stars with that class is indirect.

No clear distinction between the various subtypes can be made based on the available spectral features, but it is very likely that all stars are of a late O type (∼O6–O8). This is supported by the following three facts. First, the presence of the O V λ1371 feature indicates a spectral type earlier than $\lesssim$O8 (Smith Neubig & Bruhweiler 1997). Second, the weakness of the Si III λ1300 feature, which appears in the wing of O I + Si II λ1304, excludes much later types. Finally, the N V $\lambda\lambda$1239, 1243 feature is weaker than C IV $\lambda\lambda$1548, 1551, which is only seen in O types $\geq$O6–O7 or alternatively in OC stars (Walborn & Panek 1985).

Star #5 shows some puzzling emission features in its spectrum ($\lambda\lambda$1480, 1508, 1616, and 1640 Å), at least one of which, He II λ1640, is apparently part of a P-Cyg profile. It should be stressed though that the S/N ratio is not high enough to be absolutely certain about their presence. If these were indeed wind induced features, their presence would confirm the fact that the C IV $\lambda\lambda$1548, 1551 profile has a particularly marked emission component compared to the other stars of the sample. Since both of the He II λ1604 and S V λ1502 lines show P-Cyg profiles in Of and Wolf-Rayet spectra (Walborn et al. 1985; Willis et al. 1986), star #5 appears to be an Of or WR candidate in N81.

3.2. Stellar parameters and wind properties

To constrain the stellar wind properties we have examined the line profiles of the strongest UV lines. The best indications for velocity shifts come from the C IV λ1548, 1551 feature. The profiles of stars #1 and #2 show blue-shifted absorption reaching up to velocities of ∼1700 and 2000 km s^{-1} respectively. These values are compatible with terminal velocity measurements in other SMC O stars of similar spectral type (Walborn et al. 1995b; Prinja & Crowther 1998). For star #5 we derive a terminal velocity of 1000 km s^{-1}, while blue-shifts with smaller velocities are seen in the remaining profiles. However, these profiles also show asymmetries which are more important on the red side. Further investigations will be necessary to understand the detailed behavior of the line profiles.

Using an effective temperature derived from the estimated spectral types (O6–O8), in particular the one from Vacca et al. (1996) for dwarfs, and the absolute magnitudes from Table 1, we place the N81 stars (filled circles) in an HR-like diagram (Fig. 3). For further comparison we also include the mean M_V magnitudes for O3–B0 dwarfs based on a compilation by Vacca et al. (1996), as well as the mean M_V relation of Walborn (1972) used by Walborn & Blades (1997) for 30 Doradus stars. Figure 3 clearly shows that most of the stars in N81 are sub-luminous compared to the mean M_V for dwarfs. This finding still holds even if the spectral types are shifted by 1–2 subtypes towards later types. Compared to the so-called Vz luminosity class, the sub-luminosity of the N81 stars is more pronounced. Our targets are up to ∼2 mag fainter in M_V than the mean relation for dwarfs! Although this is not

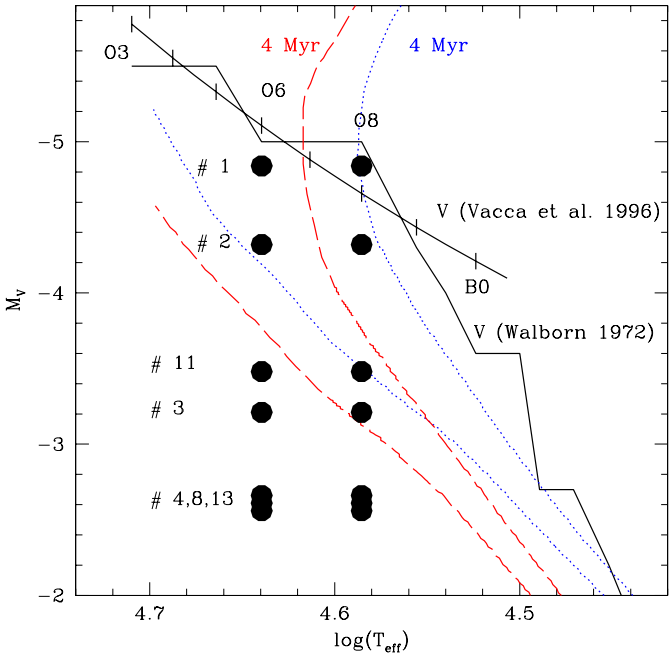

Fig. 3. The absolute M_V magnitude versus effective temperature diagram of the N81 stars is compared to the zero age main sequence (ZAMS) and 4 Myr isochrones at various metallicities. The $T_{\rm eff}$ of the stars has been estimated using an O6 or O8 spectral type and the Vacca et al. (1996) scale. The ZAMS and 4 Myr isochrones for a metallicity of 1/20 $Z_\odot$ ($Z = 0.001$) are indicated by long-dashed lines while the same pair for 1/5 $Z_\odot$ ($Z = 0.004$) is plotted with dotted lines. The ZAMS curves are not plotted for $\log(T_{\rm eff}) \geq 4.7$ due to lack of an appropriate conversion to M_V. Also shown, as solid lines, are the M_V–$T_{\rm eff}$ calibration for dwarfs from Vacca et al. (1996) as well as the one from Walborn (1972). Note that four of the observed stars are situated in the HRD-like diagram in a locus suggesting that they are either on the ZAMS or that they have a young age. The lower luminosity stars (#4, 8, 13) are possibly hotter than the ZAMS.

the defining characteristic of the Vz class, the above indications as well the weakness of the UV wind lines further attest to the possibility that these stars belong to the Vz class.

Two sets of ZAMS and isochrones of 4 Myr are presented in Fig. 3 using the Geneva stellar evolution tracks for metallicities bracketing approximately that of the SMC (Lejeune & Schaerer 2001). One set has been computed for a metallicity 1/20 Solar ($Z = 0.001$) and is marked with a long-dashed line, while the second has a metallicity of 1/5 Solar ($Z = 0.004$) and is marked with a dotted line. The observed M_V and spectral types are roughly compatible with positions close to the theoretical ZAMS or young ages. Given mostly the lack of an accurate spectral subtype determination we cannot firmly establish if the lower luminosity stars (#8, #13) are really hotter than the ZAMS. Atmospheric modeling is in progress to obtain more accurate stellar parameters of these unique young stars in the SMC (Martins et al., in preparation). Based on the $Z = 0.004$ tracks, the ZAMS luminosities and

masses corresponding to the observed M_V are between $\log L/L_\odot \sim 4.2$–5.5 and $\sim$14–50 $M_\odot$ respectively.

4. Discussion

The *HST* spectra of N81 presented here are the first ones ever obtained from a tight cluster of stars in a HEB. The reason is that these stars, embedded in a compact emission nebula, have not been reachable by ground-based telescopes. And even with recent developments in ground-based instruments, taking spectra of individual stars in the visible remains still practically infeasible. As a result, contrary to other massive stars in the SMC that have been observed from space in the UV (Walborn et al. 1995b, 2000; Smith Neubig & Bruhweiler 1997), the N81 stars lack high quality spectra in the visible. Our low-resolution *HST* spectra in the visible, imposed by stringent time allocation constraints, were intended to be a first exploratory attempt.

Massive stars observed from the ground and also with *HST* are typically much brighter than the ones seen in N81 and comparably they are much less affected by nebular emission and dust. The decoupling from nebulae is presumably due to the evolutionary state of these stars; they have had enough time to entirely and/or effectively disrupt their H II regions and the associated dust. This means that those bright stars are older than the N81 members, as supported by their spectra. Among the 15 SMC stars studied by Walborn et al. (2000), 9 are clearly giants, 5 are peculiar and have already developed emission line features of N IV λ 4058, N III λ 4640, or C III λ 4650 (two of them being on the main sequence), and the last one is a pure main sequence.

The fact that all the observed exciting stars of N81 display the Vz characteristics further supports the very young age of the cluster (Paper I). This observed concentration of Vz stars in a small region is intriguing since in the LMC region of 30 Doradus only 6 of the 104 O and early B stars classified by Walborn & Blades (1997), that is $\sim$6%, belonged to the Vz category. If we assume that all 20 bright stars we detected towards N81 (Paper I) are of O or B type, then the lower limit for the fraction of Vz stars in N81 is nearly 35%, which is quite considerable!

The exact nature and evolutionary stage of Vz stars is still unknown. Presumably these objects are close to a transition from their formation locus in the HR diagram to the main sequence. However, several issues regarding their properties, which are relevant to our observations of compact low-metallicity H II regions, remain open:

1. *Why do these stars show such weak stellar winds?* Are their mass loss rates compatible with expectations from "normal" O stars, i.e. due to their reduced luminosity compared to stars with similar effective temperatures and representative for massive stars in their earliest evolutionary stage?
2. *Are these objects truly on the ZAMS, blueward or redward of it?* The presence or absence of massive stars on the ZAMS – corresponding to the locus of completely homogeneous objects initiating H-burning – yields information on the star formation process. Indeed, the apparent lack of Galactic OB stars close the ZAMS could be due to the hiding of such stars in their parental cocoon (Garmany et al. 1982) or explained by the progressive redward bending of the upper part of the birthline due to moderate mass accretion rates in an accretion scenario for these stars (Bernasconi & Maeder 1996). In the former case the position of the "earliest" star visible thus provides constraints on the duration of the hidden phase. For the latter scenario, the position of the bluest stars constrains the accretion rate $\dot{M}_{\rm acc}$; the existence of massive stars close to the ZAMS requires high values of $\dot{M}_{\rm acc}$ (Norberg & Maeder 2000; Behrend & Maeder 2001).
   Given the present uncertainties on the $T_{\rm eff}$ determination of the N81 stars, one may speculate that some of the objects are indeed *hotter* than the ZAMS, as indicated by Fig. 3. If true, this "blue straggler" like behavior could be indicative of stellar collisions (e.g. Benz & Hills 1987), and thus a signature of formation of massive stars via this process, as advocated among others by Bonnell et al. (1998).
3. *Could some of the N81 stars still be accreting pre-main sequence objects?* The stars with smaller M_V magnitudes (#3, 4, 8, 11, and 13) have estimated luminosities slightly above the probable high luminosity Herbig Ae/Be pre-main sequence stars found by Lamers et al. (1999) and de Wit et al. (2001) in the LMC and SMC. Their location in the HRD also coincides with the region where the predicted birthlines follow quite closely the ZAMS. Given the strong indications for a very young age of N81, it is thus conceivable that our objects are still accreting mass as part of their formation process. The redshifted C IV profiles in the above cited objects could be an indication of ongoing accretion.
4. *Are Vz stars related to low metallicity?* Vz stars have also been detected in the Milky Way by Walborn and co-workers (private communication). Therefore, it appears unlikely that they are due to a simple metallicity effect.

While at present these answers remain fairly speculative, our upcoming determinations of stellar and wind parameters and further studies of similar objects should hopefully shed more light onto these issues related to the formation and early evolution of massive stars.

5. Conclusions

Our *HST*/STIS observations of the brightest massive stars powering the high excitation compact H II region SMC N81 reveal that the stars have strikingly weak wind profiles and a pronounced sub-luminosity which are clear indications of their early evolutionary state. Most likely they belong to the Vz category of massive Magellanic

Cloud stars (Walborn & Parker 1992; Walborn & Blades 1997), which are very young stars just arriving at the ZAMS or already located near it. These stars may also serve as templates for newborn massive stars of distant metal-poor galaxies which cannot be individually resolved. Therefore, a more detailed study and modeling of their properties is highly desirable as it will help shed some more light on the intricacies and consequences of the early stages in stellar evolution.

Acknowledgements. We would like to thank the referee for a critical reading of the paper which contributed to its improvement. We are also grateful to Dr. Nolan R. Walborn (Space Telescope Science Institute) for very helpful comments and suggestions. VC would like to acknowledge the financial support for this work provided by NASA through grant number GO-8246 from the STScI, which is operated by the Association of Universities for Research in Astronomy, Inc., under NASA contract 26555. DS, FM, and MH-M received partial support from the French "Programme National de Physique Stellaire" (PNPS).

References

Beech, M., & Mitalas, R. 1994, ApJS, 95, 517
Behrend, R., & Maeder, A. 2001, A&A, 373, 122
Benz, W., & Hills, J. G. 1987, ApJ, 323, 614
Bernasconi, P. A., & Maeder, A. 1996, A&A, 307, 829
Bonnell, I. A., Bate, M. R., & Zinnecker, H. 1998, MNRAS, 298, 93
Churchwell, E. 1990, A&AR, 2, 79
Davies, R. D., Elliott, K. H., & Meaburn, J. 1976, MNRAS, 81, 89
de Wit, W. J., Beaulieu, J. P., Lamers, H. J. G. L. M., Lesquoy, E., & Marquette, J.-B. 2001, A&A, submitted
Di Benedetto, G. P. 1997, ApJ, 486, 60
Garmany, C., Conti, P. S., & Chiosi, C. 1982, ApJ, 263, 777
Garmany, C., Conti, P. S., & Chiosi, C. 1985, ApJ, 293, 407
Hanson, M. M., Conti, P. S., & Rieke, M. J. 1996, ApJS, 107, 281
Henize, K. G. 1956, ApJS, 2, 315
Heydari-Malayeri, M., Le Bertre, T., & Magain, P. 1988, A&A, 195, 230
Heydari-Malayeri, M., Rosa, M., Zinnecker, H., Deharveng, L., & Charmandaris, V. 1999, A&A, 344, 848 (Paper I)
Heydari-Malayeri, M., Charmandaris, V., Deharveng, L., Rosa, M. R., & Zinnecker, H. 1999b, A&A, 347, 841
Heydari-Malayeri, M., Rosa, M. R., Charmandaris, V., Deharveng, L., & Zinnecker, H. 1999c, A&A, 352, 665
Heydari-Malayeri, M., Charmandaris, V., Deharveng, L., et al. 2001a, A&A, 372, 495
Heydari-Malayeri, M., Charmandaris, V., Deharveng, L., et al. 2001b, A&A, 372, 527
Hutchings, J. B. 1982, ApJ, 255, 70
Israel, F. P., & Koornneef, J. 1988, A&A, 190, 21
Israel, F. P., & Koornneef, J. 1991, A&A, 248, 404
Israel, F. P., Johansson, L. E. B., Lequeux, J., et al. 1993, A&A, 276, 25
Kaltcheva, N. T., & Georgiev, L. N. 1992, MNRAS, 259, 166
Lamers, H. J. G. L. M., Beaulieu, J. P., & de Wit, W. J. 1999, A&A, 341, 827
Lejeune, T., & Schaerer, D. 2001, A&AS, 366, 538
Martins, F., et al. 2001, in preparation
Norberg, P., & Maeder, A. 2000, A&A, 359, 1025
Palla, F., & Stahler, S. W. 1990, ApJ, L47
Prinja, R. K., & Crowther, P. A. 1998, MNRAS, 300, 828
Relyea, L. J., & Kurucz, R. L. 1978, ApJS, 37, 45
Shu, F. R., Adams, F. C., & Lizano, S. 1987, ARA&A, 25, 23
Smith Neubig, M. M., & Bruhweiler, F. C. 1997, AJ, 114, 1951
Smith Neubig, M. M., & Bruhweiler, F. C. 1999, AJ, 117, 2856
Vacca W. D., Garmany C. D., & Shull, J. M. 1996, ApJ, 460, 914
Walborn, N. R. 1972, AJ, 77, 312
Walborn N. R., & Blades, J. C. 1997, ApJS, 112, 457
Walborn, N. R., & Fitzpatrick, E. L. 1990, PASP, 102, 379
Walborn, N. R., & Panek, R. J. 1985, ApJ, 291, 806
Walborn, N. R., & Parker, J. Wm. 1992, ApJ, 399, L87
Walborn, N. R., Nichols-Rohlin, J., & Panek, R. J. 1985, International Ultraviolet Explorer Atlas of O-Type Spectra from 1200 to 1900 Å (NASA RP-1155)
Walborn, N. R., Parker, J. Wm., & Nichols, J. S. 1995a, International Ultraviolet Explorer Atlas of B-Type Spectra from 1200 to 1900 Å (NASA RP-1363)
Walborn, N. R., Lennon, J. L., Haser, S. M., et al. 1995b, PASP, 107, 104
Walborn, N. R., Lennon, J. L., Heap, S. R., et al. 2000, PASP, 112, 1243
Werner, K., & Rauch, T. 2001, in Eta Carinae and other Mysterious Stars, ASP Conf. Ser., ed. T. Gull, et al. [astro-ph/0102006]
Willis, A. J., van der Hucht, K. A., Conti, P. S., & Garmany, D. 1986, A&AS, 63, 417
Woodgate, B. E. 1998, PASP, 110, 1183
Yorke, H. W., & Krügel, E. 1977, A&A, 54, 183

Chapter 7

Stellar and puzzling wind properties of young massive stars in SMC-N81

French summary

Ce chapitre est dédié à l'étude quantitative des étoiles de N81 présentées ci-dessus. Les paramètres stellaires et de vent sont déterminés au moyen de modèles d'atmosphères calculés avec le code CMFGEN.

Une étude quantitative de ces étoiles est intéressante tout d'abord pour tenter de mieux caractériser les étoiles Vz (à la condition que les étoiles de N81 fassent bien partie de cette classe ce qui n'est pas complètement établi). En effet, l'existence d'étoiles proches de la séquence principale d'âge zéro doit permettre de contraindre les scenarios de formation stellaire qui prévoient parfois l'absence de telles étoiles à cause de l'allumage des réactions nucléaires au sein des étoiles massives alors même qu'elles sont encore en train d'accréter (Bernasconi & Maeder, 1996). Par ailleurs, la détermination des paramètres de vent d'étoiles du SMC doit permettre d'adresser la question de la dépendance avec la métallicité de la perte de masse.

Notre analyse quantitatives de ces étoiles conduit aux résultats suivants:

- Les étoiles de N81 sont des étoiles jeunes d'âge de lordre de 3 à 4 millions d'années.
- Leur sous-luminosité par rapport à des étoiles naines classiques est confirmée. Elles sont en effet moins brillantes que ce que l'on at-

tendrait des tables de calibrations de Vacca, Garmany & Schull (1996).

- Les taux de perte de masse de ces étoiles sont de l'ordre de $10^{-8..-9}$ $M_\odot$ yr^{-1}, bien en deçà de ce que l'on avait observé jusque là pour des étoiles Galactiques. Ces pertes de masse sont également bien inférieures à ce que prédit la théorie, même avec une métallicité réduite telle que celle du SMC.

- Les quantités de mouvement modifiées sont entre 1 et 2 ordres de grandeur plus faibles que ce qui n'a jamais été déterminé pour des étoiles de luminosité similaire. Cela peut révéler une rupture de pente de la relation quantité de mouvement modifié - luminosité pour les faibles luminosités, ou bien indiquer une pente plus forte de cette relation à faible métallicité. Toutefois, les raisons d'une rupture de pente restent inconnues, et aucune des prédictions théoriques actuelles basées sur des simulations hydrodynamiques ne prévoit un changement de pente pour une métallicité typique du SMC. Par ailleurs, nous montrons qu'il existe au moins une étoile de la Galaxie qui montre le même comportement (faiblesse du vent et faible luminosité).

- Diverses possibilités pour tenter d'expliquer ce comportement étrange des vents sont discutées. Un phénomène de découplage entre ions absorbants et ions passifs semble pouvoir être exclu. La non prise en compte de gradients dans le structure en vitesse et l'approximation Sobolev dans les simulations numériques pourrait partiellement expliquer une sur-estimation des prédictions de perte de masse d'étoiles naines de faible luminosité. De même, la paramétrisation de l'accélération au moyen du formalisme CAK pourrait ne plus être valide dans certains cas extrêmes. Enfin, il pourrait exister un lien entre la jeunesse de l'étoile et la faiblesse du vent puisque l'on pourrait assister aux premiers instants du développement des vents radiatifs (donc avec de faibles pertes de masse) dans de jeunes étoiles massives.

Quelle que soit l'origine de la faiblesse des vents de ces étoiles, cette propriété intriguante montre que les vents radiatifs des étoiles massives reste un domaine complexe.

This chapter is dedicated to the quantitative analysis of the stellar and wind properties of the SMC-N81 stars. Atmosphere models are run to put constraints on the effective temperatures and mass loss rates (among others). The analysis confirm the weakness of the winds mentioned in the previous section.

In the previous section, we have seen that the massive stars of the star forming region SMC-N81 showed intriguing properties. In the context of the formation of massive stars, the N81 components turn out to be young massive stars with a lower luminosity compared to classical O dwarfs. This characteristic is interesting since it may be an indication that these massive stars are less evolved than typical dwarfs, and hence closer to the ZAMS. The existence of massive stars in this part of the HR diagram is particularly important since the absence of observations of massive stars on or close to the ZAMS has often been claimed to be the result of the ignition of the H burning in a massive stars still in the process of formation (via accretion, see e.g. Bernasconi & Maeder, 1996). In that case, a ZAMS does not exist since the star is already evolved when it reaches its final mass. The absence of massive stars on the ZAMS has also been interpreted as the fact that the the early evolution of a massive star happens while the star is still embedded in its parental cloud (Wood & Churchwell, 1989). Finding massive stars close to the ZAMS would then put constraints on the timescales required for a massive star to emerge from its parental cloud. And the existence of ZAMS massive stars would certainly help to better understand the formation process of massive stars. Hence, a quantitative analysis of the N81 objects should be rewarding.

As for the wind properties, the weakness of the wind lines observed in the STIS spectra is indicative of extremely low mass loss rates. Even typical O dwarfs in the SMC do not show such weak features (see Fig. 1.6). The mass loss rates are certainly very low, and at least lower than expected according to a simple scaling with global metallicity. Or this may reveal that the reduction of the wind strength with Z is much higher than currently believed from hydrodynamical simulations. Whatever the answer to this surprising behaviour of the wind properties, a quantitative study is also required to put constraints on the rates of mass loss of these massive stars.

We have carried out such an analysis through the modelling of the atmospheres of the SMC-N81 stars with the code CMFGEN already used in the first part of this thesis. The results are given in the following paper, and are summarised below:

- The SMC-N81 stars are young massive stars with an age of $\sim$ 3-4 Myr.

- We confirm the subluminosity of these objects which are found to be fainter compared to the calibration of Vacca, Garmany & Schull (1996) for O dwarfs.

- With values of the order of $10^{-8..-9}$ $M_{\odot}$ yr^{-1} the mass loss rates are much lower than observed for Galactic O dwarfs and predicted by the current generation of radiatively driven wind models, even for an SMC metallicity.

- The modified wind momenta are 1 to 2 orders of magnitude lower than ever observed for stars of the same luminosity. This may be indicative of a break-down of the modified wind momentum - luminosity relation at low luminosity or of a steeper slope of this relation at low metallicity. However, the reason for a break-down are not known and the effect of metallicity is not supported by the current hydrodynamical models which do not predict any variation of the slope of the WLR at SMC metallicity. Moreover, we show that some Galactic stars have the same behaviour.

- The weakness of the winds may be related to the youth of the stars and we may be seeing the onset of radiatively driven winds in recently formed stars.

Whatever the exact reason for it, the results presented here are one of the first strong indication that the wind properties of low luminosity stars are certainly more complex than previously believed and calls for a deeper investigation.

7.1 Puzzling wind properties of young massive stars in SMC-N81

A&A 420, 1087–1106 (2004)
DOI: 10.1051/0004-6361:20034509

Astronomy & Astrophysics

Puzzling wind properties of young massive stars in SMC-N81⋆

F. Martins[1,2], D. Schaerer[2,1], D. J. Hillier[3], and M. Heydari-Malayeri[4]

[1] Laboratoire d'Astrophysique, Observatoire Midi-Pyrénées, 14 Av. E. Belin, 31400 Toulouse, France
[2] Observatoire de Genève, 51 Chemin des Maillettes, 1290 Sauverny, Switzerland
[3] Department of Physics and Astronomy, University of Pittsburgh, 3941 O'Hara Street, Pittsburgh, PA 15260, USA
[4] LERMA, Observatoire de Paris, 61 Avenue de l'Observatoire, 75014 Paris, France

Recieved 14 October 2003 / Accepted 16 March 2004

Abstract. We present a quantitative study of massive stars in the High Excitation Blob N81, a compact star forming region in the SMC. The stellar content was resolved by HST, and STIS was used to obtain medium resolution spectra. The qualitative analysis of the stellar properties presented in Heydari-Malayeri et al. (2002a) is extended using non-LTE spherically extended atmosphere models including line-blanketing computed with the code CMFGEN (Hillier & Miller 1998), and the wind properties are investigated. The main results are the following:

– The SMC-N81 components are young (∼0–4 Myrs) O stars with effective temperatures compatible with medium to late subtypes and with luminosities lower than those of average Galactic O dwarfs, rendering them possible ZAMS candidates.
– The winds are extremely weak: with values of the order of $10^{-8}/10^{-9}$ $M_\odot\,\mathrm{yr}^{-1}$ the mass loss rates are lower than observed so far for Galactic dwarfs. Only the recent study of SMC stars by Bouret et al. (2003) show the same trend. The modified wind momenta ($\dot{M}\,v_\infty\,\sqrt{R}$) are also 1 to 2 orders of magnitude lower than observed for Galactic stars. Both the mass loss rates and the modified wind momenta are lower than the predictions of the most recent hydrodynamical models.

The accuracy of the UV based mass loss rate determination, relying in particular on the predicted ionisation fractions, are carefully examined. We find that $\dot{M}$ could be underestimated by a factor of up to 10. Even in this unlikely case, the above conclusions remain valid *qualitatively*.
The reasons for such weak winds are investigated with special emphasis on the modified wind momenta:

– There may be a break-down of the wind momentum-luminosity relation (WLR) for dwarf stars at low luminosity ($\log L/L_\odot \lesssim 5.5$). However, reasons for such a breakdown remain unknown.
– The slope of the WLR may be steeper at low metallicity. This is predicted by the radiation driven wind theory, but the current hydrodynamical simulations do not show any change of the slope at SMC metallicity. Moreover, there are indications that some Galactic objects have wind momenta similar to those of the SMC stars.
– Decoupling may take place in the atmosphere of the SMC-N81 stars, leading to multicomponent winds. However, various tests indicate that this is not likely to be the case.

The origin of the weakness of the wind observed in the SMC-N81 stars remains unknown. We suggest that this weakness may be linked with the youth of these stars and represents possibly the onset of stellar winds in recently formed massive stars.

Key words. stars: winds, outflows – stars: atmospheres – stars: mass-loss – stars: early-type – stars: fundamental parameters – ISM: HII region

1. Introduction

Massive stars play key roles in various astrophysical contexts all along their evolution: they ionise ultra-compact HII regions while still embedded in their parental molecular cloud; they create ionised cavities and shape the surrounding interstellar medium during the main fraction of their lifetime; they experience strong episodes of mass loss when they become Luminous Blue Variables and Wolf-Rayet stars, revealing their core and enriching the ISM in products of H and He burning; they end their life as supernovae, producing the heavy elements and releasing large amounts of mechanical energy. During all these phases, massive stars lose mass through winds driven by radiation pressure on metallic lines. This affects not only their evolution (e.g., Chiosi & Maeder 1986) but also the surrounding interstellar medium in which the release of mechanical

Send offprint requests to: F. Martins,
e-mail: fabrice.martins@obs.unige.ch
⋆ Appendix A is only available in electronic form at
http://www.edpsciences.org

energy can trigger instabilities leading to the collapse of molecular clouds and to star formation. Moreover, bubbles and superbubbles observed on galactic scales are powered by such mass ejections. Hence, various astrophysical fields require the knowledge of quantitative wind properties of massive stars.

Several studies have been carried out in the last two decades to determine these properties. At solar metallicity, the observational determinations (e.g., Howarth & Prinja 1989; Puls et al. 1996; Herrero et al. 2000) are on average in good agreement with the most recent hydrodynamical predictions based on the radiation driven wind theory (Vink et al. 2000), both in terms of mass loss rate and of the modified wind momentum-luminosity relation (WLR; e.g., Puls et al. 1996) which quantifies the strength of the wind. At nonsolar metallicities, we expect the wind properties to vary with Z due to the modified radiative acceleration through metallic lines. In particular, the mass loss rate should be proportional to Z^r (Abbott 1982; Puls et al. 2000) and the WLR should be shifted towards lower values and should have a steeper slope. The most recent theoretical results predict $r \sim 0.8$ (Vink et al. 2001) but no change in the slope of the WLR, at least for $Z > 10^{-3}\ Z_\odot$ (Hoffmann et al. 2002; Kudritzki 2002). Observational studies indicate a reduction of the mass loss rate and of the terminal velocity in the Magellanic Clouds, but given the small number of objects studied so far, the behaviour of the WLR at low metallicity is still poorly understood. Several groups are currently analysing stars in subsolar (Crowther et al. 2002; Hillier et al. 2003; Bouret et al. 2003) and supersolar (Najarro et al. 1997; Figer et al. 2002) regions for a better understanding of wind properties in different environments. The present work on SMC-N81 stars takes part in this effort.

The SMC-N81 region belongs to the class of the "High Excitation Blobs" (HEB) first introduced by Heydari-Malayeri & Testor (1982). These blobs are compact regions of star formation in the Magellanic Clouds (see Heydari-Malayeri (2002b) for a complete review). They have a typical radius of a few pc and display the features of starforming regions: HII cavities, turbulent structures, ionisation fronts and shocks. Recent HST observations (Heydari-Malayeri et al. 1999) have revealed for the first time its stellar content, 4 of the brightest stars being grouped in the central 2″ wide region. Subsequently spectra of the main exciting stars have been obtained with STIS onboard HST. The qualitative analysis of these spectra, presented in Heydari-Malayeri et al. (2002a, hereafter Paper I), has already revealed interesting properties. First, the stars have been identified as mid O dwarfs with surprisingly low luminosities compared to "classical" dwarfs. Second, the UV spectra have shown signatures of very weak winds, even weaker than those usually observed in the SMC. These characteristics have led Heydari-Malayeri et al. (2002a) to propose that the SMC-N81 stars could belong to the class of Vz stars, which are massive stars thought to lie very close to the ZAMS (Walborn & Parker 1992).

As such the properties of these stars, showing unusually weak winds compared to other SMC O stars, seem already quite interesting. Furthermore the association of these objects with a compact star forming region, presumably indicative of a very young age, also allows one to obtain unique constraints on properties of very young massive stars shortly after their birth. In fact such observations appear crucial for a better understanding of the earliest evolutionary phases of massive stars and for constraining their formation process which is still under debate (they may form by accretion on a protostellar core – Norberg & Maeder 2000; Behrend & Maeder 2001 – or by collisions between low mass components in dense stellar clusters – Bonnell et al. 1998).

With such objectives in mind we have carried out a quantitative study of the UV spectra of the SMC-N81 stars. First results have been presented in Martins et al. (2002a). In fact we are able to determine upper limits on the mass loss rates of four O stars in this region, which turn out to be surprisingly low (typically $\dot{M} \lesssim$ a few $10^{-9}\ M_\odot\ \mathrm{yr}^{-1}$) compared to predictions of the radiation driven wind theory, even when taking metallicity effects into account. Although no precise physical explanation is found for this behaviour we strongly suggest that this behaviour is related to the very youth of these massive stars.

The remainder of the paper is structured as follows. Section 2 briefly summarises the observations and data reduction. Section 3 describes the main ingredients of the modeling. In Sect. 4 we explain how interstellar lines are taken into account. The main results are given in Sect. 5 and discussed in Sects. 6 (nebular and stellar properties) and 7 (wind properties). Finally, Sect. 8 summarises the main results.

2. Observations and data reduction

Ten SMC N81 stars were observed with STIS onboard HST on 28 and 31 October 1999 (General Observer Program No 8246, PI M. Heydari-Malayeri). The spectra in the wavelength range 1120−1715 Å were obtained through the G140 L grating on the Multi-Anode Microchannel Array (MAMA) detector. The $52'' \times 0.2''$ entrance slit was used. The effective resolution was 0.6 Å per pixel of 25 μm which corresponds to a dispersion of 24 Å mm^{-1} or a resolution of 1.2 Å. The exposure times were chosen to equalize the *S/N* ratios, which are of the order 20 for the 4 stars studied here. The other stars have lower *S/N* ratio which precludes any quantitative analysis. Optical spectra, also obtained with STIS for 6 objects, were of insufficient quality (too low spectral resolution) and are therefore not used here.

Details concerning the data reduction can be found in Paper I.

3. CMFGEN: Basic concepts

The modeling of realistic atmospheres of massive stars requires the inclusion of three main ingredients: 1) due to the high luminosity of these stars, radiative processes are dominant and a non-LTE treatment must therefore be done; 2) mass loss creates an atmosphere which can extend up to several tens of stellar radii which renders the use of spherical geometry unavoidable; 3) the inclusion of metals (mostly iron) is fundamental to reproduce realistic atmospheric structures and emergent spectra (line-blanketing effect).

We are now in an area where powerful tools including most of the above ingredients with progressively fewer

approximations are becoming available. Examples are the codes TLUSTY (Hubeny & Lanz 1995), WM-BASIC (Pauldrach et al. 2001) and FAST-WIND (Santolaya-Rey et al. 1997). For our study, we have chosen to use the program CMFGEN (Hillier & Miller 1998) now widely used for spectroscopic studies of massive stars. The main ingredients taken into account in CMFGEN are the following:

- non-LTE approach: the whole set of statistical equilibrium equations and radiative transfer equations is solved to yield the level populations and the radiative field;
- wind extension: all equations are written in spherical geometry with the assumption of spherical symmetry and include all velocity terms due to the expanding atmosphere;
- line-blanketing: metals are included in the statistical equilibrium equations so that accurate level occupation numbers can be derived. A super-level approximation consisting in gathering levels of close energy into a unique super-level is used to reduce the computational cost;
- radiative equilibrium: the temperature structure in the atmosphere is set by the condition of radiative equilibrium. Other heating/cooling sources are optional and can be included (adiabatic cooling, X-rays);
- hydrodynamical structure: at present, CMFGEN does not compute the velocity and density structure so that they have to be taken as input data or have to be parameterised. In our approach, they are computed by other atmosphere codes. We use either the ISA-WIND code which uses the hydrodynamical equations together with a grey LTE temperature to yield the density and velocity in the atmosphere (see also Martins et al. 2002b), or TLUSTY which, thanks to a more accurate description of the pressure terms, gives a good description of the photospheric structure which is connected to a wind velocity structure represented by a classical β law ($v = v_\infty(1 - \frac{R_*}{r})^\beta$). Tests made with stellar and wind parameters typical of our stars have shown that the two methods give similar results for dwarfs in terms of emergent UV spectra.

Several input parameters have to be specified, the main ones being:

- stellar parameters: luminosity (L), radius (R), mass (M);
- wind parameters: mass loss rate ($\dot{M}$, terminal velocity v_∞). Note that the slope of the velocity field in the wind (the so-called β parameter) is chosen when the velocity structure is computed so it is also an input parameter (with default value 0.8). CMFGEN also gives the possibility to include clumping. This is done by the inclusion of a volume filling factor f of the form $f = f_\infty + (1 - f_\infty)e^{-\frac{v}{v_{\rm init}}}$ where f_∞ is the value of f in the outer atmosphere and $v_{\rm init}$ the velocity at which clumping appears (30 km s^{-1} by default in our computations);
- abundances/elements: in most of our models, the metallicity has been chosen to be 1/8 solar where solar refers to the values by Grevesse & Sauval (1998). This metallicity is thought to be typical of stars in the SMC and in N81 in particular (Venn 1999; Hill 1999; Vermeij et al. 2002), although the exact value remains uncertain. The ions included in our computations are given in Table 1;
- turbulent velocity: a value of 20 km s^{-1} was chosen for the calculation of the populations and of the temperature structure. Martins et al. (2002b) have shown that reasonable changes of $v_{\rm turb}$ had few effects on this part of the calculation. For the formal solution of the radiative transfer equation leading to the final detailed emergent spectrum, the value of $v_{\rm turb}$ has been determined to give the best fit as shown in Sect. 5.5 and is found to be of the order of 5 km s^{-1}.

Table 1. Ions included in the atmosphere models. Numbers in parentheses indicate species which, for given $T_{\rm eff}$, are trace ions and then are not taken into account.

Element	Ionisation state							
H	I	II						
He	I	II	III					
C		(II)	III	IV	V			
N		(II)	III	IV	V	VI		
O		(II)	III	IV	V	VI	(VII)	
Si		(II)	(III)	IV	V			
S			(III)	IV	V	VI	(VII)	
Fe			(III)	IV	V	VI	VII	(VIII)

4. Interstellar lines

The determination of mass loss rates relies on the fit of emission or P-Cygni lines (see Sect. 5.2). The synthetic profiles are quite sensitive to the value of $\dot{M}$, so that a reliable estimate of this quantity requires the best possible knowledge of the stellar and wind spectrum. Consequently, the contaminating interstellar (IS) lines must be identified, which is easy in high resolution spectra where these IS lines appear as narrow absorptions in the P-Cygni profiles. However, in our medium resolution observations the IS components are diluted in the stellar features so that the exact stellar + wind profiles are uncertain. Of course, this depends on the line: as N v is a trace ion in the interstellar medium, stellar N v λ1238,1242 is weakly affected by this problem. But this is not the case for C iv $\lambda\lambda$1548,1551 which is all the more contaminated given that the wind feature is weak in the observed N81 spectra. It is therefore crucial to estimate the contribution of the interstellar absorption to derive reliable mass loss rates.

The interstellar absorption originates both in the Galaxy and the local SMC environment. To estimate the interstellar C iv column densities, we have proceeded as follows:

– First, we have used high resolution HST-STIS spectra of 8 SMC stars (AV 69, AV 75, AV 80, AV 327, NGC 346 355, NGC 346 368, NGC 346 113, NGC 346 12), for which UV spectra have been obtained from the HST archive, to determine the C iv column densities in the direction of the NGC 346 region and the southwest part of

Table 2. Determination of CIV column densities.

Component	Log (N(C IV))	Reference
Galactic	$14.4/14.5^{+0.10}_{-0.10}$	Mallouris et al. (2001)
	14.4	Fitzpatrick & Savage (1983)
	$14.35^{+0.06}_{-0.06}$	Sembach & Savage (1992)
	$14.28^{+0.10}_{-0.13}$	SMC stars, this work
SMC	$14.4/14.5^{+0.10}_{-0.10}$	Mallouris et al. (2001)
	>14.5	Fitzpatrick & Savage (1983)
	$14.43^{+0.20}_{-0.40}$	SMC stars, this work

the SMC. For that purpose, the Galactic and SMC interstellar profiles have been fitted with a Gaussian profile (with a shift of 140 km s^{-1} – the receding velocity – for the SMC component). Two parameters are needed to achieve such a fit: the column density and the *FWHM* of the Gaussian profile (for which a typical value of 20 km s^{-1} was chosen). The mean column densities derived from this study are the following: log (N(C IV)) = $14.28^{+0.10}_{-0.13}$ for the Galactic component, and log (N(C IV)) = $14.43^{+0.20}_{-0.40}$ for the SMC component. The higher dispersion in the case of the SMC component is probably due to the fact that we are looking at different parts of the SMC, whereas only one line of sight is used for the Galaxy.

– Second, we have taken various determinations of the C IV column density from the literature. Several methods were used (curve of growth, line fitting, apparent optical depth) and give consistent results.

Table 2 summarises the various column density estimates. For the Galactic case, the results from our determination are consistent with more accurate determinations (within the errors). For subsequent analysis, we adopt log (N(C IV) = 14.4 as a representative value for the Galactic absorption. For the SMC, the results are also in good agreement. As the reddening of the SMC-N81 stars is similar to that of the other 8 SMC stars used for this study (the values of $E(B-V)$ are of the order of 0.12 for all stars), the properties of the interstellar matter on the different lines of sight towards the SMC sampled here must be the same. This absence of local extinction was noted by Heydari-Malayeri et al. (1988) in the first detailed study of SMC-N81. Then the value of log (N(C IV) = 14.5 derived on average for the SMC regions in Table 2 is chosen to be typical of the CIV column density in the direction of N81.

With these column densities, we have created synthetic profiles of the interstellar C IV absorption lines. The method used was the same as that employed to estimate the column densities from the spectra of the 8 SMC stars mentioned above. We have then added these interstellar contributions to the CMFGEN profiles. Figure 1 shows an example of such a correction. The typical uncertainties in the column densities translate to modifications of the depth of the corrected absorption profile of the order of 0.05.

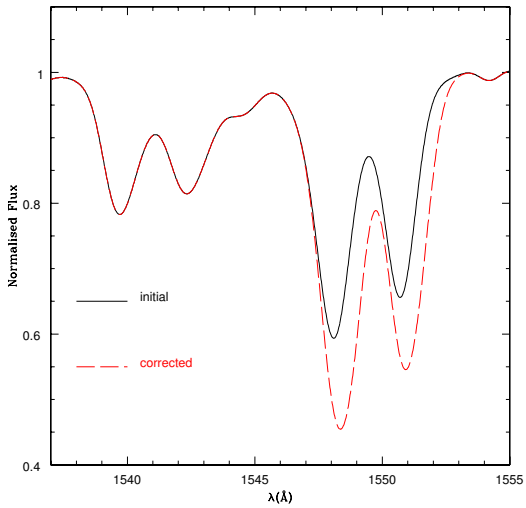

Fig. 1. Interstellar C IV component addition: the black solid line shows the C IV $\lambda\lambda$1548,1551 profile of a CMFGEN model, and the red long dashed line is the resulting profile after including the IS absorption. A convolution has been performed to take into account the instrumental resolution (1.2 Å). The parameters used to model the interstellar component are: log (N(C IV)$_{\rm gal}$) = 14.4, log (N(C IV)$_{\rm SMC}$) = 14.5 and $v_{\rm SMC}$ = 140 km s^{-1}.

5. Detailed analysis of individual stars

In this section, we present the results of the quantitative analysis of the UV spectra of our target stars. Constraints on the effective temperature, the luminosity, the terminal velocity of the wind and the mass loss rate constitute the main outputs. Secondary constraints on the slope of the velocity field or the amount of clumping are also given. The method used is explained in detail for the case of star 2, while for the other stars the results are summarised in Sect. 5.7 and in Table 4.

5.1. Effective temperature

The most reliable $T_{\rm eff}$ diagnostics for O stars remain the photospheric helium lines in the optical. Unfortunately, optical spectra of the SMC-N81 stars are not available so that we had to rely on the UV. Two types of indicators were used in this spectral range: the shape of the SED and the strength of several lines.

5.1.1. UV colour index

As O stars emit most of their luminosity in the UV, the shape of the spectral energy distribution at these wavelengths is sensitive to the effective temperature just as is the optical spectrum in the case of cooler stars. A colour index in the UV can then make it possible to determine $T_{\rm eff}$. This has been done observationally by Fanelli et al. (1992) who have computed various spectral indices based on IUE spectra for different groups of stars.

We have used the recent grid of O dwarf models by Martins et al. (2002b) recomputed for an SMC metallicity (Z = 1/8 $Z_\odot$) completed by various models at this low Z to derive a relation

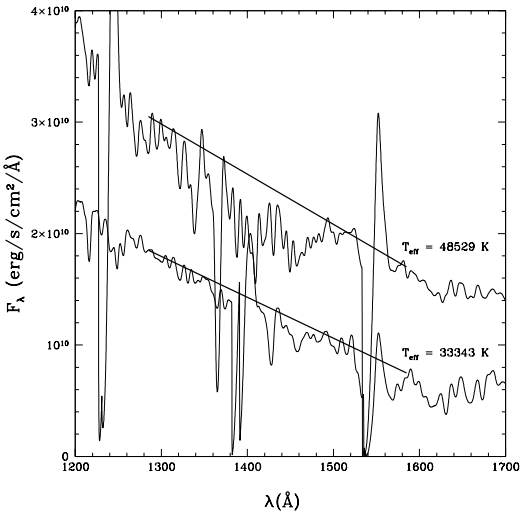

Fig. 2. UV flux distribution of two O dwarf models at 33 343 K and 48 529 K. Whereas the slope $F_{1285} - F_{1585}$ increases with $T_{\rm eff}$ the ratio $\frac{F_{1285}}{F_{1585}}$ decreases. The bold lines are to guide the eye and to show the variations of the slope.

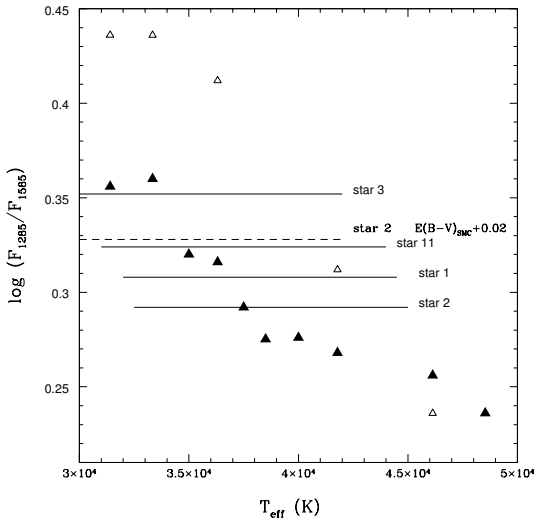

Fig. 3. Effective temperature indicator: colour index method. The colour index is define by $\frac{F_{1285}}{F_{1585}}$ where F_{1285} (F_{1585}) is the mean flux at 1285 Å (1585 Å). Filled (open) triangles are for models with Z = 1/8 $Z_\odot$ ($Z = Z_\odot$). Horizontal lines indicate the colour index for N81 stars which, by comparisons with the theoretical values, give an estimate of the effective temperature. Note that this method is strongly metallicity-dependent. The dashed line show the position of star 2 for an SMC extinction increased by 0.02.

between effective temperature and a synthetic colour index defined by $\frac{F_{1285}}{F_{1585}}$ where F_{1285} (F_{1585}) is the mean flux in an artificial 20 Å wide box-shaped filter centered on 1285 Å (1585). The choice of these wavelengths was a compromise between having fluxes in distant wavelength ranges (to get a ratio significantly different from 1) and avoiding metallicity effects (see below). In the UV part of the spectrum of interest to us, an increase of $T_{\rm eff}$ translates to a decrease of $\frac{F_{1285}}{F_{1585}}$ (whereas the slope of the spectrum, $F_{1285} - F_{1585}$, increases). This is illustrated in Fig. 2 where we see that an increase of $T_{\rm eff}$ from 33 343 K to 48 529 K induces a decrease of $\frac{F_{1285}}{F_{1585}}$ from ∼2.5 to ∼1.8 while the slope increases (see the bold lines). This is confirmed observationally by Fanelli et al. (1992).

Figure 3 shows the correlation between our UV colour index and $T_{\rm eff}$. The determination of the UV colour index from the dereddened flux distribution of the SMC-N81 stars together with this theoretical relation allows us to estimate $T_{\rm eff}$ of the observed stars. In the case of star 2, we found a value of ∼37 500 K.

This method suffers from various problems. The most important is probably the extinction which modifies the slope of the SED and renders the UV colour index uncertain. The dashed line in Fig. 3 shows the position of star 2 if its SMC extinction was increased by 0.02 (compared to the extinction derived from photometry): in that case, the estimated $T_{\rm eff}$ would be ∼34 000 K. This may seem surprising, as naively a higher $T_{\rm eff}$ could be expected for a higher extinction. However, this behaviour is simply due to the fact for a "normal" extinction law (e.g., Prévot et al. 1984) an increase of $E(B-V)$ translates into an increase of $F^{1285}_{\rm dered}/F^{1585}_{\rm dered}$ which corresponds to a lower $T_{\rm eff}$ as discussed above. Figure 3 shows that a typical error of 0.02 on $E(B-V)$ (i.e. an error on the flux determination) translates to an uncertainty of the order of 3000/4000 K in $T_{\rm eff}$ based on the UV colour index method.

The UV SED is also shaped by many metallic (mostly iron) lines and thus metallicity can affect the determination of UV magnitudes. This is clearly demonstrated in Fig. 3 where the effect of increasing the metallicity from 1/8 $Z_\odot$ to $Z_\odot$ strongly steepens the slope of the relation UV colour index – $T_{\rm eff}$. Both the slope of the continuum and the "line forests" are responsible for such a behaviour. Our choice of filters centered at 1285 Å and 1585 Å (where the density of metallic lines is weaker than in other wavelength ranges) was made to try to minimise the latter effect.

Finally, the slope of the SED also depends on the gravity (e.g., Abbott & Hummer 1985). However, for dwarf stars, this dependence is weak: a test case run for a model with $\log g = 4.1$ and 4.4 has shown a change of the ratio $\frac{F_{1285}}{F_{1585}}$ of less than 2%.

Given the above uncertainties, the UV colour index method can only give an indication of the effective temperature which needs to be confirmed by other indicators.

5.1.2. spectral lines

Several spectral features can be used as $T_{\rm eff}$ indicators in the UV.

- O IV $\lambda\lambda$1339,1343/O V λ1371:

O IV $\lambda\lambda$1339,1343 is present in the spectra of most O dwarfs while O V λ1371 appears only in stars earlier than O6 (Walborn et al. 1995) so that their presence/absence and relative strength

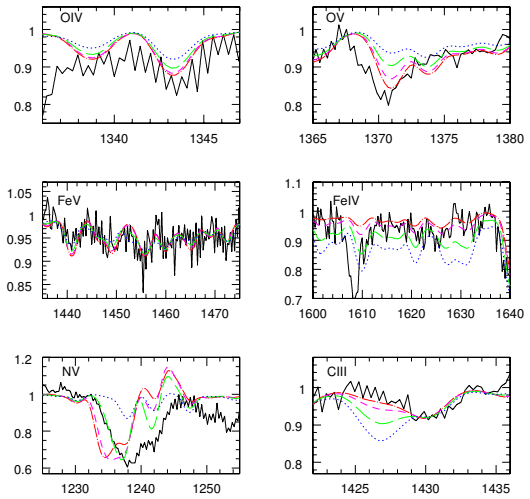

Fig. 4. Spectroscopic $T_{\rm eff}$ indicators. The black solid line is the observed spectrum of star 2. Coloured lines are four different models with $T_{\rm eff}$ 42 000 K (red, dot-long dashed line), 40 000 K (magenta, short dashed line), 37 500 K (green, long dashed line), 35 000 K (blue, dotted line). The mass loss rate is fixed at a constant value of $10^{-8.5}$ $M_\odot$ yr^{-1}. See text for discussion.

is a good $T_{\rm eff}$ estimator. Figure 4 shows comparisons between models of different $T_{\rm eff}$ and the observed spectrum of star 2. An increase of $T_{\rm eff}$ increases the strength of both lines which are reproduced for $T_{\rm eff} \geq 40\,000$ K.

O V λ1371 alone has been used by de Koter et al. (1998) as a $T_{\rm eff}$ indicator for early O stars. Nonetheless, as mentioned by these authors, this line is always predicted too strong compared to observations above ~40 000 K. Below this limit, the situation seems better. Recently, Bouret et al. (2003) have claimed that clumping could help to solve this well known problem (see Schaerer et al. 1996; Pauldrach et al. 2001): the line is weaker in a clumped model than in a homogeneous wind. As O V λ1371 (together with O IV $\lambda\lambda$1339,1343) depends also on $\dot{M}$, our $T_{\rm eff}$ estimate relies on the relative strength of both lines in homogeneous winds. This estimate must be confirmed by stronger indicators.

- Fe IV/Fe V:

Iron line forests exist all over the UV range. In particular, Fe IV lines are present between 1600 Å and 1640 Å, while Fe V lines are found between 1430 Å and 1480 Å. The iron ionisation increases with $T_{\rm eff}$ so that Fe IV lines weaken relatively to Fe V lines between 35 000 and 42 000 K. As Fe V is the dominant ionisation state of Fe in this temperature range, Fe V lines are saturated and little affected by an increase of $T_{\rm eff}$ whereas Fe IV lines weaken. This is shown in Fig. 4. For star 2, a value of at least 40 000 K is necessary to reproduce the observed spectrum.

The determination of $T_{\rm eff}$ from this line ratio can be hampered mainly by two effects:

– the iron abundance (and more generally metallicity) can change the strength of the Fe absorption. This effect is twofold. First, increasing the iron abundance will immediately increase the absorption of *all* Fe ions, although differently depending on the position of the lines on the curve of growth. Consequently, the ratio of lines from two successive ionisation states will be modified. Second, increasing the iron abundance will strengthen the line-blanketing effect and thus will increase the local temperature in the line formation region. The ionisation will be increased, leading to a higher $T_{\rm eff}$ estimate. The effects of metallicity due to line-blanketing on the effective temperature of O stars have been estimated by Martins et al. (2002b) and turn out to be of the order of 1000 to 2000 K depending on the spectral type for metallicities ranging from solar to 1/8 solar. We have run test models for a global metallicity of $Z = 1/5\,Z_\odot$. Its main effect is to strengthen the Fe IV lines, leaving the Fe V lines unchanged as they are almost saturated in the temperature range of interest here. Quantitatively, this change of Z is equivalent to a decrease of $T_{\rm eff}$ by ~2000 K as regards the iron lines behaviour;
– the so-called turbulent velocity "artificially" strengthens the absorption profiles as shown in Fig. 12 where $v_{\rm turb}$ increases from 5 to 15 km s^{-1}. Fe IV and Fe V lines deepen differently when $v_{\rm turb}$ increases, so that their relative strength remains turbulent-velocity dependent. Nonetheless, the effect is smaller than the effect on individual lines so that a reasonable estimate of $T_{\rm eff}$ can be drawn from the study of the relative strength of these iron forests. Note that if the effective temperature is known, the iron lines can be used to determine the turbulent velocity (see Sect. 5.5).

- C III $\lambda\lambda$1426,1428:

As noted by Walborn et al. (1995) in their IUE atlas of O star spectra, this blend of C III lines strengthens towards later types. Figure 4 shows that in the case of star 2 a value of at least 42 000 K is required to fit the observed spectrum. Changing slightly the carbon content can affect this determination. Quantitatively, a reduction of the C abundance from 1/8 $C_\odot$ to 1/10 $C_\odot$ (as discussed in Sect. 5.2.2) is equivalent to an increase of $T_{\rm eff}$ by ~1500 K.

- N V λ1238,1242:

This resonance line is known to be strongest around spectral type O4 (Smith-Neubig & Bruhweiler 1997) and to weaken at later spectral types or equivalently when $T_{\rm eff}$ decreases. Quantitatively, a $T_{\rm eff} > 35\,000$ K is required to account for the N V λ1238,1242 absorption profile in star 2. Nonetheless, the strong mass loss dependence of this line makes it a poor and only secondary $T_{\rm eff}$ indicator: a high mass loss associated with a relatively low $T_{\rm eff}$ can mimic the NV profile of a star with a lower mass loss rate but a higher $T_{\rm eff}$.

Table 3 summarises the results of these $T_{\rm eff}$ estimates, which all point to an effective temperature of the order 40 000 K for star 2. A real dispersion exists and is mostly due to the multi-parameter dependence of most of the indicators used.

Table 3. Effective temperature estimates.

Star	Estimator	$T_{\rm eff}$ (K)	Adopted $T_{\rm eff}$ (K)
1	UV colour index	37 000	
	OIV/OV	36 000	
	Fe IV/Fe V	≳38 500	
	N V	–	
	C III	38 500	
			38 500
2	UV colour index	37 500	
	O IV/O V	≳40 000	
	Fe IV/Fe V	40 000	
	N V	>35 000	
	C III	42 000	
			40 000
3	UV colour index	34 000	
	O IV/O V	≲37 500	
	Fe IV/Fe V	36 000	
	N V	<37 500	
	C III	36 000	
			36 000
11	UV colour index	35 000	
	O IV/O V	37 000	
	Fe IV/Fe V	≳37 000	
	N V	<37 000	
	C III	37 000	
			37 000

5.1.3. Estimation of uncertainty on $T_{\rm eff}$

Table 3 shows that for a given star the dispersion in the $T_{\rm eff}$ estimators is of the order of ±2500 K in the worst cases. A possible additional source of uncertainty comes from the rectification of the spectra. We estimate it to be lower than 0.05 in terms of normalised flux, which from Fig. 4 (especially the FeV plot) can lead to an error on $T_{\rm eff}$ of the order of ±1500 K.

The uncertainties due to variations of the global metallicity and carbon content have been estimated above and are of the order of 2000 K.

To estimate the efficiency of our $T_{\rm eff}$ determination method, we have applied it to a star for which optical and UV analysis have given strong constraints on $T_{\rm eff}$. For this purpose, 10 Lac was chosen (see Sect. 7.2). The UV colour index method indicates a value of 39 000 K, while the spectral lines point to values of the order 35 000/36 000 K. As the accepted $T_{\rm eff}$ for 10 Lac is close to 36 000 K, the error on the $T_{\rm eff}$ estimate is not more than ±3000 K. This example also shows that the spectral line method is more accurate than the colour index method. For that reason we have given more weight to the $T_{\rm eff}$ estimates based on the line method in our final estimate (as can be shown in Table 3).

From the above discussion, we conclude that on average, the uncertainty on our $T_{\rm eff}$ determination is of the order of ±3000 K.

5.2. Mass loss rate

The determination of the mass loss rate remains one of the main goals of this study. As already noted, the spectra of N81 stars show very weak wind features with no emission. As emission, contrary to absorption, is entirely formed in the wind, our constraints on $\dot{M}$ have been set by the requirement that no emission is produced in the model spectra (as observed in the STIS spectra). Thus, we have derived only upper limits on the mass loss rates as models with $\dot{M}$ below this limit never produce emission. The main mass loss indicators in the UV are the N V λ1238,1242, C IV $\lambda\lambda$1548,1551 and O V λ1371 lines.

5.2.1. Primary determinations

- O V λ1371:

O V λ1371 develops a P-Cygni profile in the earliest supergiants while only an absorption is seen in dwarfs (Walborn et al. 1995). Figure 5 reveals that the profile deepens when $\dot{M} \geq 10^{-8}\ M_\odot\ {\rm yr}^{-1}$ but remains roughly unchanged below this value. Fitting the observed spectrum of star 2 requires a mass loss rate lower than $10^{-8}\ M_\odot\ {\rm yr}^{-1}$. As mentioned in the previous section, O V λ1371 is sensitive to $T_{\rm eff}$ so that a degeneracy $\dot{M}/T_{\rm eff}$ exists. X-rays can also affect this line by increasing the Oxygen ionisation to produce O VI (observed in the EUV) by Auger ionisation of O IV.

- N V λ1238,1242:

This line is present in dwarfs of spectral type earlier than O8 (Walborn et al. 1995; Smith-Neubig & Bruhweiler 1997) and shows a strong P-Cygni profile in early dwarfs. It is mostly formed in the wind so that it is one of the best mass loss rate indicators of the UV part of the spectrum. This is illustrated in Fig. 5 where we see the profile changing from a well developed P-Cygni shape to a weak absorption when $\dot{M}$ is reduced by two orders of magnitudes. A mass loss rate lower than $10^{-9}\ M_\odot\ {\rm yr}^{-1}$ is necessary to produce no emission. However, in that case the absorption profile is too weak. Increasing $\dot{M}$ by a factor of 3 improves the fit of this absorption part but induces an emission (see Sect. 7 for a discussion of the shape of these wind profiles). Nonetheless, as emission is only produced in the wind whereas absorption can originate both in the wind and in the photosphere, we adopt $\dot{M} = 10^{-9}\ M_\odot\ {\rm yr}^{-1}$ as a reasonable upper limit.

N V λ1238,1242 is also $T_{\rm eff}$ sensitive as seen in Sect. 5.1.2 so that any error on $T_{\rm eff}$ can lead to an error on $\dot{M}$. Another problem comes from the X-rays (supposed to be created by shocks in the outer wind, e.g., Owocki et al. 1988; Feldmeier et al. 1997) which can increase the ionisation of nitrogen, thus leading to modifications of the N V λ1238,1242 profile. A very accurate determination of $\dot{M}$ based on N V λ1238,1242 would then require the inclusion of X-rays in the models. However,

Table 4. Summary of the stellar and wind properties derived for the N81 stars. The spectral types are estimated from the optical spectra of the models giving the best UV fits. As we have only lower limits on the terminal velocities, we have adopted $v_\infty/v_{\rm esc} = 2.6$ to compute both the modified wind momenta and the theoretical mass loss rates of Vink et al. (2001). The Si, S and Fe abundances are 1/8 solar and n(He)/n(H) is 0.1. The gravity adopted for our computation was log $g = 4.0$ as it is typical of dwarf stars (Vacca et al. 1996) and as we have no diagnostics to estimate the value of this parameter.

	Star 1	Star 2	Star 3	Star 11
$m_{\rm V}$	14.38	14.87	16.10	15.74
$E(B-V)$	0.07	0.06	0.10	0.07
Spectral type	O7	O6.5	O8.5	O7.5
$M_{\rm V}$	−4.84	−4.32	−3.21	−3.48
$T_{\rm eff}$ [K]	38 500	40 000	36 000	37 000
log $(L/L_\odot)$	5.32	5.16	4.59	4.73
$R/R_\odot$	10.3	7.9	5.0	6.9
$M/M_\odot$	32	30	19	21
$V \sin i$ [km s^{-1}]	200	300	250	250
log $\dot{M}$ [$M_\odot$ yr^{-1}]	$\lesssim$−8.0	$\lesssim$−8.0	$\lesssim$−8.5	$\lesssim$−9.0
v_∞ [km s^{-1}]	$\geq$1500	$\geq$1800	$\geq$300	$\geq$600
$v_{\rm esc}$	1088	1203	1204	1077
log $(\dot{M} v_\infty \sqrt{R})$	$\lesssim$26.76	$\lesssim$26.75	$\lesssim$26.14	$\lesssim$25.67
f_∞	0.01	0.01	1	1
log Q_0 [s^{-1}]	48.85	48.76	47.99	48.41
log $\dot{M}_{\rm Vink}$ [$M_\odot$ yr^{-1}]	−6.96	−7.25	−8.31	−8.04
C/C$_\odot$	1/10	1/8	1/10	1/10
N/N$_\odot$	1/20	1/8	1/20	1/20
O/O$_\odot$	1/5	1/8	1/5	1/5

tests have revealed that the inclusion of X-rays does not modify our conclusions. It is also unlikely that X-ray emission is important since any emission in the wind of the SMC-N81 stars seems to be very weak as shown by the UV spectra.

- C IV $\lambda\lambda$1548,1551:

This line is the other strong UV mass loss indicator of O dwarfs. It is seen in all O dwarfs with a strength increasing towards early types (Walborn et al. 1995). In Fig. 5 we see that it shifts from a P-Cygni profile to an absorption profile when $\dot{M}$ decreases. The absence of emission, required by the observation, is obtained for $\dot{M} \leq 10^{-7.5}\ M_\odot\ {\rm yr}^{-1}$. Contrary to N V λ1238,1242, a significant absorption profile can remain even when the emission disappears. But this absorption is mainly photospheric and the wind part turns out to be too weak compared to the observed spectra. A change of $T_{\rm eff}$ does not lead to any improvement (a lower $T_{\rm eff}$ implies an emission in C IV $\lambda\lambda$1548,1551 and a too weak N V λ1238,1242 line, and a higher $T_{\rm eff}$ weakens further the C IV $\lambda\lambda$1548,1551 line).

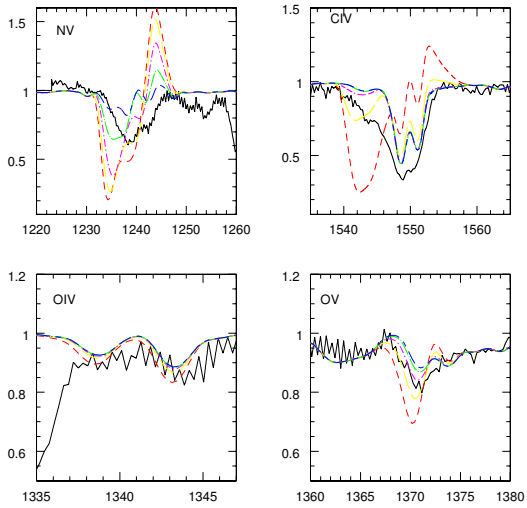

Fig. 5. Mass loss rate indicators: the black solid line is the observed profile while coloured lines are taken from models with $T_{\rm eff}$ = 40 000 K and various $\dot{M}$ ($-\log(\dot{M})$ = 7 (red, short dashed line), 7.5 (yellow, long dashed line), 8 (magenta, dot-short dashed line), 8.5 (green, dot-long dashed line), 9 (blue, short dashed – long dashed line)). See text for discussion.

5.2.2. Improving the $\dot{M}$ determinations: Effects of β, clumping, adiabatic cooling and abundances

One difficulty in fitting the UV lines (especially C IV $\lambda\lambda$1548,1551 and N V λ1238,1242) is to produce a

significant absorption extending up to velocities ≥1800 km s^{-1} without any emission. In the following, we concentrate on C IV $\lambda\lambda$1548,1551 as the discrepancy is highest for this line, but the discussion applies equally to N V λ1238,1242.

The absence or weakness of absorption at high velocity in the models showing no emission results from a lack of absorbers (i.e. C IV ions) which may come either from a too low density, and hence from a too low mass loss rate, or from a too high ionisation of carbon (CV being the dominant ionisation state in the wind). The first possibility can be ruled out because a higher mass loss rate will produce an emission which is not observed. Relying on the second hypothesis, we have sought for mechanisms that could lead to a reduction of the ionisation in the wind. This can be achieved if recombination rates are increased, i.e. if the density is higher (recombination scales as ρ^2). As the density is given by $\rho = \frac{\dot{M}}{4\pi r^2 v f}$ where f is the filling factor ($f = 1$ in an homogeneous atmosphere), a higher density at a given radius can be obtained by either a higher mass loss rate (which is excluded), or a clumped wind ($f < 1$) or a lower velocity which, as v_∞ is fixed, implies a softer slope of the velocity field (the β parameter). Recombinations can also be increased when the temperature in the outer wind is reduced. Adiabatic cooling may induce such a reduction as in these low density winds it can become an important cooling process. Last, abundances can of course modify the strength of the wind profiles. In the following, we present investigations of the influence of these various parameters on the line profiles and the mass loss rate determinations.

- β effects:

β is usually determined through the shape of hydrogen emission lines in the optical range (e.g., Hillier et al. 2003). However, as optical spectra are not available and as the optical lines probably have absorption profiles due to the weakness of the winds, we have no constraints on this parameter. We have thus run test models with $\beta = 2.0$ (the default value in all our computations being 0.8). The results are displayed in Fig. 6. C IV $\lambda\lambda$1548,1551 is not modified since it is almost purely photospheric in the models shown here, while N V λ1238,1242 shows narrower and stronger absorption and emission when β is higher. This behaviour can be explained in terms of the size of the interaction region which is the region in which, due to the wind velocity induced doppler shift, a photon can interact with a given line. The size of this region is proportional to the Sobolev length (see Lamers & Cassinelli 1999) which scales as $(\mathrm{d}v/\mathrm{d}r)^{-1}$ in the inner wind, so that a higher β will lead to larger Sobolev length (the acceleration being smaller). The interaction region is then wider which leads to a stronger absorption or emission in the center of the line. In the outer atmosphere, the radial Sobolev length is proportional to $\beta^{-1} r^2/v$ (for a β velocity law) and smaller for higher β so that the emission/absorption are reduced at high velocity[1]. Illustrations of the dependence of the size of the interaction region can be seen in Fig. 8.6 of Lamers & Cassinelli (1999).

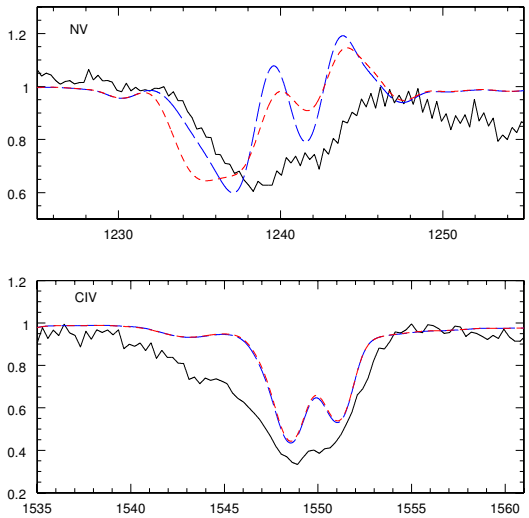

Fig. 6. Influence of the slope of the velocity field (β) on the mass loss rate diagnostic lines. Models with $\beta = 2.0$ (blue short dashed line) and $\beta = 0.8$ (red long dashed line) are compared to the observed profiles of star 2 (black solid line). Models are for $T_{\rm eff} = 40\,000$ K, $\dot{M} = 10^{-8.5}\ M_\odot\ \mathrm{yr}^{-1}$ and $V \sin i = 300$ km s^{-1}. The C IV $\lambda\lambda$1548,1551 line is almost unchanged while the N V λ1238,1242 line shows narrower absorption and emission when β is higher.

In our case, low values of β seem to be preferred as the observed N V λ1238,1242 profile does not show a double absorption line. However, $\beta = 2.0$ reproduces better the blue edge of the absorption profile. As $\beta = 0.8$ is closer to the predictions of the radiation driven wind theory, we adopt this value as typical of the SMC-N81 stars. But whatever the exact value of β, the mass loss rate determination is not strongly modified as the level of emission remains roughly the same (see Fig. 6).

- Clumping effects:

As already mentioned, there are indications that the winds of O stars are clumped (Crowther et al. 2002; Hillier et al. 2003; Bouret et al. 2003; Repolust et al. 2004), although there exist no quantitative constraints. The effects of inhomogeneous winds are twofold: first, due to the presence of overdensities, the emission of density-sensitive lines is strengthened; second, the higher density in clumps increases the recombination so that the ionisation is reduced. The competition between the two effects can lead to either stronger or weaker emission. To investigate deeper the effect of clumping on the wind profiles, we have run test models with $f_\infty = 0.01$ (recall that the filling factor f is given by $f = f_\infty + (1 - f_\infty)\mathrm{e}^{\frac{-v}{v_{\rm init}}}$). The main effects on the N V λ1238,1242 and C IV $\lambda\lambda$1548,1551 lines are shown in Fig. 7. We see that the strength of N V λ1238,1242 is reduced and that the C IV $\lambda\lambda$1548,1551 absorption is increased in the outer part of the atmosphere. This is attributed to a reduced ionisation in the outer wind (N V recombines to N IV and C V to C IV), which improves the fits. Hence, there is no doubt that

[1] When β increases, the transverse Sobolev length, which is proportional to $(v/r)^{-1}$, increases too. However, the decrease of the radial Sobolev length is greater than the increase of the transverse Sobolev length so that globally, the size of the interaction region is reduced.

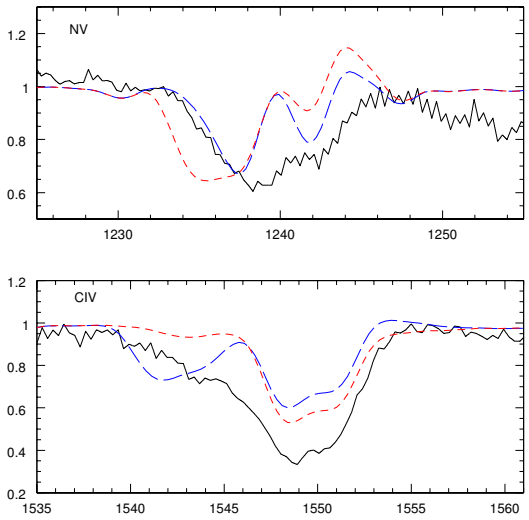

Fig. 7. Influence of clumping on the mass loss rate diagnostic lines. Models with a volume filling factor of 0.01 (blue long dashed line) and 1.0 (red short dashed line, no clumping) are compared to the observed profiles of star 2 (black solid line). Models are for $T_{\rm eff}$ = 40 000 K and $\dot{M}$ = $10^{-8.5}$ $M_{\odot}\,{\rm yr}^{-1}$ and V sin i = 300 km s^{-1}. The strength of N V λ1238,1242 is reduced and the absorption of C IV $\lambda\lambda$1548,1551 is increased when clumping is included.

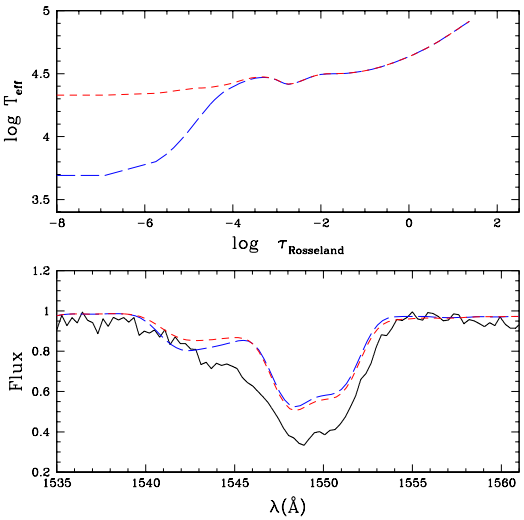

Fig. 8. Effect of the inclusion of adiabatic cooling in model computations on the temperature structure (*top*) and the C IV $\lambda\lambda$1548,1551 profile (*bottom*; blue long dashed line: model with adiabatic cooling; red short dashed line: model without adiabatic cooling). While the temperature is strongly reduced in the outer parts, the C IV $\lambda\lambda$1548,1551 profile is only slightly affected. Other wind lines do not show any change.

the inclusion of clumping is crucial to reproduce the observed features. Whether this is a proof of the inhomogeneity of O star winds or just a trick to simulate the correct ionisation is not clear, but this parameter turns out to be an important ingredient of the modeling. As regards the mass loss determination, Fig. 7 shows that the emission is slightly reduced when clumping is included so that the upper limit on $\dot{M}$ must be slightly increased.

- Adiabatic cooling:

In low density winds, due to the reduction of any cooling processes based on atomic mechanisms, adiabatic cooling is expected to be important to set the temperature structure (e.g., Drew 1985). Figure 8 demonstrates that this is indeed the case: a model with adiabatic cooling (long dashed line) shows a strong drop in temperature in the outer wind. However, as in this part of the atmosphere populations are mostly governed by radiative processes, the influence on the line profiles is reduced: the C IV $\lambda\lambda$1548,1551 line shows a slightly enhanced absorption which improves the fit but remains marginal. We conclude that adiabatic cooling is not a crucial parameter *as regards the fit of UV wind lines*.

- Abundances:

Metallicity in our models has been chosen to be 1/8 solar, and the individual abundances have simply been scaled according to this global metallicity. A better assumption would have been to take abundances typical of the SMC molecular clouds since the N81 stars are young and their atmospheres probably not contaminated by stellar nucleosynthesis products. Such initial abundances can be obtained by studies of either main sequence stars which have not yet experienced internal mixing, or HII regions. However, few of the former have been undertaken and they are often uncertain (Venn 1999, and references therein), and studies of nebular abundances can lead to underestimates due to the depletion of material on dust grains. Nonetheless, reasonable agreement between these two types of determinations can sometimes be obtained (see Venn 1999, for a discussion) and point to the following values: C/C$_{\odot}$ = 1/10, N/N$_{\odot}$ = 1/20 and O/O$_{\odot}$ = 1/5 (Venn 1999; Heap 2003; Vermeij 2002). Adopting these abundances in our computations leads to weaker N V λ1238,1242 and C IV $\lambda\lambda$1548,1551 profiles for a given $\dot{M}$. This means that our upper limit on the mass loss rate necessary to remove emission in the wind lines has to be increased. Recently, Asplund (2003) has revised the solar N abundance. With his new value, the SMC-N81 N abundance derived by Vermeij et al. (2002) is 1/30 solar, meaning that the upper limits on $\dot{M}$ have again to be increased a little.

From the above discussion the result is that if the CNO abundances are reduced and set to more realistic values and if clumping is included, the upper limit on $\dot{M}$ has to be increased by ∼1.0 dex (the effect of abundances being dominant). Clumping also helps to get better shapes of the wind lines. β and adiabatic cooling have almost no influence on the $\dot{M}$ determination. As a consequence, we adopt an upper limit on the mass loss rate of star 2 of $10^{-8.0}$ $M_{\odot}\,{\rm yr}^{-1}$.

5.3. Reliability of the mass loss rate determination

In view of the low values of $\dot{M}$ derived, we may wonder whether our determination is not hampered by any modeling

problem. In particular, what is really determined through fits of UV wind lines is the product of the mass loss rate times the ionisation fraction (q_i) of the absorbing/emitting ion. Any problem with the prediction of these ionisation fractions would translate into an error in $\dot{M}$. To investigate this point, two kinds of tests have been pursued.

- H_α vs. UV mass loss determination:

H_α is much less sensitive to the model predictions concerning the ionisation than UV resonance lines, so that we have compared the values of $\dot{M}$ derived from the fit of UV lines on the one hand and H_α on the other hand. To this aim we have chosen as a test case the star HD 217086 (O7Vn) for which constraints on the mass loss rate (Puls et al. 1996; Repolust et al. 2004) and the ionisation fractions of several ions (Lamers et al. 1999) exist. The low density of the wind (see Lamers et al. 1999) and the effective temperature of the order of 37 000 K make this star similar to the SMC-N81 stars, although the wind is less weak. We have computed various models to fit simultaneously the H_α profile and the UV resonance lines.

Figure 9 shows the results of the fits of the wind-sensitive lines. Two types of conclusions can be drawn depending on the value of the β parameter (slope of the wind velocity field):

- if we adopt $\beta = 0.8$ as derived by Repolust et al. (2004), the H_α profile is best fitted for $\dot{M} = 10^{-6.4}\ M_\odot\ \mathrm{yr}^{-1}$ (dot-dashed line) but in that case the UV lines (especially N IV λ1718) are too strong. A value of $\dot{M}$ of $10^{-7.2}\ M_\odot\ \mathrm{yr}^{-1}$ (long dashed line) has to be adopted to improve the fit of these UV lines, but now the H_α absorption is too strong. Mass loss rates derived from the UV seem then to be lower by a factor 6 compared to the H_α determination. Note that the predictions of Vink et al. (2001) give $\dot{M} = 10^{-6.1}\ M_\odot\ \mathrm{yr}^{-1}$ for HD 217086;
- when we increase β to 1.7, a mass loss rate of $10^{-7.0}\ M_\odot\ \mathrm{yr}^{-1}$ gives a reasonable – although not perfect – agreement between observations and models for both H_α and the UV lines (dotted line in Fig. 9).

While the conclusions of the case $\beta = 0.8$ point to a problem with the ionisation fractions predicted by the CMFGEN models, the case $\beta = 1.7$ indicates that this problem partly disappears when β is increased. This does not necessarily mean that $\beta = 1.7$ (the determination of this parameter in low-density winds is difficult, see e.g., Puls et al. 1996), but it is a way to produce the ionisation throughout the wind leading to an overall good fit of the observed profile[2]. Practically, as we do not have any constraint on β (see Sect. 5.2.2) we can conclude that *in the worst case $\dot{M}$ derived from UV lines is underestimated by a* ***factor 6***, at least if we take the mass loss rate from H_α as the correct one. In fact, if we take the case $\beta = 1.7$ as representative of the real conditions in the wind, the error we make when we only look at the UV spectrum (as for our SMC-N81 stars) and adopt $\beta = 0.8$ is 0.2 dex, or less than a factor 2^3. Moreover, in their recent study of SMC dwarfs with weak winds, Bouret et al. (2003) have been able to fit simultaneously lines of different ionisation stages of the same element with CMFGEN models, which indicates that the wind ionisation was predicted correctly.

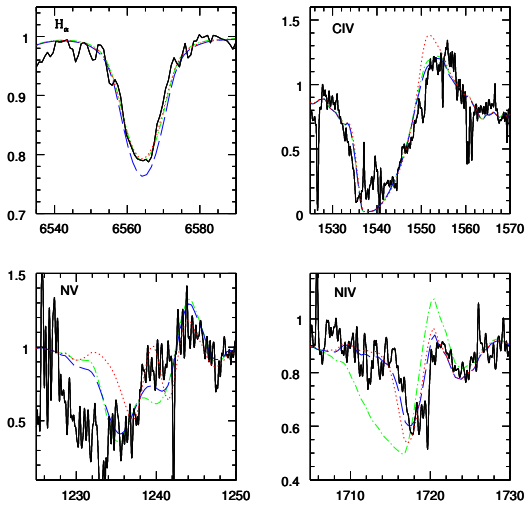

Fig. 9. H_α versus UV lines $\dot{M}$ determinations. The solid line is the observed profile of wind sensitive lines of HD 217086. Other lines are CMFGEN models at 37 000 K with $\beta = 0.8$ and $\dot{M} = 10^{-6.4}\ M_\odot\ \mathrm{yr}^{-1}$ (dot-dashed line), $\beta = 0.8$ and $\dot{M} = 10^{-7.2}\ M_\odot\ \mathrm{yr}^{-1}$ (long dashed line) and $\beta = 1.7$ and $\dot{M} = 10^{-7.0}\ M_\odot\ \mathrm{yr}^{-1}$ (dotted line). A rotational velocity of 290 km s^{-1} has been adopted. For $\beta = 0.8$ values of $\dot{M}$ different by one order of magnitudes are required to fit H_α on the one hand and the UV lines on the other hand, while for $\beta = 1.7$ a reasonable fit of all lines is achieved. See text for discussion.

- SEI method:

We have applied the SEI method (Lamers et al. 1987) to our SMC N81 star 2. This method leads to the determination of $\dot{M} \times q_i$. Basically, the SEI method solves the radiative transfer in an expanding atmosphere for which the source functions are calculated in the Sobolev approximation. The main input parameters are the velocity field and a function giving the optical depth of the line as a function of velocity. The main output is the value of $\dot{M} \times q_i$. The best fit to the C IV $\lambda\lambda$1548,1551 line of star 2 is shown in Fig. 10. The corresponding value of $\log(\dot{M} \times q_i)$ is −9.68. We also show in this figure the influence of the underlying photospheric absorption: as expected, the low-velocity part of the C IV $\lambda\lambda$1548,1551 absorption profile is sensitive to this photospheric absorption. As the interstellar contamination renders the true stellar absorption uncertain (see above), we do not give too much weight to this part of the profile which can always be fitted by tuning the photospheric absorption. The important point is that the wind profile ($0.4 \leq \Delta v/v_\infty \leq 1.0$) is insensitive to the amount of photospheric absorption and only depends on the wind parameters.

[2] As mentioned in Sect. 5.2.2 clumping can also modify the ionisation in the wind. However, several tests have shown that it was not possible to fit simultaneously H_α and UV lines with clumped models.

[3] Compared to the value given by Repolust et al. (2004) – $\dot{M} = 10^{-6.64}\ M_\odot\ \mathrm{yr}^{-1}$ –, our best determination ($\dot{M} = 10^{-7.0}\ M_\odot\ \mathrm{yr}^{-1}$, $\beta = 1.7$) is a factor ∼2 lower.

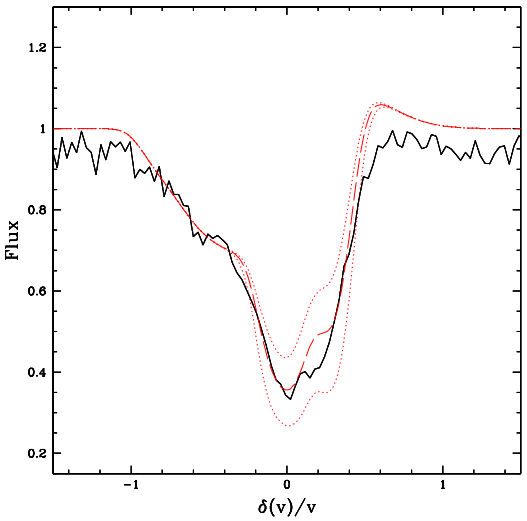

Fig. 10. Fit of C IV $\lambda\lambda$1548,1551 line with the SEI method. The solid line is the observed profile and the dashed line is the best fit. The parameters for the velocity law are $\beta = 1.0$ and $v_\infty = 1800$ km s^{-1}. A photospheric component has been used. The optical depth has the following velocity dependence: $\tau(w) = T_{\rm tot}(1-(w)^{1/\beta})(w)^{0.2}$ with $w = v/v_\infty$ and $T_{\rm tot} = \int_{0.01}^{1}\tau(w)$. The derived value of $\dot{M}\times q_{\rm i}$ is $10^{-9.68}$. Dotted lines show the influence of an increased or reduced photospheric component: the wind part of the absorption is not affected by this component.

Our estimation of $\dot{M}\times q_{\rm i}$ with the SEI method can then be regarded as reliable.

To compare this value to that deduced from our model giving the best fit for star 2, we have computed the ionisation fraction of C IV using the definition of Lamers et al. (1999):

$$q_{\rm i} = \frac{\int_{x_0}^{x_1} n_{\rm i}(x){\rm d}x}{\int_{x_0}^{x_1} n_{\rm E}(x){\rm d}x} \quad (1)$$

where $n_{\rm i}$ is the population of the absorbing ion, $n_{\rm E}$ the population of the element, x_0 (x_1) the lower (higher) integration limit (x being $r/R_\star$). We found $\log q_{\rm C\,IV} = -1.36$ which, together with a mass loss rate of $10^{-8.5}\,M_\odot$ yr^{-1} gives $\log(\dot{M}q_{\rm i}) = -9.86$, in reasonable agreement with the SEI result. This shows that the value of $\dot{M}\times q_{\rm i}$ obtained by fitting the CMFGEN model profiles to the observations is correct. Thus it follows that if $\dot{M}$ is underestimated, the C IV ionisation fraction is overestimated. To investigate this point, we have compared our ionisation fractions to those derived by Lamers et al. (1999). For stars of different stellar and wind properties, they found a mean $q_{\rm C\,IV}$ of the order $10^{-2.5}$ which is ∼a factor of 10 lower than the CMFGEN value. An error by such a factor in $q_{\rm i}$ translates to an underestimate of $\dot{M}$ by the same factor. This confirms the result of the previous section where a possible underestimate of $\dot{M}$ by a factor 6 was highlighted.

An interesting comment to make is that if we simply *assume* that the derived mass loss rate is correct, the mean density in the wind (as defined by Lamers et al. 1999) is of the order $10^{-16...-17}$ g cm^{-3} which is well below the lowest density probed by the Lamers et al. sample (see their Fig. 3). As their analysis indicates an increase of the C IV ionisation fraction with decreasing mean density, it is conceivable that for very weak winds $q_{\rm C\,IV}$ may reach values of the order of 0.1, which would reconcile the CMFGEN and Lamers et al. ionisation fractions. Moreover, it should be noted that the study of Lamers et al. includes radio and H$_\alpha$ mass loss rates which did not take clumping into account. Since the inclusion of clumping leads to lower $\dot{M}$ (e.g., Hillier et al. 2003), it is conceivable that some of the Lamers et al. ionisation fractions are underestimated.

The main conclusion of these two types of studies (H$_\alpha$/UV and SEI) is that there are indications that the ionisation fractions predicted by CMFGEN may be wrong, but by no more than a factor of ∼10 (leading in that case to an underestimation of $\dot{M}$ by the same factor). However, in both studies we have also found means to explain the observations with the CMFGEN predictions (changing the value of β in the study of HD 217086, extrapolating the trend $q_{\rm C\,IV}$ – mean density in the SEI study). It is thus not clear if the ionisation fraction predictions of the CMFGEN models are erroneous or not, especially given that we are in a range of parameters never explored before (weak winds). However, if these predictions are wrong, they do not *qualitatively* modify the conclusion concerning the weakness of the winds (see Sect. 7).

5.4. Terminal velocity

The terminal velocity of the winds of O stars is usually derived from the blueward extension of UV resonance lines. Here, due to the weakness of the outer wind density, the absorption may not extend up to v_∞ so that with the above method one can only derive lower limits for the terminal velocities. As shown in Table 4, these limits can even be lower than the escape velocity (which is of the order 1100 km s^{-1}), reinforcing the fact that the absorption probably does not extend up to v_∞. Moreover, the relatively low signal to noise ratio of our spectra coupled to the uncertainty in the flux normalisation introduces an uncertainty in the exact position of the most blue-shifted absorption. Figure 11 shows the N V λ1238,1242 and C IV $\lambda\lambda$1548,1551 profiles of models with $v_\infty = 1500$ and 1800 km s^{-1} compared to the observed line. The N V λ1238,1242 profile is not affected by the change of v_∞ while the C IV $\lambda\lambda$1548,1551 profile is hardly modified. In view of this result, and as the fit with the SEI method requires a value of 1800 km s^{-1} for the terminal velocity, we adopt this value as representative for star 2. The values for the other stars are given in Table 4.

5.5. Turbulent velocity/rotational velocity

The turbulent velocity in O stars is thought to increase from values of a few km s^{-1} near the photosphere to ∼10% of the terminal velocity in the outer atmosphere. As mentioned in Sect. 5.1, iron lines are sensitive to $v_{\rm turb}$ so that once $T_{\rm eff}$ is known, they can be used to determine the turbulent velocity. Figure 12 shows the comparison of iron lines of a model with $T_{\rm eff} = 40\,000$ K but different $v_{\rm turb}$. For each model, spectra convolved with rotational velocities of 200, 250 and 300 km s^{-1}

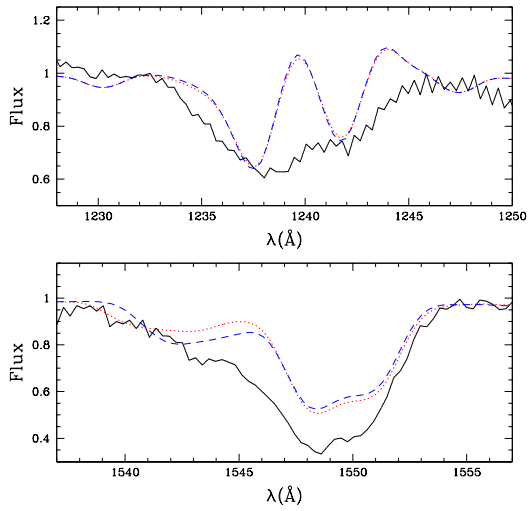

Fig. 11. Determination of v_∞. The solid line is the observed spectrum while the dotted (dashed) line is a model with v_∞ = 1800 (1500) km s^{-1}. No change is seen in N V λ1238,1242, and C IV $\lambda\lambda$1548,1551 is hardly affected. See text for discussion.

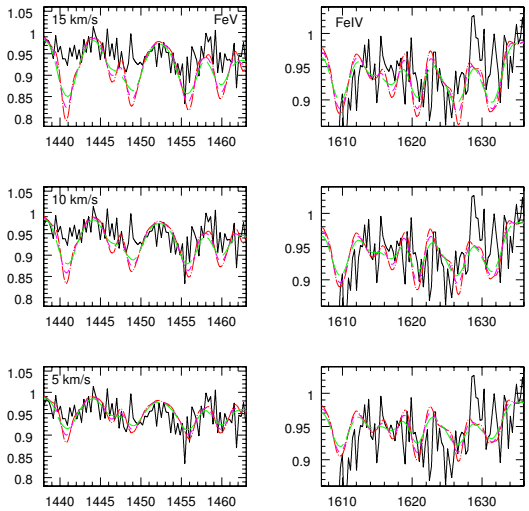

Fig. 12. Effect of microturbulence and rotation on the iron spectrum. The three left panels show Fe V lines while the Fe IV lines are shown in the right panels. The turbulent velocity decreases from 15 to 5 km s^{-1} from top to bottom. Each model is convolved with a rotational velocity of 100 (dot – long dashed line), 200 (short dashed line) and 300 km s^{-1} (long dashed line). The lower panels ($v_{\rm turb}$ = 5 km s^{-1}) give the best fit.

are shown. The best fit is obtained for a turbulent velocity of 5 km s^{-1}. For higher values, the Fe V lines deepen too much compared to the observed spectrum. The Fe IV lines behave similarly but also weakly. Tests have been run with a turbulent velocity varying from 5 km s^{-1} near the photosphere up to 100 km s^{-1} in the outer wind and have revealed very little change in the blue part of wind profiles. This is explained by the weakness of the wind in which absorption is likely to take place up to velocities lower than the terminal velocity of the wind. Figure 12 also reveals that the rotational velocity of the star is of the order 300 km s^{-1}. Indeed, lower velocities lead to narrow and deep profiles which are not observed.

5.6. Luminosity

The luminosity of the stars has been estimated from the absolute visual magnitude $M_{\rm V}$ and a bolometric correction calculated for the estimated $T_{\rm eff}$ of the star according to

$$\log \frac{L}{L_\odot} = -0.4\left(M_{\rm V} + BC - M_\odot^{\rm bol}\right) \quad (2)$$

where $M_\odot^{\rm bol}$ = 4.75 (Allen 1976). M_V was derived in Paper I from the observed visual magnitude and the estimated extinction. BC, which is essentially model-independent when calculated as a function of $T_{\rm eff}$, is derived from the relation of Vacca et al. (1996)

$$BC(T_{\rm eff}) = 27.66 - 6.84 \times \log T_{\rm eff}. \quad (3)$$

The uncertainty is 0.01 for the observed visual magnitude (Paper I), 0.05 for the extinction (from an uncertainty of 0.01 on $E(B-V)$), 0.025 for the distance modulus (di Benedetto 1997) and finally 0.25 for BC for a typical error on $T_{\rm eff}$ of 3000 K. On average, the uncertainty in L is therefore of the order of 0.12 dex.

5.7. Summary and results for other stars

Stellar and wind parameters for 3 other stars of SMC-N81 have been determined with a similar analysis. Here we summarise the results of this analysis and give the results in Table 4. The best fits are shown in the Appendix. For the remaining stars presented in Paper I, no constraints have been derived due to the poor quality of the spectra. For all the stars, β = 0.8 and Si, S and Fe abundances equal to 1/8 solar have been chosen. The masses have been derived from the HR diagram presented in Fig. 14.

5.7.1. Star 2

The main results have been given in the previous sections. In contrast to all other stars, we stress that the fits of the C IV $\lambda\lambda$1548,1551 and N V λ1238,1242 lines for star 2 are improved when the abundances are taken to be 1/8 solar. Choosing the lower values indicated by the nebular analysis (see Sect. 5.2.2) leads to too weak absorptions even when clumping is included. The best fits are achieved with a filling factor at the top of the atmosphere of 0.01[4].

5.7.2. Star 1

For this star, $T_{\rm eff}$ is found to be ~38 500 K. The upper limit on the mass loss rate is $10^{-8.0}$ $M_\odot$ yr^{-1} and v_∞ is at least 1500 km s^{-1}. Clumping is necessary to improve the fit

[4] Recall that in the present parameterisation of clumping in CMFGEN, this means that f goes from 1 at the photosphere to 0.01 when $v = v_\infty$.

of the C IV $\lambda\lambda$1548,1551 line (f_∞ = 0.01). A reasonable fit is achieved with the nebular CNO abundances.

5.7.3. Star 3

Star 3 is the coolest of the 4 stars studied ($T_{\rm eff}$ = 36 000 K). The determination of the mass loss rate is very difficult because the N V λ1238,1242 line is almost absent due to the low $T_{\rm eff}$ and the C IV $\lambda\lambda$1548,1551 line is almost entirely photospheric. Hence, secondary indicators such as O IV $\lambda\lambda$1339,1343 have been used to estimate $\dot{M}$ (which is found to be lower than $10^{-8.5}$ $M_\odot\,{\rm yr}^{-1}$). We want to stress that this determination is probably the most uncertain of our sample, especially since the the observed spectrum is noisy. The very small value for the terminal velocity reflects the low density of the wind: the number of absorbants in the wind is so low that the wind lines are essentially absent. The nebular CNO abundances give the best fits.

5.7.4. Star 11

We have estimated an effective temperature of 37 000 K for this star. An upper limit of $10^{-9.0}$ $M_\odot\,{\rm yr}^{-1}$ is estimated from the N V λ1238,1242 and C IV $\lambda\lambda$1548,1551 lines. The terminal velocity we derive (600 km s^{-1}) is again a lower limit. The nebular CNO abundances give reasonable fits and clumping is not necessary.

6. Nebular and stellar properties

In this section we first go back to the nebular properties of N81 and then investigate the evolutionary status of the individual stars together with the consequences of their weak winds.

6.1. Nebular properties/Ionising fluxes

A meaningful way of testing our results concerning the stellar properties of the N81 individual components is to compare them to the integrated properties of the cluster.

First, Heydari-Malayeri et al. (1999) derived a mean extinction of $A_{\rm V}$ = 0.40 from the observed H_α/H_β ratio in the nebula, and they used this value to correct the observed flux in H_β and to estimate the number of Lyman continuum photons – Q_0 – emitted by the N81 stars (under the assumption that the HII region is ionisation bounded). They find Q_0 = 1.36×10^{49} photons s^{-1}. From this and from the calibration of Vacca et al. (1996), they conclude that a single main sequence star of spectral type O6.5 or O7 can lead to such an ionising flux. We have estimated the total amount of ionising photons released by the N81 stars from the SEDs of the models giving the best UV fit. As the N81 stars studied here are the most luminous and hottest of the region, they are likely to provide essentially all the ionising flux. We found from the models Q_0 = 1.64×10^{49} photons s^{-1} in good agreement with the values derived from the nebular properties. The lower value of the estimate of Heydari-Malayeri et al. (1999) can be partly explained by the fact that the HII region may be density bounded so that a part of the ionising flux may escape the cavity.

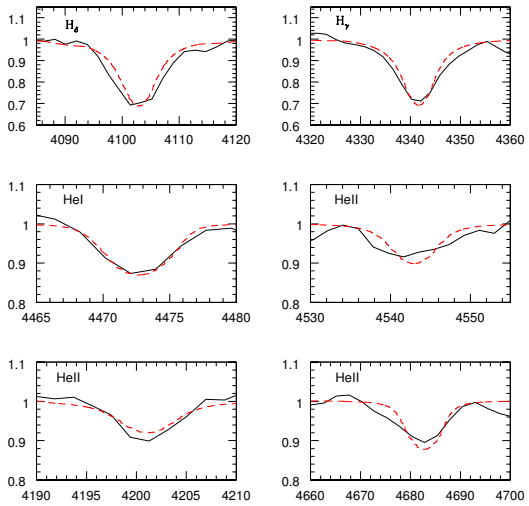

Fig. 13. Comparison between observed optical spectrum of the N81 cluster corrected for nebular lines (solid line) and sum of the optical spectra of the models giving the best UV fits (dashed line). Each optical spectrum from the models has been convolved with rotational velocities derived from the UV spectra. The agreement is very good, showing that our determination of the stellar parameters of the N81 stars is reliable.

Second, we have integrated optical spectra of the N81 cluster that have been corrected for the nebular contamination so that they give the total stellar spectrum which can be compared to the sum of the individual stellar optical spectra of the models giving the best UV fits. Figure 13 shows that there is again a good agreement between the observed and modeled spectra. From the strength of the He lines, a "mean" spectral type O7 is found (which is in fact similar to the spectral type of the two most luminous stars of the cluster, namely stars 1 and 2). This indicates that despite the difficulties in estimating the stellar properties of the individual stars (in particular $T_{\rm eff}$), our results are reliable. Moreover, the He II λ4686 line is reasonably fitted by the models. As this line is usually filled by wind emission, this may be an indication of not too high mass loss rates.

6.2. Evolutionary status

We have placed the N81 stars on an HR diagram constructed with Geneva evolutionary tracks without rotation for Z = 0.004 (Fig. 14). All the stars are compatible with an age ≤5 Myrs. While star 1 seems to be slightly older, the 3 other stars (especially star 3 and 11) lie close to the ZAMS and have an age between 0 and 4 Myrs. There seems to be an age dispersion of the order 1 or 2 Myrs in the cluster, which is reasonable. The inclusion of rotation is known to move the ZAMS towards lower $T_{\rm eff}$ (see Meynet & Maeder 1997), reducing the age estimates for stellar populations compared to the non-rotating case. However, this effect becomes significant only for rotational velocities close to the critical velocity. As the SMC-N81 stars have $V \sin i$ of only 200−300 km s^{-1} (which corresponds to ∼1/3 of the break velocity), our results are

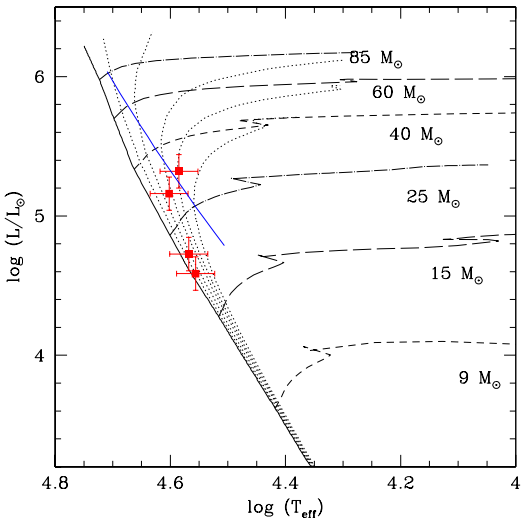

Fig. 14. HR diagram for $Z = 0.004$ without rotation. Different Geneva evolutionary tracks for various masses are indicated, together with the ZAMS and isochrones for 1, 2, 3, 4 and 5 Myrs (data from Lejeune & Schaerer 2001). The filled squares give the position of the SMC-N81 stars with the typical errors on their position. The calibration $\log L - \log T_{\rm eff}$ of Vacca et al. (1996) for dwarfs is also shown by the long dashed line. Note the underluminosity of most of the SMC-N81 stars.

probably not strongly hampered by the use of stellar tracks without rotation.

Based on the equations governing the dynamical evolution of HII regions (Dyson 1978) with the typical values $\dot{M} = 3 \times 10^{-9}\ M_\odot\,{\rm yr}^{-1}$ $v_\infty = 1500\ {\rm km\,s}^{-1}$, $n_0 = 400\ {\rm cm}^{-3}$ (gas density, see Heydari-Malayeri et al. 1988) and a radius of the HII region of 3 pc, one can derive an age of ~1.4 Myr for the N81 region. This assumes that star 1 and 2 provide most of the mechanical energy ($\frac{1}{2}\dot{M}v_\infty$). Previous age estimates based on the decrement of H_β equivalent width by Heydari-Malayeri et al. (1988) were of 1 to 2.5 Myr assuming a stellar cluster of solar metallicity. However, for clusters with a small number of ionising stars this method is inherently inaccurate due to statistical fluctuations.

If we compare the positions of the SMC-N81 stars with the calibration $L - T_{\rm eff}$ for dwarfs of Vacca et al. (1996) based on studies of Galactic O stars (long dashed line in Fig. 14), we note that except star 1, the other components are all underluminous compared to "normal" O dwarfs. This result based on the quantitative study of the stellar properties confirms the conclusion of Paper I in which the subluminosity of most of the stars was already highlighted and interpreted as an indication of the youth of the stars.

In Paper I it was argued that the SMC-N81 stars could belong to the class of Vz stars. Figure 14 shows that although young, the stars do not lie perfectly on the ZAMS. This may be an indication that either Vz stars are not strictly ZAMS stars but more probably "young" stars less evolved than "normal" dwarfs, or that our objects are not "true" Vz stars (we recall that we do not dispose of optical spectroscopy to firmly establish if the SMC-N81 stars are Vz stars or not). A deeper investigation of the properties of this interesting class of objects will be presented in a forthcoming paper.

7. Puzzling wind properties

7.1. Comparison to previous observations and theoretical predictions

One of the most surprising feature of the spectra of the SMC-N81 stars is the shape of the wind lines (mainly N V λ1238,1242 and C IV $\lambda\lambda$1548,1551): while they show no emission, they display a blueshifted absorption profile. This is quite puzzling: how can we produce such an absorption without any emission? Theoretically, in an extended atmosphere, the absorption in the P-Cygni profile comes from the removal of photons from the observer's line of sight, and the emission is due to photons that have been scattered isotropically on sight lines not parallel to that of the observer. Globally, the amount of "absorbed" photons is then equal to the number of "emitted" photons. If the atmosphere is only weakly extended (i.e. its height is smaller than the stellar radius), then roughly half the photons are backscattered towards the star and destroyed, so that the emission is reduced compared to the absorption (the ratio between them being 1/2). This is even more true if there is an underlying photospheric absorption which increases the absorption with respect to the emission. This points to the behaviour observed in our spectra, but the absence of emission remains a puzzle.

A possible explanation for the absence of emission may be an enhanced backscattering of photons towards the photosphere, so that the emission is even more reduced compared to the absorption. But the physical reason for such a process is not known. Another possibility is a strongly non-spherically symmetric wind. Rotation is known to increase the mass loss near the poles and to reduce it at the equator (Bjorkmann & Cassinelli 1993; Maeder & Meynet 2000). If a star rotates sufficiently fast to induce a strong contrast between the polar and equatorial ejection, and if we can observe it pole-on, then we can obtain the kind of profile we have: the blueshifted absorption comes from the high density polar flow while the (absence of) emission corresponds to the low density "equatorial" atmosphere. However, as *all* the SMC-N81 stars show such profiles and as the probability to see all of them pole-on is low, this explanation is not satisfying. Moreover, as the projected rotational velocities of the N81 stars are of the order 200/300 km s^{-1}, it is not likely that they are seen pole-on.

In spite of these curious features, we have been able to place constraints on the wind properties of the SMC-N81 stars, the main results being that they lose mass at an extremely low rate. Whether this is typical or not of O dwarfs at low metallicity remains to be established. Indeed, this is one of the first quantitative determinations of mass loss rates for such objects and consequently few comparisons are possible. To our knowledge, the only previous studies of wind parameters of O dwarfs in the SMC have been performed by Puls et al. (1996), Bouret et al. (2003) and very recently Massey et al. (2004). Puls et al. (1996) only derived upper limits on the mass loss rates for four SMC dwarfs. This is mainly due to the fact that their method

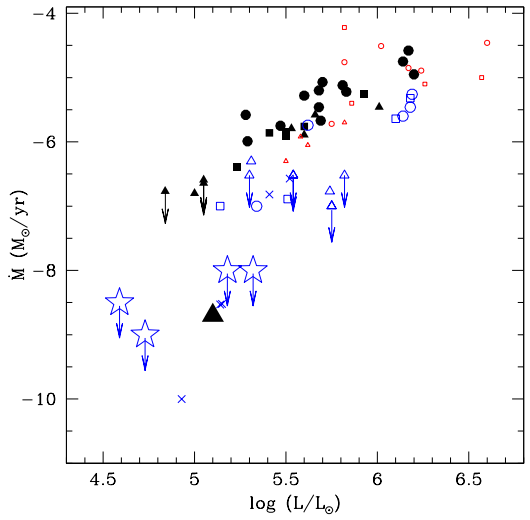

Fig. 15. Mass loss rate as a function of stellar luminosity for O stars. Filled (open) symbols are Galactic (LMC, small red/SMC, blue) objects. Triangles (squares, circles) are for luminosity class V (III, I). Crosses are the SMC stars of Bouret et al. (2003). Data are from Puls et al. (1996), Herrero et al. (2000), Crowther et al. (2002), Repolust et al. (2004), Hillier et al. (2003) and Massey et al. (2004). The star symbols are for the SMC-N81 stars. Note the low mass loss rates of the SMC objects with $\log \frac{L}{L_\odot} \leq 5.5$ and of 10 Lac (large filled triangle).

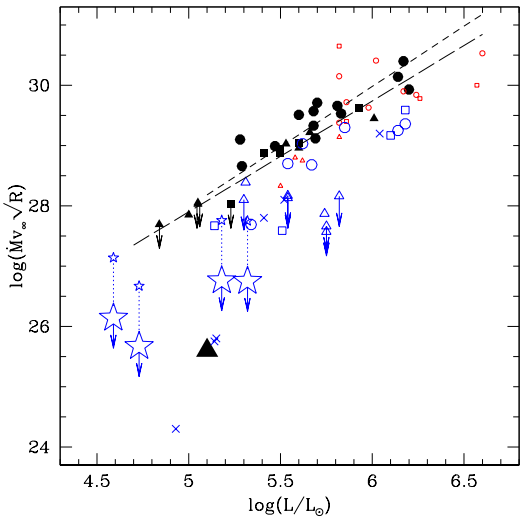

Fig. 16. Modified wind momentum-luminosity relation. Data and symbols are the same as in Fig. 15. The SMC-N81 stars (for which we have adopted $v_\infty = 2.6\, v_{\rm esc}$ to compute the modified wind momentum) confirm the trend of either a reduced modified wind momentum at low luminosity or a steeper slope of this relation at low metallicity. The small star symbols show the position of the SMC-N81 stars if $\dot{M}$ was systematically underestimated by a factor 10. The long-dashed (short-dashed) line gives the mean relation for luminosity clas V−III (I) stars from Repolust et al. (2004). The position of 10 Lac is also indicated by the large filled triangle.

relies on the the strength of the H_α emission whereas the H_α profile in SMC dwarfs is mostly in absorption. Their upper limits are of the order $10^{-7}\ M_\odot\ {\rm yr}^{-1}$ which is roughly 10 times higher than our estimates for the SMC-N81 stars. The recent work by Bouret et al. (2003) includes 5 SMC O dwarfs of which three (with spectral type between O9.5 and O6) have mass loss rates between 10^{-10} and $3 \times 10^{-9}\ M_\odot\ {\rm yr}^{-1}$. Our results agree very well with these estimates (we recall that the SMC-N81 stars have mid to late spectral types). The dwarfs studied by Massey et al. (2004) are more luminous than the N81 stars and have therefore higher mass loss rates. Figure 15 shows mass loss rates as a function of luminosity for Galactic and SMC dwarfs from different studies. The results of this work and of Bouret et al. (2003) indicate a strong reduction of the mass loss rate of stars with $\log \frac{L}{L_\odot} \lesssim 5.5$.

How do these results compare to theoretical calculations? The most recent predictions of wind parameters as a function of metallicity are the extensive calculations by Vink et al. (2001). Using their cooking recipe to estimate the mass loss rate as a function of stellar parameters and metallicity, we found $\dot{M}$ of the order $10^{-7...8}\ M_\odot\ {\rm yr}^{-1}$ for the SMC-N81 stars (the exact values are given in Table 4). The derived mass loss rate are more than 30 times lower. Even if we take into account a possible error in the ionisation fraction of the CMFGEN models (which would lead to an increase of the $\dot{M}$ determinations by a factor of $\lesssim$10) the mass loss rates are still lower than predicted (with perhaps the exception of star 3 for which we recall that the $\dot{M}$ determination is uncertain). There is thus no doubt that the winds of the SMC-N81 stars show unusual weakness.

This result is even more striking in terms of modified wind momentum. This quantity defined by $\dot{M} v_\infty \sqrt{R}$ is predicted to be a power law of the sole stellar luminosity (e.g., Kudritzki & Puls. 2000) to give the so-called modified wind momentum-luminosity relation (hereafter WLR)

$$\dot{M} v_\infty \sqrt{R} \propto L^{\frac{1}{\alpha}}. \quad (4)$$

Figure 16 shows the observed relation for Galactic and MC stars. For Galactic stars, the correlation is well defined and is slightly different for luminosity class I stars and LC class III−V stars (as demonstrated by the regression curves). For the MC objects however, the relation seem to be different from that followed by the Galactic objects, at least for the LC V stars. Indeed, our results indicate that the SMC-N81 stars (star symbols if Fig. 16) have modified wind momenta lower by ∼2 orders of magnitudes compared to Galactic objects of the same luminosity and following the LC III−V relation, which simply reflects the weakness of the winds[5]. Bouret et al. (2003) indicate a similar trend. Note that even if the mass loss rates are underestimated by a factor 10 (see Sect. 5.2.2) there is still a significant difference compared to Galactic objects (except in the case of star 3) as shown by the small star symbols in Fig. 16. We have also compared the derived wind momenta with those expected for B and A

[5] To compute the modified wind momenta of the SMC-N81 stars, we have adopted $v_\infty = 2.6\, v_{\rm esc}$ since we have not been able to derive the true terminal velocities due to the weakness of the winds.

supergiants (e.g., Kudritzki et al. 1999): it turns out that the SMC-N81 momenta are weaker. This confirms the extreme weakness of the winds of the SMC-N81 stars.

7.2. Possible origin of the low $\dot{M}$/wind momentum

Several possibilities can be invoked to explain the low wind momenta observed for the SMC-N81 stars: first, there may be a breakdown of the modified wind momentum-luminosity relation at low luminosity for dwarfs; second, metallicity can affect this relation; third, ion runaway may happen in the wind, reducing the mass loss rate. In the following, we investigate these different hypotheses. Finally we will speculate on the possible relation between these "unusual" wind properties and the youth of these stars.

1) *Breakdown of the wind momentum-luminosity relation at low luminosities:*

Let us first consider the case of Galactic stars. The study of Puls et al. (1996) showed that in the luminosity range $5.2 < \log L/L_\odot < 5.5$ several of their stars seemed to indicate a weaker modified wind momentum than expected from the relation followed by higher luminosity stars, indicating a possible break in the slope of the WLR. However, the recent reanalysis of these stars by Repolust et al. (2004) does not show this trend any more if their upper limits are taken as the true values for $\dot{M}$. As their mass loss determinations are based on H_α fitting and as this line becomes insensitive to $\dot{M}$ below $\sim 10^{-8}\ M_\odot\ \mathrm{yr}^{-1}$ (e.g., Herrero et al. 2002), one cannot rule out the possibility of low wind momenta for these low luminosity objects. UV analysis of these stars could certainly shed more light on this question.

Concerning low metallicity objects, few LMC stars have been studied so far, all of them being furthermore of high luminosity. More SMC stars have been studied (including the SMC-N81 objects). For objects with $\log L/L_\odot > 5.5$, the wind momenta are lower than for Galactic stars, but the WLR seems to have the same slope. The low luminosity stars show a clear reduction of the wind momenta which imply a steeper slope of the WLR in this luminosity range. Nonetheless, most of the high L objects are giants or supergiants while low L objects are all dwarfs. As the WLR may be different for different luminosity classes, the existence of a real breakdown is unclear.

Moreover, reasons for such a possible breakdown of the wind momentum-luminosity relation are not known. Is it linked with the driving mechanism? One possibility could be a change of the ions responsible for the radiative acceleration with the consequence of the modification of the efficiency of the driving, but this would be linked to the change of the ionisation in the atmosphere and then more to $T_{\rm eff}$ than to L. Is this breakdown of the wind momentum luminosity relation only due to the low luminosities of the stars? There are in fact other objects, central stars of planetary nebulae, which are much less luminous than any O stars and which seem to follow the mean relation for Galactic objects with $\log \frac{L}{L_\odot} \geq 5.5$ (see Kudritzki & Puls 2000). This renders the behaviour of the low luminosity O stars even more puzzling.

Another possibility is that the current formalism of the radiation theory may be erroneous in the case of massive stars with weak winds. Indeed, Owocki & Puls (1999) have shown that in such winds the curvature of the velocity field near the sonic point could lead to an *inward* directed flux of the diffuse radiation field that can significantly reduce the total radiative acceleration compared to the CAK approach (see their Fig. 7). As a consequence, the mass loss rates are also reduced compared to the predictions based on the CAK formalism for radiative acceleration. For stars with high luminosity and/or low gravity, the density scale height just above the photosphere is higher[6] so that line thermalisation near the sonic point may suppress the above effect (see Owocki & Puls 1999). This may explain why giants/supergiants and dwarfs with high luminosity are not sensitive to the effects of the curved velocity field and show a more classical behaviour. This possibility is attractive since it could explain why only dwarfs with low luminosities seem to have wind properties deviating from the predictions of the CAK theory.

Puls et al. (2000) have made a detailed study of the line statistics and its effect on the radiative driving and have shown that under certain conditions, the parameterisation of the radiative acceleration with the CAK formalism ($g \propto (\frac{\mathrm{d}v}{\mathrm{d}r})^\alpha$) is not valid, and thus the predictions based on this formalism are erroneous. This would happen if both the level density of the ions responsible for the driving were much higher *and* the distribution of the oscillator strengths were much steeper. However, they argue that the atomic physics of the driving ions should not lead to such extreme conditions.

In summary, the above discussion presents evidence that the current predictions of the radiation driven wind theory may fail to explain the winds of low luminosity O dwarfs due to subtle effects negligible in the winds of stars studied so far.

2) *Metallicity effect:*

The wind momentum-luminosity relation may be different at low metallicity. Such a dependence, though quite weak, is in fact predicted by the radiation driven wind theory. The inverse of the luminosity exponent in Eq. (4) (α) is linked to the line strength distribution function. But this function depends on metallicity, α being lower at low Z (e.g., Abbott 1982; Puls et al. 2000). It turns out that the wind momentum-luminosity relation should have a steeper slope at subsolar metallicities. The reduction of the number of lines effectively driving the wind also leads to a global shift of the relation towards lower modified wind momenta. Our results tend to indicate a steeper slope of the WLR, together with the Puls et al. (1996) SMC objects and the Bouret et al. (2003) results. Nonetheless, the real form of the WLR is

$$\dot{M} v_\infty \sqrt{R} \propto (M(1-\Gamma))^{\frac{3}{2}-\frac{1}{\alpha}}\ L^{\frac{1}{\alpha}} \qquad (5)$$

where Γ is the ratio of radiative acceleration to gravitational acceleration. For solar metallicity, $\alpha \sim 2/3$ so that the dependence on the effective mass $M(1-\Gamma)$ vanishes. Values

[6] The density scale height is proportional to $R_\star^2/M(1-\Gamma)$ where $R_\star$ is the stellar radius and Γ the ratio of electron scattering to gravitational acceleration.

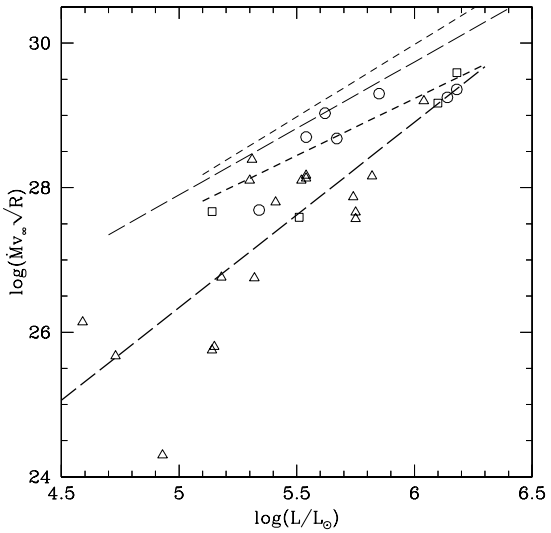

Fig. 17. Modified wind momentum-luminosity relation for SMC stars. Data are from Puls et al. (1996), Bouret et al. (2003), Massey et al. (2004) and the present work. Dwarfs (giants, supergiants) are shown by triangles (squares, circles). The long-dashed (short-dashed) curves are regressions for supergiants (giants/dwarfs) of the Galaxy (light curves, from Repolust et al. 2004) and the SMC (bold curves). SMC giants and dwarfs may indicate a steeper slope of the modified wind momentum-relation at low metallicity, but the scatter is considerable and more studies are needed to confirm this trend.

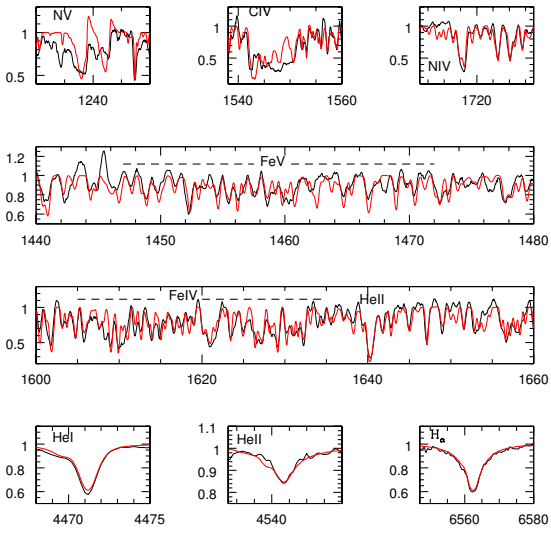

Fig. 18. Fit of the UV and optical spectra of 10 Lac (light curve: observation; bold curve: model). The parameters of the models are: $T_{\rm eff}$ = 36 000 K, $\log g = 4.1$, $\dot{M} = 2\times10^{-9}\ M_\odot\,{\rm yr}^{-1}$ $v_\infty = 1070\,{\rm km\,s}^{-1}$. A turbulent velocity increasing from 5 km s^{-1} near the photosphere to 100 km s^{-1} in the outer wind has been adopted. Abundances are from Herrero et al. (2002) for He, Villamariz et al. (2002) for CNO and have been set to the solar value (Grevesse & Sauval 1998) for the other metals. A rotational velocity of 40 km s^{-1} has been adopted.

of $\alpha < 2/3$ bring back this dependence, which should lead to a large scatter of the WLR for low Z objects and then to a more difficult calibration of this relation. Figure 17 shows the modified wind momentum-luminosity relation for the SMC stars studied so far: the scatter is indeed significant. Indicative regression curves are given and reveal a possibly steeper slope ($\alpha \sim 0.4$) for giants/dwarfs while for the supergiants α may be close to 2/3. More studies are needed to confirm this trend of a steeper slope at lower metallicities.

However, two points may impede this explanation. First, the most recent hydrodynamical simulations do not show any change of the slope of the WLR at metallicities typical of the Magellanic Clouds (Vink et al. 2001; Hoffmann et al. 2002). Furthermore, Kudritzki (2002) has shown that only for extremely low metal content – $10^{-3}\ Z_\odot$ – a difference appears, although his calculations were made at high luminosities ($\log L/L_\odot > 6$) where most of the driving is thought to be done by H and He lines, leading to a weaker metallicity dependence of the wind properties. Second, some Galactic stars are known to display signatures of weaker than normal winds (Walborn et al. 1995) but none has been analysed quantitatively so far.

We have carried out a detailed study of the wind properties of one of them: 10 Lac. This O9V star has often been considered as a standard dwarf star for its stellar properties. We have run models to fit its IUE and optical spectra taking the the stellar parameters from Herrero et al. (2002)[7] and the CNO abundances from Villamariz et al. (2002). A microturbulent velocity increasing from 5 km s^{-1} near the photosphere up to 100 km s^{-1} in the outer atmosphere was used. Figure 18 shows the results of our best fit model for which $\dot{M} = 2\times10^{-9}\ M_\odot\,{\rm yr}^{-1}$ and $v_\infty = 1070\,{\rm km\,s}^{-1}$. This value of $\dot{M}$ is lower than estimates of Howarth & Prinja (1989, $10^{-6.7}\ M_\odot\,{\rm yr}^{-1}$ based on line profile fitting with a Sobolev code), of Leitherer (1988, $10^{-6.83}\ M_\odot\,{\rm yr}^{-1}$ based on H_α) and lower than the prediction of Vink et al. (2001) – $10^{-6.2}\ M_\odot\,{\rm yr}^{-1}$ – but it is in agreement with the more recent upper limit of Herrero et al. (2002) based on H_α fits ($10^{-8}\ M_\odot\,{\rm yr}^{-1}$). The important point is that the wind momentum of this star is as low as that of the SMC-N81 stars (see Fig. 16). The metal content of 10 Lac being near solar (10 Lac belongs to the nearby association Lac OB1, and its CNO abundances being between 0.5 and 0.9 the solar values – see Villamariz et al. 2002), this indicates that metallicity is not uniquely responsible for the weakness of the winds observed in the present work.

The above discussion shows that our understanding of the metallicity effects on the wind properties of massive stars is still partial and that both observational and theoretical efforts are needed to improve this situation.

3) *Decoupling:*
Finally, an alternative answer to the puzzling wind properties of the low luminosity O stars is that a decoupling between the absorbing ions and the passive plasma may occur. In classical radiatively driven winds, ions from metals gain momentum

[7] $T_{\rm eff}$ = 36 000 K, $\log g = 3.95$, and the He abundance $\epsilon = 0.09$.

from the photons they absorb and redistribute this momentum to the passive plasma through friction. However, if the density in low enough, friction may become inefficient so that the absorbing ions are the only species to be accelerated. Due to their low abundances compared to H and He (constituting most of the passive plasma), the mass loss is greatly reduced.

Various studies have been pursued to determine the conditions under which such decoupling may take place (e.g., Babel 1995, 1996; Krtička & Kubát 2000). Springmann & Pauldrach (1992) have estimated that decoupling occurs when radiative acceleration is not compensated by frictional braking. We have applied their Eq. (15) to the case of our SMC-N81 stars and we found that decoupling is expected to happen only in the outer region of the wind where the outflow velocity has almost reached the terminal velocity. In the transsonic region, where the mass loss rate is set, decoupling is not predicted to take place. More recently, Owocki & Puls (2000) gave an estimate of the wind velocity at which maximal coupling occurs as a function of stellar and wind parameters. If this velocity is greater than the terminal velocity, then the wind can be described by a single component fluid. In the SMC-N81 stars, this maximal drift is predicted to happen at velocities of the order v_∞ so that decoupling is not expected to happen. Even more recently, Krtička et al. (2003) have estimated the metallicity below which decoupling should occur due to the reduced wind density for a given set of stellar parameters. In the case of the SMC-N81 stars, this limit is of the order $1/100\ Z_\odot$ which is well below the metallicity of the SMC. As a consequence, it seems that decoupling cannot explain the weakness of the winds.

After these considerations the most likely explanation for the weak winds of the analysed stars is therefore that a breakdown of the modified wind momentum-luminosity relation exists at low luminosity for dwarfs (1), possibly independently of metallicity. A possible mechanism responsible for such a behaviour may exist (cf. above) although no realistic calculations have been done for parameters appropriate to the objects considered here. In any case, it is not clear what parameter(s) would determine that some O dwarf stars have such weak winds in comparison to other O stars of similar luminosity. Possible relevant parameters could be a higher gravity, higher mass/light ratio, or others (such as the presence of magnetic fields). From the current limited sample of objects showing such puzzling wind properties we speculate that the low mass loss rate is probably intrinsically related to the youth of the stars. It is conceivable that we are beginning to witness the "onset" of radiatively driven winds in young, still somewhat underluminous O stars shortly after their formation. Further systematic studies of Vz stars and related objects with indications of weak winds will be necessary to resolve these issues.

8. Conclusion

Based on UV spectra obtained with STIS/HST we have analysed the stellar and wind properties of the four main exciting stars of the High Excitation Blob SMC-N81 using extensive calculations of spherically expanding non-LTE line blanketed atmosphere models with the code CMFGEN.

The main results are the following:

- The stellar properties (L, $T_{\rm eff}$) indicate that the SMC-N81 components are young (~0–4 Myrs old) O stars which show, with perhaps the exception of star 1, a lower luminosity than "normal" Galactic O dwarfs. This, together with the closeness to the ZAMS for star 3 and 11, confirms the conclusion of Paper I that they may belong to the Vz class (Walborn & Parker 1992).
- The UV spectra of the N81 stars show unusually weak stellar winds. The upper limits on mass loss rates are of the order a few $10^{-9}\ M_\odot\ {\rm yr}^{-1}$ which is low compared to 1) Galactic stars of the same luminosity and 2) the most recent predictions of $\dot{M}$ as a function of stellar parameters and metallicity. Point 1) could be qualitatively understood due to the reduced metallicity of the SMC but point 2) indicates that this reduction is higher than expected.
  Although the mass loss rates derived from the UV line analysis are potentially affected by uncertainties in the modeled ionisation fractions, various tests indicate that the above conclusions remain qualitatively valid.
- Our objects show modified wind momenta ($M_\odot v_\infty R^{1/2}$) which are, for the same luminosity L, lower by typically two orders of magnitude compared to the "normal" O star samples. Similarly low wind momenta have also been found by Bouret et al. (2003) for 3 SMC stars in NGC 346. The modified wind momentum-luminosity relation of all the SMC objects could be interpreted as showing a breakdown at low luminosities or a different slope than the Galactic relation. The current sample of SMC stars may indeed indicate a steeper slope at least for giants and dwarfs, but the scatter is still too large to firmly establish this trend. However, the most recent hydrodynamical models (Vink et al. 2001; Kudritzki 2002; Hoffmann et al. 2002) do not predict such a change in the slope between solar and SMC metallicities. Furthermore we present the first indications that some Galactic objects also have low wind momenta, comparable to the SMC dwarfs. This also tends to exclude explanations based uniquely on metallicity.
- Possible explanations for a breakdown of the modified wind momentum-luminosity relation at low luminosities are discussed. Ionic decoupling appears unlikely according to various estimates. A failure of the CAK parameterisation in high density atmospheres, discussed by Owocki & Puls (1999), might be invoked to explain a lower acceleration in the transsonic region where the mass loss rate is set.
  Although the physical mechanism leading to such weak winds remains currently unknown, we speculate that the low mass loss rate is probably intrinsically related to the youth of the stars, possibly testifying to a phase of the "onset" of radiatively driven winds in young O stars shortly after their formation.

Further studies of very young massive stars, Vz stars, and related objects with indications of weak winds will be of great interest to attempt to understand these puzzling wind properties and to provide interesting constraints on the development of stellar winds in the early phases of massive star evolution or possibly even on the final phases of their birth.

Acknowledgements. We thank Jean-Claude Bouret, Luc Dessart, Claus Leitherer, André Maeder, Georges Meynet and Stan Owocki for useful discussions. We also thank Artemio Herrero and Gerard Testor who kindly provided respectively the optical spectra of 10 Lac and the integrated optical spectra of SMC-N81 corrected for nebular contamination. Artemio Herrero is also acknowledged for his constructive comments as the referee of the paper. The present results rely heavily on generous allocation of computing time from the CALMIP and IDRIS centers. F.M., D.S., and M.H.-M. thank the French "Programme National de Physique Stellaire" (PNPS) for support. Part of this work was also supported by the French "Centre National de Recherche Scientifique" (CNRS) and by the Swiss National Fund.

References

Abbott, D. C. 1982, ApJ, 259, 282
Allen, C. W. 1976, Astrophysical Quantities (London: Athlone)
Abbott, D. C., & Hummer, D. G. 1985, ApJ, 294, 286
Asplund, M. 2003, in CNO in the Universe, ed. C. Charbonnel, D. Schaerer, & G. Meynet, ASP Conf. Ser., 304, 279
Babel, J. 1995, A&A, 301, 823
Babel, J. 1996, A&A, 309, 867
Behrend, R., & Maeder, A. 2001, A&A, 373, 190
Bjorkmann, J. E., & Cassinelli, J. P. 1993, ApJ, 409, 429
Bonnell, I. A., Bate, M. R., & Zinnecker, H. 1998, MNRAS, 298, 93
Bouret, J. C., Lanz, T., Hillier, D. J., et al. 2003, ApJ, in press [arXiv:astro-ph 0301454]
Chiosi, C., & Maeder, A. 1986, ARA&A, 24, 329
Crowther, P. A., Hillier, D. J., Evans, C. J., et al. 2002, ApJ, 579, 774
de Koter, A., Heap, S. R., & Hubeny, I. 1998, ApJ, 509, 879
di Benedetto, G. P. 1997, ApJ, 486, 60
Drew, J. E. 1985, MNRAS, 217, 867
Dyson, J. E. 1978, A&A, 62, 269
Fanelli, M. N., O'Connell, R. W., Burstein, D., & Wu, C. 1992, ApJS, 82, 197
Feldmeier, A., Kudritzki, R. P., Palsa, R., Pauldrach, A. W. A., & Puls, J. 1997, A&A, 320, 899
Figer, D. F., Najarro, F., Gilmore, D., et al. 2002, ApJ, 581, 258
Fitzpatrick, E. L., & Savage, B. D. 1983, ApJ, 267, 93
Grevesse, N., & Sauval, A. 1998, Space Sci. Rev., 85, 161
Heap, S. R. 2003, in CNO in the Universe, ed. C. Charbonnel, D. Schaerer, & G. Meynet, ASP Conf. Ser., 304, 41
Herrero, A., Puls, J., & Villamariz, M. R. 2000, A&A, 354, 193
Herrero, A., Puls, J., & Najarro, F. 2002, A&A, 396, 949
Heydari-Malayeri, M., & Testor, G. 1982, A&A, 111, L11
Heydari-Malayeri, M., Le Bertre, T., & Magain, P. 1988, A&A, 195, 230
Heydari-Malayeri, M., Rosa, M. R., Zinnecker, H., Deharveng, L., & Charmandis, V. 1999, A&A, 344, 848
Heydari-Malayeri, M., Rosa, M. R., Schaerer, D., Martins, F., & Charmandis, V. 2002a, A&A, 381, 951 (Paper I)
Heydari-Malayeri, M., Charmandis, V., Deharveng, L., et al. 2002b, in A massive star odyssey: from main sequence to supernova, ed. K. A. van der Hucht, A. Herrero, & C. Esteban, IAU Symp., 212, 553
Hill, V. 1999, A&A, 345, 430
Hillier, D. J., & Miller, D. L. 1998, ApJ, 496, 407
Hillier, D. J., Lanz, T., Heap, S. R., et al. 2003, ApJ, 588, 1039
Hoffmann, T. L., Pauldrach, A. W. A., & Puls, J. 2002, in A massive star odyssey: from main sequence to supernova, ed. K. A. van der Hucht, A. Herrero, & C. Esteban, IAU Symp., 212, 206
Howarth, I. D., & Prinja, R. K. 1989, ApJS, 69, 527
Hubeny, I., & Lanz, T. 1995, ApJ, 439, 875
Krtička, J., & Kubát, J. 2000, A&A, 359, 983
Krtička, J., Owocki, S. P., Kubát, J., Galloway, R. K., & Brown, J. C. 2003, A&A, 402, 713
Kudritzki, R. P., Puls, J., Lennon, D. J., et al. 1999, A&A, 350, 970
Kudritzki, R. P., & Puls, J. 2000, ARA&A, 38, 613
Kudritzki, R. P. 2002, ApJ, 577, 389
Lamers, H. J. G. L. M., Cerruti-Sola, M., & Perinotto, M. 1987, ApJ, 314, 726
Lamers, H. J. G. L. M., Haser, S., de Koter, A., & Leitherer, C. 1999, ApJ, 516, 872
Lamers, H. J. G. L. M., & Cassinelli, J. P. 1999, Introduction to stellar winds (Cambridge University Press)
Leitherer, C. 1988, ApJ, 533, 626
Lejeune, T., & Schaerer, D. 2001, A&A, 366, 538
Mallouris, C., Welty, D. E., York, D. G., et al. 2001, ApJ, 558, 133
Maeder, A., & Meynet, G. 2000, ARA&A, 38, 143
Martins, F., Schaerer, D., & Heydari-Malayeri, M. 2002a, in A massive star odyssey: from main sequence to supernova, ed. K. A. van der Hucht, A. Herrero, & C. Esteban, IAU Symp., 212, 564
Martins, F., Schaerer, D., & Hillier, D. J. 2002b, A&A, 382, 999
Massey, P., Bresolin, F., Kudritzki, R. P., Puls, J., & Pauldrach, A. W. A. 2004, ApJ, in press
Meynet, G., & Maeder, A. 1997, A&A, 321, 465
Najarro, F., Krabbe, A., Genzel, R., et al. 1997, A&A, 325, 700
Norberg, P., & Maeder, A. 2000, A&A, 359, 1025
Owocki, S. P., Castor, J. I., & Rybicki, G. B. 1988, ApJ, 335, 914
Owocki, S. P., & Puls, J. 1999, ApJ, 510, 355
Owocki, S. P., & Puls, J. 2000, ApJ, 568, 965
Pauldrach, A. W. A., Kudritzki, R. P., Puls, J., Butler, K., & Husinger, J. 1994, A&A, 283, 525
Pauldrach, A. W. A., Hoffmann, T. L., & Lennon, M. 2001, A&A, 375, 161
Prévot, M. L., Lequeux, J., Maurice, E., Prévot, L., & Rocca-Volmerange, B. 1984, A&A, 132, 389
Puls, J., Kudritzki, R. P., Herrero, A., et al. 1996, A&A, 305, 171
Puls, J., Springmann, U., & Lennon, M. 2000, A&AS, 141, 23
Repolust, T., Puls, J., & Herrero, A. 2004, A&A, 415, 349
Santolaya-Rey, A. E., Puls, J., & Herrero, A. 1997, A&A, 323, 488
Schaerer, D., de Koter, A., Schmutz, W., & Maeder, A. 1996, A&A, 312, 475
Sembach, K. R., & Savage, B. D. 1992, ApJS, 83, 147
Smith-Neubig, M., & Bruhweiler, F. 1997, AJ, 114, 1951
Springmann, U. W. E., & Pauldrach, A. W. A. 1992, A&A, 262, 515
Vacca, W. D., Garmany, C. D., & Shull, J. M. 1996, ApJ, 460, 914
Venn, K. A. 1999, ApJ, 518, 405
Vermeij, R., & van der Hulst, J. M. 2002, A&A, 391, 1081
Villamariz, M. R., Herrero, A., Becker, S. R., & Butler, K. 2002, A&A, 388, 940
Vink, J., de Koter, A., & Lamers, H. J. G. L. M. 2000, A&A, 362, 295
Vink, J., de Koter, A., & Lamers, H. J. G. L. M. 2001, A&A, 369, 574
Walborn, N., & Parker, J. 1992, ApJ, 399, L87
Walborn, N., Nichols-Bohlin, J., & Panek, R. J. 1995, IUE Atlas of O-Type stellar spectra

Online Material

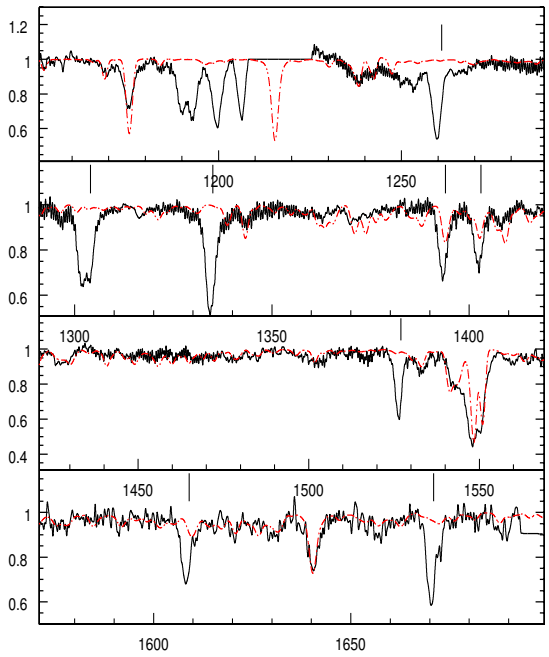

Fig. A.1. Best fit model for star 1. The model parameters are: $T_{\rm eff}$ = 38 500 K, $\dot{M}$ = $10^{-8.5}$ $M_\odot\,{\rm yr}^{-1}$, v_∞ = 1500 km s^{-1}, $V \sin i$ = 200 km s^{-1}, f = 0.01. The abundances are the following: n(He) = 0.1 n(H), C/C$_\odot$ = 1/10, N/N$_\odot$ = 1/20, O/O$_\odot$ = 1/5, and Si, S and Fe abundances are 1/8 the solar values. Solid line: observations; dot-dashed line: model. The vertical lines indicate the main interstellar lines.

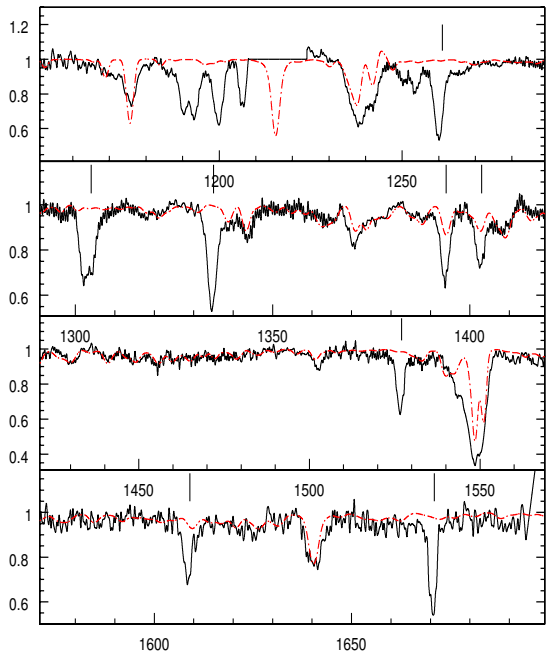

Fig. A.2. Best fit model for star 2. The model parameters are: $T_{\rm eff}$ = 40 000 K, $\dot{M}$ = $10^{-8.5}$ $M_\odot\,{\rm yr}^{-1}$, v_∞ = 1800 km s^{-1}, $V \sin i$ = 300 km s^{-1}, f = 0.01. The abundances are the following: n(He) = 0.1 n(H), and C, N, O, Si, S and Fe abundances are 1/8 the solar values. Solid line: observations; dot-dashed line: model. The vertical lines indicate the main interstellar lines. The poor fits of the C IV $\lambda\lambda$1548,1551 and N V λ1238,1242 lines comes from the difficulty to have important absorption without emission.

Appendix A: Best fits

Figures A.1– A.4 give the best fits achieved for star 1, 2, 11 and 3 respectively. For each figure, the model parameters are given and the main interstellar lines are indicated. The interstellar CIV absorption has been added to the synthetic spectra as described in Sect. 4. Even with this correction, the fit of the C IV $\lambda\lambda$1548,1551 line remains poor for star 2, showing the difficulty to produce significant absorption without emission. The normalisation of the observed spectra below 1200 Å is very uncertain so that any comparison with models in this wavelength range is irrelevant.

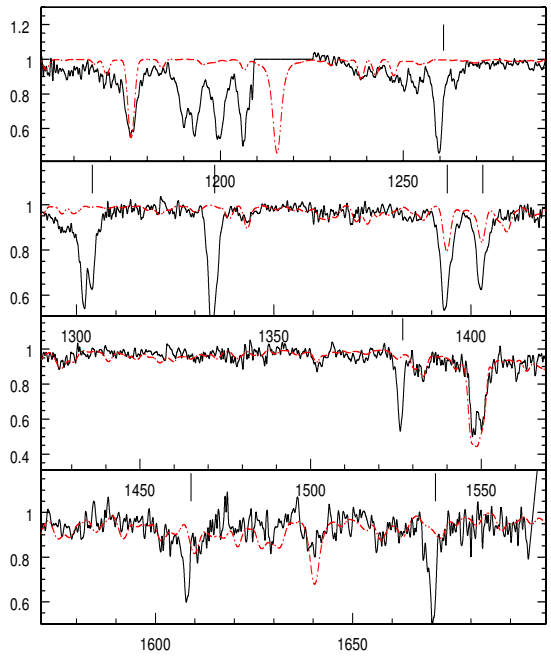

Fig. A.3. Best fit model for star 3. The model parameters are: $T_{\rm eff}$ = 36 000 K, $\dot{M}$ = $10^{-8.5}$ $M_\odot\,{\rm yr}^{-1}$, v_∞ = 300 km s^{-1}, $V \sin i$ = 250 km s^{-1}. The abundances are the following: n(He) = 0.1 n(H), C/C$_\odot$ = 1/10, N/N$_\odot$ = 1/20, O/O$_\odot$ = 1/5, and Si, S and Fe abundances are 1/8 the solar values. Solid line: observations; dot-dashed line: model. The vertical lines indicate the main interstellar lines.

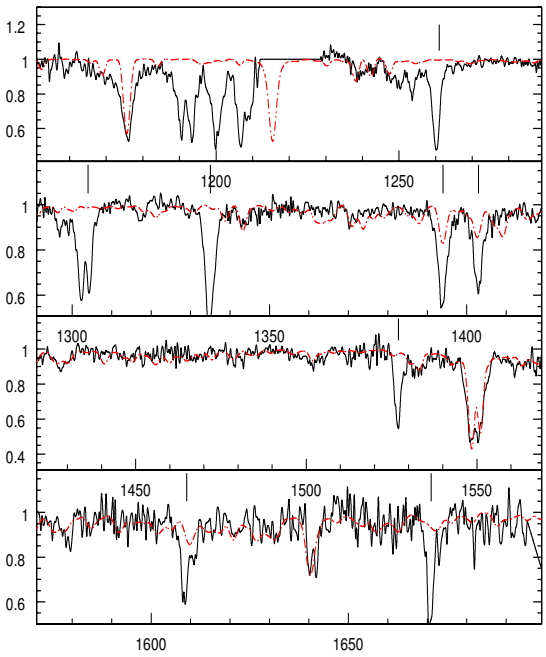

Fig. A.4. Best fit model for star 11. The model parameters are: $T_{\rm eff}$ = 37 000 K, $\dot{M}$ = $10^{-9.5}$ $M_\odot\,{\rm yr}^{-1}$, v_∞ = 600 km s^{-1}, $V \sin i$ = 250 km s^{-1}. The abundances are the following: n(He) = 0.1 n(H), C/C$_\odot$ = 1/10, N/N$_\odot$ = 1/20, O/O$_\odot$ = 1/5, and Si, S and Fe abundances are 1/8 the solar values. Solid line: observations; dot-dashed line: model. The vertical lines indicate the main interstellar lines.

7.2 Possible explanations for the weakness of the winds of the SMC-N81 stars

In this section, we want to go back in more detail to several possible explanations to the puzzling weakness of the winds observed in the SMC-N81 stars.

7.2.1 Radiative acceleration in hydrodynamical simulations

In this section, we go back to the various possibilities invoked in the above paper (Martins et al., 2004) to explain the weakness of the winds observed in the SMC-N81 stars. We first have a look at the possible failure of the hydrodynamical simulations currently predicting the wind properties of massive star winds.

Diffuse radiation field

We have mentioned in the above paper (Martins et al., 2004) that the diffuse radiation field near the sonic point could strongly modify the radiative transfer and thus change the value of the mass loss rate which is set in this region. This has been shown by Owocki & Puls (1999). The basic idea is the following: in the classical hydrodynamical simulations, the curvature of the velocity field is assumed to be negligible. This is not strictly correct and the existing gradients in the velocity field create an inward directed radiative acceleration due to diffuse radiation field which in turn modify the radiative acceleration. The global effect is a reduction of the mass loss rate.

To understand more clearly this effect, let us first go back to the classical approximation of the hydrodynamical simulations. In a massive star atmosphere, the velocity gradients are usually high (the velocity increases from a few km s^{-1} to a few thousands km s^{-1} over $\sim$ 100 stellar radii). This property can be used to simplify the various equations, especially the radiative transfer equation. In simple term, we have already seen that due to these velocity gradients, a photon emitted with a given frequency at a given point can be absorbed far from its emission point by a line of lower frequency because of the Doppler shifts experienced in the accelerating atmosphere. The interaction region of this photon with the "new" line is extended, which means that resolving the transfer is a global problem. However in practice the size of the interaction region is finite: due to the high velocity gradients, the wavelength range in which the photon can interact with the line (i.e. the width of the line) is covered within a short fly of the photon: the velocity gradient is so high that a small displacement of the photon corresponds to a huge wavelength shift which makes the

photons go out of the width of the line. This boils down to say that the interaction region is very small, and is even a point if we push the approximation at maximum. This last case is called the Sobolev approximation and was first introduced by Sobolev (1960). This approximation greatly simplifies the radiative transfer equation, rendering the problem local while it is initially a global problem. Let us show how this approximation is used for the derivation of the optical depth in the atmosphere. The definition of the optical depth is

$$\tau_\nu(z) = \int_z^\infty \kappa_\nu \rho(z) dz \tag{7.1}$$

where κ_ν is the absorption coefficient and ρ the density.

This expression can be developed as follows:

$$\tau_\nu(z) = \frac{\pi e^2}{m_e c} f_l \int_z^\infty n_l(z) \left\{ 1 - \frac{n_u}{n_l} \frac{g_l}{g_u} \right\} \Phi(\Delta\nu) dz \tag{7.2}$$

where the symbols have their usual meanings and Φ is the line profile. The Doppler shift is expressed by

$$\Delta\nu(z) = \nu \left\{ 1 - \frac{v}{c} \right\} - \nu_0 \tag{7.3}$$

This allows to rewrite Eq. 7.2

$$\tau_\nu(z) = \frac{\pi e^2}{m_e c} f_l \int_{\Delta_\nu(z)}^{\Delta_\nu(z=\infty)} n_l(z) \left\{ 1 - \frac{n_u}{n_l} \frac{g_l}{g_u} \right\} \Phi(\Delta\nu) \frac{dz}{d(\Delta_\nu)} d(\Delta_\nu) \tag{7.4}$$

If we now make the approximation that the interaction region is very small, and even reduced to one point (which boils down to say that the interacting line has an infinitely small width) this expression simplifies and gives

$$\tau_\nu(z) = \frac{\pi e^2}{m_e c} f_l n_l(r) \left\{ 1 - \frac{n_u}{n_l \frac{g_l}{g_u}} \right\}_r \left(\frac{dz}{d(\Delta_\nu)} \right)_r \tag{7.5}$$

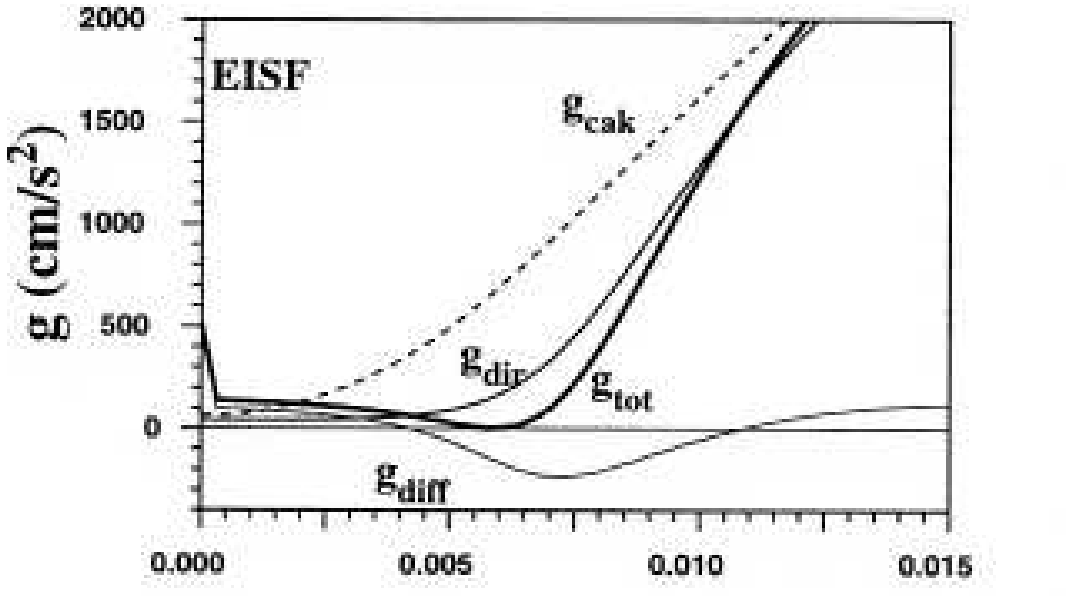

Figure 7.1: Radiative acceleration computed with different methods as a function of height ($= \frac{r}{R_\star} - 1$) in the atmosphere. g_{cak} is the radiative acceleration computed with the standard CAK formalism. The other lines give the total (g_{tot}), direct (g_{dir}) and diffuse (g_{diff}) radiative acceleration computed with the escape integral source function method of Owocki & Puls (1999). The acceleration due to the diffuse radiation field is negative in the transsonic region, which reduces the total acceleration compared to the CAK acceleration. From Owocki & Puls (1999).

where r is the position of the interaction region.

This expression of the Sobolev optical depth is then further used for the computation of the radiative acceleration (see lamers & Cassinelli 1999 for a detailed description). At present, this is how the radiative acceleration (see Eq. 5.9) is computed in most of the hydrodynamical simulations.

However, as we have mentioned in the introduction to this section, this description of the radiative acceleration may be erroneous in some cases. The reason is that the velocity field has important gradients on short length scales, so that the gradient just below the interacting point may be different from the velocity gradient just above the interacting point. This means that a photon interacting with the line will not have the same probability to escape outward or inward, whereas the Sobolev approximation implies the equality of these probabilities. How does this pattern translates in terms of radiation field. Owocki & Puls (1999) have given a simple description of what happens: the diffuse radiation field depends on the balance between the source and loss of radiation within the resonance line. The source depends on the amount of continuum radiation intercepted by the line and is thus directly proportional to the velocity gradient just below the

interaction region. The loss of radiation on the other hand depends on both the velocity gradient below and above the interaction region (through the escape probabilities). In the atmosphere near the transition region between photosphere and wind, the velocity gradient increases, so that the source of radiation is reduced compared to the loss. It results that the diffuse radiation field increases with velocity. The acceleration being directly proportional to the intensity of the radiation field, this means that an ion will feel a stronger acceleration from the layer above it than the acceleration from the layer below it: the resulting total acceleration on this ion is then *inward* directed. This reduces the global acceleration (due to the diffuse field + acceleration due to the direct radiation coming from the star) in the transsonic region and then leads to a lower mass loss rate. This qualitative picture is confirmed by the computations of Owocki & Puls (1999) and shows that the use of the Sobolev approximation may lead to overestimates of the total radiative acceleration. Fig. 7.1 shows the result of such calculations in which we clearly see the negative acceleration due to the diffuse radiation field leading to a global acceleration lower than in the Sobolev (noted cak) case.

Is this diffuse radiative field always so important? In fact, previous tests of the validity of the Sobolev approximation used in the CAK formalism were made by Pauldrach et al. (1986) and did not reveal such discrepancies. Owocki & Puls (1999) have argued that the more exact treatment of radiative transfer in the simulations of Pauldrach et al. (1986) may explain the differences. Indeed, the latter included the coupling of lines with a continuum radiation and took into account the possibility for lines to thermalise at great depth, which is not the case of the Owocki & Puls (1999) simulations. In that case, the diffuse radiation field disappears or at least becomes negligible, so that the global acceleration resembles that of the Sobolev approach. However, if the density in the wind is low enough, the effect of the diffuse radiation field may become important. Practically, to what type of stars do we refer when we say "low density winds"? The density near the sonic point is given by the pseudo-hydrostatic approximation:

$$\rho(r) = \rho_0 e^{-\frac{r-r_0}{H_0}\frac{r_0}{r}} \tag{7.6}$$

with the density scale height H_0

$$H_0 \propto \frac{1}{g_0} = \frac{r_0^2}{GM(1-\Gamma)} \tag{7.7}$$

r_0 is the radius at the base of the photosphere and g_0 the gravity at this point. Hence the density will be lower for higher gravity stars, or for stars with the same gravity for lower luminosity stars (since lower L implies lower Γ). This is in particular the case of O dwarfs with low luminosities.

Hence, from the above discussion, it seems that a possible explanation to the puzzle of the weak winds of the SMC-N81 stars may come from the overestimation of the mass loss rates in present hydrodynamical simulations using the Sobolev approximation. However, the reduction of $\dot{M}$ predicted by Owocki & Puls (1999) [1] if the diffuse radiation field is correctly taken into account are only of a factor 1.46 whereas we find reduction by more than a factor 10. More sophisticated hydrodynamical simulations should help to better quantify the exact effect of the diffuse radiation field.

Radiative acceleration and line strength distribution

In the previous section we have seen that the current formalism used to compute the radiative acceleration in radiatively driven winds may miss the important contribution of the diffuse radiation field. Here, we focus on another possible weakness of the CAK approach: the parameterisation of the radiative acceleration. Indeed, in this approach, the basic assumption is that the radiative acceleration can be expressed as a power law of the optical depth parameter t, the exponent being related to the *local* slope of the line strength distribution function. More precisely, this means that the exponent α entering the expression of the radiative acceleration (g $\propto t^{-\alpha}$) is related to the slope of the line strength distribution function *at the point where the line strength is equal to* $k_1 = t^{-1}$. But what happens if it is no more the case?

As we have shown in Sect. 5, the radiative acceleration due to lines is directly proportional to $t^{-\alpha}$ where α is linked with the slope of the line strength distribution function ($\alpha - 2$). However, in this derivation, we have *assumed* that this line strength distribution function was indeed a power law with exponent α -2. Let us now examine the more general case of an unknown line strength distribution function. Such a function is represented in Fig. 7.2 and a differential form of this function is

$$dN(\nu, k_L) = -f(k_L, \nu) d\nu dk_L \tag{7.8}$$

Following Puls, Springmann & Lennon (2000) we now define k_- and k_+ such as $N(k_L)$ is roughly a power law with slope $\alpha - 1$ in between (and N_- and N_+ the corresponding N values), we have

[1] the model parameters for their computations are $\log \frac{L}{L_\odot} = 5.84, R = 19 R_\odot$ and $M = 40 M_\odot$

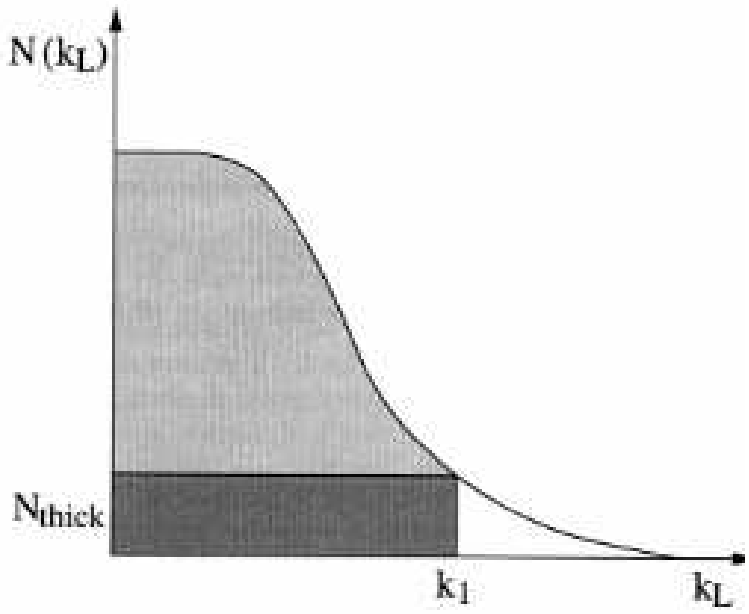

Figure 7.2: Cumulative line number as a function of line strength in a general case. The contribution of optically thick lines ($k_L > k_1$) is shown by the dark area and the contribution of optically thin lines ($k_L < k_1$) by the gray area.

$$\begin{aligned} N(k_L) &= N_+ k_+^{1-\alpha} k_L^{\alpha-1} \qquad \text{for} \qquad \mathrm{k_- < k_L < k_+} \\ \alpha &= 1 + \frac{\log(N_+/N_-)}{log(k_+/k_-)} \end{aligned} \tag{7.9}$$

Using this expression together with Eq. 5.13, and making once again the separation between optically thin and thick lines, one easily finds

$$g_{rad}^{tot} = \left\{ \bar{N}_{\{0,k_-\}} - \frac{N_+}{\alpha} \left(\frac{k_+}{k_-} \right)^{1-\alpha} \right\} k_- + \left(\frac{N_+ k_+^{1-\alpha}}{\alpha} \right) k_1^{\alpha} \tag{7.10}$$

where

$$N_{\{0,k_-\}} = \int_0^{k_-} N(k_L) dk_L \tag{7.11}$$

Form this, it is easy to see that the total radiative acceleration is proportional to $t^{-\alpha}$ (recall that $t = k_1^{-1}$) if the first term in Eq. 7.10 is negligible

compared to the second one. In that case, the α parameter is directly related to the slope of the line strength distribution function (see Eq. 7.9).

Puls, Springmann & Lennon (2000) have shown that it is usually the case as long as $\alpha > 0$ (condition for which the first term of Eq. 7.10 is greater than the second one) or equivalently when the line strength distribution function is not too steep. If on the other hand this slope is too steep, the radiative acceleration can no longer be parameterised by $g_{rad} \propto t^{-\alpha}$. Under which conditions do we have such a case?

Again, the answer was given by Puls, Springmann & Lennon (2000) in their very detailed study of the line statistics. They have shown that the slope of the line strength distribution function of an ensemble of lines of different elements is rather constant for a large range of t, but then increases when we go to the lower values of the t parameter (or equivalently large k_1, see also Fig. 7.3). In practise, this corresponds to low densities in the atmosphere (since t is directly proportional to the density, see Eq. 5.7). But the "low t" part of the line distribution function (where the slope is steeper) is governed by two factors:

- the slope of the *oscillator strength* distribution function (different from the *line strength* distribution function function, see Puls, Springmann & Lennon (2000) for the definition of each quantities).
- the excitation of the ions (or equivalently the population of high energy levels).

Hence, the break down of the classical parameterisation happens when both the oscillator strength distribution function is much steeper and the density of excited levels is much higher (see the complex determination in Puls, Springmann & Lennon (2000)). In simple terms, this means that we need to have at the same time much more transitions with high oscillator strengths and much more levels with high excitation energy. Note that the recent calculations of Kudritzki (2002) take into account the "non linear" shape of the line strength distribution function and in particular the fact that α may be different at different depth due to this curvature. Indeed, in the above derivation, α is the local slope of the line strength distribution function, i.e. the slope around $k_L = k_1$. But if we move through the atmosphere, k_1 changes. As the line strength distribution function is not strictly linear in the log-log plane (see Fig. 7.3) the local slope varies according to the position in the atmosphere. The computations of Pauldrach et al. (1986) and Kudritzki (2002) take this effect into account. However, the radiative accelerations are still computed under the assumption that $g_{rad}^{tot} \propto t^{-\alpha}$, even if the slope of the line strength distribution function is steep. The inclusion of the depth variation of α are certainly an improvement, but if the conditions mentioned above are gathered, the parameterisation of the radiative acceleration with $t^{-\alpha}$ (even if α is not constant) may become invalid.

Nonetheless, our current knowledge of the line statistics of elements do not point to such a situation. Practically, this means that the classical parameterisation $g_{rad}^{tot} \propto t^{-\alpha}$ seems to be valid.

7.2.2 Metallicity effects

The effects of a lower metallicity on the wind properties of massive stars have been discussed in Sect. 7. Here, we just want to give more detail on the derivation of the expected behaviour at low metallicity.

As already mentioned several times, the reduction of the metal content will reduce the total radiative acceleration due to line absorption since metals are the main drivers. This will then modify the wind strength, with the consequence of a reduction of the mass loss rate and terminal velocity. Part of the quantitative explanation of this behaviour have been given in Sect. 5. There are mainly two effects highlighted very precisely by Puls, Springmann & Lennon (2000):

- direct effect: the change of the metal content modifies the populations of the energy levels, which in turn modifies the dimensionless line strength (k_L). As demonstrated by Eqs. 5.10 and 5.11 this boils down to a change of the normalisation constant N_0 and then of the mass loss rate according to Eq. 5.47.

- indirect effect: this effect is more subtle than the previous one and is more complex to disentangle. It is rooted in the behaviour of the line strength distribution function which can be separated in two parts: the strong line strength part of the distribution is dominated by the contribution of light ions (mainly H and He), while the low line strength part depends essentially on the Iron group elements. It is the contribution of the former elements which governs the decline of the distribution at large line strength mentioned in the previous section. Changing the metallicity leads to a change of the abscissa scale of this distribution (the line strength being modified according to $k_L(z) = zk_L(z_\odot)$, see Fig. 7.3. This is the first point. Now, the α parameter entering the radiative acceleration calculation is equal to the α parameter of the slope of the line strength distribution *at the point where* $k_L = k_1$. Since the line strength distribution function is shifted because of the change of the abscissa scale, at this point, the local slope is different if the metallicity is changed. In practice, lowering Z shifts the distribution towards the left, and the slope increases, so that α decreases (k_1 being situated closer to the light element dominated part of the distribution). On the contrary, if Z is increased, the distribution is shifted towrds the right and the slope does not change too much (as k_1 gets closer to the Iron group dominated part of the distribution). This

general behaviour is clearly seen in Fig. 7.3.

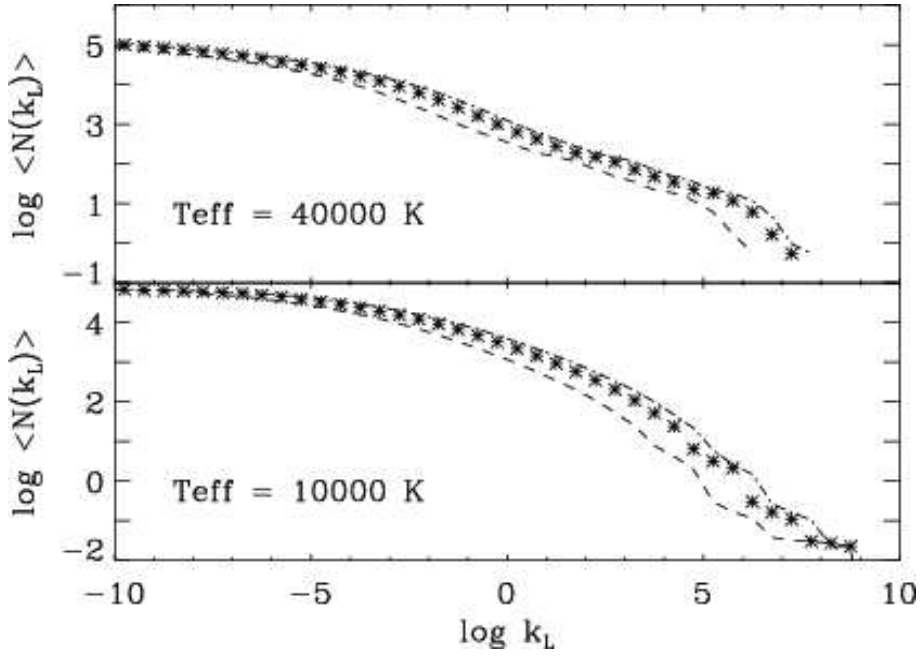

Figure 7.3: Effect of metallicity on the line strength distribution function. The asterisk symbols show the line strength distribution function at solar metallicity, while the dashed (dot-dashed) line is for Z = 0.1 (3.0) $Z_\odot$. Reducing the metal content boils down to shift the relation towards the left. This has important consequences for the wind properties (see text for discussion). From Puls, Springmann & Lennon (2000).

What can we conclude from the above discussion? First, if the metal content is increased, the only effect will be an increase of the mass loss rate according to Eq. 5.47. The α parameter is not expected to change, and consequently the terminal velocity should remain almost identical. This should translate to a global shift of the modified wind momentum - luminosity relation upward, but the slope should be the same as at solar metallicity. We highlight here once again that this expected behaviour has not been tested so far. Now, if the metal content is reduced, both the direct and indirect effects must exist. The mass loss rate AND the α parameter are expected to be reduced. As a consequence, the terminal velocity which depends directly on α should be reduced too, and the slope of the WLR should be steeper. On the observational side, the terminal velocities of O stars of any luminosity class and of B supergiants have been found in the last decades to be $\sim$ 20% lower in the SMC than in the Galaxy (Garmany & Conti, 1985; Walborn et al., 1995; Kudritzki & Puls, 2000; Urbaneja et al., 2002). However, a recent study by Evans et al. (2004) revealed similar terminal velocities for early type stars in the Galaxy and the SMC. As regards the modified wind momentum - luminosity there

are indications of metallicity effects (see the discussion in Martins et al. (2004), Sect. 7.1). But the results presented in Sect. 8 seem to confirm the finding highlighted in Sect. 7.1 that Galactic stars show reduced modified wind momenta, which renders the picture more complicated and the effects of metallicity more difficult to disentangle.

7.2.3 Multicomponent winds

We have mentioned in Sect. 7 (Martins et al., 2004) that a mechanism which could explain the reduction of the wind strength is the so-called "ion decoupling" leading to multicomponent winds. The origin of this phenomenon has already been put forward, but we recall the basics here.

In a classical wind, the radiative acceleration comes form only a part of the ions present in the atmosphere, say the part responsible for most of the absorption of radiation. But these absorbing ions are surrounded by passive ions with which they interact through Coulomb interactions. As a result of these interactions, ions initially accelerated by the gain of momentum from photons speed down while the passive ions are accelerated by the Coulomb interactions. The result is that all ions in the wind end with the same velocity, so that the atmosphere is globally lifted as if it was composed of the same ions independently of their ability to absorb photons. However, if the density in the wind becomes too low, the Coulomb interactions will be weaker, so that the transfer of momentum from the absorbing ions to the passive plasma will be reduced. In that case, we may be left with a multicomponent wind in which absorbing ions are accelerated and passive ions remain static.

The first study of this effect was lead by Babel (1995) and Babel (1996). Springmann & Pauldrach (1992) ran hydrodynamical simulations which included the resolution of the momentum conservation equation for the various species, say the absorbing ions, passive ions and electrons. They took into account the frictional forces between exerted by species k and species j with the following expression:

$$R_{jk} = -n_j n_k k_{jk} G(x_{jk}) \tag{7.12}$$

where n_i is the density of ion i and k_{jk} is the coefficient of friction

$$k_{jk} = \frac{4\pi ln\Lambda q_j^2 q_k^2}{kT} \frac{v_j - v_k}{|v_j - v_k|} \tag{7.13}$$

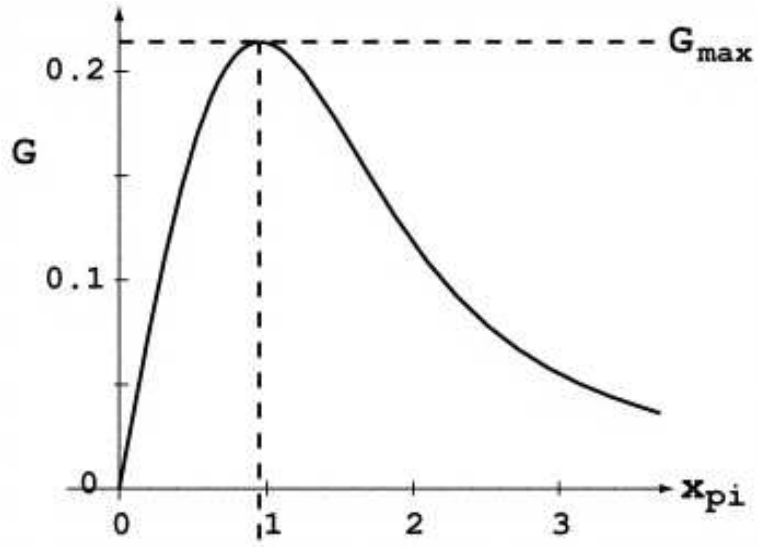

Figure 7.4: Chandrasekhar function. This function enters the friction force due to Coulomb interactions. It is alsmost linear in x before x = 1 and then behaves roughly as $1/x^2$. See text for discussion. From Owocki & Puls (2002).

v_i is the velocity of ion i, q_i its charge and ln Λ a constant. $x_{jk} = \sqrt{A_j A_k/(A_j + A_k)}|v_j - v_k|/a_p$ where A_i is the atomic mass number and $a_p = \sqrt{2kT/m_p}$ is the thermal velocity of protons. The function G is the Chandrasekhar function and behaves as displayed in Fig. 7.4. The interesting thing to note is that beyond the maximum of the function, an increase of the velocity difference of the two species (drift velocity) leads to a lower frition force, which then increases further the drift velocity! This is the runaway regime in which absorbing ions are accelerated and expelled while passive ions remain essentially static, or at least are much less accelerated.

Springmann & Pauldrach (1992) have derived the expression of the radiative line acceleration over the gravitational acceleration (Γ_L):

$$\Gamma_L = 5.24\beta v_\infty^2 R/M(1 - R/r)^{2\beta-1} \tag{7.14}$$

which is given for a classical β law for the velocity in the wind. R and M are in solar units, and v_∞ is in units of 10^3 km s^{-1}.

They also give the value of this acceleration when the drift velocity reaches the thermal speed, i.e. when $x_{jk} = 1$:

$$\Gamma_B = 810^6 Y_i Z_i^2 ln\Lambda \frac{\dot{M}}{TMv} \tag{7.15}$$

With this definitions, we see that if the radiative acceleration is higher than the value when $x_{jk} \simeq 1$, the drift velocity becomes higher than the thermal speed and we go into the regime where G decreases when x increases: we are in the runaway regime. Practically, the condition for decoupling is:

$$\Gamma_B < \Gamma_L \tag{7.16}$$

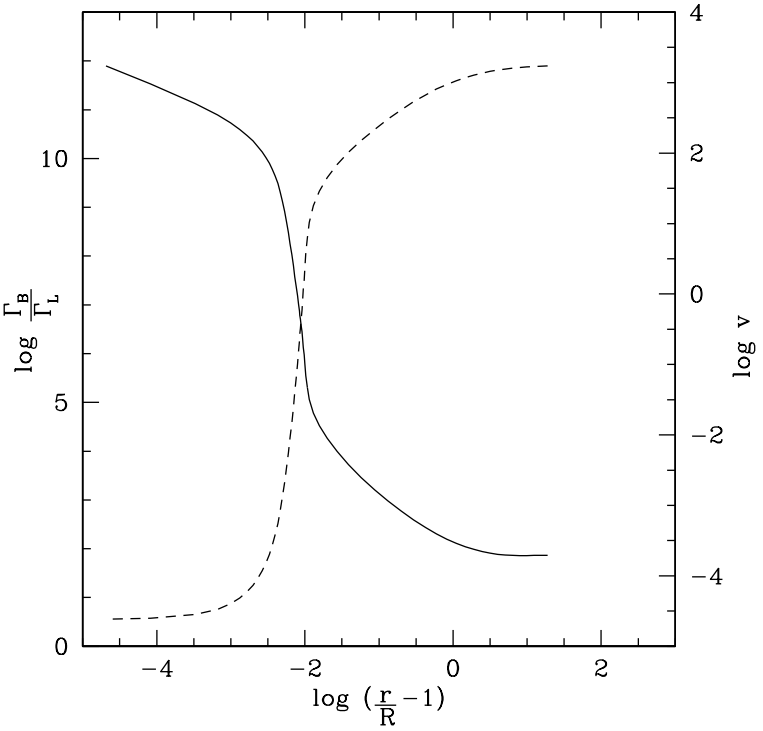

Figure 7.5: Test of the condition for ion runaway. The solid line gives the ratio Γ_B/Γ_L which must be lower than unity for decoupling. The dashed line gives the velocity in the atmosphere as a function of height. From this test, we see that decoupling should not occur in this model ($\dot{M}$= $10^{-8.5}$ $M_\odot$ yr^{-1}).

In order to test whether this condition was met in the wind of the SMC-N81 stars, we have computed the ratio of Γ_B over Γ_L and plotted the log of the result in Fig. 7.5 as a function of the atmosphere height. decoupling should occur if $\Gamma_B/\Gamma_L < 1$ which is not the case in the example we show here. For the model shown, the mass loss rate is $10^{-8.5}$ $M_\odot$ yr^{-1}. For lower values of $\dot{M}$, decoupling can occur but only in the outer wind, well above the transsonic point near $\log(r/R - 1) = -2$ as shown by the dashed line

in Fig. 7.5. As the mass loss rate is set in this region, the derived $\dot{M}$ is not affected by multicomponent wind effects according to the criterion of Springmann & Pauldrach (1992).

The above test relies on the fact that the friction force is reduced in the superthermal velocity range which, according to an intuitive expectation, should lead to a stronger acceleration of the absorbing ions and to an ion runaway, the passive plasma remaining almost static. However, Kritčcka & Kubát (2000) have shown that the reduction of the drift force leads in fact to a slower acceleration of the absorbing ions *and* of the passive plasma which is still accelerated. Owocki & Puls (2002) have shown that the reason for this surprising behaviour was that the radiative acceleration is directly balanced by the friction force, so that a reduction of the latter implies also a reduction of the former. Does it mean that ion runaway should never occur? In fact, Owocki & Puls (2002) also showed that for non-stationary winds, instabilities could develop even before the drift velocity has reached the thermal velocity, leading to an ion runaway. But the models run by Owocki & Puls (2002) are, according to the authors themselves, still incomplete, so that the question of the exact condition under which ion runaway should occur remains unanswered.

Recently, Kritčka et al. (2003) have tackled the problem under a different angle. They have estimated the metallicity below which the effects of multicomponent winds become important, i.e. the metallicity below which the different ions start to behave differently from each other, without necessarily reaching the state of ion runaway in which one or a few species are expelled while others remains almost static. Indeed, we have shown that the wind density should decrease when metallicity decreases. This may naturally lead to a lower momentum transfer between absorbing and passive ions and thus to decoupling. They have run multicomponent wind models for which they adopting simple scaling relation for the wind parameters as a function of Z. In particluar, they chose $\dot{M} \propto Z^{1/2}$. Using the condition that decoupling should occur when the drift velocity reaches the thermal velocity, they establish that the metallicity below which multicomponent effects become important is, for a given set of stellar parameters, given by:

$$\frac{Z}{Z_\odot} \simeq 4\ 10^{-3} \frac{T^{2/3} M^{4/2}}{R^{1/3} L} \tag{7.17}$$

where R is in 10^{12} cm units, T in 10^4 K, M in 100 $M_\odot$ and L in 10^6 $L_\odot$.

If we adopt R = 8 $R_\odot$, T = 40000 K, M = 30 $M_\odot$ and L = 10^5 $L_\odot$ as typical of the SMC-N81 stars, we find that the critical metallicity given by Eq. 7.17 is ~ 0.024 $Z_\odot$. This is much lower than the typical metallicity of the Small Magellanic Cloud, as we have mentioned in Sect. 7.

Chapter 8

Study of Galactic stars with weak winds

French summary

Dans ce chapitre, nous poursuivons notre l'étude précédente en nous intéressant à un échantillon d'étoiles Galactiques de divers type spectraux. Les buts sont 1) de voir s'il existe d'autres étoiles Galactiques montrant des vents faibles comme c'est le cas de 10 Lac (cf. chapitre pécédent), et 2) de mieux cerner les propriétés de ces étoiles. En particulier, nous testons la possibilité d'un lien entre la jeunesse et la faiblesse du vent en incluant quelques étoiles Vz dans notre échantillon.

L'analyse spectroscopique se fait au moyen de données tirées des archives de l'ESO, de l'Observatoire de La Palma et du satellite IUE qui sont complétées par des données obtenues sur le télescope NTT de l'ESO dans le cadre du programme 72.D-0038(A). Des modèles calculés avec le code CMFGEN sont utilisés pour analyser diverses raies optiques (incluant H_α) et UV afin de déterminer les paramètres stellaires et de vent des étoiles de notre échantillon.

Les principaux résultats peuvent être résumés comme suit:

- Les étoiles de notre échantillon sont âgées de 1 à 2 millions d'années pour les plus brillantes, et de 2 à 4 millions d'années pour les moins lumineuses. La majorité d'entre elles suit assez bien la relation $T_{\rm eff}$ - luminosité de Vacca, Garmany & Schull (1996).

- Les étoiles les plus lumineuses ont des taux de perte de masse environ 5 fois plus faibles que les prédictions théoriques de Vink, de Koter & Lamers (2001). Les deux étoiles en commun avec l'étude de Repolust, Puls & Herrero (2004) ont aussi des pertes de masse plus

faibles que celles dérivées de leur étude basée uniquement sur H_α. Cette réduction de la perte de masse s'explique principalement par l'inclusion de clumping dans nos modèles, inclusion nécessaire pour reproduire les raies O V λ1371 et N IV λ1718 .

- Le sous-échantillon d'étoiles de faible luminosité montre des vents exceptionnellement faibles comparé aux prédictions théoriques: $\dot{M}$ peut être jusqu'à 2 ordres de grandeur plus faible. Les vitesses terminales sont elles aussi réduites.

- La relation quantité de mouvement modifiée - luminosité montre une rupture de pente autour de $\log \frac{L}{L_\odot} = 5.2$. En dessous de cette luminosité de transition, la pente correspond a $\alpha' \sim 0.2$ alors qu'au dessus, la pente est similaire aux études basées sur H_α uniquement.

- L'origine des vents faibles dans les étoiles de faible luminosité reste inconnue, mais nous pouvons écarter un effet de métallicité car à la fois des étoiles Galactiques et du SMC montrent cette tendance. Par ailleurs, la jeunesse des étoiles ne semble pas non plus être une explication convaincante car les étoiles de faible luminosité de notre échantillon sont aussi presques toutes déjà relativement âgées.

Ainsi, le mystère entourant les vents des étoiles de faible luminosité reste entier. Des études théoriques au moyen de simulations hydrodynamiques seraient à mener pour tester l'hypothèse d'une sur-estimation de la force des vents dans les étoiles naines de faible luminosité, comme cela peut être le cas d'après Owocki & Puls (1999). D'autre part, de plus amples analyses spectroscopiques sont nécessaires pour calibrer la relation quantité de mouvement modifiée - luminosité puisqu'à la fois le clumping et la faible luminosité semblent être des facteurs déterminants.

In this chapter, we study the stellar and wind properties of Galactic O dwarfs. We show that several stars have winds as weak as the N81 stars. This reveals that metallicity is probably not the main reason for the weakness of the wind, as already suspected.

Astronomy & Astrophysics manuscript no. WW˙Gal February 23, 2005
(DOI: will be inserted by hand later)

O stars with weak winds: the Galactic case ⋆

Fabrice Martins[1,2,3], Daniel Schaerer[1,2], D. John Hillier[4], Frédéric Meynadier[5], Mohammad Heydari-Malayeri[5], and Nolan R. Walborn[6]

[1] Observatoire de Genève, 51 Chemin des Maillettes, CH-1290 Sauverny, Switzerland
[2] Laboratoire d'Astrophysique, Observatoire Midi-Pyrénées, 14 Av. E. Belin, F-31400 Toulouse, France
[3] Max Planck Institüt für Extraterrestrische Physik, Postfach 1312, D-85741 Garching, Germany
[4] Department of Physics and Astronomy, University of Pittsburgh, 3941 O'Hara Street, Pittsburgh, PA 15260, USA
[5] LERMA, Observatoire de Paris, 61 Rue de l'Observatoire, F-75012 Paris, France
[6] Space Telescope Science Institute, 3700 San Martin Drive, Baltimore, MD 21218, USA

submitted 23 Feb. 2005 / accepted ...

Abstract.
We study the stellar and wind properties of a sample of Galactic O dwarfs to track the conditions under which weak winds (i.e mass loss rates lower than $\sim 10^{-8}$ $M_\odot$ yr^{-1}) appear. The sample is composed of low and high luminosity dwarfs including Vz stars and stars known to display qualitatively weak winds. Atmosphere models including non-LTE treatment, spherical expansion and line blanketing are computed with the code CMFGEN (Hillier & Miller 1998). Both UV and Hα lines are used to derive wind properties while optical H and He lines give the stellar parameters. We find that the stars of our sample are usually 1 to 4 Myr old. Mass loss rates of all stars are found to be lower than expected from the hydrodynamical predictions of Vink et al. (2001). For stars with $\log \frac{L}{L_\odot} \gtrsim 5.2$, the reduction is by less than a factor 5 and is mainly due to the inclusion of clumping in the models. For stars with $\log \frac{L}{L_\odot} \lesssim 5.2$ the reduction can be as high as a factor 100. The inclusion of X-ray emission (possibly due to magnetic mechanisms) in models with low density is crucial to derive accurate mass loss rates from UV lines, while it is found to be unimportant for high density winds. The modified wind momentum - luminosity relation shows a significant change of slope around this transition luminosity. Terminal velocities of low luminosity stars are also found to be low. Both mass loss rates and terminal velocities of low L stars are consistent with a reduced line force parameter α. However, the physical reason for such a reduction is still not clear although the finding of weak winds in Galactic stars excludes the role of a reduced metallicity. There may be a link between an early evolutionary state and a weak wind, but this has to be confirmed by further studies of Vz stars. X-rays, through the change in the ionisation structure they imply, may be at the origin of a reduction of the radiative acceleration, leading to lower mass loss rates. A better understanding of the origin of X-rays is of crucial importance for the study of the physics of weak winds

Key words. stars: winds - stars: atmospheres - stars: massive - stars: fundamental parameters

1. Introduction

Massive stars are known to develop winds so intense that mass loss rate turns out to be the main factor governing their evolution (e.g. Chiosi & Maeder 1986). The mechanism responsible for such strong outflows was first pointed out by Milne (1926) when observations of winds were not yet available: the radiative acceleration in these bright objects was suspected to be large enough to overtake gravitational acceleration, creating expanding atmospheres. The first quantitative description of this process was given by Lucy & Solomon (1971) who computed mass loss rates due to radiative acceleration through strong UV resonance lines. Castor, Abbott & Klein (1975) made a significant improvement in the understanding of winds of massive stars in their detailed calculation of radiative acceleration including an ensemble of lines by means of their now famous formalism and found mass loss rates ~ 100 times larger than Lucy & Solomon (1971). The theory of radiation driven winds developed by Castor, Abbott & Klein was further improved by Pauldrach et al. (1986) and Kudritzki et al. (1989) who included the effect of the finite size of the star in the radiative acceleration.

In parallel to theoretical studies, observational constraints on the wind properties of massive stars were ob-

Send offprint requests to: F. Martins, martins@mpe.mpg.de

⋆ Partly based on observations collected with ESO-NTT telescope (program 72.D-0038(A))

tained. Most methods relied on either the measurement of infrared and radio excess emitted in the wind of such stars (Howarth & Prinja 1989, Leitherer 1988, Lamers & Leitherer 1993), or on the analysis of UV and optical emission or P-Cygni lines (e.g. Leitherer 1988, Haser 1995, Puls et al. 1996). The results confirmed the prediction of the theory that the mass loss rate should scale mainly with a power law of luminosity (e.g. Howarth & Prinja 1989) and that the terminal velocities are directly proportional to escape velocities (e.g. Lamers et al. 1995). Another success of the radiation driven wind theory came from the so called modified wind momentum - luminosity relation (hereafter WLR). Kudritzki et al. (1995) showed that the quantity $\dot{M}v_\infty\sqrt{R}$ (with $\dot{M}$ the mass loss rate, v_∞ the terminal velocity and R the stellar radius) should depend only on luminosity (contrary to $\dot{M}$ which also depends slightly on the star mass) which was soon confirmed by the spectroscopic analysis of O and B stars (Puls et al. 1996, Kudritzki et al. 1999). This finding was quite exciting since once calibrated, the WLR could be used as a distance indicator up to several Mpc (Kudritzki 1998). Recent determinations of wind parameters with sophisticated atmosphere codes confirm the good agreement between observational constraints and theoretical predictions for bright O stars, both in term of mass loss rate (for which the most recent predictions are those of Vink et al. 2000, 2001) and WLR (see Herrero, Puls & Najarro 2002, Crowther et al. 2002, Repolust et al. 2004).

In spite of these encouraging results, the behaviour of the wind properties of O stars with relatively low luminosity seems to be a little more complicated. Martins et al. (2002b, 2004, hereafter paper I) have shown that the stellar components of the star forming region N81 of the SMC are O dwarfs with low luminosities and surprisingly weak winds: the mass loss rates are lower than 10^{-8} $M_\odot$ yr^{-1} and the modified wind momenta are nearly 2 orders of magnitude lower than expected from the WLR obtained for bright stars. Bouret et al. (2003) also found low mass loss rates for the faintest of the NGC 346 dwarfs they analysed. Although all stars were in the SMC, we showed in paper I that metallicity may not be the only factor responsible for such a strong reduction of the wind strength. In particular, we showed that a Galactic star - 10 Lac - displayed a similar weak wind. One of the explanations we highlighted was a possible link with the youth of the stars since most of them were (or were suspected to be) Vz stars, i.e. young stars lying close to the ZAMS (Walborn & Parker 1992). Another possibility was a break down of the scaling relations (especially the WLR) at low luminosity. This reduction of the wind strength at low luminosities was in fact already mentioned by Chlebowski & Garmany (1991) more than a decade ago.

In this paper, we try to investigate more deeply the wind properties of low luminosity Galactic stars. The aim is 1) to see if one can exclude the effect of metallicity to explain the weakness of the winds, 2) to test the hypothesis of the link between the weakness of the wind and the youth of the stars and 3) to quantify the wind properties of faint O stars and the luminosity below which such weak winds are observed. For this, we study a sample of O dwarfs with both low and high luminosities. Stars known to display qualitatively weak winds are included together with stars belonging to the Vz subclass. We selected stars showing weak UV lines usually sensitive to winds (from the IUE atlas of Walborn et al. 1985) and/or with low mass loss rates from the study of Chlebowski & Garmany (1991). We also included Vz stars (N. Walborn, private communication) and bright stars (two in common with the Repolust et al. 2004 sample) to examine the dependence of the wind properties on luminosity. Finally, stars from the young star forming region in the Rosette nebula were included.

The remainder of the paper is organised as follows: In Sect. 2 we give information about the observational data we used; Sect. 3 explains how we derived the stellar and wind parameters; Sect. 4 gives the results for individual stars; Sect. 5 highlights the importance of X-rays and magnetic fields in weak wind stars, while Sect. 6 discusses possible sources of uncertainty; the results are discussed in Sect. 7 and the conclusions are given in Sect. 8.

2. Observations

2.1. Optical

Various sources have been used to get the optical spectra of the stars studied here. First, the VLT archive provided UVES spectra for HD 152590, HD 38666 and HD 46202. The instrumental resolution varies between 0.04 Å and 0.1 Å, due to different slit widths. The UVES pipeline was used for the reduction of the data. Second, optical data for HD 34078 and HD 15629 were retrieved from the La Palma archive. Spectra obtained with the instrument ISIS on the WHT were reduced using standard procedures under the ESO/MIDAS environment. The spectral resolution is 0.9 Å. Third, spectra of HD 93204, HD 93250 (EMMI) and HD 15629 (La Palma) were provided by Artemio Herrero and Danny Lennon and have a typical resolution of 0.95 Å. Finally for stars HD 93146, HD 93028, HD 46223 and HD 42088, we used EMMI spectra obtained during the nights of 29, 30 and 31 December 2003 on the ESO/NTT in La Silla, under the program 72.D-0038(A) (PI Martins). These spectra were obtained in the red mode of the instrument and provided the Hα profiles. The IRAF package was used for the data reduction. For a few stars, we were left with several spectra of the same wavelength range. In that case, we always chose the spectra with the best resolution. The signal to noise ratio depends on the instrument used but is usually larger than 100 in most lines of interest.

2.2. UV

The IUE archive was used to retrieve the UV spectra of all the stars of this study. Spectra in the range 1150-2000 Å obtained with the Short Wavelength Spectrograph (SWS) were selected. The typical instrumental resolution is 0.2 Å

and a S/N ratio of the order of 10. The normalisation was made "by eye" and turned out to be somewhat uncertain below 1200 Å.

Hence, we also retrieved FUSE spectra when available from the MAST archive. The data are provided already reduced by the CALFUSE pipeline, and we simply normalised them by eye. Due to the strong Galactic interstellar absorption, many broad absorption bands form H_2 render the bluest part of the FUSE spectra useless for our purpose (e.g. Pellerin et al. 2002). We mostly used the 1100-1180 Å range which has a better signal to noise ratio than the IUE spectra for such wavelengths and extends to shorter wavelengths.

3. Method

Our main concern is to derive wind parameters (mass loss rates, terminal velocities) and modified wind momenta. However, such determinations require reliable stellar parameters, especially effective temperatures. Indeed, any uncertainty on $T_{\rm eff}$ can lead to an error on $\dot{M}$. We thus first estimate the stellar parameters using the optical spectra, and then we use the UV range + Hα line to determine the wind properties.

3.1. Stellar parameters

The main stellar parameters have been determined from blue optical spectra. As such spectra contain diagnostic lines which are formed just above the photosphere and are not affected by winds, plane-parallel models can be used for a preliminary analysis. Hence, we have taken advantage of the recent grid of TLUSTY spectra (OSTAR2002, Lanz & Hubeny 2002). This grid covers the log g - $T_{\rm eff}$ plane for O stars and includes optical synthetic spectra computed with a turbulent velocity of 10 km s^{-1}. The models include the main ingredients of the modelling of O star atmospheres (especially non-LTE treatment and line-blanketing) except that they do not take the wind into account (see Hubeny & Lanz 1995 for details).

Our method has been the following:

- V *sini :* First we adopted the rotational velocities from the literature (mostly Penny 1996).

- $T_{\rm eff}$ *:* Then the ratio of He I λ4471 to He II λ4542 equivalent widths gave the spectral type which was used to estimate $T_{\rm eff}$ from the $T_{\rm eff}$-scale of Martins et al. (2002a). Then, TLUSTY spectra with effective temperatures bracketing this value were convolved to take into account the rotational velocity and instrumental resolution, and the resulting spectra were compared to the observed profiles of the He I λ4471 and He II λ4542 lines. The best fit led to the constraint on $T_{\rm eff}$. As the OSTAR2002 grid has a relatively coarse sampling (2500 K steps), we have often interpolated line profiles of intermediate temperatures. A simple linear interpolation was used. For the stars for which the He I λ4471 and He II λ4542 lines were not available, we used He I λ5876 and He II λ5412 as the main indicators.

Secondary $T_{\rm eff}$ diagnostic lines such as He I λ4388, He I λ4713, He I λ4920 He I λ4144 He I λ5016 and He II λ4200 were also used to refine the determination (when available). The uncertainty on $T_{\rm eff}$ depends on the resolution of the spectra and on the rotational broadening. Indeed, the broader the profile, the lower the precision of the fit of the line. The typical error on $T_{\rm eff}$ is usually of $\pm$ 2000 K but can be reduced when many optical He lines are available.

We also checked that our final models including winds computed with CMFGEN fitted correctly the optical lines. it turns out that the agreement between TLUSTY and CMFGEN is very good as already noticed in previous studies (e.g. Bouret et al. 2003). The problem recently highlighted by Puls et al. (2005) concerning the weakness of the He I singlet lines between 35000 and 40000 K is in fact related to subtle line blanketing effects and is solved when both the turbulent velocity is reduced and other species (Neon, Argon, Calcium and Nickel) are added in the models (see Sect. 4.9).

- $\log g$ *:* Fits of the wings of Hγ led to constraints on log g. Once again, interpolations between the OSTAR2002 spectra were made to improve the determination as the step size of the OSTAR2002 grid is 0.25 in log g. Hβ, which behaves similarly to Hγ, was used as a secondary indicator. The typical uncertainty on log g is 0.1 dex.

Once obtained, these parameters have been used to derive L, R and M:

- *Luminosity :* with $T_{\rm eff}$ known, we have estimated a bolometric correction according to

$$BC(T_{\rm eff}) = 27.66 - 6.84 \times \log T_{\rm eff} \quad (1)$$

which has been established by Vacca et al. (1996). Visual magnitudes together with estimates of the reddening and the distance modulus of the star have then lead to M_V and L from:

$$\log \frac{L}{L_\odot} = -0.4(M_{\rm V} + BC - M_\odot) \quad (2)$$

the error on $T_{\rm eff}$ leads to a typical error of 0.2 dex on BC. Note that we have recently revised the calibration of bolometric corrections as a function of $T_{\rm eff}$ (see Martins et al. 2005), but it turns out that due to line-blanketing effects, BCs are reduced by only 0.1 dex, which translates to a reduction of $\log L$ by 0.04 dex, which is negligible here given the uncertainty on the distance.

The solar bolometric magnitude was taken as equal to 4.75 (Allen 1976). We want to caution here that for most of the stars of this study, the distance is poorly known (with sometimes a difference of 1 magnitude on the distance modulus between existing determinations). This leads to an important error on the luminosity.

As this last parameter is crucial for the calibration of the modified wind momentum - relation, we decided to take the maximum error on L by adopting the lowest (resp. highest) luminosity (derived from the lowest -resp. highest- extinction, distance modulus and bolometric correction) as the boundaries to the range of possible luminosities. The typical error on L is $\sim \pm$ 0.25 dex, and the main source of uncertainty is the distance.

- *Radius :* Once $T_{\rm eff}$ and L are known, R is simply derived from

$$R = \sqrt{\frac{L}{4\pi\sigma T_{\rm eff}^4}} \quad (3)$$

where σ is the Stefan Boltzmann constant. Standard errors have been derived according to

$$\Delta \log R = 0.5\sqrt{(\Delta \log L)^2 + (4\Delta \log T_{\rm eff})^2} \quad (4)$$

- *M :* The (spectroscopic) mass is derived from g and R according to

$$M = \frac{gR^2}{G} \quad (5)$$

and the standard error is given by

$$\Delta \log M = \sqrt{(\Delta \log g)^2 + (2\Delta \log R)^2} \quad (6)$$

With this set of stellar parameters, we have run models including winds to derive the mass loss rate and the terminal velocity (see next section). The stellar parameters giving the best agreement between observations and models with winds were adopted as the final stellar parameters.

3.2. Wind parameters

UV (and FUV when available) spectra and Hα profiles were used to constrain the wind parameters. In the case where mass loss rates were low, prority was given to UV indicators since Hα becomes much less sensitive to $\dot{M}$: for such situations, we checked that the Hα line given by our models with $\dot{M}$ estimated from UV was consistent with the observed line. We want to stress here that it is only because metals are now included in a reliable way in new generation atmosphere models that such a study is possible. Indeed, UV metallic lines now correctly reproduced allow to push the limits of mass loss determination below $\sim 10^{-8}$ M$_\odot$ yr^{-1}.

Models including stellar winds were computed with the code CMFGEN (Hillier & Miller 1998). This code allows for a non-LTE treatment of the radiative transfer and statistical equilibrium equations in spherical geometry and includes line blanketing effects through a super-level approach. The temperature structure is computed under the assumption of radiative equilibrium. At present, CMFGEN does not include the hydrodynamics of the wind so that the velocity and density structures must be given as input. In order to be as consistent as possible with the optical analysis, we have used TLUSTY structures for the photosphere part and we have connected them to a classical β law ($v = v_\infty(1 - \frac{R_*}{r})^\beta$) representing the wind part. We chose $\beta = 1.0$ as the default value for our calculation since it turns out to be representative of O dwarfs (e.g. Massa et al. 2003). The TLUSTY structures have been taken from the OSTAR2002 grid or have been linearly interpolated from this grid for $T_{\rm eff}$ not included in OSTAR2002. This method has also been used by Bouret et al. (2003) and has shown good consistency between CMFGEN and TLUSTY photospheric spectra.

Clumping can be included in the wind models by means of a volume filling f factor parameterised as follows: $f = f_\infty + (1 - f_\infty)e^{-\frac{v}{v_{\rm init}}}$ where f_∞ is the value of f at the top of the atmosphere and $v_{\rm init}$ is the velocity at which clumping appears. As in Bouret et al. (2003), we chose $v_{\rm init} = 30$ km s^{-1}.

A depth independent microturbulent velocity can be included in the computation of the atmospheric structure (i.e. temperature structure + population of individual levels). We chose a value of 20 km s^{-1} as the default value in our computations. Several tests (Martins et al. 2002a, Bouret et al. 2003) indicate that a reasonable change of this parameter has little effect on the emergent spectrum, except for some specific lines (see Sect. 4.9). For the computation of the detailed spectrum resulting from a formal solution of the radiative transfer equation (i.e. with the populations kept fixed), a depth dependent microturbulent velocity can be adopted. In that case, the microturbulent velocity follows the relation $v_{turb}(r) = v_{min} + (v_{max} - v_{min})\frac{v(r)}{v_\infty}$ where v_{min} and v_{max} are the minimum and maximum microturbulent velocities. By default, we chose $v_{min} = 5$ km s^{-1} in the photosphere, and v_{max} = min (0.1 v_∞, 200) km s^{-1} at the top of the atmosphere. For some stars, we had to increase v_{min} from 5 to 10/15 km s^{-1} to be able to fit correctly the observed spectra.

CMFGEN allow the possibility to include X-ray emission in the models. In some cases (see next Section), we had to include such high energy photons. Practically, as X-rays are thought to be emitted by shocks distributed in the wind, two parameters are adopted to take them into account: one is a shock temperature (equal to $3 10^6$ K) to set the wavelength of maximum emission, and the other is a volume filling factor which is used to set the level of emission. With this formalism, X-ray sources are distributed throughout the atmosphere and the emissivities are taken from tables computed by a Raymond & Smith code (Raymond & Smith 1977). We included such X-rays in the models for the four faintest stars as explained in Sect. 5 using measured X-ray fluxes or a canonical value of $L_{\rm X}/L_{\rm bol} = -7.0$.

The main wind parameters we have determined are the mass loss rate ($\dot{M}$) and the terminal velocity (v_∞). Constraints on the amount of clumping were also derived

when possible. The terminal velocities have been estimated from the blueward extension of the absorption part of UV P-Cygni profiles. We define the terminal velocity as the velocity for which the flux in the blueward absorption of the P-Cygni line reaches the continuum level. Other definitions exist (e.g. Prinja, Barlow & Howarth 1990). The typical uncertainty on our determination of v_∞ is 200 km s^{-1} (depending on the maximum microturbulent velocity we adopt).

Fits of strong UV lines such as N V λ1240 C IV $\lambda\lambda$1548,1551 Si IV $\lambda\lambda$1394,1403 O V λ1371 and N IV λ1718 have led to constraints on $\dot{M}$. Hα is also sensitive to $\dot{M}$: in dwarfs with weak winds, a quasi photospheric profile is expected but the line can be used to estimate upper limits on the mass loss rate as it is filled by emission when $\dot{M} \gtrsim 10^{-8}$ M$_\odot$ yr^{-1}. Also, in the case of weak winds C IV $\lambda\lambda$1548,1551 is actually the only line showing some sensitivity to wind and was in several cases our best $\dot{M}$ estimator. Given this, we tried to adjust the mass loss rate (and clumping parameters) to get the best fit of both the UV wind sensitive lines and Hα.

As regards the abundances, we have taken as default values the solar determinations of Grevesse & Sauval (1998) since the stars of this study are are all Galactic stars. CNO solar abundances have been recently revised downward by Asplund (2004). However, we preferred to rely on the Grevesse & Sauval abundances since they have been widely used in previous studies of massive stars and are therefore more suited for comparisons. When necessary, we indicate if these abundances have been changed to get a better fit.

4. Results

In this Section, we present the results of the analysis for each star and highlight the main difficulty encountered in the fitting process. The derived stellar and wind parameters, together with the observational quantities, are gathered in Table 1, while results from previous studies of wind properties are given in Table 2. The observed properties (magnitudes, colors, distances) come from the following sources: the Simbad compilation, the Hipparcos database, the Webda cluster [1] database, Humphreys (1978), Maíz-Apellániz et al. (2004), Bernabeu et al. (1989), Howarth & Prinja (1989).

Spectra from atmosphere models are convolved to include the instrumental resolution of the observational data and the projected rotational velocity of the star. The wavelength range between $\sim$ 1200 and $\sim$ 1225 Å is not used in the spectral analysis since it suffers from a strong interstellar Lyman absorption.

4.1. HD38666

HD 38666 (also μ Col) is an O9.5V runaway star located east of Orion. HD 38666 has been observed by Hipparcos which found a parallax of 2.55 $\pm$ 0.55 mas from which Maíz-Apellániz et al. (2004) derived a distance of 531 pc, or a distance modulus of $8.63^{+0.93}_{-0.63}$. Humphreys (1978) gives $DM = 8.50$ assuming that HD 38666 belongs to the

[1] http://obsww.unige.ch/webda

Table 2. Comparison between our derived wind parameters ($\dot{M}$, v_∞, shown in bold text) and previous determinations. (1) Leitherer (1988), (2) Bernabeu et al. (1989), (3) Howarth & Prinja (1989), (4) Prinja et al. (1990), (5) Chlebowski & Garmany (1991), (6) Lamers & Leitherer (1993), (7) Lamers et al. (1995), (8) Puls et al. (1996), (9) Howarth et al. (1997), (10) Lamers et al. (1999), (11) Repolust et al. (2004), (12) Markova et al. (2004).

HD	log $\dot{M}$	v_∞
38666	< -7.22 (1), -7.8 (3)	2000 (1), 1000 (3)
	-8.31 (5)	
	-9.5	**1200**
34078	-6.6 (3)	750 (3)
	-9.5	**800**
46202	< -6.87 (1), -7.2 (3)	2100 (1), 750 (3)
	-8.10 (5)	1150 (5), 1590 (2)
	-8.9	**1200**
93028	-7.0 (3)	1500 (3), 1780 (2)
	-9.0	**1300**
152590	-6.9 (3), -7.36 (5)	2150 (3), 2300 (5)
		1785 (9)
	-7.78	**1750**
93146	-6.9 (3)	2975 (3), 3200 (2)
		2565 (4), 2640 (9)
	-7.25	**2800**
42088	-6.35 (1), -7.0 (3)	2550 (1), 2030 (3)
	-6.82 (5), -6.42 (12)	2300 (5), 2420 (2)
		2155 (4), 2215 (9)
		2200 (12)
	-8.0	**1900**
93204	-6.1 (3)	3250 (3), 3180 (2)
		2890 (4), 2900 (7)
	-6.75	**2900**
15629	-5.89 (11)	3200 (11), 3220 (2)
		2810 (9)
	-6.5	**2800**
46223	-5.75 (1), -5.8 (3)	3100 (1), 3100 (3)
	-5.62 (5), -5.85 (6)	3100 (5), 2800 (6)
	-5.68 (10)	2800 (10), 3140 (2)
		2910 (4), 2900 (7)
	-6.5	**2800**
93250	-4.9 (8), -4.6 (3)	3250 (8), 3350 (3)
	-5.46 (11)	3250 (11), 3470 (2)
		3230 (9)
	-6.25	**3000**

Table 1. Stellar and wind parameters of Galactic stars. The escape velocities were computed from the spectroscopic derived mass, radius and luminosity. The evolutionary masses have been estimated from the isochrones of Lejeune & Schaerer (2001).

HD number	38666	34078	46202	93028	152590	93146	42088	93204	15629	46223	93250
ST	O9.5V	O9.5V	O9V	O9V	O7.5Vz	O6.5V	O6.5Vz	O5V	O5V	O4V	O3.5V
V	5.15	5.99	8.18	8.36	8.44	8.43	7.55	8.44	8.42	7.27	7.38
E(B-V)	0.05	0.54	0.49	0.26	0.46	0.34	0.46	0.42	0.74	0.54	0.48
DM	8.63	8.24	10.85	12.09	10.72	12.09	11.20	12.34	11.38	10.85	12.34
M_V	−3.64	−3.92	−4.14	−4.54	−3.71	−4.70	−4.66	−5.20	−5.25	−5.25	−6.45
$T_{\rm eff}$ [K]	33000	33000	33000	34000	36000	37000	38000	40000	41000	41500	44000
log g	4.0	4.05	4.0	4.0	4.10	4.0	4.0	4.0	3.75	4.0	4.0
V sin$i$ [km s^{-1}]	111	40	30	50	66	80	60	130	90	130	110
log $\frac{L}{L_\odot}$	4.66	4.77	4.87	5.05	4.79	5.22	5.23	5.51	5.56	5.57	6.12
R [R$_\odot$]	6.58	7.47	8.38	9.71	6.42	9.97	9.56	11.91	12.01	11.86	19.87
$M_{spectro}$ [M$_\odot$]	16	23	26	34	19	36	33	52	30	51	144
M_{evol} [M$_\odot$]	19	20	21	25	22	30	31	41	44	45	105
v_{esc} [km s^{-1}]	920	1043	1046	1112	1015	1106	1100	1178	799	1157	1461
v_∞ [km s^{-1}]	1200	800	1200	1300	1750	2800	1900	2900	2800	2800	3000
$\dot{M}$ [M$_\odot$ yr^{-1}]	−9.5	−9.5	−8.9	−9.0	−7.78	−7.25	−8.0	−6.75	−6.5	−6.5	−6.25
f_∞	1.0	1.0	1.0	1.0	1.0	1.0	1.0	0.1	0.1	0.1	0.01
$\dot{M}_{Vink}$ [M$_\odot$ yr^{-1}]	−7.41	−7.38	−7.23	−6.97	−7.15	−6.58	−6.17	−6.11	−5.74	−5.97	−5.25
$\dot{M}v_\infty\sqrt{R}$	24.79	24.64	25.44	25.41	26.67	27.50	26.57	28.05	28.29	28.28	28.68

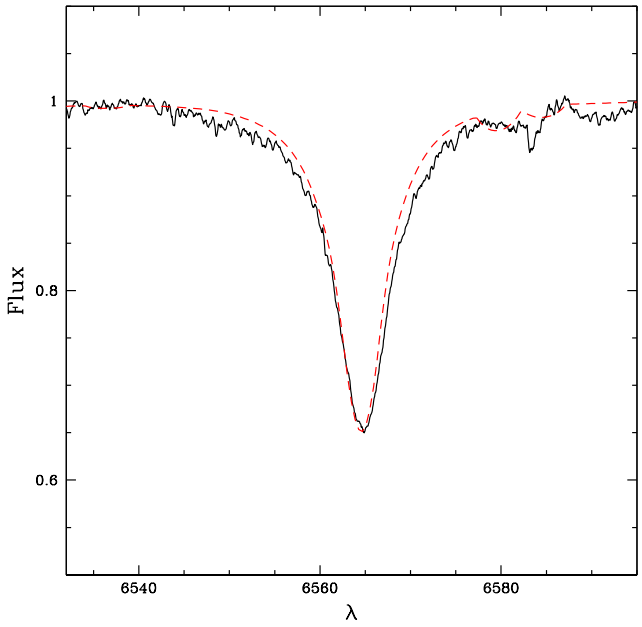

Fig. 2. Best fit (red dashed line) of the observed Hα line (black solid line) of HD 38666. We have derived $\dot{M} = 10^{-9.5}$ M$_\odot$ yr^{-1} and v_∞ was 1200 km s^{-1}.

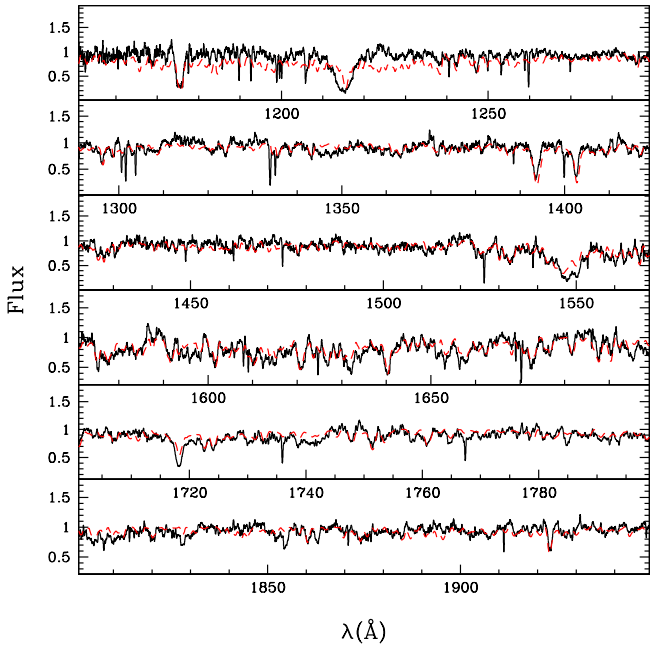

Fig. 3. Best fit (red dashed line) of the UV spectrum (black solid line) of HD 38666. For this model, $\dot{M} = 10^{-9.5}$ M$_\odot$ yr^{-1}, $v_\infty = 1200$ km s^{-1} and $\log L_{\rm X}/L_{\rm bol} = -6.87$

association Ori OB1. We adopt the Hipparcos measurement and error bars in the following since they encompass the value of Humphreys (1978).

The visual magnitude of 5.15 and the $B-V$ color of −0.27 imply $M_V = -3.64^{+0.60}_{-0.93}$ (adopting $(B-V)_0 = -0.32$, e.g. Schmidt-Kaler 1982). We derive an effective temperature of 33000 K from the fit of the optical He lines shown in Fig. 1. Due to the high quality of the data the uncertainty on $T_{\rm eff}$ is of the order 1000 K. Chlebowski & Garmany (1991) found $T_{\rm eff} = 34900$ K, while Howarth & Prinja (1989) give 33000 K, in good agreement with our result. The bolometric correction is then $BC = -3.25^{+0.10}_{-0.08}$,

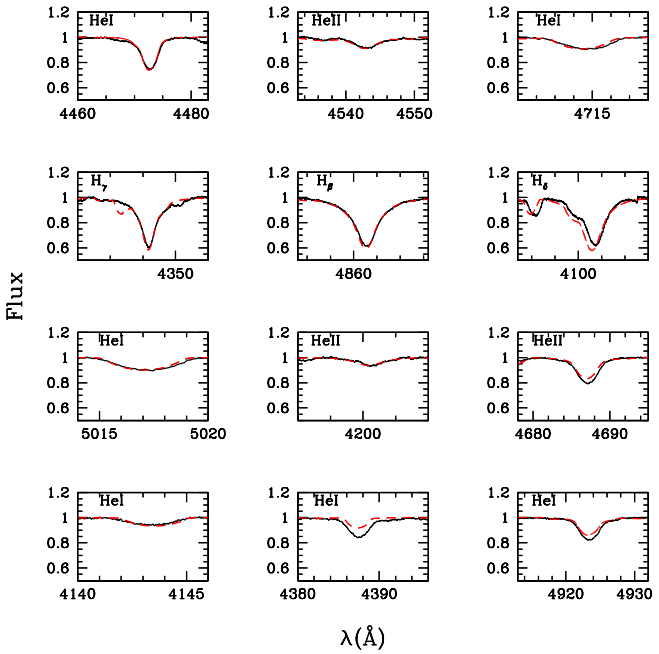

Fig. 1. Best fit (red dashed line) of the optical spectrum (black solid line) of HD 38666. The effective temperature is 33000 K, $\log g = 4.0$ and $V \sin i = 110$ km s^{-1}.

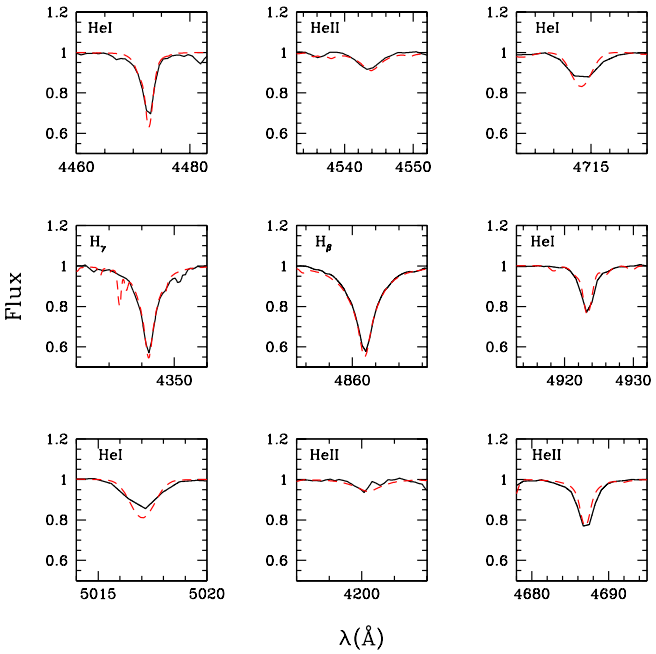

Fig. 4. Best fit (red dashed line) of the optical spectrum (black solid line) of HD 34078. Here, $T_{\rm eff} = 33000$ K, $\log g = 4.05$ and $V \sin i = 40$ km s^{-1}.

leading finally to $log\frac{L}{L_\odot} = 4.66^{+0.40}_{-0.30}$ and $R = 6.58^{+3.89}_{-2.45}$ R$_\odot$. A value of $\log g = 4.0 \pm 0.1$ is derived from the Balmer lines, so that $M = 16^{+25}_{-10}$ M$_\odot$. The uncertainties on R is very large, but once again, this is due to our choice to maximise the error on L in order to cover the entire range of possible luminosities for the stars studied here.

The Hα and UV fits are given in Fig. 2 and Fig. 3. The best fits are obtained for $\dot{M} = 10^{-9.5}$ M$_\odot$ yr^{-1} and $v_\infty = 1200$ km s^{-1}. An important point is that X-rays have been included in the modelling, with $\log \frac{L_{\rm X}}{L_{\rm bol}} = -6.87$ as indicated by the observed X-ray emission (see Table 3). If this high energy component is not included, we need a mass loss rate 10 times lower to fit the C IV $\lambda\lambda$1548,1551 line. The reason for this is that the ionisation structure of the wind is increased when X-rays are present, leading to a lower C IV ionisation fraction, and thus requiring a higher mass loss rate to reproduce the observed line profile (see Sect. 5 for a more complete discussion). An increase of $\dot{M}$ by a factor of 3 leads to a too strong Si IV $\lambda\lambda$1394,1403 and C IV $\lambda\lambda$1548,1551 line. Note that the fit of the C IV $\lambda\lambda$1548,1551 profile is not perfect. This is due to the presence of interstellar absorption which adds to the photospheric component. However, the fit of the blueshifted wind part of the line is good and is not affected by interstellar absorption (see also Martins et al. 2004). Hence, we are confident that our values of $\dot{M}$ and v_∞ are not too far from reality. A higher terminal velocity leads to a too-much-extended blueward absorption in C IV $\lambda\lambda$1548,1551. The value of v_∞ we derive is just above the escape velocity. Leitherer (1988) estimated $v_\infty = 2000$ km s^{-1} while Howarth & Prinja (1989) found 1000 km s^{-1} illustrating the uncertainty on the exact value of the terminal velocity of HD 38666. Concerning the mass loss rate, Leitherer found $\dot{M} < 10^{-7.22}$ M$_\odot$ yr^{-1}, Howarth & Prinja give $\dot{M} = 10^{-7.80}$ M$_\odot$ yr^{-1} and Chlebowski & Garmany (1991) claim $\dot{M} = 10^{-8.31}$ M$_\odot$ yr^{-1}. Our estimate is lower than all these determinations. The determination of Leitherer (1988) relies only on the Hα wind emission, which in the case of low mass rates is very small and difficult to disentangle from the photospheric absorption. The studies of Chlebowski & Garmany (1991) and Howarth & Prinja (1989) are based on the fit of UV resonance lines with the following method: the optical depth as a function of the velocity (only for unsaturated profiles) is determined by profile fitting; from this, the determination of the mass loss rate requires the adoption of an ionisation structure which may or may not be representative of the real ionisation in the atmosphere. This assumption may affect the $\dot{M}$ determination.

4.2. HD34078

HD 34078 (also AE Aur) is a runaway O9.5V star possibly formed as a binary (with μ Col, see Hoogerwerf et al. 2001) and ejected after a binary - binary interaction with ι Ori (see Sect. 4.1). The Hipparcos parallax for this star is quite uncertain and corresponds to a distance of 446^{+220}_{-111} pc, or a distance modulus $DM = 8.25^{+0.87}_{-0.62}$.

The visual magnitude is $5.99^{+0.01}_{-0.04}$, $B-V$ is $0.22^{+0.01}_{-0.02}$ so that the absolute visual magnitude is $M_V = -3.92^{+0.69}_{-0.96}$. Fig. 4 shows the best fit of the optical spectrum. From this best fit model, we derive an effective temperature of 33000

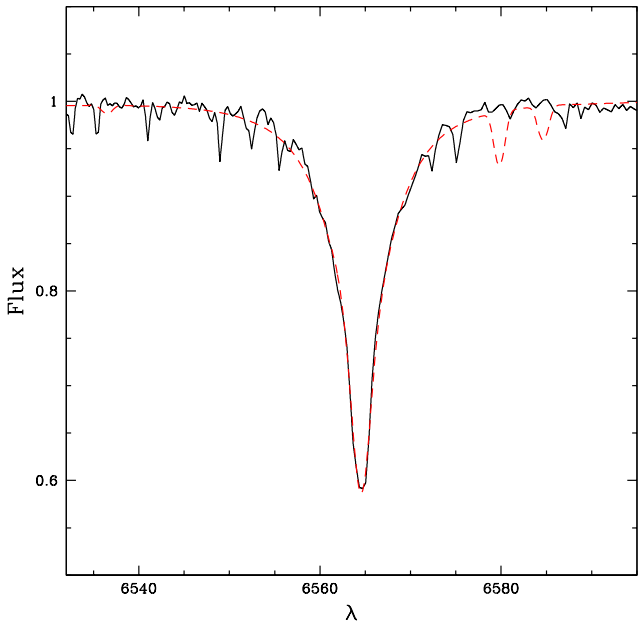

Fig. 5. Best fit (red dashed line) of the observed Hα line (black solid line) of HD 34078. Here, $\dot{M} = 10^{-9.5}$ M$_\odot$ yr^{-1} and $v_\infty = 800$ km s^{-1}.

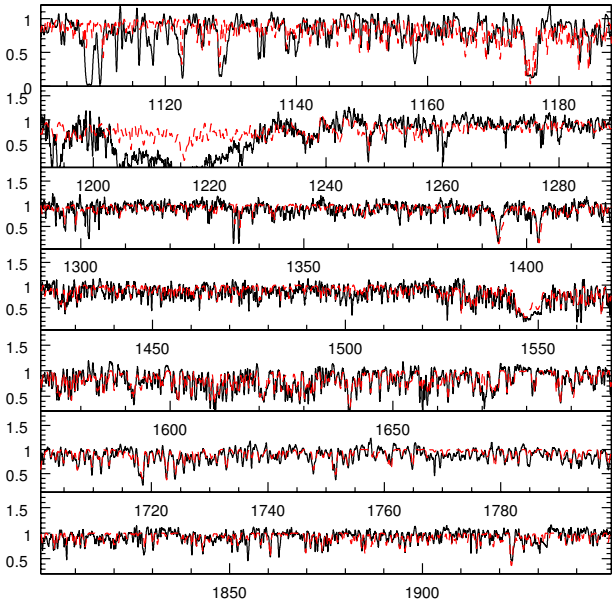

Fig. 6. Best fit (red dashed line) of the UV spectrum (black solid line) of HD 34078. The wind parameters are: $\dot{M} = 10^{-9.5}$ M$_\odot$ yr^{-1}, $v_\infty = 800$ km s^{-1} and $\log L_X/L_{bol} = -7.0$

K. This is confirmed by the good fit of the iron lines shown in Fig. 7. Our $T_{\rm eff}$ is slightly lower than previous determinations (35500 K for Howarth & Prinja 1989 and 36500 K for Villamariz et al. 2002), mainly due to the inclusion of line-blanketing in our study. The rotational velocity has been derived by various authors: Penny (1996) finds 25 km s^{-1} together with Howarth & Prinja (1989), whereas Howarth et al. (1997) give 30 km s^{-1} and Villamariz et al. (2002) prefer a value of 40 km s^{-1}. Our modelling indicates that the latter value seems to better reproduce the observation, especially the optical spectra and we adopt it for V sin$i$. With this rotational velocity and the instrumental resolution (of the order of 0.9 Å), our estimate of $T_{\rm eff}$ has a typical uncertainty of the order of ± 1000 K. Hence, the bolometric correction is $BC = -3.25^{+0.10}_{-0.08}$, the luminosity is $log\frac{L}{L_\odot} = 4.77^{+0.41}_{-0.32}$ and the radius is $R = 7.47^{+4.55}_{-2.83}$ R$_\odot$. The gravity determined by Villamariz et al. (2002) gives a good fit of the Balmer lines, so that we adopt $\log g = 4.05 \pm 0.1$. This leads to $M = 23^{+38}_{-11}$ M$_\odot$.

Figs. 5 and 6 show the fit of the Hα line and UV spectrum of HD 34078. As we have shown that X-rays seem to be important for weak winds (see also next stars) and as HD 34078 shows no sign of a strong wind, we have used an X-ray emission such as $\log L_X/L_{bol} = -7.0$. Indeed, no X-ray measurement exists for HD 34078 and we have thus adopted the classical value for O stars (e.g. Chlebwoski & Garmany 1991). A reasonable agreement between the two types of mass loss indicators (Hα and UV lines) is found for $\dot{M}$= $10^{-9.5}$ M$_\odot$ yr^{-1}and a terminal velocity of 800 km s^{-1}. Howarth & Prinja (1989) found $\dot{M} = 10^{-6.6}$ M$_\odot$ yr^{-1}, a value much higher than ours, but deduced from a method suffering from several assumptions, especially as regards the ionisation fractions. They also deduced v_∞ = 750 km s^{-1}, in good agreement with our determination. A comment must be made here: the terminal velocity is similar to or even lower than the escape velocity (1043 km s^{-1}). However, given the large error on M and R, the escape velocity is also very uncertain. Also, a value of v_∞ lower than v$_{esc}$ is possible since the escape velocity quoted here is the photospheric escape velocity, and a velocity in the wind of the order v_∞ is obtained only in the outer atmosphere where the local escape velocity is much lower.

For HD 34078, we have used the He and CNO abundances of Villamariz et al. (2002). They are nearly solar, except for C which is found to have an abundance of ∼ 1/2 solar.

4.3. HD46202

HD 46202 is an O9 V star situated in the Rosette nebula. The distance to the young cluster in the center of this famous region is 1445 pc from the Webda database, corresponding to a distance modulus of 10.80. Humphreys (1978) gives $DM = 11.03$ for HD 46202, and $DM = 10.91$ as a mean value for the cluster. Hence, we adopt the mean value $DM = 10.85 \pm 0.05$.

The visual magnitude of HD 46202 is 8.18 ± 0.02, and $B - V = 0.17 \pm 0.01$. This leads to $M_V = -4.19 \pm 0.10$. An effective temperature of 33000 K gives the best fit of the optical He lines as shown in Fig. 8. Howarth & Prinja (1989) derived $T_{\rm eff} = 34000$ K and Chlebowski & Garmany (1991) found $T_{\rm eff} = 35900$ K. This is a rather good agree-

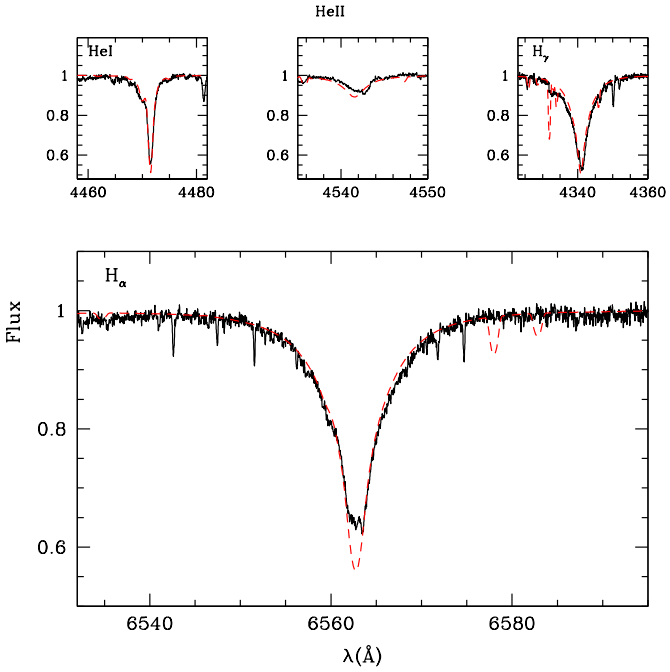

Fig. 8. Best fit (red dashed line) of the optical spectrum (black solid line) of HD 46202. Here, $T_{\rm eff}$ = 33000 K, $\log g$ = 4.0, V sin$i$ = 30 km s^{-1}, $\dot{M}$ = $10^{-8.9}$ M$_\odot$ yr^{-1} and v_∞ = 1200 km s^{-1}. The observed core of Hα is likely contaminated by small interstellar emission.

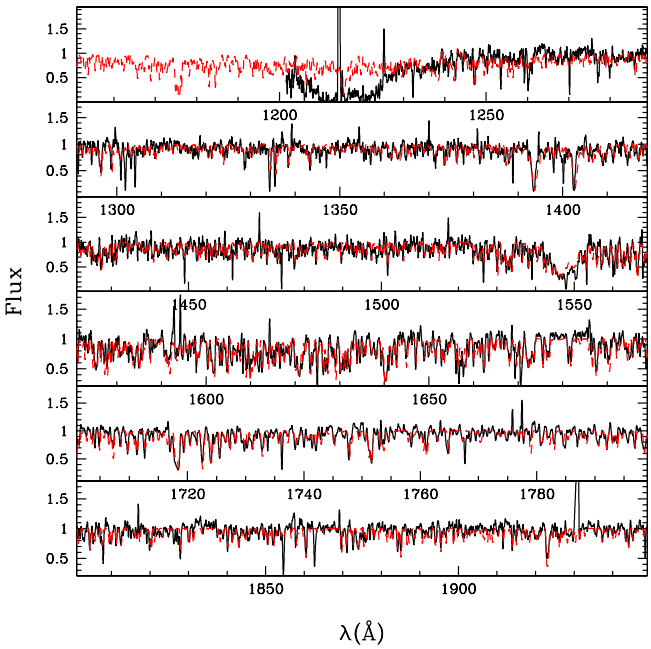

Fig. 9. Best fit (red dashed line) of the UV spectrum (black solid line) of HD 46202. The wind parameters are: $\dot{M}$ = $10^{-8.9}$ M$_\odot$ yr^{-1} and v_∞ = 1200 km s^{-1}. X-rays are included so that $\log L_{\rm X}/L_{\rm bol} = -6.05$. The IUE spectrum below 1200 Å is not shown since the low S/N ratio does not allow any reliable comparison.

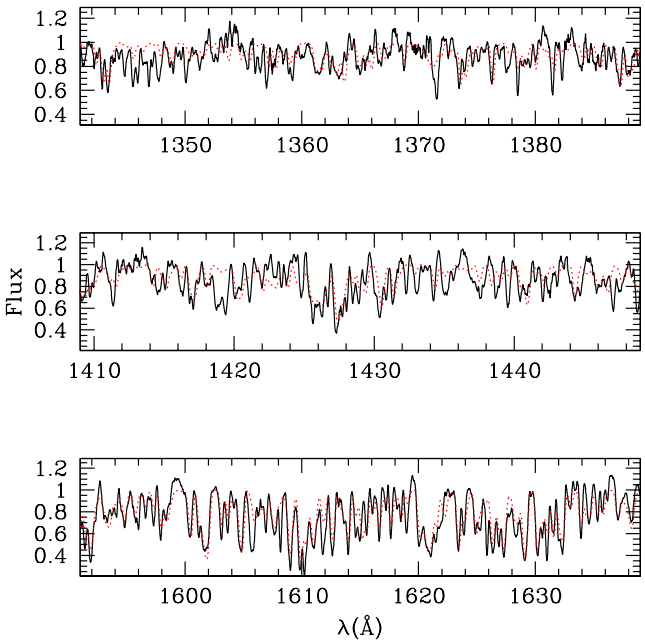

Fig. 7. Zoom on the Iron line forests from Fig. 6 showing the good agreement between the predicted spectrum (dotted line) and the observed spectrum (solid line) and confirming the $T_{\rm eff}$ estimate.

ment with our estimate since these two last values relied on atmosphere models without line blanketing, and since for late O spectral types, the reduction of $T_{\rm eff}$ due to line-blanketing is between 1000 and 2000 K (e.g. Martins et al. 2002a). The typical uncertainty is ± 1000 K. In our models, we adopted V sin$i$ = 30 km s^{-1}since Penny (1996) gives 26 km s^{-1}and Howarth et al. (1997) give 37 km s^{-1}. A gravity of $\log g = 4.0$ gives a good fit of the Hγ line (see Fig. 8). The bolometric correction is $BC = -3.25^{+0.10}_{-0.08}$ and the luminosity is thus $log\frac{L}{L_\odot} = 4.87 \pm 0.07$. The derived radius is $R = 8.38^{+0.88}_{-0.81}$ R$_\odot$ and the mass is $M = 26^{+9}_{-7}$ M$_\odot$.

Fig. 8 and 9 show the fit of the wind sensitive lines from which we derive a mass loss rate of $10^{-8.9}$ M$_\odot$ yr^{-1} and a terminal velocity of 1200 km s−1. According to the X-ray detection, we have chosen $\log\frac{L_{\rm X}}{L_{\rm bol}} = -6.10$ (see Table 3). If X-rays are not included, a value of $\dot{M}$ as low as 10^{-10} M$_\odot$ yr^{-1} is required to fit the wind part of C IV $\lambda\lambda$1548,1551. Note that the core of the Hα line is stronger in the model, but as the observed profile seems to be somewhat contaminated (possibly by a small nebular contribution), we did not try to fit this core. As C IV $\lambda\lambda$1548,1551 is the main $\dot{M}$ indicator and as $\log\frac{L_{\rm X}}{L_{\rm bol}}$ is quite high for this star, we have run test models including the high ionisation states C V and C VI to check if the C ionisation was modified. They show that the C ionisation is indeed slightly increased, which implies to increase $\dot{M}$ by a factor of $\sim$ 2 in order to fit C IV $\lambda\lambda$1548,1551. Hence, given the uncertainty in $\log\frac{L_{\rm X}}{L_{\rm bol}}$ (due to both uncertainties in $L_{\rm X}$ and $L_{\rm bol}$), we think this effect is negligible compared

to other sources of errors for the $\dot{M}$ determination (see Sect. 6). Howarth & Prinja (1989) found $\log \dot{M} = -7.2$, Leitherer (1988) gives $\log \dot{M} \leq -6.87$ and Chlebowski & Garmany (1991) derived $\log \dot{M} = -8.10$. All these values are higher than our estimate. As for v_∞, Howarth & Prinja (1989) give 750 km s^{-1}, Chlebowski & Garmany (1991) 1150 km s^{-1}, Bernabeu et al. (1989) 1590 km s^{-1}and finally Leitherer (1988) 2100 km s^{-1}. Our estimate is within the very wide range of values derived for this star. The low terminal velocity will be discussed in Sect. 7.2.1.

4.4. HD46223

HD 46223 belongs to the Rosette cluster (NGC 2244) and has a spectral type O4V. The distance modulus of the cluster has been derived in the previous Section and is chosen to be $DM = 10.85 \pm 0.05$. Humphreys (1978), Maíz-Apellániz et al. (2004) and the Simbad database agree to give $B - V = 0.22$, corresponding to $E(B - V) = 0.54$, and according to the same sources, the visual magnitude is $V = 7.27^{+0.05}_{-0.02}$. The resulting absolute magnitude is thus $M_V = -5.25^{+0.1}_{-0.07}$. Penny (1996) quotes a projected rotational velocity of 103 km s^{-1}, Howarth et al. (1997) give 82 km s^{-1}and Howarth & Prinja (1989) claim 140 km s^{-1}. From these estimates and our own fits of optical lines, we adopt V sin$i$ = 130 km s^{-1}as a reliable value. The upper panels of Fig. 10 show the fit of He optical lines with a model for which $T_{\rm eff}$ = 41500 K. The typical uncertainty of our $T_{\rm eff}$ determination is of ± 2000 K since we do not have many indicators. Note that the effective temperature adopted from the optical gives a reasonable fit of the UV spectrum (see Fig. 11). The associated bolometric correction is $BC = -3.93 \pm 0.15$ which implies $log\frac{L}{L_\odot} = 5.57^{+0.09}_{-0.10}$ and $R = 11.86^{+1.78}_{-1.58}$. As we do not have reliable gravity indicators, we adopt once again $\log g = 4.0 \pm 0.1$. This leads to $M = 51^{+22}_{-16}$ M$_\odot$.

As regards the terminal velocity, we find v_∞ = 2800 km s^{-1}from the UV resonance lines. This is in fairly good agreement with previous estimates which give values between 2800 and 3140 km s^{-1}(Bernabeu et al. 1989, Howarth et al. 1997, Prinja et al. 1990, Lamers et al. 1993, 1995, 1999, Chlebowski & Garmany 1991, Leitherer 1988, Howarth & Prinja 1989). The mass loss rate is derived from Hα and the UV resonance lines. The adopted value for $\dot{M}$ is $10^{-6.5}$ M$_\odot$ yr^{-1}. However, a comment is necessary here. Indeed, to fit reasonably all the UV lines, we had to use clumped models. This is especially true for O V λ1371 since as previously shown by Bouret et al. (2003) this line is predicted too strong in homogeneous models. In our case, the use of clumping with the law given in Sect. 3.2 and $f_\infty = 0.1$ improves the fit of O V λ1371, as shown in Fig. 11. As the inclusion of clumping leads to mass loss rates lower than in homogeneous winds, this explains partly why our estimate is nearly a factor 5 lower than most previous estimates for this star which did not use clumping: Chlebowski & Garmany (1991) derived $\dot{M} = 10^{-5.62}$ M$_\odot$ yr^{-1}, Leitherer (1988) gives $10^{-5.75}$ M$_\odot$ yr^{-1}, Howarth & Prinja (1989) $10^{-5.8}$ M$_\odot$ yr^{-1}, Lamers et al. (1993) $10^{-5.68}$ M$_\odot$ yr^{-1}and Lamers et al. (1999) $10^{-5.85}$ M$_\odot$ yr^{-1}. Note that in our models, the inclusion of clumping reduces the strength of N V λ1240 which is then less well fitted than in the case of the homogeneous model. However, the very blue part of the absorption profile is contaminated by interstellar Lyman absorption rendering the exact line profile uncertain.

4.5. HD93146

HD 93146 is an O6.5V star in the Carina nebula and belongs to the cluster Cr 228. The WEBDA database gives d = 2200 pc (corresponding to $DM = 11.71$), while Massey et al. (2001) give $d = 3100$ pc ($DM = 12.46$). Humphreys (1978) claim an intermediate value with $DM = 12.18$ for the cluster. Adopting the median value (corresponding to $d = 2490$ pc), we have $DM = 12.09 \pm 0.37$.

The visual magnitude is 8.43 ±0.02 (from Maíz-Apellániz et al. 2004, Massey et al. 2001 and the Simbad database), and the color excess is $E(B - V) = 0.34^{+0.01}_{-0.02}$. This leads to an absolute visual magnitude $M_V = -4.70 \pm$ 0.45. Penny (1996) derived a projected rotational velocity of 83 km s^{-1} whereas Howarth et al. (1997) found V sin$i$ = 79 km s^{-1}. We adopt V sin$i$ = 80 km s^{-1}. Fig. 12 shows our best fit to the optical spectrum of HD 93146. The corresponding effective temperature is 37000 K as derived form the fit of He lines between 5000 and 6000 Å. Notice that this fit is not perfect, but it is actually the best we could get. Increasing $T_{\rm eff}$ may help reduce the He I absorption, but it increases too much the He II strength. Besides this, the UV photospheric lines are very well reproduced with this $T_{\rm eff}$ (see Fig. 13). Due to the small number of $T_{\rm eff}$ indicators, the uncertainty is ± 2000 K leading to a bolometric correction $BC = -3.59^{+0.13}_{-0.15}$. We have thus the following range for the luminosity: $log\frac{L}{L_\odot} = 5.22^{+0.23}_{-0.25}$. The corresponding radius is $R = 9.97^{+3.29}_{-2.49}$ R$_\odot$. As we do not have reliable gravity estimators, we assume $\log g = 4.0 \pm 0.1$ since this value is typical of dwarfs (e.g. Vacca et al. 1996). This allows to estimate the mass of HD 93146: $M = 36^{+31}_{-17}$ M$_\odot$.

Fig. 13 shows our best fit of the (extreme) UV spectrum of HD 93146. The terminal velocity is 2800 km s^{-1}and the mass loss rate is $10^{-7.25}$ M$_\odot$ yr^{-1}. For higher values, N IV λ1718 displays a too strong blueshifted absorption. The Hα profile of Fig. 12 confirms partly this value of $\dot{M}$ since the line is correctly reproduced, under the uncertainty of the exact depth of the core which is contaminated by nebular emission. The only mass loss rate determination for HD 93146 was made by Howarth & Prinja (1989) who found $\log \dot{M} = -6.9$, only a factor $\sim$ 2 higher than our estimate. Concerning v_∞ Bernabeu et al. (1989) found 3200 km s^{-1}, Howarth et al. (1997) 2640 km s^{-1}, Howarth & Prinja (1989) 2975 km s^{-1}and Prinja et al. (1990) 2565 km s^{-1}. All these values are in good agreement with our determination.

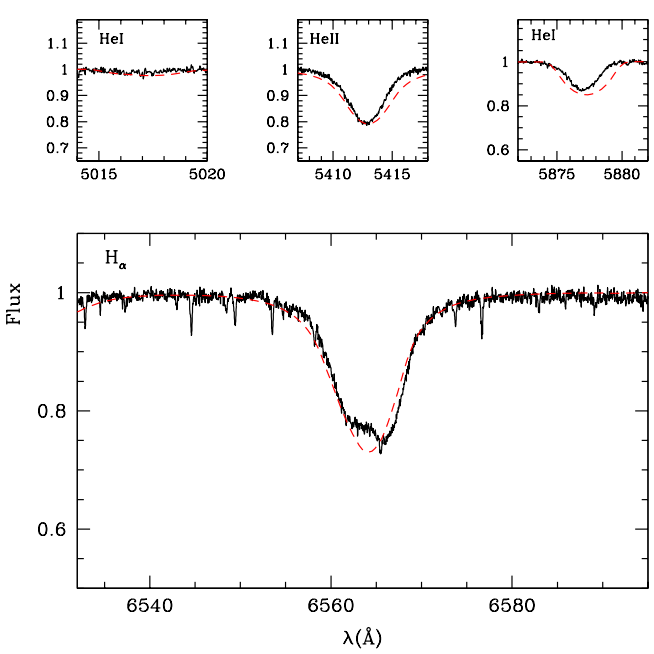

Fig. 10. Best fit (red dashed line) of the observed He and Hα lines (black solid line) of HD 46223. The effective temperature is 41500 K, $\log g = 4.0$ and $V \sin i = 130$ km s^{-1}.

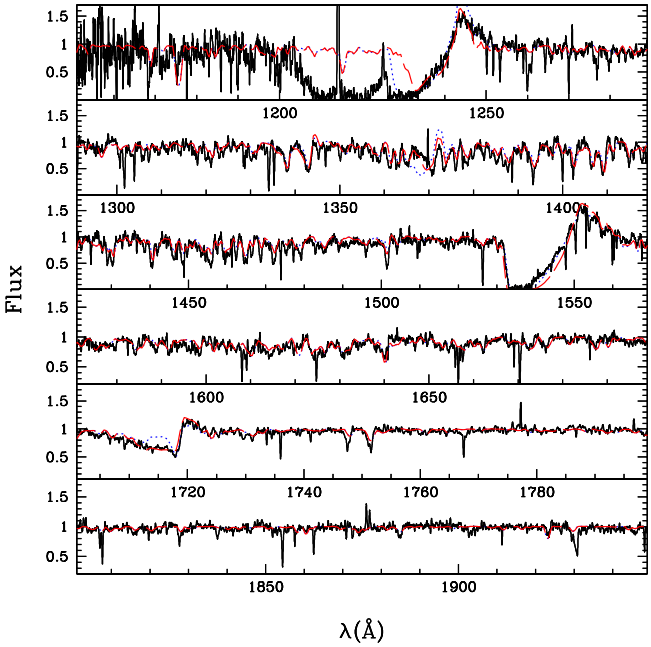

Fig. 11. Best fit of the UV spectrum (black solid line) of HD 46223. For this model, $\dot{M} = 10^{-6.5}$ M$_\odot$ yr^{-1}and $v_\infty = 2800$ km s^{-1}. The red dashed line is a clumped model with $f_\infty = 0.1$ and the blue dotted line is a homogeneous model.

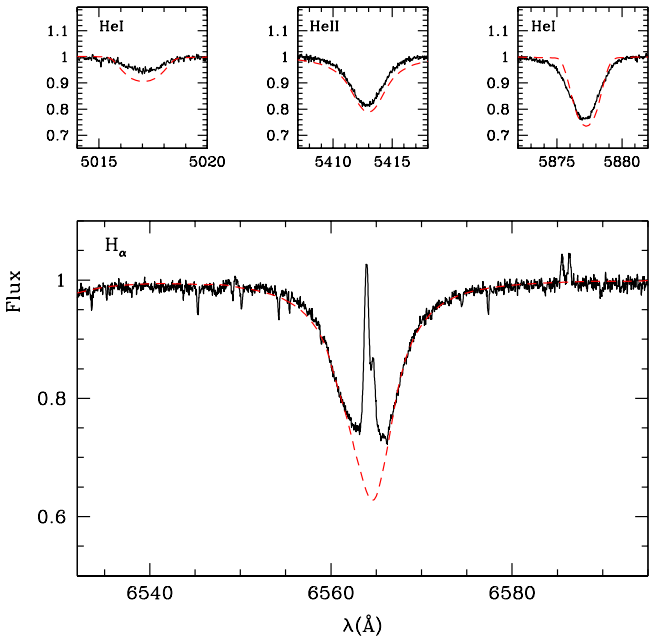

Fig. 12. Best fit (red dashed line) of the observed He and Hα lines (black solid line) of HD 93146. The effective temperature is 37000 K, $\log g = 4.0$ and $V \sin i = 80$ km s^{-1}.

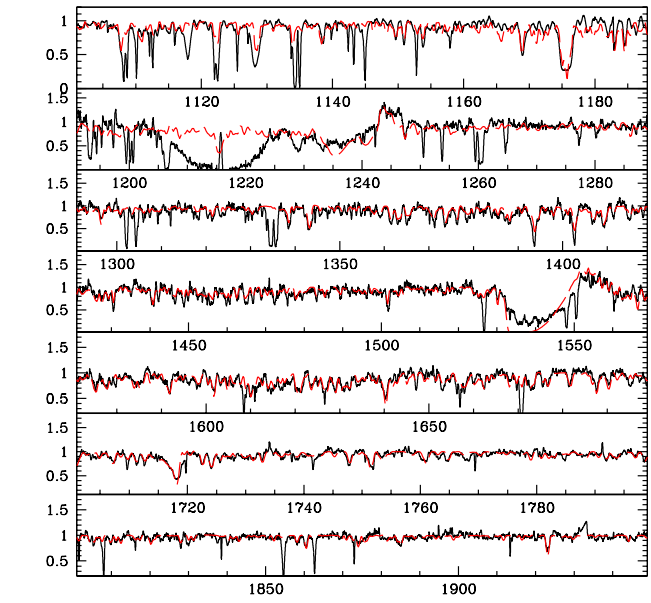

Fig. 13. Best fit (red dashed line) of the UV spectrum (black solid line) of HD 93146. For this model, $\dot{M} = 10^{-7.25}$ M$_\odot$ yr^{-1}and $v_\infty = 2800$ km s^{-1}.

4.6. HD93028

HD 93028 has a spectral type O9V and, as HD 93146, belongs to the young cluster Collinder 228 in the Carina nebula. Hence the discussion concerning the distance is the same as for HD 93146 and we adopt $DM = 12.09^{+0.37}_{-0.38}$.

With $V = 8.36$ (Maíz-Apellániz et al. 2004, Massey et al. 2001, the Simbad database and Humphreys 1978) and $E(B-V) = 0.26$, the absolute magnitude is $M_V =$

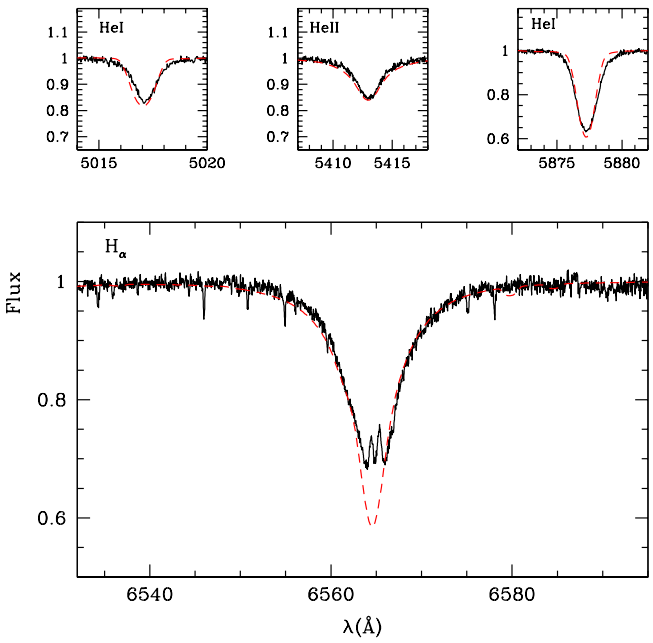

Fig. 14. Best fit (red dashed line) of the observed He and Hα lines (black solid line) of HD 93028. The effective temperature is 34000 K, $\log g = 4.0$ and $V \sin i = 50$ km s^{-1}.

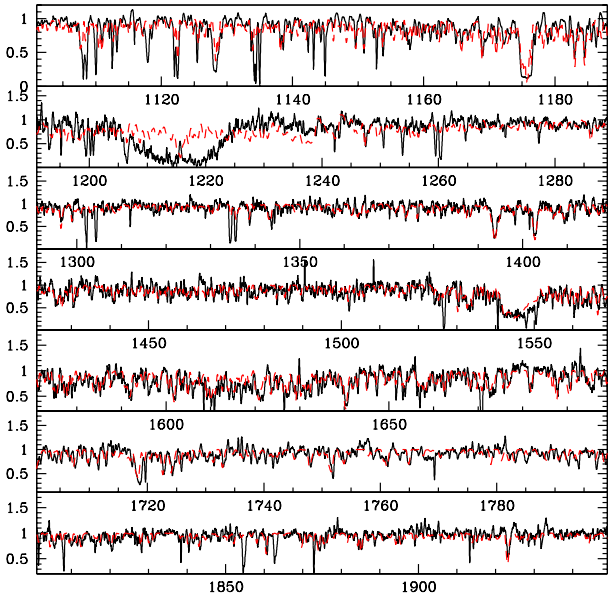

Fig. 15. Best fit (red dashed line) of the UV spectrum (black solid line) of HD 93028. For this model, $\dot{M} = 10^{-9.0}$ M$_\odot$ yr^{-1}, $v_\infty = 1300$ km s^{-1}and we adopted $\log \frac{L_X}{L_{bol}} = -7.0$.

$-4.54^{+0.38}_{-0.37}$. The rotational velocity given by Penny (1996) is 43 km s^1 and Howarth et al. 1997 give a similar value (42 km s^{-1}), while Howarth & Prinja (1989) derive $V \sin i$ = 80 km s^{-1}. From these estimates and our own fits, we adopt a value of 50 km s^{-1}. The effective temperature we derive from He optical lines is 34000 K with a typical uncertainty of ± 2000 K. Fig. 14 shows our best fit of the $T_{\rm eff}$ diagnostic lines. We deduce a bolometric correction $BC = -3.34^{+0.18}_{-0.17}$ which leads to $log\frac{L}{L_\odot} = 5.05 \pm 0.22$ and $R = 9.71^{+3.11}_{-2.38}$. Again, a gravity such as $\log g = 4.0 \pm 0.1$ is adopted and gives $M = 34^{+28}_{-16}$ M$_\odot$.

From the C IV $\lambda\lambda$1548,1551 line, we derive a terminal velocity of 1300 km s^{-1}, slightly lower than the estimate of Bernabeu et al. (1989, 1780 km s^{-1}) and Howarth & Prinja (1989, 1500 km s^{-1}). We find that a mass loss rate of $10^{-9.5}$ M$_\odot$ yr^{-1} gives a good fit of the extreme UV, far UV Hα spectrum without X rays. However, as we have shown previously, X-rays influences strongly the determination of $\dot{M}$ in stars with weak winds (see Sect. 4.1, 4.3). Hence, although there is no measurement of X-rays for HD 93028, we adopted the classical value $\log \frac{L_X}{L_{bol}} = -7.0$ (Chlebowski & Garmany citechleb) and then derived $\dot{M}$ = $10^{-9.0}$ M$_\odot$ yr^{-1} as shown in Figs. 14 and 15. The core of Hα is a little too strong in our best fit model, but the observed line shows evidences of interstellar contamination, which is natural in a star forming region (see also the Hα profile of HD 93146). The only previous determination of mass loss rate for HD 93028 was made by Howarth & Prinja (1989) who found $\dot{M} = 10^{-7}$ M$_\odot$ yr^{-1}, more than two orders of magnitude higher than our value.

4.7. HD93204

HD 93204 (O5V((f))) is a member of the young cluster Trumpler 16 in the Carina complex. Several values for the distance modulus to the cluster exist: 12.15 (Humphreys 1978), 12.55 (Massey et al. 2001), 12.79 (DeGioia et al. 2001), 12.07 (Mason et al. 1998) and 12.13 (WEBDA database). We adopt the mean value as representative: $DM = 12.34^{+0.45}_{-0.27}$.

The visual magnitude and visual color excess are respectively 8.44±0.02 and 0.42±0.01, leading to M_V = $-5.20^{+0.34}_{-0.48}$. Penny(1996) finds a projected rotational velocity of 130 km s^{-1}, Howarth et al. (1997) give 137 km s^{-1}and Howarth & Prinja (1989) derive 155 km s^{-1}. We adopt the value 130 km s^{-1} for $V \sin i$ in our fits, which helps to derive an effective temperature of 40000 K, with an uncertainty of ± 2000 K (see Fig. 16) corresponding to $BC = -3.82^{+0.14}_{-0.16}$. Lamers et al. (1995) found $T_{\rm eff}$ = 44300 K and Howarth & Prinja (1989) gave $T_{\rm eff}$ = 45500 K. The use of line-blanketing in our models explains the difference with our determination. A gravity of $\log g = 4.0 \pm 0.1$ is compatible with the observed Balmer lines. Hence, we derive $log\frac{L}{L_\odot} = 5.51^{+0.25}_{-0.20}$, $R = 11.91^{+4.23}_{-3.14}$ R$_\odot$ and $M = 52^{+47}_{-25}$ M$_\odot$.

Fig. 17 shows the fit of the UV spectrum. As for HD 46223, the inclusion of clumping is required to fit the O V λ1371 and N IV λ1718 lines which are too strong in homogeneous winds (see also Bouret et al. 2005). Reducing $T_{\rm eff}$ does not solve the problem since in that case O V λ1371 is weaker but N IV λ1718 gets stronger. We derive a mass loss rate of $10^{-6.75}$ M$_\odot$ yr^{-1} and a terminal velocity of

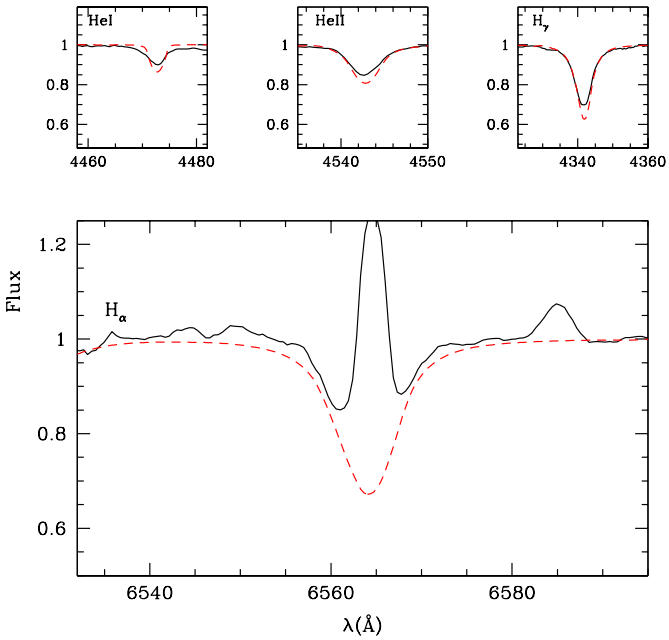

Fig. 16. Best fit (red dashed line) of the observed He and Hα lines (black solid line) of HD 93204. The effective temperature is 40000 K, $\log g = 4.0$, $V \sin i = 130$ km s^{-1} and $\dot{M} = 10^{-6.75}$ M$_\odot$ yr^{-1}.

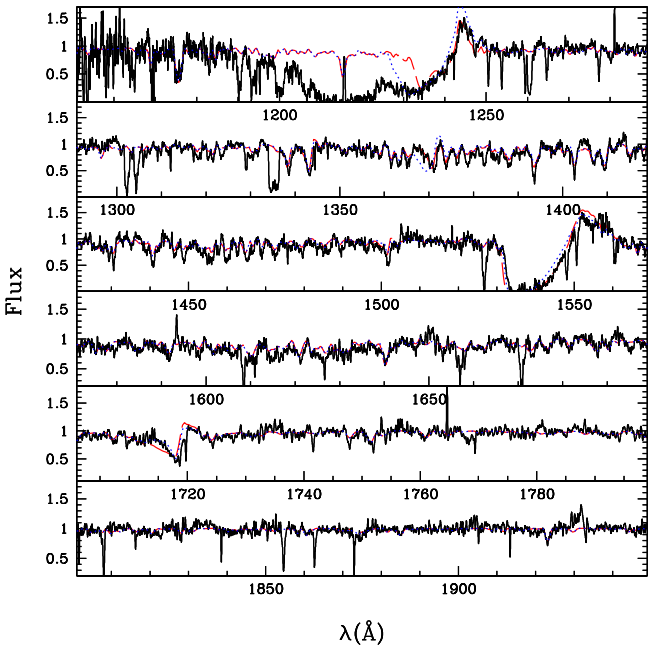

Fig. 17. Best fit of the UV spectrum (black solid line) of HD 93204. For this model, $\dot{M} = 10^{-6.75}$ M$_\odot$ yr^{-1}and $v_\infty = 2900$ km s^{-1}. The red dashed line is a clumped model with $f_\infty = 0.1$ and the blue dotted line is a homogeneous model.

2900 km s^{-1}. Due to the high level of nebular contamination of Hα, we can not use this line to constrain $\dot{M}$ (see Fig. 16). The only previous value for $\dot{M}$ we found in the literature is that of Howarth & Prinja (1989): $10^{-6.1}$ M$_\odot$ yr^{-1}. Concerning the terminal velocity, Bernabeu et al. (1989) found 3180 km s^{-1}, Howarth et al. (1997) and Prinja et al. (1990) 2890 km s^{-1}, Lamers et al. (1995) 2800 km s^{-1}and Howarth & Prinja (1989) 3250 km s^{-1}. Our estimate is well within the range of values previously derived.

4.8. HD93250

HD 93250 is a well studied O dwarf of the Trumpler 16 cluster in the Carina region. It is a prototype of the recently introduced O 3.5 subclass (Walborn et al. 2002). We adopt the same distance modulus as HD 93204 (another Trumpler 16 member): $DM = 12.34^{+0.45}_{-0.27}$.

With a visual magnitude $V = 7.38 \pm 0.02$ and a visual extinction $A_V = 1.49$, the bolometric magnitude is $M_V = -6.45^{+0.29}_{-0.48}$. Several authors derived the projected velocity $V \sin i$: Penny (1996) found 112 km s^{-1}, Howarth et al. (1997) 107 km s^{-1}, Howarth & Prinja (1989) 100 km s^{-1}and Repolust et al. (2004) 130 km s^{-1}. All these values are in good agreement, and we adopt 100 km s^{-1} as a reasonable value. Using optical He lines, we estimate the effective temperature to be $\sim$ 46000 K, mainly from the strength of He I λ4471(see Fig. 18). However, Fe line forests in the UV are more consistent with a value of 42000-44000 K as displayed in Fig. 20. For such a $T_{\rm eff}$ He I λ4471 is a little too strong in the model. However, this seems to be the case of all H and He optical lines, possibly due to the fact that HD 93250 may be a binary (see Repolust et al. 2004) which may also be advocated from the fact that the absorption of C IV $\lambda\lambda$1548,1551 is not black despite the strength of the line. Hence, we rely mainly on the UV and we adopt a value of 44000 K for the effective temperature of HD 93250, with an uncertainty of $\pm$ 2000 K. This value is in reasonable agreement with the determination of Repolust et al. (2004) who found 46000 K. Previous estimates led to higher values (52500 K for Howarth & Prinja 1989, 50500 K for Puls et al. 1996 and 51000 K for Vacca et al. 1996) but they relied on unblanketed models which are known to overestimate effective temperatures by nearly 4000 K for early type dwarfs (Martins et al. 2002a). Given that, the bolometric correction is $BC = -4.10 \pm 0.12$ and leads to $\log \frac{L}{L_\odot} = 6.12^{+0.25}_{-0.17}$, in reasonable agreement with other determinations (6.4 for Howarth & Prinja 1989, 6.01 for Repolust et al. 2004 and 6.28 for Puls et al. 1996). This corresponds to $R = 19.87^{+6.98}_{-3.87}$ which, with a gravity of $\log g = 4.0 \pm 0.1$ taken from Repolust et al. (2004) and consistent with our fits, finally leads to $M = 144^{+130}_{-56}$ M$_\odot$. Notice that this mass estimate is very high, but also very uncertain !

The determination of the wind parameters relies on Hα and on several strong UV lines: N V λ1240, O IV $\lambda\lambda$1339,1343, O V λ1371, C IV $\lambda\lambda$1548,1551, He II λ 1640 and N IV λ1718. The terminal velocity deduced mainly from C IV $\lambda\lambda$1548,1551 is 3000 km s^{-1}, slightly lower

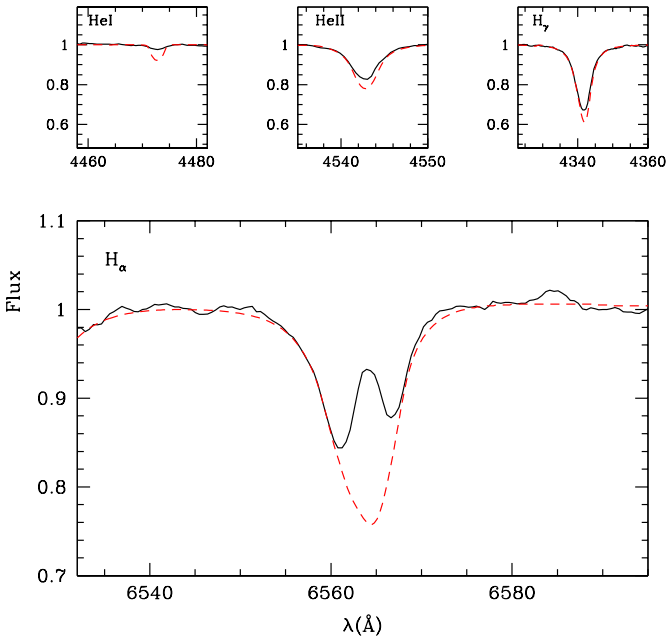

Fig. 18. Best fit (red dashed line) of the observed He and Hα lines (black solid line) of HD 93250. The effective temperature is 46000 K, $\log g = 4.0$, $V \sin i = 110$ km s^{-1} $\dot{M} = 10^{-6.25}$ M$_\odot$ yr^{-1}, $v_\infty = 3000$ km s^{-1} and $f_\infty = 0.01$.

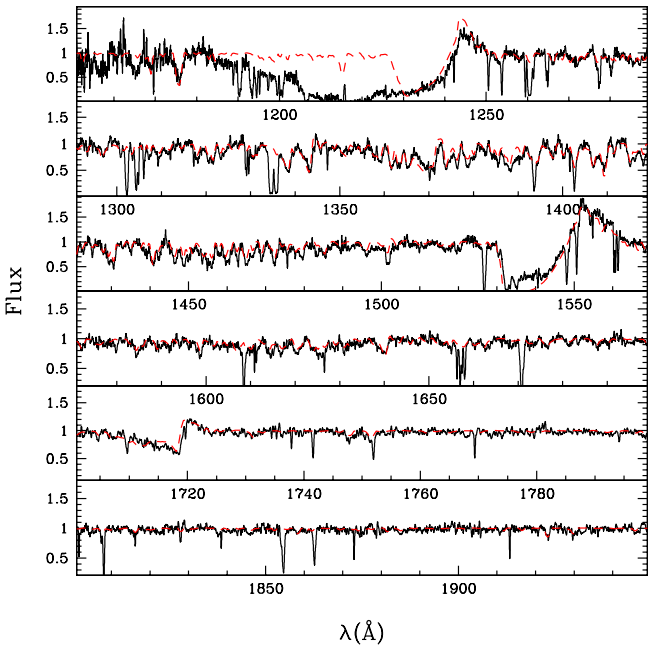

Fig. 19. Best fit of the UV spectrum (black solid line) of HD 93250. For this model (red dashed line) $\dot{M} = 10^{-6.25}$ M$_\odot$ yr^{-1}, $v_\infty = 3000$ km s^{-1}and $f_\infty = 0.01$.

than the previously derived values which are between 3250 km s^{-1}(Repolust et al. 2004) and 3470 km s^{-1} (Bernabeu 1989). However, we use a microturbulent velocity of 200 km s^{-1}in the outer part of our model atmosphere for this star, so that in practice, the absorption extends up to 3200 km s^{-1}. As regards the mass loss rate, we actually found that it was impossible to find a value for $\dot{M}$ which would produce reasonable fits of all UV lines in homogeneous winds. Indeed, O V λ1371 was always too strong and N IV λ1718 too weak. Reducing the effective temperature does not improve the situation, since values as low as 40000 K are required to fit O V λ1371, and in that case the other UV lines are not correctly fitted so that again, we had to include clumping. In the end, we find that a mass loss rate of $10^{-6.25}$ M$_\odot$ yr^{-1}with a clumping factor $f_\infty = 0.01$ gives a reasonable fit, as displayed in Fig. 19. This value of $\dot{M}$ is lower than the determination of Repolust et al. (2004) – $10^{-5.46}$ M$_\odot$ yr^{-1}– relying only on Hα. We will return to this in Sect. 7.2.2.

4.9. HD152590

HD 152590 is an O7.5Vz star. Its distance is rather difficult to estimate: it is possibly a member of the cluster Trumpler 24 in which case its distance modulus is 10.28 (WEBDA database), or a member of NGC 6231 for which the distance modulus is 10.47. Humphreys (1978) derived $DM = 11.41$ for the Sco OB1 association to which HD 152590 may be also related. Given the uncertainty on the distance, we simply adopt the mean value $10.72^{+0.69}_{-0.44}$.

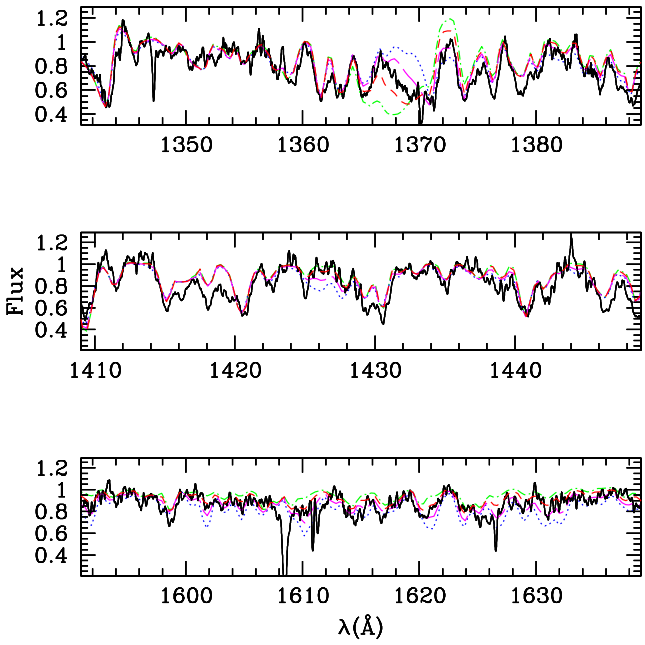

Fig. 20. Determination of effective temperature from UV Fe line forests. Solid line is the observed spectrum, dotted line a model with $T_{\rm eff} = 40000$ K, long dashed line a model with $T_{\rm eff} = 42000$ K, short dashed line a model with $T_{\rm eff} = 44000$ K and dot-dashed line a model with $T_{\rm eff} = 46000$ K. See text for discussion

The visual magnitude is much more constrained: $V = 8.44 \pm 0.2$ from various sources (Maíz-Apellániz 2004,

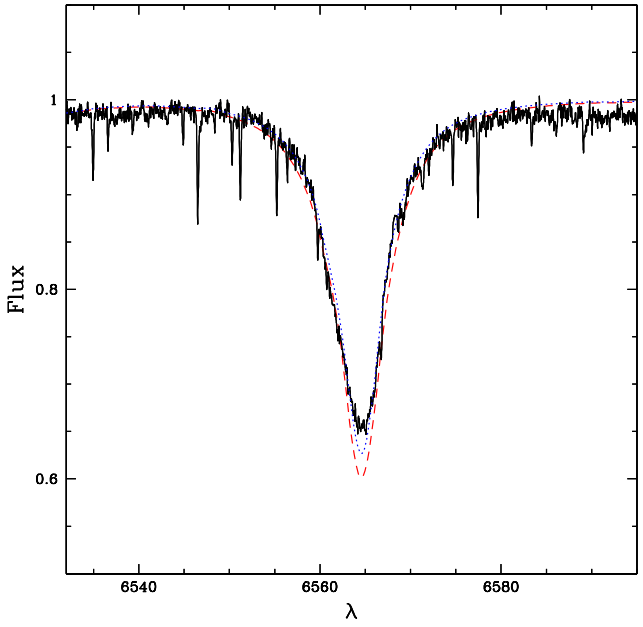

Fig. 22. Fits of the observed Hα line (black solid line) of HD 152590 for a model with $\dot{M} = 10^{-7.78}$ M$_\odot$ yr^{-1} (blue dotted line) and for a model with $\dot{M} = 10^{-8.75}$ M$_\odot$ yr^{-1} (red dashed line). The terminal velocity in both models is 1750 km s^{-1}. Note the insensitivity of Hα line profile to the mass loss rate.

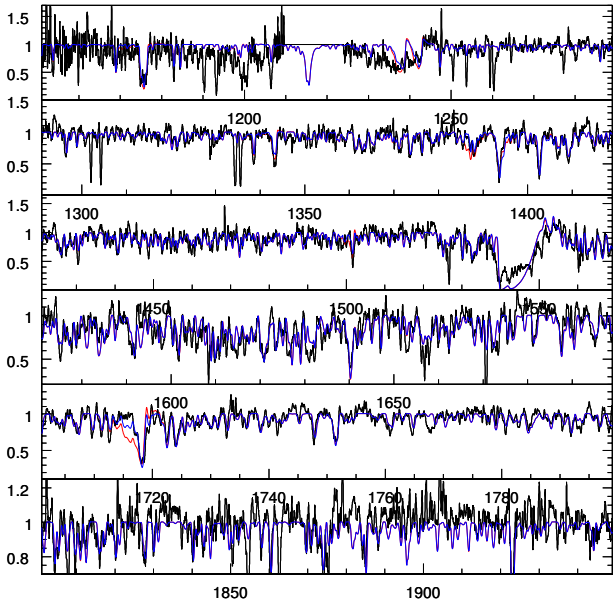

Fig. 23. Same as Fig. 22 for the UV range.

Humphreys 1978 and the Simbad database), and the color excess is $E(B-V) = 0.46 \pm 0.1$. This gives a bolometric magnitude $M_V = -3.71^{+0.51}_{-0.74}$. Penny (1996) determined a rotational velocity of 66 km s^{-1} and Howarth et al. (1997) found 60 km s^{-1}. In our fits, we adopt the value of Penny fot the convolution of our spectra. The optical spectrum shown in Fig. 21 is correctly reproduced with an effective temperature of 36000 K. Note that initially, we had a problem to reproduce the He I singlet lines which were too weak in our models wheras all other lines were very well reproduced. This problem has been recently noted by Puls et al. (2005) when they put forward a discrepancy between CMFGEN and FASTWIND for these lines between 36000 and 41000 K for dwarfs. However, a more complete treatment of line blanketing appeared to solve this problem. Indeed, if we reduce the microturbulent velocity from 20 to 10 km s^{-1} in the computation of the atmospheric structure AND if we add some more species (Neon, Argon, Calcium and Nickel) we greatly improve the fit of the He I singlet lines without modifying the strength of other H and He lines (Hillier et al. 2003 already noted that the He I singlet lines were much more sensitive to details of the modelling than the triplet lines). This is shown in Fig. 21. Hence, we attribute the origin of the discrepancy pinpointed by Puls et al. (2005) to a subtle line-blanketing effect in this particular temperature range, and concerning only the He I singlet lines. Note that reducing v_{turb} without including additional metals strengthens the singlet lines, but not enough to fit the observed spectrum. Hence the additional line-blanketing effects of Ne, Ar, Ca and Ni, although small (most lines are unchanged) is crucial to fit the he I lines around $T_{\rm eff} = 36000$ K.

Due to the good quality of the data and the number of indicators, the uncertainty on this determination is $\pm$ 1000 K. This leads to $BC = -3.51 \pm 0.08$, $\log \frac{L}{L_\odot} = 4.79^{+0.33}_{-0.24}$ and $R = 6.42^{+3.00}_{-2.05}$ R$_\odot$. We found that a gravity $\log g = 4.10 \pm 0.1$ gives the best fit of the Balmer lines (in particular Hγ) which gives $M = 19^{+23}_{-10}$ M$_\odot$.

The terminal velocity of HD 152590 estimated from C IV $\lambda\lambda$1548,1551 is 1750 km s^{-1}, in good agreement with Howarth et al. (1997) - 1785 km s^{-1} - but lower than values derived by Howarth & Prinja (1989) and Chlebowski & Garmany (1991) - 2300 km s^{-1}. The estimate of the mass loss rate is much more difficult for this star. In fact, we have not been able to fit simultaneously the UV lines and Hα. If the former are correctly reproduced (with $\dot{M}$ = $10^{-8.75}$ M$_\odot$ yr^{-1}), then the later has a too strong absorption in its core, and if Hα is fitted (with $\dot{M} = 10^{-7.78}$ M$_\odot$ yr^{-1}), C IV $\lambda\lambda$1548,1551 is too strong. This is shown in Fig. 22 and 23. We have tried without success to increase the β parameter to improve the fit (an increase of β leading to a weaker Hα absorption). The fits of Fig. 22 and 23 are for $\beta = 1.2$ and even for this quite high value for a dwarf star, the Hα core is not perfectly reproduced. A possible explanation is the presence of a companion for HD 152590 (Gieseking 1982). In that case, Hα may be diluted by the continuum of this secondary whereas the UV spectrum may be unaffected provided the companion is a later type star than HD 152590 without strong

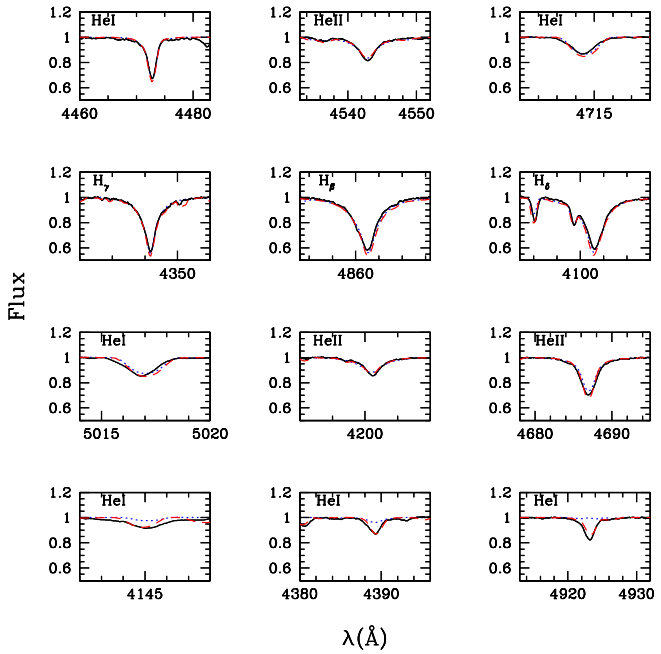

Fig. 21. Best fit of the optical spectrum (black solid line) of HD 152590. The effective temperature is 36000 K, $\log g = 4.1$ and $V \sin i = 66$ km s^{-1}. The blue dotted line is for a standard model while the red dashed line is for a model with $v_{turb} = 10$ km s^{-1} and additional metals (Ne, Ar, Ca and Ni). We see that this improved model leads to better fits of the He I singlet lines, leaving all other lines basically unchanged.

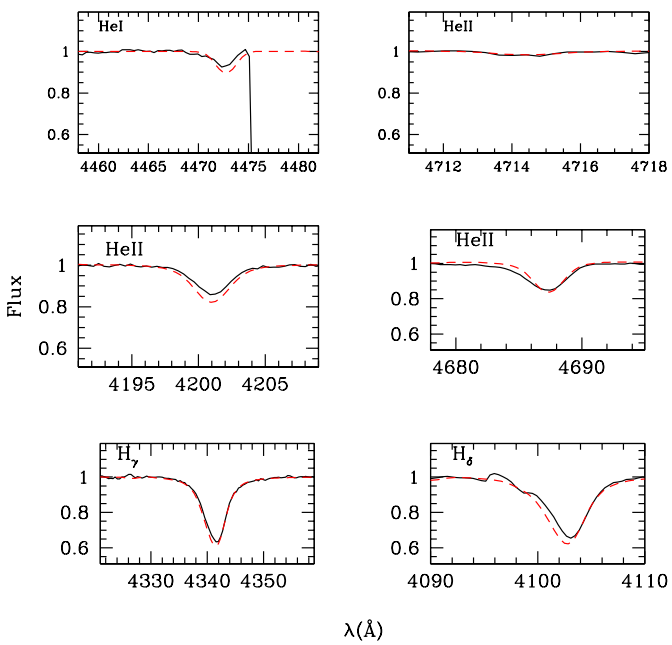

Fig. 26. Best fit (red dashed line) of the observed He and H lines (black solid line) of HD 15629. The effective temperature is 41000 K, $\log g = 3.75$ and $V \sin i = 90$ km s^{-1}.

UV lines. However, adopting a conservative approach, we adopt the Hα mass loss rate ($10^{-7.78}$ M$_\odot$ yr^{-1}) as typical, keeping in mind that it may well be only an upper limit. Howarth & Prinja (1989) derived $\dot{M} = 10^{-6.9}$ M$_\odot$ yr^{-1}and Chlebowski & Garmany (1991) found $\dot{M} = 10^{-7.36}$ M$_\odot$ yr^{-1}.

4.10. HD42088

HD 42088 is a O6.5 V star associated with the H II region NGC 2175. It also belongs to the class of Vz stars. Taking the mean values of the distance modulus between the results of Markova et al. (2004), from Humphreys (1978) and from the distance of NGC 2175 from the WEBDA database, we adopt $DM = 11.20^{+0.30}_{-0.23}$. Note that the distance (and thus luminosity) is the least well known of all stars of our sample.

Given the visual magnitude (7.55) and the visual extinction (1.04) we find $M_V = -4.66^{+0.30}_{-0.33}$. The rotational velocity is chosen to be 60 km s^{-1}in view of the determinations of Penny (1996) - 62 km s^{-1} - and Howarth et al. (1997) - 65 km s^{-1}. The fit of optical He lines above 5000 Å leads to an estimate of the effective temperature which is found to be $\sim$ 38000 K as shown by Fig. 24. This estimate also relies on the fit of UV lines since the number of optical indicators is small. The typical uncertainty is $\pm$ 2000 K. We have thus $BC = -3.67^{+0.16}_{-0.15}$, $\log \frac{L}{L_\odot} = 5.23 \pm 0.19$, $R = 9.56^{+2.61}_{-2.07}$ and, adopting $\log g = 4.0 \pm 0.1$, $M = 33^{+24}_{-14}$ M$_\odot$.

The terminal velocity is derived from the blueward extension of the absorption in C IV $\lambda\lambda$1548,1551 and is 1900 km s^{-1}. Previous determinations go from 2030 km s^{-1}to 2550 km s^{-1}(Leitherer 1988, Howarth & Prinja 1989, Chlebowski & Garmany 1991, Howarth et al. 1997, Bernabeu 1989, Markova et al. 2004). Given the fact that we adopted a microturbulent velocity of 190 km s^{-1}in the outer wind (10 % of v_∞), the absorption actually extends up to 2100 km s^{-1}in the model, in good agreement with other determinations. Concerning the mass loss rate, it turns out that a value of 10^{-8} M$_\odot$ yr^{-1}gives a reasonable fit of the main UV lines and Hα, although for the latter the very core is not correctly fitted but may suffer from nebular contamination (see Fig. 24). The best fit model is shown in Fig. 25. Markova et al. (2004) found $\dot{M} = 10^{-6.42}$ M$_\odot$ yr^{-1} from Hα, Leitherer (1988) $10^{-6.35}$ M$_\odot$ yr^{-1} (Hα), Chlebowski & Garmany (1991) $10^{-6.82}$ M$_\odot$ yr^{-1} (from UV) and Howarth & Prinja (1989) $10^{-7.00}$ M$_\odot$ yr^{-1} (UV). Hence, our determination based on both Hα and UV lines gives a much lower value than ever found for this star. But the UV lines produced by models with mass loss rates much higher than our adopted value are much too strong compared to the observed spectrum, forcing us to adopt such a low $\dot{M}$.

4.11. HD15629

HD 15629 is classified as O5V((f)) and belongs to the star cluster IC 1805 for which the WEBDA database gives

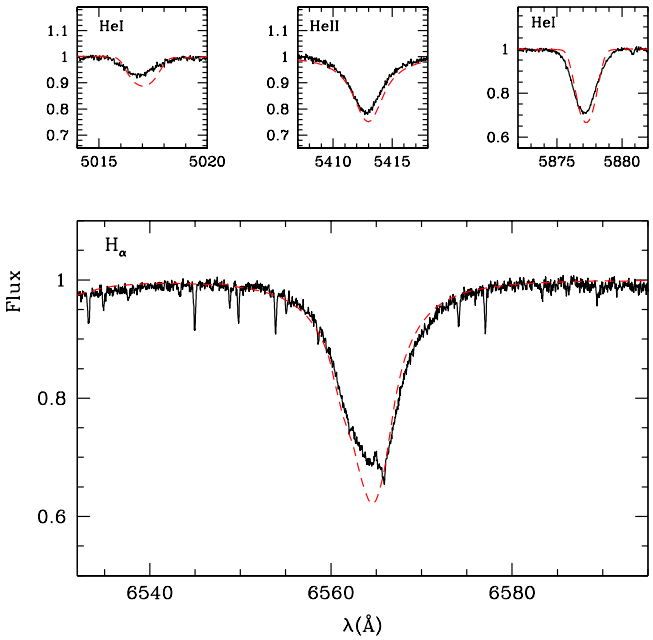

Fig. 24. Best fit (red dashed line) of the observed He and Hα lines (black solid line) of HD 42088. The effective temperature is 38000 K, $\log g = 4.0$ and $V \sin i = 60$ km s^{-1}.

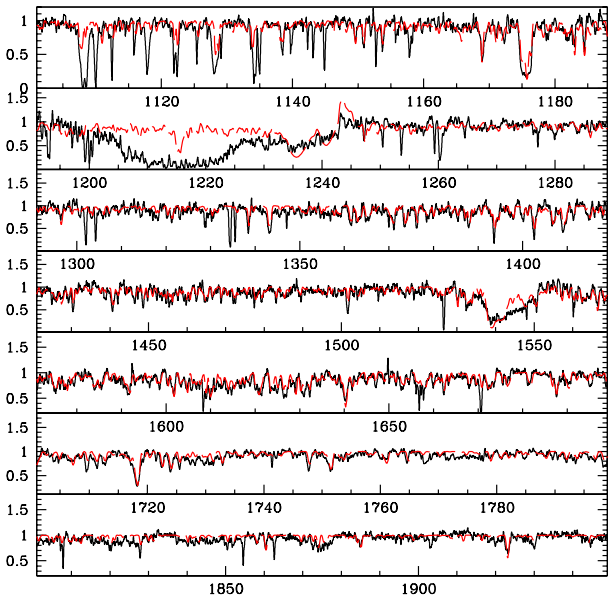

Fig. 25. Best fit (red dashed line) of the UV spectrum (black solid line) of HD 42088. For this model, $\dot{M} = 10^{-8}$ M$_\odot$ yr^{-1}and $v_\infty = 1900$ km s^{-1}.

a distance modulus of 11.38. Humphreys (1978) found DM=11.71 relying on a calibration of absolute magnitude as a function of spectral type. As individual stars may deviate from this relation, we prefer to rely on the result of WEBDA. Hence, we choose $DM = 11.38 \pm 0.3$ to be a reasonable approximation.

With a visual magnitude of 8.42 (Simbad + Maíz-Apellániz et al. 2004) and a visual extinction of 2.29, the absolute magnitude of HD 15629 is -5.25 ± 0.3. The projected rotational velocity is found to be 90 km s^{-1} by Howarth et al. (1997), Penny (1996) and Repolust et al. (2004). We adopted this value in our fits. The optical spectrum presented in Fig. 26 indicates an effective temperature of 41000 K with a conservative uncertainty of $\pm$ 2000 K. This is in good agreement with the recent determination of Repolust et al. (2004) who found 40500 K. The corresponding bolometric correction is -3.89 ± 0.15 which finally leads to $\log \frac{L}{L_\odot} = 5.56 \pm 0.18$ and $R = 12.01^{+3.08}_{-2.47}$ R$_\odot$. We adopted $\log g = 3.75 \pm 0.1$ since it gives a reasonable fit of Balmer lines (Fig. 26) and it is close to the value derived by Repolust et al. (2004) who derived $\log g = 3.70$. This finally leads to $M = 30^{+20}_{-12}$ M$_\odot$.

The best fit model of the UV spectrum is shown in Fig. 28, and Hα is displayed in Fig. 27. The main parameters for this model are $\dot{M} = 10^{-6.5}$ M$_\odot$ yr^{-1}, $v_\infty = 2800$ km s^{-1} and $f_\infty = 0.1$. We also show on these figures a model without clumping and with the mass loss rate of Repolust et al. (2004) which is higher - $10^{-5.89}$ M$_\odot$ yr^{-1}- than our derived value. Once again the inclusion of clumping is necessary to correctly reproduce both O V λ1371 and N IV λ1718. With the Repolust et al. (2004) $\dot{M}$ and no clumping, CNO abundances have to be reduced by a factor of 3 to give reasonable fits, and even in that case the O V λ1371 line is too strong. Such a reduction of the abundances is unlikely for a Galactic star. For our best fit, we have adopted the CNO solar abundances recently claimed by Asplund (2004) since they are slightly lower than those of Grevesse & Sauval (1998) and allow a fit of the UV lines with a slightly higher (0.25 dex) mass loss rate compared to the later values. Note that in our final best fit, the core of Hα is not perfectly fitted. However, we suspect that the strange squared shape of the observed line core is probably contaminated by weak nebular emission. By the way, if we adopt the mass loss rate of Repolust et al. (2004), the flux level in the line core is correct, but the line is slightly narrower in the remainder of the profile compared to the observed profile, while with our $\dot{M}$, the line is well fitted excepted in the very core. Increasing the flux level in the core in models with our $\dot{M}$ requires the adoption of $\beta = 1.7$ which is high for a dwarf. In that case again, although the flux level in the core is correct, the synthetic line profile is too narrow. We are then rather confident that the observed line core is somewhat contaminated and that our mass loss rate is correct. The use of clumping explains partly the discrepancy with the result of Repolust et al. (2004). Concerning the terminal velocities, Repolust et al. (2004) found 3200 km s^{-1}, Howarth et al. (1997) 2810 km s^{-1} and Bernabeu et al. (1989) 3220 km s^{-1}. Given the fact that we again used a microturbulent velocity of 200 km s^{-1}in the outer wind, our estimate of v_∞ (2800 km s^{-1}) is in reasonable agreement with the later determinations.

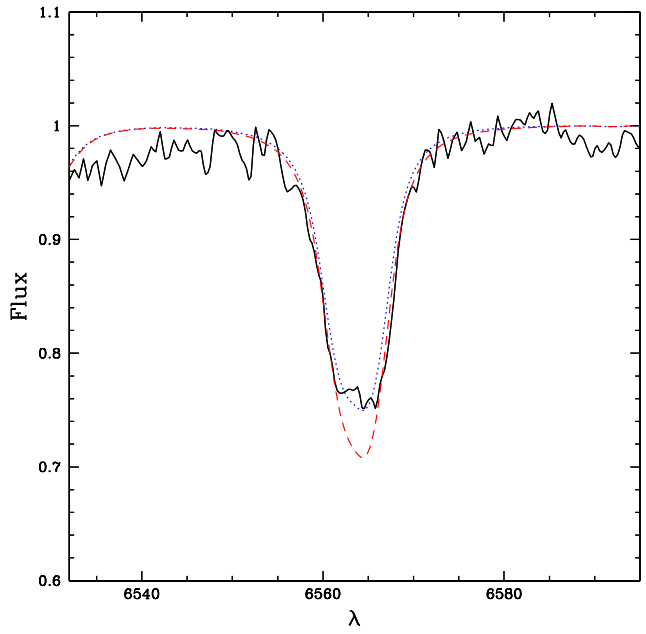

Fig. 27. Best fit (red dashed line) of the observed Hα line (black solid line) of HD 15629. For this model, $\dot{M} = 10^{-6.5}$ M$_\odot$ yr^{-1}, $v_\infty = 2800$ km s^{-1} and $f_\infty = 0.1$. We also show a model with $\dot{M} = 10^{-5.89}$ M$_\odot$ yr^{-1} and no clumping (blue dotted line) as derived by Repolust et al. (2004).

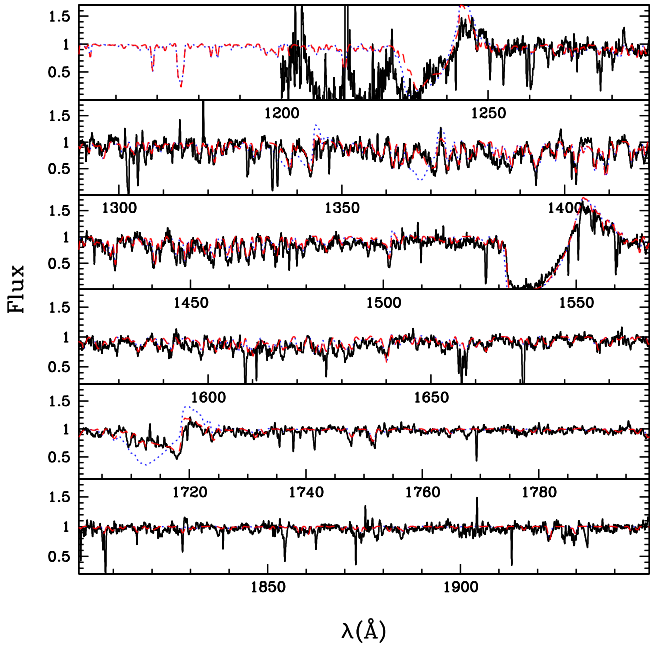

Fig. 28. Best fit (red dashed line) of the UV spectrum (black solid line) of HD 15629. The wind parameters are the same as in Fig. 27. The IUE spectrum below 1200 Å is not shown since the low S/N ratio does not allow any reliable comparison. The blue dotted line is the model with the Repolust et al. (2004) parameters.

5. Role of X-rays and magnetic field in weak-wind stars

Several of our sample stars have published X-ray fluxes. Chlebowski & Garmany (1991) report X-ray measurements for HD 38666, HD 46202, HD 152590, HD 42088 and HD 46223, while Evans et al. (2003) give X-ray luminosities for HD 93204 and HD 93250. These high energy fluxes may have important consequences on the atmosphere structure since, as shown by MacFarlane et al. (1994), the ionisation fractions may be significantly altered. These authors also demonstrated that the effect of X-rays was higher in low-density winds: ionisation in early O stars is almost unchanged by X-rays, while in early B-stars changes as large a factor 10 can be observed between models with and without X-rays. The reason for such a behaviour is that 1) X-rays produce higher ionisation state through Auger process and 2) the ratio of photospheric to X-ray flux decreases when effective temperature decreases, implying an increasing role of X-rays towards late type O and early B stars (see MacFarlane et al. 1994). Moreover, the lower the density, the lower the recombinations to compensate for the Auger ionisation so that we expect qualitatively an even stronger influence of X-rays in stars with low mass loss rate. Since some of our sample stars are late type O stars with low density winds, X-rays can not be discarded in their analysis. Indeed, the Carbon ionisation fraction – and thus the strength of the C IV $\lambda\lambda$1548,1551 line and the derived mass loss rates – can be altered.

In this context, we have first run test models for HD 46202 and HD 93250. For HD 93250, the inclusion of X-rays did not lead to any significant change of the ionisation structure as expected from the above discussion. However, the atmosphere structure of HD 46202 is affected which leads to a weaker C IV $\lambda\lambda$1548,1551 line (for a given $\dot{M}$) as displayed in Fig. 29. Indeed, the ionisation fraction of C IV is reduced. Fitting C IV $\lambda\lambda$1548,1551 thus requires a higher mass loss rate. In practice, the change in the C IV $\lambda\lambda$1548,1551 profile when X-rays are included is equivalent to a reduction of the mass loss rate by a factor of ~ 10 in models without X-rays. Given this result, we have included X-rays in our modelling of the atmosphere of HD 38666, HD 46202, HD 34078 and HD93028. For the two former stars, X fluxes from the literature have been used while for the two latter ones, we simply adopted $\log \frac{L_X}{L_{bol}} = -7.0$.

A question which remains to be answered concerning the X properties of such weak wind stars is the origin of the X-ray emission. Indeed, it is usually believed that shocks in the wind due to instabilities in the line driving mechanism are responsible for the production of such high energy photons (Lucy & White 1980, Owocki, Castor & Rybicki 1988). However, recent observations by Chandra have revealed that for the B0V star τ Sco and for the Trapezium stars, most of the lines emitted in the X-ray range were too narrow to have been produced in the wind up to velocities of the order v_∞ as expected in the wind-

shock scenario (see Cohen et al. 2003, Schulz et al. 2003). And these lines are also not formed very close to the photosphere as predicted by a model in which the X-ray emission is due to a hot corona (e.g. Cassinelli & Olson 1979). Actually, such lines are more likely to be formed in an intermediate region. This may be explained in the context of magnetically confined winds: in this scenario, the presence of a magnetic field confines the outflow and chanels it into the equatorial plane where shocks produce X-ray emission above the photosphere but not in the upper atmosphere (See Babel & Montmerle 1997). This model has been recently refined by Ud'Doula & Owocki (2002) who have investigated the structure of both the wind outflow and the magnetic field through time dependent hydrodynamic simulations. In particular, they estimated from simple arguments the strength of the magnetic field required to confine the wind (hereafter B') and thus to lead to shocks in the equatorial plane.

In Table 3, we have gathered different properties of the stars of our sample showing X-ray emission: the X-ray luminosity ($L_{\rm X}$), the mechanical wind luminosity ($L_{\rm wind} = \frac{1}{2}\dot{M}v_\infty^2$) for our $\dot{M}$ and $\dot{M}$ from Vink et al. (2001), and B' again considering our derived $\dot{M}$ and Vink's $\dot{M}$. We see that for weak winds, $\frac{L_{\rm X}}{L_{\rm wind}}$ becomes of the order unity which shows the increasing importance of X-rays as the wind becomes less and less dense. Moreover, the magnetic field strength required to confine the wind is low for weak-wind stars, showing the increasing role of magnetic field when $\dot{M}$ decreases. Given these results and the above discussion, we may speculate that our weak wind stars may have magnetically confined winds (although no detections of magnetic field exist for them). In that case, one may wonder how our results would be modified. Fig. 8 of Ud'Doula & Owocki (2002) shows that the mass flux (ρv) is reduced close to the pole and enhanced near the equator, but their Table 1 reveals that the total mass loss is only reduced by a factor < 2 even in the case of strong confinement. Hence, using classical 1D atmosphere models should lead to correct values for the mass loss rates within a factor of two, even if magnetic confinement exists.

6. Sources of uncertainty for the $\dot{M}$ determination

In this section, we investigate the various sources of uncertainty of our determinations of mass loss rates both on the observational side and on the modelling side.

6.1. Observational uncertainties

Under the term "observational uncertainty", we gather all the effects which can influence the shape of the observed line profiles, especially Hα. The first source of uncertainty is the S/N ratio. However, in most of the stars studied here, this ratio is good ($\sim$ 100) and does not affect the analysis. The second source of uncertainty comes from the normalisation of the spectra. This is a general and well known problem which can affect the strength of lines, especially in the case of weak lines. In our spectra the main difficulties arise in the N v λ1240 and Hα regions. For the former, this is due to the presence of the broad Lyman α absorption around 1216 Å which renders uncertain the exact position of the continuum. We simply check that the strength of the emission part of the profile in the models is on average consistent with the observed line, leaving aside the bluest part of the absorption. The case of Hα is more critical. The normalisation can be hampered by the S/N ratio: a low ratio will not allow a good identification of the continuum position. The use of echelle spectra renders also difficult the identification of the continuum since the wavelength range around the line of interest in a given order is limited to $\sim$ 60 Å. We estimate that taken together, these effects induce an uncertainty $\lesssim$ 0.02 on the absolute position of the Hα core. Of course, Hα is also contaminated by nebular emission. When present, such an emission precludes any fit of the very core of the line. But the high resolution of our spectra allows a fit of $\sim 80-90\%$ of the stellar profile, excluding the very core.

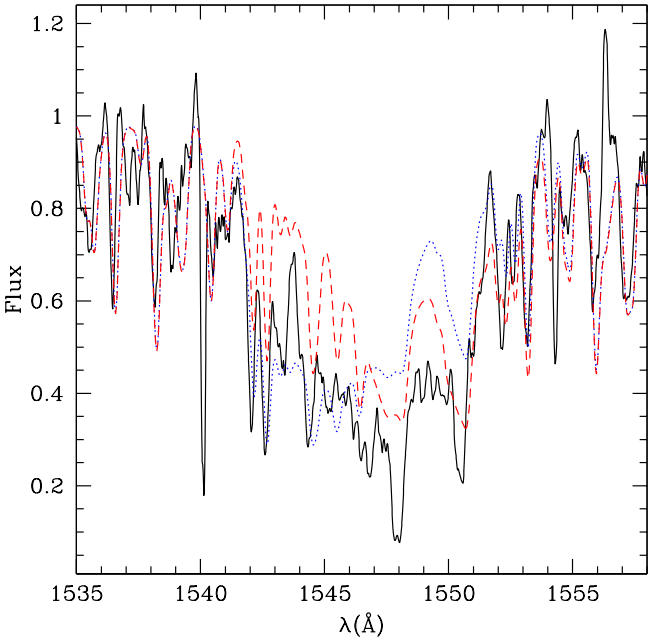

Fig. 29. Effect on X-rays on the C IV $\lambda\lambda$1548,1551 line. The observed profile is the solid line, the initial model is the dotted line and the model with X-rays and the same $\dot{M}$ is the dashed line. See text for discussion.

6.2. Photospheric Hα profile

Our estimates of $\dot{M}$ rely on the fit of both the UV wind sensitive lines *and* Hα. In low density winds, Hα is essentially an absorption profile for which only the central core is sensitive to mass loss rate. In order to derive reliable values of $\dot{M}$ it is thus important to know how robust the prediction of the photospheric profile is, since it will dominate over the wind emission. This is of much less importance in high density winds where the lines are dominated by wind emission.

Table 3. X properties of our sample stars with known X-rays fluxes. $L_{\rm X}$ is from Chlebowski & Garmany (1991) for HD 38666, HD 46202, HD 152590, HD 42088 and HD 46223, and from Evans et al. (2003) for HD 93204 and HD 93250. $L_{\rm wind}$ is the mechanical wind luminosity. Values with "Vink" are those for which $\dot{M}$ is taken from Vink et al. (2001) mass loss reciepe. B' is the value of the magnetic field for which confinement begins (corresponding to $\eta = 1$ in the formalism of Ud'Doula & Owocki 2002).

HD	$\log L_{\rm X}$ [egs s^{-1}]	$\log \frac{L_{\rm X}}{L_{\rm bol}}$	$\log L_{\rm wind}$ [egs s^{-1}]	$\log L_{\rm wind}^{Vink}$ [egs s^{-1}]	$\log \frac{L_{\rm X}}{L_{\rm wind}}$	$\log \frac{L_{\rm X}}{L_{\rm wind}^{Vink}}$	B' [G]	B'_{Vink} [G]
38666	31.37	-6.87	32.16	34.25	-0.79	-2.88	7	75
46202	32.40	-6.05	32.76	34.43	-0.36	-2.03	11	72
152590	32.51	-5.86	34.20	34.83	-1.69	-2.32	60	125
42088	32.38	-6.43	34.06	35.89	-1.68	-3.51	33	269
93204	32.06	-7.03	35.67	36.31	-3.61	-4.25	137	286
46223	32.62	-6.53	35.89	36.42	-3.27	-3.80	180	332
93250	33.22	-6.53	36.20	37.20	-2.98	-3.98	153	485

To check the CMFGEN prediction in a low density wind, we have compared the Hα line with that predicted by FASTWIND, the other non-LTE atmosphere code including wind and line-blanketing widely used for optical spectroscopic analysis of massive stars (see Santolaya-Rey et al. 1997, Repolust et al. 2004). The test model was chosen with the following parameters: $T_{\rm eff}$ = 35000 K, $\log g = 4.0$, $\dot{M} = 10^{-9}$ M$_\odot$ yr^{-1} and $\beta = 0.8$. This set of parameters is typical of the stars with weak winds analysed in the present study, and Hα should not be too much contaminated by wind emission. The result of the comparison between CMFGEN and FASTWIND is given in Fig. 30. We see that the agreement between both codes is very good. This is not a proof that the predicted profile is the correct one, but it is at least a kind of consistency check. Note here that a first comparison between both codes also revealed a problem in the He I singlet lines which were much weaker in CMFGEN than in FASTWIND. This problem has been highlighted by Puls et al. (2005) and appears for $T_{\rm eff}$ between 36000 and 41000 K for dwarfs. However, we have shown in Sect. 4.9 that this problem was solved when a microturbulent velocity of 10 km s^{-1} was chosen in model atmosphere including also Neon, Argon, Calcium and Nickel. The resulting additional line-blanketing effect strengthens the singlet lines, leaving all other lines basically unchanged. This improvement has a strong cost in term of computational time and that is the reason why we usually have to work with more standard models with v_{turb} = 20 km s^{-1} and only Iron.

We have also investigated another effect which can alter the shape of the Hα line core: the number of depth points included in the models. Indeed, the finner the spatial sampling, the better the line profile. This means that a too coarse spatial grid should introduce errors in the determination of $\dot{M}$ from Hα. We have run a test model taking the best fit model for HD 34078 and increasing the number of depth points from 72 to 90: a finner spatial grid leads to a slightly less deep line core, but the difference is only of 0.01 in terms of normalised flux. This is lower than any other observational uncertainty (see Sect. 6.1) so that we have adopted $\sim$ 70 depth points in all our computations [2].

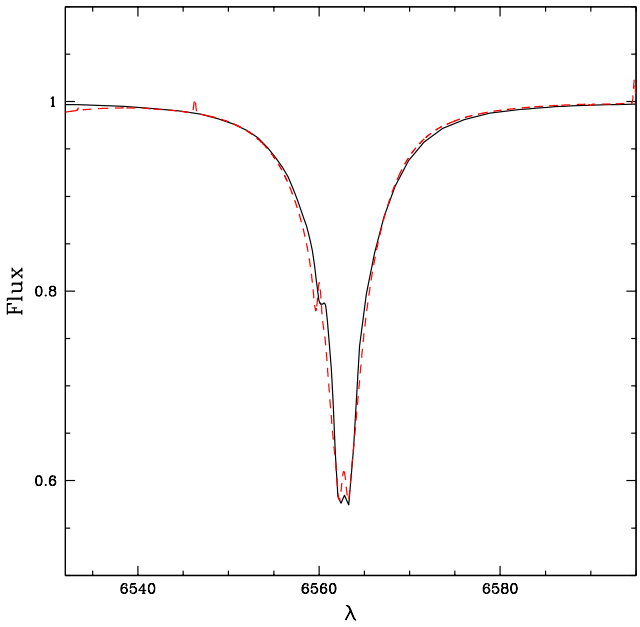

Fig. 30. Comparison between CMFGEN (red dashed line) and FASTWIND (black solid line) Hα profile. The model is for $T_{\rm eff}$ = 35000 K, $\log g = 4.0$, $\dot{M} = 10^{-9}$ M$_\odot$ yr^{-1} and $\beta = 0.8$. The agreement between both codes is good.

In conclusion, there is no evidence that the photospheric Hα profile is not correctly predicted by our models.

6.3. Ionisation fraction

In the low density winds, which correspond to late O type dwarfs in the present study, the final word concerning the mass loss rate is often given by C IV $\lambda\lambda$1548,1551. Indeed, Hα becomes almost insensitive to $\dot{M}$ in these cases, and

[2] choosing 90 depth points significantly increases the resources required for the computation

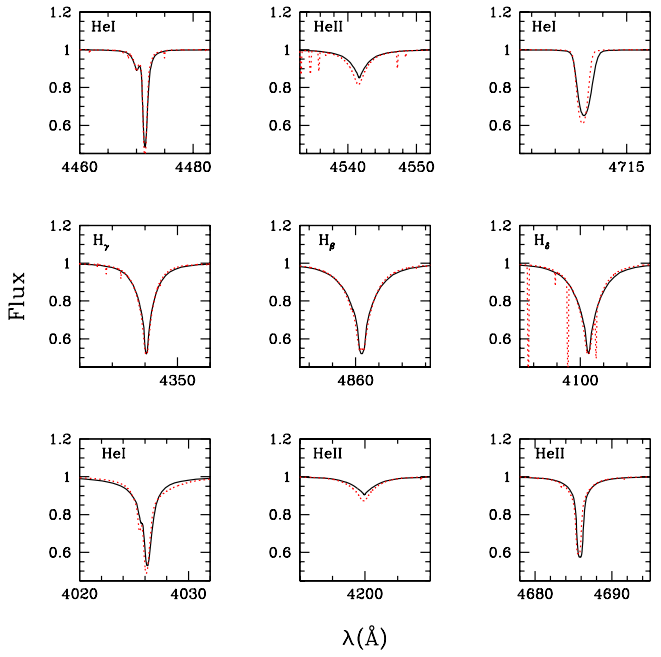

Fig. 31. Same as Fig. 30 but for H and He optical lines. With the exception of the singlet He I lines and He I λ6678, the agreement between both codes is good.

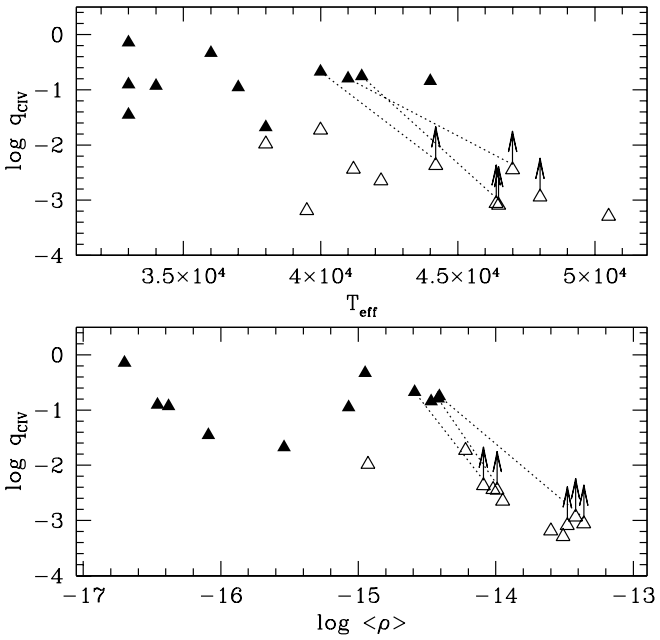

Fig. 33. C IV ionisation fractions in CMFGEN models (filled symbols) and from Lamers et al. 1999 (open symbols) for dwarfs as a function of effective temperature (upper panel) and mean wind density (lower panel). The dotted lines link objects in common between this work and the study of Lamers et al. (1999). See text for discussion.

the other main wind sensitive UV line, N V λ1240, is almost absent from the spectra due to the reduced effective temperature. Other indicators such as Si IV $\lambda\lambda$1394,1403 or N IV λ1718 are still present, but they are weaker than C IV $\lambda\lambda$1548,1551 and become rapidly insensitive to any change of the mass loss rate. Hence, the final constraint on $\dot{M}$ is set by C IV $\lambda\lambda$1548,1551. For more standard winds, almost all indicators can be used together to derive $\dot{M}$. We show in Fig. 32 the variation of the C IV $\lambda\lambda$1548,1551 line profile when the mass loss rate is decreased from $10^{-8.5}$ down to $10^{-9.5}$ $M_\odot$ yr^{-1} for the case of star HD 46202. We clearly see that C IV $\lambda\lambda$1548,1551 is still sensitive to changes in $\dot{M}$ even for such low values. In parallel, we see that Hα is essentially unchanged in this regime of $\dot{M}$.

However, relying on only one line to assign final mass loss rates may be risky. We have highlighted in paper I that erroneous mass loss rates may be derived in the case where the C IV ionisation fraction is incorrectly predicted. This is still true here, since fitting the observed profile gives the right value of $\dot{M} \times q_{C\ IV}$ ($q_{C\ IV}$ being the ionisation fraction of C IV) but not necessarily the right $\dot{M}$. In Fig. 33, we compare the ionisation fractions predicted by the CMFGEN best fit models to the values derived by Lamers et al. 1999 (hereafter L99) for dwarfs. The ionisations fractions are defined by

$$q_{C\ IV} = \frac{\int_{0.2}^{1} n_{C\ IV}(x)dx}{\int_{0.2}^{1} n_C(x)dx} \quad (7)$$

where $x = \frac{v}{v_\infty}$ and $n_{C\ IV}$ and n_C are the number densities of C IV and C respectively. At first glance, the CMFGEN ionisation fractions seem to be $\sim$ 2 orders of magnitude higher than the L99 results, and that in spite of the few lower limits in the latter data. However, several comments can be made:

- First, the work of L99 is based on previous mass loss rate determinations, mainly from Hα (Puls et al. 1996, Lamers & Leitherer 1993) or from predictions for their dwarf subsample (Lamers & Cassinnelli 1996). In the latter case, $\dot{M}$ is derived from the modified wind momentum - luminosity relation, so that any error in the calibration can lead to incorrect mass loss rate. Moreover, the uncertainty of such a method due to the fact that a given star can deviate from a mean relation may introduce a bias in the derived ionisation fraction. Concerning the mass loss rates derived from Hα, Lamers & Leitherer (1993) use the line emission strength to determine $\dot{M}$. However, in most O dwarfs Hα is in absorption so that the determination of the emission part of the line filling the photospheric profile may be uncertain. Puls et al. (1996) also use Hα to derive $\dot{M}$ but give only upper limits in the cases of thin winds. As L99 adopt these upper limits as the real values, we should expect the derived ionisation fractions to be lower limits.

- Second, there is a significant shift in terms of parameter space sampled by our results and that of L99: we have stars with $33000 < T_{\rm eff} < 44000$ K and $-17.3 < \log < \rho >< -14.4$ while L99 have $38000 < T_{\rm eff} < 50500$ K and $-15 < -log < \rho >< -13.4$, although both studies have stars of late and early O spectral types. Concerning effective temperatures, part of the discrepancy comes from the

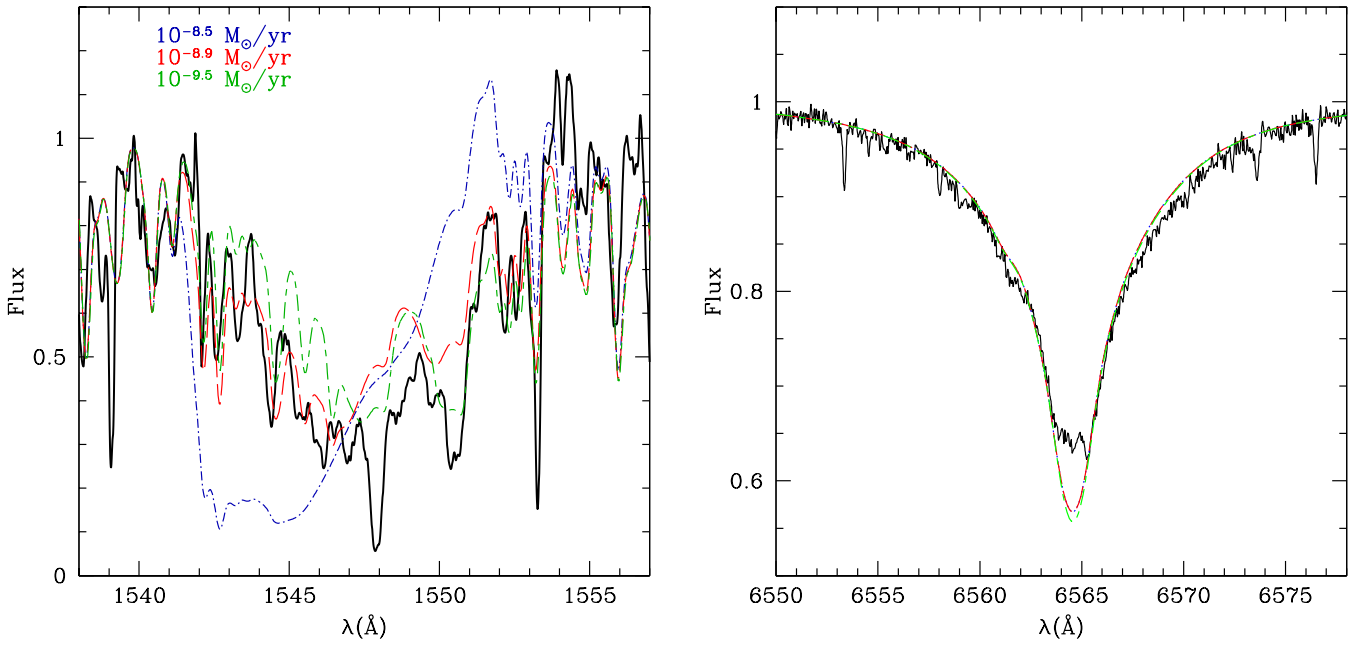

Fig. 32. Determination of $\dot{M}$ in low density winds (HD 46202). (a) shows the variation of the C IV $\lambda\lambda$1548,1551 line profile when $\dot{M}$ is reduced (solid line: observed line; dash-dotted line: $\dot{M} = 10^{-8.5}$ M$_\odot$ yr^{-1}; long dashed line: $\dot{M} = 10^{-8.9}$ M$_\odot$ yr^{-1}; short-dashed long-dashed line: $\dot{M} = 10^{-9.5}$ M$_\odot$ yr^{-1}). Notice that the weaker the line, the more prominent the presence of photospheric lines (mostly from iron) superimposed to the C iv absorption. (b) shows the behaviour of Hα under the same changes. See text for discussion.

use of line-blanketing in our models, which is known to reduce $T_{\rm eff}$ compared to unblanketed studies. But for densities, the explanation may again come from the fact that the adopted mass loss rates (and consequently the densities) in one or the other study are not correct. Can we discriminate between them? An interesting point is that 3 stars are common to our study and that of L99: they are shown linked by dotted lines in Fig. 33. If we consider the fact that line-blanketing may explain the lower $T_{\rm eff}$ in our study, and the fact that for these stars the ionisation fractions derived by L99 are only lower limits, then the ionisation fractions predicted by CMFGEN are not necessarily too high. And if in addition we argue that our study investigates a density range not explored by L99, then we can not conclude that the ionisation fractions predicted by CMFGEN are wrong since no comparison can be made for very low mean densities.

How could we test more strongly the wind ionisation fractions of our atmosphere models? One possibility is offered by the analysis of far UV spectra. Indeed, this wavelength range contains a number of lines *formed in the wind* from different ions of the same elements. Such a test will be done in a subsequent paper, based on FUSE observations of Vz stars in the LMC. But we can already mention that several studies of supergiants in the Magellanic Clouds using FUSE + optical data do not reveal any problem with the CMFGEN wind ionisation fractions, except that clumping must be used to reproduce a couple of (but not all) lines (see Crowther et al. 2002, Evans et al. 2004). Hence in the following, we assume that the ionisation fractions given by CMFGEN are correct.

6.4. Abundances

Although our mass loss determination relies on both Hα and UV lines, we usually give more weight to the UV diagnostics the absorption profile of Hα can be shaped by other parameters than $\dot{M}$ (β, clumping). But the UV lines depend more strongly on abundances than Hα. Hence, we have to estimate the error we make on the $\dot{M}$ determination from UV lines due to uncertain abundances. We have already seen in Sect. 4.11 that adopting the CNO abundances of Asplund (2004) instead of those of Grevesse & Sauval (1998) – which corresponds on average to a reduction by a factor of $\sim 3/4$ – leads to an increase of $\dot{M}$ by 0.25 dex. We have also run test models for a low luminosity star (HD 46202). It turns out that reducing the CNO abundances by a factor 2 implies an increase of the mass loss rate of the order of 2-2.5 in order to fit C IV $\lambda\lambda$1548,1551 since this line is not saturated in low density winds and thus its strength is directly proportional to the number of absorbers..

How different from solar could the CNO abundances of our sample stars be ? Given the estimated distances,

it turns out that all stars are within 3 kpc from the the sun. Determinations of abundances through spectroscopic analysis of B stars (Smartt et al. 2001, Rolleston et al. 2000) reveal the following gradients: −0.07 dex/kpc for C, O and Si, and −0.06 to −0.09 dex/kpc for N. Similarly, Pilyugin et al. (2003) derive an Oxygen abundance gradient of −0.05 dex/kpc from studies of HII regions. Taken together, these results indicate that on average we do not expect variation of CNO abundances by more than ± 0.25 dex for our sample stars. This means that adopting a solar metallicity leads to an error of at most 0.3 dex on the mass loss rate determination.

Given the above discussion, we estimate the error on $\dot{M}$ due to uncertainties in the CNO abundances to be of $\sim$ 0.3 dex.

6.5. Advection / adiabatic cooling

In low density winds, two processes may affect the ionisation structure: advection and adiabatic cooling. The former is rooted in the fact that for low densities, the timescale for recombinations becomes longer than the timescale for transport by advection. Thus the ionisation structure can be significantly changed. The latter process (adiabatic cooling) lowers the temperature in the outer part of the atmosphere where the heating processes (mainly photoionisations) are less and less efficient due to the low density, implying also a modification of the ionisation structure (see also Martins et al. 2004). We have tested the influence of those two effects in one of our low $\dot{M}$ models for HD 46202. Their combined effects lead to an increased ionisation in the outer atmosphere, the mean ionisation fraction of C IV being lowered by $\sim$ 0.1 dex (which does not modify the conclusions of Sect. 6.3). This slightly changes the UV line profiles, especially C IV $\lambda\lambda$1548,1551 which for a given $\dot{M}$ shows a smaller absorption in the bluest part of the profile. Quantitatively, the inclusion of advection and adiabatic cooling is equivalent to an increase of $\dot{M}$ by $\sim$ 0.15 dex. We have thus included these two processes in our models for low density winds (HD 38666, HD 34078, HD 46202, HD 93028).

Given the above discussions, we think our $\dot{M}$ determinations have a very conservative error bar of ±0.7 dex (or a factor ± 5). This is a quite large uncertainty which however does not modify qualitatively our results, namely the weakness of O dwarfs with low luminosity (see Sect. 7.2.2).

7. Discussion

7.1. Evolutionary status

Fig. 34 shows the HR diagram of the our sample stars. Overplotted on Fig. 34 is our new calibration $T_{\rm eff}$ - luminosity (Martins et al. 2005, solid line) for dwarfs: most stars of our sample agree more or less with this relation (within the error bars). The latest type stars of our sample, which are also the stars showing the weakest winds, may be slightly younger than "standard" dwarfs of the same spectral type (or $T_{\rm eff}$). Notice that this does not mean that these stars are the youngest in terms of absolute age, but that they are less evolved than classical dwarfs. Indeed, the youngest stars of our sample are those of Trumpler 16 (HD 93250 and HD 93204) for which we derive an age of 1 to 2 Myrs, compatible with the $L-T_{\rm eff}$ relation. In comparison, HD 38666 and HD 34078 may be 2 to 4 Myrs old according to our HR diagram (although given the error bars, we can not exclude younger ages), slightly less than for standard late type dwarfs. In the scenario where these two stars originated from a binary and were ejected in a dynamical interaction, Hoogerwerf et al. (2001) estimate a travel time of 2.5 Myrs, while van Rensbergen et al. (1996) found travel times of $\sim$ 3.5 Myrs for HD 38666 and $\sim$ 2.5 Myrs for HD 34078. These estimates are in good agreement with our results. We also derive an age of $\sim$ 3-5 Myrs HD 46202, one of our weak wind stars. Note that this star is in the same cluster as HD 46223 which is likely 1-2 Myrs old according to Fig. 34. A similar age should be expected for these two stars in case of a burst of star formation, but an age spread of 1-2 Myrs (common in star clusters) can explain the difference. The same is true for the stars of Cr 228: HD 93146, the brightest star, may be slightly younger than HD 93028.

Besides this, HD 152590 behaves differently, being less luminous than other dwarfs of same $T_{\rm eff}$. It is interesting to note that this star is classified as Vz. Taking literaly the result of Fig. 34, it seems indeed that it is younger than other dwarfs (but again, the error bars are large), confirming the fact that Vz stars are supposed to lie closer to the ZAMS than typical dwarfs. However, HD 42088 is another Vz star of our sample, and it has a more standard position on the HR diagram. This poses the question of the exact evolutionary status of Vz stars. Indeed, they are defined by stars having He II λ4686 stronger than any other He II lines which is thought to be a characteristic of youth since this line is filled with wind emission when the star evolves. In fact the Vz characteristics may be more related to the wind properties than to the youth of the star. Indeed, HD 42088 seems to have the same stellar properties as HD 93146, but the former is classified Vz (not the latter) and has a weaker wind ($\dot{M} = 10^{-8}$ $M_\odot$ yr^{-1} compared to $10^{-7.25}$ $M_\odot$ yr^{-1} for HD 93146. Note however that the distance (and thus luminosity) of HD 42088 is highly uncertain. Obviously, more studies are required to better understand the physics of Vz stars.

To summarise, there may be a hint of a link between a relative youth and the weakness of the wind *if by youth we mean an evolutionary state earlier than for standard stars and not an absolute age*, standard stars meaning stars with the average properties of dwarfs studied so far. But the present results are far from being conclusive. A forthcoming study of Vz stars in the LMC will probably shed more light on this issue.

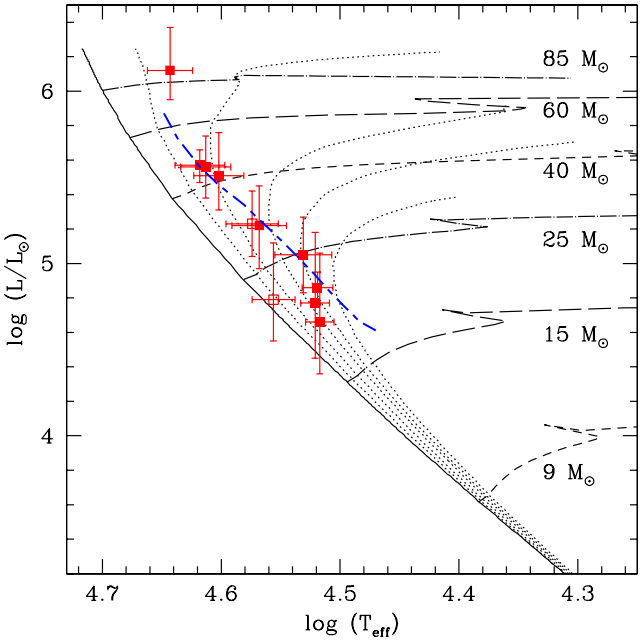

Fig. 34. HR diagram of the Galactic stars. Evolutionary tracks are from Lejeune & Schaerer (2001) and Z = Z$_\odot$. Isochrones for 0, 1.. 5 Myrs are indicated together with evolutionary paths of stars of different masses. The blue dashed line is our new relation $T_{\rm eff}$ - luminosity for dwarfs (Martins et al. 2005). Squares are the stars studied here (open symbols are for Vz stars).

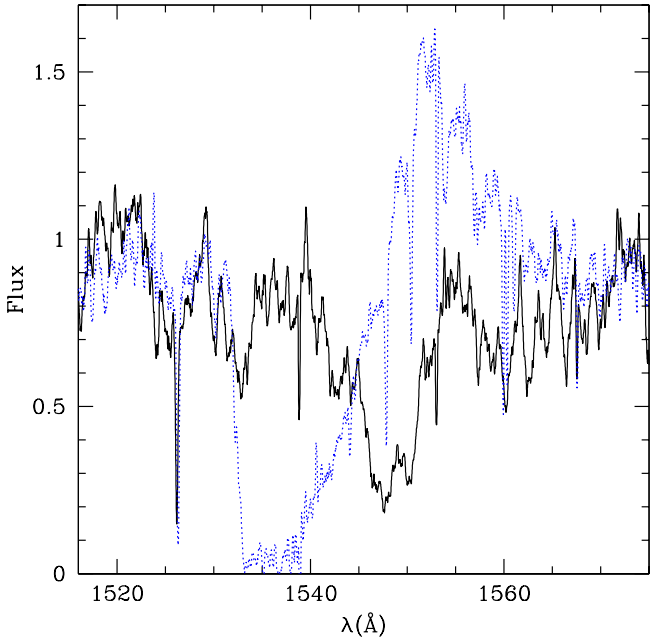

Fig. 35. Comparison between C IV $\lambda\lambda$1548,1551 line profiles in a star with weak (HD 38666, solid line) and strong (HD 46223, dotted line) wind. The rise of the flux level in the very blue part of the absorption features is slightly shallower in HD 38666. See text for discussion.

7.2. Wind properties

7.2.1. Terminal velocities

Some of the terminal velocities we derive are surprisingly low (see Table 1) reaching values lower than the escape velocity in a one case (HD 34078). What could explain this behaviour? First, the most obvious reason could be an underestimation of v_∞. We have argued in paper I that in stars with weak winds the density in the upper parts of the atmosphere may be so low that almost no absorption takes place in strong lines usually formed up to the top of the atmosphere. This explanation was also given by Howarth & Prinja (1989) to justify the low v_∞ they obtained in some stars. If this is indeed the case, one would expect a smooth decrease of the absorption strength in the blue part of P-Cygni profiles due to the reduction of the density as we move outwards, and not a steep break as seen in dense winds. Is there such a transition? Fig. 35 shows the C IV $\lambda\lambda$1548,1551 line profiles of HD 34078 and HD 46223 and reveals that although the increase of the flux level from the deepest absorption to the continuum level in the bluest part of the profile extends over a slightly larger range in the case of the weak wind star (3 Å for HD 38666 instead of 2 Å for HD 46223), it is difficult to draw any final conclusion as regards the reduction of the C IV $\lambda\lambda$1548,1551 absorption in the outer wind of low density wind stars from this simple eye estimation given also that blending is clearly apparent in the line of HD 38666.. More information is given by Fig. 36 which shows the derived terminal velocities as a function of mean density in the wind (see Sect. 6.3 for definition). There is an obvious trend of lower terminal velocities with lower wind densities. This is not a proof of the fact that absorption in strong UV lines extends to larger velocities since low densities also mean low mass loss rate and correspond to stars with lower radiative acceleration. However, it is an indication that underestimations of v_∞ are certainly more likely to happen in such low density stars.

In view of the above discussion, it is not clear whether the lower density in the outer atmosphere of weak wind stars is responsible for an underestimation of the terminal velocities. Let us now assume for a moment that the derived values are real terminal velocities: what are the implications? The radiation driven wind theory predicts that v_∞ is tightly correlated to the escape velocity (v_{esc}) according to

$$v_\infty^2 = v_{esc}^2 I(\alpha) \frac{\alpha}{1-\alpha} \quad (8)$$

where α is the usual parameter of the Castor, Abbott & Klein (1975) formalism and $I(\alpha)$ is a correction factor to take into account effects of the finite cone angle of the star disk (see Kudritzki et al. 1989). In practice, it is possible to derive values of α from this equation once the stellar parameters and v_∞ are known. The only problem comes from $I(\alpha)$ which is a complex function of (among other parameters) α. However, it is possible to solve this problem with the following procedure: we first assume a given

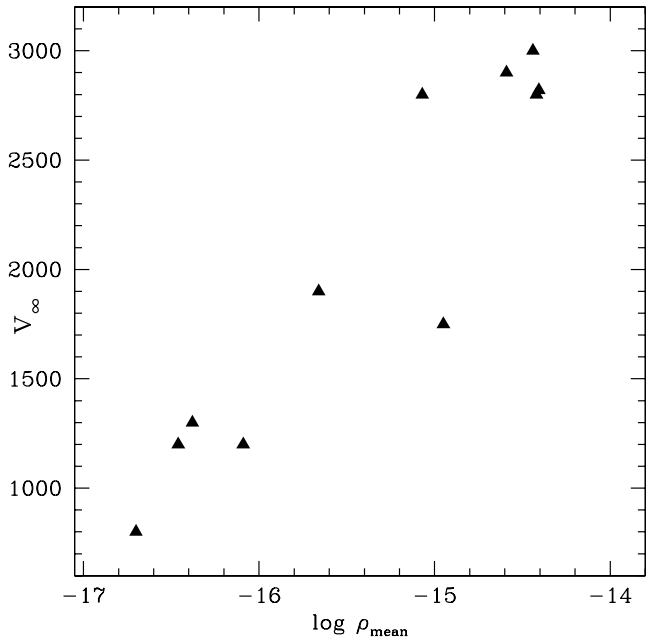

Fig. 36. Terminal velocity as a function of mean density in the wind for the stars studied here. There is a clear trend of lower v_∞ in lower density stars.

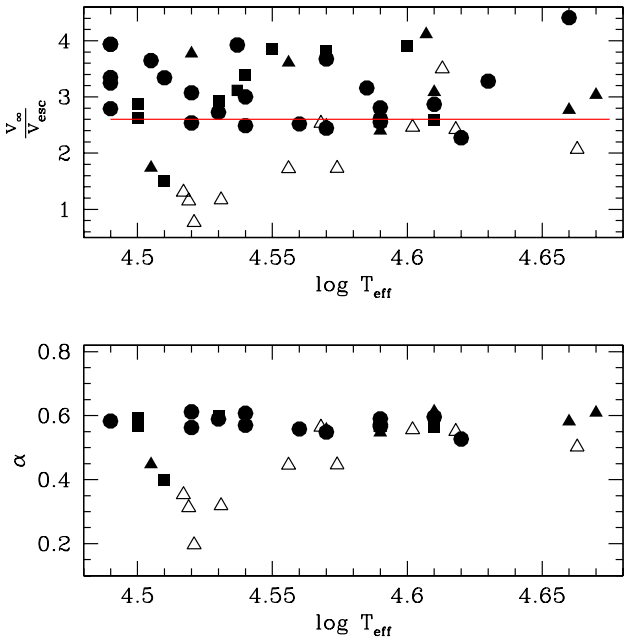

Fig. 37. Upper panel: ratio of terminal to escape velocity in our sample stars (open symbols) and stars studied by Herrero et al. 2000, 2002, Repolust et al. 2004 and Markova et al. 2004 (filled symbols). The solid line indicates the classical value 2.6 derived for stars hotter than 21000 K (Lamers et al. 1995). Dwarfs (giants, supergiants) are shown by triangles (squares, circles). Lower panel: derived α parameter from the estimated terminal and escape velocities. See text for discussion.

value of α, then estimate $I(\alpha)$ which is subsequently used to find a new α using

$$\alpha = \frac{\frac{v_\infty^2}{v_{esc}^2}}{I + \frac{v_\infty^2}{v_{esc}^2}} \quad (9)$$

A few iterations should lead to the final value of the α parameter. We have used such a scheme to estimate α for our sample stars and for a number of stars studied elsewhere. Solutions are usually found with less than 10 iterations (and are essentially independent on the starting value of α), except in the cases where $v_\infty/v_{esc}$was larger than ~ 3: in that case, the iterative process did not converge but kept oscillating between two distinct values. The results for the cases where solutions could be found are shown in Fig. 37 (lower panel). A majority of cases lead to $\alpha \sim 0.5 - 0.6$, in reasonable agreement with (although slightly lower than) theoretical expectations (Puls, Springmann & Lennon 2000). However, for the stars of this work with weak winds (and low v_∞), lower values are deduced ($\alpha \sim 0.3$). Hence, *if the derived low terminal velocities correspond to real* v_∞, they may be due to low values of the α parameter (given Eq. 8.) If true, this may also have important implications for the scaling relations involving mass loss rates (see next section). Again, it may be possible that we underestimate the terminal velocities, but the above possibility is worth being discussed in view of the puzzle of the weak winds. Note that we have also plotted in Fig. 37 the ratio of terminal to escape velocity which is usually of the order 2.6 for O stars with $T_{\rm eff} >$ 21000 K (Lamers et al. 1995). We see that hottest stars of our sample follow this general trend whereas stars with weak winds have much lower ratios.

Another very interesting explanation for the low terminal velocities we derive is the effect of X-rays. Indeed, Drew et al. (1994) highlighted the fact the cooling time in the outer atmosphere of massive stars with relatively weak winds (late O / B stars) can become relatively high so that in the case where X-rays possibly emitted by shocks heat the outer atmosphere, this region remains hot. In that case, the ionisation structure is strongly modified compared to the inner atmosphere and in practice, the radiative force becomes negligible in this hot region. This means that the wind keeps expanding at the velocity reached at the tope of the "cool" region which is lower than the value predicted by the radiation driven wind theory. This effect should be checked in future hydrodynamical simulations.

7.2.2. Mass loss rates and modified wind momenta

The mass loss of O stars has been known for a long time to depend on luminosity since due to the basic mechanism of radiatively driven winds, the more photons are available, the larger the acceleration and the larger the mass loss rate (e.g. Castor, Abbott & Klein 1975, Kudritzki & Puls 2000). Fig. 38 shows mass loss rates for our sample stars (filled symbols) and stars from other studies (Herrero et al. 2000, 2002, Repolust et al. 2004 and Markova et al. 2004,

open symbols) as a function of luminosity. One sees that there is a good correlation between $\dot{M}$ and L for bright stars. Note however that our sample stars seem to show lower $\dot{M}$ than what could be expected from the other studies (see also Table 2). For low luminosity stars, the correlation still exists, but the scatter is much larger. Moreover, the slope of the relation seems to be steeper for these objects, the transition luminosity being $\log \frac{L}{L_\odot} \sim 5.2$. Although our work is the first to show such a behaviour based on quantitative modelling of atmosphere of O stars, this trend was previously mentioned by Chlebowski & Garmany (1991) and Lamers & Cassinelli (1996). This result confirms our finding of paper I in which we showed that the stellar components of the star forming region SMC-N81 displayed winds weaker than expected from the relation $\dot{M}$ - L at high luminosities. In paper I, we mentioned that a possible explanation of such a weakness was the reduced metallicity of the SMC, but we also showed that the Galactic star 10 Lac had the same low mass loss rate. Here, we confirm that several Galactic stars with low luminosity indeed show low $\dot{M}$, rendering unlikely the effect of metallicity alone.

We also showed in paper I that the winds were weaker than predicted by the current hydrodynamical simulations. Fig. 39 extends this trend for the Galactic stars studied here: in the "worst" cases, the difference between our derived $\dot{M}$ and the mass loss rates predicted by Vink et al. (2001) can reach 2 orders of magnitude! Note that even for bright stars our values are lower than the predictions but only by a factor $\lesssim 5$. This is mainly due to the introduction of clumping in our models for these stars which naturally leads to reduced mass loss rates (Hillier et al. 2003, Bouret, Lanz & Hillier 2005). We will come back to this below.

One may also wonder why our values of $\dot{M}$ are lower than other previous studies. Indeed, as shown by Table 2 our mass loss rates are systematically lower than derived so far for all stars of the sample. How can we explain this behaviour? First, let us recall that the mass loss rates gathered in Table 2 are estimated from either pure Hα analysis (Leitherer 1988, Lamers & Leitherer 1993, Puls et al. 1996, Repolust et al. 2004, Markova et al. 2004) or from pure UV analysis (Howarth & Prinja 1989, Chlebowski & Garmany 1991). The Hα study of Leitherer (1988) and Lamers & Leitherer (1993) relied on measurement of Hα emission equivalent widths. They are linked with Hα luminosities which are themselves related to mass loss rates. The relation L(Hα) - $\dot{M}$ is based on estimates of the population of the third level of Hydrogen for which departure coefficients from LTE are taken from the pure H He computations of Klein & Castor (1978). The Hα emission equivalent width is calculated from the total equivalent width to which a photospheric profile from the plane-parallel pure H He models of Auer & Mihalas (1972) is subtracted. This procedure may suffer from various approximations: the use of pure H He models may introduce errors in the prediction of departure coefficients since line-blanketing is known to affect the ionisation (and excitation) structure; moreover, photospheric profiles based on H He plane-parallel models may also be different from line-blanketed spherically extended models. In the case of stars with Hα in absorption, the estimate of the emission part may be risky since it may suffer from uncertainties in the photospheric component subtraction, from contamination by interstellar lines or from errors in normalisation process. Leitherer (1988) himself argues that the wind emission part of the global (wind + photospheric) profile becomes almost undetectable in stars with Hα in absorption. Hence, the Hα mass loss rates of such objects based on this method may be rather uncertain. Another method relying on Hα is that of Puls et al. (1996) and Markova et al. (2004). It is again based on the emission part of Hα which is related to mass loss rate through an estimate of the H departure coefficient under the Sobolev approximation. Their method is accurate for values of their parameter A $> 10^{-4}$ (see Eq. (3) of Puls et al. for a definition of A) which, for typical values of the stellar parameters of O stars, corresponds roughly to $\dot{M} > 10^{-7}$ M$_\odot$ yr^{-1}. This is mainly the reason why the authors give only upper limits for stars with Hα in absorption. Finally, Repolust et al. (2004) used FASTWIND (see Sect. 6.2) to fit the Hα profile and estimate $\dot{M}$. In the case of weak winds, this method becomes less and less accurate since Hα is almost entirely photospheric and hardly depend on mass

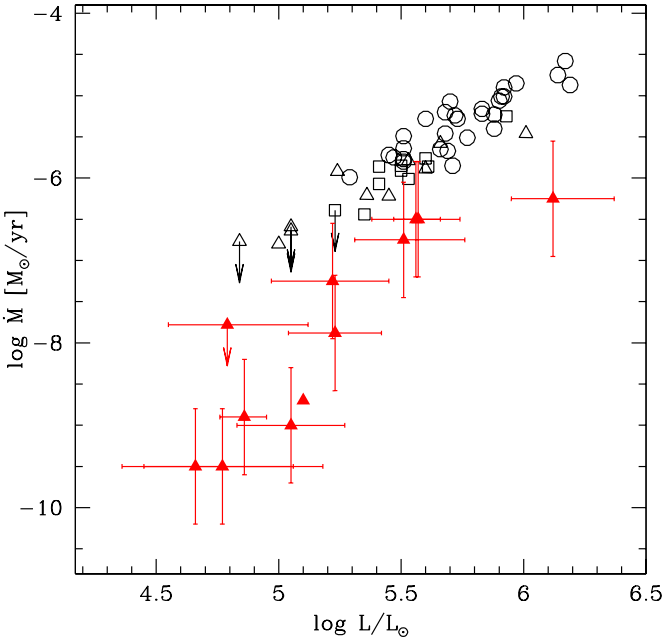

Fig. 38. Mass loss rates as a function of Luminosity for Galactic O stars. The filled triangles are the dwarfs studied in the present paper (+ 10 Lac from paper I displayed by the filled triangle without error bars). Open symbols are data from Herrero et al. (2000, 2002), Repolust et al. (2004) and Markova et al. (2004). Triangles (squares, circles) are for dwarfs (giants, supergiants).

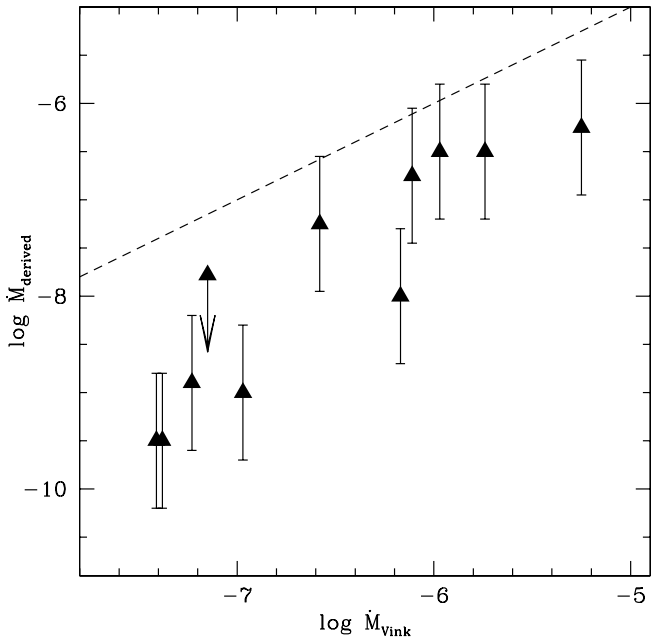

Fig. 39. Comparison between derived mass loss rates and predictions of hydrodynamical simulations (Vink et al. 2001).

loss. Here again, the authors only give upper limits on $\dot{M}$ in those cases.

Concerning UV based determinations of the mass loss rate, Howarth & Prinja (1989) use the column densities in several UV lines to estimate $\dot{M} \times qi$ (qi being the ionisation fraction of the ion responsible for the line studied). Under the approximation that the ionisation fraction is independent of luminosity, they derive $\dot{M}$. The latter approximation may introduce errors in the mass loss rates estimate. Indeed, our modelling of massive stars atmospheres reveals that the ionisation fractions are not constant when $T_{\rm eff}$ changes among dwarf stars (which in this case reduces to a change of luminosity, see Fig. 33). Since the largest ionisation fractions of C IV given by Howarth & Prinja (1989) are of the order $10^{-2.5}$ (see their Fig. 16) while we find values as high as $\sim 10^{-0.5}$, a factor of 100 between their $\dot{M}$ and ours is possible. The other UV analysis to which our results are compared is that of Chlebowski & Garmany (1991). The authors use fits of the UV lines using the method of Olson (1982) which is similar to the SEI method (Lamers et al. 1987). Basically, this method uses a parameterisation of the optical depth through the line profile to produce synthetic profiles which, once compared with observed spectra, allow a determination of $\dot{M}$. However, this latter step requires a few approximations. In particular, the ionisation fraction has to be estimated which involves the use of SED at high energies (i.e. close to ionisation thresholds of C IV and N V): a blackbody distribution is used in the computations of Chlebowski & Garmany (1991). Moreover, only photoionisation and recombinations from/to the ground states are taken into account. Hence, once again the ionisation fractions may not be correctly predicted leading to errors on $\dot{M}$. However, it is interesting to note that the approach of Chlebowski & Garmany (1991) is more accurate than that of Howarth & Prinja (1989) as regards the ionisation fractions and leads to lower mass loss rates (see Table 2), so that if, as we can expect, the ionisation fractions are better predicted in the current atmosphere models and are in fact higher, lower mass loss rates are not too surprising.

Another important point highlighted in paper I was the behaviour of the so called modified wind momentum - luminosity relation (WLR) at low luminosities. Indeed, we showed that there seemed to be a breakdown of this relation below $\log \frac{L}{L_\odot} \simeq 5.2$, at least for stars of the SMC (including the stars of paper I and 3 stars of NGC 346 studied by Bouret et al. 2003). The Galactic star 10 Lac also showed a reduced wind momentum, indicating that this property could not be related to metallicity alone. In the present study, several characteristics of the WLR are highlighted.

We first confirm that there is a breakdown - or at least a steepening- of the WLR below $\log \frac{L}{L_\odot} \simeq 5.2$. Indeed, Fig. 41 shows that most stars below this transition luminosity have wind momenta lower that what one could expect from a simple extrapolation of the WLR for bright stars. Indeed, for $\log \frac{L}{L_\odot} \sim 5.0$, the relation for dwarfs + giants found by Repolust et al. (2004) gives wind momenta of the order 10^{28} while we find values as low as 10^{25}! There is in fact only one object which is marginally in agreement with the relation of Repolust et al. (2004), but we have only an upper limit for $\dot{M}$ for this star (HD 152590).

Second, we find that for the bright stars of this study, the modified wind momenta are reduced compared to the pure Hα analysis on which the WLR is established. The difference is on average a factor of between 5 and 10, especially for the two objects we have in common (HD 15629 and HD 93250). The explanation of this discrepancy comes from the use of clumping in our models for these stars. Indeed, it is necessary to use inhomogeneous winds to correctly fit a number of UV lines, especially O V λ1371 and N IV λ1718. In Fig. 40 we show the UV + Hα spectra of HD 93250 and two models: one with the mass loss rates derived by Repolust et al. (2004) from Hα only ($\dot{M} = 10^{-5.46}$ M$_\odot$ yr^{-1}), and the other with our estimation of $\dot{M}$ relying on both Hα and UV lines and taking clumping into account ($\dot{M} = 10^{-6.25}$ M$_\odot$ yr^{-1}). One sees clearly that although both models are acceptable for Hα (in view of the nebular contamination one can not exclude one or the other possibility), UV lines are overpredicted with $\dot{M} = 10^{-5.46}$ M$_\odot$ yr^{-1}. Note that Repolust et al. (2004) put forward the fact that the presence of clumping may lead to an overestimation of the derived mass loss rates if unclumped models are used. Their argument is mainly based on the larger modified wind momenta of stars with Hα in emission compared to stars with Hα in absorption which can be explained by the neglect of clumping in the former. However, they do not exclude the existence of clumping in the latter, but claim that its ef-

fects can not be seen due to low optical depth. In our case, all stars have Hα in absorption, and we deduce the presence of clumping from UV lines.

Note that in our study, we had to include clumping only in the brightest stars to correctly fit the UV spectra. Does it mean that the winds of fainter stars are homogeneous? Not necessarily. Indeed, clumping is required to reproduce O V λ1371 and N IV λ1718. But it turns out that in late type O stars (i.e. low L stars) O V λ1371 is absent and N IV λ1718 is mainly photospheric so that homogeneous winds give reasonable fits. Clumping may be present, but it can not be seen from the UV and optical spectra. In any case, if clumping were to be included in the models, the mass loss rates would have to be reduced to fit the observed spectra (see above). Thus, $\dot{M}$ would have to be further reduced compared to the already low values we obtain, making the winds of low luminosity O dwarfs even weaker!

In spite of the global shift of our WLR for bright O dwarfs compared to pure Hα studies when clumping is included, the slope of the relation is roughly the same as that found by Repolust et al. (2004). This is important since it shows that the breakdown of the WLR we find at low luminosities is not an artifact of our method. Equivalently, this means that even if we underestimate the mass loss rates (due to ionisation fractions, see Sect. 6.3), there is however a qualitative change of the slope of the WLR near $\log \frac{L}{L_\odot} \sim 5.2$.

Can we estimate the value of the slope of the WLR in this low L range? The number of stars studied is still too low to give a reliable value, but if we do a simple eye estimate, excluding star HD 152590 (due again to the fact that it is a possible member of a binary), we find a slope of the order of 4.3. As this slope is in fact equal to $1/\alpha'$ (e.g. Kudritzki & Puls 2000), where $\alpha' = \alpha - \delta$ and $\delta = 0.005..0.1$, we deduce $\alpha' \sim 0.25$ and $\alpha \sim 0.30$ which is very low compared to the classical value of ~ 0.6, but which is consistent with our finding based on the ratio of terminal to escape velocities (Sect. 7.2.1). This does not mean that α is indeed this low for these stars since both v_∞ and $\dot{M}$ may be underestimated, but it is at least a kind of consistency check.

7.2.3. Origin of weak winds

In view of the above results, what can we conclude as regards the origin of the weakness of the winds observed in some O dwarfs? The main possibilities have been detailed in paper I. Among them, metallicity was the first to come to mind since at that time, as most stars with weak winds were found in the SMC (paper I, Bouret et al. 2003). The present study clearly shows that metallicity cannot explain the reduced wind strength observed since several Galactic stars show mass loss rates and terminal velocities as low as SMC objects. On the contrary, it becomes more and more evident that there is a transition in the wind properties near $\log \frac{L}{L_\odot} = 5.2$, although the reasons

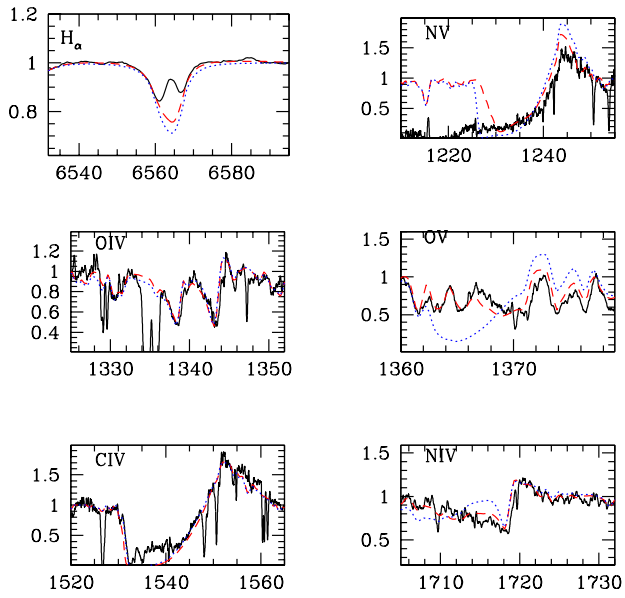

Fig. 40. Influence of clumping on the determination of $\dot{M}$ of HD 93250. The solid line is the observed spectrum, the dotted line is a model with $\dot{M} = 10^{-5.46}$ M$_\odot$ yr^{-1}(mass loss rate derived by Repolust et al. 2004 from Hα) and no clumping, and the dashed line is a model with $\dot{M} = 10^{-6.25}$ M$_\odot$ yr^{-1}and $f_\infty = 0.01$. The inclusion of clumping leads to a reduction of the mass loss rate derived from both UV lines and Hα. See text for discussion.

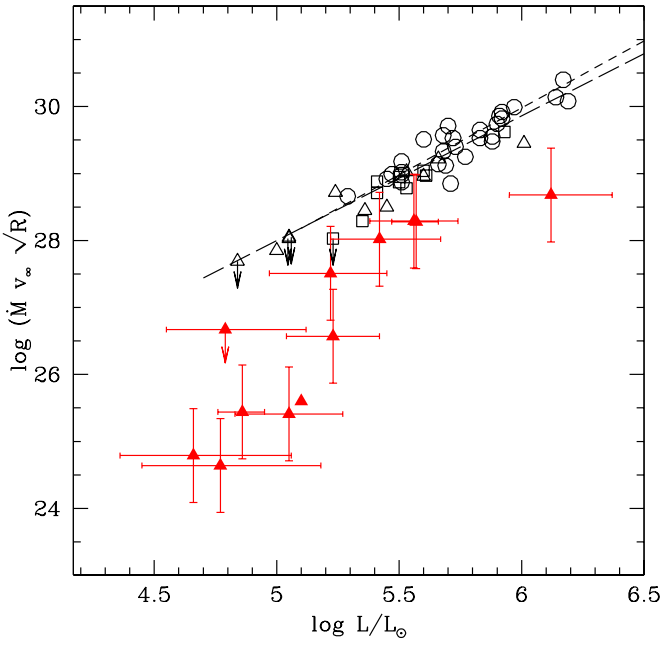

Fig. 41. WLR for Galactic stars. Symbols and data are the same as in Fig. 38. Note the breakdown of the relation below $\log \frac{L}{L_\odot} \sim 5.2$. See text for discussion. The short (long) dashed line is the regression curve for supergiants (giants + dwarfs) of Repolust et al. (2004).

for such a change of behaviour remain unclear at present. To say things more clearly, we do not state that metallicity has no effect on the wind strength (this is now well established): we simply show that low luminosity dwarf O stars have winds much weaker than expected from hydrodynamical simulations and than so far observed for O stars, *independent of metallicity*.

A possible explanation is the reduction of the α parameter which, if it were as low as ~ 0.25, could explain both the reduced mass loss rates and terminal velocities. However, what could be the reason for such a low α ? A nice possibility was highlighted by Puls et al. (2000) in their very detailed analysis of the line statistics. They first show that under fairly general conditions, the classical α parameter, i.e. the one entering the slope of the line strength distribution function, and the $\hat{\alpha}$ parameter used to express the radiative acceleration according to

$$g^{rad} \propto t^{-\hat{\alpha}} \tag{10}$$

in the CAK formalism (see Castor, Abbott & Klein 1975) are the same (this is the basics of the radiation driven wind formalism). However, the line strength distribution function may not have a constant slope, and in that case the value of α such that $\hat{\alpha} = \alpha$ must be derived at the point where the line strength is equal to t^{-1}. This has two important consequences: first, since $t = s_e v_{th} \frac{\rho}{dv/dr}$ (with s_e the Thomson scattering opacity and v_{th} the typical thermal velocity), it will be different from star to star; and second, t is not constant in a given star's atmosphere. In practise, this means that α should be different not only from star to star, but also from point to point in the atmosphere of a given star! However, Puls et al. (2000) have shown that the slope of the line strength distribution function is constant over a large range of t values, implying that α keeps a constant value close to 0.6. But in extreme cases, we may reach a range where this slope varies: in that case, α is reduced. This is shown by Fig. 27 of Puls et al. (2000) where we see that for t lower than 10^{-6} α deviates significantly from 0.6. the interesting thing is that this situation corresponds to low densities (see the definition of t above). In conclusion, $\alpha < 0.6$ is expected in low density winds, which is consistent with our findings.

Given this fact, the main problem would come from the strong disagreement between the results of spectroscopic analysis and the predictions of hydrodynamical simulations. Could such simulations overestimate mass loss rates? It is indeed possible since they neglect velocity curvature terms in the computation of radiative accelerations (Owocki & Puls 1999), which can affect the final results. As discussed in paper I, O dwarfs with low luminosity are the most sensitive to such effects but test models for a 40 $M_\odot$ star performed by Owocki & Puls (1999) lead to downward revision of the mass loss rate by only a factor 1.5 while we would need a factor ~ 100!

One can also wonder what is the effect of X-rays on the driving of winds. We have already seen in Sect. 7.2.1 that low terminal velocities can be expected when X-rays are present due to changes in the outer atmosphere ionisation structure. Further insights can be found in Drew et al. (1994). These authors have studied two B giants and have found mass loss rates 5 times lower than values expected for a simple extrapolation of the $\dot{M}$ - L relation of Garmany & Conti (1984) established for O stars. They also detected X-ray emission in both stars, and argued that such X-rays, likely formed in the outer atmosphere, can propagate towards the inner atmosphere and change the ionisation structure here too, reducing the total radiative acceleration and thus the mass loss rate. This may partly explain why the mass loss predictions of Vink et al. (2001), which does not take X-rays into account, are higher than our derived values. Obviously, hydrodynamical models including X-rays are needed to test this attractive hypothesis.

We highlighted in paper I that decoupling may be an alternative explanation although no conditions for it to take place were fulfilled in the N81 atmospheres. Here, the stellar and wind parameters of the weak winds stars being similar to those of the N81 stars, we have checked that such a process is not likely to be at work either.

8. Conclusion

We have derived the stellar and wind properties of Galactic O dwarfs with the aim of tracking the conditions under which weak winds such as observed in SMC-N81 (Martins et al. 2004) develop. Atmosphere models including non-LTE treatment, spherical expansion and line-blanketing were computed with the code CMFGEN (Hillier & Miller 1998). Optical H and He lines provided the stellar parameters while both UV lines and Hα were used to determine the wind properties. The main results can be summarised as follows:

- ◇ The O dwarfs studied here are 1 to 2 Myrs old for the hottest and 2 to 4 Myrs old for the coolest. Except for the faintest, they have luminosities in reasonable agreement with the new calibration $T_{\rm eff}$ - Luminosity of Martins et al. (2005).
- ◇ Stars with luminosities below a certain transition luminosity ($\log \frac{L}{L_\odot} \lesssim 5.2$) have mass loss rates of the order of $10^{-8..-9.5}$ $M_\odot$ yr^{-1} and low terminal velocities (down to 800 km s^{-1}). The mass loss rates are lower by nearly a factor of 100 compared to the hydrodynamical predictions of Vink et al. (2001). Uncertainties in the determination of $\dot{M}$, discussed here in detail, are not expected to qualitatively alter the results.
- ◇ Stars with $\log \frac{L}{L_\odot} \gtrsim 5.2$ are found to have reduced mass loss rates compared to both hydrodynamical predictions and previous analysis based only on Hα. The main reason is the inclusion of clumping in our models in order to fit O V λ1371 and N IV λ1718 in the IUE range. The adoption of pure Hα based mass loss rates does not allow fits of most of the UV lines.
- ◇ The modified wind momentum - luminosity relation shows a break down around $\log \frac{L}{L_\odot} = 5.2$. Below this

transition value, the slope corresponds to a value of the α parameter of the order of 0.3, which is consistent with the low terminal velocities observed. Such a low α is expected in low density winds (Puls et al. 2000).

- ◇ The origin of the weakness of the winds in low luminosity stars compared to hydrodynamical simulations is still unknown, but metallicity effects can be excluded since all the stars of the present study are Galactic stars and show reduced winds similar to SMC stars (Bouret et al. 2003, Martins et al. 2004). An earlier evolutionary state than in standard dwarfs may be responsible or not for the weakness: the present results can not resolve this issue given the error bars in the age estimates.
- ◇ Although their origin remains unclear, X-rays appear to play a very important role in the physics of weak winds. They may be due to magnetic mechanisms and affect the ionisation structure. This can possibly reduce the driving force and partly explain the low terminal velocities and low mass loss rates. Hydrodynamical simulations including X-rays should give more quantitative results.

The low luminosity objects of our sample have not been studied individually with quantitative spectroscopy before since the atmosphere models allowing the analysis of weak wind stars have only been available for a few years. Indeed, the detailed modelling of UV wind sensitive lines requires a reliable treatment of line-blanketing since most of these lines are from elements heavier than He. This also explains why a number of previous quantitative analysis relied essentially on Hα.

Now that the existence of weak winds has been established observationally both in the SMC and in the Galaxy, it would certainly be suitable to investigate the problem from a theoretical point of view with new hydrodynamical simulations. Apart from that, we still have to make sure that the ionisation fractions predicted by CMFGEN are correct since thay may alter the mass loss rate determinations. We will conduct such an investigation in a forthcoming paper using FUSE data.

Acknowledgements. We thank the ESO staff in La Silla for their help during the observations. FM and DS aknowledge financial support from the FNRS. We thank J. Puls for providing FASTWIND models and A. Herrero and D.J. Lennon for the Hα spectra of HD 93204, HD 93250 and HD 15629. JDH thanks Janos Zsargo for interesting discussions on the effects of X-rays.

References

Abbott, D.C., 1982, ApJ, 259, 282
Allen, C.W., 1976, Astrophysical Quantities, (London: Athlone)
Asplund, M., 2004, A&A. 417, 751
Auer, L.H. & Mihalas, D., 1972, ApJS, 24, 193
Babel, J. & Montmerle, T., 1997, ApJ, 485, L29
Bernabeu, G., Magazzù, A. & Stalio, R., 1989, A&A, 226, 215
Bouret, J.C., Lanz, T., Hillier, D.J., Heap, S.R., Hubeny, I., Lennon, D.J., Smith, L.J., Evans, C.J., 2003, ApJ, 595, 1182
Bouret, J.C., Lanz, T., Hillier, D.J., 2005, A&A, in press, astro-ph/0412346
Cassinelli, J.P. & Olson, G.L., 1979, ApJ, 229, 304
Castor, J., Abbott, D.C., Klein, R., 1975, ApJ, 195, 157
Chiosi, C. & Maeder, A., 1986, ARA&A, 24, 329
Chlebowski, T. & Garmany, C.D., 1991, ApJ, 368, 241
Cohen, D.H., de Messières, G., MacFarlane, J.J., Miller, N.A., Cassinelli, J.P., Owocki, S.P., Liedahl, D.A., 2003, ApJ, 586, 495
Crowther, P.A., Hillier, D.J., Evans, C.J., Fullerton, A.W., De Marco, O., Willis, A.J., 2002, ApJ, 579, 774
DeGioia-Eastwood, K., Throop, H. & Walker, G., 2001, ApJ, 549, 578
Drew, J.E., Denby, M., Hoare, M.G., 1994, MNRAS, 266, 917
Evans, N.R., Seward, F.D., Krauss, M.I., Isobe, T., Nichols, J., Schlegel, E.M., Wolk, S.J., 2003, ApJ, 589, 509
Evans, C.J., Crowther, P., Fullerton, A.W., Hillier, D.J., 2004, ApJ, in press (astroph/0404231)
Garmany, C.D. & Conti, P.S., 1984, ApJ, 284, 705
Garmany, C.D. & Stencel, R.E., 1992, A&AS, 94, 211
Gieseking, F, 1982, A&AS, 49, 673
Grevesse, N. & Sauval, A., 1998, Space Sci. Rev, 85, 161
Grigsby, J.A., Morrison, N.D. & Anderson, L.S., 1992, ApJS, 78, 205
Haser, S.M., 1995, PhD thesis, Universitäts-Sternwarte der Ludwig-Maximillian Universität, München
Herrero, A., Puls, J., Villamariz, M.R., 2000, A&A, 354, 193
Herrero, A., Puls, J., Najarro, F., 2002, A&A, 396, 949
Hillier, D.J. & Miller, D.L., 1998, ApJ, 496, 407
Hillier, D.J., Lanz, T., Heap, S.R., Hubeny, I., Smith, L.J., Evans, C.J., Lennon, D.J., Bouret, J.C., 2003, ApJ, 588, 1039
Hoogerwerf, R., de Bruijne, J.H.J. & de Zeeuw, P.T., 2001, A&A, 365, 49
Howarth, I. & Prinja, R.K., 1989, ApJS, 69, 527
Howarth, I.D., Siebert, K.W., Hussain, G.A.J., Prinja, R.K., 1997, MNRAS, 284, 265
Hubeny, I. & Lanz, T., 1995, ApJ, 439, 875
Humphreys, R.M., 1978, ApJS, 38, 309
Kendall, T.R., Lennon, D.J., Brown, P.J.F, Dufton, P.L., 1995, A&A, 298, 489
Klein, R.I. & Castor, J.I., 1978, ApJ, 220, 902
Kudritzki, R.P., Pauldrach, A., Puls, J., Abbott, D.C., 1989, A&A, 219, 205
Kudritzki, R.P., Lennon, D.J., Puls, J., 1995, in "Science with the VLT", Proc. of the ESO workshop held at Garching, Germany, 28 June - 1 July 1994, Eds J.R. Walsh & I.J. Danziger, Berlin, Springer-Verlag, p. 246
Kudritzki, R.P., 1998, in "Stellar astrophysics in the Local Group: first step to the Universe", Proc of the 8$^{\rm th}$ Canary Island winter school, Eds. A. Herrero, A. Aparicio, F. Sanchez, Cambridge University press
Kudritzki, R.P., Puls, J., Lennon, D.J., Venn, K.A., Reetz, J., Najarro, F., McCarthy, J., 1999, A&A, 350, 970
Kudritzki, R.P. & Puls, J., 2000, ARA&A, 38, 613
Lamers, H.J.G.L.M., Cerruti-Sola, M., Perinotto, M., 1987, ApJ, 314, 726
Lamers, H.J.G.L.M. & Leitherer. C., 1993, ApJ, 412, 771
Lamers, H.J.G.L.M., Snow, T.P. & Lindholm, D.M., 1995, ApJ, 455, 269

Lamers, H.J.G.L.M. & Cassinnelli, J.P., 1998, in "From Stars to Galaxies: the impact of stellar physics on Galaxy evolution", ASP conf. series 98, eds. C. Leitherer, U. Fritze-Von Alvensleben & J. Huchra, p. 162
Lamers, H.J.G.L.M., Haser, S., de Koter, A., et al., 1999, ApJ, 516, 872
Lanz, T. & Hubeny, I., 2002, ApJS, 146, 417
Leitherer, C., 1988, ApJ, 326, 356
Lejeune, T. & Schaerer, D., 2001, A&A, 366, 538
Lucy, L.B. & Solomon, P.M., 1971, ApJ, 159, 879
Lucy, L.B. & White, 1980, ApJ, 241, 300
MacFarlane, J.J., Cohen, D.H., Wang, P., 1994, ApJ, 437, 351
Maíz-Apellániz, J., Walborn, N.R., Galué, H.Á., Wei. L.H., 2004, ApJS, 151, 103
Markova, N, Puls, J., Repolust, T., Markov, H, 2004, A&A, 413, 693
Massa, D., Fullerton, A.W., Sonneborn, G., Hutchings, J.B., 2003, ApJ, 586, 996
Martins, F., Schaerer, D., Hillier, D.J., 2002, A&A, 382, 999
Martins, F., Schaerer, D., Heydari-Malayeri, M., in "A massive star odyssey: from main sequence to supernova", eds K.A. van der Hucht, A. Herrero, C. Esteban , IAU symp. 212, p. 564
Martins, F., Schaerer. D., Hillier, D.J., Heydari-Malayeri, M., 2004, A&A, 420, 1087 (paper I)
Martins, F., Schaerer, D., Hillier, D.J., 2005, A&A, submitted
Massey, P., DeGioia-Eastwood, K., Waterhouse, E., 2001, ApJ, 421, 1050
Mason, B.D., Gies, D.R., Hartkopf, W.I., Bagnuolo, W.G., Brummelarr, T.T., McAlister, H.A., 1998, ApJ, 115, 821
Pellerin, A., Fullerton, A.W., Robert, C., et al., 2002, ApJS, 143, 159
Milne, E.A., 1926, MNRAS, 86, 459
Olson, G.L., 1982, ApJ, 255, 267
Owocki, S.P., Castor, J.I., Rybicki, G.B., 1988, ApJ, 335, 914
Owocki, S.P. & Puls, J., 1999, ApJ, 510, 355
Pauldrach, A., Puls, J., Kudritzki, R.P., 1986, A&A, 164, 86
Pilyugin, L.S., Ferrini, F., Shkvarun, R.V., 2003, A&A, 401, 557
Penny, L. R., 1996, ApJ, 463, 737
Prinja, K.R., Barlow, M.J. & Howarth, I.D., 1990, ApJ, 361, 607
Puls, J., Kudritzki, R.P., Herrero, A., et al., 1996, A&A, 305, 171
Puls, J., Springmann, U., Lennon, M., 2000, A&AS, 141, 23
Puls, J., Urbaneja, M. A., Venero, R., Repolust, T., Springmann, U., Jokuthy, A., Mokiem, M.R., 2005, A&A, submitted
Raymond, J.C. & Smith, B.W., 1977, ApJS, 35, 419
Repolust, T., Puls, J., Herrero, A., 2004, A&A, 415, 349
Rolleston, W.R.J., Smartt, S.J., Dufton, P.L., Ryans, R.S.I., 2000, A&A, 363, 537
Santolaya-Rey, A.E., Puls, J. & Herrero, A., 1997, A&A, 323, 488
Schmidt-Kaler, T., 1982, in Landoldt-Börnstein, New Series, Group, VI, Vol.2, eds. K. Schaifers & H.H. Voigt (Berlin: Srpinger-Verlag), 1
Schulz, N.S., Canizares, C., Huenemoerder, D., Tibbets, K., 2003, ApJ, 595, 365
Smartt, S.J., Venn, K.A., Dufton, P.L., Lennon, D.J., Rolleston, W.R.J., Keenan, F.P., 2001, A&A, 367, 86
Ud'Doula, A. & Owocki, S.P., 2002, ApJ, 576, 413
Vacca, W.D., Garmany, C.D. & Shull, J.M., 1996, ApJ, 460, 914
van Rensbergen, W., Vanbeveren, D., de Loore, C., 1996, A&A, 305, 825
Villamariz, M.R., Herrero, A., Becker, S.R., et al., 2002, A&A, 388, 940
Vink, J., de Koter, A. & Lamers, H.J.G.L.M., 2000, A&A, 362, 295
Vink, J., de Koter, A. & Lamers, H.J.G.L.M., 2001, A&A, 369, 574
Walborn, N. & Parker, J., 1992, ApJ, 399, L87
Walborn, N., Nichols-Bohlin, J., Panek, R.J., 1985, IUE Atlas of O-Type stellar spectra, NASA RP 1155
Walborn, N.R., Howarth, I.D., Lennon, D.J., Massey, P., Oey, M.S., Moffat, T., Skalkowski, G., Morrell, N.I., Drissen, L., Parker, J.W., 2002, AJ, 123, 2754

Chapter 9

Conclusion

9.1 Summary

In this thesis, we have explored the possibilities offered by the new generation of atmosphere models for massive stars. We have first studied the quantitative effects of line blanketing and second, we have applied these models to the analysis of massive stars with weak winds. We recall the main results we have obtained in the following.

Line blanketing:

The various effects of line blanketing were known qualitatively before the atmosphere models included this ingredient in a reliable way. This was due to both theoretical expectations and results from exploratory analysis with approximated models. The code CMFGEN is the first one which includes line blanketing in a direct way, almost without approximation: the energy levels of metals are included in the calculation as H and He levels, and their detailed populations are computed through the resolution of statistical equations. The only approximation is the grouping of levels of close energy in super-levels to reduce the computational cost. However, this approximation can be easily dropped, provided that the computational resources are available. We have estimated for the first time the quantitative effects of line blanketing on model atmosphere of O stars as predicted by CMFGEN, a code devoted to the modelling of massive stars atmospheres. The main results can be summarised as follows:

- ◇ The expected effects of line blanketing on the emergent spectrum and the atmospheric structure are confirmed quantitatively (see Chap. 3). First, the inclusion of numerous transitions from metals increases the scattering of photons which renders the radiation field more isotropic. This means that on average, less photons are emitted towards the exterior of the atmosphere, and consequently that the energy transfer is reduced. In order to maintain the flux (which is fundamental to

evacuate the energy produced in the interior) the solution found by the star is to increase its temperature gradient to compensate for the increased isotropy of the radiation field. The direct consequence is a heating of the deeper layers, an effect called backwarming and from which the term line blanketing was created (the metals behave as a blanket which heats the underlying layers by reducing the transfer of energy). The increase of temperature produces a higher ionisation in the inner parts of the atmospheres where LTE is still valid. However in the outer atmosphere, the ionisation is reduced. The reason is that it is dominated by radiative processes. But due to the metal opacities (including bound-free opacities) the ionising radiation (essentially below 912 Å) is blocked and leads to a lower ionisation in the outer atmosphere. The combination of the blocking of (extreme) UV radiation and the backwarming effect makes the short wavelength flux be redistributed at longer wavelengths (since the energy must go out by any means). For O stars, this redistribution takes primarily place below the Lyman break (912 Å).

◇ The modification of the atmospheric structure due to line blanketing leads to a revision of the effective temperature scale for O stars (see Sect. 3.3). Indeed, as the ionisation is increased in the formation region of diagnostic lines used for the spectral classification of O stars, for a given effective temperature an earlier spectral will be assigned to a model with line blanketing compared to a model without metals. Equivalently, this means that a lower effective temperature is required to achieve the same ionisation, i.e. the same spectral type. This boils down to a downward revision of the relation between effective temperature and spectral type. Quantitatively, this reduction goes from $\sim$ 1500 K at the later spectral types to $\sim$ 4000 K at spectral type O3 for dwarfs.

Independently of our study, this result has been confirmed by several groups for other luminosity classes (giants and supergiants, see Crowther et al., 2002a; Herrero, Puls & Najarro, 2002; Repolust, Puls & Herrero, 2004; Markova et al., 2004). Our theoretical study (in the sense that it is only based on models without confrontation to observations) is confirmed by spectroscopic analysis of massive stars (Sect. 3.3.2). The agreement between our prediction and effective temperatures of O dwarfs is good for spectral types later than O5, whereas for earlier spectral types, the situation is not clear and requires more stars to be studied.

◇ The expected metallicity dependence of the effects of line blanketing and of the effective temperature scale of O stars is shown quantitatively for the first time on the basis of atmosphere models including

line-blanketing (Sect. 3.3.3). As line blanketing relies on the effects of the inclusion of metals in the atmosphere models, reducing the metal content should reduce the effect of line blanketing. For a metallicity typical of the Small Magellanic Cloud ($Z = 1/8\ Z_\odot$) the reduction of the effective temperature due to line blanketing is $\sim$ half the reduction obtained for solar metallicity.

- ◇ The ionising radiation of O stars is influenced by line blanketing (see Sect. 4.1). This is especially true for the He II ionising flux which is strongly reduced when metals are included since metals have most of their bound-free transitions in the (extreme) UV range. The He I ionising flux is much less reduced and the Lyman flux is almost unchanged for a given $T_{\rm eff}$. This explanation comes from the fact that the flux redistribution imposed by the blocking of radiation is essentially done below the Lyman break. However, the ionising fluxes as a function of spectral types are reduced, due to the cooler effective temperature scale of O stars. The ionisation of nebulae should be strongly affected by such changes.

  We have shown the importance of the inclusion of all lines in the radiative transfer problem (Sect. 4.2), since interactions between lines can modify the ionisation and consequently the emergent flux. This is especially true in the case of He II λ304 which controls the He ionisation. This shows that the inclusion of line blanketing through statistical methods (opacity sampling, opacity distribution functions) may miss important radiative transfer processes.

  We have tested the spectral energy distribution of O stars with the help of mid-IR emission lines in compact Galactic HII regions (Sect. 4.3). Such lines are produced in the nebula but depend on the ionisation radiation of the star(s) powering the HII region. Compared to previous models without line blanketing, the new generation of atmosphere models including winds and metals give a much better agreement with observations. Moreover, the metallicity of both the gas and the stellar atmospheres is a crucial parameter to understand the observed nebular lines.

Our studies of the effect of the inclusion of line-blanketing in the atmosphere models of O stars have revealed that line-blanketing was an important ingredient which could change quantitatively our knowledge of the properties of O stars.

Winds of O stars

Once the main effects of the inclusion of line blanketing in massive star atmosphere models were known, we applied these new models to the

quantitative analysis of stellar and wind properties of young massive stars. We first concentrated on the components of the star forming region SMC-N81 and then extended our study to Galactic dwarfs. The aims were to study the stellar content of one of the High Excitation Blobs found in the Magellanic Clouds (N81) and to investigate the metallicity dependence of the wind properties of massive stars. The results of these different studies are summarised below:

- ◇ The cluster powering the HII region of the HEB SMC-N81 is composed of young massive stars with surprisingly weak winds (Chap. 6). These stars are mid to late O dwarfs with a lower luminosity compared to classical dwarfs and are probably 3-4 Myrs old. Their winds are extremely weak as first shown by their UV spectra with no emission lines in the traditionally wind sensitive features (Sect. 7.1). This puts upper limits on their mass loss rates of the order of $10^{-8..-9}$ $M_\odot$ yr^{-1}. The weakness of the wind associated with the subluminosity may render the SMC-N81 stars Vz components, i.e. dwarfs thought to lie closer to the ZAMS than "normal" luminosity class V stars (younger stars). However, the absence of optical spectra (from which the Vz character can be established) and the estimated age of the stars do not allow a firm statement.

- ◇ The study of Galactic O dwarfs including true Vz stars indicates that weak winds also exist in the Galaxy (Chap. 8). The combined analysis of UV and optical spectra reveals mass loss rates as low as 10^{-10} $M_\odot$ yr^{-1}. However, there seems to be a trend for weak wind stars to have low luminosities, and at least luminosities lower than $\sim 10^{5.2} L_\odot$. This was already noticed a decade ago by Chlebowski & Garmany (1991) in their study of Galactic stars. However, they used the method of Olson (1982) which is similar to the SEI method explained in Sect. 7.1 and which allows determinations of mass loss rates through fits of UV wind sensitive lines under several approximations concerning the shape of the radiation field (blackbody), the ionisations (one or two ions gathering the populations of the whole element) and the radiative transfer (Sobolev approximation).

- ◇ The modified wind momentum - luminosity relation of O dwarfs shows a new behaviour at low luminosities (Sect. 7.1 and Chap 8). The discovery of stars with weak winds translates to a steeper slope or a breakdown of the WLR below $\sim 10^{5.2} L_\odot$. This behaviour was mentioned (although without emphasis) by Puls et al. (1996) in view of the upper limits on $\dot{M}$ they obtained for a few low luminosity dwarfs, but a recent reanalysis of the same objects with improved atmosphere models (Repolust, Puls & Herrero, 2004) do not show any more this trend *although the values of $\dot{M}$ for the low luminosity*

stars are still only upper limits which does not contradict our results. Above this transition luminosity, the WLR seems to have the same slope for all luminosity classes, although the exact absolute position of the relation is still uncertain.

◇ The weakness of the winds observed in O dwarfs with low luminosities is puzzling. Indeed, such low $\dot{M}$ have never been determined before (except for 3 stars recently analysed by Bouret et al., 2003). The reason is that the improved atmosphere models are much more reliable and produce more realistic spectra allowing to disentangle the effects of mass loss down to $10^{-10..-11}$ $M_\odot$ yr^{-1} in wind sensitive lines. The access to the extreme UV range (in particular thanks to FUSE) also reveals new mass loss rate indicators. Finally, the low density of the winds of such stars renders other methods (i.e. other than detailed atmosphere modelling) unreliable (e.g. "H_α method" of Puls et al. (1996), radio measurements).

◇ For the few high luminosity stars we have studied, we find more standard mass loss rates, although they are still a factor of $\sim 3-5$ lower than $\dot{M}$ derived from H_α only. This is an indication that there is no systematic trend in our analysis to find low mass loss rates since for high L stars, $\dot{M}$ is closer to what has already been observed while for low L stars, the difference is much higher.

The mass loss rates we find are also lower than the predictions of the current generation of hydrodynamical models (Vink, de Koter & Lamers, 2001). Moreover, such simulations do not indicate any variation of the slope of the WLR with luminosity or luminosity class. For high luminosity stars, the lower mass loss rates we derive are simply the result of the use of clumped models. Indeed, introducing clumping leads to a reduction of $\dot{M}$ (e.g. Hillier et al., 2003; Repolust, Puls & Herrero, 2004). Moreover, there are more and more observational and theoretical evidences that the winds of O stars are clumped (e.g. Crowther et al., 2002a; Bouret et al., 2003) so that the use of inhomogeneous models is relevant. Concerning low luminosity O stars, possible explanations for the weakness of the winds are:

→ a metallicity effect: this hypothesis was raised during our study of the SMC-N81 stars (Sect. 7.1) since at that time, the only stars with weak winds were the N81 components and the NGC 346 stars studied by Bouret et al. (2003), all SMC stars. As the wind properties are expected to depend on the metal content, this explanation was natural. And indeed, the radiation driven wind theory predicts a lowering of the α parameter at low Z, which means a steeper slope of the WLR (Sect. 7.2.2). However, the discovery of stars with weak winds in the Galaxy seems to exclude this possibility. This is confirmed by the hydrodynamical simulations which do not predict any

variation of the slope of the WLR at metallicities typical of the Small Magellanic Cloud.

→ decoupling: in winds with low densities, the Coulomb interactions between the ions absorbing photons and the passive plsama may be insufficient to redistribute momentum, resulting in a decoupling between absorbing species and non absorbing species. In that case, multicomponent winds may develop for which the predictions of traditional simulations may be inappropriate. However, we have tested several conditions for decoupling to occur in radiatively driven winds, and they do not reveal the onset of multicomponents winds in the stars we have studied (Sect. 7.2.3).

→ youth of the stars: one possibility is that the weakness of the wind may be related to the youth of the stars (Sect. 7.1). In young objects, we may witness the onset of radiatively driven winds which are known to get stronger as the star evolves and which may be weak in the earliest phases of the evolution. However, in our study we find "normal" dwarfs showing weak winds and Vz stars with more standard mass loss rates (Chap. 8). Hence, the physical parameters responsible for the weakness of the wind have not yet been identified.

→ approximations of hydrodynamical models: one of the main point of the puzzle comes from the disagreement between results of spectroscopic analysis with atmosphere models and predictions of hydrodynamical simulations. Although both models are certainly not perfect, several assumptions of the hydrodynamical simulations may have an effect on the predictions. In particular, the use of the Sobolev approximation to compute the radiative acceleration may overestimate this acceleration (Sect. 7.2.1). The presence of a diffuse radiation field in stars with relatively low densities may indeed reduce the total acceleration and consequently the mass loss rate. However, the studies of this effect lead so far point to an overestimation of $\dot{M}$ by a factor of 2, much lower than the factor needed to reconcile our results with the predicted values. Similarly, the basic assumption that the radiative acceleration can be written $g \propto t^{-\alpha}$ may break down in certain extreme cases (Sect. 7.2.1).

Our studies have revealed the existence of weak winds in O dwarfs of the Magellanic Clouds and the Galaxy. There seems to be a trend of weak winds with low luminosity dwarfs, at least for stars with $L \lesssim 10^{5.2} L_{\odot}$. There is almost no star of other luminosity class below this luminosity, so that it is not possible to say if this behaviour is characteristic of dwarfs or concerns all O stars. The exact reason for such a weakness is not clear and the physical parameters responsible for it have not yet been identified.

9.2 Perspective

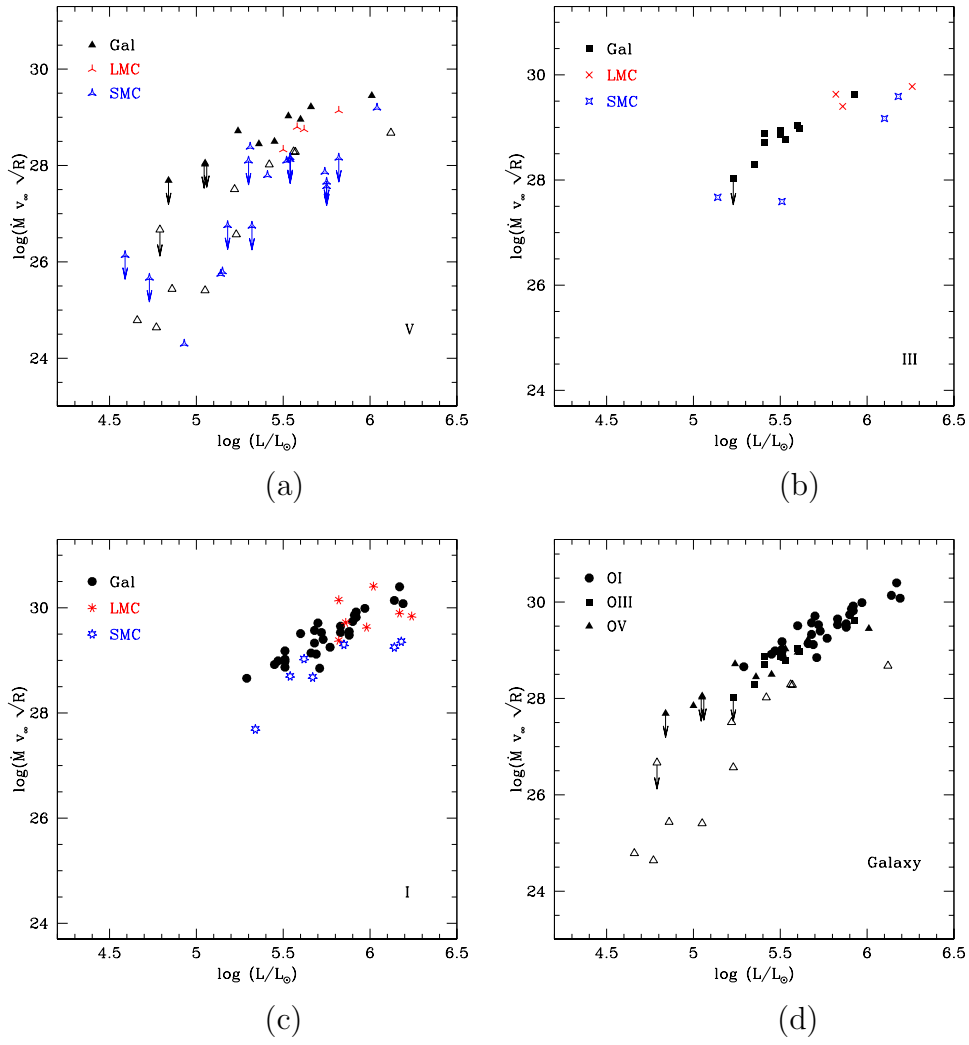

Figure 9.1: Modified wind momentum - luminosity relation for Galactic and Magellanic Clouds stars. (a) shows the relation for dwarfs, (b) for giants and (c) for supergiants. (d) shows the WLR for Galactic stars of all luminosity classes. The stars studied in this thesis are marked by open triangles in (a) and (d). For clarity, error bars have not been added to our points in (a) and (d). Data are from Herrero, Puls & Najarro (2002); Crowther et al. (2002a); Bouret et al. (2003); Hillier et al. (2003); Repolust, Puls & Herrero (2004); Markova et al. (2004); Massey et al. (2004) and this thesis.

Given the questions that were raised in the introduction, can we say that an answer was brought? Not for all, certainly. This is especially true as for the formation of massive stars. Indeed, we expected that the stars

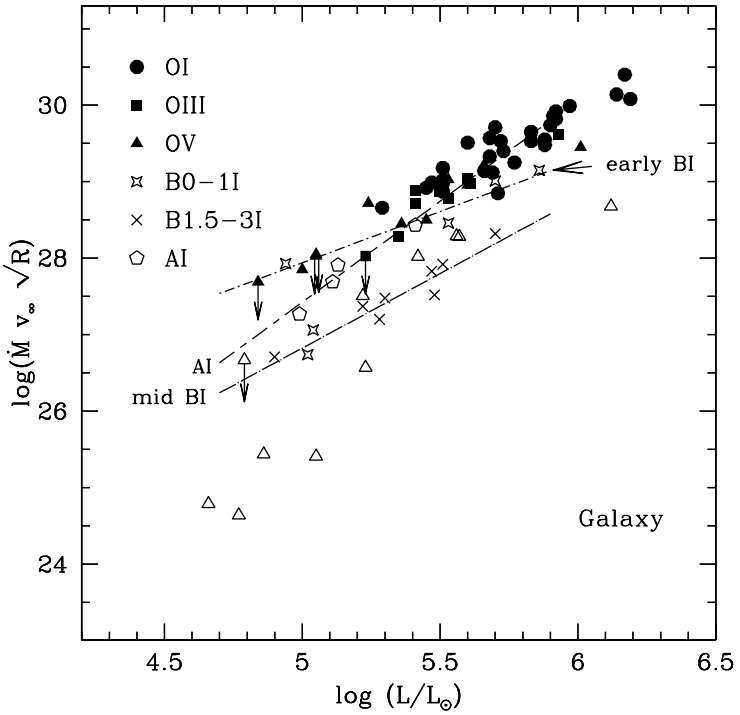

Figure 9.2: Modified wind momentum - luminosity relation for Galactic O, B and A stars. Filled circles (rectangles, triangles) are O supergiants (giants, dwarfs) and open triangles are the O dwarfs studied in this thesis. Open stars are B0-1 supergiants, open pentagons are B1.5-3 supergiants and crosses are A supergiants. Various regression curves are also shown: long dashed line for O supergiants, short dashed line for O giants + dwarfs (from Repolust, Puls & Herrero, 2004), dot - short dashed line for B0-1 supergiants, short dash - long dashed line for B1.5-3 supergiants and dot - long dashed line for A supergiants. Data are from Kudritzki et al. (1997); Herrero, Puls & Najarro (2002); Crowther et al. (2002a); Bouret et al. (2003); Hillier et al. (2003); Repolust, Puls & Herrero (2004); Markova et al. (2004); Massey et al. (2004) and this thesis .

observed in the HEB N81 would help us constrain the properties of massive stars just emerging from their parental cloud. But it turns out that these stars are already 3-4 Myrs old, which means that they have already evolved from the ZAMS. Does it mean that HEBs are not the ideal objects to catch massive stars at birth? Again, the answer is probably no, since there is a variety of HEBs and the stellar content is not so easy to distinguish in all of them. This may due to the fact that some of them are less evolved in the sense that the stellar cluster they harbour have not yet blown the surrounding interstellar medium: in that case young stars may still be present in the HEB. Or this may be an indication that the stellar content

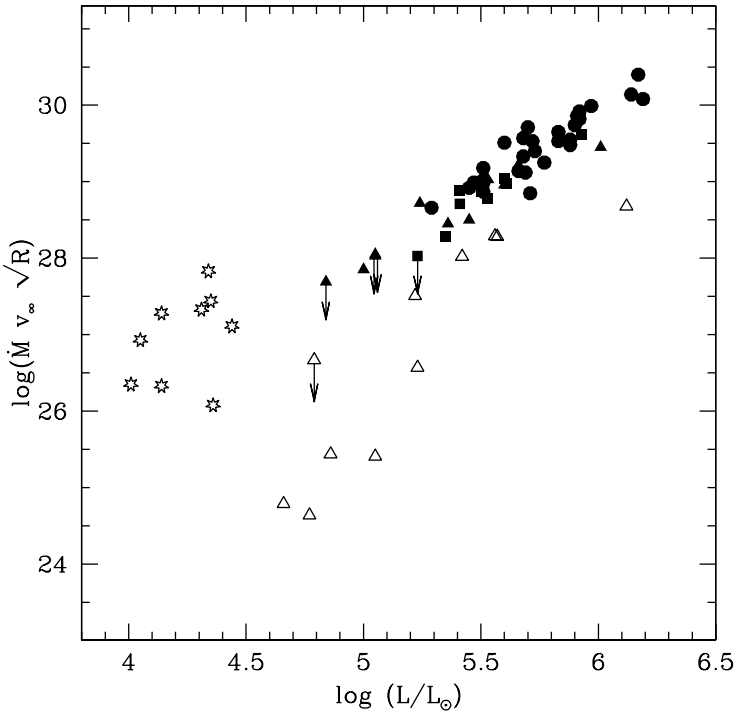

Figure 9.3: Modified wind momentum - Luminosity relation for Galactic O stars and central Stars of Planetary nebulae (CSPN). Symbols for O stars are the same as in Fig. 9.2 and open asterisks are for CSPNs. The modified wind momenta of CSPNs fall on the WLR established for luminous O stars and the O dwarfs studied in this thesis have again weaker winds than CSPNs. Data for O stars are the same as in Fig. 9.2 and are from Kudritzki et al. (1997) for CSPNs.

is different (number of stars, nature of stars...), implying a different release of mechanical energy and then a different aspect of the region. In any case, this indicates that if we want to observe (very) young massive stars, we have to concentrate on HEBs where the stellar content is still not visible or on more compact regions where massive stars are still somewhat embedded in the molecular cloud. In that case, the use of IR spectroscopy seems to be unavoidable. The other possibility is to investigate more deeply young massive clusters such as NGC 3603 in the Galaxy or R 136 in the LMC: these clusters are young (1-2 Myrs, de Koter et al., 1998; Sung & Bessel, 2004) but already accessible in the optical range, probably due to the fact that they contain a number of "very" massive (60-80 $M_{\odot}$) stars which have already blown the interstellar medium.

What about the effects of winds in star formation? The discovery of stars with weak winds may have several implications. First, we have mentioned that massive stars may be at the origin of second generation star

formation events because their strong release of mechanical energy can trigger the collapse of neighbouring molecular clouds. Can low mass loss rates in low luminosity dwarfs affect this picture? Probably not. Indeed, most of the release of mechanical energy happens in the supergiants and later stages of evolution and in the supernova explosion. Moreover, second generation star formation is usually triggered by the presence of a cluster of massive stars, which means that high luminosity stars including supergiants are present. Hence, the existence of weak winds for the faintest dwarfs may not strongly modify the global release of mechanical energy in a cluster. However, the reduced mass loss rates may be of prime importance for the formation of individual massive stars. Indeed, a wind may interact with the accretion flow if massive stars are formed by accretion. And the weaker the wind, the weaker the interaction. This means that the influence of winds in the formation process of massive stars may be reduced for the lowest luminosity massive stars. This is of course purely qualitative and speculative since no study of the possible effects of the wind of the star in simulations of individual star formation has been done so far.

The reduction of the wind strength may also have implications for the dynamics of bubbles and HII regions. Indeed, a reduced mechanical energy input will slow down the expansion of the wind blown bubble surrounding massive stars. Using the analysis of Dyson (1978), one can estimate that a reduction of the mass loss rate by a factor of 10 will double the time required to reach a given radius. Equivalently, this means that ages of HII regions may be underestimated if one adopt traditional mass loss rates. But this is only true for HII regions harbouring O dwarfs with low luminosity.

One of the main question we wanted to tackle in this thesis was the metallicity dependence of the radiatively driven winds. Do we have a clearer picture of this question? The discovery of weak winds in SMC-N81 added to the study of Bouret et al. (2003) who concentrated on NGC 346 stars first indicated that indeed winds seemed to be much weaker in the Small Magellanic Cloud than in the Galaxy (before those studies, the sample of SMC stars was too small to draw conclusions). But the fact that Galactic stars show winds as weak as the SMC stars casts doubt on this metallicity dependence. In fact, what can we say?

To answer, we have constructed in Fig. 9.1 the modified wind momentum - luminosity relation of a large sample of Galactic stars and all the Magellanic Cloud stars studied so far. We clearly see that for dwarfs (panel (a)) the breakdown of the WLR at low luminosities affects both Galactic and SMC stars, and that there is not any significant difference between both type of objects in this L range. For higher luminosities, the number of objects is still to small to draw any final conclusion, but it seems that

the wind momenta are reduced in the SMC compared to the Galaxy. The slope of the WLR may also be steeper in view of the few points available. Panel (b) of Fig. 9.1 focuses on the WLR of giants (to which we have note contributed) and reveals that too few stars have been studied so far in the Magellanic Clouds (and even the Galaxy) to put forward any trend with metallicity. The situation is a little better for supergiants (panel (c)) which reveals that the WLR of SMC supergiants seems to have the same slope as the Galactic relation, but is shifted downward by ~ 0.5 dex. Note that there is no supergiant with $\log \frac{L}{L_\odot} < 5.2$ so that the existence or not of a breakdown of the WLR for supergiants below this luminosity can not be established at present. The same can be said for giants since there is only one galactic star (however with an upper limit on its modified wind momentum) and one SMC stars with $5.1 < \log \frac{L}{L_\odot} < 5.3$. In panel (d) of Fig. 9.1, we gather the WLR of Galactic dwarfs, giants and supergiants. It shows more clearly the reduced modified wind momenta for stars with $\log \frac{L}{L_\odot} < 5.2$. Above this luminosity, the relation is quite well established (see Kudritzki & Puls, 2000; Repolust, Puls & Herrero, 2004; Markova et al., 2004). From this discussion, we can conclude that no final conclusion as regards the Z dependence of wind properties can be drawn, and more studies are still required. But the picture is now complicated by the presence of stars with weak winds!

How weak are the winds of O dwarfs studied in this thesis in terms of modified wind momenta? Part of the answer has been given in Sect. 7.1 and 8: the modified wind momenta are lower by nearly 2 orders of magnitude compared to what is would be expected if the stars followed the WLR established for higher luminosity stars. Thus, the winds are indeed much weaker than previously observed in O stars. But what about later type stars, say B and A stars? Kudritzki et al. (1999) have studied the WLR of Galactic B and A supergiants which are shown in Fig. 9.2 together with the O stars of Fig. 9.1(d). It is clear from this figure that the winds of the O dwarfs studied in this thesis are also weaker than the winds of B and A supergiants. The interesting point of this figure is that there are stars with "low" luminosities showing more standard wind properties than displayed by the O dwarfs of our sample. However, the spectroscopic studies of Kudritzki et al. (1999) were made with unblanketed atmosphere models and rely only on optical lines. In our study, we have shown that the use of UV lines lead to lower mass loss rates than given by optical lines. Moreover, the inclusion of line-blanketing has important effects, although for B and A stars they are much lower than for O stars.

Central stars of planetary nebulae have also been claimed to follow the WLR since their winds are radiatively driven (Kudritzki et al., 1997). Indeed, these authors have used the method developed by Puls et al. (1996) to derive mass loss rates of a sample of Galactic planetary nebulae and

have shown that they nicely fall on the WLR determined for O stars with the same method. This is shown in Fig. 9.3 if we extend the WLR of luminous O stars to low luminosities. Note however that there is an important scatter in the points related to planetary nebulae. Anyway, this figure shows once again that the winds of O dwarfs with low luminosities have winds weaker than any other objects supposed to have radiatively driven winds.

In view of these results, what could be the next steps to undertake? First, there is no doubt that the origin of the weakness of the winds must be tracked. In this context, one can imagine to run improved hydrodynamical simulations to test the hypothesis raised previously, especially the importance of the diffuse radiative field. This is certainly not trivial, but deserve special care since this ingredient seems to play a role for dwarfs with low luminosity, just those for which we observe weak winds. This does not mean that atmosphere models should not be improved. Indeed, several major assumption remains which may influence the results. One of them is spherical symmetry. Although massive stars rotate with high velocities and rotation is known to break the spherical symmetry, introducing a latitude dependence of the stellar and wind properties, all current atmosphere models us a 1D geometry. A better treatment of rotation is currently under development in CMFGEN, and it will certainly be useful for new studies thanks to improved line profiles formed in the wind and across which the tangential rotational velocity increases with distance to the star. The ratio of emission to absorption in P-Cygni lines will be also modified depending on the inclination of the star since mass loss will depend on latitude. Of course, ideally the other important improvement of the atmosphere models would be a consistent treatment of the hydrodynamics. This always exists in one code (WM-BASIC Pauldrach et al., 1994; Pauldrach, Hoffmann & Lennon, 2001) but at the cost of a more approximated radiative transfer than in CMFGEN.

As for the metallicity dependence of wind properties, a larger sample of MC object is required to establish the exact nature of this dependence. The completion of a ESO large programme with the VLT in the next month (PI S. Smartt, IoA) and the analysis of the obtained spectra will certainly shed more light on this issue. Studies in super-solar environment are also under way in different groups to investigate the behaviour of winds at high metallicity. The calibration of the WLR at different metallicity will also benefit from such studies and in the end may effectively turn out to become a distance indicator.

Concerning the effects of line blanketing, an important thing to do in the future will be a complete and homogeneous re-calibration of the stellar parameters of O stars as a function of spectral type. This can be done either observationally by means of spectroscopic analysis of massive stars,

the problem being to have a sample sufficiently large to cover the whole range of spectral types and luminosity classes. Of course, more and more studies are being carried on and the total sample of stars studied increases, but the methods used are sometimes different which may introduce differences in the results. Alternatively, a study relying only on models (tested on "real" stars to ensure that they give correct results) can be done. We have started such a study and hope to produce such a new calibration in the next months.

At the end of this thesis, we can say that new results concerning the physics of massive stars have been obtained ($T_{\rm eff}$-scale, wind properties...). But, as it is often the case in science, new questions have also been raised! The next step is to answer them.

Chapter 9

Conclusion

9.1 Résumé

Dans cette thèse, nous avons exploré diverses possibilités offertes par les nouveaux modèles d'atmosphères pour étoiles massives. Nous avons dans un premier temps étudié quantitativement les effets du line-blanketing, puis nous avons appliqué ces nouveaux modèles à l'analyse d'étoiles massives avec vents faibles. Dans ce qui suit, nous rappelons les principaux résultats obtenus.

Line blanketing:

Les divers effets du line-blanketing sont connus qualitativement depuis plusieurs années et en tout cas leur découverte est antérieure à l'inclusion du line-blanketing de façon sûre dans les modèles d'atmosphères. Cela est dû à la fois aux prédictions théoriques et à des résultats exploratoires de la précédente génération de modèles. Le code CMFGEN est le premier à inclure le traitement du line-blanketing d'une manière directe, quasiment sans approximation: les niveaux d'énergie des métaux sont inclus dans les calculs comme ceux de l'Hydrogène et de l'Hélium, et leurs populations sont obtenues par la résolution des équations d'équilibre statistique. La seule approximation réside dans le regroupement de niveaux d'énergies voisines en un seul "super-niveau" et ce afin de réduire la consommation en ressources informatiques. Toutefois, cette approximation peut facilement être abandonnée du moment que ces ressources sont disponibles. Nous avons estimé pour la première fois les effets quantitatifs du line-blanketing sur les modèles d'atmosphères d'étoiles massives tels qu'ils apparaissent dans la nouvelle génération de modèles et en particulier dans le cas des modèles CMFGEN. Les principaux résultats sont résumés ci-dessous:

- ◇ Les effets attendus du line-blanketing sur le spectre émergent et la structure de l'atmosphère sont confirmés quantitativement (chapitre 3.3). Tout d'abord, l'inclusion de nombreuses raies de métaux aug-

mente la diffusion des photons ce qui rend le champ de rayonnement beaucoup plus isotrope. Cela implique qu'en moyenne, moins de photons sont transportés vers l'extérieur de l'atmosphère, et donc que le transfert d'énergie est réduit. Afin de conserver le flux au même niveau (dans le but d'évacuer l'énergie produite à l'intérieur de l'étoile) la solution trouvée par l'étoile est d'augmenter les gradients de température au sein de son atmosphère qui vont ainsi compenser l'isotropie accrue du champ de rayonnement. La conséquence directe de cette hausse de température est un chauffage des couches intérieures de l'atmosphère, un effet appelé "backwarming" et qui est à l'origine du terme line-blanketing (blanket signifiant couverture en anglais, et une couverture étant utilisée pour conserver la chaleur en ralentissant les pertes par rayonnement). La hausse de température génère une plus grande ionisation dans les parties internes où l'équilibre thermodynamique local est encore valide. En revanche, dans les couches externes, l'ionisation est réduite. La raison en est que les phénomènes radiatifs sont prépondérants dans cette région. A cause des opacités continues des métaux, le flux ionisant (en dessous de 912 Å) est bloqué, ce qui conduit naturellement à une plus faible ionisation là où ce flux joue un rôle important. La combinaison du blocage du flux ionisant et du backwarming conduit à une redistribution du flux émis aux faibles longueurs d'onde vers des longueurs d'onde plus grandes (et ce car l'énergie doit sortir d'une manière ou d'une autre). Cette redistribution se produit essentiellement en-dessous de la discontinuité de Lyman (912 Å) pour les étoiles O.

◇ La modification de la structure de l'atmosphère due au line-blanketing conduit à une révision de l'échelle de température effective des étoiles O (section 3.3.1). En effet, comme l'ionisation dans les zones de formation des raies utilisées pour la classification spectrale est augmentée, il s'en suit qu'un modèle avec line-blanketing indiquera un type spectral plus précoce qu'un modèle équivalent sans les métaux. De manière similaire, cela signifie qu'une température effective plus basse est requise pour atteindre le même degré d'ionisation, soit le même type spectral. Cela se traduit par une échelle de température effective plus froide. Quantitativement, la réduction va de environ 1500 K pour les types spectraux les plus tardifs à 4000 K pour le type spectral O3, et ce pour des étoiles naines.

Indépendamment de notre étude, ce résultat a été confirmé par d'autres groupes pour d'autres classes de luminosité (géantes et supergéantes, voir Crowther et al., 2002a; Herrero, Puls & Najarro, 2002; Repolust, Puls & Herrero, 2004; Markova et al., 2004). Notre étude théorique (dans le sens où elle est basée sur des modèles sans

confrontation directe avec les observations) est confirmée d'autre part par l'analyse spectroscopique d'étoiles massives. L'accord entre notre prédiction pour les naines O et la température effective dérivée de l'analyse est satisfaisant pour les types spectraux plus tardifs que O5, tandis que pour les types spectraux plus précoces, la situation reste indécise et demande des analyses complémentaires (section 3.3.2).

◇ La dépendance des effets du line-blanketing et de l'échelle de température des étoiles O avec la métallicité est montrée quantitativement pour la première fois. (section 3.3.3). Comme le line-blanketing repose sur le contenu en métaux de l'atmosphère, réduire la métallicité doit conduire à réduire ses effets. Pour une métallicité typique du Petit Nuage de Magellan ($Z = 1/8\ Z_{\odot}$) la réduction de la température effective due au line-blanketing est environ la moitié de ce qu'elle est dans le cas d'un contenu en métaux solaire.

◇ Le flux ionisant des étoiles O est influencé par le line-blanketing (section 4.1). C'est particulièrement vrai pour le flux ionisant He II qui est fortement réduit quand les métaux sont inclus car ceux-ci ont une grande partie de leurs seuils d'ionisation dans le domaine (extrême) UV. Le flux ionisant He I est beaucoup moins réduit, et le flux ionisant H est quasiment inchangé pour une température donnée. L'explication tient au fait que la redistribution du flux imposée par le blocage à courtes longueurs d'onde se fait principalement dans le domaine UV, sous la discontinuité de Lyman. En revanche, les flux ionisants Lyman sont modifiés si on les considère en fonction du type spectral, et ce à cause du changement de l'échelle de température.

Nous avons montré l'importance de l'inclusion de toutes les raies dans le transfert de rayonnement car des interactions peuvent se produire entre elles avec des conséquences pour la structure d'ionisation (section 4.2). C'est en particulier le cas pour la raie He II λ304 qui contrôle l'ionisation de l'Hélium. Cela montre que l'inclusion du line-blanketing avec des méthodes statistiques (échantillonnage d'opacités, fonction de distribution des opacités) peut conduire à l'omission de processus de transfert radiatifs importants.

Nous avons testé la distribution spectrale d'énergie des étoiles O au moyen de raies infrarouge moyen émises par des régions HII compactes de la Galaxie (section 4.3). De telles raies sont produites dans la nébuleuse et dépendent du flux ionisant émis par la ou les étoiles présentes dans le région HII. En comparaison des modèles précédents sans line-blanketing, la nouvelle génération de modèles incluant les vents et les métaux donne un meilleur accord avec les observations. De plus, la métallicité à la fois du gaz et de l'étoile apparaissent

comme des paramètres fondamentaux pour expliquer les raies observées.

Vents des étoiles O

Une fois que nous avons mieux compris les effets des métaux sur les modèles d'atmosphères d'étoiles massives, nous avons appliqué ces modèles à l'analyse quantitative des propriétés stellaires et de vent d'étoiles massives jeunes. Nous nous sommes tout d'abord penchés sur le cas des composantes du "High Excitation Blob" N81 dans le Petit Nuage de Magellan, puis nous avons étendu l'étude à des étoiles naines Galactiques. Les buts étaient d'une part de mieux connaître le contenu stellaire des HEBs, et d'autre part de contraindre la dépendance en métallicité des vents des étoiles O. Les résultats de ces différentes études sont résumés comme suit:

- ◇ L'amas à l'origine de la région HII du HEB SMC-N81 est composé de jeunes étoiles massives montrant des vents étonnamment faibles (chapitre 6). Ces étoiles ont un type spectral O moyen à tardif et sont des naines de luminosité inférieure à celle des naines classiques. Leur âge est de l'ordre de 3-4 millions d'années. Leurs vents sont extrêmement faibles comme en témoignent leurs spectres UV sans aucune émission dans les raies traditionnellement sensibles à la perte de masse. Cela conduit à mettre une limite supérieure de $10^{-8...-9}$ $M_\odot$ yr^{-1} sur leur perte de masse (section 7.1). La faiblesse du vent associée à la sous-luminosité fait de ces étoiles de possibles candidats pour appartenir à la classe Vz qui regroupe des étoiles de classe de luminosité V situées proche de la ZAMS (et donc jeunes) dans le diagramme HR. Néanmoins, l'absence de spectres optiques (à partir desquels le caractère Vz peut être établi) et l'âge estimé ne permet pas d'affirmer complètement une telle appartenance.

- ◇ L'étude d'étoiles Galactiques naines O incluant de réelles étoiles Vz montre que les vents faibles existent aussi dans la Galaxie (chapitre 8). L'analyse combinée de spectres UV et optiques révèle des taux de perte de masse aussi bas que 10^{-10} $M_\odot$ yr^{-1}. Il semble qu'il existe une tendance à observer des vents faibles pour des étoiles de luminosités inférieure à $10^{5.2}$ $L_\odot$. Cela avait été indiqué il y a plus de 10 ans par Chlebowski & Garmany (1991), mais cela reposait alors sur une méthode développée par Olson (1982) et qui s'apparente à la méthode SEI utilisée dans la section 7.1. Cette méthode permet de déterminer le taux de perte de masse au moyen de l'ajustement de profils de raies UV avec toutefois un certain nombre d'approximations relatives au champ de rayonnement (corps noir), à l'ionisation (un ou deux ions sont supposés contenir toute la population de l'élément) et au transfert de rayonnement (approximation Sobolev).

◇ La relation quantité de mouvement modifiée - luminosité pour les naines O montre un nouveau comportement à faible luminosité (section 7.1 et chapitre 8). La découverte d'étoiles avec des vents faibles se traduit par une pente plus forte de cette relation et/ou une rupture de pente sous $10^{5.2}$ $L_\odot$. Ceci fut prudemment mentionné par Puls et al. (1996) sur la base de limites supérieures de perte de masse obtenues pour des étoiles O peu lumineuses, mais une récente réanalyse de ces mêmes objets au moyen de modèles d'atmosphères plus sophistiqués (Repolust, Puls & Herrero, 2004) ne montre plus cette tendance, *du moins si l'on se réfère aux limites supérieures adoptées pour les taux de perte de masse de ces étoiles.* Au dessus de cette luminosité de transition, la WLR semble avoir la même pente pour toutes les classes de luminosité, bien que la position exacte en valeur absolue soit toujours incertaine.

◇ La faiblesse des vents observée dans les naines O de faible luminosité est intriguante. En effet, les taux de perte de masse estimés sont plus faibles que ce qui a jamais été observé (exception faite des 3 étoiles de NGC 346 analysées par Bouret et al., 2003). Cela tient au fait que les modèles d'atmosphères actuels montrent une précision accrue et produisent des spectres plus réalistes permettant de pousser les limites de détection des effets de vent jusqu'à des taux de perte de masse de l'ordre de $10^{-10..-11}$ $M_\odot$ yr^{-1}. De plus, l'accès à de nouvelles fenêtres spectrales comme l'UV extrême avec le satellite FUSE a révélé de nouveaux indicateurs de perte de masse. Enfin, la faible densité des vents des étoiles avec faible perte de masse rend impossible l'utilisation de méthodes autres que la modélisation détaillée de l'atmosphère ("méthode H_α" de Puls et al. (1996), déterminations basées sur l'émission radio).

Par ailleurs, les taux de perte de masse que nous déterminons sont aussi plus faibles que ce que prédisent les simulations hydrodynamiques actuelles (Vink, de Koter & Lamers, 2001). Et de plus, ces simulations n'indiquent quasiment aucune variation de la pente de la WLR avec la luminosité ou la classe de luminosité. De possibles explications sont les suivantes:

→ un effet de métallicité : cette hypothèse a été mise en avant lors de notre étude des étoiles de N81 (section 7.1 car à ce moment, les seules étoiles montrant des vents faibles étaient ces dernières et celles étudiées par Bouret et al. (2003) dans NGC 346, autre région du SMC. Comme les propriétés de vent doivent varier avec la métallicité, cette explication était assez naturelle. En effet, la théorie des vents radiatifs prédit une diminution du paramètre α à faible Z, ce qui correspond à une

plus grande pente de la WLR (section 7.2.2). Néanmoins, la découverte d'étoiles avec vents faibles dans la Galaxie semble exclure cette possibilité. Cela est d'ailleurs confirmé par les simulations numériques qui ne montrent pas de variation de la pente de la WLR pour des métallicités typiques du SMC.

→ découplage : dans des vents de faible densité, les interactions de Coulomb entre les espèces absorbantes et les ions passifs peuvent être insuffisantes pour redistribuer la quantité de mouvement gagnée au dépend des photons. Il en résulte un découplage entre espèces absorbantes et espèces passives conduisant au développement de vent multi-composantes pour lesquelles les prédictions des simulations traditionnelles peuvent ne pas être valables. Toutefois, nous avons testé diverses conditions de découplage, et toutes se sont avérées négatives dans les étoiles que nous avons étudiées (section 7.2.3).

→ jeunesse des étoiles : une possibilité est qu'il existe un lien entre entre jeunesse de l'étoile et vent faible (section 7.1). Dans des objets jeunes, il se peut que l'on observe l'émergence des vents radiatifs qui deviendront plus forts au cours de l'évolution mais qui peuvent être relativement faibles dans les phases les plus précoces de l'évolution. Cependant, nous avons trouvé dans notre étude des étoiles naines "normales" montrant des vents faibles et des étoiles Vz montrant des vents plus typiques (chapitre 8). Les paramètres physiques responsables de la faiblesse du vent n'ont donc pas encore été identifiés.

→ approximation des modèles hydrodynamiques : un des points principaux du problème vient du désaccord entre les pertes de masse dérivées des observations et celles prédites par les modèles hydrodynamiques. Bien sûr, les modèles d'atmosphères et les modèles hydrodynamiques sont certainement imparfaits tous les deux. Toutefois, certaines approximations des derniers pourraient affecter les prédictions. En particulier, l'utilisation de l'approximation Sobolev pour le calcul de l'accélération radiative peut conduire à une surestimation de cette dernière (section 7.2.1). La présence d'un gradient négatif du champ diffus de rayonnement dans les étoiles avec des atmosphères de densité relativement faible peut réduire l'accélération radiative globale et donc le taux de perte de masse. Mais la réduction est de l'ordre d'un facteur 2, beaucoup moins que le facteur requis pour reconcilier nos observations et les résultats hydrodynamiques. De façon similaire, l'hypothèse que l'accélération radiative puisse s'écrire $g \propto t^{-\alpha}$ peut s'avérer incorrecte dans certains cas extrêmes (section 7.2.1).

Nos études ont ainsi révélé l'existence de vents faibles dans les étoiles O naines des Nuages de Magellan et de la Galaxie. Il semble y avoir une tendance à l'observation de ces vents faibles dans des étoiles de luminosité inférieure à $10^{5.2}$ $L_{\odot}$. La raison exacte de cette faiblesse reste méconnue.

9.2 Perspectives

Au vu des questions qui avaient été soulevées dans l'introduction, pouvons-nous dire que nous avons apporté des réponses, mêmes partielles ? Certainement, la réponse est "pas pour toutes". C'est notamment le cas pour la formation des étoiles massives. En effet, nous nous attendions à ce que les étoiles du HEB N81 puissent nous aider à mieux contraindre les propriétés des étoiles massives émergeant juste de leur nuage moléculaire parent. Or il se trouve que ces étoiles ont un âge de l'ordre de 3 à 4 millions d'années, autrement dit, elles sont déjà significativement évoluées. Cela veut-il dire que les HEBs ne sont pas de bons candidats pour l'observation d'étoiles massives jeunes ? Non, car les différents HEBs connus n'ont pas tous la même apparence : certains ont un contenu stellaire plus difficile à voir probablement à cause du fait que le gaz n'a pas encore été totalement dissipé autour d'eux. Ceci peut s'expliquer par un âge plus bas, impliquant que les étoiles présentes dans l'amas au cœur du HEB n'ont pas encore soufflé la matière interstellaire environnante. Cela peut également être dû à un contenu stellaire différent (nombre d'étoiles, nature des étoiles) à l'origine d'une éjection d'énergie mécanique différente conduisant elle-même à une apparence différente. Quoi qu'il en soit, cela montre que si l'on veut vraiment voir des objets jeunes, il faut regarder les HEBs les plus compactes ou des régions équivalentes, là où les étoiles sont encore partiellement enfouies. Dans ce cas, le recours aux observations infrarouges est inévitable afin de percer le nuage moléculaire restant. Une autre solution est d'observer des amas plus massifs tels que NGC 3603 dans la Galaxie ou bien R 136 dans le Grand Nuage de Magellan: ces amas sont en effet jeunes (1-2 Myrs, de Koter et al., 1998; Sung & Bessel, 2004) mais sont déjà observables dans le domaine optique, probablement à cause du fait qu'ils contiennent des étoiles très massives (60-80 masses solaires) qui ont un vent suffisamment puissant pour avoir déjà soufflé la matière envorinnante.

Qu'en est-il des effets des vents dans la formation des étoiles massives ? La découverte d'étoiles avec vents faibles peut avoir plusieurs implications. Tout d'abord, nous avons la possibilité que les étoiles massives puissent être à l'origine d'une seconde génération de formation stellaire du fait du fort dépôt d'énergie mécanique dans les nuages moléculaires voisins. Est-ce que l'apparition de vents faibles peut changer cette image ? Probablement non. En effet, la plus grande quantité de l'énergie mécanique est

relâchée lors des phases avancées de l'évolution et lors de la supernova. De plus, une seconde génération de formation stellaire est généralement le fait d'un amas dans lequel on trouve des étoiles massives très lumineuses (dont des supergéantes). La présence de naines avec vents faibles ne doit donc pas modifier quantitativement l'effet de l'amas sur son environnement. En revanche, la réduction de la perte de masse peut être d'importance primordiale pour la formation d'étoiles individuelles. En effet, un vent peut interagir avec un flot d'accrétion, dans le cas où une étoile massive se forme par accrétion. La réduction du vent implique une réduction de cette interaction et donc une croissance de la masse de l'étoile en formation favorisée. Ceci est bien sûr purement spéculatif car aucune étude de l'effet des vents dans les modèles de formation d'étoiles massives n'a encore été réalisée à ce jour.

La réduction de la force du vent peut aussi avoir des implications pour la dynamique des bulles et aures régions HII. En effet, une réduction du dépot d'énergie mécanique va ralentir l'expansion de la bulle entourant l'étoile massive. D'après l'étude de Dyson (1978) on estime qu'une réduction d'un facteur 10 de la perte de masse double le temps nécessaire à la bulle pour atteindre un rayon donné. Cela revient à dire que l'âge d'une région HII peut être sous-estimé si on adopte un taux de perte de masse plus traditionnel. Ceci n'est bien sûr vrai qu'autour d'une étoile naine O de faible luminosité.

Une des questions fondamentales que nous souhaitions aborder dans cette thèse était la dépendance avec la métallicité des vents radiatifs. Avons-nous une meilleure vue de la question ? La découverte d'étoiles avec vents faibles dans le HEB SMC-N81 ajoutée à l'étude de Bouret et al. (2003) qui s'était concentrée sur NGC 346 semblait indiquer des vents beaucoup faibles dans le Petit Nuage de Magellan que dans la Galaxie. Mais le fait que de tels vents existent aussi dans la Galaxie remet en doute un seul effet de métallicité. Que peut-on donc dire finalement ?

Pour tenter de répondre, nous avons construit la Fig. 9.1 qui montre la WLR pour un large échantillon d'étoiles Galactiques et toutes les étoiles des Nuages de Magellan analysées à ce jour. Nous voyons clairement que pour les étoiles naines (encart (a)) la rupture de la pente de la WLR se produit à la fois pour les étoiles galactiques et pour les étoiles du Petit Nuage de Magellan. D'autre part, il n'y a pas de différence significative entre les quantités de mouvement modifiées des étoiles Galactiques et du SMC dans ce domaine de faible luminosité. Pour les objets à plus forte luminosité, le nombre d'étoiles étudiées reste faible, mais il semble que la WLR soit légèrement décalée vers le bas dans le cas du SMC. La pente de la relation peut aussi être plus faible au vu des points disponibles à l'heure actuelle. L'encart (b) de la Fig. 9.1 montre la WLR pour les étoiles géantes (à laquelle nous n'avons pas contribué) et révèle que le nombre

d'objets étudié est trop faible pour montrer une quelconque dépendance en métallicité. La situation est un peu plus décantée en ce qui concerne les étoiles supergéantes (encart (c)) pour lesquelles la WLR dans le SMC semble avoir la même pente que dans la Galaxie, mais en étant décalée de ~ 0.5 dex vers le bas. Notons au passage qu'aucune étoile supergéante avec une luminosité $\log \frac{L}{L_\odot} < 5.2$ n'a été analysée à ce jour, laissant en suspens la question d'une rupture de pente de la WLR pour les supergéantes en dessous de cette luminosité. C'est d'ailleurs la même chose pour les géantes puisqu'une seule étoile galactique (avec une limite supérieure sur la valeur de la perte de masse toutefois) et une seule étoile du SMC avec des luminosités $5.1 < \log \frac{L}{L_\odot} < 5.3$ ont été analysées. L'encart (d) de la Fig. 9.1 rassemble les données des étoiles galactiques et montre clairement la réduction de la quantité de mouvement modifiée pour les étoiles de luminosité inférieure à $10^{5.2} L_\odot$. Au-dessus de cette valeur, la relation est mieux établie (see Kudritzki & Puls, 2000; Repolust, Puls & Herrero, 2004; Markova et al., 2004). De ce qui précède il ressort qu'aucune conclusion définitive quant à la dépendance avec la métallicité de la WLR ne peut être établie pour le moment, et ce d'autant plus que l'existence d'étoiles montrant des vents faibles complique le problème.

Quel est le niveau de faiblesse du vent de ces étoiles en terme de quantité de mouvement modifiée ? Nous avons partiellement répondu à cette question dans les sections 7.1 et 8 : les quantités de mouvement modifiées sont plus faibles d'un facteur 10 à 100 comparé à ce que l'on attendrait d'une simple extrapolation de la WLR établie pour les étoiles de plus forte luminosité. Les vents de ces naines sont donc beaucoup plus faibles que pour toutes les autres étoiles O observées jusqu'à présent. Qu'en est-il par rapport à des étoiles de type plus tardif comme les étoiles B et A ? Kudritzki et al. (1999) ont étudié la WLR d'étoiles supergéantes de type A et B et les résultats sont montrés dans la Fig. 9.2, superposés à ceux de la Fig. 9.1(d) pour les étoiles O. On voit très bien sur cette figure que les étoiles naines O étudiées dans cette thèse ont des vents plus faibles que les supergéantes B et A. Le point intéressant de cette figure est que l'on voit qu'il existe des étoiles de faible luminosité montrant des vents plus "normaux" que notre échantillon de naines O, révélant qu'il doit exister une raison physique à la faiblesse des vents que nous observons différenciant le comportement des naines O et des supergéantes B et A. Notons toutefois ici que les résultats concernant les étoiles supergéantes B et A ont été obtenus au moyen de modèles d'atmosphère n'incluant pas le line-blanketing et reposent uniquement sur les raies de Balmer observées dans le domaine optique. Nous avons montré que l'utilisation des raies UV pouvait conduire à des valeurs de taux de perte de masse plus faibles que les seules raies optiques, et que le line-blanketing avait une importance considérable pour les étoiles O, mais il est vrai plus réduite pour les étoiles

de type plus tardif.

Kudritzki et al. (1997) ont aussi montré que les étoiles centrales de nébuleuses planétaires suivaient la WLR puisque leur vents sont supposés être générés par l'accélération radiative due aux raies. Ces auteurs ont utilisés la méthode développée par Puls et al. (1996) pour déterminer les taux de perte de masse des étoiles centrales de nébuleuses planétaires et ont montré que ces objets suivaient la relation obtenue pour les étoiles O de forte luminosité. C'est ce que l'on voit sur la Fig. 9.3. On constate toutefois une importante dispersion pour les points des nébuleuses planétaires. Quoi qu'il en soit, cette figure montre une fois encore que les vents des étoiles naines de type O sont plus faibles que ceux de n'importe quel autre objet ayant un vent radiatif.

Au vu de ces résultats, quelles sont les pistes à explorer dans le futur ? En priorité, la recherche de l'origine de la faiblesse de vents des étoiles naines de faible luminosité doit être entreprise. Dans ce cadre, on peut imaginer de tester des modèles hydrodynamiques améliorés et incluant les ingrédients mentionnés auparavant, notamment le champ radiatif diffus. Cela n'est probablement pas trivial mais mérite que l'on s'y attache. Par ailleurs, les modèles d'atmosphères pourront eux aussi être améliorés dans l'avenir car ils incorporent encore un certain nombre d'approximations. L'une d'entre elles est l'hypothèse d'une symétrie sphérique qui est faite. Or, on sait que les étoiles massives tournent vite sur elles-mêmes et que la rotation brise cette symétrie en introduisant une dépendance en latitude des propriétés stellaires et de vent. Un traitement de ces effets de rotation est en cours de développement dans CMFGEN et devrait permettre d'obtenir des profils de raie encore plus précis dans un futur proche, notamment pour les raies formées dans le vent et pour lesquelles la vitesse tangentielle de rotation ($V \sin i$) varie dans le profil puisqu'elle est directement proportionnelle à la distance du centre de l'étoile. D'autre part, le rapport de l'émission à l'absorption dans les profils P-Cygni sera modifié par la prise en compte de la dépendance en latitude de la perte de masse, conduisant à des profils de raies de meilleure qualité. Par ailleurs, une importante amélioration serait la construction de modèles cohérents entre l'hydrodynamique et le transfert radiatif. Actuellement, seule une tentative a été faite (code WM-BASIC Pauldrach et al., 1994; Pauldrach, Hoffmann & Lennon, 2001) mais le transfert de rayonnement n'est pas aussi performant que dans CMFGEN (qui reste pour le moment la référence dans le domaine des étoiles massives avec vents).

En ce qui concerne la dépendance en métallicité des propriétés de vent, un plus grand échantillon d'objets des Nuages de Magellan est requis. Actuellement, un large programme d'observations de tels objets avec le VLT (P.I. S. Smartt, IoA) est sur le point d'être bouclé. Nul doute qu'il servira à avancer sur la question. Diverses études dans des environnements

supersolaires sont également en cours. La calibration de la WLR pour diverses métallicités bénéficiera elle aussi des ces programmes et pourra peut-être finalement servir d'indicateur de distance.

Pour ce qui est des effets de line-blanketing, une chose importante à envisager est une recalibration des propriétés stellaires des étoiles O en fonction du type spectral. Cela peut être fait observationnellement grâce à l'analyse spectroscopique d'un grand nombre d'étoiles massives. Le problème dans ce cas est d'avoir un échantillon suffisamment large pour couvrir tout le domaine de types spectraux et de classes de luminosités. De plus, les méthodes utilisées peuvent être différentes d'une étude à l'autre avec de possibles effets sur les résultats. Alternativement, on peut imaginer une étude basée uniquement sur des modèles. Nous avons commencé une telle étude et espérons produire des résultats dans les prochains mois.

En fin de compte, cette thèse aura permis d'amener de nouveaux résultats concernant la physique des étoiles massives (échelle de température, propriétés de vent). Mais, comme c'est souvent le cas en science, elle aura aussi posé de nouvelles questions auxquelles il faut désormais répondre !

Appendix A

Sketch of CMFGEN behaviour

This appendix gives a schematical view of the cpmplex behaviour of the atm‘osphere code CMFGEN. It has been built by John Hillier. More information concerning CMFGEN can be found at the following URL:

http://kookaburra.phyast.pitt.edu/hillier/web/CMFGEN.htm

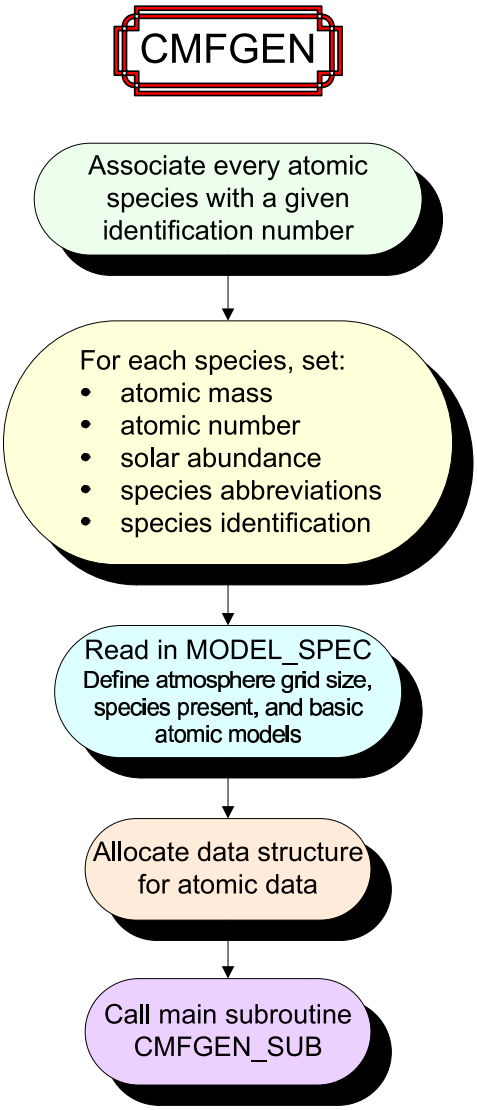
CMFGEN
Associate every atomic species with a given identification number
For each species, set:
• atomic mass
• atomic number
• solar abundance
• species abbreviations
• species identification
Read in MODEL_SPEC
Define atmosphere grid size, species present, and basic atomic models
Allocate data structure for atomic data
Call main subroutine CMFGEN_SUB

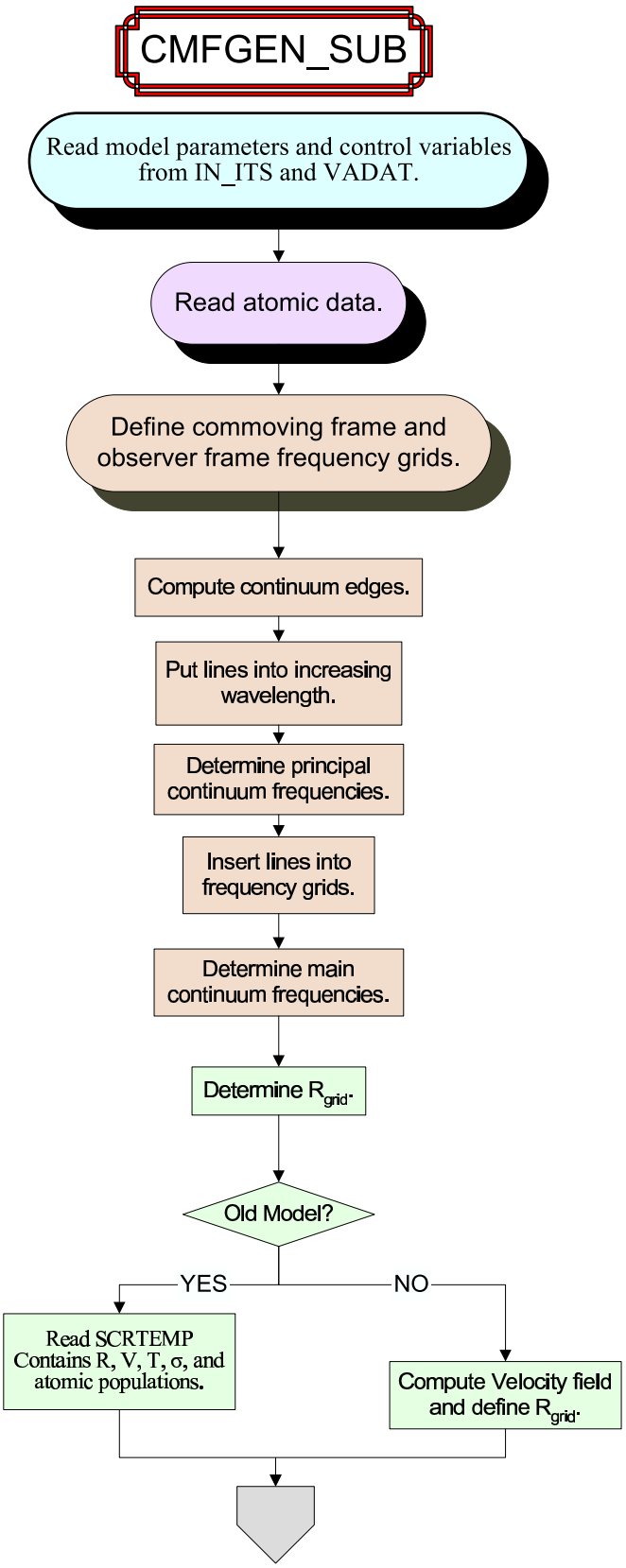
CMFGEN_SUB
Read model parameters and control variables from IN_ITS and VADAT.
Read atomic data.
Define commoving frame and observer frame frequency grids.
Compute continuum edges.
Put lines into increasing wavelength.
Determine principal continuum frequencies.
Insert lines into frequency grids.
Determine main continuum frequencies.
Determine R_{grid}.
Old Model?
YES
NO
Read SCRTEMP Contains R, V, T, σ, and atomic populations.
Compute Velocity field and define R_{grid}.

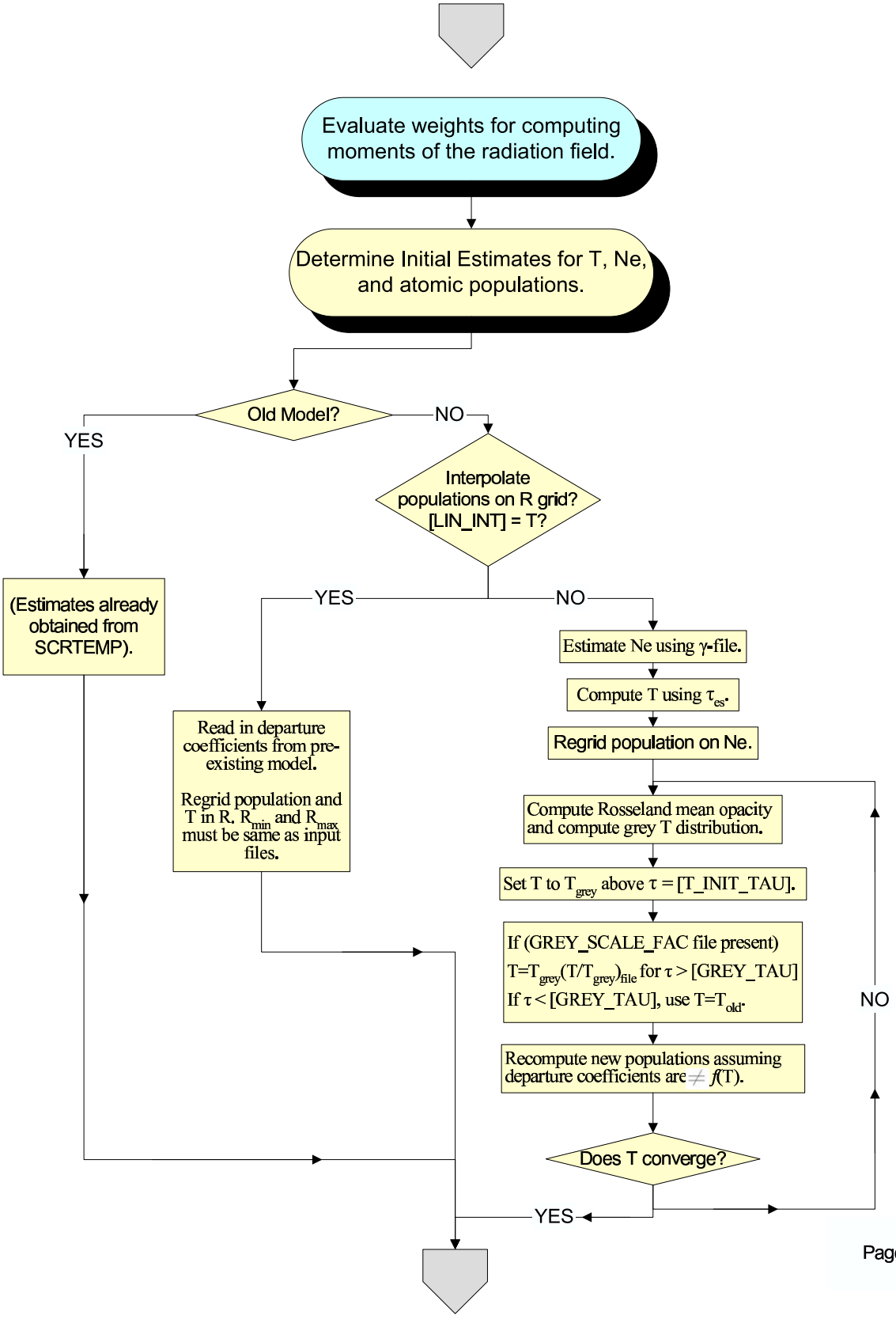
Evaluate weights for computing moments of the radiation field.
Determine Initial Estimates for T, Ne, and atomic populations.
Old Model?
YES
NO
(Estimates already obtained from SCRTEMP).
Interpolate populations on R grid? [LIN_INT] = T?
YES
NO
Read in departure coefficients from pre-existing model.
Regrid population and T in R. R_{min} and R_{max} must be same as input files.
Estimate Ne using γ-file.
Compute T using τ_{es}.
Regrid population on Ne.
Compute Rosseland mean opacity and compute grey T distribution.
Set T to T_{grey} above τ = [T_INIT_TAU].
If (GREY_SCALE_FAC file present)
$T=T_{grey}(T/T_{grey})_{file}$ for τ > [GREY_TAU]
If τ < [GREY_TAU], use $T=T_{old}$.
Recompute new populations assuming departure coefficients are ≠ f(T).
Does T converge?
NO
YES

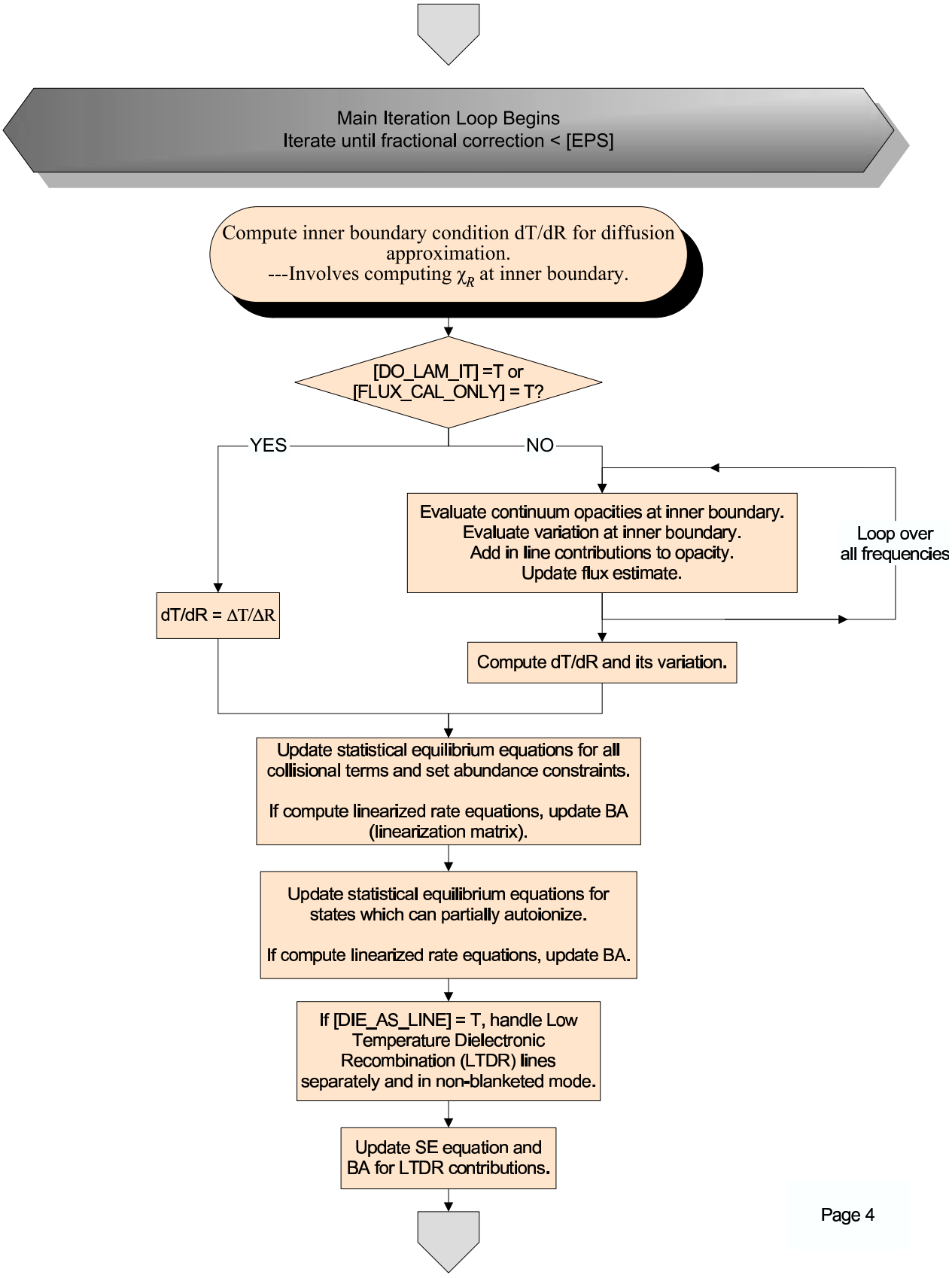
Main Iteration Loop Begins
Iterate until fractional correction < [EPS]
Compute inner boundary condition dT/dR for diffusion approximation.
---Involves computing χ_R at inner boundary.
[DO_LAM_IT] =T or [FLUX_CAL_ONLY] = T?
YES
NO
Evaluate continuum opacities at inner boundary.
Evaluate variation at inner boundary.
Add in line contributions to opacity.
Update flux estimate.
Loop over all frequencies
dT/dR = ΔT/ΔR
Compute dT/dR and its variation.
Update statistical equilibrium equations for all collisional terms and set abundance constraints.
If compute linearized rate equations, update BA (linearization matrix).
Update statistical equilibrium equations for states which can partially autoionize.
If compute linearized rate equations, update BA.
If [DIE_AS_LINE] = T, handle Low Temperature Dielectronic Recombination (LTDR) lines separately and in non-blanketed mode.
Update SE equation and BA for LTDR contributions.

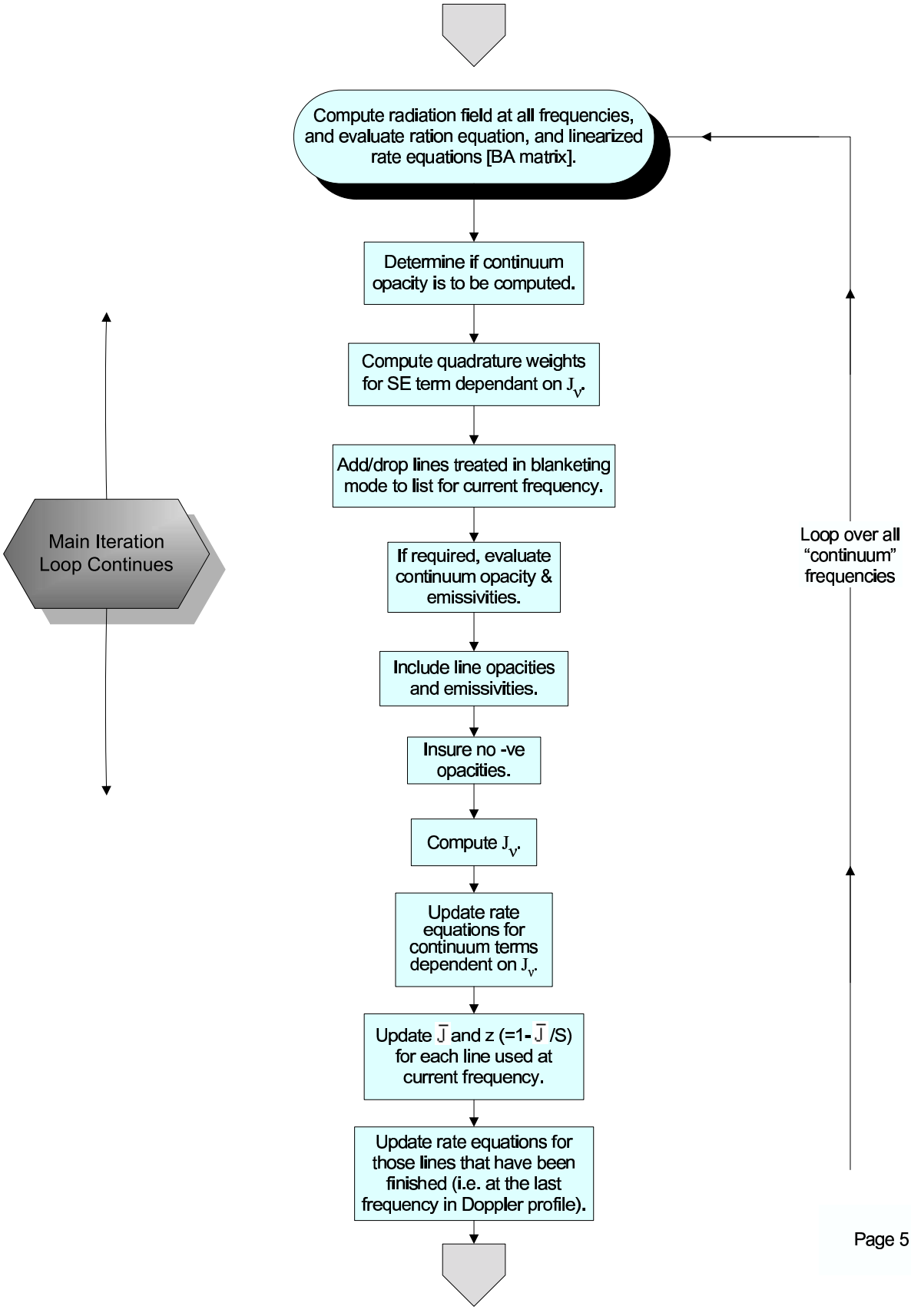
Compute radiation field at all frequencies, and evaluate ration equation, and linearized rate equations [BA matrix].
Determine if continuum opacity is to be computed.
Compute quadrature weights for SE term dependant on J_ν.
Add/drop lines treated in blanketing mode to list for current frequency.
If required, evaluate continuum opacity & emissivities.
Include line opacities and emissivities.
Insure no -ve opacities.
Compute J_ν.
Update rate equations for continuum terms dependent on J_ν.
Update $\bar{J}$ and z (=1- $\bar{J}$ /S) for each line used at current frequency.
Update rate equations for those lines that have been finished (i.e. at the last frequency in Doppler profile).
Loop over all "continuum" frequencies
Main Iteration Loop Continues

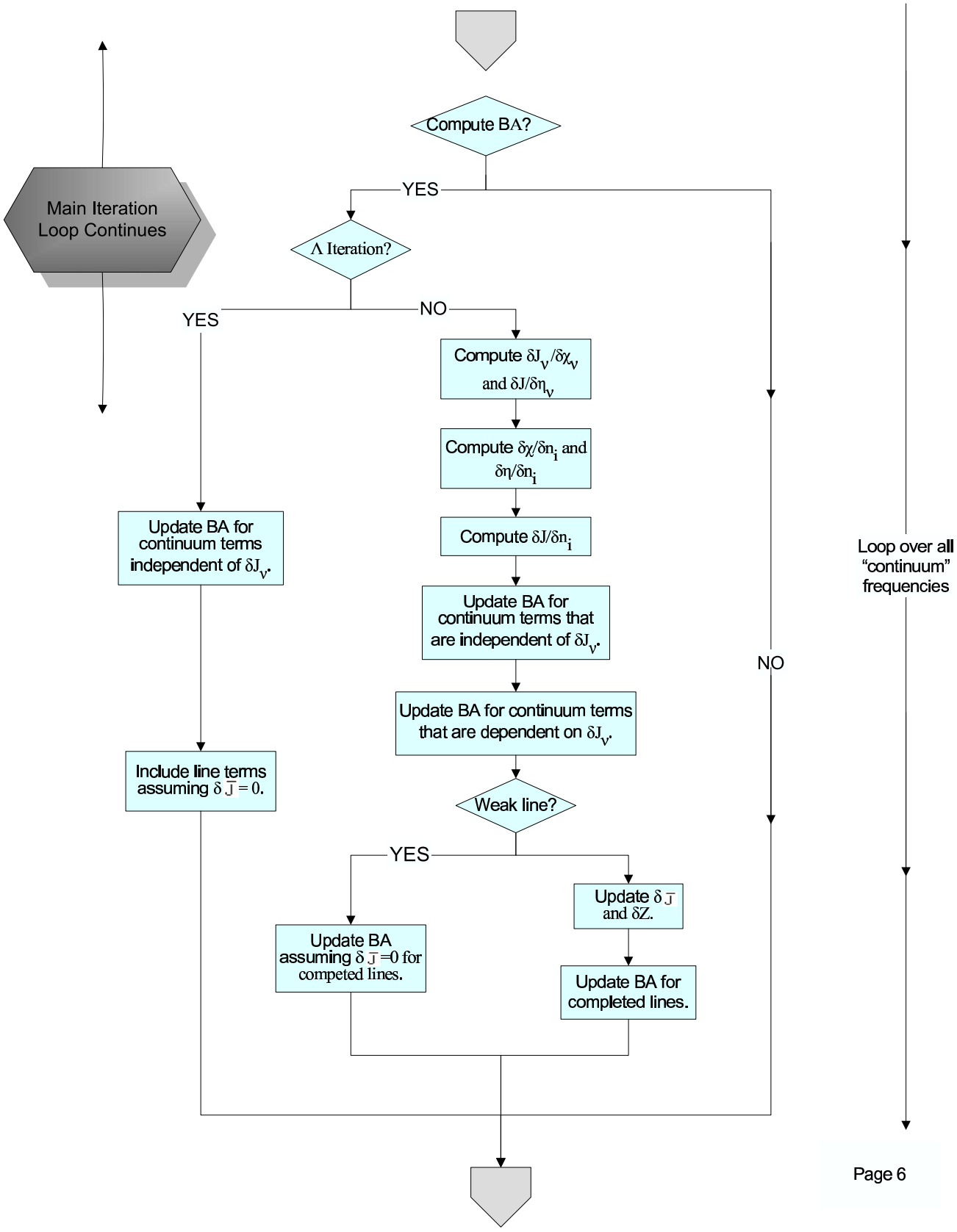
Main Iteration Loop Continues
Compute BA?
YES
NO
Λ Iteration?
YES
NO
Compute $\delta J_\nu/\delta\chi_\nu$ and $\delta J/\delta\eta_\nu$
Compute $\delta\chi/\delta n_i$ and $\delta\eta/\delta n_i$
Compute $\delta J/\delta n_i$
Update BA for continuum terms that are independent of δJ_ν.
Update BA for continuum terms independent of δJ_ν.
Update BA for continuum terms that are dependent on δJ_ν.
Include line terms assuming $\delta\bar{J}=0$.
Weak line?
YES
Update $\delta\bar{J}$ and δZ.
Update BA assuming $\delta\bar{J}=0$ for competed lines.
Update BA for completed lines.
Loop over all "continuum" frequencies

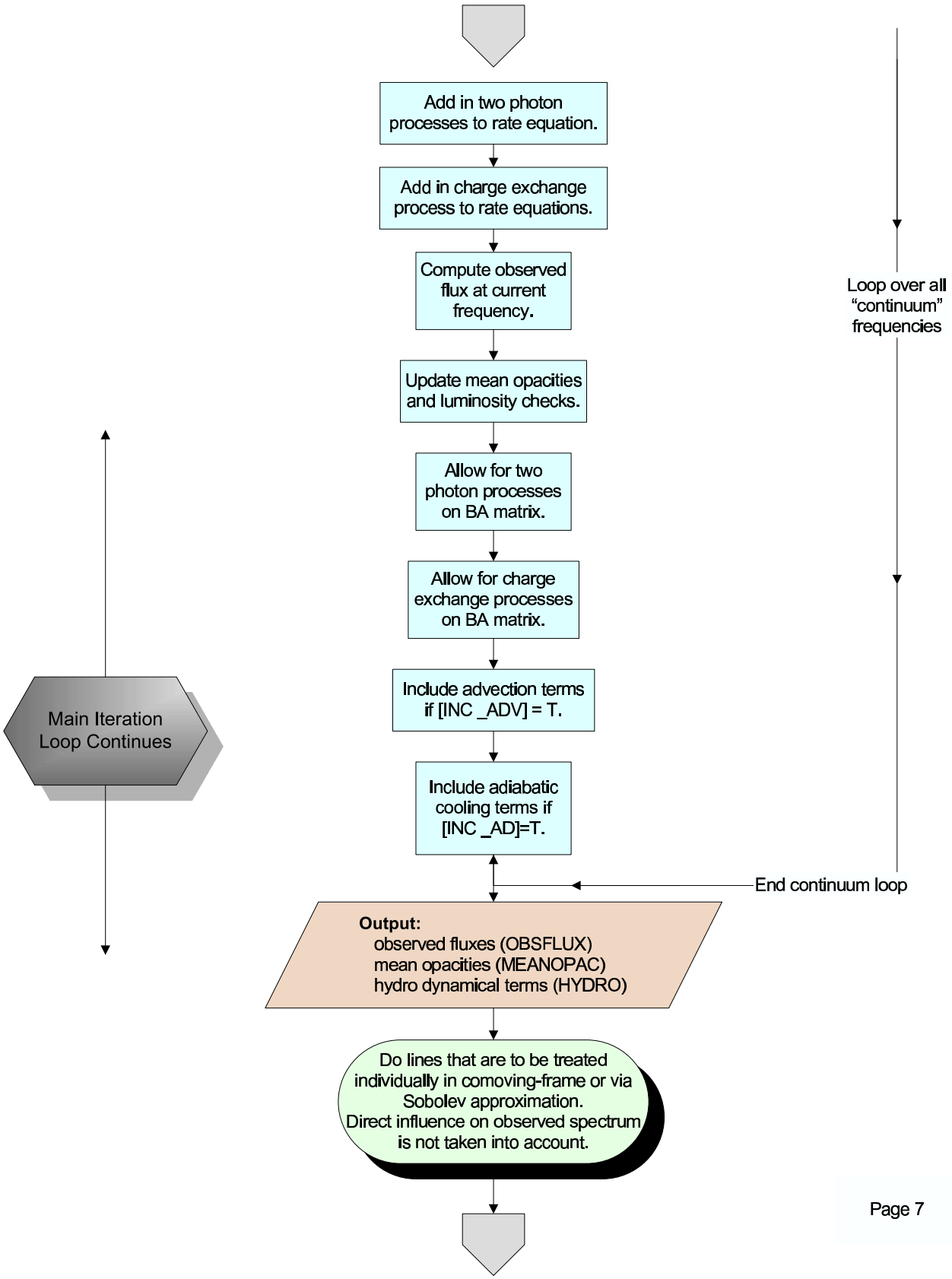
Add in two photon processes to rate equation.
Add in charge exchange process to rate equations.
Compute observed flux at current frequency.
Update mean opacities and luminosity checks.
Allow for two photon processes on BA matrix.
Allow for charge exchange processes on BA matrix.
Include advection terms if [INC _ADV] = T.
Include adiabatic cooling terms if [INC _AD]=T.
Loop over all "continuum" frequencies
End continuum loop
Main Iteration Loop Continues
Output:
observed fluxes (OBSFLUX)
mean opacities (MEANOPAC)
hydro dynamical terms (HYDRO)
Do lines that are to be treated individually in comoving-frame or via Sobolev approximation.
Direct influence on observed spectrum is not taken into account.

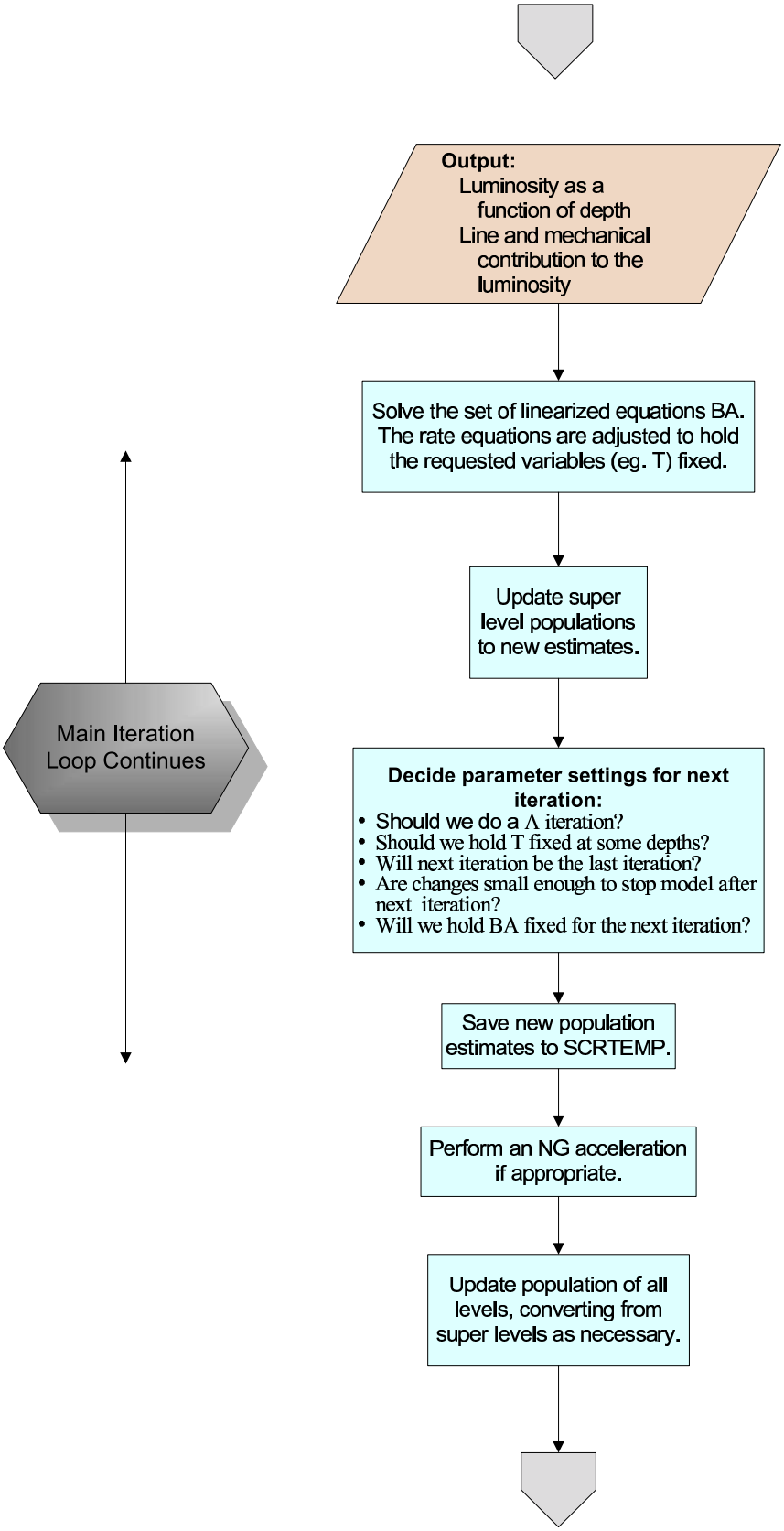
Output:
Luminosity as a function of depth
Line and mechanical contribution to the luminosity
Solve the set of linearized equations BA. The rate equations are adjusted to hold the requested variables (eg. T) fixed.
Update super level populations to new estimates.
Main Iteration Loop Continues
Decide parameter settings for next iteration:
• Should we do a Λ iteration?
• Should we hold T fixed at some depths?
• Will next iteration be the last iteration?
• Are changes small enough to stop model after next iteration?
• Will we hold BA fixed for the next iteration?
Save new population estimates to SCRTEMP.
Perform an NG acceleration if appropriate.
Update population of all levels, converting from super levels as necessary.

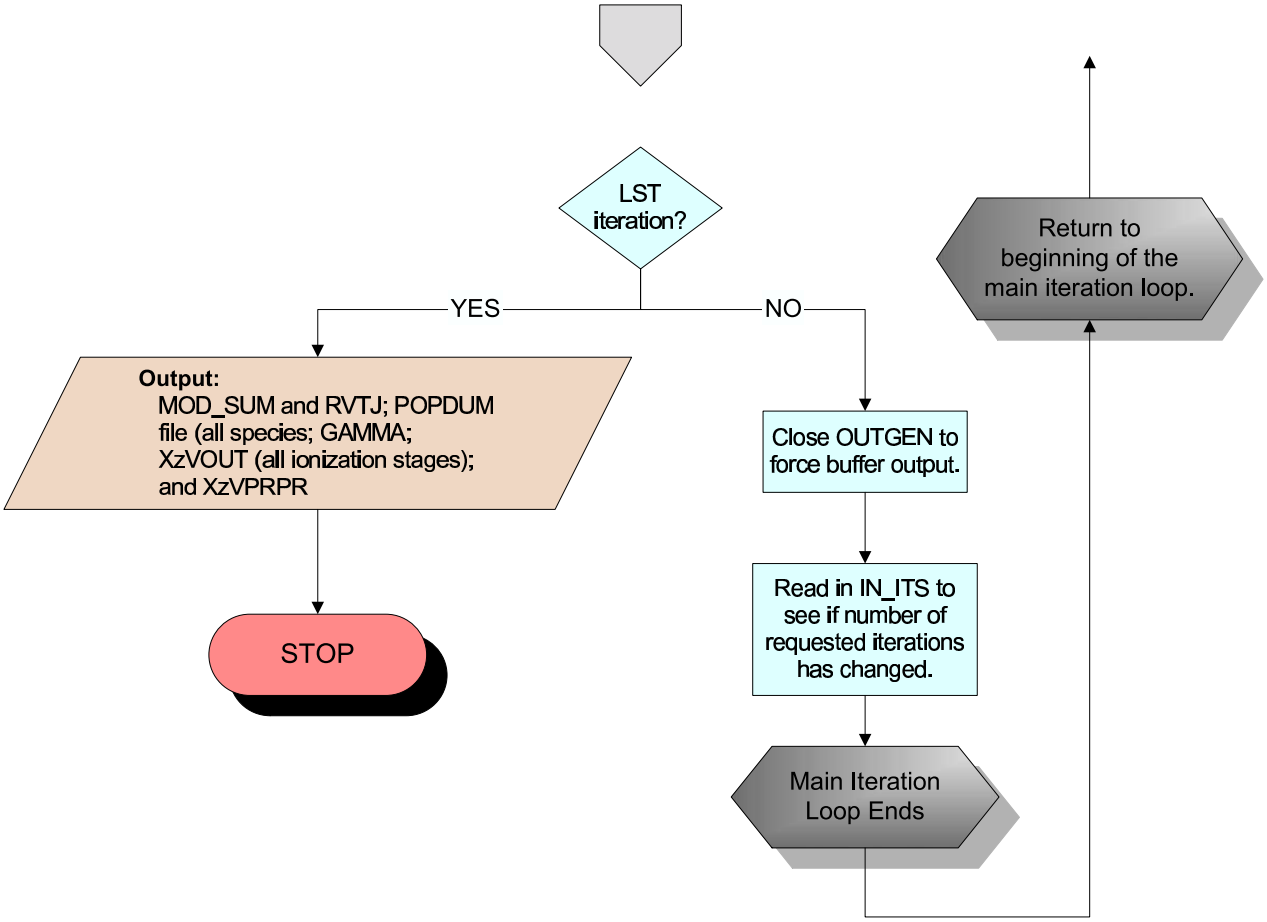
LST iteration?
YES
NO
Output:
MOD_SUM and RVTJ; POPDUM file (all species; GAMMA; XzVOUT (all ionization stages); and XzVPRPR
STOP
Close OUTGEN to force buffer output.
Read in IN_ITS to see if number of requested iterations has changed.
Main Iteration Loop Ends
Return to beginning of the main iteration loop.

Appendix B

Example of input file with modelling parameters

In the following pages, we give a typical example of an input file containing the modelling parameters (file VADAT). Its shows the number of options available for the computation of a model. The different groups of parameters have been highlighted in Sect. 2.4. In practise, most of them are held fixed between different models. The physical parameters (mass, radius, luminosity, mass loss rate, terminal velocity, clumping parameters, abundances...) are modified. Options for improving the convergence are also useful, but other parameters are usually not changed except for tests.

More informations can be found on the CMFGEN web page
http://kookaburra.phyast.pitt.edu/hillier/web/CMFGEN.htm

VADAT

44.6832	[RSTAR]	!Rp 125
100	[RMAX]	!Rmax/Rp
7	[VEL_LAW]	!Velocity Law
RVSIG_COL	[VEL_OPT]	
0.001	[VCORE]	!Core
0.1	[VPHOT]	!Photospheric velocity
1728.6	[VINF]	!Terminal (km s^{-1})
0.02	[SCL_HT]	!Scale Height
1.0	[BETA]	!Gamma (i.e. Beta=speed of velocity law)
1.660E-8	[MDOT]	!Mass loss rate
6.16595D+4	[LSTAR]	!Luminosity (Lo)
1.895D+1	[MASS]	!Stars Mass (Mo)
F	[DO_CL]	!Allow for clumping in the model?
EXPO	[CL_LAW]	!Law to evaluate clumping factors.
2	[N_CL_PAR]	!Number of clumping parameters
0.1	[CL_PAR_1]	!1st clumping parameter (X at Vinf)
30	[CL_PAR_2]	
1.0	[HYD/X]	!H/X abundance (by number)
0.1	[HE/X]	!He/X abundance (by number)
3.310D-4	[CARB/X]	!C/X abundance (by number)
8.320D-5	[NIT/X]	!N/X abundance (by number)
6.760D-4	[OXY/X]	!O/X abundance (by number)
3.550D-5	[SIL/X]	!SIL/X abundance
2.140D-5	[SUL/X]	!SUL/X abundance
3.160D-5	[IRON/X]	!IRON/X abundance
F	[RD_CF_FILE]	!Read in continuum frequencies from file
3.49897D-3	[MIN_CF]	!Minimum continuum frequency if calculating NU
50.000D0	[MAX_CF]	!Maximum continuum frequency if calculating NU
1.10D0	[FRAC_SP]	!Fractional spacing for small frequencies
1.05D0	[AMP_FAC]	!Amplification factor for large frequency ranges
0.10D0	[MAX_BF]	!Maximum frequency spacing close to bf edge
T	[DO_DIS]	!Allow for level dissolution
200.0D0	[dV_LEV]	!Spacing in km s^{-1} on low side of bf edge.
1.4	[AMP_DIS]	!Amplification factor on low side of bf edge.
0.1	[MIN_DIS]	!Minimum frequency for level disolution.

```
F           [CROSS]
750.0       [V_CROSS]
0.5         [EXT_LINE_VAR]      !Extent of variation region beyond resonance zone
0.01        [ZNET_VAR_LIM]      !Iterate on net rates when
                                ABS(ZNET-1) < ZNET_VAR_LIM.

T           [WNET]              !Iterate on net rates for weak lines.
T           [DIF]               !Diffusion approx.
T           [COH_ES]            !Assume coherent electorn scattering?
F           [OLD_J]
F           [MIX_COH]           !Mix coherencies in variation of J
0.1         [ES_FAC]            !How close RJ and RJ_ES to use COH

ZERO        [METHOD]            !Use log interp to compute chi.LOGLOG
N_ON_J      [N_TYPE]            !How to handle N in MOM_J_CMF
INT/INS     [FG_OPT]            !Solution options for FG
T           [THK_CONT]          !Thick boundary condition for continuum ?
T           [TRAP_J]            !Use trapazoidal wights to compute J ?

2.0D0       [TDOP]              !Temperature for Doppler profile
4.0D0       [AMASS_DOP]         !Atomic mass for Doppler profile
20.0D0      [VTURB]             !Turbulent Velocity

6.0         [MAX_DOP]           !Max. half-width of resonace zone
1.0D0       [FRAC_DOP]          !Spacing in CMF resonace zone [in Doppler widths]
200.0       [dV_CMF_PROF]       !Spacing (in km s^-1) across CMF profile.
400.0       [dV_CMF_WING]       !Spacing in e.s. line wings of CMF profile.
2500.0      [ES_WING_EXT]       !Ext. of non-coh e.s. wings beyond res. zone (in Vinf)
3.0         [R_CMF_WING_EXT]    !Ext. of coh. e.s. wings beyond res. zone (in Vinf)
1.1         [OBS_EXT_RAT]       !Half-Width of Observed profile in Vinf (>= 1.0)
30.0        [dV_OBS_PROF]       !Spacing (in km s^-1) across observed profile (km s^-1).
200.0       [dV_OBS_WING]       !Spacing in e.s. line wings (km s^-1).
2000.0      [dV_OBS_BIG]        !Spacing between lines (km s^-1).

F           [FLUX_CAL_ONLY]     !Do a flux calculation only?
F           [EXT_FRM_SOL]       !Extend formal solutiona factor of 10 in R
T           [INS_F_FRM_SOL]     !Insert extra frequencies in the formal sol?
INT         [FRM_OPT]
F           [DO_SOB_LINES]      !Compute rates for SObolev transitions in flux mode?
F           [SOB_FREQ_IN_OBS]   !
```

BLANK	[GLOBAL_LINE]	!Global line switch (BLANK, SOB, CMF, NONE)
F	[LAM_SET]	!Swith to SOB for long wavelengths?
0.0E+03	[F_LAM_BEG]	!Lambda to begin flux calculation.
7.0E+03	[F_LAM_END]	!Lambda to end flux calculation.
BLANK	[GLOBAL_LINE]	!Global line switch (BLANK, SOB, CMF, NONE)
F	[LAM_SET]	!Swith to SOB for long wavelengths?
0.0E+03	[F_LAM_BEG]	!Lambda to begin flux calculation.
7.0E+03	[F_LAM_END]	!Lambda to end flux calculation.
5.0D-3	[GF_CUT]	!Omit lines with gf ¡ GFCUT and lower lev
9	[GF_LEV_CUT]	!> GF_LEV_CUT
10	[MIN_TRANS]	!Minimum number of trans from level before cut.
T	[THK_LINE]	!Thk line boundary condition ?
T	[CHK_L_POS]	!Check for negative line opacity?
SRCE_CHK	[NEG_OPAC_OPT]	!Negative opacity option
F	[He2_RES=0]	!Set rates in He2 resonance lines to zero?
26	[AT_CUT]	
F	[ALLOW_OL]	!Include line overlap?
50.0	[OL_DIF]	!Max velocity dif for overlap (km s^{-1})?
F	[INC_CHG]	!Include charge exchange reactions
T	[INC_TWO]	!Include two photon transitions
F	[INC_AD]	!Include adiabatic cooling
T	[SCL_LN]	!Scale line cooling/heating rates
2.0	[SCL_LN_FAC]	
F	[INC_XRAYS]	
1.0E-08	[FIL_FAC]	
300	[T_SHOCK]	
400	[V_SHOCK]	
F	[RD_IN_R_GRID]	!Read in a predetermined R grid ?
F	[LIN_INT]	!Regrid pops (set F if NEW model) (T≥ no Temp iteration)
T	[POP_SCALE]	!Scale pops to satisfy abundance Eq.
T	[IT_ON_T]	!Iterate on initial T distribution ?
0.5	[T_INIT_TAU]	!For INIT_TEMP guess
0.5	[GREY_TAU]	!Set T to TGREY for tau > ?
F	[TDEK]	!Option to read T in Dekoter's file
CMF	[TRANS_HI]	!Method for treating Hydrogen lines ?

CMF	[TRANS_HeI]	!Method for treating HeI lines ?
CMF	[TRANS_He2]	!Method for treating He2 lines ?
CMF	[TRANS_CI]	!Method for treating CI lines ?
CMF	[TRANS_C2]	!Method for treating C2 lines ?
CMF	[TRANS_CIII]	!Method for treating CIII lines ?
CMF	[TRANS_CIV]	!Method for treating CIV lines ?
CMF	[TRANS_NI]	!Method for treating NI lines ?
CMF	[TRANS_N2]	!Method for treating N2 lines ?
CMF	[TRANS_NIII]	!Method for treating NIII lines ?
CMF	[TRANS_NIV]	!Method for treating NIV lines ?
CMF	[TRANS_NV]	!Method for treating NV lines ?
SOB	[TRANS_OI]	!Method for treating OIII lines ?
SOB	[TRANS_O2]	!Method for treating OIII lines ?
SOB	[TRANS_OIII]	!Method for treating OIII lines ?
SOB	[TRANS_OIV]	!Method for treating OIV lines ?
SOB	[TRANS_OV]	!Method for treating OV lines ?
SOB	[TRANS_OSIX]	!Method for treating OSIX lines ?
SOB	[TRANS_Sk2]	!Method for treating SiII lines ?
SOB	[TRANS_SkIII]	!Method for treating SiIII lines ?
SOB	[TRANS_SkIV]	!Method for treating SiIV lines ?
SOB	[TRANS_SIII]	!Method for treating SIII lines ?
SOB	[TRANS_SIV]	!Method for treating SIV lines ?
SOB	[TRANS_SV]	!Method for treating SV lines ?
SOB	[TRANS_SSIX]	!Method for treating SSIX lines ?
SOB	[TRANS_FeIII]	!Method for treating feIII lines ?
SOB	[TRANS_FeIV]	!Method for treating feIII lines ?
SOB	[TRANS_FeV]	!Method for treating feIII lines ?
SOB	[TRANS_FeSIX]	!Method for treating feIII lines ?
SOB	[TRANS_FeSEV]	!Method for treating feIII lines ?
F	[DIE_AS_LINE]	!Treat dielectronic as non-overlapping lines
1000.0D0	[VSM_DIE]	!Smoothing velocity (km s^{-1})
F,F	[DIE_HI]	!Include LTDR for HI (Use WI calcs?)

```
F,F   [DIE_He2]     !Include LTDR for He2 (Use WI calcs?)

T,F   [DIE_CI]      !Include LTDR for CI (Use WI calcs?)
T,F   [DIE_C2]      !Include LTDR for CIII (Use WI calcs?)
T,T   [DIE_CIII]    !Include LTDR for CIII (Use WI calcs?)
F,F   [DIE_CIV]     !Include LTDR for CIV (Use WI calcs?)

F,F   [DIE_NI]      !Include LTDR for NI (Use WI calcs?)
T,T   [DIE_N2]      !Include LTDR for N2 (Use WI calcs?)
F,F   [DIE_NIII]    !Include LTDR for NIII (Use WI calcs?)
T,T   [DIE_NIV]     !Include LTDR for NIV (Use WI calcs?)
F,F   [DIE_NV]      !Include LTDR for NV (Use WI calcs?)

T,F   [DIE_OI]      !Include LTDR for OI (Use WI calcs?)
T,F   [DIE_O2]      !Include LTDR for O2 (Use WI calcs?)
T,F   [DIE_OIII]    !Include LTDR for OIII (Use WI calcs?)
T,F   [DIE_OIV]     !Include LTDR for OIV (Use WI calcs?)
T,T   [DIE_OV]      !Include LTDR for OV (Use WI calcs?)
F,F   [DIE_OSIX]    !Include LTDR for OSIX (Use WI calcs?)
F,F   [DIE_Sk2]     !Include LTDR for Sk2 (Use WI calcs?)
F,F   [DIE_SkIII]   !Include LTDR for SkIII (Use WI calcs?)
F,F   [DIE_SkIV]    !Include LTDR for SkIV (Use WI calcs?)

F,F   [DIE_SIII]    !Include LTDR for SIII (Use WI calcs?)
F,F   [DIE_SIV]     !Include LTDR for SIV (Use WI calcs?)
F,F   [DIE_SV]      !Include LTDR for SV (Use WI calcs?)
F,F   [DIE_SSIX]    !Include LTDR for SSIX (Use WI calcs?)
F,F   [DIE_FeIII]   !Include LTDR for SIV (Use WI calcs?)
F,F   [DIE_FeIV]    !Include LTDR for SIV (Use WI calcs?)
F,F   [DIE_FeV]     !Include LTDR for SIV (Use WI calcs?)
F,F   [DIE_FeSIX]   !Include LTDR for SIV (Use WI calcs?)
F,F   [DIE_FeSEV]   !Include LTDR for SIV (Use WI calcs?)

0     [FIX_HI]      !Fix ? levels for HI
0     [FIX_HYD]     !Fix ? levels for HII
0     [FIX_HeI]     !Fix ? levels for HeI
0     [FIX_He2]     !Fix ? levels for He2
0     [FIX_HE]      !Fix ? levels for HeIII

0     [FIX_CI]      !Fix ? levels for CI
0     [FIX_C2]      !Fix ? levels for CIII
```

```
0   [FIX_CIII]      !Fix ? levels for CIII
0   [FIX_CIV]       !Fix ? levels for CIV
0   [FIX_CARB]      !Fix ? levels for CV

0   [FIX_NI]        !Fix ? levels for NI
0   [FIX_N2]        !Fix ? levels for N2
0   [FIX_NIII]      !Fix ? levels for NIII
0   [FIX_NIV]       !Fix ? levels for NIV
0   [FIX_NV]        !Fix ? levels for NV
0   [FIX_NIT]       !Fix ? levels for NSIX

0   [FIX_OI]        !Fix ? levels for OIels for O2
0   [FIX_OIII]      !Fix ? levels for OIII
0   [FIX_OIV]       !Fix ? levels for OIV
0   [FIX_OV]        !Fix ? levels for OV
0   [FIX_OSIX]      !Fix ? levels for OSIX
0   [FIX_OXY]       !Fix ? levels for OSEV

0   [FIX_Sk2]       !Fix ? levels for Sk2
0   [FIX_SkIII]     !Fix ? levels for SkIII
0   [FIX_SkIV]      !Fix ? levels for SkIV
0   [FIX_SIL]       !Fix ? levels for Silicon

0   [FIX_OI]        !Fix ? levels for OIels for O2
0   [FIX_OIII]      !Fix ? levels for OIII
0   [FIX_OIV]       !Fix ? levels for OIV
0   [FIX_OV]        !Fix ? levels for OV
0   [FIX_OSIX]      !Fix ? levels for OSIX
0   [FIX_OXY]       !Fix ? levels for OSEV

0   [FIX_Sk2]       !Fix ? levels for Sk2
0   [FIX_SkIII]     !Fix ? levels for SkIII
0   [FIX_SkIV]      !Fix ? levels for SkIV
0   [FIX_SIL]       !Fix ? levels for Silicon
0   [FIX_SIII]      !Fix ? levels for SIII
0   [FIX_SIV]       !Fix ? levels for SIV
0   [FIX_SV]        !Fix ? levels for SV
0   [FIX_SSIX]      !Fix ? levels for SSIX
0   [FIX_SUL]       !Fix ? levels for SUL

0   [FIX_FeIII]     !Fix ? levels for SIV
```

0	[FIX_FeIV]	!Fix ? levels for SIV
0	[FIX_FeV]	!Fix ? levels for SIV
0	[FIX_FeSIX]	!Fix ? levels for SIV
0	[FIX_FeSEV]	!Fix ? levels for SIV
0	[FIX_IRON]	!Fix ? levels for SIV
F	[FIX_NE]	!Fixed Electron density ?
F	[FIX_IMP]	!Fix impurity species automatically ?
F	[FIX_T]	!Fixed T ?
T	[FIX_T_AUTO]	!Automatic variable T
0.0	[TAU_SCL_T]	!Fix T for this optical depth. 1.0?
TRIDIAG	[SOL_METH]	!Msol (bmgsit)
MAJOR	[SCALE_OPT]	!Scaling option (MAJOR, LOCAL, NONE, or GLOBAL)
5.0D-02	[EPS_TERM]	!Terminate when % frac change smaller
10.0D0	[MAX_LIN]	!Maximum fractional change allowed for linearization.
1.0D+10	[MAX_LAM]	!Maximum fractional change allowed for LAMBDA iteration.
1.0D+200	[MAX_CHNG]	!Terminate with error if % frac change > number MAX_CHNG
F	[COMP_BA]	!Compute BA matrix
T	[STORE_BA_INV]	!Write BA matrix out
T	[WR_PRT_INV]	!Write BA matrix out
2	[N_FIX_BA]	!Number of iterations to hold BA fixed:
T	[STORE_BA]	!Write BA matrix out
1.0D-04	[BA_CHK_FAC]	!$\ll$ 1 (Values close to 1 reduce BA compuattion)
10.0D0	[FIX_BA]	!Fix BA if % change smaller
400.0D0	[LAM_VAL]	!Do LAMBDA iterations if % change > .
2	[NUM_LAM]	!Number of Lambda iteration per full linearization.
F	[RD_SOL]	!Read in solution matrix
T	[JC_W_EDD]	!Use Eddington factors to compute continuum J
T	[JBAR_W_EDD]	!Use Eddington factors to compute JBAR
for lines. F	[INC_GRID]	!Do an error calculation ?
F	[ALL_FREQ]	!
3.19	[ACC_END]	!
2	[N_INS]	!NPINS
1	[ST_INT]	!Interpolate from 1 to ?
30	[END_INT]	!Interpolate from 1 to ?
50	[ND_QUAD]	!Quadratic interpolation from 50 to ND
LOG	[INTERP_TYPE]	!LOG or LIN plane

```
2000            [N_PAR]          !Rate of BA incremantation by BA_PAR.

F               [COMP_F]         !Compute new Continuum f values ?
1.0D-04         [ACC_F]          !Convergence accuracy for F

T               [DO_NG]          !Use NG acceleration
10.0D0          [BEG_NG]         !Start NG when percentage change <
6               [ITS/NG]         !Number of iterations per NG aceleration
Not handeled?
SOB             [TRANS_GS_He2]   !Method for treating He2(g.s) lines ?
```

Appendix C

List of publications

• Refereed Journals:

1) Martins, F., Schaerer, D., Hillier, D.J., Heydari-Malayeri, M., Meynadier, F., Walborn, N., *Stellar and wind properties of Vz stars*, 2004, A&A, in preparation

2) Martins, F., Schaerer, D., Hillier, D.J., Meynadier, F., Heydari-Malayeri, M., Walborn, N., *O stars with weak winds: the Galactic case*, 2004, A&A, to be submitted

3) Martins, F., Schaerer, D., Hillier, D.J., *A new calibration of Galactic O star parameters*, 2004, A&A, submitted

4) Martins, F., Schaerer, D., Hillier, D.J., Heydari-Malayeri, M., *Puzzling wind properties of young O stars in SMC-N81*, 2004, A&A, 420, 1087

5) Morisset, C., Schaerer, D., Bouret, J.C., Martins, F., *Mid-IR observations of galactic HII regions: constraining ionising spectra of massive stars and the nature of the observed excitation sequences*, 2004, A&A, 415, 577

6) Martins, F., Schaerer, D., Hillier, D.J., *On the effective temperature scale of O stars*, 2002, A&A, 382, 999-

7) Heydari-Malayeri, M., Rosa, M.R., Schaerer, D., Martins, F., Charmandis, V., *STIS spectroscopy of newborn massive stars in SMC-N81*, 2002, A&A, 381, 951

• Conference proceedings:

8) Martins, F., Schaerer, D., M. Heydari-Malayeri, D.J. Hillier, 2003, in "Star formation at high angular resolution", Eds M.G. Burton, R. Jayawardhana, T.L. Bourke, IAU symposium 221

9) Martins, F., Schaerer, D., M. Heydari-Malayeri, D.J. Hillier, 2003, SF2A: journées de l'astrophysique française, Eds F. Combes, T. Contini, D. Barret, EDPS conference serie Vol. 226, p. 543

10) Martins, F. & Schaerer, D., 2002, in "A massive stars odyssey: from main sequence to supernova", Eds K.A. van der Hucht, A. Herrero, C. Esteban, IAU symposium 212, p. 212

11) Martins, F., Schaerer, D., Heydari-Malayeri, M., 2002, in "A massive stars odyssey: from main sequence to supernova", Eds K.A. van der Hucht, A. Herrero, C. Esteban, IAU symposium 212, p. 564

12) Martins, F. & Schaerer, D., 2002, in "Stellar atmosphere modeling", Eds I. Hubeny, D. Mihalas, K. Werner, ASP conference serie Vol. 288, p. 267

13) Morisset, C., Bouret, J.C., Schaerer, D., Martins, F., 2002, in "Stellar atmosphere modeling", Eds I. Hubeny, D. Mihalas, K. Werner, ASP conference serie Vol. 288, p. 271

14) Martins, F. & Schaerer, D., 2001, SF2A: journées de l'astrophysique française, Eds F. Combes, D. Barret, F. Thévenin, EDPS conference serie Vol. 189

• Other publications

15) Schaerer, D., Blum, R.D., Heydari-Malayeri, M., Martins, F., *Narrow band adaptive optics imaging in the Arches cluster*, 2001, Canada-France-Hawaii Telescope Information Bulletin, No 43, p. 8

Bibliography

Abel, T., Anninos, P.A., Norman, M.L. & Zhang, Y., 1998, ApJ, 508, 518

Abbott, D.C., 1978, ApJ, 225, 893

Abbott, D.C., 1982, ApJ, 259, 282

Abbott, D.C., Hummer, D.G., 1985, ApJ, 294, 286

Abbott, D.C. & Lucy, L.B., 1985, ApJ, 288, 679

Allen, C.W., 1976, Astrophysical Quantities, (London: Athlone)

Anderson, L., 1991, in "Stellar atmospheres: beyond classical models, eds. L. Crivellari, I. Hubeny & D.G. Hummer, NATO ASI Ser. C, 341, 29

Asplund, M., 2003, in "CNO in the Universe" eds C. Charbonnel, D. Schaerer, G. Meynet, ASP Conf. Series, Vol. 304, p. 279

Auer, L.H. & Mihalas, D., 1972, ApJS, 205, 24

Babel, J., 1995, A&A, 301, 823

Babel, J., 1996, A&A, 309, 867

Behrend, R. & Maeder, A., 2001, A&A, 373, 190

Bernasconi, P.A. & Maeder, A., 1996, A&A, 307, 829

Bianchi, L. & Garcia, M., 2002, ApJ, 581, 610

Bohannan, B., Abbott, D.C., Voels, S.A., Hummer, D.G., 1986, ApJ, 308, 728

Bonnell, I.A., Bate, M.R., Zinnecker, H., 1998, MNRAS, 298, 93

Bouret, J.C., Lanz, T., Hillier, D.J., Heap, S.R., Hubeny, I., Lennon, D.J., Smith, L.J., Evans, C.J., 2003, ApJ, 595, 1182

Bromm, V., Coppi, P.S. & Larson, R.B., 1999, ApJ, 527, L5

Bromm, V. & Larson, R.B., 2004, ARA&A, in press (astro-ph/0311019)

Castor, J.I., 1970, MNRAS, 149, 111

Castor, J.I., Abbott, D.C., Klein, R.I., 1975, ApJ, 195, 157

Chini, R., Hoffmeister, V., Kimeswenger, S., Nielbock, M., Nürnberg, D., Schmidtobreick, L., Sterzik, M., 2004, Nature, 429, 155

Chiosi, C. & Maeder, A., 1986, ARA&A, 24, 329

Chlebowski, T. & Garmany, C.D., 1991, ApJ, 368, 241

Churchwell, E., 2002, ARA&A, 40, 27

Conti, P.S. & Alschuler, W.R., 1971, ApJ, 170, 325

Conti, P.S., 1973, ApJ, 179, 181

Conti, P.S., 1975, in "HII regions and related objects", eds. T. Wilson & D. Downes (Heidelberg: Springer), 207

Conti, P.S., 1988, in "O stars and Wolf-Rayet stars", eds. P.S. Conti & A.H. Underhill (Washington D.C.: NASA SP-497), 81

Crowther, P.A., Hillier, D.J., Evans, C.J., Fullerton, A.W., De Marco, O., Willis, A.J., 2002a, ApJ, 579, 774

Crowther, P.A., Dessart, L., Hillier, D.J., Abbott, J.B., Fullerton, A.W., 2002b, A&A, 392, 653

de Koter, A., 1996, " Studies of the variability of Luminous Blue Variables", PhD thesis, University of Utrecht, The Netherlands

de Koter, A., Heap, S.R. & Hubeny, I., 1998, ApJ, 509, 879

Deharveng, L., Peña, M., Caplan, J., Costero. R., 2000, MNRAS, 311, 329

Deharveng, L., Zavagno, A., Salas, L., Porras, A., Caplan, J., Cruz-González, I., 2003a, A&A, 399, 1135

Deharveng, L., Lefloch, B., Zavagno, A., Caplan, J., Withworth, A.P., Nadeau, D, Martin, S., 2003b, A&A, 408, L25

Dyson, J.E., 1978, A&A, 62, 269

Evans, C.J., lennon, D.J., Trundle, C., Heap, S.R., Lindler, D.J., 2004, ApJ, 607, 451

Friend, D.B. & Abbott, D.C., ApJ, 311, 701

Gabler, R., Gabler, A., Kudritzki, R.P., Puls, J., Pauldrach, A.W.A., 1989, A&A, 226, 162

Garcia, M & Bianchi, L., 2004, ApJ, 606, 497

Garmany, C.D. & Conti, P.S., 1985, ApJ, 293, 407

Gies, D.R., 2002, in "A massive star odyssey: from main sequence to supernova", eds K.A. van der Hucht, A. Herrero, C. Esteban , IAU symp. 212, p. 91

Grevesse, N. & Sauval, A., 1998, Space Sci. Rev, 85, 161

Grosdidier, Y., Moffat, A.F.J., Joncas, G., Acker, A., 1998, ApJ, 506, 127

Herrero, A., Kidritzki, R.P., Vilchez, J.M., Kunze, D., Butler, K., Haser, S., 1992, A&A, 261, 209

Herrero, A., Puls, J., Villamariz, M.R., 2000, A&A, 354, 193

Herrero, A., Puls, J., Najarro, F., 2002, A&A, 396, 949

Heydari-Malayeri, M. & Testor, G., 1982, A&A, 111, L11

Heydari-Malayeri, M., Le Bertre, T., Magain, P., 1988, A&A, 195, 230

Heydari-Malayeri, M., Rosa, M.R., Charmandis, V., Deharveng, L., Zinnecker, H. 1999a, A&A, 344, 848

Heydari-Malayeri, M., Rosa, M.R., Zinnecker, H., Deharveng, L., Charmandis, V., 1999b, A&A, 352, 665

Heydari-Malayeri, M., Charmandis, V., Deharveng, L., Rosa, M.R., Zinnecker, H., 1999c, A&A, 347, 841

Heydari-Malayeri, M., Charmandis, V., Deharveng, L., Rosa, M.R., Schaerer, D., Zinnecker, H., 2001, A&A, 372, 527

Heydari-Malayeri, M., Rosa, M.R., Schaerer, D., Martins, F., Charmandis, V., 2002a, A&A, 381, 951 (paper I)

Heydari-Malayeri, M. et al., 2002b, in "A massive star odyssey: from main sequence to supernova", eds K.A. van der Hucht, A. Herrero, C. Esteban, IAU symp. 212, p. 553

Heydari-Malayeri, M., Charmandis, V., Deharveng, L., Meynadier, F., Rosa, M.R., Schaerer, D., Zinnecker, H., 2002c, A&A, 381, 941

Hilditch, R.W., Harries, T.J., Bell, S.A., 1996, 314, 165

Hill, V., 1999, A&A, 345, 530

Hillier, D.J., 1987a, ApJS, 63, 987

Hillier, D.J., 1987b, ApJS, 63, 965

Hillier, D.J. & Miller, D.L., 1998, ApJ, 496, 407

Hillier, D.J., Lanz, T. Heap, S.R., Hubeny, I., Smith, L.J., Evans, C.J., Lennon, D.J., Bouret, J.C., 2003, ApJ, 588, 1039

Hoare, M.G., Gibb, A.G., Wyrowski, F., Mundy, L., 2003, in "Star formation at high angular resolution", eds Burton, M. & Jayawadrhana, R., IAU symp. 221

Hoffmann, T.L., Pauldrach, A.W.A., Puls, J., 2002, in "A massive star odyssey: from main sequence to supernova", eds K.A. van der Hucht, A. Herrero, C. Esteban , IAU symp. 212, p. 206

Hofner, P., Kurtz, S., Churchwell, E., Walmsley, C.M., Cesaroni, R., 1996, ApJ, 460, 359

Howarth, I.D. & Prinja, R.K., 1989, ApJS, 69, 527

Howarth, I.D., Siebert, K.W., Hussain, G.A.J., Prinja, R.K., 1997, MNRAS, 284, 265

Hubeny, I. & Lanz, T., 1995, ApJ, 439, 875

Hubeny, I., Heap, S.R., Lanz, T., 1998, ASP Conf. Series, Vol. 131, 108

Hubeny, I., 1999, in "Physique et modélisation des atmosphères stellaires", Proc. of the Ecole d'Aussois 1999, eds. C. Catala & J.P. Zahn

Jaffe, D.T., Zhu, Q., Lacy, J.H., Richter, M., 2003, ApJ, 596, 1053

Krabbe, A., Genzel, R., Eckart, A., Najarro, F., Lutz, D., Cameron, M., Kroker, H., Tacconi-Garman, L.E., Weitxel, L., Drapatz, S., Geballe, T., Sternberg, A., Kudritzki, R., 1995, ApJ, 447, L95

Kritčka, J. & Kubát, J., 2000, A&A, 359, 983

Kritčka, J., Owocki, S.P., Kubát, J., Galloway, R.K., Brown, J.C., 2003, A&A, 403, 713

Kudritzki, R.P., 1980, A&A, 85, 174

Kudritzki, R.P., 1988, in "Radiation in moving gaseous media", Proc. of the 18$^{\text{th}}$ Saas-Fee school, eds. Y. Chmielewski & T. Lanz, Geneva Observatory publications

Kudritzki, R.P., Pauldrach, A., Puls, J., Abbott, D.C., 1989, A&A, 219, 205

Kudritzki, R.P. & Hummer, D.G., 1990, ARA&A, 28, 303

Kudritzki, R.P., Lennon, D.J. & Puls, J., 1995, in "Science with the VLT", Proc. of the ESO workshop held at Garching, Germany, 28 June - 1 July 1994, Eds. J.R. Walsh & I.J. Danziger, Berlin: Springer-Verlag, p. 246

Kudritzki, R.P., Mendez, R.H., Puls, J., Mc Carthy, J.K., 1997, in "Planetary Nebulae", eds. H.J. Habing and H.J.G.L.M. Lamers, IAU symp. 180, p. 64

Kudritzki, R.P., 1998, in "Stellar astrophysics in the Local Group: first step to the Universe", Proc. of the 8$^{\rm th}$ Canary Island winter school, eds. A. Herrero, A. Aparacio, F. Sanchez, Cambridge University Press.

Kudritzki, R.P., Puls, J., Lennon, D.J., Venn, K.A., Reetz, J., Najarro, F., McCarthy, J., 1999, A&A, 350, 970

Kudritzki, R.P. & Puls, J., 2000, ARA&A, 38, 613

Kudritzki, R.P., 2002, ApJ, 577, 389

Kurtz, S., Cesaroni, R., Churchwell, E., Hofner, P., Walmsley, C.M., 2000, in "Protostars and Planets IV", eds. V. Mannings, A.P. Boss & S.S. Russell, p. 299

Kurucz, R.L., 1979, ApJS, 40, 1

Lada, C.J., 1987, in "Star forming regions", eds M. Peimbert & J. Jugaku, IAU symp. 115

Lamers, H.J.G.L.M., 1981, ApJ, 245, 593

Lamers, H.J.G.L.M. & Leitherer, C., 1993, ApJ, 412, 771

Lamers, H.J.G.L.M., Snow, T.P. & Lindholm, D.M., 1995, ApJ, 455, 269

Lamers, H.J.G.L.M., Haser, S., de Koter, A., Leitherer, C., 1999, ApJ, 516, 872

Lamers, H.J.G.L.M. & Cassinelli, J.P., 1999, "Introduction to stellar winds", Cambridge University Press

Larson, R.B. & Starrfield, S., 1971, A&A, 13, 190

Leitherer, C., 1988, ApJ, 326, 356

Leitherer, C. & lamers, H.J.G.L.M., 1991, ApJ, 373, 89

Leitherer, C., Robert, C. & Drissen, L., 1992, ApJ, 401, 596

Leitherer, C., Chapman, J.M., Koribalski, B., 1995, ApJ, 450, 289

Lucy, L.B. & Salomon, P.M., 1971, ApJ, 159, 879

Lucy, L.B. & Abbott, D.C., 1993, ApJ, 405, 738

Maeder, A., 1992, A&A, 264, 105

Maeder, A. & Conti, P.S., 1994, ARA&A, 32, 227

Maeder, A. & Meynet, G., 2000, ARA&A, 38, 143

Markova, N, Puls, J, Repolust, T, Markov, H., 2004, A&A, 413, 693

Martín-Hernández, L., Peeters, E., Morisset, C., Tielens, A.G.G.M, Cox, P., Roelfsema, P.R., Baluteau, J.-P., Schaerer, D., Mathis, J.S., Damour, F., Churchwell, E., Kessler, M.F., 2002, A&A, 381, 606

Martins, F, Schaerer, D. & Hillier, D.J., 2002, A&A, 382, 999

Martins, F., Schaerer, D., Hillier, D.J., Heydari-Malayeri, M., A&A, 420, 1087

Massey, P., Lang, C.C., DeGioia-Eastwood, K., Garmany, C.D., 1995a, ApJ, 438, 188

Massey, P., Johnson, K.E., DeGioia-Eastwood, K., 1995b, ApJ, 454, 151

Massey, P. & Hunter, D.A., 1998, ApJ, 493, 180

Massey, P., Bresolin, F., Kudritzki, R.P., Puls, J., Pauldrach, A.W.A., 2004, ApJ, in press

Massey, P., 2004, ARA&A, in press

Mathys, G., 1988, A&AS, 76, 427

Mc Erlean, N.D., lennon, D.J. & Dufton, P.L., 1997, A&A, 329, 613

Mihalas, D. & Auer, L.H., 1970, ApJ, 160, 1161

Mihalas, D., 1972, ApJ, 176, 139

Mihalas, D., 1978, "Stellar atmospheres", 2nd edition, W.H. Freeman and Co., San Fransisco

Milne, E.A., 1926, MNRAS, 86, 459

Mokiem, M.R., Martín-Hernández, N.L., Lenorzer, A., de Koter, A., Tielens, A.G.G.M., 2004, A&A, 419, 319

Morton, D.C., Jenkins, E.B., Bohlin, R.C., 1968, ApJ, 154, 661

Nakamura, F. & Umemura, M., 1999, ApJ, 515, 239

Najarro, F., Hillier, D.J., Kudritzki, R.P., Krabbe, A., Genzel, R., Lutz, D., Drapatz, S., Geballe, T.R., 1994, A&A, 285, 573

Najarro, F., Krabbe, A., Genzel, R., Lutz, D., Kudritzki, R.P., Hillier, D.J., 1997, A&A, 325, 700

Nazé, Y., Chu, Y.H., Guerrero, M.A., Oey, M.S., Gruendl, R.A., Smith, R.C., 2002, AJ, 124, 3325

Olson, L.O., 1982, ApJ, 255, 267

Owocki, S.P., Castor, J.I., Rybicki, G.B., 1988, ApJ, 335, 914

Owocki, S.P. & Puls, J., 1999, ApJ, 510, 355

Owocki, S.P. & Puls, J., 2002, ApJ, 568, 965

Oey, M.S., 2004, Ap&SS, 289, 269

Pauldrach, A., Puls, J. & Kudritzki, R.P., 1986, A&A, 164, 86

Pauldrach, A.W.A., Kudritzki, R.P., Puls, J., Butler, K., Husinger, J., 1994, A&A, 283, 525

Pauldrach, A.W.A., Hoffmann, T.L., Lennon, M., 2001, A&A, 375, 161

Pittard, J.M., Stevens, I.R., Williams, P.M., Pollock, A.M.T., Skinner, S.L., Corcoran, M.F., Moffat, A.F.J., 2002, A&A, 388, 335

Prinja, R.K., Barlow, M.J. & Howarth, I.D., 1990, ApJ, 361, 607

Prinja, R.K. & Massa, D.L., 1998, Proc. 2nd Boulder-Munich workshop, PASPC, 22, 167

Puls, J., Kudritzki, R.P., Herrero, A., Pauldrach, A.W.A., Haser, S.M., Lennon, D.J., Gabler, R., Voels, S.A., Vilchez, J.M., Wachter, S., Feldmeier, A., 1996, A&A, 305, 171

Puls, J., Springmann, U., Lennon, M., 2000, A&AS, 141, 23

Rana, N.C., 1991, ARA&A, 29, 129

Rauw, G., Vreux, J.M., Stevens, I.R., Gosset, E., Sana, H., Jamar, C., Mason, K.O., 2002, A&A, 388, 552

Repolust, T., Puls, J., Herrero, A., 2004, A&A, 415, 349

Rolleston, W.R.J., Smartt, S.J., Dufton, P.L., Ryans, R.S.I., 2000, A&A, 363, 537

Sana, H., Stevens, I.R., Gosset, E., Rauw, G., Vreux, J.M., 2004, MNRAS, 350, 809

Santolaya-Rey, A.E., Puls, J., Herrero, A., 1997 A&A, 323, 488

Schaerer, D. & Schmutz, W., 1994, A&A, 288, 231

Schaerer, D., de Koter, A., Schmutz, W, Maeder, A., 1996, A&A, 310, 837

Schaerer, D. & de Koter, A., 1997, A&A, 322, 598

Schaerer, D., 2002, A&A, 382, 28

Schaerer, D., 2003, A&A, 397, 527

Schmidt-Kaler, T., 1982, in Landoldt-Börnstein, New Series, Group, VI, Vol.2, eds. K. Schaifers & H.H. Voigt (Berlin: Srpinger-Verlag), 1

Schmutz, W., 1998, in "Boulder-Munich II: Properties of Hot, Luminous stars", Ed. I. D. Howarth, ASP Conf. Series, 131, 119

Shaver, P.A., McGee, R.X., Newton, L.M., Danks, A.C., Pottasch, S.R., 1983, MNRAS, 204, 53

Shepherd, D.S., Yu, K.C., Bally, J., Testi, L., 2000, ApJ, 535, 833

Shimada, M.R., et al., 1994, in "Pulsation, rotation and mass loss in early type stars", eds. L. Balona et al. (Dordrecht: Kluwer), p. 487

Smith, K.C., & Howarth, I.D., MNRAS, 299, 1146

Sobolev, V., 1960, in "Moving envelopes of stars", Cambridge MA: Harvard University press (Russian edition, 1947)

Sokasian, A., Yoshida, N., Abel, T., Hernquist, L., Springel, V., 2004, MNRAS, 350, 47

Springmann, U.W.E. & Pauldrach, A.W.A., 1992, A&A, 262, 515

Stecklum, B., Henning, T., Eckart, A., Howell, R.R., Hoare, M.G., ApJ, 1995, 445, 153

Sung, H. & Bessel, M.S., 2004, AJ, 127, 1014

Urbaneja, M.A., Herrero, A., Kudritzki, R.P., Bresolin, F., Corral, L.J., Puls, J., 2002, A&A, 386, 1019

Vacca, W.D., Garmany, C.D., Shull, J.M., 1996, ApJ, 460, 914

Venn, K.A., 1999, ApJ, 518, 405

Vermeij, R. & van der Hulst, J.M., 2002, A&A, 391, 1081

Villamariz, M.R. & Herrero, A., 2000, A&A, 357, 597

Villamariz, M.R., Herrero, A., Becker, S.R., Butler, K., 2002, A&A, 388, 940

Vink, J., de Koter, A., Lamers, H.J.G.L.M., 1999, A&A, 350, 181

Vink, J., de Koter, A., Lamers, H.J.G.L.M., 2000, A&A, 362, 295

Vink, J., de Koter, A., Lamers, H.J.G.L.M., 2001, A&A, 369, 574

Voels, S.A., Bohannan, B., Abbott, D.C., Hummer, D.G., 1989, ApJ, 340, 1073

Walborn, N.R. & Parker, J.W., 1992, ApJ, 399, L87

Walborn, N.R., Lennon, D.J., Haser, S.M., Kudritzki, R.P., Voels, S.A., 1995, PASP, 107, 104

Walborn, N., Barbá, R.H., Brandner, W., Rubio, M., Grebel, E.K., Probst, R.G., 1999, AJ, 117, 225

Walborn, N.R., Maíz-Apellániz, J. & Barbá, R.H., 2002, AJ, 124, 1601

Walborn, N.R., Morell, N.I., Howarth, I.D., Crowther, P.A., Lennon, D.J., Massey, P., Arias, J.I., 2004, ApJ, 608, 1028

Wolfire, M.G. & Cassinelli, J.P., 1986, ApJ, 310, 207

Wolfire, M.G. & Cassinelli, J.P., 1987, ApJ, 319, 850

Wood, D.O.S. & Churchwell, E., 1989, ApJS, 69, 831

Woosley, S.E. & Weaver, T.A., 1995, ApJS, 101, 181

New atmosphere models for massive stars: line-blanketing effects and wind properties of O stars

Atmosphere models for massive stars have become very realistic since the recent inclusion of line-blanketing. In the first part of this thesis we have studied quantitatively the effects of metals on the atmospheric structure and emergent spectrum of models computed with the code CMFGEN. We have first shown that the effective temperature scale of O dwarfs was cooler than previous calibrations based on H He models. We have also shown that line-blanketing modifies the spectral energy distribution of O stars: the flux below ~ 500 Å is reduced due to the inclusion of bound-free opacities. Finally, we have tested these new SEDs thanks to the study of nebular lines emitted in compact Galactic HII regions and observed by ISO and we have found that the inclusion of line-blanketing leads to significant improvement, although the agreement with the observations is still not perfect.

In the second part of this thesis, we have studied the stellar and wind properties of O dwarfs in order to quantify their mass loss rates and modified wind momenta and their dependence on metallicity and luminosity. We have been especially interested in stars with weak winds since they have never been analysed through quantitative spectroscopy before. We have shown thar both the stellar component of the High Excitation Blob N81 in the Small Magellanic Cloud (O stars possibly members of the Vz class) and faint Galactic O dwarfs display very weak winds with mass loss rates of the order of 10^{-9} $M_\odot$ yr^{-1}. Such $\dot{M}$ are lower than ever observed and lower than predicted by hydrodynamical simulations. The same can be said about modified wind momenta so that the modified wind momentum - luminosity relation displays a break-down around $\log \frac{L}{L_\odot} = 5.2$. Several possibilities to explain such weak winds are investigated, but the exact physical reason remains unknown.